

REVIEW OF CO₂ CAPTURE TECHNOLOGIES AND SOME IMPROVEMENT OPPORTUNITIES

Sean I. Plasynski

US DOE National Energy Technology Laboratory
and

Zhong-Ying Chen

Science Applications International Corporation

KEYWORDS: Carbon Dioxide Capture, Gas Separation, Climate Change

ABSTRACT

Reducing CO₂ emissions for addressing climate change concerns is becoming increasingly important as the CO₂ concentration in the atmosphere has increased rapidly since the industrial revolution. Many mitigation methods, including CO₂ sequestration and novel CO₂ utilization, are currently under investigation. Most of these processes require CO₂ in a concentrated form. However the CO₂ from large sources such as fossil fueled power plants is mixed with nitrogen, water vapor, oxygen, and other impurities. A typical CO₂ concentration from coal fired power plants is around 15 %, while CO₂ concentrations for natural gas fired plants are less than 10 %. Therefore, capturing CO₂ from flue gas is an important common link for many mitigation methods.

The current commercial operations for capturing CO₂ from flue gas use a chemical absorption method with Monoethanol Amine (MEA) as the sorbent. The method is expensive and energy intensive. The cost of capturing a ton of CO₂ including removing impurities and compressing CO₂ to supercritical pressure using existing MEA technology would be in the order of \$40, and the power output would be significantly reduced by the energy consumption in capturing and compressing CO₂. The high capture cost and energy consumption would be a major barrier for implementing CO₂ mitigation methods. Alternative technologies may offer improvement. This paper reviews several separation technologies applicable to capture CO₂ from flue gas, and discusses improvement opportunities and research needs.

INTRODUCTION

Concern over the increased concentration of CO₂ in the atmosphere and its effect on global climate change has increased the awareness and investigation for reducing CO₂ emissions. Most of the methods for mitigation require CO₂ in a concentrated form, while the CO₂ from fossil fueled power plants is mixed with nitrogen, water vapor, oxygen, and other impurities and has low concentrations (15 % for coal fired power plants, and less than 10 % for natural gas fired plants). Therefore, capturing CO₂ from flue gas is an important common link.

The current commercial operations for capturing CO₂ from flue gas use a chemical absorption method with Monoethanol Amine (MEA) as the sorbent. The method is expensive and energy intensive. An estimate by Pergman *et al* [1] using data from an ABB/Lummus Crest brochure [2] indicated the cost of capturing a ton of CO₂ including removing impurities and compressing CO₂ to a supercritical pressure would be in the order of \$40. While compression is an energy intensive and expensive component, the capture part of MEA method actually uses more energy and costs more than compression. The high capture cost is a major barrier for implementing near term carbon sequestration methods such as injecting CO₂ for enhanced oil recovery [1].

The other major shortcoming of the current technology is its high-energy consumption. The amine based method uses a large amount of low-pressure steam for sorbent regeneration, and the total power output is significantly reduced. It could lead to 20% reduction in electricity production for a PC plant (107MW/554MW) as a study by Booras and Smelser indicated [3].

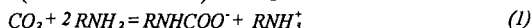
Following is a preliminary analysis of several separation technologies applicable to CO₂ capture, new power generation configurations that may simplify CO₂ capture, as well as a discussion of some improvement opportunities

GAS SEPARATION METHODS APPLICABLE FOR CO₂ CAPTURE

Capturing CO₂ from the flue gas is essentially a gas separation process. Several separation methods, including Chemical Absorption, Physical Absorption, Physical Adsorption, Membrane Technologies, and Cryogenic Separation, can achieve such a goal. The judging criteria are capture effectiveness, process economy, energy consumption, and other technical and operational issues. Other measures such as modifying of power generation configurations by using O₂/CO₂ Combustion mode and oxygen blown Gasification Combined Cycle, could alter the flue gas composition and pressure that could help the CO₂ capture. Such strategy has some benefit but also raises new technical challenges.

Chemical Absorption

Chemical Absorption with MEA as the sorbent is currently used for separating CO₂ from flue gas [Eq.1]. This method was originally used for removing CO₂ from other gases such as methane, hydrogen, etc. Chemical absorption uses the different reactivities of various gases with sorbents to separate them. The reactions need be reversible so that the spent sorbent can be regenerated. For separating CO₂ from flue gas, chemical absorption appears appropriate because CO₂ is acidic and the majority of the rest of flue gas, nitrogen, is not. CO₂ can be absorbed by many basic sorbents including alkali carbonate, aqueous ammonia, and alkanolamines. The attention needs to be paid is how the sorbents can be regenerated. The binding between sorbent molecules and CO₂ generally is strong and this offers a fast and effective removal of most of CO₂ in one stage of absorption. However, the strong binding between CO₂ and the sorbent molecules is also one of the causes for high regeneration energy requirement. Second concern is the control of impurities and miner components in the flue gas including SO₂, oxygen, etc. that may degrade the sorbents. These components have to be removed before the gas enters the absorber, or treated with appropriate measures. Lastly, because many sorbents are corrosive, only diluted solutions (around 18% for MEA) are used.



where R is the Monoethanol group. A schematic flow diagram is given at Figure 1.

In addition to the regenerator, a reclaiming operation is conducted periodically to recover amine by decomposing heat stable salts and to dispose of degradation products.

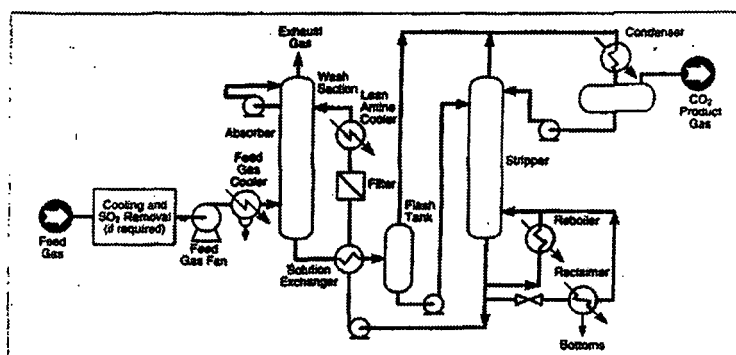


Figure 1. CO₂ Recovery Process Schematic Diagram [Ref. 2]

Physical Absorption

In physical absorption, the gas CO_2 molecules are dissolved in a liquid solvent, and no chemical reaction takes place. The binding between the CO_2 molecules and solvent molecules, being either Van der Waals type or electrostatic, is weaker than that of chemical bonds in chemisorption. The amount of gas absorbed is linearly proportional to its partial pressure (Henry's law). Figure 2 gives the CO_2 gas loading in several sorbents vs. CO_2 partial pressure. The curves show linear relations between the partial pressure and CO_2 loading for physical sorbents, and nonlinear relations for chemical sorbents. Thus the physical absorption is more effective when the partial pressure of the gas to be absorbed is high. The amount of gas absorbed also depends on the temperature. The lower the temperature, and more gas is absorbed (see methanol curves at different temperatures in Figure 2). Typical sorbents for CO_2 are methanol, N-methyl-2-pyrrolidone, polyethylene, glycol dimethyl ether, propylene carbonate and sulfolane [6].

The desorption can be achieved either by lowering pressure as in the pressure swing absorption (PSA), or raising the temperature as in the temperature swing absorption (TSA). Physical absorption has been used in gas production processes [5] to separate CO₂ from hydrogen and CO. These processes include: Rectisol that uses methanol as solvent, Selexol that uses dimethyl ether of polyethylene glycol (DMPEG), Sepsolv that uses n-oligoethylene glycol methyl isopropyl ethers (MPE), Purisol that uses N-methyl-2-pyrrolidone (NMP), and Gasolan that uses N-methylcaprolactam (NMC).

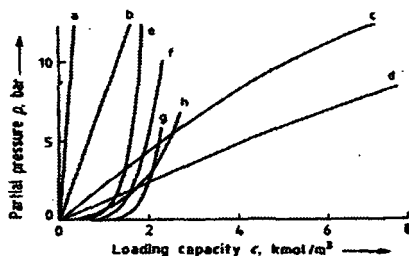


Figure 2. Equilibrium Curves of CO₂ in Various Solvents [Ref. 5]

Physical Absorption: a) H₂O (30 °C); b) N-methyl-2-pyrrolidone (110 °C); c) Methanol (-15 °C); d) Methanol (-30 °C); Chemical Absorption: e) Hot potassium carbonate solution (110 °C); f) Sulfinol solution (50 °C); g) 2.5 molar diethanolamine solution (50 °C); h) 3 molar Amisol DETA solution.

Physical Adsorption

In physical adsorption, gas is adsorbed on the solid surface by a Van der Waals force. Most important adsorbents are activated carbon, zeolite, silica gel, and aluminum oxide [4]. The separation is based on the difference in gas molecule sizes (Steric Effect), or different binding forces between gas species and the adsorbent (Equilibrium Effect or Kinetic Effect)[4]. Like physical absorption, two types of processes: Pressure Swing Adsorption and Temperature Swing Adsorption are used. Because the gas molecules are attached on the solid surface and form mono or multi-layers in *physical adsorption*, the gas loading capacity could be lower than in *physical absorption*, even though many adsorbents have large surface area per unit volume. Because of the large volume of CO₂ in the flue gas, it appears physical adsorption might not be an effective and economical solution for separating CO₂ from flue gas. The other limit in using physical adsorption for this purpose is the low gas selectivity of available sorbents [6]. However in combining with other capture methods, physical adsorption may become attractive. Such applications include membrane technologies.

Membrane Technologies

Many membranes are made with similar materials used for physical adsorbents, because the physical quality, such as porous structure and selective gas affinity, are also useful for making membranes. Membranes are microscopic sieves. Under an applied pressure some molecules will pass through the micropores in membranes, and some molecules will be stopped.

The driving forces for gas separation using membranes are generally hydrostatic pressure and concentration gradient. There has been some work done in electrically driven separation of gases via ion conduction. Two types of membrane technologies can be used for separating CO₂ from other gases: *gas separation membranes* and *gas absorption membranes*. In using gas separation membranes a hydrostatic pressure is applied and the difference in permeability of gas species leads to separation of these gases. Although using separation membranes to separate CO₂ from light hydrocarbons has met with considerable success in the petroleum, natural gas and chemical industries, this technology may not be preferable to separate CO₂ from flue gas because of the large volume of the flue gas and the compression energy requirement. A study shows that a good separation using a two-stage system would cost twice much of the conventional amine separation processes [6].

In using gas absorption membranes, a liquid sorbent is used to carry away CO₂ molecules that diffuse through the membranes, and no high hydrostatic pressure is required. In this technology, the membranes serve as an interface between the feed gas and liquid sorbent. The membranes can be made in the forms of parallel hollow fibers, and feed gas and sorbent are moving on the opposite sides of the fibers. This configuration provides significantly greater liquid-gas contact area than packed absorbers, and can reduce the size, and possibly the cost of the absorber. Additional benefits include the independent control of gas and liquid flows, and minimization of flooding, channeling, or foaming of liquid sorbent in the absorber [6]. This configuration was under investigation by Norwegian researchers as a choice for offshore operation where the space and weight of the absorber are important factors. Considerable research is still required to

address issues such as how to deal with possible clogging of hollow fibers by fine particles in the flue gas.

Cryogenic Separation

Cryogenic separation of gas mixtures uses the difference in boiling points of various gas species to separate them. Because all gas species have a distinctive boiling temperature, the cryogenic method can provide effective gas separation. The critical temperature and triple point of CO₂ are 31.6 °C and -56.8 °C respectively. Between these temperatures, CO₂ can be liquefied by compression and cooling. The major disadvantage of cryogenic method is the high-energy consumption and costs associated with gas compression and cooling. For CO₂ sequestration, liquid CO₂ is required in many cases, and the work spent on liquefying CO₂ is not wasted. However, since the concentration of CO₂ in flue gas is about 15 % or less, the energy used to compress the rest 85% of flue gas is substantial. A simple calculation for the energy requirement for liquefying CO₂ by isothermally compressing the flue gas near the critical temperature to 74 bar would spend about 30% total power output in compressing 85% of the remaining gases, and this is about 50% more than MEA process. Methods to recover that amount of compression energy spent on 85% gas components could lower total energy consumption. Generally speaking, unless novel process schemes can be developed, cryogenic separation is an energy intensive operation.

New Configurations

Reduction of capture cost may be achieved in new power plants by designs that integrate CO₂ capture with power generation. In oxygen/CO₂ combustion mode, the flue gas would consist of mostly CO₂, and its capture is simplified. The oxygen production is also expensive and energy intensive, but the benefits from oxygen combustion including better thermal efficiency, reduction in the volume of flue gas and heat loss, and simplification or elimination of NO_x control [6] can partially offset the costs. A more advanced configuration can be an oxygen-blown coal gasification combined cycle plant. In order to achieve more than 90% removal of CO₂ that would be emitted from the gas turbine by combusting the syngas, shift reactors are included to turn CO and water vapor to CO₂ and H₂. In this configuration, CO₂ needs to be separated from H₂. Because the gasifier operates at an elevated pressure, a physical separation, such as Selexol can be used. As no steam will be required to regenerate the sorbent, and no additional compression is required for the absorption process, the energy consumption for CO₂ capture is small. Booras and Smelser [3] indicated the energy consumption for 90% CO₂ removal together with compressing the captured CO₂ to a supercritical pressure would reduce power production by about 12 %, and the majority of it is spent on compressing captured CO₂ to the supercritical pressure.

Because the existing oxygen production is energy intensive and will also generate a large amount CO₂, efforts should be dedicated to the reduction of energy consumption in oxygen production such as developing oxygen separating membranes.

As the vast majority of fossil power plants will not retire for many years, developing effectively CO₂ capture technologies applicable for existing plants is an urgent task. For those plants, because of the large volume of flue gas and the low partial CO₂ pressure, chemical absorption appears to be a rational choice, as compared with other method. Productive approaches in the near term would be tapping the potentials for improving the chemical absorption, incorporating new membrane technologies, and encouraging innovative ideas.

DISCUSSION - IMPROVEMENT OPPORTUNITIES IN CHEMICAL ABSORPTION

A major limitation of using MEA as a sorbent is its high heat of absorption with CO₂ (72 KJ/mole [8], equivalent to 18% of the combustion heat of carbon (393.5 KJ/mole)). Second, the concentration of MEA is used at 15 - 20%; this means energy has to be applied to heat the solution in the stripper and to evaporate some water. The total regeneration energy required is about 900 kcal/kg CO₂ [9] or 165 KJ/mole CO₂, equivalent to 42% heat from burning a mole of carbon, and 25% of the total combustion energy generated by burning coal. Although the stripper uses a low grade steam and some heat it contains was not used for generating power anyhow, it still causes 20% reduction of power generation for a PC power plant. Several aspects should be explored to improve this process.

Search for new sorbents

New sorbents that have high CO₂ loading capacity and lower heat of absorption should be studied. Some amines are less corrosive and can be used at a higher concentration. For example

Diglycol amine (DGA) can be used at 40% concentration thus has twice as much CO₂ loading capacity as MEA (currently used at 18%). A search should be directed to amines that have a lower heat of regeneration. Several sterically hindered amines have been examined and it is found that some hindered amines can reduce the heat of regeneration by 20 % [9]. Sterically hindered amines use geometrical effect to weaken the binding between the CO₂ and amine molecules. An alternative approach is to search for amines that have weaker chemical bindings with CO₂ molecules. Other non-amine sorbents and mixture of sorbents should also be evaluated.

Increase loading of sorbent

Increasing the amine concentration could reduce the amount of sorbent solution and the requirement of regeneration heat. Ref [10] indicated that regeneration energy requirement of a 50% MEA solution will be 40% lower than a 30% MEA solution. Additional benefits of using higher sorbent loading include reduced sorbent circulation, the size of reactors, and associated costs. Using higher series amines together with increasing the sorbent concentration may offer even better benefits. Regeneration energy requirements for a 50% MDEA (Methyldiethanolamine) solution would be 50 % less than those of a 30% MEA solution [10]. Current commercial restrictions on using higher MEA concentrations are related to excessive corrosion and solvent chemistry [10]. Assessment of the material requirements, performance of concentrated solutions, overall improvement in energy consumption, and costs need to be conducted.

Improve gas-liquid contact

Better gas-liquid contact can reduce the size of absorber and costs, improve practical CO₂ loading, and reduce the sorbent circulation and regeneration energy requirement. This becomes more important for new sorbents that have lower reaction rate constants along with their lower regeneration energy requirements. A study indicated that structured packing in an absorber can provide a much higher overall mass transfer coefficient than the currently used random packing [11]. Using the membrane technology can reduce absorber size because membranes provide large contact surface between the gas and liquid. A study indicated that an absorber using membrane technology can reduce its size by 72% and its weight by 66% compared with a conventional absorption column [12].

SOME CURRENT EFFORTS IN THE US AND OTHER COUNTRIES

Because CO₂ capture is critical for CO₂ sequestration, many countries are actively engaged in research in this area. Japanese researchers are testing various sorbents and have reported sterically hindered amines that save 20% in regeneration energy. Japan is also studying membrane materials to separate CO₂ from N₂ [13]. It has also reported a Cardo polyamide that has a higher selective permeability for CO₂/N₂, and hollow fiber membranes utilizing the Cardo polyamide were tested. In addition, a pilot plant with capacity of 1000 m³N/h (~30 TPD) was set up [7]. Canadian scientists at the University of Regina in Saskatchewan built a 1.77m high absorption column, and tested new sorbents and absorber packings [11]. The Norwegian efforts include increasing amine loading, testing new chemical sorbents, using hollow fiber membranes to reduce the size of absorber, modifying reactor designs for reducing corrosion, and reducing sorbent degradation [12]. In the Netherlands, hollow fiber membrane absorber and new sorbents were studied for capturing CO₂ for feeding a greenhouse [14].

The United States built the first commercial plant capturing CO₂ from flue gas using MEA for industrial application in Trona, California. Another facility in Poteau, Oklahoma used the similar technology to produce chemical grade and food grade CO₂ from flue gas. The National Energy Technology Laboratory (NETL) has initiated a study to improve the MEA-based absorption method. Current efforts include testing hindered amines and improving gas-liquid contact in the absorber. NETL has also supported studies of innovative approaches for capturing CO₂ including "CO₂ Capture from Industrial Process Gases by High-Temperature Pressure Swing Adsorption" by Air Products, "A Novel CO₂ Separation Systems" by TDA Research Inc., "Oxygen Enriched Combustion" By CANMET, and "CO₂ Separation using Thermally Optimized Membranes" by a team led by Los Alamos National Laboratory.

SUMMARY

Recognizing improvement potential

Present operations for separating CO₂ from flue gas are used for commercial CO₂ production in which the CO₂ can be utilized for producing a revenue (carbonation of liquids, enhanced oil recovery, etc.). The new demand from climate change concerns would stimulate research efforts to examine new opportunities. Capturing CO₂ for climate change also offers more flexibility

than industrial separation because high CO₂ capture and purity may not be necessarily required. Technologies not suited for industrial applications can still serve as a candidate for climate change concerns if the costs and energy consumption are favorable.

Improved chemical absorptions

A high priority in the near term would be tapping improvement potentials in chemical absorption to reduce the energy requirement. Significant reduction in cost and energy consumption could be achieved by studying new sorbents, increasing loading, improve gas/liquid contact, etc.

Physical absorption can be incorporated in advanced IGCC plants

Physical absorption can be effective when the partial gas pressure is high and the temperature is low. In integrating CO₂ capture in the power or fuel generation cycles, physical absorption will be a good choice. Examples include the O₂-blown pressurized gasifier and combined cycles.

Collaboration with Industry

Capturing CO₂ for climate change poses a new challenge for the gas separation industry, and provides new incentives and opportunities. The progress made in improving CO₂ capture in turn will benefit other gas separations. There could be many potential collaborations between DOE sponsored research and industrial interests that would speed up the progress in developing advanced CO₂ capture technologies.

REFERENCES

1. Bergman, P. D., E. M. Winter, and Z.-Y. Chen, "Disposal of Power Plant CO₂ in Depleted Oil and Gas Reservoirs in Texas", *Energy Convers. Mgmt* Vol.38, Suppl., pp. S211-216, 1997.
2. ABB Lummus Crest, Inc. CO₂ Recovery from Flue Gas - Kerr McGee Lummus Carbon Dioxide Recovery Technology, Technical Brochure.
3. Booras, G.S., and S.C. Smelser, "An Engineering and Economic Evaluation of CO₂ Removal from Fossil-Fuel-Fired Power Plants", *Energy* Vol. 16, No11/12, pp. 1295-1305, 1991.
4. Mersmann, A., "Adsorption" in *Ullmann's Encyclopedia of Industrial Chemistry*, Vol. B3, pp. 9-1 to 9-52, VCH publishers, New York, 1988.
5. Hiller, H., et al, "Gas Production" in *Ullmann's Encyclopedia of Industrial Chemistry*, Vol. A 12, pp. 251-265, VCH publishers, New York, 1989.
6. Meisen, A., and X. Shuai, "Research and Development Issues in CO₂ Capture" *Energy Convers. Mgmt* Vol.38, Suppl., pp. S37-S42, 1997.
7. Arashi, N., N. Oda, M. Yamada, H. Ota, S. Umeda, and M. Tajika, "Evaluation of Test Results of 1000 m³ N/h Pilot Plant for CO₂ Absorption Using an Amine-based Solution", *Energy Convers. Mgmt* Vol. 38, Suppl., pp. S63-S68, 1997.
8. Chakma, A., "CO₂ Capture Processes- Opportunities for Improved Energy Efficiencies", *Energy Convers. Mgmt* Vol. 38, Suppl., pp. S51-S56, 1997.
9. Mimura, T., H. Simayoshi, T. Suda, M. Iijima, and S. Mituoka, "Development of Energy Saving Technology for Flue Gas Carbon Dioxide Recovery in Power Plant by Chemical Absorption Method and Steam System", *Energy Convers. Mgmt* Vol.38., Suppl., pp. S57-S62, 1997.
10. Leci, C. L., "Development Requirement for Absorption Processes for Effective CO₂ Capture from Power Plants", *Energy Convers. Mgmt* Vol.38, Suppl., pp. S45- S50, 1997.
11. Aroonwilas, A., and P. Tontiwachwuthikul, "Mass Transfer Studies of High Performance Structured Packing for CO₂ Separation Processes", *Energy Convers., Mgmt* Vol. 38, Suppl., pp. S75-S80, 1997.
12. Falk-Petersen, O., and H. Dannstrom, "Separation of Carbon Dioxide from Offshore Gas Turbine Exhaust", *Energy Covers., Mgmt* Vol.38, Suppl., pp. S81-S86, 1997.
13. Tokuda, Y., E. Fujisaa, N. Okabayashi, N. Matsumiya, K. Takagi, H. Mano, K. Haraya, and M. Sato, "Development of Hollow Fiber Membranes for CO₂ Separation", *Energy Convers. Mgmt* Vol. 38, Suppl., pp. S111-S116, 1997.
14. Feron, P. H. M., and A. E. Jansen, "The Production of Carbon Dioxide from Flue Gas by Membrane Gas Absorption", *Energy Convers. Mgmt* Vol. 38, Suppl., pp. S93-S98, 1997.

Study of CO₂ Absorption and Desorption in a Packed Column

James T. Yeh and Henry W. Pennline
National Energy Technology Laboratory
U.S. Department of Energy

Kevin P. Resnik
Parsons Project Services, Inc.

P. O. Box 10940
Pittsburgh, PA 15236

ABSTRACT

Carbon dioxide, a major greenhouse gas, may need to be removed from flue gas produced by combustion of fossil fuels in order to manage future climate changes. Although conventional wet scrubbing techniques exist for removal of carbon dioxide from gas streams, the wet scrubbing techniques must improve to process large volumes of flue gas at acceptable thermal efficiencies and minimal costs. Amine scrubbing is one such technique to remove CO₂. In order to make the process more efficient, two areas of improvement were investigated: gas-liquid contacting area and the type of reactant. Pertaining to the former, various absorption tests with conventional packing material and structured packings were conducted with mono-ethanolamine (MEA), a traditional solvent, as well as with novel amines. Significant improvements in CO₂ removal were obtained with the structured packing. With respect to the amine investigation, a key to improved efficiency is the ease of regeneration of the CO₂-loaded solvent. Testing with a sterically hindered amine, 2-amino-2-methyl-1-propanol, revealed that, although absorption was somewhat less as compared to MEA, thermal regeneration was far easier. The impact of various process parameters on the absorption and desorption steps will also be discussed.

INTRODUCTION

Chemical solvent absorption is based on reactions between CO₂ and one or more basic absorbents such as aqueous solutions of mono-, di-, or tri-ethanolamine. An advantageous characteristic of absorption is that it can be reversed by sending the CO₂-rich absorbent to a desorber (or stripper) where the temperature is raised. In the case of physical absorption, CO₂ is absorbed under pressure, and the gas desorption can be achieved at reduced pressure. The regenerated absorbent is then returned to the absorber thereby creating a continuous recycling process. The disadvantages of chemical absorption processes include their limited loadings and high energy requirements resulting from the reaction stoichiometry and the heats of absorption, respectively. There are also problems of corrosion and degradation. Physical solvents include methanol, polyethylene glycol, dimethylether, and others.

All currently available CO₂ separation processes are energy intensive. In ranking energy penalty of the processes, combustion with pure oxygen is the least energy intensive (about 30% energy penalty), and is followed by chemical solvent absorption processes (about 35% energy penalty) [2]. Also it has been concluded that even the current most efficient technology will reduce energy efficiency of utility steam plants by about 30% and will increase the price of electricity by 80%, even before disposal costs are added. These results are consistent with an EPRI study on CO₂ capture and disposal [3]. Combustion with pure oxygen requires redesign of the entire combustion and boiler system, and therefore, can not be retrofitted. The chemical solvent absorption process for CO₂ capture can be retrofitted in existing boiler systems and provides a rationale to pursue near-term evolutionary capture techniques. Emerging and future electricity generation technologies and novel CO₂ capturing methods have the potential to significantly reduce electricity costs if the control of CO₂ emissions is mandated.

EXPERIMENTAL

Absorption

Figure 1 shows a typical liquid chemical absorption process for CO₂ capture. The flowsheet represents a continuous absorption/regeneration cycling process. CO₂ is captured in the absorber at approximately 38 °C and is released from the regenerator at approximately 121 °C at a much higher concentration.

In our investigation, the experimental apparatus consists of a packed-column absorber to promote

gas-liquid contact and reaction in a counter-current flow pattern. Figure 2 shows the schematic diagram of the packed column absorber. The glass absorber is 7.7-cm ID and packing height varied from 18 to 71 cm during this series of tests. It has an exterior jacket with hot water flowing in this outer jacket for absorber temperature control. The heat-jacketed section is 82.6-cm high. CO₂ absorbent enters from the top of the absorber through a spray nozzle to ensure good initial liquid distribution to the packing material. The spray nozzle, which delivers fine mists, is placed 1 inch above the packing. The liquid is electrically preheated to the reactor control temperature in the stainless steel inlet line. The baseline absorber temperature is normally set at 38 °C during CO₂ absorption. Liquid flow rate is controlled by a MicroMotion mass flowmeter. Flow rate data are continuously stored in a computer at a predetermined time interval.

Simulated flue gas enters from the bottom of the absorber. Gas flow rate is controlled by a mass flow meter controller manufactured by Tylan General. Gas flow rate data are also stored in computer files. The baseline gas composition is 15% CO₂ and 85% N₂. Sulfur oxides, hydrogen chloride, nitrogen oxides, and oxygen are not included in the simulated flue gas to avoid possible interferences with the test objectives for this series of experiments. These acid gases are known to cause degradation of the solvents. Coal-fired flue gas nominally consists of 15% CO₂ on a dry basis when the combustion takes place with 20% excess air.

The initial objectives of the experiments are: (1) to obtain first-hand data on the effect of structured packing versus traditional random (or dumped) packing on the CO₂ capture rate; (2) to obtain CO₂ capture rate data by monoethanolamine (MEA) and by a sterically hindered amine; and (3) to compare CO₂ stripping rates between CO₂-rich MEA and CO₂-rich sterically hindered amine. The sterically hindered amine used during this test series was 2-amino-2-methyl-1-propanol (AMP). AMP is a tertiary amine which reacts with CO₂ at a slower rate than MEA. Though AMP reacts with CO₂ at a slower rate, less energy is required to drive out CO₂ from its CO₂-rich solution [1]. There is a wide selection of sterically hindered amines. Recently, in Japan, Kansei Electric Power Company, in conjunction with Mitsubishi Heavy Industries Limited, has developed a sterically hindered amine specifically for CO₂ recovery from flue gas [4]. TNO, in the Netherlands, also is developing liquid absorbents for flue gas applications [5]. However, the identities of those absorbents were not disclosed.

The basic reaction chemistry for monoethanolamine and CO₂ is represented by the following reversible reaction:



This is an exothermic reaction and 72 KJ of thermal energy is released per mole of CO₂ absorbed in MEA solution. Absorption usually takes place at 38 °C. During regeneration, more thermal energy (about 165 KJ/mole CO₂) is added to the solution to release the CO₂, because a large amount of water in the 20% by weight aqueous solution must be heated to regeneration temperature. Regeneration usually takes place at 121 °C. It has been estimated that up to 80% of total cost in the CO₂ absorption/regeneration cycle is due to the regeneration procedure.

Three types of column packings are compared for their CO₂ absorption rates at identical test conditions: Intalox saddle (ceramic, random packing), 1.9-cm and the smallest available from the supplier (Norton Chemical Process Products); Flexipac structured packing supplied by Koch Engineering Company; and BX Gauze structured packing also supplied by Koch Engineering Company. Structured packing provides more gas-liquid contact surface area per unit packed volume than random packings. Thus the overall CO₂ capturing capacity and rate by the liquid absorbent is increased. The packing height ranged approximately 18 cm to 71 cm during this series of tests.

CO₂ Absorption Rate Determination

Inlet nitrogen flow, inlet CO₂ concentration (vol%), and outlet CO₂ concentration (vol%) are used to calculate instantaneous absorption rates every 10 seconds during an absorption test. The nitrogen flow is measured by a mass flow controller. The inlet and outlet CO₂ concentrations are measured by an Horiba infrared gas analyzer, which is calibrated immediately before the test. The inlet CO₂ flow rate is calculated using the following equation:

$$G_1 = [(F \times D/M)/(1 - y_1)]y_1 \quad (1)$$

where

G_i = CO₂ inlet flow rate, lb-mol/hr
 F = nitrogen gas flow rate, ft³/hr
 D = density of nitrogen, lb/ft³, at standard conditions
 M = molecular weight of nitrogen
 y_i = CO₂ mole fraction at inlet of absorber, vol%

The inlet CO₂ concentration, y_i , is averaged for the 20 data points (232 s) recorded immediately before solvent flow is initiated and is assumed constant throughout the test duration. The CO₂ inlet flowrate is controlled by a mass flow controller. The calculated flow rate, G_i , is used in the absorption calculation for data accuracy purposes. Since nitrogen gas is inert in the absorber, the outlet CO₂ flowrate is calculated using the nitrogen flow rate and outlet CO₂ concentration using the following equation:

$$G_o = [(F \times D/M)/(1 - y_o)]y_o \quad (2)$$

where

G_o = CO₂ outlet flow rate, lb-mol/hr
 y_o = CO₂ mole fraction at outlet of absorber, vol%

The CO₂ absorption rate is the difference between the inlet and outlet CO₂ flow rates. Total CO₂ absorbed in the absorber can be obtained by integrating the instantaneous rates over a selected time period. Efficiency of CO₂ absorption is defined as $[(y_i - y_o)/y_i] \times 100\%$ at steady state.

Regeneration

The CO₂ - rich liquid chemical absorbent can be regenerated by heating. CO₂ evolves from the rich liquid absorbent during the heating. This regenerated liquid absorbent is CO₂ - lean and recirculated to the absorber for reuse. The regeneration temperature is usually set at 121 °C under slightly elevated pressure in the carbon dioxide industry. In our investigation, the uniqueness of the laboratory regenerator is that the absorber was used as the regenerator during the regeneration phase of the absorption/regeneration cycle. The only difference is that higher temperature is maintained in the packed column in order to drive away CO₂ from the rich amine solution. The structured packing accelerates the CO₂ release from the CO₂ - rich amine solution. The CO₂ - rich solution, which is sprayed into the reactor, is trickling in a thin film down the extensive surface area provided by the packing. No purge gas is required during the regeneration; the recovered CO₂ is pure after condensing out the vapor. A bag meter is used to measure the total mass of CO₂ evolving from a known amount of CO₂ - rich amine solution; the time at every 2830 cm³ (0.1 ft³) advance at the bag meter is manually recorded.

RESULTS AND DISCUSSIONS

Absorber Efficiencies

Effects of absorbent (MEA) flow rate and packing type on CO₂ absorption efficiencies are compared. The test results are shown in Table 1. Higher absorbent flow rate increases CO₂ absorption efficiency as expected. Absorbent utilization is defined as efficiency divided by the stoichiometric ratio. Since it takes 2 moles of MEA to react with one mole of CO₂, the stoichiometric ratio for MEA is equal to the mole ratio divided by 2.

Three types of packings were studied for their effectiveness in CO₂ absorption: BX gauze, Flexipac, and random saddle (ceramic) packings. BX gauze and Flexipac structured packings are the products of Koch Engineering Company. At an absorbent to CO₂ mole ratio of 1.4, BX gauze improves packed column absorber efficiency by about 50% over the use of random saddle packing. Flexipac minimally improved efficiency over random saddle packing.

Comparison of CO₂ Absorption Rates

Table 2 shows that the sterically hindered amine, AMP, attained near equal CO₂ absorption rate using structured packing as compared to random saddle packing for MEA processing. In these tests, 29.2 wt% of AMP solution is used while only 20 wt% of MEA solution is used, because the molecular weight of AMP is larger than MEA. Thus equal mole concentration is maintained for both MEA and AMP in the absorbent solution, respectively. Flexipac structured packing did not significantly improve the CO₂ absorption rates.

Rate of CO₂ Regeneration: AMP vs MEA

To compare CO₂ regeneration rate between MEA and AMP, CO₂-saturated MEA and AMP solutions are prepared. The packed absorber, used as the regenerator, is only heated to 93 °C, since in the present reactor setup, this is the highest temperature that can be safely maintained to prevent the water or solution from boiling. CO₂ - saturated AMP or MEA solution is sprayed on the top of the packing, while the CO₂ releasing rate is recorded with the aid of a bagmeter. The data in Table 3 show that CO₂ releasing rate from AMP solution is about 80% faster than from MEA solution. No purge gas is used. The packed column has not been optimized, and a taller packed column is expected to improve the operation.

CONCLUSIONS

Investigations of amine-based scrubbing for CO₂ capture were performed to elucidate ways to improve this chemical absorption process. Increasing the gas-liquid contacting area has a major impact on scrubbing. Absorption tests revealed that for a particular amine, structured packing improves the absorber efficiency and absorption rate as compared to the more traditional random packing. The type of amine is also a consideration. At the same bed geometry, the conventional MEA performed much better during absorption studies than the sterically hindered amine, AMP. However, in the regeneration step, the CO₂ releasing rate from the saturated AMP solution is over 80% greater than from saturated MEA solution. By extracting information from the above results, it can be speculated that if the more easily-regenerable AMP is substituted for MEA, an overall process benefit will be obtained if a structured packing is used as compared to the random packing. Other techniques to improve the amine-based scrubbing will be investigated in the future.

DISCLAIMER

Reference in this report to any specific commercial process, product or service is to facilitate understanding and does not necessarily imply its endorsement or favoring by the United States Department of Energy.

REFERENCES

- [1] Aroonwilas, A. and P. Toniwachwuthikul. Mass Transfer of High Performance Structured Packing for CO₂ Separation Processes. Proceedings of the 3rd International Conference on Carbon Dioxide Removal, pp S75-S80. Pergamon Press, Sept. 9-11, 1996, Cambridge, MA, USA.
- [2] Herzog, H. Ed. The capture, utilization and Disposal of Carbon Dioxide from Fossil Fuel-Fired Power Plants, Vol. 1. DOE/ER-30194. 1991.
- [3] Booras, G.S. and S.C. Smelser. An Engineering and Economic Evaluation of CO₂ Removal from Fossil-Fired Power Plants, Energy, 16, pp. 1295-1305, 1991.
- [4] Mimura, T.S., M. Iijima, and S. Mitsuoka. Development on Energy Saving Technology Saving Technology for Flue Gas Carbon Dioxide Recovery by Chemical Absorption Method and Steam System in Power Plant. Proceeding of the 4th International Conference on Greenhouse Gas Control Technologies, pp 71-76. Pergamon Press, Aug.30 - Sept. 2, 1988, Interlaken, Switzerland.
- [5] Freon, P.H.M. and Jansen, A.E. Techno-economic assessment of membrane gas absorption of the production of carbon dioxide from flue gas. Proceedings of the 4th International Conference on Greenhouse Gas Control Technologies, pp 53-58. Pergamon Press, Aug. 30 - Sept. 2, 1998, Interlaken, Switzerland.

TABLE 1
Absorber Efficiency and Absorbent/CO₂ Mole Ratio

Mole ratio	Efficiency, %	Packing	Utilization, %
1.4	61.3	BX gauze	87.6
1.4	60.9	BX gauze	87.0
1.4	62.2	BX gauze	88.8
2.2	97.2	BX gauze	88.4
2.3	98.9	BX gauze	86.0
1.4	41.4	Flexipac	59.1
1.4	40.1	random saddle	57.3

Absorbent: 20 wt% MEA

Mole ratio: Mole absorbent inlet/mole CO₂ inlet

Absorber temp: 38 °C

Absorber ht: 53 cm

TABLE 2
Packing Type and Absorbent Effects on CO₂ Absorption Rate

CO ₂ Absorption Rate, kg-mol/s x 10 ⁶	Absorbent	Packing
2.65	MEA	BX gauze
1.78	MEA	Random Saddle
1.88	AMP	BX gauze
1.23	AMP	Flexipac
1.15	AMP	Random Saddle

Absorbent: 20 wt% MEA
 Absorbent: 29.2 wt% AMP
 Mole Ratio: 1.4 (for both MEA and AMP)

Absorber temp: 38 °C
 Absorber ht: 53 cm

TABLE 3
Rate of CO₂ Regeneration, AMP versus MEA

	MEA (20 wt%)	AMP (29.25 wt%)	CO ₂ regeneration rate ratio AMP/MEA
CO ₂ regeneration rate, kg-mol/s x 10 ⁶	0.56	1.03	1.83
Regeneration temp °C	93	93	N/A
CO ₂ saturated absorbent flow, lb/hr	10.7	10.7	NA

Structured packing ht: 53 cm (BX gauze)

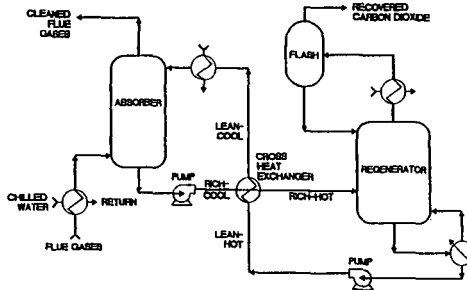


FIGURE 1 FLOWSHEET FOR THE RECOVERY OF CO₂ FROM FLUE GAS USING CHEMICAL ABSORPTION.

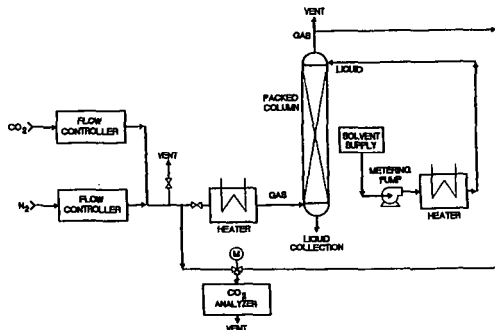


FIGURE 2. SIMPLIFIED FLOWSHEET FOR CO₂ SCRUBBING

NOVEL SOLID AMINE SORBENTS AND APPLICATIONS FOR CARBON DIOXIDE REMOVAL

Sunita Satyapal¹*, Tom Filburn², John Trela¹, and Jeremy Strange²

¹United Technologies Research Center, 411 Silver Lane, East Hartford, CT 06108

²Hamilton Sundstrand Division, One Hamilton Road, Windsor Locks, CT 06096

KEY WORDS: Carbon dioxide removal, space life support systems, solid amines

ABSTRACT

In this paper, we report on our solid amine sorbent (HSC⁺) previously developed and used for space life support applications, which may also be of interest for CO₂ removal in greenhouse gas control and other industrial processes. Adsorption capacities of the material for CO₂ pickup were determined, and long term test data show excellent performance. In addition, we have determined the heat of adsorption associated with CO₂ pickup by HSC⁺ and the effect of moisture, using isothermal flow calorimetry. We have also performed thermal gravimetric analyses on the materials to gain insight into the stability of the material and determine the temperatures at which CO₂ and constituents of HSC⁺ desorb from the surface.

INTRODUCTION

In order for CO₂ capture to be implemented as a method for climate change mitigation, technologies must be developed that are efficient, cost-effective, environmentally benign, and easily applicable. Liquid amines, used as sorbents for removing CO₂ in the natural gas industry for roughly 50 years, represent the primary competing commercial technology (lowest cost to date). However, there are several disadvantages in the use of liquid amines¹:

- High temperatures are required for regeneration (typically 100-120 °C)
- Equipment costs and maintenance for pumping or spraying liquids
- Corrosive effects of liquid amines and byproducts (corrosion inhibitors and high maintenance costs required); particularly accelerated by contaminants and acid gases
- Loss of amine due to evaporation (continual maintenance) and latent energy penalty
- Difficulty in handling liquids (as compared to solids)
- Amines must typically be maintained at <20% (occasionally up to 30%) concentration (to reduce corrosion), thereby compromising CO₂ removal capacity^{2,3}
- Additives are required to prevent foaming; and
- Oxygen typically has to be limited to prevent reaction with the solvent¹ (<8%)

The focus of our work has been on solid amine sorbents⁴⁻⁶, originally developed for space life support systems, but with several key advantages rendering them attractive for other applications: high capacity, low regeneration costs, long-term stability, intrinsically fast kinetics, no need for moisture removal from gas stream, and ease of handling. Through our Hamilton Sundstrand Space Systems International (HSSSI) Division, we previously developed a regenerable sorbent consisting of solid amine beads, known as HSC⁺. This material contains a liquid amine bonded to a high surface area, solid acrylic-based, polymeric support, followed by a coating to enhance the rate of CO₂ adsorption and desorption. Because a solid bed of material is used instead of liquids, there is minimal corrosion, and no equipment is needed to circulate or spray liquids. Our original use was for removing low concentrations of CO₂ at atmospheric pressure (typically less than 1%) and thus a key advantage is applicability to either high or low CO₂ partial pressures- i.e., compression of waste gas such as flue gas above atmospheric pressures is not mandatory. In addition, the sorbent may be made from low cost, commercially available amines and

the consumer cost is anticipated to be roughly the same as that for conventional liquid amines. Due to the anticipated long term stability of the material, periodic addition of amine, which is a necessity in conventional liquid amine systems, should not be required.

In order to design sorbents with higher capacities and favorable kinetics, a detailed study of the currently used sorbent, HSC⁺ is essential. In this paper, we report on a preliminary experimental investigation of thermodynamic data for HSC⁺ such as heats of adsorption, adsorption capacity, and thermal gravimetric analyses. Due to the exothermic nature of the CO₂ absorption reaction and the variability of CO₂ capacity with temperature, physical property data is essential to optimize system parameters (power, weight and volume). Our overall goal is to maximize the cyclic CO₂ capacity of the system while adhering to system power, weight and volume specifications. By reporting on fundamental property data, this sorbent may also be found applicable for other CO₂ removal processes as well.

EXPERIMENTAL

The adsorption capacity for CO₂ and temperature increase associated with adsorption was determined using a flow apparatus, consisting of a pyrex tube packed with HSC⁺. A thermocouple was placed at the center of the bed, the concentration of CO₂ was measured at the inlet and exit of the tube using an infra red detector (Horiba, model PIR-2000), and the mass of the tube was measured after equilibrium to determine equilibrium adsorption capacities. In order to determine the thermal stability of HSC⁺, thermal gravimetric methods (TA Instruments, model 2950) were used. All TGA experiments were taken under consistent conditions and typical sample sizes varied between 20 and 50 mg. The runs were initiated at room temperature (approximately 25°C), and the temperature was increased at a ramp rate of 10°C per minute. Nitrogen was used as a purge gas at a flow rate of roughly 70 ml/min throughout all experiments. We have also measured heats of adsorption using isothermal flow microcalorimetry. This highly sensitive technique is valuable for thermochemical measurements in which equilibrium is attained in a relatively short time. Rather than maintaining adiabatic conditions (i.e., eliminating heat flow to or from the sample cell), we maintain isothermal conditions and measure heat flow to or from the cell. Integration of the heat flow over the time period of the adsorption process provides the heat of adsorption. The instrument (CSC, model 4400) is a differential (dual cell) unit and can measure heat flows as low as 0.1 μ W (25 nanocalories/sec). Operating temperatures range from 0 to 100 °C with an adsorbent bed volume of approximately 3 cm³.

RESULTS

Figure 1 shows a typical breakthrough curve using an initial mass of 11.4 g of HSC⁺, packed in a 1 inch-diameter tube. The flow rate of CO₂ (2% in N₂) was varied between ~0.5 and 2 slpm. The maximum temperature determined in the center of the bed was 53 °C, and the maximum adsorption capacity was found to be roughly 4% by mass. These experiments employed a bed packed solely with beads of HSC⁺, whereas in practical applications, the use of a reticulated aluminum foam provides several advantages: the foam acts as a heat transfer and a bed retention medium, allowing for small scale changes in sorbent size without introducing a short-circuit path for channeling. These features are also in-place with the full-scale cycling sorbent system on-board the space shuttle orbiters.

TGA (thermal gravimetric analysis) data allow us to determine the range of temperatures at which CO₂, the coating material, and the amine(s) leave the surface of HSC⁺ under controlled conditions. As shown in Figure 2, the initial peak in the mass loss derivative curve (at ~ 60 °C) is due to removal of CO₂, with a maximum rate in mass loss between 60 and 70 °C. The second peak at ~ 200 °C is due to removal of both amine and coating.

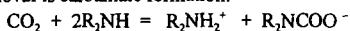
There is a change in the mechanism beginning at roughly 230 °C and complete decomposition occurs at ~ 450 °C. It is clear that loss of additional components (e.g., amine or coating) do not begin to take place until over 100 °C, illustrating thermal stability under the operating conditions we employ for space life support systems.

Figure 3 shows heat of adsorption data for the adsorption of CO₂ (2% in air) on HSC*. In this example, an approximately 0.6 g sample of HSC* was exposed to a 2% mixture of CO₂ in N₂, at a flow rate of 30 ml/min. The heat of adsorption was calculated to be -94 (±8) kJ/mol CO₂ which is consistent with results anticipated for amine + CO₂ reactions. The value we have reported is an average for 5 sample trials, and the mass % of CO₂ adsorbed is 3.7 (±0.4) %. One of the predominant sources of error is believed to be incomplete degassing to remove CO₂ and moisture, and absorption of CO₂/H₂O during material handling and sample transfer. Note that the heat of adsorption reported here represents a total heat of adsorption for adsorption of the maximum concentration of CO₂, rather than a differential or isosteric heat of adsorption for a specific CO₂ coverage.

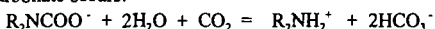
DISCUSSION

In order to design CO₂ scrubbers for various applications, detailed performance studies of the sorbent are essential. We have performed a set of preliminary experiments to determine thermophysical properties and reactivity of the solid amine sorbent HSC*. Some of the key issues to address in designing improved sorbents are: capacity, ease of reversibility, and stability. TGA and capacity measurements have shown the material to be favorable for space life support applications although a detailed understanding of the mechanism is still lacking. This is the first report of a direct measurement of the heat of adsorption of CO₂ on the material which may provide insight into the mechanism and ease of reversibility of the process.

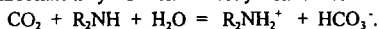
The mechanism for CO₂ removal using amines is known to be dependent on the presence of water^{7,8}. Without moisture present, the main reaction believed to account for CO₂ removal is carbamate formation:



This shows that for every one mole of amine, only ½ a mole of CO₂ is removed. However, when moisture is present, further reaction of the carbamate ion to form bicarbonate occurs:



Bicarbonate may also form directly from the amine + CO₂ + water reaction:



Therefore, in the presence of water, one mole of amine is effective in removing one mole of CO₂. This mechanism has been discussed in the literature for several years⁷. In our results, based on a measurement of mass increase alone, it appears as if roughly 3 times more CO₂ is removed in the presence of water as compared to the absence of water. An additional possibility is that reaction on the surface, and/or moisture adsorption, allows more of the active sites of the material to be available for CO₂ removal.

Measuring heats of adsorption can also provide important information on the interaction between CO₂ and the sorbent. For the case of water vapor on HSC* ΔH was found to be -47.2 (±1.0) kJ/mol H₂O, with nearly 17% mass capacity for water. As anticipated, a physisorptive process typically results in a ΔH similar to the heat of condensation of the adsorbed gas (ΔH ~ -44.0 kJ/mol at 25 °C for water). The heat released during adsorption of CO₂ is significantly larger (-94 (±8) kJ/mol CO₂) than the heat of condensation of water vapor, indicative of a strong interaction between the CO₂ and the amine surface. An illustration of mechanistic differences is shown by the measurement of mass % adsorbed in the presence of water versus in the absence of water. In the case of a dry (CO₂, N₂ mixture), there is a 3.7 (±.4) % mass gain; while the gain is 16.8 (± 3.6)% in the case of

pure water vapor, and 27.3 (\pm 2.2)% in the case of CO₂ + water vapor. It is therefore clear that higher CO₂ capabilities are achieved by coadsorption of water. Future studies will investigate the mechanism by which coadsorption aids in carbon dioxide removal and on optimizing solid amine sorbents.

CONCLUSIONS

We have measured the equilibrium CO₂ adsorption capacity for HSC⁺ to be \sim 4 % at ambient pressures, and have shown that the sorbent may be regenerated using vacuum desorption at \sim 1 Torr. Thermal gravimetric analysis was used to show that the amine is strongly bonded to the substrate and the material does not begin to lose amine/coating components until over 100 °C, while CO₂ is desorbed at roughly 60°C in a non pressure swing adsorption mode. The material has been tested for hundreds of cycles with no loss in performance.

ACKNOWLEDGEMENTS

We would like to thank Phil Birbara, Joe Genovese, and Harvey Michels for discussions related to this work and are very grateful to Larry Pryor for set up of the TGA instrument.

REFERENCES

1. M. Halmann, M. Steinberg, *Greenhouse Gas Carbon Dioxide Mitigation*, Lewis Publishers, (1999)
2. H. Herzog, D. Golomb and S. Zemba, "Feasibility, Modeling and Economics of Sequestering Power Plant CO₂ Emissions In The Deep Ocean", *Environ. Prog.*, **10**(1), 64-74, (1991)
3. C.R. Pauley, "CO₂ Recovery from Flue Gas", *Chem. Eng. Progress*, **80**, 59-62 (1984)
4. S. Satyapal, T. Filburn, H. Michels, J. Graf, "A Unique Solid Amine Sorbent useful for Capturing Low Concentrations of Carbon Dioxide", *Greenhouse Gas Control Technologies*, ed. P. Riemer et al, 113-117, Elsevier Science (1999)
5. T. Filburn, J. Genovese, T. Nalette and G. Thomas, "Advanced Regenerable CO₂ Removal Technologies Applicable to Future EMUs" SAE 961484, presented at 26th International Conference on Environmental Systems (July 1996)
6. T. Filburn, J. Genovese, L. McNamara and G. Thomas, "Rapid Cycling Amine Development Test" presented at the 48th International Astronautical Congress, (October 1997)
7. Goodridge, F., 1955, " Kinetic Studies in Gas-Liquid Systems", *Trans. Far. Soc.*, p. 1703.
8. 10. Otsubo, K., 1992, "Carbon Dioxide Adsorption Characteristics of Solid Amine", In Proceedings of International Symposium on Space Technology and Science, Tokyo, Japan, May 17-22.

Carbon Dioxide Concentration and Temperature Profiles

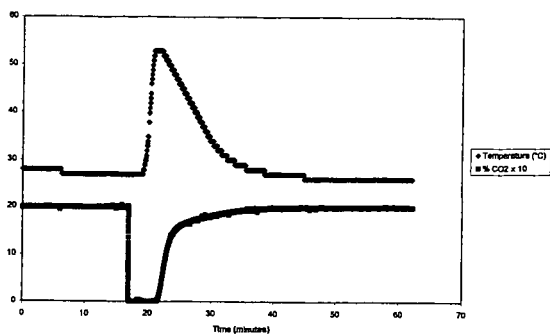


Figure 1.

TGA Data

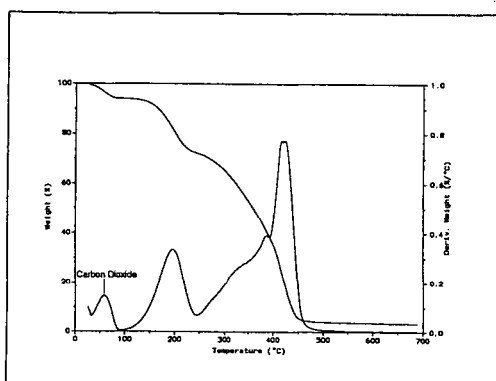


Figure 2.

* HSC* + 2% CO₂ in N₂

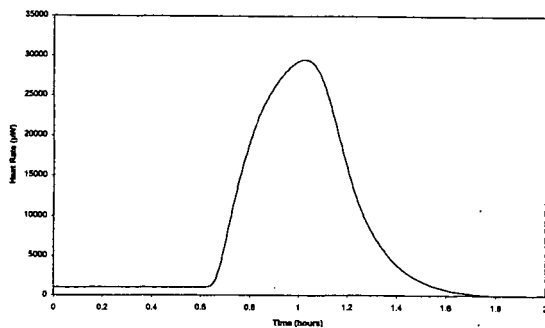


Figure 3.

DUAL ALKALINE APPROACHES FOR THE CAPTURE AND DISPOSAL OF CO₂

H.P. Huang and S.G. Chang
Environmental Energy Technology Division
Lawrence Berkeley National Laboratory
University of California
Berkeley, CA 94720

KEYWORDS: Ammonia, Activated Carbon, and Carbon Dioxide

Abstract

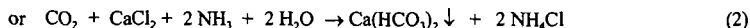
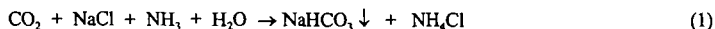
A new method being investigated to capture CO₂ uses a dual alkaline approach with the use of chloride salts in an alkaline solution. The capture of CO₂ leads to the precipitation of environmentally benign bicarbonate salts, which can be safely disposed of in the ground or ocean. A secondary alkaline is then employed to regenerate the first alkaline at ambient temperatures. During regeneration of the secondary alkaline, hydrochloric acid is produced which is subsequently injected into the ground to produce calcium chloride. The aqueous solution of calcium chloride can be either safely stored in the ground or pumped out as a salt source for the initial capture step. Another source of salt is the sodium chloride naturally available in the ocean. The dual alkaline approach offers an alternative method for CO₂ capture, separation, and disposal with the advantage of being able to avoid any new environmental problems that might occur as a result of the storage of supercritical CO₂ liquid.

1. Introduction

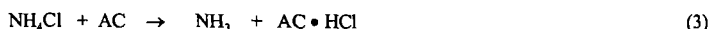
The existing approach for the sequestration of CO₂ from stationary power plants involves two steps: 1. The use of an amine (as an alkaline) to capture CO₂ from flue gas followed by steam stripping of the absorbed CO₂ at high temperatures, 2. The concentrated CO₂ gas is then pressurized to a supercritical CO₂ liquid for disposal in geologic formations and/or the deep ocean. It is known that both steps are energy intensive, especially the first step which accounts for two thirds to three fourths of the entire cost. Also, the reagent loss is substantial if flue gas contains a large amount of SO₂ and NO_x due to the difficulty in regenerating amines from heat stable salts such as amine sulfates or nitrates. Additional energy is also needed to pressurize the CO₂ gas into supercritical liquid for injection into the ground or deep-ocean. Besides the high cost of implementing the existing CO₂ sequestration approach, there is a concern about the ecological consequence resulting from the storage of CO₂ in the ocean and geological formations.

An alternative approach is the conversion of CO₂ to carbonate salts that can be safely returned to the environment. Weathering of alkaline rocks is a natural method of CO₂ sequestration. To enhance the rate of the natural process, Kojima et al. suggested that alkaline minerals could be pulverized, dissolved, and reacted with power plant CO₂ to form magnesium and calcium carbonates. Lackner et al. has extensively investigated the thermodynamics and processes of using chlorides to accelerate the carbonate formation from various minerals, including Serpentinite and Peridotites.

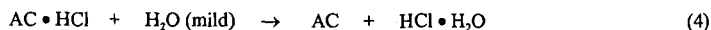
With previous research on the conversion of CO₂ to benign carbonate in mind, a new method is addressed, a dual alkaline approach. The approach involves the use of a salt in an alkaline solution, such as ammonia, to capture CO₂, leading to the formation of a bicarbonate salt.



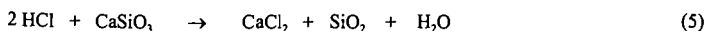
We have found that an activated carbon (AC), a secondary alkaline in solid form, can then be employed to regenerate the first alkaline at ambient temperature (25°C).



The AC can then be regenerated by the extraction of the adsorbed hydrochloric acid with water washing at a mild temperature (<100°C).



The hydrochloric acid extracted by the water may then be injected into the ground where it would react with calcium silicate minerals to produce calcium chloride.

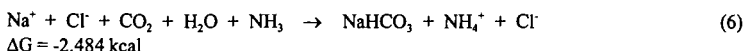


The aqueous solutions of calcium chloride produced underground can either be safely stored in the ground or provide a source of salts for the first step as shown in Eq. (2). In addition to the man-made salts produced by Eq. 5, another source of salt is brine (NaCl), which can be obtained from the ocean.

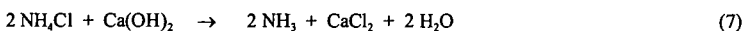
The dual alkaline approach requires low temperatures and little heat input in the regeneration of bases. The approach is self-sustaining, the needed chloride salt is supplied by the ground (Eq. 5) or can be obtained at low costs from the ocean (about \$5/ton sodium chloride based on Encyclopedia of Chemical Technology, Kirk-Othmer, Vol 21), which is especially suitable for power plants located near the coast.

Proven Process

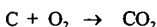
Ammonia has been demonstrated to be an effective catalyst for the reaction of CO₂ with sodium chloride in the production of sodium carbonate (the Solvay process). The reaction was performed by first saturating brine with ammonia, and then with carbon dioxide.



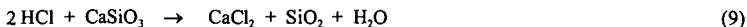
Following the reaction, sodium bicarbonate, which is fairly insoluble, was separated by filtration. Sodium carbonate is subsequently obtained by heating sodium bicarbonate. The ammonia was recovered by the reaction of ammonium chloride with lime, Ca(OH)₂ where limestone served as the source of lime



However, this scheme poses several drawbacks when applied to coal-fired power plants. Among others, the use of limestone for the regeneration of ammonia renders the process ineffective mainly because for every mole of CO₂ captured and transformed, two moles of NaCl are consumed, wasting a mole of NaCl that is needed to react with CO₂ produced during the calcination of limestone to lime:



To circumvent these drawbacks, activated carbon is used as a base to replace lime for the regeneration of ammonia. The HCl subsequently produced may be disposed of by reacting it with silicate minerals to produce benign CaCl₂ and SiO₂. This reaction is performed in subsurface areas by injecting HCl underground, where silicates are abundant in the Earth's crust. Plagioclase (NaAlSi₃O₈ or CaAl₂Si₂O₈), Feldspar (KAlSi₃O₈), and Amphibole [(Ca, Mg, Fe)₇Si₈O₂₂(OH)₂] constitute about 42%, 22%, and 5% in vol, respectively.



The soluble CaCl₂ salt may be pumped out of the ground for use in the fixation of additional CO₂ according to Eq. (2).

2. Experimental Approaches and Results

The use of an aqueous solution of ammonia and sodium chloride for the reaction with CO₂ to produce sodium bicarbonate precipitate is a proven process as mentioned previously. After the reaction and the separation of a sodium bicarbonate precipitate, the remaining solution contains ammonium chloride.

We have discovered that ammonium chloride can be separated into hydrochloric acid and ammonia. Experiments were performed by passing an aqueous solution of ammonium chloride ($\text{pH} = 4.7$) through a column of activated carbon. The resultant liquid was analyzed by ion chromatography. Results indicated that the liquid after the column contained more ammonium ions than chloride ions (Figure 1). The pH of the liquid also increased from 4.7 to as high as 9.5, indicating that the ammonia is regenerated from the ammonium chloride solution.

The kinetics of the decomposition of ammonium chloride and subsequent adsorption of hydrochloric acid by the acid adsorbent was studied. It was found that the reaction order was first order and 0.617 order with respect to the concentration of the adsorbent and ammonium chloride, respectively (Figure 2). The temperature dependence on the adsorption of hydrochloric acid from an ammonium chloride solution was investigated. The Van't Hoff plot indicates that the adsorption is exothermic (-2.48 kcal/mol).

The regeneration of the activated carbon with water as a function of temperature was also investigated. The kinetics of the desorption of hydrochloric acid from the adsorbent was studied at 298, 313, 333, 353, and 373°K (Figure 4). The desorption rate increased with an increase in temperature. The Van't Hoff plot showed that the enthalpy of the desorption of hydrochloric acid was 6.25 kcal. This energy was substantially less than that (47.85 kcal) required in the regeneration of MEA from an MEA-carbamate.

The capability of repeated use of the activated carbon was also demonstrated. Several cycles were performed (Figure 5). The results show that the cyclic process can sustain itself.

3. Conclusion

The research performed has demonstrated that: 1. It is feasible to capture CO_2 and directly transform it into a bicarbonate precipitate using an aqueous mixture of an alkaline and a chloride, 2. It is possible to regenerate ammonia from an ammonium chloride solution using an activated carbon. Future work includes the study of the effectiveness of different types of activated carbon and adsorbents for the regeneration of ammonia from ammonium chloride solutions.

Acknowledgments

This work was supported by the Assistant Secretary for Fossil Energy, U.S. Department of Energy, under Contract DE-AC03-76SF00098 through the National Energy Technology Laboratory.

Reference

1. Kojima, T., Nagamine, A., Ueno, N., Uemiya, S., Absorption and Fixation of Carbon Dioxide by Rock Weathering, *Energy Convers. Mgmt.*, 38, S461, 1997.
2. Lackner, K.S., Wendt, C. H., Butt, D. P., Joyce, E. L., and Sharp, D. H., Carbon Dioxide Disposal in Carbonate Minerals, *Energy*, 20, 1153, 1995.

Fig. 1 Production of NH_3 from NH_4Cl using Carbon

Conditions: 10 g AC, 100 ml 10 mM NH_4Cl solution was pumped at 1 ml/min flow rate at room temp.

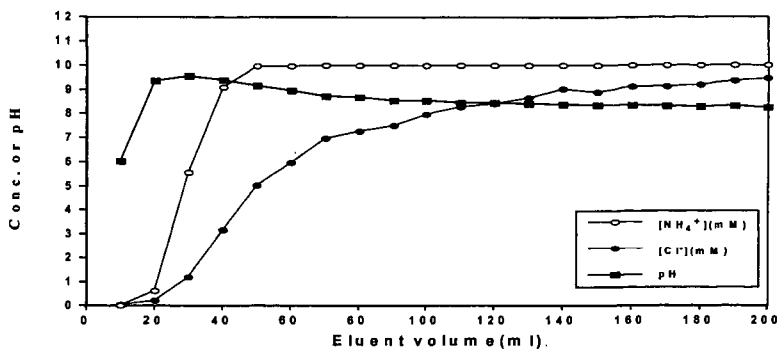


Fig. 2 Reaction order for the adsorption of HCl from NH_4Cl by Carbon

Conditions: 2g AC, 100ml NH_4Cl solution, room temp., stirring speed: 800 rpm

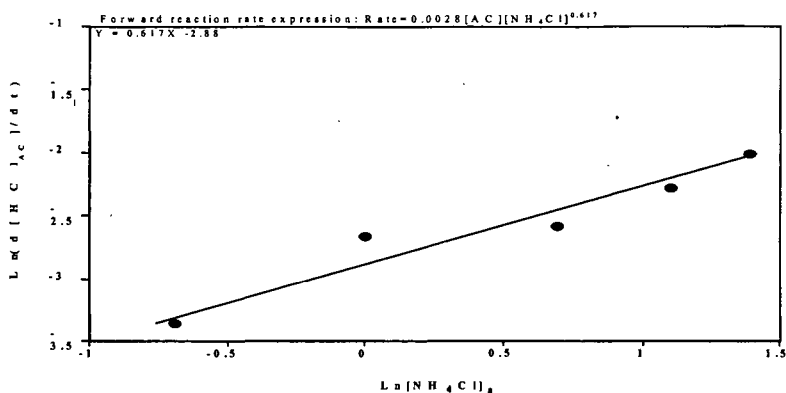


Fig. 3 Van't Hoff plot for adsorption of HCl on Carbon from NH_4Cl solution

Conditions: 10 g AC, 500 ml 12 mM NH_4Cl solution, stirring speed: 800 rpm at 293, 313, 333, 353 K, respectively

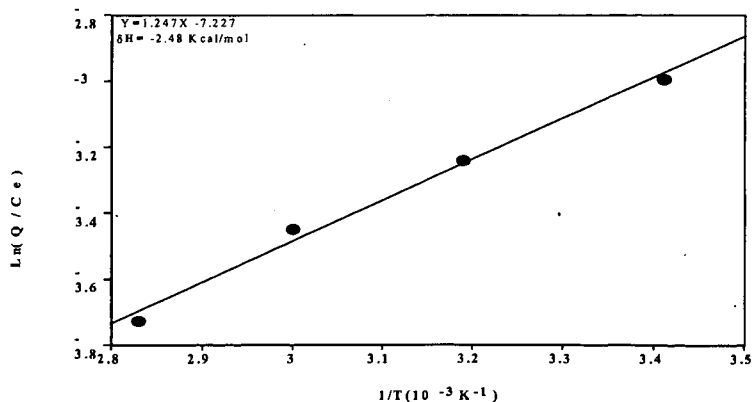


Fig. 4 Van't Hoff plot for desorption of HCl from Carbon in water

Conditions: 10 g AC, 500 ml, 2 mM NH_4Cl solution, stirring speed: 800 rpm at 298, 313, 333, 353, 373 K, respectively

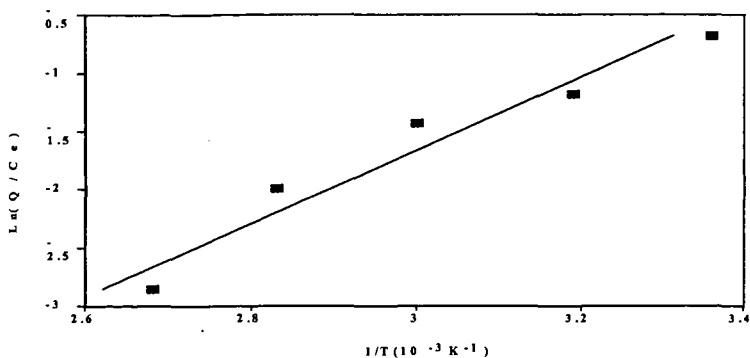
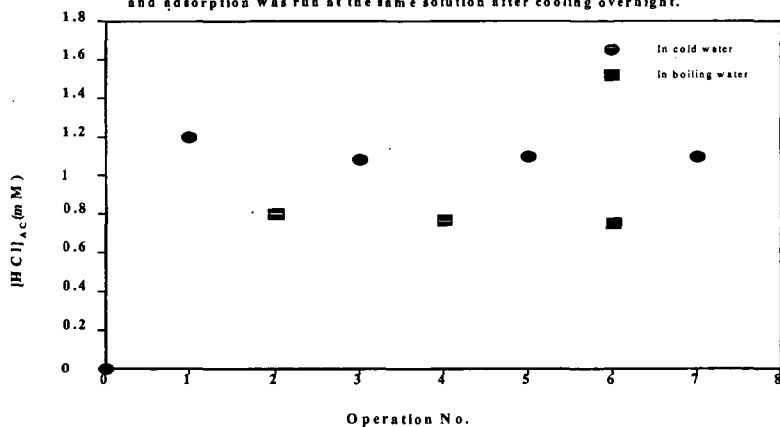


Fig. 5 Regenerability of Carbon for HCl adsorption

Conditions: 2 g AC adsorbed 1.225 mM HCl from 100 ml 1.3 mM HCl solution at room temp. The desorption was run at 100 ml boiling water, and adsorption was run at the same solution after cooling overnight.



A.S.Kovvali, H.Chen, G. Obuskovic, S. Majumdar and K.K. Sirkar

Center for Membrane Technologies

Department of Chemical Engineering, Chemistry and Environmental Science
New Jersey Institute of Technology, Newark, NJ 07102.**Keywords:** CO₂, Separation, Liquid membranes**Introduction**

Gas separation using facilitated transport membranes (FTM) has been extensively investigated. Major advantages of FTM over conventional polymeric membranes include higher permeabilities for reacting species like CO₂ and the resultant high selectivities over nonreacting species like N₂. This is due to the facilitating reaction mechanism in FTMs compared to the solution-diffusion mechanism in polymeric membranes. FTMs are particularly attractive at low reacting species concentrations where the driving force is very low. This is especially advantageous for removal and sequestration of carbon dioxide when it is present in low concentrations. Facilitated transport membranes include immobilized liquid membranes (ILMs) where the carrier in a solvent, usually water, is immobilized in the pores of the membrane.

Despite the obvious advantages offered by the ILMs, commercialization of these membranes is restricted because of the inherent limitation of stability of the liquid membrane. The reasons for the ILM instability are: (a) absence of any chemical bonding to the support matrix; (b) evaporation of the solvent liquid into gas phases during operation; (c) lower breakthrough pressures. To improve the ILM stability, the feed and sweep sides are completely humidified minimizing solvent loss by evaporation. Another alternative is to use low-volatile and hygroscopic solvents for the ILM preparation.

We have been studying replacement of water by glycerol in the ILMs for separating CO₂ from N₂ streams (Chen et al., 1999, 2000). Since glycerol is very viscous when dry and has higher viscosity than polyethylene glycol (PEG) 400 at ambient temperatures, we can expect lower permeabilities for the non-reacting species like N₂ and higher selectivity for the reacting species like CO₂. The general objective of this work is to investigate CO₂ permeation characteristics through glycerol-based ILMs using different carriers like sodium carbonate and sodium salt of glycine.

Both carriers mentioned above require a solvent, either water or glycerol, to dissolve them. The use of novel carrier liquids/oligomers which do not require any additional solvent was also explored. These carrier liquids are non-volatile and have high densities of reactive functional groups for CO₂ separation. Such carrier liquids eliminate the necessity of a solvent; the liquid membranes formed can be inherently stable.

Experimental Details

Hydrophilized polyvinylidene fluoride (PVDF) and hydrophilized polypropylene Celgard 2500 were used as flat membrane substrates; hydrophilized polysulfone was used as the hollow fiber substrate. ILMs were prepared by immersion or coating techniques. After immersing the substrate in the solution for a pre-determined period of time, it was removed from the solution: the extra liquid on the substrate surface was wiped away. If the immersion time is long enough, the ILMs prepared can be assumed to fill the entire pore length of the substrate. For hollow fibers, immobilization was carried out on the shell side before the fibers were placed in a shell casing.

The CO₂/N₂ permeances were measured by the flow cell technique which involved passing an inert sweep gas on the permeate side whose flow rate and compositions were continuously monitored. The feed gas stream was humidified with water before passing into the cell. For feed gas relative humidities (RHs) less than 100%, dry and humidified gases were blended to achieve the required RH. Sweep gas used was dry helium. The experimental procedure consisted of setting the feed gas flow rate such that the partial pressure of CO₂ remained essentially constant along the feed side of the membrane which had a small area. The sweep flow rate was set to keep the partial pressure of CO₂ in the permeate relatively small, yet high enough for accurate measurement. The permeation rates of CO₂ and N₂ were determined from their concentrations in the sweep gas and sweep gas flow rate.

Results and Discussion

Glycerol-based ILMs having average thicknesses ranging from 15 to 100 microns were studied. The concentrations of carriers examined were: 0 to 4.0 mol/dm³ for sodium carbonate, 0.3-5 mol/dm³ for glycine-Na. While 1M sodium carbonate solution was clear and stable, higher carbonate concentrations in glycerol led to turbid solutions at room temperature. Most of the glycine-Na based ILMs were prepared using less than 3M solutions; higher concentration solutions tend to be turbid. An oligomer providing high liquid density of reactive functional groups was also studied with and without the presence of glycerol as solvent in the ILM.

Table 1 compares the effect of carrier concentration of sodium carbonate and glycine-Na in glycerol systems in hydrophilized PVDF membranes. The entering feed gas was completely humidified with water. For a sodium carbonate concentration of 0.1M, the CO₂ permeability through the ILM increased by a factor of nearly 100 compared with that through pure glycerol. In the higher carrier concentration range, the permeability of carbon dioxide did not increase proportional to the carrier concentration, but there was an increase in the selectivity of ILM for CO₂, possibly due to increase in solution viscosity and ionic strength and the resultant decrease in solubility and diffusivity of N₂ in the ILM. Similar behavior was observed for glycine-Na-glycerol based ILMs also. Some data were obtained for membranes having both carriers, glycine-Na and sodium carbonate. The mixed carriers-based ILMs gave CO₂/N₂ permeation performances close to the glycine-Na based ILMs of corresponding concentration.

Table 1. ILM performance in hydrophilized PVDF membranes: effect of carrier concentration

Carrier concentration (M)	CO ₂ partial pressure (cm Hg)	CO ₂ permeability (Barrer)	N ₂ Permeability (Barrer)	CO ₂ /N ₂ Selectivity
Na₂CO₃				
0	0.55	14	3.83	3.7
0.1	0.55	1420	3.98	359
1	0.55	2880	3.34	850
4	0.55	2540	1.75	1460
Glycine-Na				
0.3	0.44	4280	1.98	2210
2.25	0.41	9730	1.89	5140
3.5	0.42	8510	1.16	7310
5.0	0.38	7370	1.27	5780
1.0 M Na ₂ CO ₃ + 1.0 M Glycine-Na	0.48	4980	2.22	2240

The partial pressure of carbon dioxide affected the CO₂ permeance according to the expected facilitated transport behavior. At lower CO₂ partial pressures, the CO₂ permeance of sodium carbonate-glycerol ILM or glycine-Na-glycerol ILM is greater than those of DEA-PEG 400 ILM (Saha and Chakma, 1995), but lower than MEA-water ILM (Teramoto et al., 1996). At higher CO₂ partial pressures, fixed-carrier membranes (Quinn and Laciak, 1997) achieve higher CO₂ permeances than these ILMs.

The glycine Na-glycerol ILMs were operated for more than 600 hours with no change in performance. The mechanical stability of the glycerol-based ILMs was studied by subjecting the ILMs to different feed inlet relative humidities. In one such experiment, a 0.6 M sodium carbonate-glycerol ILM was subjected to feed inlet relative humidity varying with time to observe any deterioration in performance. The feed stream was 10.6% CO₂-balance N₂ gas mixture. The feed RH was 100% for the first 48 hrs. Then it was decreased to 13% and maintained at that level for 100 hours. Finally, the feed RH was increased to 100% again. The ILM was not at all damaged during the 100 hour flow of very low RH feed stream: the ILM performance could be restored to normal levels when the feed RH was increased to 100% again. The low volatility and highly hygroscopic nature of glycerol are responsible for the observed stability, which is a marked improvement over water-based ILMs. Glycine-Na-glycerol based ILMs also demonstrated similar behavior.

Table 2 shows the performances for glycerol based ILMs in hydrophilized Celgard 2500 membranes. The permeabilities obtained in the Celgard-based ILMs were lower than those obtained in PVDF membrane based ILMs. The Celgard-based membranes in general showed lower selectivities which may be attributed to imperfect hydrophilization.

Table 3 presents the results for hollow fiber based ILMs. The effective CO₂ permeance for a 0.53% CO₂-balance N₂ feed gas mixture can be as high as 3.13×10^{-5} cc/cm².s.cmHg with CO₂/N₂ separation factors in the range of 2000-2700. These data represent so far the highest carbon dioxide permeances observed in this study for hollow fiber membranes. Further, they compare very well with the highest CO₂ permeances obtained with flat film ILMs in our studies. The stability of these ILMs was excellent over the period studied, namely, 300 hours with no apparent deterioration in CO₂ permeance or CO₂/N₂ selectivity.

Table 2. Effect of carrier concentration on the ILM performance in hydrophilized Celgard 2500 membranes

Carrier concentration	CO ₂ partial pressure (cm Hg)	CO ₂ permeability (Barrer)	N ₂ Permeability (Barrer)	CO ₂ /N ₂ Selectivity
1 M Na ₂ CO ₃	0.52	863	1.24	698
2.25M Glycine-Na	0.46	3920	2.23	1770

Table 3. Performance of hydrophilic polysulfone fiber modules for 3.0 M glycine-Na-glycerol solution.

Δp_{CO_2} cmHg	Feed in/out RH %	$(Q/t)_{eff,N_2}$ cc/cm ² .s.cmHg	$(Q/t)_{eff,CO_2}$ cc/cm ² .s.cmHg	CO ₂ /N ₂ selectivity
0.335	91.7/n.a.	1.34e-8	3.13e-5	2330
0.390	100/n.a.	2.54e-8	2.93e-5	1150
0.410	87.6/50.0	1.54e-8	2.98e-5	1930
0.410	93.0/66.0	1.36e-8	3.08e-5	2260
0.410	92.3/32.4	1.14e-8	2.81e-5	2460

The novel use of non-volatile highly functionalized oligomers for selective CO₂ separation was also studied. Pure oligomer was used as the ILM. The results were remarkable. The CO₂-N₂ separation factor could go very close to 19,000 at a low CO₂ partial pressure of 0.36 cm Hg. The corresponding CO₂ permeability was 4100 Barrers. At higher CO₂ partial pressures of about 30 cmHg, the CO₂-N₂ separation factor was around 700. This behavior reflects the classical carrier saturation behavior of facilitated transport membranes. This particular ILM was used continuously for more than 35 days without any visible signs of any membrane leaks or instability. During this period, the ILM was subjected to different carbon dioxide partial pressures, transmembrane pressures, and feed inlet relative humidities. The oligomer-based ILMs appear to function almost as a molecular gate for CO₂ vis-à-vis other inert gases, N₂, O₂ etc at low partial pressures and high feed RHs. Addition of glycerol to the oligomer in forming the ILM tends to reduce the CO₂-N₂ selectivity because of higher N₂ solubility in glycerol.

Conclusions

- 1) Glycerol-based immobilized liquid membranes provide mechanically stable performance even when exposed to low humidity feed gases. The performance of the ILM can be restored to the normal levels once higher feed humidity is reintroduced. This is a radical improvement over conventional water-based ILMs.
- 2) ILMs were operated for more than 600 hrs continuously without any deterioration in performance.
- 3) Increase in partial pressure of CO₂ reduces the CO₂ permeability and its selectivity as expected for the facilitated transport mechanism.
- 4) Novel non-volatile oligomeric liquids having high density of reactive functional groups appear to function as a CO₂-selective molecular gate, yielding very high CO₂-N₂ selectivities at low CO₂ partial pressures and high feed side RHs.

References

- H.Chen, A.S.Kovvali, S.Majumdar and K.K.Sirkar, "Selective CO₂ separation from CO₂-N₂ mixtures by immobilized carbonate-glycerol membranes", *Ind.Eng.Chem.Res.* 38 (1999) 3489.
- H.Chen, A.S.Kovvali, K.K.Sirkar, Selective CO₂ separation from CO₂-N₂ mixtures by immobilized glycine-Na-glycerol membranes, *Ind.Eng.Chem.Res.*, In press (2000).
- R. Quinn and D.V.Laciak, "Polyelectrolyte membranes for acid gas separations", *J.Membr. Sci.*, 131(1997) 49.
- S.Saha and A.Chakma, "Selective CO₂ separation from CO₂/C₂H₆ mixtures by immobilized diethanolamine/PEG membranes", *J.Membr.Sci.*, 98(1995)157.
- M.Teramoto, K.Nakai, N.Ohnishi, Q.Huang, T.Watari, and H.Matsuyama, "Facilitated transport of carbon dioxide through supported liquid membrane of aqueous amine solutions", *Ind.Eng.Chem.Res.*, 35(1996)538.

ADSORPTION OF CO₂ ON MOLECULAR SIEVES AND ACTIVATED CARBON

Ranjani Siriwardane, Ming Shen, Edward Fisher, James Poston, and Duane H. Smith

U.S. Department of Energy, National Energy Technology Laboratory, 3610 Collins Ferry Road,
P.O.Box 880, Morgantown, WV 26507-0880

Key Words - Volumetric adsorption of CO₂, Pressure swing adsorption of CO₂, Adsorbents for CO₂ separation and removal

INTRODUCTION

Fossil fuels supply more than 98% of the world's energy needs. However, the combustion of fossil fuels is one of the major sources of the green house gas CO₂. It is necessary to develop technologies that will allow us to utilize the fossil fuels while reducing the emissions of green house gases. Commercial CO₂ capture technology that exists today is very expensive and energy intensive. Improved technologies for CO₂ capture are necessary to achieve low energy penalties. Pressure swing adsorption (PSA) is one of the potential techniques that could be applicable for removal of CO₂ from high pressure gas streams such as those encountered in Integrated Gasification Combined Cycle (IGCC) systems.

PSA processes are based on preferential adsorption of the desired gas (eg. CO₂) on porous materials at a high pressure. When the pressure is decreased, the gas is desorbed from the porous sorbent and the sorbent can be reused for subsequent adsorption. PSA technology has gained interest due to low energy requirements and low capital investment costs. Development of regenerable sorbents that have high selectivity for CO₂ and high adsorption capacity for CO₂ is critical for the success of the PSA process.

In this work three sorbents from United Catalyst, namely, molecular sieve 13X, molecular sieve 4A, and activated carbon were utilized to study the adsorption of CO₂. Volumetric adsorption studies of CO₂, N₂, or H₂ with the three sorbents were conducted at 25 °C up to a pressure of 300 psi (~2x 10⁶ Pa).

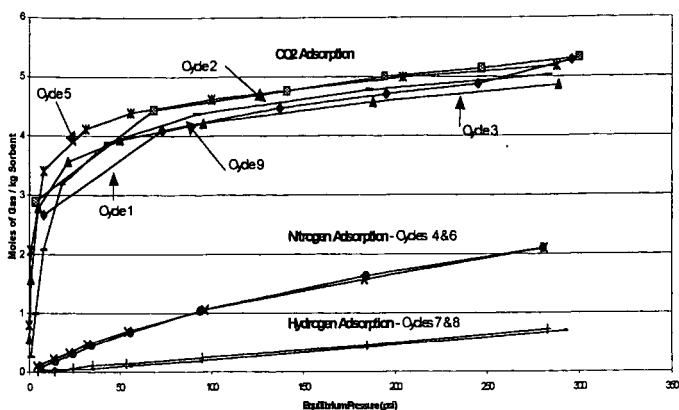
EXPERIMENTAL

The sorbents Zeochem-Z10-02/13X molecular sieve, Z4-01/4A molecular sieve and activated carbon were obtained from United Catalysts, Inc. Adsorption isotherms at 25 °C of pure CO₂, N₂, or H₂ on molecular sieve 13X, molecular sieve 4A, and activated carbon were measured up to an equilibrium pressure of about 300 psi (~2x 10⁶ Pa) utilizing volumetric adsorption apparatus. Approximately 10 ml of the sorbent materials were placed in the sample chamber, which was evacuated to ~5x10⁻⁵ Torr. The amount of CO₂ adsorbed was calculated utilizing the pressure measurements before and after the exposure of the sample chamber to CO₂. Base line data with CO₂ were obtained utilizing 10 ml of glass beads. A total of 9-10 adsorption cycles were performed with each sorbent. After each cycle the sorbent was evacuated overnight. After two cycles, each, were performed with hydrogen and nitrogen, a final cycle was performed with CO₂ to evaluate whether the adsorption was affected by the adsorption of the other gases.

RESULTS AND DISCUSSION

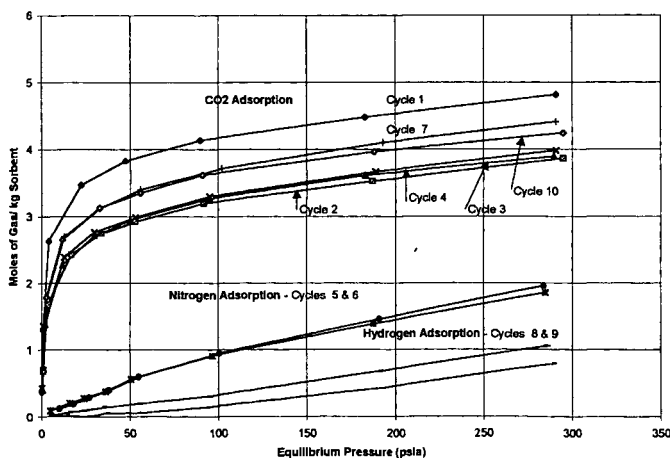
Volumetric adsorption isotherms of CO₂, N₂ and H₂ on molecular sieve 13X at 25 °C are shown in Figure 1. Up to 50 psi the CO₂ adsorption increased rapidly when the pressure was increased. The increase in CO₂ adsorption after 50 psi appeared to be gradual. The adsorption isotherms for repeated cycles were very similar. This indicated that the adsorption is fully reversible and complete regeneration can be obtained by evacuation of the material after adsorption. At all pressures, adsorption isotherms of nitrogen were lower than those of the CO₂, and adsorption isotherms of hydrogen were significantly lower than those of CO₂. Both nitrogen and hydrogen isotherms were completely reversible. Preferential adsorption of CO₂ indicates that this material can be used for separation of CO₂ from some gas mixtures. The final adsorption isotherm (cycle 9-which was obtained after the adsorption experiments with nitrogen and hydrogen) was conducted with CO₂ and it is very similar to the previous adsorption isotherms with CO₂. This indicates that the sorbent was not affected by the adsorption of nitrogen and hydrogen.

Figure 1 - Adsorption Isotherms on ZEOCHEM-Z1042P13



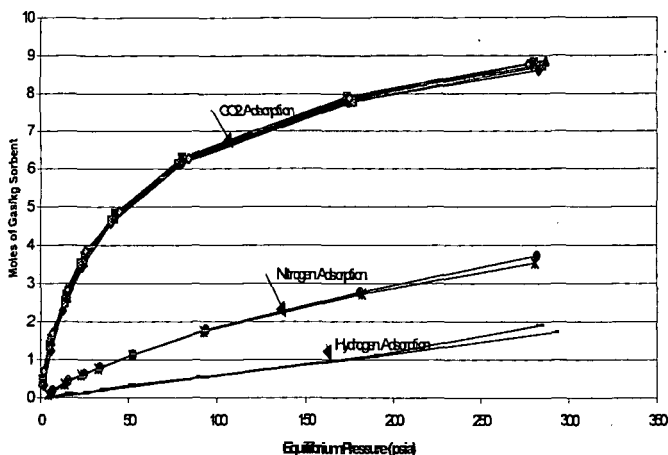
The volumetric adsorption isotherms for molecular sieve 4A(Zeochem Z4-01-4A) are shown in Figure 2. The adsorption isotherms indicate that the uptake of CO₂ is higher than the uptakes of the other two gases, nitrogen and hydrogen. This preferential uptake of CO₂ makes this sorbent suitable for the separation of CO₂ from gaseous mixtures. The adsorption isotherms of CO₂ for molecular sieve 4A are not highly reproducible, indicating that the adsorption is not completely reversible. The adsorption at the first cycle was the highest. The uptake of CO₂ for molecular sieve 4A was lower than that of molecular sieve 13X at all equilibrium pressures up to 250 psia. However, both nitrogen and hydrogen adsorption isotherms of molecular sieve 4A appear to be similar to those of molecular sieve 13X. The adsorptions of nitrogen and hydrogen did not affect the final adsorption isotherm of CO₂.

Figure2 - Adsorption Isotherms of ZEOCHEM Z4-01-4A/4x8



The adsorption isotherms for activated carbon are shown in Figure 3. It is interesting to note that all the isotherms are extremely reproducible, which indicates the excellent reversibility of adsorption. The CO_2 uptake for activated carbon was lower than that of the two molecular sieves at lower pressures (< 50 psi), but at higher pressures the CO_2 uptake for activated carbon was higher than that of the molecular sieves. Nitrogen and hydrogen adsorption isotherms appear to be very reproducible. The final CO_2 adsorption cycle (cycle 10) was very similar to the first cycle, which indicated that the sorbent was not affected by the adsorption of other gases.

Figure 3-Adsorption isotherms of Activated Carbon



CONCLUSIONS

All three sorbents, molecular sieves 13X and 4A, and activated carbon, showed preferential adsorption of CO_2 over nitrogen or hydrogen at all pressures up to 250 psia. The molecular sieve 13X showed better CO_2 uptake than molecular sieve 4A. At lower pressures activated carbon had a lower CO_2 uptake than the uptakes of the molecular sieves, but at higher pressures the adsorption was higher for activated carbon than for the molecular sieves.

SEPARATION AND RECOVERY OF CO₂ FROM EXHAUSTED GAS BY HYDRATES

Fumio KIYONO

National Institute for Resources and Environment, MITI, Japan

16-3, Onogawa, Tsukuba, Ibaraki, 305-8569, Japan

E-mail : kiyono@nire.go.jp

Keywords: Separation, Phase equilibrium, Hydrate

ABSTRACT

Hydrates have the peculiar crystal structure that one guest molecule is surrounded with a cage composed by water molecules. These water molecules are connected by the hydrogen bonding each other, but there is no chemical bonding between the guest molecule and the water molecules. In this paper I will show the possibility of hydrate's application to solve environmental problems. The cage-like structure of hydrates can be utilized as an environmental pollutant gas separation method since in mixture hydrates the molar fraction of components in a hydrate phase is different from that in a gas phase. Firstly properties of hydrates concerning with the separation technology are summarized concisely. Potential function between the water molecules and the guest molecule is calculated for CO₂, N₂ and O₂. And hydrate-gas equilibrium in CO₂-N₂-O₂ mixture is predicted. Then, based on these data, the separation technology with hydrates is demonstrated.

INTRODUCTION

Hydrates have been classified as one of clathrate compounds and show the peculiar structure that one gas molecule exists in the cage composed by water molecules. The molecule in the cage is called a guest molecule and many kinds of gas molecules like argon, oxygen, nitrogen, xenon, carbon dioxide, nitric monoxide, sulfur dioxide, and hydrogen sulfide may become a guest molecule. The forming condition of hydrates is generally in low temperature and high pressure, and this condition is different with the type of the guest molecule.

Recently, the separation technology that uses the functional material having recognition ability of molecules has been attracting many attentions. For instance, Crown ether, shown in Fig.1, can recognize and capture a molecule that fits the molecular space of the crown ether. This property of the crown ether can be utilized in the separation technology. In that case recognition and capture of the molecule are carried out based upon the molecular size. On the other hand, hydrates have the recognition ability based upon the potential energy between the guest molecule and water molecules in addition to the ability based upon the molecular size.

In this paper I take the possibility of hydrates as the functional material having the molecular recognition ability and report the result of applying this ability of hydrates to the separation of the carbon dioxide from the exhausted gas. Firstly the properties of hydrates concerning separation are introduced and the separation process using hydrates is explained. Then in relation to the molecular recognition ability of hydrates, the potential functions between the guest molecule and water molecules are presented for each guest molecule of carbon dioxide, oxygen or nitrogen. Some examples of the phase equilibrium calculation that can be used to recover carbon dioxide from the exhausted gas are shown. Lastly experimental apparatus demonstrating this technology is introduced and some experimental results are shown.

HYDRATES

Fig.2 shows models of the cage composed by water molecules and Table 1 indicates structural properties and geometric constants of the cage. Water molecules occupy summits of the polygon and are connected by the hydrogen bonding each other. And each cage contains one guest molecule. Though there are many kinds of molecules that can be held in the cage, some

restrictions exist to be contained in the cage. At first, the size of the molecule must be proper to be inside of the cage because the diameter of the cage is constant and fixed. In other words, hydrates have the molecular recognition ability depending on the molecular size. And the molecule whose size is extremely smaller than the cage size cannot make hydrates. Next, it is necessary not to make the hydrogen bonding between water molecules. Table 2 shows guest molecules that make hydrates and their van der Waals diameter.

SEPARATION BY HYDRATES

Each cage of hydrates contains one guest molecule, but considering bulk hydrates, there is no need for all guest molecules to be same. In other words, mixture hydrates exists. Mixture hydrates means the situation that different kinds of molecules are scattered in hydrates cages. Mixture gas that consists of many components shown in table 2 can form mixture hydrates.

The separation technology by hydrates is based on the fact that molar fraction of components in the hydrate phase is different from that in the gas phase. Fig 3 illustrates this situation conceptually. In this case, the gas phase contains same number of black molecules and white molecules but the hydrates phase includes larger number of black molecules. That is to say, the stability of the hydrate cage is different according to the type of the guest molecule.

Fig.4 expresses the situation illustrated in Fig.2 by a diagram. This figure is also conceptual. In this figure a vapor line and a hydrate line are drawn. By utilizing this figure we can design the separation process. For instance, the dotted line in this figure indicates that the vapor in which the molar fraction of black molecules is 0.5 forms hydrates at pressure P_1 and that the molar fraction of black molecules in the hydrates phase is 0.79. When dissolving these hydrates, you can obtain the vapor in which the molar fraction of black molecules is 0.79. The dashed line shows that the vapor in which the molar fraction of black molecules is 0.79 forms hydrates at pressure P_2 and that the molar fraction of black molecules in hydrates phase is 0.95. By same procedure in the former case, dissolving these hydrates, you can recover the vapor in which the molar fraction of black molecules is 0.95. The repeating process between forming and dissolving hydrates is necessary to separate mixture gas by hydrates.

MOLECULAR RECOGNITION BY HYDRATES

Molecular recognition of hydrates is carried out by two mechanisms. One is based upon molecular size and the other is based upon the difference of the potential function between the guest molecule and water molecules. Let assume that mixture gas is composed by carbon dioxide, oxygen and nitrogen, in this case each molecule can be clathrated in the cage as shown in Table 2. So next factor of the separation is the difference of potential functions among these three components. Fig.5 shows potential functions between the guest molecule and water molecules for carbon dioxide, oxygen and nitrogen. It is obvious from this figure that the depth of the potential well with carbon dioxide is deep comparing with that of oxygen and nitrogen. This fact suggests that the carbon dioxide molecule is easier to be captured in the hydrate cage than other two components.

To design the separation process for the mixture of carbon dioxide, oxygen and nitrogen, the phase equilibrium diagram for $\text{CO}_2\text{-N}_2\text{-O}_2$ mixture is necessary. After removing NO_x and SO_x , main components of exhausted gas are nitrogen, carbon dioxide, oxygen and water. Hydrate phase equilibrium calculation was carried out for the exhausted gas of this component. Fig.6 and Fig.7 demonstrate results of the phase equilibrium calculation based upon the van der Waals and Platteeuw theory. If the molar fraction of carbon dioxide in the exhausted gas is 0.12, carbon dioxide is separated and recovered by two steps of forming and dissolving hydrates.

EXPERIMENTAL APPARATUS AND RESULTS

Fig.8 illustrates the experimental apparatus. The high-pressure vessel was made by sus303

and its diameter was 150mm. The molar fraction of mixture gas was controlled by mass flow meters. The mixture gas was pressurized by a booster pump then introduced to the vessel. Hydrates were made by the spray method. Pressurized water was jetted out from a nozzle. Temperature was measured by platinum resistance thermometers and pressure was gauged by a pressure transducer. The molar fraction of the mixture gas and hydrates was measured by a gas chromatograph.

Table 3 shows one example of experimental results. Obviously the molar fraction of carbon dioxide in the hydrate phase is higher than that in the gas phase. But there is a gap between theoretical predictions and experimental results.

CONCLUSION

Properties of hydrates concerning with the separation were briefed. Potential function between the water molecules and the guest molecule was calculated for carbon dioxide, oxygen and nitrogen. And hydrate-gas equilibrium in CO₂-N₂-O₂ mixture was predicted. Then, based on these data, the separation technology with hydrates was demonstrated.

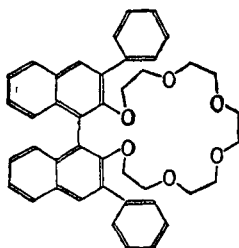


Fig.1 Crown ether

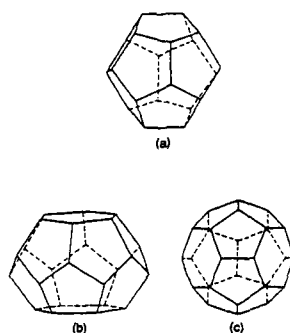


Fig.2 Cages of gas clathrate hydrates
(a) small cage. (b)(c) large cage

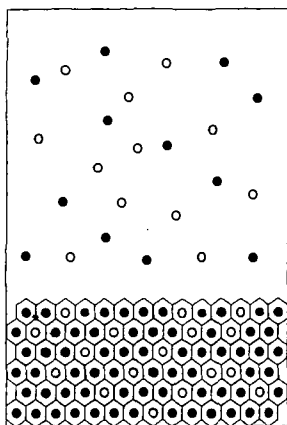


Fig.3 Mixture hydrates with vapor phase

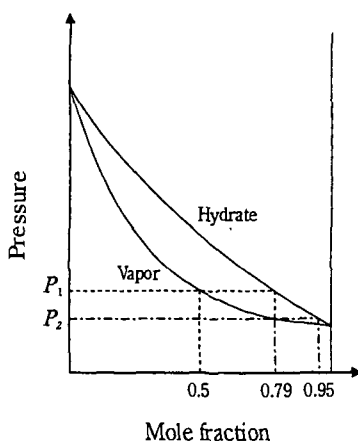


Fig.4 Hydrate-Vapor Equilibrium

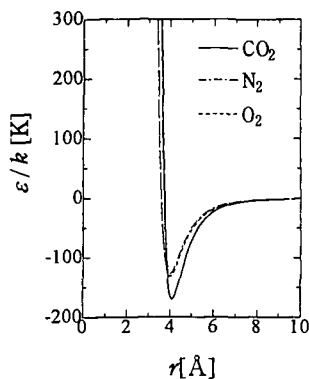


Fig.5 Potential function for the guest molecule

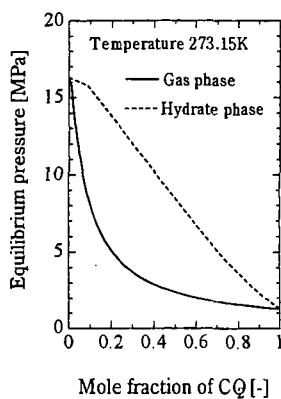


Fig.6 Phase equilibrium for $\text{CO/N}_2\text{-O}_2$ mixture hydrate where NO_2 is constant at 97.7:2.3

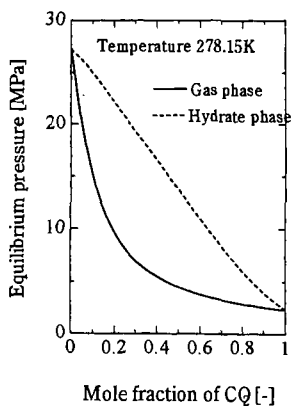


Fig.7 Phase equilibrium for $\text{CO/N}_2\text{-O}_2$ mixture hydrate where NO_2 is constant at 97.7:2.3

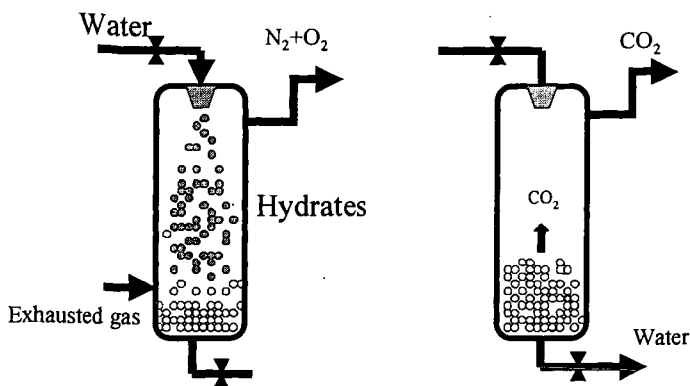


Fig.8 Experimental apparatus

Table 1 Geometry of cages

Crystal structure	I		II	
Cavity type	Small	Large	Small	Large
Description	5 ¹²	5 ¹² 6 ⁴	5 ¹²	5 ¹² 6 ⁴
Average cavity radius [nm]	0.395	0.433	0.391	0.473
Coordination number	20	24	20	28
Number of cavities per water molecule	1/23	3/23	2/17	1/17

Table 2 Guest molecules that make hydrates

Largest van der Waals Diameter [nm]	
0.70	C_4H_4
0.65	Furan Acetone
0.60	Tetrahydrofuran
0.55	1,3-Dioxolane
0.50	C_2H_4 C_3H_4
0.45	N_2O SO_2
0.40	CO_2 Xe
0.35	N_2 H_2S CH_4 Kr O_2 Ar

Table 3 Experimental results

Temperatuer:276.75K		Pressure:9.33MPa		
		N_2	O_2	CO_2
Injection port (control of WFC)		50.0%	20.0%	30.0%
Measurement of gas component before injection		51.1%	21.1%	27.9%
Collection port (measurement of gas chromatograph)		41.8%	19.1%	39.1%

COPOLYMERIZATION REACTIONS OF CARBON DIOXIDE

Ramesh K. Sharma and Edwin S. Olson

Energy & Environmental Research Center, University of North Dakota

PO Box 9018, Grand Forks, ND 58202-9018

KEYWORDS: copolymerization, sequestration, carbon dioxide

ABSTRACT

Polymerization reactions of carbon dioxide were investigated with a view toward utilization of vast amounts as a chemical feedstock. Copolymerization of carbon dioxide with formaldehyde and paraformaldehyde in the presence of a variety of catalysts was investigated. In the presence of amine catalysts or Lewis acid catalysts, carbon dioxide copolymerizes with formaldehyde or paraformaldehyde to give a water-soluble polymer of polycarbonate structure. A 1:1 alternating copolymer is proposed from its infrared spectra showing a strong ester band at 1750 cm^{-1} . From high-pressure liquid chromatography analysis, number-averaged molecular weight was determined to be about 20,000. However, mixing in 25% of a comonomer spacer (ethylene glycol) gave a polymer with twice the molecular weight. The addition of boric acid resulted in cross-linking of the polymer and a significant increase in the viscosity of the aqueous solution.

INTRODUCTION

Since 1969 when Inoue and coworkers (1, 2) first reported the synthesis of high-molecular-weight poly(propylene carbonate) by copolymerization of CO_2 and propylene oxide using organozinc catalysts, copolymerization of carbon dioxide has been widely studied (3). Because of the low cost and accessibility of the monomers and the attractive properties of polycarbonates, there has been considerable recent interest in the development of catalysts for the alternating copolymerization of carbon dioxide with epoxides (3-7). Recently, Chiang (8) reported copolymerization of carbon dioxide and formaldehyde to give a 1:1 alternating copolymer. The nature of the product from alternating copolymerization of CO_2 with carbonyl compounds in the presence of a variety of acid and base catalysts is reported here.

EXPERIMENTAL

Reactions were conducted in a 300-mL pressurized Parr autoclave with generally 16 g of CO_2 and an equimolar amount of aldehyde equivalent with 5% by weight of catalyst. Products were worked up differently depending on the solvent for the reaction. In a typical run, a mixture of aqueous formaldehyde (37%), catalyst, and dry ice was placed in a 300-mL Parr reactor. The reactor was sealed under nitrogen and heated at the desired temperature for the desired time period. The reaction products were soluble in the water solvent used for the reaction. For the reactions of paraformaldehyde and trioxane, methyl *tertiary* butyl ether (MTBE) or dioxane were used as solvents.

Polymer products were analyzed by infrared (IR) spectroscopy and gel permeation chromatography (GPC). Aqueous solutions of the polymeric products were analyzed with high-pressure GPC on a TSK30 gel column with water eluent and ultraviolet (UV) detection at 210 nm, and dioxane solutions were analyzed with a mixed pore size photoluminescence gel column in tetrahydrofuran (THF) solvent. Molecular weights (M_w) were calibrated using retention times of proteins and polymer standards with narrow M_w distributions. Reaction yields were also determined on the GPC column. The copolycarbonate peak area was calibrated using a known concentration of a standard consisting of a purified copolycarbonate sample.

RESULTS AND DISCUSSION

Base Catalysis

A comparison of the catalytic effects of a series of organic bases was conducted on the reactions of carbon dioxide with aqueous formaldehyde to form the acetal copolycarbonate ester (Figure 1). The reactions were performed in a pressurized autoclave at 120°C using organic bases, triethylamine (TEA), dimethylaminopyridine (DMAP), and diazabicyclooctane (DABCO) as catalysts for the reactions (Table 1). Chiang used TEA as the catalyst (8). The DMAP and DABCO are much more basic and were expected to exert a better catalytic effect.

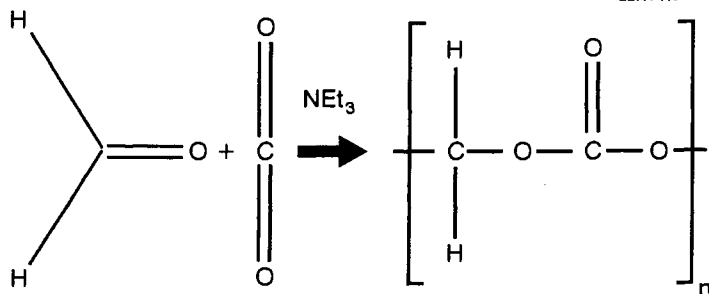


Figure 1. Acetal copolycarbonate formation.

TABLE I

Reactions of Formaldehyde							
Aldehyde	Catalyst	Solvent	Temp., °C	Time, hr	Polymer	Solubility	M _w (yield)
HCHO (37%, 40 mL)	TEA (2 g)	Water	120	100	Very viscous oil (4.01 g)	Somewhat soluble in water	23,000 (1%) 20,000 (17%) 16,000 (19%) 12,000 (8%)
HCHO (37%, 40 mL)	DMAP (2.3 g)	Water	120	100	Very viscous oil (6.2 g)	Somewhat soluble in water	22,000 (8%) 14,000 (27%) 11,500 (15%) 1000 (20%) <1000 (rest)
HCHO (37%, 40 mL)	DABCO (2.24 g)	Water	120	100	Very viscous oil (5.1 g)	Somewhat soluble in water	22,000 (22%) 1000 (17%) <1000 (rest)

* HCHO = formaldehyde.

The product from aqueous formaldehyde reaction was water-soluble. Extraction of the product with ether recovered about 70% of the base catalyst. The amount of the acetal polycarbonate was determined by GPC. Polymer peaks eluted early, and molecular weights and amounts were determined from retention times and peak areas. Low-molecular-weight oligomers were also present in the products, as evidenced by the presence of a late GPC peak. The results in Table I show that higher yields of polymer were obtained from the reaction using the more powerful base DMAP. TEA gave the lowest yield and is the most volatile.

Water was removed from the reaction products by low-vacuum distillation. The impure reaction products were tacky solids with good water and ethanol solubility, but poor solubility in THF and dioxane. IR spectroscopy of the products indicated that substantial amounts of aliphatic ester carbonyl groups were present, verifying that the desired incorporation of CO₂ to form the polycarbonate ester had occurred.

A comparison of the reaction conditions was also performed for the reaction in aqueous formaldehyde using the basic catalyst, DMAP. This reaction matrix varied temperature (120° to 200°C) and the reaction time (12 versus 24 hr). Relevant data are given in Table 2. For the 12-hr series of runs, polycarbonate yields increased with temperature as follows: 120°C, 4%; 150°C, 5%; 175°C, 9%; 200°C, 11%. Increasing the reaction time to 24 hours at 150°C increased the yield from 5% to 7%. The molecular weight of the polymer products was about 20,000 daltons for most of the reactions, but was 40,000 for the reaction at 175°C.

Two disadvantages of the aqueous formaldehyde became obvious during these initial studies: 1) the product polymers are not easily separated from the reactant formaldehyde and oligomers, owing to similarity in solubility and difficulty in distilling the formaldehyde off without decomposition; 2) the aqueous formaldehyde contains methanol (normally 5%–15% present in commercial formalin solution) that could cap the ends of the chains as an acetal linkage. Methanol and formic acid are also formed as byproducts in the reaction via the Cannizzaro reaction of aldehydes in base. Although it is displaceable from the end formaldehyde unit, it would inhibit the reaction and prevent the reaction with the CO₂.

TABLE 2

Reactions of Aqueous Formaldehyde							
Aldehyde	Catalyst	Solvent	Temp, °C	Time, hr	Polymer	Solubility	M _w (yield)
Formaldehyde (40 mL, 37%) + Ammonium Carbonate (42 g)	DMAP (2.37 g)	Water	120	24	Orange solution (1.21 g)*	Water	20,000 (58%) 19,500 (42%)
Formaldehyde (40 mL, 37%) + Dry Ice (16 g)	DMAP (2.37 g)	Water	120	24	Orange solution (1.21 g)*	Water	20,000 (58%) 19,500 (42%)
Formaldehyde (40 mL, 37%) + Dry Ice (16 g)	DMAP (2.37 g)	Water	150	12	Orange solution (1.63 g)*	Water	85,000 (2%) 20,000 (98%)
Formaldehyde (40 mL, 37%) + Dry Ice (16 g)	DMAP (2.37 g)	Water	150	24	Orange solution (2.24 g)*	Water	16,000 (51%) 15,500 (49%)
Formaldehyde (40 mL, 37%) + Dry Ice (16 g)	DMAP (2.37 g)	Water	175	12	Orange solution (2.84 g)*	Water	40,000 (100%)
Formaldehyde (40 mL, 37%) + Dry Ice (16 g)	DMAP (2.37 g)	Water	200	12	Orange solution (3.1 g)*	Water	21,000 (48%) 20,000 (52%)

* Yield based on GPC data.

Paraformaldehyde Reactions

An investigation of the reactions of paraformaldehyde with CO₂ was conducted in ether and ester solvents at 120°C (see Table 3). The products were compared for reactions with two basic catalysts, DMAP and DABCO, in two solvents, MTBE and dioxane. The molecular weights of the products were determined by high-pressure GPC. In MTBE solvent, the stronger of the base catalysts, DMAP, resulted in the highest yields of polycarbonate, but the molecular weight of the product (12,000) was lower than that obtained with DABCO (19,000 and 23,000, two peaks). Yields in dioxane were similar for the two bases. Reactions in the ester solvent (ethyl acetate) gave no polymer product. The reaction products had limited solubility in dioxane, so were easily separated as a viscous liquid by decantation of the solvent. This product exhibited high water and ethanol solubility. IR spectroscopy confirmed its polycarbonate structure.

TABLE 3

Reactions of Paraformaldehyde							
Aldehyde	Catalyst	Solvent	Temp., °C	Time, hr	Polymer	Solubility	M _w (yield)
Paraformaldehyde (15 g) + Dry Ice (16 g)	DMAP (2.37 g)	Dioxane (40 mL)	120	48	Viscous oil (6.5 g)	Water	85,000 (16%) 23,000 (48%) 22,000 (37%)
Paraformaldehyde (15 g) + Dry Ice (16 g)	DMAP (2.37 g)	Dioxane (40 mL)	120	24	—	—	—
Paraformaldehyde (15 g) + Dry Ice (16 g)	DABCO (3.58 g)	Dioxane (40 mL)	120	24	Viscous oil (3.5 g)	Water	—
Paraformaldehyde (15) + Dry Ice (16 g)	DMAP (2.3 g)	Dioxane (30 mL)	175	12	Viscous oil (10.33 g)	Water	23,000 (100%)
Paraformaldehyde (22 g) + Dry Ice (24 g)	None	Dioxane (40 mL)	120	24	—	—	—
Paraformaldehyde (15 g) + Ethanolamine (30.5 g) + Dry Ice (16 g)	DABCO (2.3 g)	Dioxane (40 mL)	120	24	Viscous oil (51 g)	Water	<1000 (86%) 19,000 (12%) 45,000 (1%)

Higher-temperature reactions of paraformaldehyde were also investigated. Reactions of paraformaldehyde with CO₂ in dioxane solvent (DMAP catalyst) at 175°C for 12 hr gave a 33% yield compared with a yield of 21% for the reaction at 120°C for 48 hr. The molecular weights were

similar for the two reactions (23,000). Thus temperature has a very significant effect in increasing the reaction yields, but does not significantly affect the molecular weights.

Paraformaldehyde gave higher yields of polymer than aqueous formaldehyde. The reaction of paraformaldehyde required the catalyzed depolymerization to the reactive monomer *in situ*. When paraformaldehyde was heated in dioxane at 120°C for 24 hr, no formaldehyde was formed. However, when paraformaldehyde was heated in dioxane in the presence of 4-dimethylaminopyridine, a significant amount of formaldehyde was formed. Quantitative analysis was not performed. Trioxane does not decompose to formaldehyde in base and therefore did not react to form polymer.

Reactions of Trioxane

Trioxane, the trimer of formaldehyde, is easily formed from formaldehyde and represents a soluble form. One reaction of trioxane was attempted with CO₂ with the DMAP catalyst at 150°C. No polymer formed in the reaction. The basic catalyst was not effective in breaking down the trioxane to formaldehyde for the copolymerization.

Reactions with Glycol Comonomer

Incorporation of ethylene glycol as a comonomer was attempted to determine if additional stability would result from the presence of the glycol or 1,2-dioxy unit in the chain. This unit would be expected to be more stable than the vicinal acetal or 1,1-dioxy unit that results from polymerization of the aldehydes. Thus, the polymerization of CO₂ with paraformaldehyde and 25% ethylene glycol in a dioxane solvent and DABCO catalyst was carried out. The ethylene glycol unit was also expected to modify the crystallinity of the chains by acting as a "spacer" group.

The copolymer products obtained with ethylene glycol contained 58% of a significantly higher-molecular-weight polymer (42,500 daltons) in addition to the normal 20,000-dalton polymer. The products were still soluble in water. Further reactions with epoxide and other comonomer mixtures are needed to understand and optimize the copolymerization reaction chemistry.

Copolymerization of Other Aldehydes

The scope of the acetal copolycarbonate reaction was expanded to include other aldehydes. Reactions of acetaldehyde were conducted with carbon dioxide in dioxane (DMAP catalyst) at 150°C (see Table 4). A low yield of polymer was obtained. The condensation product, crotonaldehyde, and low-molecular-weight oligomers were present. A repetition at this temperature gave similar results. A reaction temperature of 175°C gave higher yields than the reactions at 150°C. In contrast to the formaldehyde copolycarbonates, the polymer products from the acetaldehyde polymerization were not water-soluble. The acetaldehyde copolycarbonate is in fact soluble in dioxane and THF. The molecular weight of the product from the higher-temperature reaction (19,000) was similar to that from the 150°C reaction. With the basic catalyst, the major products result from condensation rather than copolymerization. Reactions of a second aldehyde (furfuraldehyde) with CO₂ were also investigated at 120°C. The product was, however, only partially soluble and appeared to have been converted to a pitch under the reaction conditions.

TABLE 4

Reactions of Acetaldehyde							
Aldehyde	Catalyst	Solvent	Temp., °C	Time, hr	Polymer	Solubility	M _w (yield)
Acetaldehyde (22 g) + Dry Ice (16 g)	DMAP (2.37 g)	Dioxane (40 mL)	150	12	(0.73 g)*	Dioxane	86,000 (35%) 20,000 (97%)
Acetaldehyde (22) + Dry Ice (16 g)	DMAP (2.3 g)	Dioxane (40 mL)	175	12	(5.73 g)*	Dioxane	19,000 (100%)

* Yield based on GPC data.

Lewis Acid Catalysis

A large number of Lewis acid catalysts have been tested in other laboratories for the related copolymerization of epoxides with CO₂ (2-7). One of these catalysts, zinc bisanil (7), was prepared for the reactions of CO₂ with paraformaldehyde and acetaldehyde. The function of the acid catalyst is to break down the paraformaldehyde or trioxane, as well as catalyze the copolymerization.

Several forms of the Zn bisanil catalyst were investigated. The methoxide form gave a white polymeric film on top of an orange solution. The polymeric film was separated by filtration. The white film was air-dried and weighed. The orange solution was evaporated to remove solvent. Upon removal of solvent, a highly viscous orange oil was formed. The oil was completely soluble in water and was analyzed by GPC. Relevant data are given in Table 5.

TABLE 5

Zinc Bisanil Complex-Catalyzed Reactions of Paraformaldehyde and CO₂

Aldehyde	Catalyst	Solvent	Temp., °C	Time, hr	Polymer	Solubility	M _w (yield)
Paraformaldehyde (15 g)	Bisanil + NaOMe +ZnCl ₂ (1.08 g)	Dioxane (40 mL)	150	20	Orange oil (8.71 g) White solid	Water	21,500 (18%) 18,000 (6%) 1000 (52%) <1000 (rest)
Paraformaldehyde (15 g)	Bisanil ZnCl ₂ (3.54 g)	Dioxane (40 mL)	150	12	Orange oil (4.62 g)	Water	
Paraformaldehyde (15 g)	Bisanil ZnTCA (0.5 g)	Dioxane (40 mL)	150	12	Orange oil (6.26 g)	Water	85,000 (1.5%) 24,000 (3%) 21,000 (36%) 17,000 (24%) 13,000 (7%)

The methoxide form of the catalyst gave the most product, but only a portion of it was the 21,000-dalton polymer. Most was the oligomers. The chloride form gave the least product, and since it was not soluble in water, it has not yet been analyzed in the GPC system. The trichloroacetate form was reasonably successful in producing the 17,000- to 21,000-dalton product.

ACKNOWLEDGMENT

We gratefully acknowledge the support of U.S. Department of Energy (Cooperative Agreement DE-AC26-98FT40415) for this work.

REFERENCES

1. Inoue, S.; Koinuma, H.; Tsuruta, T. *J. Polym. Sci. B* **1969**, *7*, 287.
2. Inoue, S.; Koinuma, H.; Tsuruta, T. *Makromol. Chem.* **1969**, *130*, 210.
3. Rokicki, A.; Kuran, W. *J. Macromol. Sci.-Rev. Macromol. Chem.* **1981**, *C21(1)*, 135.
4. Darensbourg, D.J.; Holtcamp, N.W. *Coord. Chem. Rev.* **1996**, *153*, 155-174.
5. Super, M.S.; Beckman, E.J. *Trends. Polymer. Sci.* **1977**, *5*, 236-40.
6. Tan, C.S.; Hsu, J. *J. Macromol.* **1997**, *30*, 3147-3150.
7. Cheng, M.; Lobkovsky, B.; Coats, G.W. *J. Am. Chem. Soc.* **1998**, *120*, 11018.
8. Chiang, W.T. *Ta T'ung Hsueh Pao.* **1978**, *8*, 255.

CARBON DIOXIDE CATALYSIS IN TRANS-ESTERIFICATION REACTION FOR THE CARBAMATION OF AMINES OF INDUSTRIAL INTEREST

A. Dibenedetto⁽¹⁾, M. Aresta⁽¹⁾, E. Quaranta⁽²⁾

⁽¹⁾ Università degli Studi di Bari, Dipartimento di Chimica, Bari, Italy, m.aresta@tin.it;

⁽²⁾ Università degli Studi di Bari, Dipartimento di Chimica e Centro MISO.

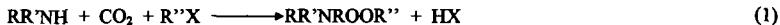
Abstract: Developing clean synthetic methodology for the production of carbamates, avoiding phosgene, is a very attractive perspective. In this paper, the reactivity of industrially relevant amines, aliphatic and aromatic, towards CO₂ and alkylating agents, or dialkyl/aryl-carbonates, is discussed. We also describe the catalytic role of carbon dioxide in the carbamation of aliphatic amines and that of P-acids in the reaction of aromatic amines towards carbonates. The reaction mechanism is discussed.

Keywords: carbon dioxide, organic carbamates, amines.

Introduction

Organic carbamates are compounds of great interest used in pharmacology, agriculture, and chemical industry.¹ Their conventional syntheses are based on the use of phosgene, a chemical difficult to handle because of its toxicity. The substitution of phosgene with less noxious starting materials represents a very important target of "green chemistry" for the future. Carbon dioxide and organic carbonates are good candidates as succedaneous for phosgene.²

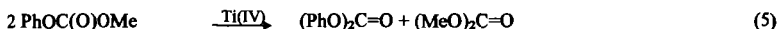
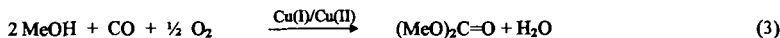
Utilisation of carbon dioxide in the synthesis of carbonate esters has been investigated for long time. We have reported about their selective synthesis from amines, CO₂ and alkylating agents³ [Eq. 1]:



Aminolysis of organic carbonates [Eq. 2] is another attractive synthetic route to carbamates, since non-phosgene routes to carbonic acid diesters are now available.



In fact, dimethylcarbonate (DMC) is produced on large-scale by oxidative carbonylation of methanol [Eq. 3], and other organic carbonates can be prepared by transesterification of DMC with phenols or long chain alcohols [Eq. 4, 5]



Carboalkoxylation of aliphatic amines requires suitable catalysts in order to observe high conversion rate and good selectivity. Lewis acids, such as AlCl₃, SnCl₂, ZnCl₂, FeCl₃, or metal (Rh, Ru) complexes, can catalytically promote the carboalkoxylation of aliphatic amines with carbonates. A major drawback is the methylation of the amine.

Recently, we have shown that carbon dioxide is an efficient catalyst for the synthesis of organic carbonates from aliphatic amines and DMC.⁴ As this synthetic approach requires mild conditions, we have extended our studies to aminofunctional silanes. The corresponding carbamates are used as modulators of physico-mechanical properties of polymeric materials.⁵ CO₂ plays again a quite interesting catalytic role.

The conventional carboalkoxylation/arylation of aromatic amines, obtained using Zn, Co, Sn, Al, Ti catalyst, has again as major drawback the alkylation/arylation of the amines. We have found that in this case organophosphorous acids can be advantageously used as very selective catalysts avoiding the alkylation/arylation process.

Experimental

All reaction and manipulation were carried out under the specified atmosphere, by using vacuum line techniques. All solvents were dried as described in literature⁶, and they were stored under dinitrogen.

Synthesis of RNHC(O)OCH₃ from aliphatic amines or aminofunctional silanes and DMC in the presence of CO₂

A solution of amine (9.15 · 10⁻³ mmol) in DMC (10 mL) was prepared under dinitrogen in an appropriate flask and, then, saturated with CO₂ (P_{CO₂} = 0.1 MPa) to give (RCH₂)₃NH₃⁺·O₂CNH(CH₂R) as white microcrystalline solid which was poorly soluble in the reaction solvent. The system was heated to 343 K for 5-7 h. After cooling to room temperatures

the reaction mixture was filtered. A small amount of unreacted $(\text{RCH}_2)_3\text{NH}_3^+\text{O}_2\text{CNH}(\text{CH}_2\text{R})$ was recovered. The solution was evaporated in vacuo and the residue fractionated on a silica gel column using a diethyl ether/hexane (2:1 v/v) eluent mixture. Solvent was evaporated from the eluted fractions and pure carbamate obtained.

When the reaction mixture was heated at 363 K, an increase of the yield (Table 1) was observed.

Table 1. Yield of carbamate esters from aliphatic amines or aminofunctional silanes and DMC in the presence of carbon dioxide

Amine	Yield (%)	Yield (%)
$(\text{PhCH}_2)_3\text{NH}_2$	50 (343 K)	92 (363 K)
$\text{C}_6\text{H}_{11}\text{NH}_2$	27 (343 K)	45 (363 K)
$\text{CH}_2=\text{CHCH}_2\text{NH}_2$	44 (343 K)	70 (363 K)
$\text{H}_2\text{N}(\text{CH}_2)_3\text{Si}(\text{OMe})_3$	70-80 (348 K)	/
$\text{H}_2\text{N}(\text{CH}_2)_3\text{Si}(\text{OEt})_3$	70-80 (348 K)	/
$\text{H}_2\text{N}(\text{CH}_2)_2\text{NH}(\text{CH}_2)_3\text{Si}(\text{OMe})_3$	100 (348 K)	/

Synthesis of mono- and di-carbamates, from aromatic di-amines and 1) diphenylcarbonate (DPC) or 2) methylphenylcarbonate (MPC), in the presence of phosphorous acids

1) A mixture of DPC (26.1 mmol), di-amine (1.35 mmol) and phosphorous acid (0.135 mmol) was heated at 363 K under stirring for 4 h. The mixture was cooled to room temperature (293 K) and the solid was extracted with diethyl ether. The white residue was analysed as pure di-carbamate. By reducing the reaction time to 30 min, it was possible to isolate the mono-carbamate (Table 2) by using the same purification procedure.

2) A mixture of MPC (6.9 mmol), di-amine (3.45 mmol) and phosphorous acid (0.347 mmol) in THF (10 mL) was stirred at 363 K for 10 h, then cooled to room temperature and the solid that precipitated was isolated by filtration and identified as $(\text{ArH}_2)(\text{O}_2\text{PPh}_2)_2$. The solution was fractionated on a silica gel column using diethyl ether/toluene for MDA and diethyl ether/hexane for TDA as eluent. Methylphenylcarbonate afforded very selectively the methylcarbamate without production of neither phenyl carbamate nor methyl-amine.

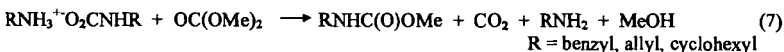
Table 2. Yield of mono- and di-carbamate synthesised from di-amines and carbonates in the presence of phosphorous acids.

Di-amine	Yield (%) of Mono-carbamate	Yield (%) of Di-carbamate	Phosphorous acid
$\text{H}_2\text{NPh}(\text{CH}_2)_2\text{PhNH}_2$	50 (DPC)	100 (DPC)	$\text{Ph}_2\text{P}(\text{O})\text{OH}$
$\text{H}_2\text{NPh}(\text{CH}_2)_2\text{PhNH}_2$	35 (MPC)	32 (MPC)	$\text{Ph}_2\text{P}(\text{O})\text{OH}$
$\text{H}_2\text{NPh}(\text{CH}_3)_2\text{NH}_2$	42 (DPC)	84 (DPC)	$\text{Ph}_2\text{P}(\text{O})\text{OH}$
$\text{H}_2\text{NPh}(\text{CH}_3)_2\text{NH}_2$	51 (MPC)	66 (MPC)	$\text{Ph}_2\text{P}(\text{O})\text{OH}$

Results

Reactivity of aliphatic amines towards DMC in the presence of carbon dioxide

Saturation of an amine solution in DMC with carbon dioxide gives the corresponding alkylammonium N-alkylcarbamate that reacts with DMC to afford N-alkylmethylcarbamates [Eqq. 6, 7].



The alkylammonium N-alkylcarbamate was prepared *in situ* and, after its precipitation, the reaction mixture was heated to the required temperature. The reaction was carried out in conventional solvents as THF, CH_2Cl_2 , and aromatics. Interestingly, the organic carbonate (DMC) could be used as reaction solvent. In order to ameliorate the reaction rate and selectivity, we have tested different reaction conditions and established that working at temperature higher than 343 K and pressure of $\text{CO}_2 = 0.1 - 0.2$ MPa produces best results. In all cases, the products have been completely characterised. By-products as ureas, N,N-substituted carbamates, secondary and tertiary amines were formed in very low yield (< 1%), if not absent. Conversely, if aliphatic amines were reacted with DMC under N_2 atmosphere the formation of carbamate esters was completely suppressed and methylation products were formed.

Reactivity of aminofunctional silanes towards DMC in the presence of carbon dioxide

Under mild condition (348 K), aminofunctional silanes as $\text{H}_2\text{N}(\text{CH}_2)_3\text{Si}(\text{OMe})_3$ (I), $\text{H}_2\text{N}(\text{CH}_2)_3\text{Si}(\text{OEt})_3$ (II), $\text{H}_2\text{N}(\text{CH}_2)_2\text{NH}(\text{CH}_2)_3\text{Si}(\text{OMe})_3$ (III) react with DMC in the presence of carbon dioxide to give the corresponding carbamate esters $\text{MeO}(\text{O})\text{CNH}(\text{CH}_2)_3\text{Si}(\text{OMe})_3$, $\text{MeO}(\text{O})\text{CNH}(\text{CH}_2)_3\text{Si}(\text{OEt})_3$, $\text{MeO}(\text{O})\text{CNH}(\text{CH}_2)_2\text{NH}(\text{CH}_2)_3\text{Si}(\text{OMe})_3$, respectively.

The carbamation reaction is very selective⁷; no formation of N-mono- or N,N'-di-methylated derivatives as by-products has been observed.

The reactivity of the di-amine (III) was higher than that of amines (I) and (II). In fact, the conversion of (III) into the corresponding carbamate was complete in less than 7 hours.

When the reactivity of silyl amines towards DMC, at 348 K, was investigated in a dinitrogen atmosphere the carbamation reaction was not observed: the formation of N-methylated species was the main process.

The development of new clean methodologies for these products is required by the fact that silyl carbamates are more and more used as silane coupling agents and as source of isocyanates, largely used in the chemical industry.

Reactivity of 4,4'-methylenedianiline (MDA) and 2,4-diaminotoluene (TDA) towards DPC or MPC in the presence of P-acids

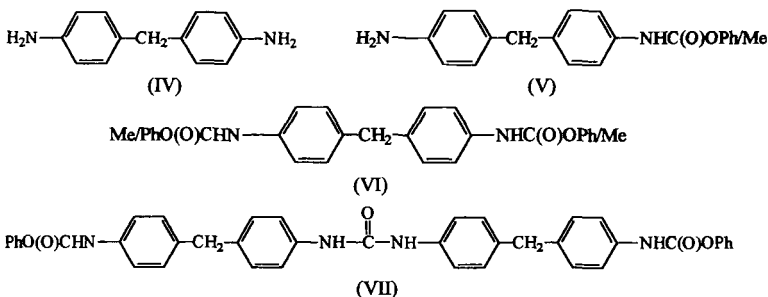
Aromatic amines show a poorer reactivity towards DPC or MPC in the presence of CO₂ with respect to aliphatic ones. This behaviour is most probably due to their low nucleophilicity. In the presence of catalysts such as Ph₂P(O)OH, (PhO)₂P(O)OH, (BuO)₂P(O)OH, (BuO)P(O)(OH)₂ aromatic mono-⁸ and di-amines^{9,10} react with DPC and DMC to give the corresponding carbamate esters with high yield and selectivity. DPC affords the phenyl carbamate, while MPC¹⁰ affords selectively the methyl carbamate and results to be a much better carboxymethylating agent than DMC.

In order to gather information about the reaction mechanism of mono- and di-carbamate of MDA (IV) with either DPC or MPC, we have carried out a kinetic study. At 363 K, mono-carbamate (V) was formed followed by di-carbamate (VI), in very good yield. In absence of the catalyst, no reaction was observed. The kinetics is first order in the amine and first order in the carbamate.¹¹

Carrying out the reaction in THF as solvent, at different temperatures (393, 363, 323 K) it was possible to establish the better reaction conditions for addressing the reaction towards the preferential formation of mono- or di-carbamate.

The temperature affects the selectivity of the reaction. In fact at 393 K, when DPC is used, the formation of urea (VII) is observed, produced by reaction of the di-carbamate with mono-carbamate. At 363 K, urea is not observed.

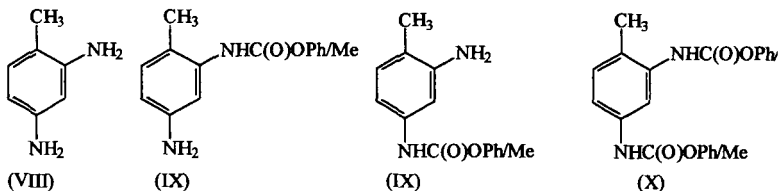
Interestingly, when MPC¹⁰ was used, urea was never detected.



The carbamation reaction was studied using solvents as diethyl ether, phenol or the carbonate itself. The use of phenol as solvent produces an inhibitory effect on the carbamation process, that results to be very selective when the carbonate is used as solvent. The conversion of the amine is quantitative.

The P-acids used as catalyst have shown a quite different activity, Ph₂P(O)OH being the most active. In the case of MPC a progressive deactivation of the catalyst was observed after sixteen hours. Further addition of catalyst results, in fact, in a significant increase of the rate of formation of both carbamates.

The P-acids show a very interesting catalytic activity also in the carbamation process of TDA (VIII). The formation of mono- (IX) and di-carbamate (X) is observed with high yield and selectivity.



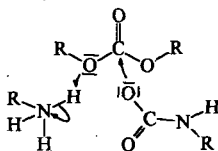
The formation of (X) involves the carbamation of two non-equivalent amino groups of the aromatic di-amine. We have demonstrated that the amino group in the *para* position is functionalised first than that in *ortho*. This is due to the hindrance of the methyl group that induces the faster reactivity of the amino group in the *para* position.

MDA and TDA carbamates have a large market as they are used as precursors of isocyanates, which are monomers for polymers.

Discussion

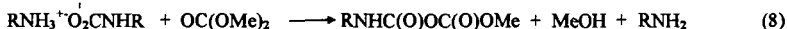
Carbon dioxide as catalyst

The results reported above, and the experiments carried out in absence and in presence of CO₂, clearly demonstrate that carbon dioxide plays a catalytic role in the carbamation of aliphatic amines. The kinetic study we have completed¹¹ shows that the rate determining step is the reaction of carbamate anion with the carbonate [Eq. 8], that bears to the formation of the mixed carbamic-carbonic anhydride RNHC(O)OC(O)OMe. Scheme 1 shows the reactive step.



Scheme 1.

Subsequently it is decarboxylated to form the carbamate ester.

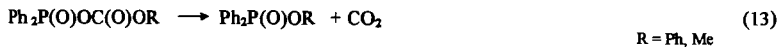
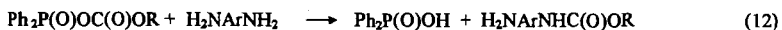
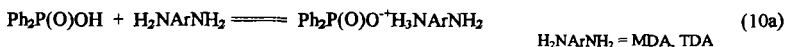


The mixed anhydride has been isolated and characterised. It is stable at low temperature and at room temperature, or higher, spontaneously converts into the carbamate with CO₂ loss. This mechanism explains why the incorporation of labelled CO₂ in the organic carbamate is not observed when RNH₃⁺O₂¹³CNHR is utilised as the starting reactant.

The reaction conditions are quite mild and selectivity is 100%.

Role of the P-acids in the carbamation process

Aromatic amines show a lower reactivity towards carbon dioxide, so the carboalkoxylation process requires suitable catalysts. Phosphorous acid can be considered as bifunctional catalysts. A plausible mechanism involves the formation of a carbonic-diphenylphosphinic mixed anhydride Ph₂P(O)OC(O)OPh, that reacts with the free aromatic amines which are converted into the carbamate esters, with regeneration of the catalyst.



R = Ph, Me

The catalyst is still active at the end of the several runs if the process involves DPC. MPC can cause a progressive deactivation of the catalyst.

This could be explained considering that in the former case the starting catalyst may be converted into Ph₂P(O)OPh, that is also a catalytic species. In the latter, the catalyst converts into Ph₂P(O)OMe that has no catalytic properties.

Conclusion

In the presence of carbon dioxide, aliphatic amines and aminofunctional silanes react with carbonates (DMC) to give the corresponding carbamate esters. The carbon dioxide catalysis is a new, useful finding. The selectivity is very high.

This methodology cannot be extended to the carboalkoxylation of aromatic amines, most probably because they show a lower reactivity towards CO₂. Aromatic amines and carbonate can be converted into the corresponding carbamate esters in the presence of P-acids as catalyst.

In both cases, the carbamation reaction is very selective and no formation of N-methyl/aryl species or ureas is observed.

Acknowledgements

This work was supported by MURST, Project no. 9803026360 and CNR-Rome. We thank ENICHEM Synthesis for a loan of DPC and DMC.

References

1. (a) Barthelemy, *J. Lyon Pharm.* **1986**, 37(6), 297; (b) Tai-The Wu, Huang, J.; Arrington, N. D.; Dill, G. M. *J. Agric. Food Chem.* **1987**, 35, 817; (c) Kato, T.; Suzuki, K.; Takahashi, J.; Kamoshita, K. *J. Pesticide Sci.* **1984**, 9, 489; (d) Picardi, P. *La Chimica e l'Industria* **1986**, 68(11), 108; (e) Rivetti, F.; Romano, U.; Sasselli, M. *U.S. Pat.* 4514339, **1985**.
2. M. Aresta and E. Quaranta, *ChemTech*, **1997**, 27(3), 32.
3. (a) M. Aresta and E. Quaranta, *J. Org. Chem.* **1988**, 53, 4153; M. Aresta and E. Quaranta, *Ital. Pat.* 1198206; M. Aresta and E. Quaranta, *Ital. Pat. Appl.* 22740 A/89.
4. M. Aresta and E. Quaranta, *Tetrahedron*, **1991**, 47, 9489; M. Aresta and E. Quaranta *Ital. Pat.* 1237207, **1993**.
5. Organofunctional Silanes - Union Carbide (Organosilicon products, System, Services) **1991**.
6. Perrin, D. D.; Armarego, W. L. F.; Perrin, D. R. *Purification of Laboratory Chemicals*; Pergamon Press: Oxford, England, **1986**.
7. M. Aresta, E. Quaranta, , *J. Appl. Organomet. Chem.* in press.
8. M. Aresta; C. Berloco; E. Quaranta, *Tetrahedron* **1995**, 51, 8073.
9. M. Aresta, A. Dibenedetto, E. Quaranta, *Tetrahedron* **54(1998)** 14145-14156.
10. M. Aresta, A. Dibenedetto, E. Quaranta, *Green Chemistry*, **1999**, 237-242.
11. M. Aresta, A. Dibenedetto, E. Quaranta, M. Boscolo and R. Larsson, submitted for publication

CAMERE PROCESS FOR CARBON DIOXIDE HYDROGENATION TO FORM METHANOL

Oh-Shim Joo

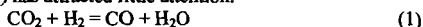
Catalysis Laboratory, Korea Institute of Science and Technology
P.O. Box 131, Cheongryang, 130-650, Seoul, South Korea

KEYWORDS: CAMERE process, methanol, CO₂ hydrogenation

INTRODUCTION

Catalytic hydrogenation of CO₂ has been one of major approaches to diminish the greenhouse gas because large amounts of CO₂ can be converted to resources such as methanol and other oxygenates compounds by the reaction. However, a direct hydrogenation of CO₂ shows low conversion, which increases the recycle gas to obtain high methanol productivity. CAMERE process (Scheme 1) has been developed to form methanol from CO₂ via a reverse-water-gas-shift reaction (1). In the CAMERE process, carbon dioxide is converted to CO and H₂O by the reverse-water-gas-shift reaction (RWReaction) and then, the produced gas (CO/CO₂/H₂) is fed to the methanol reactor after removing the water. Each reactor in the process has the recycle stream to increase CO₂ conversion to CO and carbon oxide (CO₂+CO) conversion to methanol, respectively. With the gas feeding of CO/CO₂/H₂, the water produced in the methanol reactor is chemically eliminated through a water-gas-shift reaction, increasing carbon oxide conversion to methanol and then decreasing the recycle gas in the methanol reactor. The methanol productivity in the CAMERE process depends on the CO concentration in the feed gas of the methanol reactor, which is dependent on the RWReaction conditions, especially the temperature.

A water-gas-shift reaction has been studied intensively for the last several decades in order to adjust for H₂/CO ratio in the synthesis gas (2-4). On the contrary, a reverse- water-gas-shift reaction of Eq.(1) has attracted little attention.



Besides, all the kinetic equations published on the RWReaction have been obtained over copper-containing catalysts at low temperatures (5-7). Therefore, we need to develop a mathematical model for the RWReaction at high temperature to predict the effects of operating condition changes of the RWReactor on the overall performance of the CAMERE process. A mathematical form based on a redox mechanism is obtained over Fe₂O₃/Cr₂O₃ catalyst at 773 K. Apparent activation energy for the RWReaction is calculated from an arrhenius plot of specific activities acquired over the temperature of 673-823 K, which is 109.8 kJ/mol. The CAMERE process has been evaluated based on the kinetic equation of the RWReaction to find an optimum operating condition to form methanol from CO₂.

EXPERIMENTAL

A commercial Fe₂O₃/Cr₂O₃(Fe:Cr=9:1 in molar ratio) catalyst was investigated to obtain a kinetic equation for the RWReaction over the temperature of 593-723 K. The catalyst charged in a tubular catalytic reactor is heated up to a reaction temperature in the presence of CO₂ and H₂ before the RWReaction. The RWReactions are performed under the reaction conditions of 1atm, temperature of 670-823 K, and W/F (g_{cat}.h/mol of CO₂ in the feed) of 0.05-3.7. The absence of diffusion limitations is confirmed by changing the size and the amount of the catalyst.

RESULTS AND DISCUSSION

The RWReaction is endothermic, and hence conversion of CO₂ is favored by high reaction temperature. Hence the RWReaction should be operated at high temperature above 773 K to keep CO₂ conversion up to 60%, increasing carbon oxide conversion to methanol in the second step of the CAMERE process. The kinetic studies for the RWReaction are performed in an integral plug flow reactor over Fe₂O₃/Cr₂O₃ catalyst at 773 K. A redox mechanism is derived from the best fitting of the experimental data. The surface of the Fe₂O₃/Cr₂O₃ catalyst is successively oxidized by CO₂ and reduced by H₂ by the redox mechanism. For the redox mechanism a rate expression is derived from that the step, which the catalyst surface was reduced by H₂, is a rate-determining step. The kinetic equation is expressed as follows;

$$r = \frac{P_{\text{CO}_2} P_{\text{H}_2} / P_{\text{CO}} - P_{\text{H}_2\text{O}} / K}{1/kK_1 + P_{\text{CO}_2}/kP_{\text{CO}}}$$

where, k = apparent rate constant of the RWReaction (mol h⁻¹ g_{cat}⁻¹ atm⁻¹)

K = equilibrium constant of the RWReaction (dimensionless)

K_1 = equilibrium constant of the surface oxidation step by CO₂ (dimensionless)

r = reaction rate (mol h⁻¹ g_{cat}⁻¹), P_i = partial pressure of i component (atm)

Overall apparent activation energy can be determined from the effect of temperature on the rate for the RWReaction at a constant composition. Hence the RWReaction is performed with

temperature over the W/F ($g_{cat}/h/mol$ of CO_2 in the feed) of 0.05-1.5. Figure 1 gives the experimental data and the values calculated from the kinetic equation for the RWReaction. An arrhenius type plot of $\ln(\text{rate})$ versus $1/T$ is obtained from CO_2 conversion with the reaction temperature. Figure 2 shows the activation energy of 109.77 kJ/mol for the RWReaction. The activation energy is similar to that of copper-containing catalyst (8).

The CAMERE process has been simulated based on the kinetic equation of the RWReaction and carbon oxide conversion to methanol to compare the operating conditions of the CAMERE process with those of a direct CO_2 hydrogenation. We use the published results on the carbon oxide conversion to methanol under the reaction conditions of 50 atm and 523 K (9-10). Table 1 shows the simulation results that are dependent on the presence and conditions of the RWReaction. The same amount (14.3 kgmol/hr) of CO_2 and H_2 is fed to the direct CO_2 hydrogenation and CAMERE process, respectively. In the methanol reactor the recycle gas is calculated by subtracting the purge gas (=P) from the downstream gas (=F2). To obtain methanol productivity of 2 kg mol/h, the gas of 42.82 kgmol/h should be recycled in the direct CO_2 hydrogenation process. On the other hand, the gas of 16.27 kgmol/h is recycled in the CAMERE process to form methanol of 2.06 kgmol/h where there is no recycle step in the RWReactor ($R1=0$). Moreover, the recycle gas is further reduced to 10.66 kgmol/h when the recycle ratio is the one in the RWReactor ($R1=1$). It means that the recycle gas for the same methanol production strongly depends on the CO concentration in the feed gas of the methanol reactor (F1). The CO concentration is decided by the presence of the RWReaction and the recycle ratio ($R1$). The CO concentration in the F1 stream increases when the temperature and recycle ratio of the RWReaction is increased. With the elimination of water by the RWReaction, the recycle gas of the CAMERE process is minimized compared with the direct CO_2 hydrogenation process to form the same amount of methanol. Therefore, the reactor size to obtain methanol of 2 kgmol/h in the CAMERE process can be decreased up to one fourth of the one of the direct CO_2 hydrogenation process when the product gas of 50% in the RWReactor is recycled. Table 1 indicates the relationships between CO concentrations in the feed gas with the recycle gas for the same methanol production. The water produced in direct CO_2 hydrogenation process is comparable with that in the methanol reactor of the CAMERE process, that are 2.31 kgmol/h in the direct process and 0.34 kgmol/h in the CAMERE process ($R1=1$) for the same methanol production of 2.0 kgmol/h, respectively. The pilot plant for methanol production of 5 kg/day is constructed in our laboratory.

CONCLUSIONS

A rate equation for a reverse-water-gas-shift reaction is obtained based on a redox mechanism over Fe_2O_3/Cr_2O_3 catalyst at 773 K, which apparent activation energy is 109.8 kJ/mol. The CAMERE process has been simulated based on the kinetic equation of the RWReaction and carbon oxide conversion to methanol to find an optimum operating conditions to form methanol from CO_2 . With the elimination of water by the RWReaction, the recycled gas in the CAMERE process is decreased more than four times compared with a direct CO_2 hydrogenation for the same methanol production.

REFERENCES

1. Joo, O.S., Jung, K.D., Moon, I., Rozovskii, A.Y., Lin, G.I., Han, S.H., and Uhm, S.J., *I&EC Research*, **38**, 1808 (1999).
2. Kubsh, J.E. and Dumesic, J.A., *AIChE Journal*, **28**, 793 (1982).
3. Grenoble, D.C., Estadt, M.M., and Ollis, D.F., *J. Catal.*, **67**, 90 (1981).
4. Rhodes, C., Hutchings, G.J., and Ward, A.M., *Catal. Today*, **23**, 43 (1995).
5. Herwijnen, T.V and Jong, W.A.D., *J. Catal.*, **63**, 83 (1980).
6. Gines, M.J.L., Marchi, A.J., and Apesteguia, C.R., *Appl. Catal. A*, **154**, 155 (1997).
7. Ernst, K.H., Campbell, C.T., and Moretti, G., *J. Catal.*, **134**, 66 (1992).
8. Chinen, G.C., Spencer, M.S., Waugh, K.C., and Whan, D.A., *J. Chem. Soc. Faraday Trans. I*, **83**, 2193 (1987).
9. Ushikosbi, K., Mori, K., Watanabe, T., Takeuchi, M., and Saito, M., "Advances in Chemical Conversions for Mitigating Carbon Dioxide Studies in Surface Science and Catalysis", **114**, 357 (1998).
10. Arakawa, H., Dubois, J.L., and Sayama, K., *Energy Cnvers. Mgmt.*, **33**, 521 (1992).

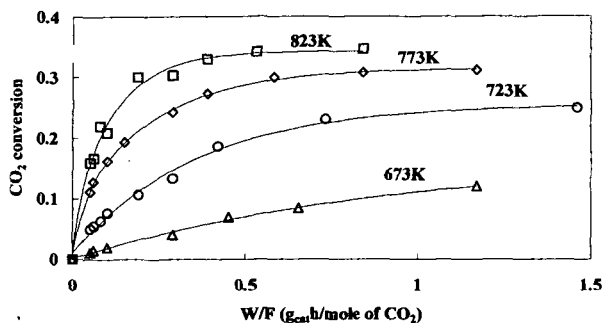


Figure 1. CO₂ conversion with reaction temperature over Fe₂O₃/Cr₂O₃ with the H₂/CO ratio of 1. The marks are experimental points; the lines are calculated values from the kinetic equation.

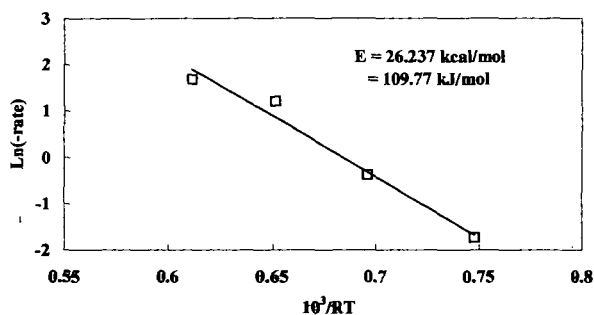
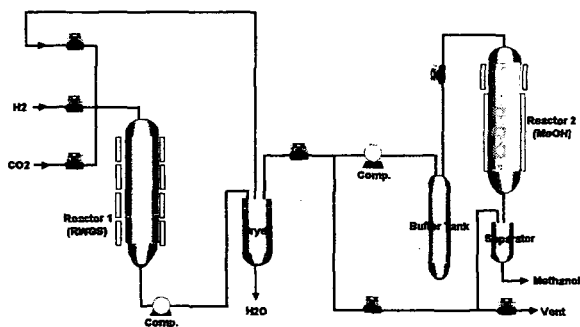


Figure 2. Arrhenius plot of specific activities for the continuous flow reaction of CO₂/H₂ of 1 over Fe₂O₃/Cr₂O₃ catalyst.



Scheme 1. CAMERE process diagram for MeOH of 5 kg/day from CO₂

Table 1. Comparison of the CAMERE process with a direct CO₂ hydrogenation.

Process	A1	R1	A2	R2	F1	F2	L1	L2	MeOH Yield	P
Direct CO ₂ Hydrogenation Process	-	-	1.0	0	14.3	11.7	1.47	0.57	16.04	11.7
	-	-	0.9481	1	24.3	20.4	2.23	0.94	26.32	10.2
	-	-	0.9243	2	32.5	27.2	2.78	1.22	34.12	9.08
	-	-	0.9100	3	38.9	32.8	3.21	1.44	40.31	8.20
	-	-	0.9003	4	44.3	37.5	3.56	1.62	45.35	7.49
	-	-	0.8930	5	48.8	41.4	3.85	1.77	49.54	6.90
	-	-	0.8874	6	52.7	44.8	4.10	1.90	53.10	6.40
	-	-	0.8829	7	56.2	47.8	4.31	2.00	56.16	5.98
	-	-	0.8790	8	59.2	50.5	4.49	2.10	58.82	5.61
CAMERE Process	0.3978	0	0.3978	0	12.2	8.66	1.30	1.10	30.80	8.66
	0.3978	0	0.4636	1	19.3	14.2	1.91	1.57	43.97	7.10
	0.3978	0	0.5050	2	24.2	18.4	2.32	1.86	51.92	6.13
	0.3978	0	0.5324	3	28.4	21.7	2.62	2.06	57.52	5.43
	0.3978	0	0.5514	4	31.7	24.4	2.85	2.21	61.81	4.89
	0.3978	0	0.5652	5	34.5	26.7	3.05	2.33	65.23	4.45
	0.3978	0	0.5753	6	36.7	28.6	3.21	2.43	68.05	4.08
	0.3978	0	0.5832	7	38.6	30.2	3.35	2.52	70.41	3.78
	0.3978	0	0.5893	8	40.3	31.6	3.46	2.59	72.43	3.52
	0.2906	1	0.2906	0	11.8	7.93	1.38	1.23	34.42	7.93
	0.2906	1	0.3487	1	18.1	12.6	2.00	1.74	48.69	6.29
	0.2906	1	0.3894	2	22.5	16.0	2.37	2.03	56.77	5.34
	0.2906	1	0.4188	3	25.6	18.7	2.64	2.22	62.16	4.69
	0.2906	1	0.4405	4	28.6	21.0	2.84	2.36	66.12	4.21
	0.2906	1	0.4569	5	30.9	22.9	3.00	2.47	69.22	3.83
	0.2906	1	0.4696	6	32.9	24.6	3.13	2.56	71.72	3.51
	0.2906	1	0.4795	7	34.5	26.0	3.24	2.64	73.81	3.25
	0.2906	1	0.4874	8	36.0	27.3	3.34	2.70	75.57	3.03

A1: CO₂ concentration in carbon oxide in the stream after RWReactor.

R1: Recycle ratio in the RWReactor.

A2: CO₂ concentration in carbon oxide in F1 stream.

R2: Recycle ratio in the methanol reactor.

F1: Feed gas for the methanol reactor (kgmol/h).

F2: Downstream gas in the methanol reactor (kgmol/h).

L1: Liquid product in the methanol reactor (kgmol/h).

L2: Methanol productivity (kgmol/h)

P: Purge gas (kg mol/h)

Methane Dry Reforming: Effects of Pressure and Promoters on Carbon Formation

Abolghasem Shamsi
U.S. Department of Energy
National Energy Technology Laboratory
P. O. Box 880
3610 Collins Ferry Road
Morgantown, WV 26505-0880

KEYWORDS: Dry reforming, Methane reforming, CO₂ utilization

INTRODUCTION

Natural gas, estimated to last well into the 21st Century, is composed mainly of methane and it is in direct competition with coal and oil as a fuel for the production of electricity. Use of natural gas which contains more hydrogen and fewer carbons than coal and oil will significantly reduce pollutants such as CO₂, SOx, NOx, and trace elements such as Sb, As, Be, Cl, Cd, Co, Cr, Pb, Hg, Mn, Ni, and Se.

In recent years there have been considerable efforts to develop catalysts for converting natural gas to fuels, fuel additives, and chemicals. Oxidative coupling of methane to ethane and ethylene and subsequent conversion of these chemicals to liquid fuel is one approach that has attracted great interest.^{1,2} A key to success for an economically viable process is the development of a catalyst that converts methane selectively into higher hydrocarbons, preferably ethylene, at a higher yield than current technology.

Early work at NETL demonstrated that it is possible to convert methane to higher hydrocarbons (C₂⁺ products) via oxidative coupling of methane, in which oxygen and methane were fed over a catalyst.^{3,4} Despite intensive efforts in this area, little progress has been achieved, mainly because the products of methane conversion, ethane and ethylene, are more reactive than methane and are converted to carbon oxides at a lower temperature compared to methane.⁶

The other method of producing fuels, fuel additives, and chemicals is via production of synthesis gas (a mixture of carbon monoxide and hydrogen) by steam reforming, partial oxidation, or dry reforming. Reforming methane combined with the water-gas shift reaction produces syngas suitable for synthesis of ammonia, methanol, Fischer Tropsch products, and chemicals. The cost of syngas production in converting natural gas to liquid fuels is more than 60% of the total cost. Therefore, reducing the cost of syngas will significantly affect the economics of gas to liquids processes. Most of these reactions are carried out catalytically and the development of new and novel catalysts is very important for utilization of natural gas, particularly for producing liquid fuels.

Recently many researchers have concentrated their efforts toward catalytic reforming of methane with carbon dioxide. This process can be very useful for converting thermal energy into chemical energy. For example, energy losses in combustion/gasification systems and in advanced gas turbines can be captured by reacting natural gas with the by-product of combustion (CO₂) over a catalyst producing syngas which can be converted into liquid fuels and chemicals, ultimately increasing the system efficiency. Although this concept has many environmental and economic incentives, unfortunately, there are no commercial processes for reforming of methane with CO₂. The main problem is that there are several carbon-forming reactions associated with this concept that deactivate the conventional steam reforming, nickel-based, catalysts. Nickel catalyzes carbon formation via hydrocarbon decomposition and CO disproportionation reactions, which greatly contributes to catalyst deactivation, specifically at higher pressures. Methane conversion decreases as the pressure increases due to water formation via the reverse water-gas shift reaction. Therefore, the challenge is to develop a catalyst which exhibits a high selectivity toward hydrogen and carbon monoxide without forming carbon. In this paper we report the preparation and testing of catalysts for dry reforming of methane to syngas at atmospheric and at higher pressures with and without promoters.

EXPERIMENTAL

Tungsten carbide catalyst was prepared as described in the U.S. patent 5321,161 by mixing 12 grams (0.03 mole) of tungsten hexachloride (WCl_6) with 8.6 grams (0.09 mole) of guanidine hydrochloride, $\text{HN}=\text{C}-(\text{NH}_2)_2\text{HCl}$.⁷ The mixture was heated from room temperature to 200 °C in two hours, held at this temperature for two hours, then the temperature was raised to 750 °C for seven and one-half hours and held at this temperature for two hours under nitrogen. Molybdenum carbide catalyst was prepared by temperature-programmed reduction of molybdenum oxide in a flow of 11.6% ethane or methane in hydrogen at a flow rate of 55 ml/min.

The nickel-based catalysts were prepared from water soluble nitrate solutions with proper metal ratios. A 0.3-m long quartz (1/2" stainless steel tube used for higher pressure) reactor tube (6.35-mm o.d., 4.0-mm i.d.) with a quartz thermocouple well was used as a fixed-bed reactor with 0.01-0.5 grams of catalyst (-28/+48 mesh) held in place by quartz wool. A thermal conductivity detector was used with a 1-m by 3.2-mm-o.d. stainless steel molecular sieve 5A column and a 3.66-m by 3.2-mm-o.d. stainless steel HayeSep C (80/100 mesh) column at isothermal oven temperatures of 120 and 50 °C, respectively. Argon was used as carrier gas at 20 ml/min.

RESULTS AND DISCUSSION

A series of carbide and Ni-based catalysts were prepared and tested at several reaction conditions for reaction of methane with CO_2 . Pure SiC was tested at 950 °C and no significant methane or CO_2 conversions were observed. Higher activity was obtained for pure tungsten carbide, which was tested at 650, 750, and 850 °C as shown in Figure 1. At temperatures of 650 and 750 °C methane and CO_2 conversions were less than 15% and H_2/CO ratio was about 0.2. A dramatic increase in CH_4 and CO_2 conversions plus a H_2/CO ratio of 1.1 was obtained at higher temperatures of 850 and 950 °C (not shown). Methane conversion of less than 15% and CO_2 conversion of less than 17% were obtained for commercially produced Mo_3C . However, when molybdenum carbide was prepared by temperature-programmed reduction of molybdenum (VI) oxide with a mixture of 11.6% ethane or methane in hydrogen, methane and CO_2 conversions of more than 90% were obtained at 950 °C and 1.0 atm. A lower H_2/CO was obtained at lower temperatures. Molybdenum carbide catalyst was tested for 16 hrs and the results are shown in Figure 2. Higher catalytic activity was observed for the catalyst prepared with ethane mixture compared to that prepared with methane mixture. Molybdenum carbide supported on TiO_2 was prepared by mixing MoO_3 with TiO_2 in an ethyl alcohol slurry. The dried mixture was reacted with 11.6 vol.% ethane in hydrogen to form carbide. About 90% of methane and 100% of CO_2 were converted to hydrogen and CO with a ratio of 1.0 and the test continued for 2.5 hours at 900 °C without deactivation or forming significant amounts of carbon.

We also tested two commercial nickel-based catalysts. The results for R-67 are shown in Figure 3. Similar results were obtained for G-56B catalyst. Although these catalysts showed a similar activity and selectivity compared to carbide and noble metal catalysts at temperatures higher than 850 °C, none of the experiments lasted more than five hours because a significant amount of carbon formed on the catalyst bed plugging the reactor tube. Zero activity in Figure 3 means that there was no flow due to carbon formation that plugged the reactor. We prepared a series of Ni-based catalysts promoted with alkali and alkali earth metals which were tested for more than 360 hours at 850 °C and at atmospheric pressure. The amount of carbon deposition was reduced significantly due to addition of alkali and alkali earth metals. The promoted catalyst was tested at 7 and 13 atm for 6 hours. Methane and CO_2 conversions decreased as the pressure increased.

CONCLUSIONS

A series of carbide and Ni-based catalysts were prepared and tested at several reaction conditions for reaction of methane with CO_2 . The Ni-based and carbide catalysts were very active and selective for producing syngas. However, a significant amount of carbon formed on the commercial Ni-based catalysts, plugging the reactor after five hours on stream. The amount of carbon deposition was reduced significantly due to addition alkali and alkali earth metals. Methane conversion decreased as the pressure increased, due to water formation via the reverse

water-gas shift reaction. Molybdenum carbide catalyst appeared to be stable for ten hours, at atmospheric pressure, and after that methane and CO₂ conversions slowly decreased due to oxidation of molybdenum carbide to molybdenum oxide.

ACKNOWLEDGMENT

Author acknowledges the natural gas processing and utilization team of NETL for funding this work. He also thanks Dr. Ranjani V. Siriwardane, James A. Poston and Elizabeth A. Frommell for carrying out the XPS, SEM and XRD measurements.

REFERENCES

1. S. Ahmed; J.B. Moffat, *Journal of Catalysis*, **1990**, 125, 54.
2. H.-F. Liu; K.Y. Liu; R.E. Johnson; J.H. Lunsford, *J. Am. Chem. Soc.* **1984**, 106(4), 117.
3. J. E. France; A. Shamsi; L.C. Headley, *Energy Progress* **1988**, Vol.8, No.4, 185.
4. A. Shamsi; K. Zahir, *Energy & Fuels*, 1989, 3(6), 727.
5. R. V. Siriwardane; A. Shamsi, *Journal of Applied Catalysis*, **1990**, 60, 119
6. A. Shamsi, *Ind. Eng. Chem. Res.* **1993**, 32, 1877
7. V. W.; Sherif, F.G.; Burk, J.H.; Gadberry, J.F. U.S. Patent 5,321,161, **1994**.

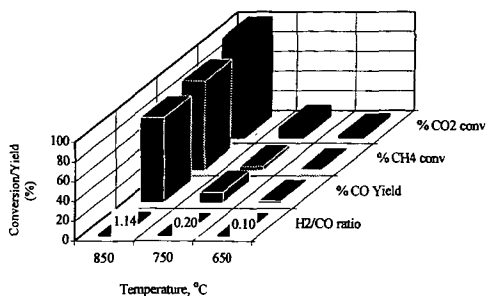


Figure 1. Effect of temperature on dry reforming of methane over Tungsten carbide, $\text{CH}_4/\text{CO}_2=1.15$, GHSV = $5040 \text{ cm}^3 \cdot \text{g}^{-1} \cdot \text{h}^{-1}$

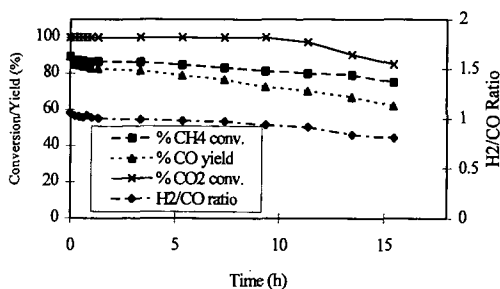


Figure 2. Dry reforming of methane over molybdenum carbide, $\text{CH}_4/\text{CO}_2=1.16$, GHSV = $5040 \text{ cm}^3 \cdot \text{g}^{-1} \cdot \text{h}^{-1}$ at 850°C

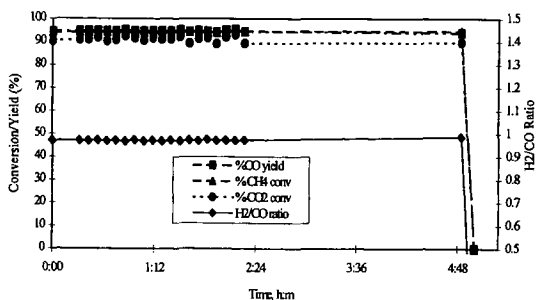


Figure 3. Dry reforming of methane over Ni-based catalyst (R-67), CH_4/CO_2 ratio = 1.1, GHSV = $5040 \text{ cm}^3 \cdot \text{g}^{-1} \cdot \text{h}^{-1}$, at 750°C , no flow after 5 hours.

CONVERTING OF CARBON DIOXIDE INTO MORE VALUABLE CHEMICALS USING CATALYTIC PLASMAS

Chang-jun Liu, Qing Xia, Yue-ping Zhang, Yang Li, Ji-jun Zou and Gen-hui Xu
State Key Laboratory of C1 Chemical Technology, Tianjin University
Tianjin 300072, P.R. China

Baldur Eliasson and Bingzhang Xue
Energy & Global Change, ABB Corporate Research Ltd.
Baden, CH5405, Switzerland

Key words: carbon dioxide, plasma, alkene, oxygenate

ABSTRACT

Experiment has confirmed that the CO_2 plasmas can generate a plentiful of active oxygen species and other active plasma species for further reaction with other reactants, like methane, low alkanes and others. These reactions leads to a formation of more valuable chemicals, like ethylene, propylene and oxygenates. The characteristics of CO_2 plasma reactions have been addressed therefore in this paper. To be our surprised, the experiment has shown that the CO_2 plasma is an excellent "catalyst" for the conversion of low alkanes to alkenes (esp., ethylene and propylene). To the knowledge of authors, this is the first report of this kind of experiments that could lead to a novel method for the utilization of CO_2 and low alkanes. The present yield of alkenes achieved has been competitive to that from the conventional catalytic dehydrogenation of low alkanes.

INTRODUCTION

Any success in research and development of a feasible utilization of carbon dioxide will signify the attainment of objectives of slowing down a build-up of greenhouse gases in the atmosphere and better carbon resource utilization. Due to the difficulty in the utilization of carbon dioxide via the conventional catalysis, plasma approaches for the CO_2 utilization have been paid more and more attentions^[1-10]. Within these plasma CO_2 utilization, an indirect utilization (via syngas) and a direct utilization have been investigated^[1]. The plasma CO_2 utilization is being demonstrated to be an efficient method. In addition, the plasma flue gas treatment has become an industrialized operation. If more valuable chemicals can be directly produced from such plasma CO_2 utilization, the CO_2 emission control will become compensable. In this presentation, the recent progresses in converting of CO_2 into more valuable chemicals using dielectric-barrier discharge (DBD) plasmas has been reported. It has been found that CO_2 is a very good reactant within gas discharge plasmas for organic synthesis.

EXPERIMENTAL

The DBD is one of non-thermal plasma phenomena, which has been considered very promising for organic chemical reactions because of its non-equilibrium properties, low input power requirement and its capacity to induce physical and chemical reactions within gases at relatively low gas temperatures^[1,4,6]. Figure 1 illustrates the reactor system. The feed gas flow is subjected to the action of the DBD in an annular gap formed between an outer stainless steel tube maintained at constant temperature and an inner quartz tube. The radial width of the discharge space was 1 mm, its length 50mm ~ 300 mm. This reactor system is very similar to the DBD reactor for methane conversion described elsewhere^[4,6]. All the experiments were conducted at atmospheric pressure. The feed and exhaust gases were analyzed by gas chromatograph (MTI M200H and HP 4890) with a thermal conductivity detector (TCD) and a flame ionization detector (FID). The exhaust gas from the reactor was first introduced into a condenser to separate

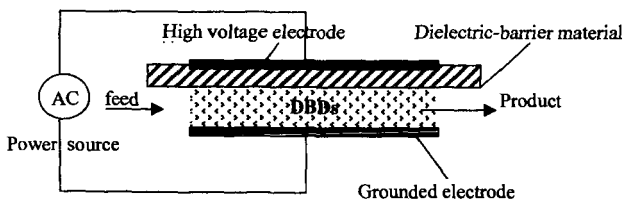


Figure 1 Schematically representative of DBD reactor system

the condensable product from the gas. The power is applied by a high voltage generator working at about 25 kHz. The power can be varied by adjusting the voltage amplitude which causes a slight change of frequency. The voltage and current measurements were conducted using a high voltage probe (Tektronix P6015) and a current probe (Tektronix CT-2) with a digital oscilloscope (Tektronix TDS 210).

RESULTS

We have previously reported a direct liquid fuel synthesis from methane and carbon dioxide via DBDs.^{1,4} During this liquid fuel synthesis, the formation of ethylene and propylene, that is very important chemicals, have been observed. Upon the feed ratio of carbon dioxide/methane, a significant amount of oxygenates has also been detected. Figure 2 shows the effect of feed ratio of CO_2/CH_4 on the conversions and selectivities. It is clear that a lower CO_2/CH_4 feed ratio leads to a higher selectivity of ethylene and propylene. The highest selectivity of ethylene and propylene presents under the feed of pure methane. However, the methane conversion with the pure methane feed is low. The addition of carbon dioxide significantly increases the methane conversion but reduces the selectivity of alkenes. A mixture of oxygenates including methanol, DME, formaldehyde and so on has thereby been produced. Table 1 shows a summary of selectivities based upon the oxygen balance. The higher CO_2 amount in the feed will induce a larger selectivity of oxygenates. Further investigations are being conducted to improve the selectivity of desired oxygenate, e.g. methanol. To get a higher selectivity of alkenes, a lower CO_2 feed amount is suggested. In addition, the use of zeolite within the DBDs and changes in other plasma reaction condition can increase the selectivity of alkenes. We will report it in the near future.

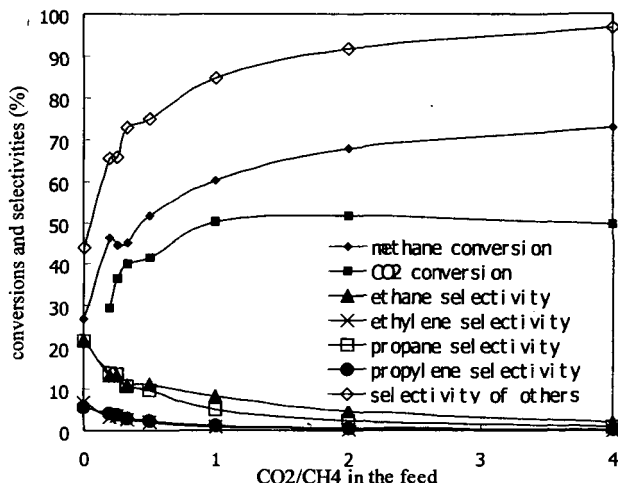
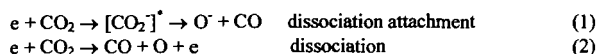


Figure 1 Effect of CO_2/CH_4 feed ratio on the selectivities based on the carbon balance (input power: 500w; feed rate: 150 ml/min; gas temperature: 150°C; gas pressure: 1 bar)

Table 1. Effect of CO_2/CH_4 feed ratio on the selectivities based on the oxygen balance

CO ₂ /CH ₄	Selectivity (%)		
	CO	H ₂ O	Oxygenates
0			
1/4	61.5	24.2	14.3
1/3	59.9	21.1	19.1
1/2	64.1	22.3	13.5
1/1	47.8	15.7	36.4
2/1	43.3	12.7	44.0
4/1	41.1	9.2	49.7
0	100.0		

It is generally accepted that the ethylene and propylene are from the secondary reactions of ethane and propane. The initiation reactions are thought to be the DBD-induced plasma dissociation of CO₂ and CH₄ to generate various radicals, like methyl, ethyl, propyl radicals and so on. A hydrocarbon chain growth reaction is thereby induced to produce ethane, propane and other higher hydrocarbons. Especially, the DBDs can generate a significant amount of active oxygen species from the following plasma CO₂ reactions:



The oxygen species O and O⁺ are being of excited state or metastable state. These plasma species are very active for the dehydrogenation of alkanes and lead to the formation of ethylene and propylene. Experimental investigations have confirmed there are at least two kind of oxygen species produced in the DBDs from carbon dioxide: one leads to the formation of alkenes and oxygenated hydrocarbons and the other induces the complete oxidation of hydrocarbons. A comparative investigation has been conducted to study the decomposition of pure carbon dioxide. It has been found that the plasma decomposition of pure carbon dioxide in some of our reactor designs is higher than that of carbon dioxide and methane or other alkanes (ethane and propane conducted in this investigation) at the same reactive conditions. For example, a CO₂ conversion is 18% with pure CO₂ feed, while the CO₂ conversion reduces to 10% with a mixture feed of carbon dioxide and low alkanes. It can be considered that the CO₂ plasma could be a good catalyst for the conversion of alkanes. A high conversion has been achieved. The challenge, however, is that plasma is a complex mixture of electrons, radicals, ions, photons and others. Especially, the products (alkenes or oxygenates) from plasma CO₂ utilization using alkanes as hydrogen sources are easily to be destroyed by plasma species. It is very necessary to exploit how to control the activity of each plasma species. A special "quenching" has been successfully applied in our investigation on the conversion of low alkanes (ethane and propane) with CO₂ plasma and a selective production of alkenes has been achieved. The high selectivity of alkenes (as high as 80%) can be competitive to the conventional catalytic conversion of low alkanes. Table 2 shows a result of effect of CO₂/C₃H₈ feed ratio on the selectivity of propylene. The products from this DBD conversion of carbon dioxide and propane only contain propylene, water, carbon monoxide and a small amount of iso-butane. Compared to hundreds of components produced^[4], this is a significant improvement in the organic synthesis via non-thermal plasmas and could lead to a practical application of plasma synthesis of more valuable chemicals from low alkanes and carbon dioxide.

Table 2 Effect of carbon dioxide/propane ratio in the feed on the selectivities

CO ₂ /C ₃ H ₈	conversions (%)		selectivities (%)		
	CO ₂	C ₃ H ₈	C ₃ H ₆	CO	iso-C ₄ H ₁₀
1/3	15.6	7.7	73.4	17.6	8.9
1/2	11.0	7.3	77.2	16.3	6.5
1/1	10.9	9.2	72.9	19.7	7.4

CONCLUSION

The potential of the utilization of CO₂ plasma has been demonstrated in this investigation. Due to the low price of present oil market, the synthesis of liquid fuel^[4] from methane and carbon dioxide would not be a good option. The production of more valuable chemicals, like ethylene and propylene, is a better choice for the utilization of carbon dioxide, together with the utilization of low alkanes, especially methane, ethane and propane. It can be considered this as an important innovative alternative technology to produce ethylene and propylene.

ACKNOWLEDGEMENT

Supports from Ministry of Education of China, the Research Fund for the Doctoral Program of Higher Education in China and ABB Corporate Research Ltd., Switzerland are very appreciated. Discussion with Dr. Richard Mallinson and Dr. Lance Lobban at the University of Oklahoma, USA and Prof. Albin Czernichowski at University of Orleans, France is also very appreciated.

REFERENCES

1. C.-J. Liu, G.-H. Xu And T. Wang; "Non-thermal plasma approaches in CO₂ utilization," *Fuel Processing Technology*, **1999**, 119□58.
2. C.-J. Liu, R.G. Mallinson and L.L. Lobban; "Comparative Investigation on plasma catalytic methane conversion to higher hydrocarbons over Zeolites," *Applied Catalysis, A.*, **1999**, 178,17.
3. C.-J. Liu; "The oxidative synthesis of higher hydrocarbons from CH₄ and CO₂ by streamer discharge," *Chemistry Letters*, **1996**, 749.
4. B. Eliasson, C.-J. Liu and U. Kogelschatz; "Direct Conversion of Methane and Carbon Dioxide to Higher Hydrocarbons Using Catalytic Dielectric-Barrier Discharges with Zeolites", *Ind. Eng. Chem. Res.*, **2000** (to be published)
5. C.-J. Liu, L. L. Lobban and R. G. Mallinson; "Modification of NaY Zeolite in a Corona Discharge and Its Application for the Reduction of Carbon Dioxide," in *Greenhouse Gas Control Technologies*, B. Eliasson, P. Riemer and A. Wokaun, eds., 1999, Elsevier, 1103.
6. B. Eliasson, U. Kogelschatz, B. Xue and L.-M. Zhou, "Hydrogenation of carbon dioxide to methanol with a discharge-activated catalyst", *Ind. Eng. Chem. Res.*, **1998**, 37, 3350.
7. M.A. Malik and X.Z. Jiang, "The CO₂ reforming of natural gas in a pulsed corona discharge reactor", *Plasma Chem. Plasma Processing*, **1999**, 19, 505.
8. O. Mutaf-Yardimci, A.V. Saveliev, A.A. Fridman and L.A. Kennedy, "Employing plasma as catalyst in hydrogen production", *Int. J. Hydrogen Energy*, **1998**, 23, 1109.
9. H. Lesueur, A. Czernichowski and J. Chapelle, "Electrically assisted partial oxidation of methane", *Int. J. Hydrogen Energy*, **1994**, 19, 139.
10. H.D. Gesser, N.R. Hunter and D. Probawono, "The CO₂ reforming of natural gas in a silent discharge reactor", *Plasma Chem. Plasma Processing*, **1998**, 18, 241.

DEVELOPING INNOVATIVE SYNTHETIC TECHNOLOGIES OF INDUSTRIAL RELEVANCE BASED ON CARBON DIOXIDE AS RAW MATERIAL

Michele Aresta and Angela Dibenedetto,

Università degli Studi di Bari, Dipartimento di Chimica and Centro METEA, Bari, Italy,
miaires@tin.it

Abstract: The reduction of carbon dioxide emission requires the implementation of several convergent technologies in different production sectors. The chemical industry can contribute to the issue with innovative synthetic technologies, that implement the principles of atom-economy, dematerialisation, energy saving, and raw material diversification with carbon recycling. The innovative synthetic methodologies merge the issues of avoiding the production of CO₂ and carbon recycling, through carbon dioxide utilisation.

In this paper, some options will be discussed, namely the synthesis of carboxylic acids, organic carbonates, and carbamates/isocyanates. The synthesis of methanol from CO₂ and CO will be compared.

Keywords: carbon dioxide, innovative syntheses

Introduction

The implementation of innovative synthetic technologies based on CO₂ can considerably contribute to the reduction of carbon dioxide emission. The avoided amount is not simply represented by the amount of CO₂ fixed. As we have already discussed, the assessment of the exact amount of avoided CO₂ requires an integrated approach which takes in consideration several parameters, as shown in Scheme 1.¹

Amount of CO₂ fixed per t reacted

$$1 - Y + Z$$

$$Y = \sum (e_r, e_{co}, e_{pi}, e_{wt}, \dots)$$

$$Z = \sum (e_{sc}, e_{vr}, e_{vpi}, e_{vwt}, \dots)$$

as CO₂ equivalent

**e_r* = energy of reaction; *e_{co}* = energy of other reagents; *e_{pi}* = energy of purification; *e_{wt}* = energy of waste treatment; *e_{sc}* = energy of substituted reagents and solvents; *e_{vr}* = variation of the reaction energy with respect to the synthesis that does not use CO₂; *e_{vwt}* = variation of waste treatment energy; *e_{vpi}* = variation of energy of purification*

Scheme 1.

The exact evaluation of each parameter can be only made by using a methodology like Life Cycle Analysis, LCA,² that demands an exhaustive basis of process-data, including emission, energy and mass data.²

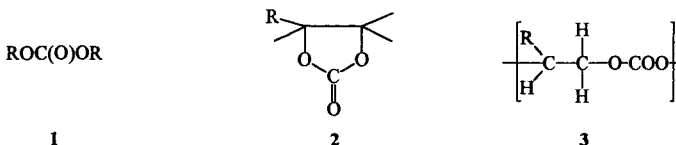
New synthetic methodologies that implement the principles of atom economy, solvent shift, waste minimisation at source, use of less noxious materials and carbon recycling, contribute to CO₂ reduction in many different ways, that cannot be discovered and quantified by simply looking at the stoichiometry of a reaction.

The target compounds considered in this paper are: organic carbonates, carboxylic acids (long-chain aliphatic, or mono- and di-carboxylic aromatic), carbamates and isocyanates. They are today prepared using quite energy- and material-intensive synthetic methodologies, while could be synthesised by using more eco-efficient and economic pathways, including those based on carbon dioxide.

The last section of the paper will be devoted to the analysis of methanol synthesis from CO₂ and CO.

Discussion

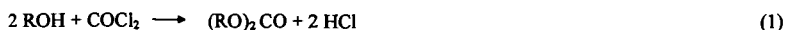
Monomeric (linear 1 and cyclic 2) and polymeric organic carbonates 3 have a market of ca. 1.8



Mt/y, bisphenol-A-polycarbonate being by far the largest commercialised product.

However, the large majority of the production of non polymeric carbonates does not reach the market, as they have a captive use as solvents and internal commodities.

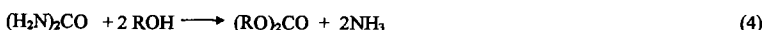
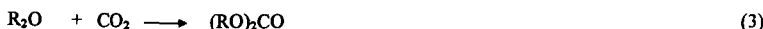
The large majority of the products is produced by the old phosgenation of alcohols, (Eq. 1)



a technology that has a positive aspect in the high reactivity of phosgene, and black spots in the high energy requirement for the synthesis of chlorine, the limitation to the transport of phosgene, the safety measures required for the use of phosgene, the chloride and halogenated solvents end-production. These aspects may be a barrier to further enlargement of the technology exploitation and to a many-purpose use. As a matter of facts, the limitation to the transport of phosgene, concentrates its use at its production site and has encouraged the building up of small-medium-units that can be mounted at the customer site. This is not the solution to problems.

Alternative syntheses are now on stream based on the oxidative-carbonylation of methanol (ENIChem and Ube processes).

The synthetic approaches proposed in this paper consider the reaction of alcohols (Eq. 2), ethers (Eq. 3), or urea with carbon dioxide (Eq. 4), the reaction of ketals with carbon dioxide and alcohols (Eq. 5), and the oxidative-carboxylation of olefins (Eq. 6).



All these syntheses are characterised by a high atom efficiency. The only by-product is water.

This is true also for reaction 5, in which the ketone and glycol can be reconverted into the ketal, that is used as promoter of the reaction of carbon dioxide with alcohol.

Reactions 3 and 5 avoid the water formation in the reaction medium, that can be crucial for equilibrium shift.

Processes based on reactions 2-6 are more eco-efficient than existing ones and are characterised by an atom economy close to 100%. The phosgene based technology (Eq. 1), quite attractive for the easy reaction conditions and high yield, as reported above, has weak points in the fact that it is energy intensive and produces undesired chloride ions and waste chlorinated solvents. These attributes may not guarantee that phosgenation will continue to be the leader technology in the future and will be able to cover the demand of carbonates that is expanding, especially for the production of speciality chemicals and DMC.

The use of carbon dioxide is a better option with respect to both phosgene and carbon monoxide. CO_2 can be recovered from industrial plants, responding, thus, to the principle of recovery and recycling, and to the international agreement of reducing greenhouse gases emission.

This goal is met not only for the recycled fraction of carbon dioxide, but also, and essentially, for the avoided use of natural resources, necessary for the synthesis of carbon monoxide or phosgene, and, the reduced production of waste.

A preliminary Life Cycle Assessment, LCA, study performed considering reactions 1, 2 and 4 has clearly shown that reaction 1 has an impact factor much higher than reactions 4 and 2, (Fig. 1) the key steps responsible for such high impact being the energy required for the synthesis of chlorine, and the production of chloride.

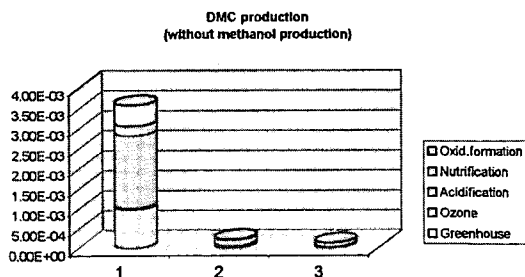
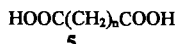
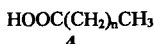


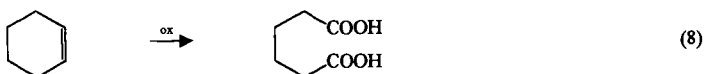
Figure 1. LCA of alternative synthetic pathways for the synthesis of DMC.

- 1: DMC from phosgene and methanol; 2: DMC from urea and methanol;
- 3: DMC from methanol and CO_2 .

Long chain mono- and di-carboxylic acids, **4** and **5** respectively, are high quality products with a major use in polymer chemistry.

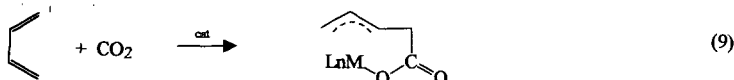


Presently, the latter are synthesised by oxidation of di-alcohols (Eq. 7) or cyclic alkanes/alkenes (Eq. 8) by oxidative ring cleavage with formation of the two carboxylic functionalities.

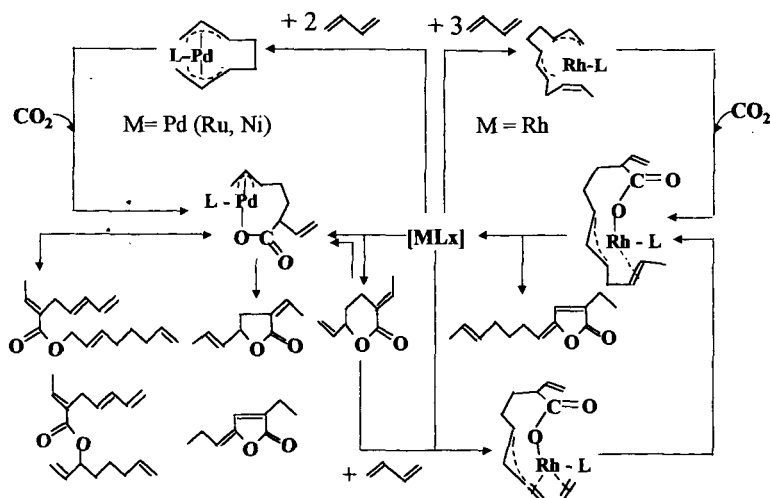


Such processes are neither atom-efficient nor selective. Such non-convergent and destructive synthetic approach, with high waste production, is a major draw-back that cancels-out the advantages of the use of heterogeneous catalysts. An analogous situation exists for long chain mono-carboxylic acids that find a wide application as additives, and in the production of surfactants.

The use of dienes and carbon dioxide as substrates (Eq. 9) brings in the great advantages of atom-economy and selectivity.⁴



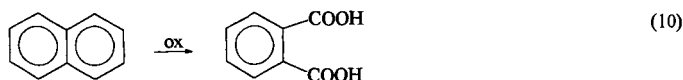
Such synthetic approaches are now known for lactones and can be also used for both the synthesis of either di- or mono-carboxylic acids, by changing the catalyst and controlling the reaction conditions. C-5 or C-9 mono-carboxylic or C-10 di-carboxylic acids can be prepared in mild conditions from butadiene and carbon dioxide. Longer chains can be also built up, according to the metal used. (Scheme 2)



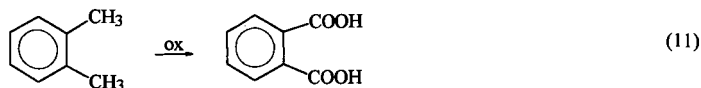
Scheme 2. Metal catalysis in butadiene- CO_2 chemistry.

The reaction is controlled through the use of specific ligands on the metal centre.

Aromatic mono- and di-carboxylic acids are prepared using drastic oxidation reactions (Eq. 10) with low atom efficiency.

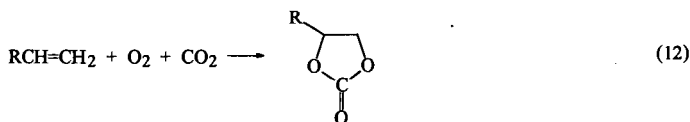


The side chain oxidation of alkyl-aromatic compounds (Eq. 11), which may yield different type of oxygenated organic chemicals, pertains to a large number of industrial intermediates addressed to the manufacture of plastics, fibres, pharmaceuticals, agrochemicals, etc.



At present, these oxidation reaction, namely to obtain the correspondent aromatic acids, are commercially carried out both in the gas and liquid phase. Gas phase processes adopt fixed or fluidised-bed, on V_2O_5 based catalysts, with air as oxidant, at temperatures ranging from 350 to 550 °C; liquid phase oxidation routes, usually with metal salt catalysts dissolved, adopt milder reaction conditions, 110-180 °C, pressure up to 2 MPa. Soluble acetates or naphthenates of Co, Mn, or Mo are generally used with bromine-based co-catalysts. Carboxylic acids, mainly acetic acid, are added as solvents. Benzoic and phthalic acids or anhydride production, accounting for more than 16 Mt/y, rely on these current technologies, by processes with relevant objections for what concerns the formation of polluting effluents, the use of corrosive conditions due to the aggressivity of the reaction medium employed, the low or moderate selectivity in the synthesis of partially oxygenated intermediates, such as ketones and aldehydes, the low or moderate conversions, due to the necessity to maintain the reaction system outside the explosion limits. In addition some of these processes are not continuous.

The oxidation of olefins with dioxygen is a process that has found a seldom exploitation like in the synthesis of ethylene oxide.³ In most other cases, peroxides are used as oxidants with high costs. The oxidation of olefins with dioxygen and CO_2 (Eq. 12) may bring in positive results.⁶



The use of sc- CO_2 may add some more benefits for what concerns critical aspects difficult to drive in solution, namely: the control of the reaction selectivity (one- or two-oxygen transfer to the substrate), yield, working conditions, eventual radical life-time control.

Moreover, the use of sc- CO_2 offers a unique opportunity of using carbon dioxide as solvent and reagent.

Another area of application for carbon dioxide is the use in the synthesis of methanol that is actually synthesised from CO/H_2 mixtures. (Eq. 13) Methanol may have a large market as fuel and chemical and its synthesis from carbon dioxide attracts the attention and interest of several research groups around the world in order to define the potential.



The use of carbon dioxide (Eq. 14) has as major draw-back the higher consumption of dihydrogen with respect to CO.



However, higher selectivity and better yields may counterbalance such apparent negative point. We have performed a LCA study of the possible synthetic methodologies of methanol⁷ and found that the most eco-efficient synthesis is based on the use of a mixture of $\text{CO}:\text{CO}_2=2:1$.

Conclusions

All the synthetic methodologies described above respond to the enviro-economics principles. They are characterised by a great level of innovation and promote the corporate image of the

chemical industry as they couple the reduction of carbon dioxide emission and waste minimisation at source with possible recycling of carbon. Their implementation is on a time scale short to medium, with great benefits for the chemical industry.

References

1. M. Aresta, I. Tommasi, *Energy Convers. Mgmt* Vol. 38, pp. S373-S378, 1997
2. M. Aresta and M. Galatola, *J. Cleaner Production*, 7, 1999, pp. 187-193
3. M. Aresta, A. Magarelli and I. Tommasi, *Appl. Organomet. Chem.*, in press
4. M. Aresta, E. Quaranta and I. Tommasi, *New J. Chem.*, 1994, 18, 133-142
5. *Union Carbide and Carbon*, U.S. P., 2,238,474 (1941); *Shell Devel*, U.S. P., 2,404,438 (1946); *Celanese Corp. of America*, U.S. P., 2,578,841 (1951)
6. M. Aresta, A. Dibenedetto and I. Tommasi, *Appl. Organomet. Chem.*, in press
7. M. Aresta, A. Caroppo, A. Magarelli, A. Dibenedetto, *GHGT-5*, in press

CARBON DIOXIDE SEQUESTRATION VIA pH REDUCTION OF RED MUD USING LIQUID CO₂

Chunmei Shi, Jianhang Xu, Eric Beckman and Robert Enick
Chemical and Petroleum Engineering
1249 Benedum Engineering Hall
University of Pittsburgh
Pittsburgh, PA 15261

KEYWORDS: red mud, steel plant dust, carbon dioxide, carbonate

ABSTRACT

The pH of red mud, waste from the Bayer process for alumina manufacture, can be lowered by contacting the aqueous red mud slurry with liquid carbon dioxide. The carbonic acid that forms in the water in the presence of liquid CO₂ (pH of 2.8 – 2.9) neutralizes the basic compounds of the red mud via the formation of metal carbonates. The pH of a 45% red mud slurry can be reduced from 12.5 to a stable value of 9.0-9.5 via the contact of liquid CO₂ at 298 K and 6.7-10 MPa. The required reaction time is 5-15 minutes if the slurry is well mixed with the liquid CO₂. The carbonates were not removed from the red mud because pH reduction was the only process requirement. The approximate amount of sequestration is about 2.3 gr CO₂ per 100 gr dewatered red mud.

INTRODUCTION

The Bayer process, developed by Karl Josef Bayer 110 years ago, remains the most widely used means of manufacturing calcined commercial alumina from bauxite (40-60% Al₂O₃). Typically, the alumina in the crushed bauxite feed is dissolved aqueous caustic soda at high temperature. Red mud, the insoluble impurities of bauxite, is then separated from the soluble alumina and caustic soda and washed. The soluble sodium aluminate is then partially hydrolyzed, yielding an aluminum trihydroxide precipitate. Calcination of the aluminum trihydroxide yields the anhydrous alumina product (Anderson and Haupin 1985). Aluminum is subsequently produced by the electrolysis of alumina.

The major by-product from the Bayer process is red mud, the insoluble residue of the alumina extraction from the bauxite (Hind et al.1999, Prasad et al.1996). Approximately 70 million tons of red mud is generated annually throughout the world. Red mud disposal methods include traditional closed cycle disposal (CCD) methods and modified closed cycle disposal (MCCD). A new class of dry stacking (DS) technology has also emerged which requires much less land. Problems associated with the disposal of red mud waste include its high pH (12-13), alkali seepage into underground water, safety in storage, and alkaline air borne dust impact on plant life. Efforts to ameliorate red mud typically and possibly, use it as a raw material usually incorporate a pH-reduction processing step (Wong and Ho 1994, Vachon et al. 1994, Koumanova, et al. 1997, Rodriguez et al.1999). Various aqueous acidic solutions have been considered for this application, including acidic industrial wastewater (Wong and Ho 1994). The use of carbonic acid has also been considered. Gas phase CO₂ or CO₂-containing flue gas has been bubbled through aqueous slurries to form carbonic acid in the aqueous phase (Sziirmai, et al. 1991). The carbonic acid results with basic components of the red mud, lowering its pH. However, the pH of water exposed to gaseous CO₂ is not likely to drop below 5.5 (approximately), and hence the rate of reaction/neutralization of the solids in the aqueous slurry is typically not fast enough to satisfy industrial needs. At the short contact times which industrial process rates demand, only a fraction of the alkaline material in red mud is neutralized using gaseous CO₂. Hence although the pH of the aqueous phase drops rapidly upon exposure to CO₂ gas, it soon rises again to unacceptable levels as additional alkaline material leaches from the mud.

The focus of this investigation was the use of high-pressure *liquid* carbon dioxide, rather than *vapor phase* carbon dioxide, for the pH reduction of red mud. The pH of water in contact with liquid CO₂ is 2.80-2.95 over the 298-343 K temperature range and 70-200 atm pressure range (Toews, et al. 1995). This is significantly lower than the pH of 5.0-5.6 that can be attained with gas-phase carbon dioxide. Therefore, we expected that a more rapid and effective neutralization of the red mud would be achieved using liquid carbon dioxide. The apparatus used for this remediation would need to operate at elevated pressures, however.

MATERIAL AND METHODS

Dewatered red mud was provided by Alcoa. Its approximate composition is provided in Table 1.

Table 1. The Composition of the Red Mud Sample

Compound	Formula	Content In Red Mud	MW
Hematite	Fe_2O_3	10-30wt%	160
Alumino-geothite	$(\text{Fe,Al})\text{OOH}$	10-30	75
Sodalite	$3\text{Na}_2\text{O} \cdot 3\text{Al}_2\text{O}_3 \cdot 6\text{SiO}_2 \cdot \text{Na}_2\text{SO}_4$	4-40	994
Tricalcium aluminate	$3\text{CaO} \cdot \text{Al}_2\text{O}_3 \cdot 6\text{H}_2\text{O}$	2-20	378
Anatase/Rutile	TiO_2	2-15	80
Calcite	CaCO_3	2-10	100
Quartz	SiO_2	0-30	60
Boehmite	$\text{Al}_2\text{O}_3 \cdot \text{H}_2\text{O}$	0-20	120
Gibbsite	$\text{Al}_2\text{O}_3 \cdot 3\text{H}_2\text{O}$	0- 5	156
Kaolinite	$\text{Al}_2\text{O}_3 \cdot 2\text{SiO}_2 \cdot 2\text{H}_2\text{O}$	0- 5	258
Muscovite	$\text{K}_2\text{O} \cdot 3\text{Al}_2\text{O}_3 \cdot 6\text{SiO}_2 \cdot 2\text{H}_2\text{O}$	0-15	796

Two slurries were prepared from this sample by mixing it with distilled water. The 45wt% red mud and 10% red mud slurries had pH values of 12.5 and 11.8, respectively. The slurry was contacted with liquid carbon dioxide at 297 K and 10 MPa in an attempt to neutralize both the free soda and bound soda in the red mud. In a typical experiment, 40 gr of the slurry and 40 ml of liquid carbon dioxide at 297 K at 10 MPa psia were introduced to a variable volume, windowed cell. This amount of carbon dioxide used was sufficient to keep the aqueous phase saturated with CO_2 , and a clear liquid carbon dioxide phase resided above the slurry in each experiment. The system was then gently mixed via rocking throughout the duration of the treatment, which ranged from 1 minute to 4 hours, at 297 K and 10 MPa. After specified reaction time had elapsed, the mixing was stopped and the liquid CO_2 was slowly vented from the top of the vessel.

In order to estimate the amount of liquid CO_2 that was sequestered during this experiment, a non-sampling, CO_2 material balance experiment was conducted. The initial pressure of this experiment was set at 5000 psia. In the control experiment, only water and CO_2 were introduced to the cell. The pressure in the cell dropped due to cooling of the vessel (which was heated as the CO_2 was compressed into the sample volume) and dissolution of the CO_2 into the aqueous phase. The experiment was then repeated with the same amount of water and carbon dioxide, but with a specified amount of dewatered red mud. The pressure in the vessel dropped more rapidly and reached a lower limiting value due to the neutralization reaction that removed CO_2 from the liquid phase and transformed it into a carbonate via the formation of carbonic acid and reaction in the aqueous phase. The additional pressure drop, temperature, initial pressure, knowledge of CO_2 density as a function of temperature and pressure and volume of liquid CO_2 , were then used to perform a material balance that indicated the amount of CO_2 that formed carbonates.

A one-liter fixed volume cell with turbine impeller mixing was employed for the neutralization experiments because of the poor mixing observed during the rocking of the smaller, variable volume view cell. Approximately 900 gr of the 45% red mud slurry was introduced to this vessel, which was then blanketed with liquid carbon dioxide. The aqueous slurry and the liquid carbon dioxide were mixed at 297 K and 6.7 MPa using several axial flow impellers spinning at 300 rpm.

RESULTS

The pH reduction results for the smaller vessel with mixing by rocking are illustrated in Figures 1 and 2. The results, shown on the following figures, indicate that

- (1) there is a reduction in pH immediately following the exposure to liquid CO_2 ,
- (2) the pH slowly rises and then levels off following the treatment due to the release of bound soda via desilication,
- (3) the 10% red mud slurries approached an equilibrium pH of approximately 9, regardless of the duration of the mixing
- (4) the efficiency of the treatment was comparable for all of the 10wt% red mud slurries
- (5) the 45% red mud slurries approached an equilibrium value, with lower pH values attained for solutions that were mixed for longer times during treatment (e.g. 4 hr. of mixing was required to attain an equilibrium pH of 9)

The material balance experimental results are shown in Figure 3. The difference between the curves represents a "sequestration" of carbon dioxide. Using the data at 5000 minutes, approximately 2.3 grams of CO_2 can be sequestered for each 100 grams of dewatered red mud.

The effect of neutralizing the red mud with more vigorous mixing is shown in Figure 4. Reaction times of 5-15 minutes were capable of lowering the ultimate pH value to approximately 9.5, as opposed to the 4 hours required to lower the pH to 9 with poor mixing (Figure 2). The pH of the treated mud reached its equilibrium value within two weeks of treatment as shown in Figure 4, while several months were required for equilibration of the sample that was poorly mixed (Figure 2).

DISCUSSION

The neutralization of red mud can be achieved with liquid carbon dioxide at ambient temperature due to the pH value of carbonic acid at high pressure being in the 2.8 - 2.9. As expected and previously reported for red mud treated with gaseous CO_2 , the pH of the red mud was close to 7 immediately after the treatment, it soon rose again as additional alkaline material leached from the mud. Effective treatment was obtained within minutes by reducing mass transfer limitations with vigorous mixing with impellers, rather than rocking the contents of the vessel. The process simultaneously remediated the red mud while sequestering about 2% (based on dewatered red mud mass) CO_2 . The process requires the use of high pressure, corrosion resistant equipment, however, and power for the operation of the high-pressure pumps.

CONCLUSIONS

Liquid carbon dioxide was more effective for pH reduction of red mud than vapor phase CO_2 because carbonic acid pH values less than 3 can be realized with high-pressure carbon dioxide (6.7 - 10 MPa in this study). The initial red mud pH of 12-13 was lowered to 7-8 immediately after treatment, then slowly rose to values of 9.0-9.5 due to desilication reactions of the treated red mud. The processing time was reduced to 5-15 minutes using vigorous mixing of the liquid carbon dioxide and aqueous red mud slurry. Approximately 2 gr of carbon dioxide per 100 gr of red mud were bound in carbonate products when the process was conducted at 297 K.

ACKNOWLEDGMENTS

We would like to thank Normex International for their financial support of this work. We would also like to thank Alcoa for supplying red mud samples.

REFERENCES

- Anderson, W.A., Haupin, W.E., "Aluminum and Aluminum Alloys," in the Kirk-Othmer Concise Encyclopedia of Chemical Technology, Wiley and Sons, New York (1985)
- Hind A.R., Bhargava, S.K., Grocott, S.C., *Colloids Surface*, 146: (1-3) 359-374 Jan 5, 1999
- Koumanova, B., Drame, M., Popangelova, M., *Resources Conservation and Recycling*, 19: (1) 11-20 Jan 1997
- Prasad, P.M., Chandwani, H.K., Mahadevan, H., *Transactions of Indian Institute of Metals*, 49: (6) 817-839 Dec 1996.
- Rodriguez, G., Rivera, F., Pendas, S., *Boletin De La Espanola De Ceramica Y Vidrio* 38: (3) 220-226 May-Jun 1999
- Szirmai, E., Babusek, S., Balogh, G., Nedves, A., Horvath, G., Lebenyi, Z., Pinter, J., "Method for the Multistage, Waste-free Processing of Red Mud to Recover Basic Materials of Chemical Industry," US Patent 5,053,144, Oct. 1 1991
- Vachon P, Tyagi R., Auclair J., Wilkinson K., *Environmental Science & Technology*, 28: (1) 26-30 Jan 1994
- Wong, J., Ho, G., *Soil Science*, 158: (2) 115-123 Aug 1994

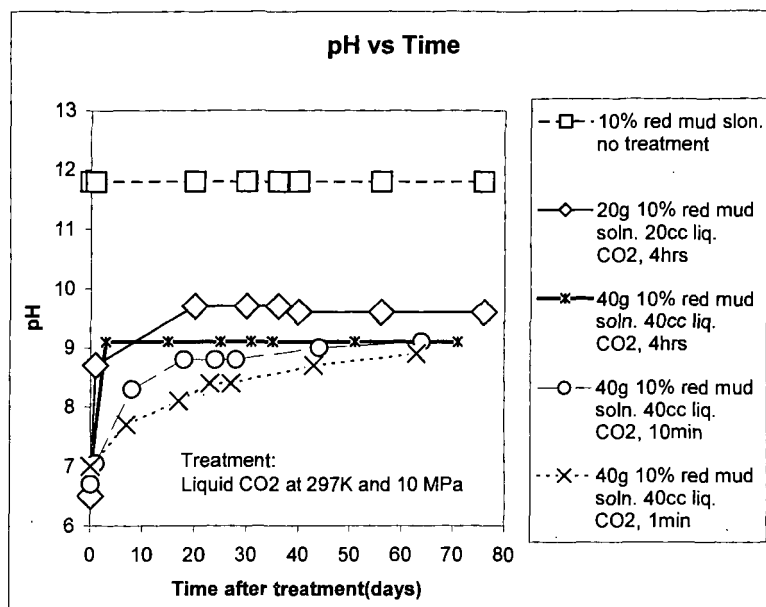


Figure 1. pH reduction of 10% Red Mud Slurries, Small Vessel, Poor Mixing via Rocking

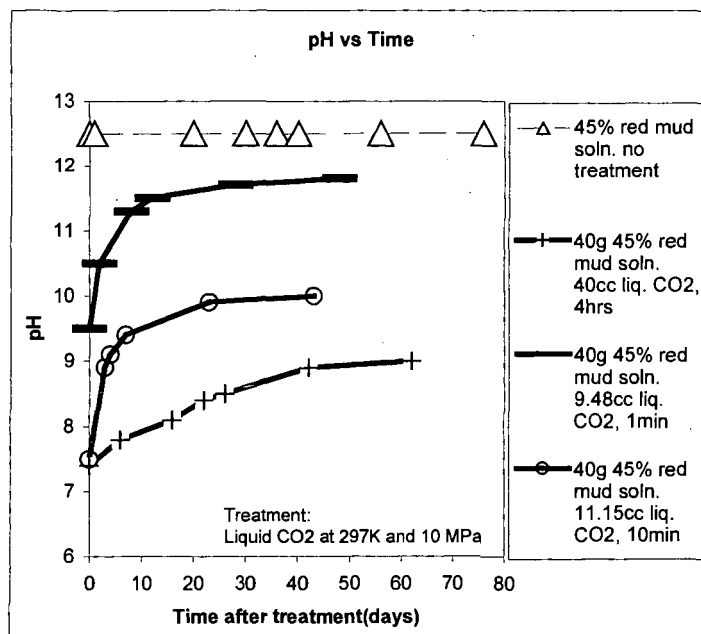


Figure 2. pH Reduction of 45% Red Mud Slurries, Small Vessel, Poor Mixing via Rocking

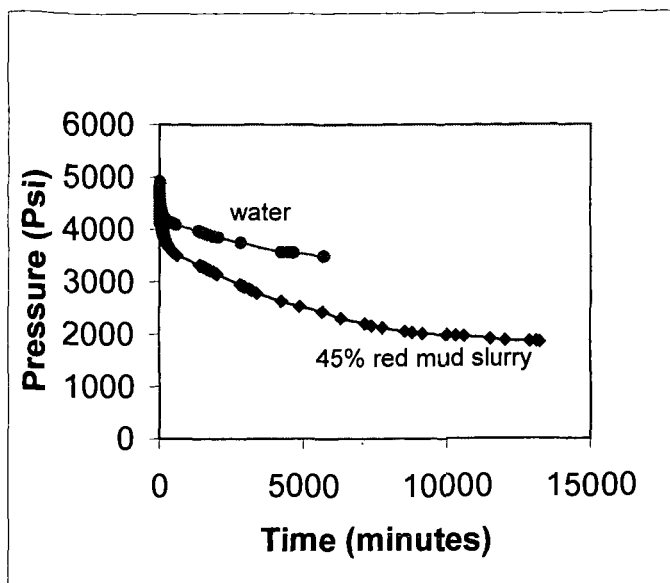


Figure 3. Pressure Decline Measurements at 298 K, 10 ml CO₂, 43 gr Water, Difference Between the Curves Corresponds to the CO₂ in Liquid CO₂ that Formed Carbonates

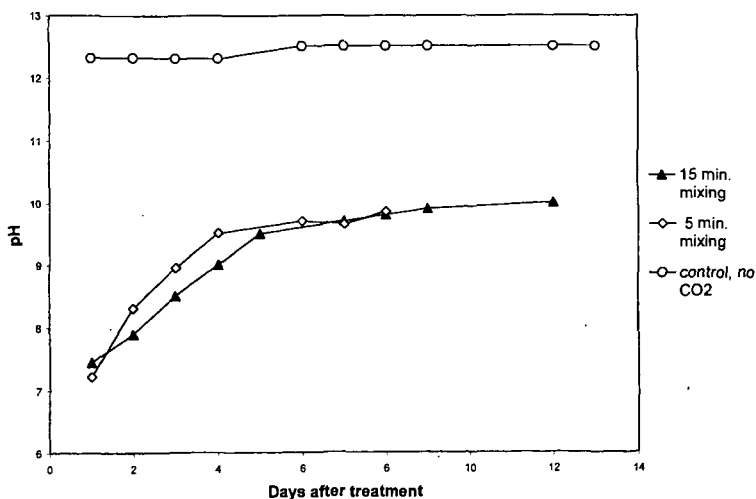


Figure 4. pH Reduction of 45% Red Mud Slurries, Large Vessel, Vigorous Mixing with Impellers, 900g slurry, 130g CO₂, 6.7 MPa

CARBON DIOXIDE STORAGE AS MINERAL CARBONATES

Daniel J. Fauth, Philip M. Goldberg, James P. Knoer, and Yee Soong
U. S. Department of Energy, National Energy Technology Laboratory (NETL)
Pittsburgh, PA 15236-0940

William K. O'Connor, David C. Dahlin, David N. Nilsen, and Richard P. Walters
U.S. Department of Energy, Albany Research Center (ARC)
Albany, Oregon 97321

Klaus S. Lackner and Hans-Joachim Ziock
Los Alamos National Laboratory (LANL)
Los Alamos, New Mexico 87545

Michael J. McKelvy
Arizona State University (ASU)
Tempe, Arizona 85287-1704

Zong-Ying Chen
Science Applications International Corporation (SAIC)
Pittsburgh, PA 15236

KEYWORDS: CO₂ sequestration, magnesium silicate, mineral carbonation

INTRODUCTION

The sequestration of greenhouse gas emissions in the 21st century, in particular carbon dioxide (CO₂), will have a profound influence on the environmental impact of electric power systems within the United States and abroad. Within the U. S., nearly one-third of all anthropogenic or human-caused CO₂ emissions are generated by electric power systems estimated at 6 GtC/year (1). Large economic benefits will continue for the U.S., when and how CO₂ sequestration technologies will be implemented, thus, securing inexpensive and plentiful sources of fossil-fuel-based electric power.

As participants in the Mineral Carbonation Study Program within the United States Department of Energy (DOE), the Mineral Carbonation Research Cluster has focused its carbon sequestration efforts on developing a long-term mitigation strategy. Our approach employs reacting abundant magnesium-rich silicate minerals in an exothermic reaction with CO₂ forming thermodynamically stable and environmentally benign mineral carbonate products. Drawing on mineral carbonation to reduce CO₂ emissions has a myriad of potential advantages. Mineral carbonation mimics the natural weathering of rock. Mineral carbonates, the principal product of the process, are known to be stable over geological time periods (millions of years). For this reason, mineral sequestration ensures permanent fixation rather than temporary storage of CO₂ guaranteeing no legacy issues for future generations. Readily accessible deposits of magnesium silicate minerals exist as ultramafic complexes along the eastern and western coastal regions of North America (2,3). Globally, these natural raw materials for binding CO₂ exist in grand quantities. Therefore, readily accessible deposits/outcrops exist worldwide in quantities that far exceed even the most optimistic estimates of coal reserves. Finally, the overall mineral carbonation process is exothermic and hence, has the potential to become economically feasible.

The aim of DOE's Mineral Carbonation Program is to generate a valuable knowledge base that can lead to development of cost-competitive mineral CO₂ sequestration methods. In achieving this goal, mechanisms, kinetics, and heat requirements of various CO₂ mineral reactions must be understood well enough to identify feasible reaction pathways and to permit engineering process development. A secondary and equally significant target is to acquire knowledge essential to understanding the reactions of CO₂ with underground minerals, in support of the U.S. DOE's geological sequestration programs where CO₂ may be injected into deep saline formations, or depleted oil or gas reservoirs. Knowledge of the reaction characteristics of CO₂ with various minerals at elevated pressures and temperatures such as those found deep underground would help predict the long-term effects of such practices.

Experiments investigating the reactivities of olivine and serpentine in aqueous and bicarbonate aqueous solutions under supercritical CO₂ pressures were conducted to help determine effects of particle size, P_{CO2}, temperature, and solution chemistry. Here we summarize published continuous-stirred-tank-reactor (CSTR) results (4,5) for reactions of ultramafic minerals with supercritical CO₂ and, for comparison, with a lignite fly ash.

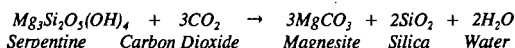
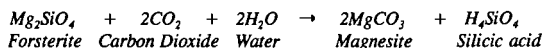
MATERIALS AND METHODS

All mineral carbonation reactions were performed in Hastelloy C-276 autoclaves. Tests were conducted at subcritical (P_{CO2} = 51 atmospheres) and supercritical CO₂ (P_{CO2} = 80, 126, and 136 atmospheres) pressures; reaction temperatures of 155°, 185°, and 230°C and residence times ranging from 3 to 144 hours. In a typical experiment, finely ground minerals and water (15-20% solids concentration) were charged into the CSTR. The CSTR was immediately sealed, purged with

gaseous CO₂, weighed (tare weight), and submerged into an ice bath. Liquid CO₂ was carefully injected through the side port of the autoclave while heating to a pre-calculated process temperature and pressure. The mineral/water/liquid CO₂ mixture was sufficiently agitated during heat up to prevent any settling of magnesium-enriched solids. A modified CSTR system to include a CO₂ gas booster pump and pressure switch was latter designed and operated under relatively constant CO₂ pressures. The addition of the gas booster pump permitted successful operation at an operating pressure of 126 atmospheres (P_{CO2} = 115 atmospheres).

RESULTS & DISCUSSION

The conceptual process for sequestering CO₂ as mineral carbonates was initially proposed by O'Connor, et. al. (4,5) utilizing olivine, water, and supercritical carbon dioxide. In this method, injected CO₂ is dissolved in a slurry of water and mineral reactant, such as olivine. The CO₂ reacts with the olivine/water mixture forming carbonic acid, which dissociates into hydrogen cations and bicarbonate anions. Reaction of carbonic acid with the solid mineral consumes most of the hydrogen cations and liberates equivalent amounts of magnesium cations. These Mg²⁺ cations react with the HCO₃⁻ to form magnesite (MgCO₃). Under supercritical CO₂ pressures, carbonic acid is continuously being generated, consumed, and regenerated. The reaction sequence is concluded: 1) when the reactive surface of the mineral particle is depleted or 2) becomes inactive by mass transfer resistance (i.e., formation of a foreign oxide coating on the surface of mineral reactant particle). The acid-base chemistry for Mg₂SiO₄ and Mg₃Si₂O₅(OH)₄ are given below:



Olivine [forsterite end member (Mg₂SiO₄)] and serpentine [Mg₃Si₂O₅(OH)₄] were identified as being solid mineral reactants for the direct carbonation reaction (4-7). A foundry-grade olivine (identified as ARC olivine), a natural olivine (Twin Sisters, Washington purchased from WARD'S Natural Science Establishment, Inc.) and a synthetic forsterite sample (Alfa Aesar, a Johnston Matthey Company) were selected based on their desired characteristics of high purity, high MgO concentration and low water content. Chemical analyses of the ARC and WARD'S natural olivine, synthetic forsterite, and Cedar Hills quarry serpentine feed samples are included in Table 1. The magnesium oxide concentration was noticeably higher in the synthetic feed material (57.8 wt %) in comparison to both the ARC olivine (49.7 wt %) and WARD'S olivine samples (51.8 wt %). The basis for the lower MgO concentration in these natural feed minerals was attributed to iron substitution for magnesium within the solid solution series. X-ray diffraction data and patterns identified forsterite (Mg₂SiO₄) as the primary phase for both natural olivine feed samples. XRD also confirmed a trace constituent, enstatite (MgSiO₃), for each of the natural olivine samples. This finding was fully anticipated for the raw materials.

Olivine carbonation results from the preliminary series of tests performed at ARC are included in Table 2. Initial results revealed the mineral carbonation reaction is extremely slow at ambient temperatures and pressures. For example, test MC-14 conducted at 150°C and 750 psi (P_{CO2} = 51 atms.) resulted in only a 17.6% conversion of olivine to magnesite after 144 hours. However, increasing both process temperature and CO₂ partial pressure helped to improve upon the kinetics of the carbonation reaction. This was demonstrated during the series of tests at different time intervals (3, 6, 12, 24, and 48 hours) under identical conditions (T = 185°C and P_{CO2} = 115 atmospheres in distilled water) using again the ARC olivine feed sample. Collectively, carbonation tests conducted within the series under relatively short reaction times (3, 6, and 12 hours) gave minor to moderate conversions of Mg₂SiO₄ to MgCO₃. Under longer residence times (24 and 48 hours), the conversion of silicate to carbonate increased with time-on-stream, achieving 51.8% and 56.1% of its stoichiometric maximum in 24 hours and 48 hours respectively. In substituting the synthetic forsterite for the solid reactant, olivine, within the series, significant improvement in terms of carbonation activity was attained. As shown in Table 2, the synthetic forsterite (MC-3) achieved carbonation to 76% of its stoichiometric maximum in just 3 hours, again at 185°C and 1,850 psig. While the chemical analysis of the synthetic material confirmed nearly exact molar concentrations of MgO and SiO₂ as compared to the natural counterparts, the presence of free periclase (MgO) and its subsequent reactivity with carbonic acid resulted in accelerating the mineral carbonation activity within the CSTR. A series of leach tests were later performed to help quantify the free MgO concentration present in the synthetic forsterite material. Results estimated the synthetic material to contain approximately 11 wt % MgO. Although preliminary in nature, these results tend to suggest MgO acts as a promoting agent within the carbonation reaction.

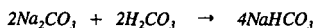
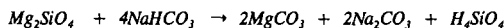
Duplicate experiments at NETL at higher process temperature and pressure (T = 230°C, P_{CO2} = 120 atm in distilled water) conditions coupled with using a minus 325 mesh raw material (WARD'S olivine feed) and a gas dispersion tube within the CSTR provided new evidence into the efficiency of the mineral carbonation reaction. Duplicate CO₂ analysis showed 28.9 weight percent of the recovered solid product as being identified as magnesium carbonate. The extent of reaction was experimentally determined to be over 80% of its stoichiometric maximum after 24 hours.

A major limitation of the CSTR mineral carbonation units at ARC and NETL was its lack of ability to introduce additional CO₂ to the reaction vessel as the carbonation reaction progressed. Hence, for longer test times, the P_{CO2} decreased with increased extent of reaction, which perhaps retarded the reaction. A modified CTSR system to include a CO₂ gas booster pump and pressure switch was designed and operated at ARC at a operating pressure of 126 atmospheres. This development lead to a major improvement in rate and extent of reaction, as illustrated by the olivine and serpentine carbonation tests shown in tables 2 and 3 respectively. Under the modified system, test MC-25 showed a 91.5% rate of conversion for a finely ground olivine (-325 mesh) mineral to MgCO₃. In view of this finding, the effects of particle size, temperature, and P_{CO2} on the olivine carbonation reaction were systematically examined.

Particle size of the silicate mineral was recognized as a key element in aiding the acceleration of the mineral dissolution reaction. This effect can be easily viewed by comparing % conversions of tests MC-4, MC-25, and MC-31 shown in Table 2. Under test conditions (T = 185°C, P_{CO2} = 115 atm. in distilled water), test MC-25 produced over a 90% conversion of Mg₂SiO₄ to MgCO₃ employing a minus 37 micron natural olivine feed. In contrast, tests MC-31 and MC-4 achieved mineral carbonation conversions of 10.6% and 51.8% respectively in 24 hours utilizing the identical feed ARC olivine with the exception of the feed particles sizes being 150 x 106 microns for test MC-31 and 106 x 75 microns for test MC-4.

Another series of completed experiments aided in defining the temperature and CO₂ partial pressure requirements for the olivine carbonation reaction. At 115°C and P_{CO2} = 80 atmospheres, test MC-42 showed no reaction had occurred after 6 hours. However, significant conversion to carbonate (68.2%) resulted in test MC-43 by increasing the process temperature to 185°C while holding CO₂ pressure identical to that in test MC-42. The extent of reaction, as exemplified in test MC-40, was enhanced further to ~85% by increasing the CO₂ process pressure to 115 atmospheres while holding the process temperature constant.

An improvement in mineral carbonation efficiency was established in modifying the solution chemistry of the liquid reactant, water. The final series of tests was conducted in a bicarbonate aqueous solution, 0.5 M NaHCO₃, 1 M NaCl, which dramatically enhanced the overall reaction rate. Sodium bicarbonate was established as a more effective CO₂ carrier, generating product solutions of nearly 20g/liter CO₂, compared to 0.5-1.0 g/liter CO₂ in tests using distilled water. The modified solution was found to be very stable, with nearly constant pre- and post-test pH values (~7.8), and relatively constant CO₂ concentrations. The following equations represent a possible reaction sequence in the bicarbonate aqueous solution.



NaHCO₃ is consumed by the mineral silicate, along with being regenerated by reaction with carbonic acid, which is also continuously regenerated due to the high P_{CO2} in the system.

A Cedar Hills serpentine sample obtained from the Pennsylvania/Maryland state line district was selected for serpentine carbonation testing. XRD determinations established antigorite as the primary constituent for the serpentine feed sample with minor elements of chrysotile, magnetite, and kaolinite. Initial carbonation tests (T = 185°C, and P_{CO2} = 115 atm.) performed for 24 hours with serpentine resulted in a much lower extent of reaction (34%) compared with identical tests conducted with the ARC olivine feed (51%). The removal of (both physically adsorption and chemically bound) inherent water present in the serpentine feed sample via heat treatment was envisioned to produce a more reactive sample. Thermogravimetric analysis (TG) and differential thermal analysis (DTA) were completed on the Cedar Hills feed sample to determine treatment temperature(s). DTA revealed three separate points of inflection, occurring at 160°C, 375°C (evolution of water of crystallization); and 614°C (evolution of constitutional water). For that reason, heat pretreatments were performed at 650°C for 2 hours.

It was also acknowledged that oxidation of the minor constituent magnetite present in the serpentine feed sample during heat treatment could potentially form a passive layer of hematite on the mineral surface, inhibiting the carbonation reaction. Thus, heat treatments on the serpentine feed sample were conducted in both air and CO₂. Chemical analysis of the air-treated products identified hematite being present, while magnetite oxidation to hematite was limited during treatments in CO₂. XRD analysis also confirms heat-treated serpentine samples were partially transformed to forsterite.

Table 3 shows both the serpentine carbonation conditions and results obtained in the series of tests performed at ARC. Tests conducted in distilled water for 24 hours showed marginal improvement in the serpentine carbonation reaction with the air-treated sample (57%) in comparison to the untreated serpentine sample (34%). Test MC-37 utilizing an air-treated serpentine feed sample showed a moderate improvement in extent of reaction (63.5%) for the serpentine carbonation test conducted in a bicarbonate aqueous solution (0.5 M NaHCO₃). The effect of gaseous atmosphere (CO₂ versus air) during heat treatments of serpentine was found significant for the carbonation tests conducted in the carbonation starting solution, 0.5 M NaHCO₃, 1 M NaCl. Extent of reaction increased to over 83% for the serpentine heat-treated in CO₂ compared to 41% for the serpentine treated in air. Both results were achieved in identical carbonation tests (T = 185°C; P_{CO2} = 115 atm) conducted for 6 hours. In contrast, test MC-44 conducted under identical conditions utilizing

an untreated serpentine feed sample showed only minor conversion of serpentine to magnesite (6.8%) after 6 hours.

Finally, studies at NETL demonstrated a lignite fly ash (16% CaO + MgO) could also be used to produce a carbonated product as identified by XRD. Recent work by Anthony et. al. (8) has shown carbonation to be rapid at FBC operating conditions for dry ashes above 400°C. Hydration of the ash promotes the carbonation reaction below this temperature. Fly ash is seen as an excellent candidate to be used solely or in conjunction with mineral silicates for sequestering CO₂ within the mineral carbonation process. Future work at NETL will utilize a Coal Combustion By-product (CCB) database system for identifying best candidates to be used in the Mineral Carbonation Study Program.

CONCLUSIONS

DOE-sponsored carbon sequestration research at NETL, ARC, LANL, and ASU is addressing important issues related to the mineral sequestration of CO₂. Experimental investigations confirm magnesium silicates, olivine and serpentine, are equally amenable to the mineral carbonation process, even though serpentine requires heat treatment. Experimental data are being sought to help facilitate and develop kinetic models that can be employed to identify large-scale, cost-effective mineral sequestration strategies and to evaluate its physical, chemical, and environmental effects on the terrestrial and underground environments.

DISCLAIMER

Reference in this report to any specific product, process, or service is to facilitate understanding and does not imply its endorsement or favoring by the United States Department of Energy.

REFERENCES

1. Freund, P., and Ormerod, W.G. "Progress Toward Storage of Carbon Dioxide." Energy Conversion Management #8:S199; 1997
2. Goff, F.; Guthrie, G.; Counce, D.; Kluk, E.; Bergfeld, D.; and Snow, M. Preliminary Investigations on the Carbon Dioxide Sequestering Potential of Ultramafic Rocks. Los Alamos, New Mexico: Los Alamos National Laboratory; LA-13328-MS; 1997, 22 pp.
3. Hunter, C.E. Forsterite Olivine Deposits of North Carolina and Georgia. Raleigh, North Carolina: North Carolina Department of Conservation and Development; Bulletin 41; 1941, 117 pp.
4. O' Connor, W.K., Dahlin, D. C., Walters, R. P., and Turner, P. C., "Carbon Dioxide Sequestration by Ex-Situ Mineral Carbonation," Proceedings, Second Annual Dixy Lee Ray Symposium, American Society of Mechanical Engineers, Washington, D.C., August 29-September 2, 1999
5. O' Connor, W.K., Dahlin, D. C., Nilsen, D. N., Walters, R. P., and "Carbon Dioxide Sequestration by Direct Mineral Carbonation with Carbonic Acid," Proceedings, 25th International Technical Conference on Coal Utilization and Fuel Systems, Coal Technology Association, Clearwater, Florida, March 6-9, 2000
6. Lackner, K. S., Butt, D. P., Wendt, C. H., and Sharp, D. H. "Carbon Dioxide Disposal in Solid Form", Proceedings of 21st International Conference on Coal Utilization and Fuel Systems, Coal Technology Association, Clearwater, FL; 1996
7. Lackner, K. S., Wendt, C. H., Butt, D. P., Joyce, E. L., and Sharp, D. H. "Carbon Dioxide Disposal in Carbonate Minerals", Energy, Vol. 20, No. 11, pp 1153-1170, 1995
8. Anthony, E.J.; et.al., "Pacification of high calcic residues using carbon dioxide", Waste Management, Vol 20, Issue 1, Feb. 2000

Table 1. Chemical composition of reactant minerals, wt %

Oxide	ARC Olivine	WARD'S Olivine	Alfa Aesar Forsterite	Cedar Hills serpentine
Al ₂ O ₃	0.208	0.148	0.264	0.156
CaO	0.070	0.130	0.661	0.028
Cr ₂ O ₃	0.044	N/A	0.012	0.037
FeO	5.966	N/A	0.009	4.333
Fe ₂ O ₃	2.558	9.059	0.000	2.629
MgO	49.677	51.789	57.845	45.843
K ₂ O	0.007	0.02	0.019	<0.002
SiO ₂	41.357	38.205	37.929	37.500
Na ₂ O	0.099	0.00	0.101	<0.002
Volatiles ¹	0.401	0.70	0.123	11.500
Total	100.387	100.051	96.963	102.026

¹ Volatile constituents include: fixed carbon, mineral carbon, water

N/A - not available

Table 2 – Olivine Carbonation Tests – Test Summary

Test	Particle size, microns	Time, Hrs	Temp., C	PCO ₂ , atm	Carbonation Starting Solution	Product Solids- CO ₂ , wt pct	Percent Stoichiometric Conversion
MC-3	-44	3	185	115	Distilled H ₂ O	32.50	76.0
MC-4	106 x 75	24	185	115	Distilled H ₂ O	18.30	51.8
MC-10	53 x 37	6	185	115	Distilled H ₂ O	1.25	3.5
MC-11	53 x 37	48	185	115	Distilled H ₂ O	19.80	56.1
MC-12	53 x 37	3	185	115	Distilled H ₂ O	0.33	0.9
MC-13	53 x 37	12	185	115	Distilled H ₂ O	6.58	18.6
MC-14	53 x 37	144	150	51	Distilled H ₂ O	6.21	17.6
MC-25 ¹	-37	24	185	115	Distilled H ₂ O	32.30	91.5
MC-31	150 x 106	24	185	115	Distilled H ₂ O	3.74	10.6
MC-40	-37	6	185	115	0.5 M NaHCO ₃ , 1 M NaCl	29.80	84.4
MC-42	-37	6	115	80	0.5 M NaHCO ₃ , 1 M NaCl	0.00	0.0
MC-43	-37	6	185	80	0.5 M NaHCO ₃ , 1 M NaCl	24.09	68.2

¹ Test MC-25 and all subsequent tests conducted in modified CSTR facility with gas dispersion

Table 3 – Serpentine Carbonation Tests – Test Summary

Test	Particle Size microns	Heat Pretreatment ¹	Time, Hrs	Temperature	PCO ₂ atmospheres	Carbonation Starting Solution	Product Solids CO ₂ , wt pct	Percent Stoichiometric Conversion
MC-32	-37		24	185	115	Distilled H ₂ O	11.40	34.2
MC-33	-37		24	185	115	Distilled H ₂ O	11.50	34.5
MC-34	-37	in air	24	185	115	Distilled H ₂ O	22.30	57.0
MC-37	-37	in air	24	185	115	0.5 M NaHCO ₃	22.60	63.5
MC-38	-37	in air	24	185	115	0.5 M NaHCO ₃ , 1 M NaCl	24.70	69.4
MC-39	-37	in CO ₂	6	185	115	0.5 M NaHCO ₃ , 1 M NaCl	28.20	83.2
MC-41	-37	in CO ₂	24	185	115	Distilled H ₂ O	20.17	59.5
MC-44	-37	in air	6	185	115	0.5 M NaHCO ₃ , 1 M NaCl	2.28	6.8
MC-45	-37	in air	6	185	115	0.5 M NaHCO ₃ , 1 M NaCl	14.45	40.6

¹ Heat treatments conducted for 2 hours at 600-650°C

DEVELOPMENT OF INTEGRATED SYSTEM FOR BIOMIMETIC CO₂ SEQUESTRATION USING THE ENZYME CARBONIC ANHYDRASE

Gillian M. Bond¹, John Stringer², Donald K. Brandvold³, F. Arzum Simsek¹, Margaret-Gail Medina¹, and Gerald Egeland¹

¹Department of Materials & Metallurgical Engineering, New Mexico Tech, Socorro, NM 87801

²Electric Power Research Institute, 3412 Hillview Avenue, Palo Alto, CA 94304

³Department of Chemistry, New Mexico Tech, Socorro, NM 87801

KEYWORDS: CO₂ sequestration, biomimetic, enzyme

INTRODUCTION

Many possible approaches to carbon sequestration are being investigated by researchers worldwide (see, e.g., Bond et al., 1999 a, b; Department of Energy, 1997; Hendriks, 1994; Herzog, 1997; Knotek and Eisenberger, 1998; Lackner et al., 1995; Yamada, 1998). This is good, because the scale of anthropogenic CO₂ emissions is so huge that sequestration of anything more than a small fraction of it is likely to require a combination of different approaches. Most sequestration studies have been based on the assumption that CO₂ would first have to be separated from the remainder of the exhaust gases from fossil-fuel combustion. It could then be disposed of, for example, in DOG (depleted oil and gas) wells, in deep saline aquifers, in the deep ocean, or through deposition into minerals such as peridotites or serpentinites. A common theme for all of these approaches is that they involve the need to concentrate and, for the most part, transport CO₂. However, whilst it is technically feasible to remove CO₂ from flue gases with existing technology (Hendriks, 1994; Yamada, 1998), the removal systems require large amounts of capital and energy, and could raise the cost of busbar electricity, for example, by 50% (Department of Energy, 1997). Transportation of CO₂ by pipeline as a supercritical fluid is a well-established technology in EOR (enhanced oil recovery), but still is not cheap.

Our present research is aimed at the development of a novel biomimetic approach to CO₂ sequestration. The intent is to develop a CO₂ scrubber that can be used to reduce CO₂ emissions from, for example, fossil-fuel-burning power plants, based on the use of an enzyme or biological catalyst. The resulting sequestration system would offer several potential advantages, including: a plant-by-plant solution to emission reduction; no costly CO₂ concentration and transportation steps; a safe, stable, environmentally benign product; and an environmentally benign process. Proof of principle has already been demonstrated (Bond et al., 1999 a, b). The present emphasis will be on the performance of the enzyme in the presence of other chemical species likely to be present in the industrial situation. It is useful first, however, to summarize the biomimetic approach, in order to put the present results in context.

Atmospheric levels of CO₂ are much lower today than they were early in the earth's history. Carbonate minerals, such as calcite, aragonite, dolomite, and dolomitic limestone, comprise a massive CO₂ reservoir, estimated (Wright et al., 1995) to contain an amount of carbon equivalent to 150,000 x 10¹² metric tons of CO₂. Thus carbonate minerals offer a geologically proven, safe, long-term repository for CO₂. If anthropogenic CO₂ can be fixed into solid carbonate form, such as calcium carbonate, then we have a stable and environmentally friendly product. The problem, of course, is one of rate.

In order to address the problem of rate, we adopted a biomimetic approach (Bond et al., 1999 a, b). It is useful to keep in mind here that we are defining a biomimetic approach as one in which a particular aspect of a biological process or structure is identified and applied to solve a specific non-biological problem (Bond et al., 1999 a). In other words, it is an approach in which:

- We have a specific engineering problem to solve.
- We identify a biological system in which an analogous engineering problem has been solved.
- We use the enabling part of that system, whether it be a structural design, a processing route, or a biochemical component, to solve our engineering problem.

In the present instance, we examined the rate-limiting step in the chemistry of CO₂ fixation into calcium carbonate in aqueous solution, and then considered what lessons could be learned from biological systems in order to accelerate that step. Calcium carbonate precipitates readily from aqueous solution given a suitable saturation of calcium and carbonate ions, and so the issue becomes one of how to produce carbonate ions rapidly from CO₂ and H₂O (Wilbur and Simkiss, 1968). One important parameter to be considered is pH, because of its strong effect on the proportions of the carbonic species present (Loewenthal and Marais, 1978), and because, at low pH, carbonates will tend to dissolve rather than precipitate. Although carbonate could be formed rapidly at high pH, this would pose both economic and environmental concerns, and hence a

process that operates at very mildly basic pH values would be desirable. Gaseous CO₂ dissolves rapidly in water, producing a loosely hydrated aqueous form (Quinn and Jones, 1936; Keene, 1993). Three additional reactions are then required to form carbonate ions at moderate pH:

- Hydration of aqueous CO₂ to produce carbonic acid (H₂CO₃).
- Dissociation of carbonic acid into bicarbonate ions and protons.
- Production of carbonate ions from bicarbonate ions.

By far the slowest of these reactions is the hydration of CO₂ (Keene, 1993).

A solution to the problem of accelerated CO₂ hydration, in fact, already exists in biological systems. The carbonic anhydrases (CAs) are a broad group of zinc metalloenzymes that are ubiquitous in nature (Brown, 1990; Dodgson et al., 1991; Pocker, 1990). They are among the fastest enzymes known, and they catalyze the reversible hydration of CO₂. The fastest CA isozyme known is the human isozyme HCA II, each molecule of which can hydrate at least 1.4×10^6 molecules of CO₂ per second (Khalifah and Silverman, 1991); the catalyzed hydration occurs at or near the diffusion-controlled limit for the encounter rate of enzyme and CO₂. Thus, if we use CA to catalyze the hydration of CO₂, it should be possible to fix large quantities of CO₂ into carbonate form, without recourse to caustic conditions. [Another group has, in fact, been looking at CA as a catalyst for short-term aqueous sequestration of CO₂ for use in completely closed systems, such as a space station (M. Trachtenberg, personal communication).]

Feasibility of our biomimetic approach was demonstrated (Bond et al., 1999 a, b), based on two types of experiment. One was designed to show acceleration of the overall process of forming a solid product (calcium carbonate) in the presence of CA. This involves a series of steps beyond the hydration of CO₂, but is vital to show potential industrial applicability. The other was designed to demonstrate the accelerated hydration of CO₂ in the presence of CA. This shows catalysis of a single reaction, and hence is applicable also to comparisons of enzyme performance for different isozymes, and under different conditions. Following the successful proof of principle, several topics were identified as needing further study, and some of these are discussed in Bond et al. (1999 a, b). One of these topics is optimization of the catalyst. The activity and lifetime of the enzyme will be influenced by a range of factors, including pH, temperature, and other ions present. The ions present will depend on the source of the water used (seawater or freshwater), as well as on the other species present in the flue gases.

Some inhibition of CA activity by various anions has been reported previously (see, e.g., Maren et al., 1976 [Δ pH]; Pocker and Stone, 1967 [*p*-NPA assay]). By the far the most potent of the inorganic anionic inhibitors of CA, however, is CN⁻, which is not an issue for the proposed application. Very small amounts (unlikely to exceed 100 ppm) of SO_x (Electric Power Research Institute, 1984) and NO_x may be present in the flue gases. Higher concentrations of anions are likely in the water used, particularly, of course, if it is seawater.

EXPERIMENTAL

A suitable catalyst (or isozyme) for an industrial-scale CO₂ scrubber will have to be fast, robust, and capable of being produced in large amounts cost effectively. The simplest and cheapest means of obtaining large amounts of CA will be by means of overexpression by a genetically modified bacterial system, and we are working with two different isozymes for which other research groups have successfully cloned genes. In the short term, however, initial experiments on anionic inhibition have been performed on BCA (bovine erythrocyte CA), purchased in purified form from Sigma Chemical Corporation.

The method that has been used to show the accelerated hydration of CO₂ is a Δ pH method (Henry, 1991). CA catalyzes the reversible hydration reaction between CO₂ and H₂O, producing HCO₃⁻ and H⁺. This production of protons leads to a change in pH as the reaction proceeds towards equilibrium. Measurement of this pH change as a function of time forms the basis of the Δ pH method. Measurements are usually made at temperatures in the range 0–5°C, to slow the enzyme-catalyzed reaction which is otherwise so rapid that initial rates are hard to measure (Henry, 1991). A World Precision Instruments Bee-Trode pH electrode and Dri-Ref system, with an ATC (automatic temperature compensation) probe, connected to an Orion Sensorlink pH data acquisition system, was used for temperature-compensated pH monitoring. Activities were measured and compared for 30 µg/ml BCA in 2.5 mM aqueous CO₂ solution, in the presence of different concentrations of Na₂SO₄ and NaNO₃, in 25 mM pH 7.4 tris buffer, at 1–3 °C. CA activity in ASW-based solution (artificial seawater) was also compared to that in deionized-water-based solution. ASW was produced by dissolution of Sigma artificial-seawater salts, 38g of which were added to 1 liter of deionized water prior to bubbling with CO₂. In this case, the weak buffering was achieved with Barbitol buffer.

A *p*-NPA assay has also been used to monitor the activity of CA, based on the enzyme-mediated hydrolysis of para-nitrophenyl acetate (Pocker and Stone, 1967). The same enzyme active site that is responsible for acceleration of CO₂ hydration also accelerates this hydrolysis reaction, which yields a bright yellow product that absorbs at 405 nm and can be determined spectrophotometrically. Due to steric factors, however, the reaction rate is much slower for the hydrolysis reaction than for the hydration of CO₂. Thus the enzyme-accelerated hydrolysis rates can be conveniently monitored without cooling (in contrast to the delta pH measurements of accelerated CO₂ hydration), making the *p*-NPA assay useful for a first look at the influence of different parameters on CA activity. Activities were measured and compared for 20µg/ml BCA in the presence of different concentrations of Na₂SO₄ and NaNO₃, in 50mM pH 7.4 tris buffer, at 25°C. Stock solutions of 0.0025g/ml *p*-NPA were prepared in acetonitrile, which was used to prevent spontaneous decomposition of *p*-NPA in air or in water. 10% (v/v) was added into each sample solution. The absorbance intensity at 405nm for the yellow product, *p*-nitrophenol, was followed versus time with a Hitachi-330 spectrophotometer. The slope of absorbance versus time was defined as the activity gradient.

RESULTS

Absorbance-versus-time plots from the *p*-NPA assay are shown for SO₄²⁻ concentrations ranging from 0.5 mM up to 200 mM in Figure 1. There is little inhibition at concentrations up to 5 mM (480 ppm), but there is significant inhibition by 50 mM. Similar plots are shown for NO₃⁻, again over a concentration range of 0.5 mM up to 200 mM, in Figure 2. Again, large-scale inhibition starts somewhere between 5 mM (310 ppm) and 50 mM.

Delta pH data for different SO₄²⁻ and NO₃⁻ concentrations, ranging from 5 mM to 200 mM, are shown in Figures 3 and 4 respectively. There is little indication of inhibition at concentrations below 100-200 mM. Figure 5 shows a comparison of enzyme activity in ASW-based solution versus DI-water-based solution. The enzyme is seen to perform well in both solutions.

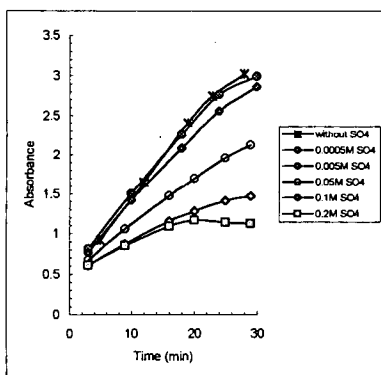


Figure 1. *p*-NPA activity of BCA in various concentrations of SO₄, in tris buffer.

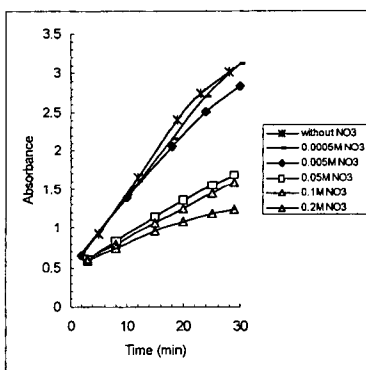


Figure 2. *p*-NPA activity of BCA in various concentrations of NO₃, in tris buffer.

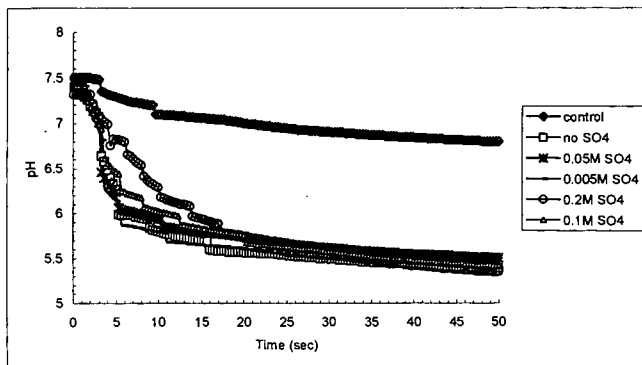


Figure 3. Delta-pH activity of BCA in various concentrations of SO₄, in tris buffer.

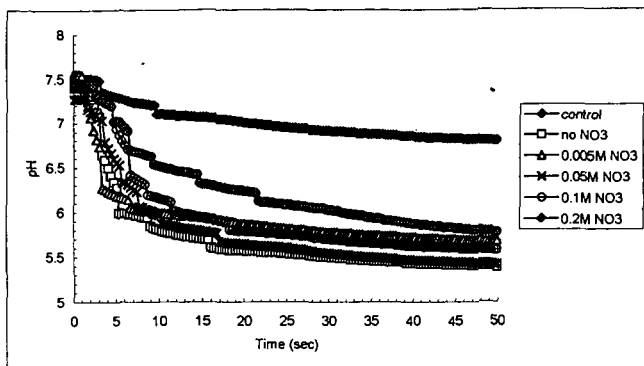


Figure 4. Delta-pH activity of BCA in various concentrations of NO_x in tris buffer.

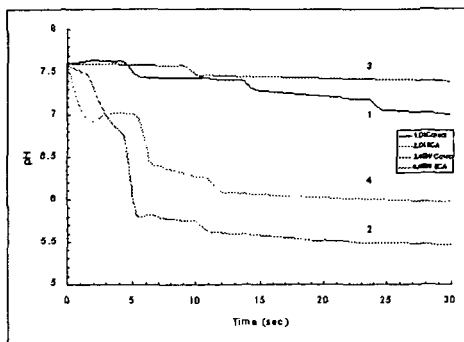


Figure 5. Delta-pH activity of BCA in artificial seawater (ASW) and de-ionized water (DI) tested in barbital buffer.

DISCUSSION

It is interesting to note that the enzyme appears to be less susceptible to inhibition as determined by the delta pH technique, than by the *p*-NPA assay. It should be remembered, however, that the enzyme is also a much less efficient catalyst for the hydrolysis of *p*-NPA than it is for the hydration of CO₂, and hence it is perhaps not surprising that that already somewhat difficult catalytic action should be more easily inhibited. It is clear that, for the present purposes of catalyst optimization, the *p*-NPA assay has a useful role to play for convenient initial screening, but the final assay should be delta pH.

Given the low levels of SO_x and NO_x that would be present in flue gases reaching a CO₂ scrubber located behind a sulfur scrubber, it appears very unlikely that either of these species would present an inhibition problem to the enzyme in such a system. It also appears unlikely that the type of water used will pose an inhibition problem, even for seawater, as represented here by the ASW-based solution. Similar experiments will be performed on the other isozymes, produced by bacterial overexpression, that we are currently investigating.

CONCLUSIONS

The enzyme, carbonic anhydrase, is the biological catalyst responsible for the interconversion of CO₂ and bicarbonate in living organisms. The present research is aimed at the development of a CO₂ scrubber that can be used to reduce CO₂ emissions from, for example, fossil-fuel-burning power plants. In this system, the enzyme works as a catalyst to accelerate the rate of CO₂ hydration for subsequent fixation into stable mineral carbonates, the counterions for which may be supplied from such sources as waste brines from desalination operations. Proof of principle has already been demonstrated. One of the requirements for the enzyme will be that it must be able to function in the presence of other chemical species likely to be present in the industrial application. The present results show excellent enzyme activity in the presence of low levels of SO_x and NO_x (that might be expected from flue gases) and also in solution representative of seawater.

ACKNOWLEDGMENT

The authors gratefully acknowledge support from EPRI under contract number WO9000-26.

REFERENCES

- Bond, G.M., G. Egeland, D.K. Brandvold, M.G. Medina and J. Stringer, pp. 763-781, in Mishra, B., editor, *EPD Congress*, TMS, Warrendale, (1999 a).
- Bond, G.M. G. Egeland, D.K. Brandvold, M.G. Medina, F.A. Simsek, and J. Stringer, *World Resource Review*, **11**, 603 (1999 b).
- Brown, R.S., pp. 145-180, in Aresta, M. and J.V. Schloss, editors, *Enzymatic and Model Carboxylation and Reduction Reactions for Carbon Dioxide Utilization*, NATO ASI Series, Series C: Mathematical and Physical Sciences, vol. 314, Kluwer Academic Publishers, Dordrecht (1990).
- Department of Energy (Office of Energy Research), *Carbon Management: Assessment of Fundamental Research Needs*, DOE, Washington, (1997).
- Electric Power Research Institute, *Field Investigation of FGD System Chemistry*, EPRI CS-3796 (12/1984).
- Dodgson, S.J., R.E. Tashian, G. Gros and N.D. Carter, editors, *The Carbonic Anhydrases: Cellular Physiology and Molecular Genetics*, Plenum Press, New York (1991).
- Hendriks, C., *Carbon Dioxide Removal from Coal-Fired Power Plants*, Kluwer Academic Publishers, Dordrecht (1994).
- Herzog, H.J., editor, *Proceedings of the Third International Conference on Carbon Dioxide Removal, Energy Conversion and Management*, **38 Suppl.** (1997).
- Keene, F.R., pp. 1-18, in Sullivan, B.P., K. Krist and H.E. Guard, editors, *Electrochemical and Electrocatalytic Reactions of Carbon Dioxide*, Elsevier, Amsterdam (1993).
- Khalifah, R.G. and D.N. Silverman, pp. 49-70, in Dodgson, S.J., R.E. Tashian, G. Gros and N.D. Carter, editors, *The Carbonic Anhydrases: Cellular Physiology and Molecular Genetics*, Plenum Press, New York (1991).
- Knotek, M. and P. Eisenberger, co-chairs, *Basic Research Needs to Attain Sustainability: The Carbon Problem*, Workshop held at Tucson, AZ (October 1998).
- Lackner, K.S., C.H. Wendt, D.P. Butt, E.L. Joyce and D.H. Sharp, *Energy*, **20**, 1153 (1995).
- Loewenthal, R.E. and G.v.R. Marais, *Carbonate Chemistry of Aquatic Systems: Theory and Application*, volume 1, chapter 3, Ann Arbor Science, Ann Arbor (second printing, 1978).
- Maren, T.H., C.S. Rayburn, and N.E. Liddell, *Science*, **191**, 469 (1976).
- Pocker, Y., pp. 129-143, in Aresta, M. and J.V. Schloss, editors, *Enzymatic and Model Carboxylation and Reduction Reactions for Carbon Dioxide Utilization*, NATO ASI Series, Series C: Mathematical and Physical Sciences, vol. 314, Kluwer Academic Publishers, Dordrecht (1990).
- Pocker, Y. and J.T. Stone, *Biochemistry*, **6**, 668 (1967).
- Quinn, E.L. and C.L. Jones, *Carbon Dioxide*, Reinhold Publishing Corporation, New York (1936).
- Wilbur, K.M. and K. Simkiss, *Comparative Biochemistry*, **26A**, 229 (1968).
- Wright, J., A. Colling and Open University Course Team, *Seawater: Its Composition, Properties and Behaviour*, 2nd Edition, Pergamon-Elsevier, Oxford (1995).
- Yamada, K., pp. 77-86, in Inui, T., M. Anpo, K. Izui, S. Yanagida and T. Yamaguchi, editors, *Advances in Chemical Conversions for Mitigating Carbon Dioxide*, *Studies in Surface Science and Catalysis*, vol. 114, Elsevier, Amsterdam (1998).

Roger C. Dahlman¹ and Gary K. Jacobs²

¹U.S. Department of Energy
Office of Science, Biological and Environmental Research
19901 Germantown Road, MS-F-240
Germantown, MD 20874-1290

²Environmental Sciences Division
Oak Ridge National Laboratory*
P.O. Box 2008
Building 1505, MS-6035
Oak Ridge, TN 37831-6035

ABSTRACT

Carbon sequestration is a growing research topic that addresses one important aspect of an overall strategy for carbon management to help mitigate the increasing emissions of CO₂ into the atmosphere. There are estimates that terrestrial ecosystems could sequester significant quantities of carbon over the next 50 years. The impact of this sequestration could help buy time for other technologies to come on-line by delaying the need for more dramatic decreases in global emissions. There is increasing interest in scientific advances that can be used to further enhance this potential sequestration of carbon in soils. This paper summarizes current research that is addressing some of the major uncertainties in the carbon cycle and introduces new research that is being initiated specifically related to carbon sequestration in terrestrial ecosystems.

KEYWORDS

Carbon sequestration, carbon cycle, climate change, AmeriFlux, ecosystem research, soil carbon

INTRODUCTION

Currently, emissions of CO₂ are increasing globally and are projected to double over the next century. [1] This excess CO₂ enters the global carbon cycle where part remains in the atmosphere, part is taken up by oceans and the terrestrial biosphere. But significant uncertainty still surrounds the quantitative description of the natural carbon cycle. A major challenge of the greenhouse gas and climate change issue is to understand what happens to the excess CO₂ generated from the burning of fossil fuels. In particular, the rate and magnitude by which excess carbon is assimilated into terrestrial and oceanic sinks will determine the balance that remains in the atmosphere. While research in this challenging area continues, there are new efforts to begin research that might help mitigate increasing CO₂ emissions through special efforts to sequester CO₂.

Carbon sequestration in terrestrial ecosystems can be defined as the net removal of CO₂ from the atmosphere into long-lived pools of carbon. The pools can be living, aboveground biomass (e.g., trees), wood products with a long, useful life created from biomass (e.g., lumber), living biomass in soils (e.g., roots and microorganisms), or recalcitrant organic and inorganic carbon in soils and deeper subsurface environments. It is important to emphasize that increasing photosynthetic carbon fixation alone is not enough. This carbon must be fixed into long-lived pools. Otherwise, one may be simply altering the size of fluxes in the carbon cycle, not increasing carbon sequestration.

THE DOE ROADMAP FOR CARBON SEQUESTRATION

The U. S. Department of Energy (DOE) has recently completed a report that details the state of science related to carbon sequestration. [2] The report also lays out future research topics that will be necessary in achieving increases in carbon sequestration. There are four main objectives that must be addressed for terrestrial ecosystems: (1) assessing ecosystem dynamics, (2)

* Oak Ridge National Laboratory is managed by UT-Battelle LLC, for the U.S. Dept. of Energy under contract DE-AC05-00OR22725. The submitted manuscript has been authored by a contractor of the U.S. Government under contract DE-AC05-00OR22725. Accordingly, the U.S. Government retains a nonexclusive, royalty-free license to publish or reproduce the published form of this contribution, or allow others to do so, for U.S. Government purposes.

increasing below-ground carbon stocks, (3) increasing the rate of growth, standing stocks of carbon, and utilization of above-ground biomass, and (4) optimizing land use for carbon sequestration. It is important to remember that while many processes occur at the molecular level (i.e., photosynthesis, formation and protection of soil organic matter, etc), management practices to enhance carbon sequestration will be implemented at the landscape scale. At this scale ecosystems are the key functional units for estimating productivity and carbon sequestration, and for assessing potentially deleterious impacts associated with efforts to increase carbon in ecosystems.

The DOE report goes on to detail examples of specific research areas that are ripe for innovations that will advance our scientific underpinnings for enhanced sequestration. The other key component of research is on developing improved measurement and monitoring systems. It will be important to be able to determine what sequestration methods are working, and current measurement techniques are lacking in sensitivity and spatial resolution. The Offices of Science and Fossil Energy of the U.S. Department of Energy are implementing research opportunities identified by the state of the science report.

CURRENT RESEARCH IN DOE

While the DOE Office of Science/Biological and Environmental Research (OBER) is embarking on a new research program focused on carbon sequestration in terrestrial ecosystems, current research efforts in OBER have been addressing the natural carbon cycle and potential impacts to ecosystems from global change for some time.

The Terrestrial Carbon Program (TCP) performs research that provides the scientific underpinnings for predicting future concentrations of CO₂ in the atmosphere. The research, which focuses on natural systems that regulate the abundance of CO₂ in the atmosphere, emphasizes (i) understanding the processes controlling exchange rate of CO₂ between atmosphere and terrestrial biosphere; (ii) developing process-based models of atmosphere-terrestrial carbon exchange; (iii) evaluating source-sink mechanisms for atmospheric CO₂; and (iv) improving reliability of global carbon models for predicting future atmospheric concentrations of CO₂. Three particularly key parts of the TCP are:

- Mechanistic terrestrial carbon models for evaluating the role of the biosphere in atmospheric CO₂ changes, and the influence of climate and other feedbacks on the biogeochemical cycle of carbon.
- AmeriFlux network of CO₂ measurements for estimating carbon cycling by terrestrial ecosystems.
- Free Air CO₂ Enrichments (FACE) experiments that evaluate the responses of terrestrial plants and ecosystems to increased concentrations of atmospheric CO₂.

AmeriFlux involves the measurement of net CO₂ exchange of representative ecosystems across United States and North America. For the present network of 35 sites, net annual CO₂ exchange is measured by eddy covariance methods producing annual estimates of net carbon gain or loss by ecosystems such as forests, grasslands and croplands. In addition to flux measurements, biological/ecological data are collected on processes such as photosynthesis, respiration, primary productivity and growth rates and the turnover of different ecosystem carbon pools. Together with flux measurements these data provide unique estimates of net ecosystem production (NEP); positive values of NEP mean the system is storing carbon and negative values indicate net loss of carbon. Initial results show that forest ecosystems are gaining carbon at the rate of 2 to 6 tons of carbon per hectare per year. This network of flux measurements, and related ecosystem and micrometeorological data collectively provide vital ground surface information about carbon sequestration. The data also help interpret other observations of atmospheric CO₂ and space-based information about ground surface processes. Research products of AmeriFlux contribute significantly to the understanding of the role of the terrestrial biosphere in the global carbon cycle, to uniquely quantify carbon sequestration by the terrestrial biosphere, and to provide vital data for evaluating the hypothesis that N. America is a significant terrestrial carbon sink.

The Program for Ecosystem Research (PER) includes both experimental and modeling research related to both the direct and indirect effects of climatic and atmospheric changes on ecosystem components and processes. Research emphasizes the detection and quantification of adjustments to global atmospheric and climatic changes (e.g., temperature, moisture, ozone, CO₂) and the

mechanisms that control the observed adjustment processes. Ecosystem responses that are studied include (1) ecological adjustments such as changes in the organized hierarchy of ecosystem processes, structure, and diversity; and (2) biological adjustments at the organism level that are manifested at the ecosystem level, including homeostatic (physiological, biochemical) and genetic responses.

NEW RESEARCH DIRECTIONS

DOE formed a new center in 1999 to focus on research related to enhancing carbon sequestration in terrestrial ecosystems. A consortium of institutions (see next section) will perform research to help determine how to increase the amount of carbon entering into "pools" that are stabilized in soil and protected against decomposition. The center will also research ways to measure, monitor and verify sequestration so that it may be appropriately accounted for in national inventories of greenhouse gas emissions.

In addition to the Centers approach, there is a solicitation for research from the scientific community involving investigator-initiated ideas and innovative research for enhancing carbon sequestration of terrestrial ecosystems. New ideas and concepts will be selected from the competition that can be expected to promote significantly increased capture and storage of carbon by terrestrial ecosystems.

THE DOE CENTER FOR RESEARCH TO ENHANCE CARBON SEQUESTRATION IN TERRESTRIAL ECOSYSTEMS (CSiTE)

The newly formed research center is known as CSiTE – Carbon Sequestration in Terrestrial Ecosystems. CSiTE performs fundamental research that supports methods that will lead to enhanced carbon sequestration in terrestrial ecosystems as one component of a carbon management strategy. The goal of CSiTE is to discover and characterize links between critical pathways and mechanisms for creating larger, longer-lasting carbon pools in terrestrial ecosystems. Research is designed to establish the scientific basis for enhancing carbon capture and long-term sequestration in terrestrial ecosystems by developing (1) scientific understanding of carbon capture and sequestration mechanisms in terrestrial ecosystems across multiple scales from the molecular to the landscape, (2) conceptual and simulation models for extrapolation of process understanding across spatial and temporal scales, (3) estimates of national carbon sequestration potential, and (4) assessments of environmental impacts and economic implications of carbon sequestration.

SUMMARY

Carbon sequestration is an important part of an overall carbon management strategy to help reduce and/or mitigate global CO₂ emissions. Research into how to enhance sequestration in terrestrial ecosystems could lead to significant beneficial practices that could be implemented during the next 20-50 years. These practices could help "buy time" for other methods of sequestration and energy technologies to come on-line. At the same time, it is essential to continue to emphasize understanding the carbon cycle which drives future global change scenarios and also can impact the efficacy of sequestration options in natural systems.

ACKNOWLEDGMENTS

Research sponsored by the U.S. Department of Energy, Office of Science, Biological and Environmental Research. This paper is a contribution from CSiTE – The Center for Research to Enhance Carbon Sequestration In Terrestrial Ecosystems.

REFERENCES

1. IPCC (Intergovernmental Panel on Climate Change), Climate Change 1995: The Science of Climate Change, J. T. Houghton, L. G. Meira Filho, B. A. Collander, N. Harris, A. Kattenberg, and K. Maskell, eds., Cambridge University Press, Cambridge, UK, 1996.
2. DOE (U.S. Department of Energy), Carbon Sequestration Research and Development, DOE/SC/FE-1, Washington, D.C., 2000.

GLOMALIN: A SOIL PROTEIN IMPORTANT IN CARBON SEQUESTRATION

Sara F. Wright¹, Matthias C. Rillig² and Kristine A. Nichols³

¹USDA-ARS-SMSL, Building 001, Room 140, BARC-W, Beltsville, MD 20705, ²University of Montana, Division of Biological Sciences, HS104, Missoula, MT 59812, ³University of Maryland, Department of Natural Resources and Landscape Architecture, College Park, MD 20742

KEYWORDS: Aggregate stability, soil organic matter, soil stability, glycoprotein

ABSTRACT

Elevated atmospheric CO₂ levels lead to greater fixation of carbon by plants and greater transfer of carbon to roots and soil. We are studying the amplification of a series of events that flow from increased inputs of carbon to plant roots and subsequently to sequestration of organic carbon in soil aggregates. Soil aggregates are groups of primary particles that adhere to each other more strongly than to surrounding soil particles. Plant roots provide carbon for growth and reproduction of a ubiquitous group of symbiotic fungi called arbuscular mycorrhizal fungi (AMF). A recent discovery shows that AMF produce copious amounts of an insoluble, hydrophobic, recalcitrant glycoprotein, named glomalin, which is important in stabilizing soil aggregates. Aggregates store and protect additional organic carbon until the aggregates break down. Thus, greater stability of aggregates leads to larger amounts of protected organic carbon in terrestrial ecosystems.

INTRODUCTION

Increases in atmospheric CO₂ (Keeling et al., 1995) highlight the need to explore ways to trap and sequester this greenhouse gas in terrestrial ecosystems. Plants fix CO₂ and allocate a part of the photosynthate to roots (Rogers et al., 1994) and soil (Jones et al., 1998). Organic carbon in soil plays an important role in soil aggregation (Kemper & Rosenau 1986). Soil aggregates are groups of primary particles that adhere to each other more strongly than to surrounding soil particles (Martin et al., 1955). Relatively labile carbon is protected in soil aggregates (Cambardella & Elliott 1992; Jastrow & Miller 1997; Six et al., 1998) and has a turnover of 140 – 412 years in a pasture soil, depending upon the aggregate size (Jastrow et al., 1996).

Increased fixation of CO₂ by plants may have a direct effect on root symbionts that utilize plant-fixed carbon for growth – the arbuscular mycorrhizal fungi (AMF). AMF are ubiquitous symbionts of the majority of land plants. AMF are also important in soil aggregate stabilization (Tisdall & Oades, 1982; Jastrow & Miller, 1997). The contribution of AMF to stabilization of aggregates was thought to be through entrapment of soil particles by fungal hyphae, the filamentous structures making up the body of the fungus. Hyphae extend several centimeters from the root into soil. Estimates of AMF extraradical hyphae vary widely (Rillig & Allen, 1999), but one of the highest estimates is 111 m cm³ in a prairie grassland soil (Miller et al., 1995).

A recent discovery of copious production of a glycoprotein, glomalin, by hyphae of AMF (Wright et al., 1996) and its role in aggregate stability (Wright & Upadhyaya 1998) has implications for enhanced carbon sequestration by soils under elevated CO₂. Recently Rillig et al. (1999) provided evidence for a change in aggregate stability under elevated CO₂ in three natural ecosystems. Increases in hyphal length and glomalin concentration in soils were shown concurrently.

This report will review glomalin and aggregate stability: (i) in disturbed and undisturbed agricultural soils, (ii) in agricultural soils in transition from plow- to no-tillage, (iii) in natural grasslands under increased CO₂ and (iv) in a tropical soil. We will also present characteristics of glomalin that indicate the unusual nature of the molecule.

MATERIALS AND METHODS

Glomalin extraction. Extractions were performed as described by Wright & Upadhyaya (1998). One-gram samples of air-dried soil were placed in 8 mL 20 mM citrate, pH 7.0 and autoclaved (121 °C) for 30 min to remove the easily-extractable glomalin (EEG). After centrifugation (10,000 x g) and removal of the supernatant, 8 mL 50 mM citrate, pH 8.0 was added to the remaining soil and heated at 121 °C for 60 min to extract total glomalin (TG). Additional extractions with 50 mM citrate were done until the supernatant was a straw color, indicating that glomalin, a red-brown color, had been removed. One mL of EEG was removed and then the remaining supernatant containing EEG was combined with all of the supernatants from the 50 mM citrate extractions. Protein was determined by the Bradford dye-binding assay with bovine serum albumin as the standard (Wright et al., 1996). An indirect enzyme-linked immunosorbent

assay (ELISA) was used to quantify the immunoreactive fraction (IREEG and IRTG). Weight of soil was corrected for non-aggregated coarse material.

Glomalin purification. Glomalin was precipitated with trichloroacetic acid (TCA) and then dialyzed against 10 mM borate, pH 8.0 as described by Wright et al. (1998). Dialyzed samples were freeze-dried.

Aggregate stability. The apparatus described by Kemper & Rosenau (1996) was used to determine water stability of air-dried aggregates. Air-dried bulk soil was sieved to remove the 1 – 2 mm and 0.5 – 1 mm aggregates. Four g of aggregates was placed in a sieve and pre-wetted by capillary action. The 1 – 2mm aggregates were in 0.25 mm sieves, and the 0.5 – 1 mm aggregates were in a 0.01 mm sieve. Aggregates were pre-wetted by capillary action and then tumbled for 5 min in a column of water. After drying remaining aggregates at 70 °C aggregate stability was calculated: % stability = (g aggregates remaining on the sieve - the coarse material/ 4 g - coarse material) x 100.

Characterization of glomalin. Various routine and specialized assays have been performed to characterize the glomalin molecule. Routine assays are Bradford protein and enzyme-linked immunosorbent assay (ELISA). Methods for these are described above. Sodium dodecyl sulfate polyacrylamide (SDS-PAGE) gel electrophoresis banding patterns on 12% T gels stained with silver are also run on a routine basis (Wright and Upadhyaya, 1996). Iron was analyzed by atomic absorption spectroscopy after microwave digestion in nitric acid.

RESULTS

We have studied undisturbed, disturbed, and soils under elevated CO₂ for the relationship between aggregate stability and glomalin (Rillig et al., 1999; Wright & Upadhyaya, 1998; Wright et al., 1999) in temperate regions. In general, undisturbed soils have the highest aggregate stability and glomalin, but soils appear to differ in the amount of glomalin they can accumulate (Table 1). Both aggregate stability and glomalin are higher in undisturbed compared with disturbed soils (Tables 2 and Fig. 1).

TABLE 1: Selected undisturbed soils that illustrate the range in values for aggregate stability and measures of easily extractable glomalin (EEG), total glomalin (TG), and the immunoreactive fractions of each (IREEG and IRTG, respectively).

Location	Soil Type (series)	Aggregate Stability (%)	TG (mg/g)	IRTG (mg/g)	EEG (mg/g)	IREEG (mg/g)
Maryland	Silt loam (Baltimore)	80	5.2	4.4	2.9	2.5
Virginia	Silt loam (Georgeville)	93	14.1	10.9	10.0	8.3
Illinois	Silty clay loam (Sable)	52	12.6	5.7	4.3	1.9
Minnesota	Sand (Nymore)	55	4.7	8.6	5.8	4.5
Texas ¹	Sandy loam (Berta, Posey)	22	3.3	1.5	1.5	0.6
Colorado ¹	Silt loam (Weld)	60	3.0	1.7	1.0	1.0

¹Alkaline soils. All other soils are acidic.

Cultivated soils have been compared with undisturbed soil under native or introduced grasses to determine the effects of disturbance on glomalin. The immunoreactive easily extractable (IREEG) fraction of glomalin is most closely correlated with aggregate stability across soil types and locations. This fraction is similar to glomalin on fresh hyphae using currently available analytical procedures (Wright & Upadhyaya, 1998) (Table 2).

TABLE 2: Immunoreactive easily extractable glomalin (IREEG) and aggregate stability of 1 – 2 mm aggregates for three geographic locations with comparisons between disturbed and undisturbed sites (SD in parentheses).

Location	Soil Type	Disturbed		Undisturbed	
		Aggregate stability (%)	IREEG ¹ (mg/g)	Aggregate stability (%)	IREEG (mg/g)
Texas ¹	Sandy loam	8.6 (0.6)	0.4 (0.2)	22.3 (3.5)	0.6 (0.2)
Colorado ¹	Silt loam	11.1 (4.3)	1.1 (0.3)	59.9 (20.1)	1.7 (1.4)
Maryland ¹	Silt loam	18.1 (3.0)	0.6 (0.0)	58.9 (3.5)	1.9 (0.3)

¹Texas – three cultivated sites were compared with three nearby rangeland sites; Colorado – 45 cultivated plots were compared with nine nearby individual grass soils; Maryland – four cultivated plots were compared with four sites from a grass buffer surrounding the plots.

Soil management affects aggregate stability and glomalin. A recent study compared no-tillage to plow-tillage over three years for a silt loam soil in Beltsville, MD corn plots (Wright et al, 1999). Both aggregate stability and glomalin increased during the transition (Fig. 1).

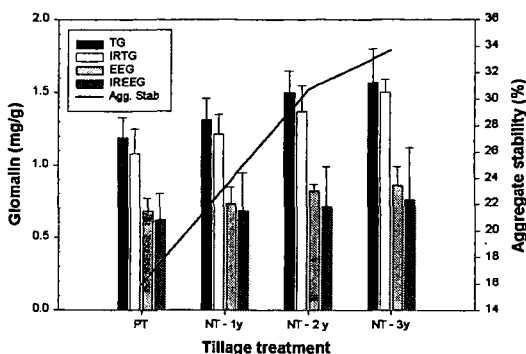


FIGURE 1: Changes in aggregate stability and glomalin during transition from plow- to no-tillage for corn production. TG = total glomalin, EEG= easily extractable glomalin and IR= immunoreactive fraction.

A chronosequence (300 years – 4.1 million years) from Hawaii was studied (manuscript in preparation) to determine glomalin levels in a tropical climate. Very large amounts of TG were found (Fig. 2).

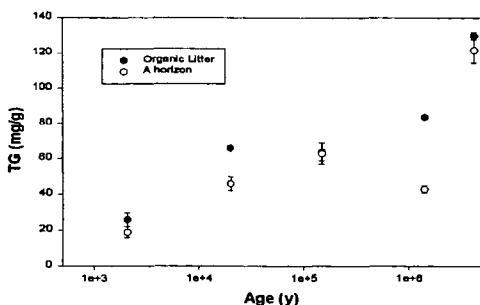


FIGURE 2: Total glomalin in the upper layers of an organic soil chronosequence from Hawaii.

Exposure of annual grassland to elevated CO₂ resulted in increases the number of aggregates as a proportion of soil mass, and increases in aggregate stability and glomalin (Rillig et al., 1999). Results of this study are summarized in Table 3.

TABLE 3: Effects of increased CO₂ on aggregates as a percent of bulk soil, water stability of aggregates, and glomalin in natural grasslands in California (Rillig et al., 1999).

	Sandstone		Serpentine	
	Ambient CO ₂	Increased CO ₂	Ambient CO ₂	Increased CO ₂
Aggregates 1-2 mm (% of soil)	14.4 (0.5)	15.1 (0.3)	16.7 (0.6)	18.1 (0.5)
Aggregates 0.25-1mm (% of soil)	17.1 (0.6)	20.0 (0.8)	26.9 (1.6)	25.6 (1.1)
Water stable 1-2 mm (%)	86.7 (1.6)	90.1 (1.3)	76.2 (1.5)	81.0 (1.3)
Water stable 0.25-1 mm (%)	88.9 (0.9)	92.8 (0.6)	84.3 (0.9)	85.3 (0.5)
Immunoreactive glomalin (mg/g)	0.7 (0.0)	0.8 (0.0)	1.0 (0.0)	1.1 (0.0)

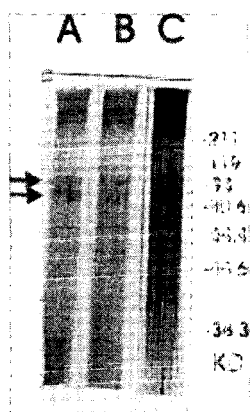
Glomalin is categorized as a glycoprotein (Wright et al., 1998). Carbon, nitrogen, and iron in glomalin from hyphae of two AMF and a soil and other soil are shown in Table 4.

TABLE 4: Total carbon, iron and nitrogen in selected glomalin samples.

Assay	Baltimore soil	Glomus intraradices UT126	Gigaspora rosea FL225
Total Carbon (%)	26.4	24.80	17.50
Fe (%)	7.2	0.5	0.5
N (%)	1.63	1.70	1.22

Similarity between glomalin on hyphae from axenic cultures and soil indicates that the substance extracted from soil is the same as that on hyphae. Raw extracts from hyphae or soil show the same banding patterns on SDS-PAGE (Fig. 3).

FIGURE 3: SDS-PAGE of glomalin extracted from hyphae of *Glomus intraradices* UT126 (A), *Gigaspora gigantea* MA453A (B), and Baltimore soil (C). Molecular weight standards (KD) are indicated. The arrow indicates the position of two bands.



DISCUSSION

Glomalin, a major component of previously unidentified organic matter in soil, reaches levels of 1.4 – 13% of air-dried mineral soils based on Bradford protein values (Table 1, Fig. 2). Comparison of amounts of humic and fulvic acids and glomalin from Hawaiian organic soil on a weight basis show that glomalin can be as high as 26% of the soil while fulvic, humic, and the mineral fraction are 2.7, 6.7, and 60.7%, respectively (unpublished data).

Levels of glomalin in soil are closely associated with aggregate stability. This was shown in undisturbed soils, undisturbed compared with disturbed soils, and during transition from plow- to no-tillage (Tables 1 and 2, Fig. 1). Since glomalin production appears to be directly linked to carbon supplied by plants, production of glomalin may be affected by increased atmospheric CO₂ (Table 3). Evidence for this was also found in a sorghum field equipped with a free-air CO₂ enrichment (FACE) system (manuscript in preparation). Measures of soil AMF hyphal length showed a strong response to CO₂ as well as one fraction of glomalin. Glomalin and AMF hyphal lengths were positively correlated with soil aggregate stability.

The structure of glomalin at present unknown, but the molecule is insoluble, hydrophobic and recalcitrant. Insolubility of the molecule is probably the reason that glomalin was not discovered until recently. We have seen evidence of insolubility and sloughing of glomalin from AMF hyphae in sand cultures of these fungi on plant roots. When cultures are harvested and fresh roots are placed in water, glomalin floats to the surface of the water and collects as a film at the air-water interface. This film entraps air bubbles and adheres to plastic surfaces. Plastic traps have been used to quantify glomalin in cultures (Wright & Upadhyaya, 1999). Residence time of glomalin in soils is currently being investigated, but preliminary results indicate that glomalin in the undisturbed Hawaiian soils (Fig. 2) lasts for 6 – 42 years (manuscript in preparation).

Other fungal proteins, hydrophobins, have characteristics similar to glomalin (Wessels, 1996). For example, the hydrophobin SC3 produced by the basidiomycete *Schizophyllum commune* is a glycoprotein (Wessels, 1997) that is insoluble in hot SDS and forms insoluble complexes (de Vries et al., 1993). Interfacial self-assembly of SC3 monomers leads to insoluble amphiphatic films about 10 nm thick that coat air bubbles (Wessels, 1996). SC3 is secreted from hyphal tips as a monomer and then flows over the hyphal surface as semi-fluid polymers (Wessels, 1996). Hydrophobic interactions of monomers and other bonds may contribute to the overall hydrophobicity of the molecules (Wessels, et al., 1991). Purified SC3 is described as a milky suspension (Wessels, 1997). However, there are no reports of any iron-containing hydrophobins at this time.

Iron in or on glomalin (Table 4) imparts a red-brown color to extracted glomalin, and we think that iron is critical to the stability of the molecule in soil and in laboratory procedures used to reveal the molecular structure. Hydrolysis for amino acid analysis requires 24 h at 150 °C, and a pre-treatment to remove some of the iron may be necessary to achieve complete hydrolysis. We

have successfully removed a large amount of iron from glomalin using 8-hydroxy quinoline, but weaker chelators are slightly effective to ineffective for removal of iron. Lactoferrin is an iron-bearing protein with similarities to glomalin. Lactoferrin is a member of a group of iron-binding glycoprotein called transferrins. Although this glycoprotein is found in animals, it shares some intriguing characteristics with glomalin. Both are approximately the same size (~80 – 90 KD), extracellular, heat and enzymatically stable and difficult to hydrolyze. Lactoferrin hyperaccumulates iron and undergoes conformational changes upon binding iron. We have evidence that glomalin hyperaccumulates iron (Table 4) and are working on dissecting the conformational changes that may occur. Lactoferrin functions in iron binding and transport and as a bacteriostatic molecule – roles that glomalin may play in the soil environment.

Currently we are working to determine amino acid and carbohydrate contents and carbohydrates in glomalin from axenic cultures and soils. This requires stripping the iron with 8-hydroxy quinoline (manuscript in preparation).

CONCLUSIONS

Glomalin is abundant in soils and is closely correlated with aggregate water-stability. Glomalin contains carbon and hence constitutes a non-trivial portion of the terrestrial carbon pool. Possibly far more importantly, however, stabilization of aggregates amplifies the role of glomalin in soils because carbonaceous compounds are protected from degradation inside of aggregates. Increased atmospheric CO₂ can lead to increased production of glomalin because of the symbiotic association that exists between plants and producers of glomalin, AMF. We have also shown that glomalin concentrations in soils are influenced by management practices, for example in agroecosystems, further highlighting the role of this protein in carbon storage. Glomalin is an unusual molecule that has proven difficult to analyze biochemically due to its recalcitrance and possible complexity. Future research will be directed towards the elucidation of its structure and the controls on its production.

REFERENCES

- Cambardella, C. A., & Elliott, E. T. (1992) *Soil Sci. Soc. Am. J.* 56, 777-783.
- De Vries, O. M. H., Fekkes, M. P., Wösten, H. A. B., & Wessels, J. G. H. (1993) *Arch. Microbiol.* 159, 330-335.
- Jastrow, J. D., & Miller, R. M. (1997) *Soil Processes and the Carbon Cycle*, pp 207-223, CRC Press, Boca Raton, FL.
- Jastrow, J. D., Boutton, T. W., & Miller, R. M. (1996) *Soil Sci. Soc. Am. J.* 60, 801-807.
- Jones, T. H., Thompson, L. J., Lawton, H. H., Bezemer, T. M., Bardgett, R. D., Blackburn, T. M., Bruce, K. D., Cannon, P. F., Hall, G. S., Hartley, S. E., Howson, G., Jones, C. G., Kampichler, C., Kandeler, E., & Ritchie, D. A. (1998) *Science* 280, 441-443.
- Keeling, C. D., Whorf, T. P., Whalen, M., & van der Plicht, J. (1995) *Nature* 375, 666-670.
- Kemper, W. D., & Rosenau, R. C. (1986) *Methods of Soil Analysis (Part I)*, pp. 425-442, American Society of Agronomy, Madison, WI.
- Martin, J. P., Martin, W. P., Page, J. B., Ranley, W. A., & De Ment, J. D. (1955) *Adv. Agro.* 7, 1-37.
- Miller, R. M., Reinhardt, D. R., & Jastrow, D. D. (1995) *Oecologia* 103, 17-23.
- Rillig, M. C., & Allen, M. F. (1999) *Mycorrhiza* 9, 1-8.
- Rillig, M. C., Wright, S. F., Allen, M. F., & Field, C. B. (1999) *Nature* 400, 628.
- Rogers, H. H., Runion, G. B., & Krupa, S. V. (1994) *Environ. Pollution* 83, 155-189.
- Wessels, J. G. H. (1996) *Trends Plant Sci.* 1, 9-15.
- Wessels, J. G. H. (1997) *Adv. Microbial Physiol.* 38, 1-45.
- Wessels, J. G. H. de Vries, O. M. H., Åsgeirsdóttir, & Schuren, F. H. J. (1991) *Plant Cell* 3, 793-799.
- Six, J., Elliott, E. T., Paustian, K., & Doran, J. W. (1998) *Soil Sci. Soc. Am. J.* 62, 1367-1377.
- Tisdall, J. M., & Oades, J. M. (1982) *J. Soil Sci.* 33, 141-163.
- Wright, S. F., & Upadhyaya, A. (1996) *Soil Sci.* 161, 575-586.
- Wright, S. F., & Upadhyaya, A. (1998) *Plant Soil* 198, 97-107.
- Wright, S. F., & Upadhyaya, A. (1999) *Mycorrhiza* 8, 283-285.
- Wright, S. F., Upadhyaya, A., & Buyer, J. S. (1998) *Soil Biol. Biochem.* 30, 1853-1857.
- Wright, S. F., Starr, J. S., & Paltineanu, I. C. (1999) *Soil Sci. Soc. Am. J.* 63, 1825-1829.

PROCESS MODELING OF CO₂ INJECTION INTO NATURAL GAS RESERVOIRS FOR CARBON SEQUESTRATION AND ENHANCED GAS RECOVERY

C.M. Oldenburg, K. Pruess, and S.M. Benson
Earth Sciences Division
Lawrence Berkeley National Laboratory
Berkeley, CA 94720

KEYWORDS: carbon sequestration, enhanced gas recovery, natural gas reservoir

ABSTRACT

Injection of CO₂ into depleted natural gas reservoirs offers the potential to sequester carbon while simultaneously enhancing CH₄ recovery. Enhanced CH₄ recovery can partially offset the costs of CO₂ injection. With the goal of analyzing the feasibility of carbon sequestration with enhanced gas recovery (CSEGR), we are investigating the physical processes associated with injecting CO₂ into natural gas reservoirs. The properties of natural gas reservoirs and CO₂ and CH₄ appear to favor CSEGR. In order to simulate the processes of CSEGR in detail, a module for the TOUGH2 reservoir simulator that includes water, brine, CO₂, tracer, and CH₄ in nonisothermal conditions has been developed. Simulations based on the Rio Vista Gas Field in the Central Valley of California are used to test the feasibility of CSEGR using CO₂ separated from flue gas generated by the 680 MW Antioch gas-fired power plant. Model results show that CO₂ injection allows additional methane to be produced during or after CO₂ injection.

INTRODUCTION

Depleted natural gas reservoirs are potentially important targets for carbon sequestration by direct carbon dioxide (CO₂) injection. The accumulation and entrapment of a light gas such as methane (CH₄) testifies to the integrity of natural gas reservoirs for containing gas for long periods of time. By virtue of their proven record of gas production, depleted natural gas reservoirs have demonstrated histories of both (i) available volume, and (ii) integrity against gas escape. The IEA (International Energy Agency) has estimated that as much as 140 GtC could be sequestered in depleted natural gas reservoirs worldwide (IEA, 1997) and 10 to 25 GtC in the U.S. alone (Riechle et al., 2000). These aspects of natural gas reservoirs for carbon sequestration are widely recognized.

Less well recognized is the potential utility of CO₂ injection into natural gas reservoirs for the purpose of enhancing CH₄ production by simple repressurization of the reservoir. The pressure support provided by the CO₂ is similar to the proven cushion gas concept used in the gas storage industry wherein expansion of cushion gases upon natural gas withdrawal aids in production from the storage reservoir (Carrière et al., 1985; Lailie et al., 1988). The concept of enhancing CH₄ production is important because it can partially offset the costs of CO₂ sequestration. This concept was first described by van der Burgt et al. (1992) and Blok et al. (1997), who used reservoir simulation to evaluate how quickly the injected CO₂ would mix with the produced natural gas. Based on the simulations they concluded that enhanced production was possible for some period before the extent of mixing was too great. Nevertheless, little attention has been given to this option for sequestration, primarily due to concerns about degrading the quality of the produced gas.

The purpose of this paper is to further explore the physical processes involved in CSEGR. To accomplish this, numerical simulations of CO₂ injection and enhanced gas recovery were carried out on a model system based on the Rio Vista Gas Field in California's Central Valley. The proposed source of CO₂ in this study is flue gas from the 680 MW power plant at Antioch, California, 20 km from Rio Vista. To carry out the simulations, we have developed capabilities for the TOUGH2 reservoir simulator (Pruess et al., 1999) for modeling gas reservoirs. Through simulations of the injection process, we show that repressurization of the methane is possible and significant quantities of methane that would otherwise be left in the reservoir can be produced while carbon dioxide is being injected.

PROCESS DESCRIPTION

CSEGR involves the injection of CO₂ into depleted gas reservoirs with simultaneous or subsequent production of repressurized CH₄. The processes of gas-phase mixing by advection, dispersion, and molecular diffusion, which will tend to mix the gaseous components and deteriorate the quality of the natural gas, are dependent on the properties of natural gas reservoirs and of the gases. Pressures in depleted natural gas reservoirs are approximately 20–50 bars, with temperatures 27–120 °C. The large volume and large areal extent of gas reservoirs decrease the potential for mixing by dispersion over practical time scales. In Table 1 we present properties of CO₂ and CH₄ relevant to CSEGR. Note that CO₂ is denser and more viscous than CH₄, and will generally be subcritical but may be supercritical in deep depleted reservoirs. The large density of CO₂ relative to CH₄ means that CO₂ will tend to migrate downwards relative to CH₄. The larger viscosity of CO₂ ensures that displacement of CH₄ by CO₂ will be a favorable mobility ratio displacement, with less tendency for the gases to finger and intermix than in displacements such as water floods in oil reservoirs. Pressure diffusivity is typically three–five orders of magnitude larger than molecular diffusivity, making repressurization occur much faster than mixing by molecular diffusion. In summary, the properties of gas reservoirs and CO₂ and CH₄ appear to favor the feasibility of CSEGR.

Table 1. Properties of CO₂ and CH₄ from Vargaftik (1975).

Property	CO ₂	CH ₄
Molecular weight	44 g/mole	16 g/mole
Critical point	31 °C, 73 bar	-83 °C, 46 bar
Density	880 kg/m ³ (50 °C, 300 bar) 140 kg/m ³ (50 °C, 60 bar)	193 kg/m ³ (50 °C, 300 bar) 39 kg/m ³ (50 °C, 60 bar)
Viscosity	0.085 cp (50 °C, 300 bar) 0.019 cp (50 °C, 60 bar)	0.023 cp (50 °C, 300 bar) 0.013 cp (50 °C, 60 bar)
Diffusivity (at 273 K, 1 bar)	1.42×10^{-5} m ² /s (in air)	1.53×10^{-5} m ² /s (in CO ₂)

MATHEMATICAL MODEL

In order to model gas reservoir processes, we have developed a module called EOS7C (Oldenburg and Pruess, 2000) for simulating gas and water flow in natural gas reservoirs within the TOUGH2 framework (Pruess et al., 1999). The module handles five components (water, brine, non-condensable gas, tracer, and methane) along with heat. The non-condensable gas can be selected by the user to be CO₂, N₂, or air. EOS7C is an extension of the EOS7R (Oldenburg and Pruess, 1995) and EWASG (Battistelli et al., 1997) modules. The EOS7C module is currently restricted to the high-temperature "gas-like" conditions for CO₂, as opposed to the high-pressure "liquid-like" conditions. Advection of gas and liquid phases is governed by a multiphase extension of Darcy's law. Molecular diffusion in the gas and liquid phases is currently modeled using a Fickian approach. The main gas species partition between the gas and liquid phases according to their temperature- and pressure-dependent solubilities (Irvine and Liley, 1984; Cramer, 1982; Pritchett, 1981), while the gas tracer volatilization is controlled by a Henry's coefficient input by the user. The selection of N₂ or air in place of CO₂ will allow the module to be used for simulating gas storage processes, including the use of inert cushion gases. Because it is a module of TOUGH2, EOS7C includes all of the multiphase flow capabilities of TOUGH2, including the ability to model water drives and gas-liquid displacements that may be present in gas reservoirs.

APPLICATION TO RIO VISTA GAS FIELD

In this section, we investigate by numerical simulation the process of CSEGR at the Rio Vista Gas Field. Rio Vista is the largest gas field in California and has been under production since 1936 (Burroughs, 1967). It is located approximately 75 km north of San Francisco in the Sacramento Basin and has an elongated dome-shaped structure extending over a 12 by 15 km area (see Figure 1). The reservoir rocks are Upper Cretaceous to Eocene and consist of alternating layers of sands and shales deposited in deltaic and marine environments. Normal faulting occurred contemporaneously with sedimentation, creating a set of sub-parallel faults trending NW through the field. The most important of these is the Midland Fault (Figures 1 and 2). In some gas-bearing strata, displacement along the faults has created structural traps. In others, particularly the thicker gas bearing sands, the smaller faults do not play as important a role in defining reservoir structure.

Since 1936 the Rio Vista Gas Field has produced over 9.3×10^{10} m³ of natural gas (at standard conditions of 1 bar, 15.5 °C [14.7 psi, 60 °F]) from 365 wells. Production peaked in 1951 with annual production of 4.4×10^9 m³ and, as shown in Figure 3, has declined steadily since then (Cummings, 1999). Production decline is caused by decreasing reservoir pressures and increased water production, particularly on the western boundary of the field.

The Domengine formation shown in Figure 2 has been the most productive pool in the Rio Vista Gas Field. It occurs at an average depth of 1150 to 1310 m with an average net thickness of 15 to 100 m. The initial reservoir pressure and temperature were approximately 120 bars and 65 °C. Other generalized reservoir properties are provided in Table 2. As shown in Figure 2, the Domengine is laterally continuous across the Rio Vista Gas Field with vertical confinement provided by the Nortonville and Capay Shales. Its western boundary is controlled by the presence of the watertable at a depth of 1325 m. For the purpose of this study we focused on CO₂ sequestration and enhanced gas recovery in the Domengine formation to the west of the Midland Fault (see Figure 4).

The source of CO₂ considered in this study is the 680 MW gas-fired power plant located in Antioch, California (20 km from Rio Vista). This plant produces 2.2×10^9 m³ (1 bar, 15.5 °C) or 4.15×10^8 kg of CO₂ annually. At this rate, a simple volumetric replacement of all of the natural gas produced from Rio Vista since 1936 suggests that approximately 80 years of sequestration capacity are available.

The simplified 2-D model system based on the Rio Vista Gas Field is shown in Figure 4. The model system is a 1 km wide cross-section with vertical dimensions 100 m and horizontal extent 6600 m of the western flank of the dome, corresponding to 1/16 of the actual length of the reservoir. The model reservoir has a roof sloping at 0.78 ° and closed right-hand side. The bottom of the gas reservoir is a horizontal water table. Note that in all simulations presented here, water drive is turned off by closing all the lower boundaries of the system. Properties of the formation are simplified for this study as shown in Table 3.

Table 2. Relevant properties of Rio Vista model gas reservoir.

Property	Value	Units
Porosity	0.35	-
Y-, Z-direction permeability	1.0×10^{-12} , 1.0×10^{-14}	m^2 , m^2
Capillary pressure m , S_{lr} , $1/\alpha$, P_{capmax} , S_{li}	van Genuchten (1980); 0.2, 0.27, 8.4×10^{-4} , 10^5 , 1.	-, -, Pa^{-1} , Pa , -
Relative permeability liquid	Van Genuchten model	-
gas	Corey model ($S_{gr} = 0.01$)	-
Molecular diffusivity in gas, liquid	1.0×10^{-3} , 1.0×10^{-10}	$\text{m}^2 \text{s}^{-1}$, $\text{m}^2 \text{s}^{-1}$
Temperature	65	$^{\circ}\text{C}$
Initial pressure at water table	126	bars

The initial condition consists of the water table at $Z = 0$ on the left-hand side of the domain at a pressure of 126 bars, with CH_4 gas and residual water ($S_w = 0.27$) in the pore space above. All simulations were done at isothermal conditions of 65°C . From this initial condition, we simulated the withdrawal of CH_4 at 1/16 the historical rate as shown in Figure 3 for the period 1936–1998.

Following the historical production, we simulated CO_2 injection at a point 15 m below the top of the reservoir at approximately $Y = 2000$ m, and CH_4 withdrawal from the upper right-hand side of the domain ($Y = 6600$ m). In all cases, CO_2 is injected into the reservoir at a rate corresponding to 1/16 the actual production of CO_2 from the 680 MW Antioch gas-fired power plant. An example simulation result is shown in Figure 7 where we show mass fraction of CO_2 along with gas velocity vectors at three different times for the case of CO_2 injection with no CH_4 production. Note the depression of the water table in response to gas injection. As gas is injected, reservoir pressure increases with limited mixing of the gases by advection and diffusion.

Summaries of the simulated pressure evolutions and mass production rates are shown in Figures 5 and 6, respectively. We simulated two different scenarios that start in 1999 (see Table 3). In Scenario I, CO_2 is injected into the reservoir for ten years starting in 1999, as shown in Figure 7. This injection serves to repressurize the reservoir. In the subsequent part of Scenario I, CH_4 is produced for ten years from the repressurized reservoir at a rate corresponding to the 1950–1960 average rate. In Scenario II, CO_2 injection is simultaneous with CH_4 production, where CH_4 is produced at constant pressure. Note in Figure 5 that in Scenario I, 99% pure CH_4 can be produced for about 5 years following CO_2 injection, and that this CH_4 production is at a very large rate. In Scenario II, 99% pure CH_4 can be produced for approximately 10 years during CO_2 injection, although the rate is smaller than in Scenario I (see Figure 6). Note that these simulations have neglected dispersion which would increase gas-phase mixing. Assuming a longitudinal dispersivity of 100 m and 20 years of CSEGR, the dispersive mixing length for these scenarios is on the order of 1 km. This estimate shows that dispersion is an important mixing mechanism, but that over the large length scale in the model gas reservoir, repressurization and production of high quality methane would still be possible. The total additional masses of CH_4 produced by CSEGR for Scenarios I and II are 1×10^9 kg (5.2×10^7 Mcf) and 1.1×10^9 kg (5.7×10^7 Mcf), respectively, as compared to a projected 1.8×10^8 kg (9.4×10^6 Mcf) without CSEGR. Note that these quantities are for the 2-D model system which is 1/16 of the whole gas field.

Table 3. CSEGR scenarios for Rio Vista case study.

Period	Inject	Produce	Rate	Cumulative mass
1936–1998	-	CH_4	Variable (1/16 historical CH_4 production)	-3.5×10^9 kg CH_4
Scenario I. 1999–2009	CO_2	-	8.2 kg/s (1/16 Antioch CO_2 production)	2.6×10^9 kg CO_2
2010–2019	-	CH_4	3.2 kg/s (1950–1960 average rate)	-9.6×10^8 kg CH_4
Scenario II. 1999–2019	CO_2	CH_4	CO_2 : 8.2 kg/s CH_4 : Variable (constant pressure of 39 bars)	5.1×10^9 kg CO_2 -1.1×10^9 kg CH_4

Finally, we present in Figure 8 a scenario to examine the process of density stratification within the reservoir for the case of no CH_4 production. In this scenario, CO_2 is injected for 10 years and then allowed to migrate as driven by density and pressure gradients. As seen in Figure 8, CO_2 moves downwards due to its greater density relative to CH_4 , a process favorable for CSEGR.

CONCLUSIONS

The Rio Vista Gas Field is a potential site for CSEGR. Properties of natural gas reservoirs and of CO_2 and CH_4 are favorable for repressurization without extensive mixing over time scales of practical interest. Simulations of the process of CO_2 injection into a depleted natural gas reservoir carried out with TOUGH2/EOS7C confirm the plausibility of CSEGR as a way to sequester carbon while enhancing methane recovery. Simulations that use realistic estimates of CO_2 produced from the Antioch gas-fired power plant show that with CSEGR, more than five times the mass of methane can be recovered relative to that which would be produced without CSEGR.

ACKNOWLEDGMENTS

The authors would like to thank Drs. P. Witherspoon and L. Myer of Lawrence Berkeley National Laboratory for fruitful discussions regarding the feasibility of carbon sequestration and enhanced gas recovery. We would also like to acknowledge the help of M. F. Cummings of the California Division of Oil and Gas in obtaining detailed production data for the Rio Vista Gas Field. Thanks are also due to Victoria Porto who helped gather the early data needed for this project. This work was supported by Laboratory Directed Research and Development Funds at Lawrence Berkeley National Laboratory under Department of Energy Contract No. DE-AC03-76SF00098.

REFERENCES

- Battistelli, A., C. Calore, and K. Pruess, The simulator TOUGH2/EWASG for modelling geothermal reservoirs with brines and non-condensable gases, *Geothermics*, 26(4), 437-464, 1997.
- Blok, K., R.H. Williams, R.E. Katofsky, and C.A. Hendriks, Hydrogen production from natural gas, sequestration of recovered CO₂ in depleted gas wells and enhanced natural gas recovery, *Energy*, 22 (2,3), 161-168, 1997.
- Bondor, P.L., Applications of carbon dioxide in enhanced oil recovery, *Energy Convers. Mgmt.*, 33 (5-8), 579-586, 1992.
- Burroughs, E., Rio Vista Gas Field. Summary of California oil fields, Vol. 53., No. 2-Part 2., pp. 25-33, State of California, Department of Conservation, Division of Oil and Gas, 1967.
- Carrière, J.F., G. Fasanino, and M.R. Tek, Mixing in underground storage reservoirs, *Society of Petroleum Engineers SPE-14202*, 9-12, 1985.
- Cramer, S.D., The solubility of methane, carbon dioxide and oxygen in brines from 0° to 300°C, U.S. Bureau of Mines, Report No. 8706, 16 pp., 1982.
- Cummings, M. F., Northern California oil and gas field production. Annual production and well Data. 1977-1998. State of California, Division of Oil, Gas and Geothermal Resources, 1999.
- IEA, Carbon Dioxide Utilization, IEA Greenhouse Gas R&D Programme, Table 6, 1997.
- Irvine, T.F. Jr., P.E. Liley, Steam and gas tables with computer equations, Academic Press, Orlando, FL, 185 pp, 1984.
- Laille, J-P., J-E. Molinard, and A. Wents, Inert gas injection as part of the cushion of the underground storage of Saint-Clair-Sur-Epte, France, *Society of Petroleum Engineers SPE-17740*, 343-352, 1988.
- Mualem, Y., A new model for predicting the hydraulic conductivity of unsaturated porous media, *Water Resour. Res.*, 12(3), 513-522, 1976.
- Oldenburg, C.M., and K. Pruess, EOS7R: Radionuclide transport for TOUGH2, Lawrence Berkeley National Laboratory Report, LBL-34868, 1995.
- Oldenburg, C.M., and K. Pruess, EOS7C: Gas reservoir simulation for TOUGH2, Lawrence Berkeley National Laboratory Report, in preparation, 2000.
- Pruess, K., C. Oldenburg, and G. Moridis, TOUGH2 user's guide, version 2.0, Ernest Orlando Lawrence Berkeley National Laboratory Report, LBNL-43134, November 1999.
- Pritchett, J.W., M.H. Rice, and T.D. Riney, Equation-of-state for water-carbon-dioxide mixtures: implications for Baca reservoir, Report DOE/ET/27163-8, UC-66-a, 53 pp, 1981.
- Riechle et al., Carbon sequestration research and development. U.S. Department of Energy, DOE/SC/FE-1, 2000.
- van der Burgt, M.J., J. Cattle, and V.K. Boutkan, Carbon dioxide disposal from coal-based IGCCs in depleted gas fields, *Energy Convers. Mgmt.*, 33 (5-8), 603-610, 1992.
- van Genuchten, M.Th., A closed form equation for predicting the hydraulic conductivity of unsaturated soils, *Soil Sci. Soc.*, 44, 892-898, 1980.
- Vargaftik, N.B., Tables on the thermophysical properties of liquids and gases, 2nd Ed., John Wiley & Sons, New York, NY, 1975.

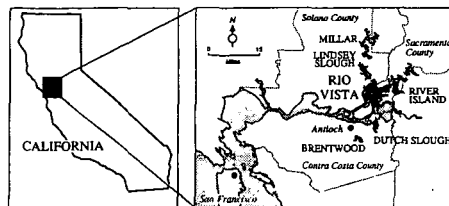


Figure 1. Rio Vista Gas Field area map showing gas fields in black.

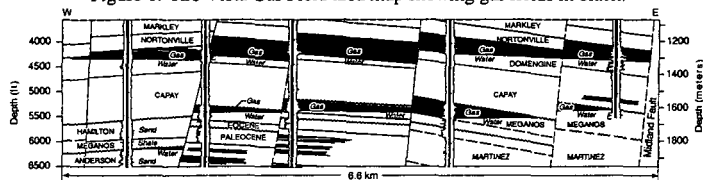


Figure 2. East-west cross section of the Rio Vista Gas Field modified from Burroughs (1967).

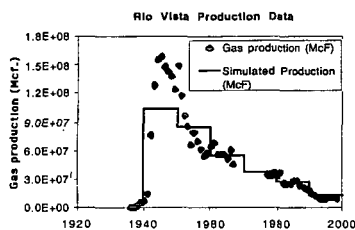


Figure 3. Production history of methane from the Rio Vista Gas Field. Production from model system is 1/16 of the 10-year-averages shown. (n.b., 1 Mcf = 10^3 cf)

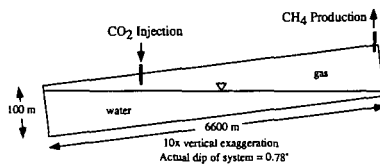


Figure 4. 2-D vertical section used in CSEGR simulations.

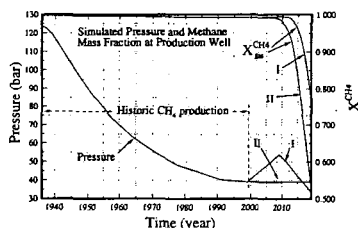


Figure 5. Pressure and CH_4 mass fraction evolution for Scenarios I and II.

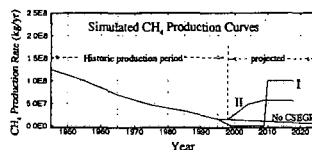


Figure 6. Simulated mass production rates of CH_4 for Scenarios I, II, and projected if no CSEGR.

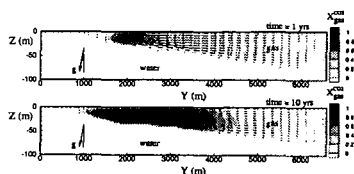


Figure 7. Mass fraction of CO_2 in the gas phase and gas velocity at $t = 1$ yr and 10 yrs with no CH_4 production.

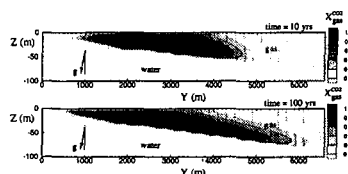


Figure 8. Mass fraction CO_2 in the gas phase and gas velocity at $t = 10$ yrs and 100 yrs for the case of gravity-driven density stratification following 10 years of CO_2 injection.

FIELD-TESTING CO₂ SEQUESTRATION AND ENHANCED COALBED METHANE RECOVERY IN ALBERTA, CANADA – A HISTORICAL PERSPECTIVE AND FUTURE PLANS

William D. Gunter and Sam Wong, Alberta Research Council, 250 Karl Clark Road, Edmonton, AB, Canada T6N 1E4; and Thomas Gentzis, National Centre for Upgrading Technology, 1 Oil Patch Drive, Suite A202, Devon, AB, Canada T9G 1A8

ABSTRACT

The Alberta Research Council is leading a program on the reduction of greenhouse gas emissions by injecting CO₂, N₂, and flue gas in a deep coal seam while enhancing the recovery factors and production rates of methane. A field test was carried out in 1998 to obtain accurate information on CO₂ storage and production of CH₄ following a CO₂ injection/soak period. Experimental data was used to calibrate simulation models for a feasibility analysis of a full-scale, 5-spot pilot study planned for 2000-2002. In late 1999, a new well was drilled and completed in order to perform a simulated flue gas micro-pilot test into the coal seam. Three additional well may be drilled in 2001. Subsequently, gases will be injected into the four wells and production will be monitored from a fifth well over a 12-month period. Full-scale commercial development could begin as early as 2003.

KEYWORDS: Coalbed methane recovery, CO₂ storage, Alberta Basin

INTRODUCTION

The coalbed methane (CBM) recoverable resources in the Plains and Foothills regions of the Western Canada Sedimentary Basin (WCSB) are estimated to be 135 to 261 trillion cubic feet (TCF) and are comparable to the marketable conventional gas endowment of 263 TCF (1). About 48.5 megatonnes (Mt) or 32% of the 151 Mt of CO₂ emissions generated in Alberta in 1996 originated from coal-fired power plants (Figure 1). The above figure also shows that coal beds in the Alberta part of the WCSB are second only to aquifers in terms of storage capacity for CO₂ (2). An abundance of deep and unminable coal seams in Alberta makes geological storage of CO₂ applicable, particularly in those areas located in close proximity to power plants emitting large quantities of CO₂, a greenhouse gas (GHG). In such a storage process, the CO₂ produced from the power plants could be injected into the coal seams to produce CBM. This could lead to null-GHG power plants that would be fuelled by methane released from the deep coals in a cyclical approach that would eliminate any release of CO₂ to the atmosphere.

The Alberta Research Council is currently leading a multi-phase study on field-testing CO₂-enhanced CBM recovery at a site near Fenn Big Valley, Alberta, Canada. Phase I encompassed a paper study of the initial assessment and proof of concept of injecting CO₂, nitrogen, and flue gas into Mannville Group coals (Lower Cretaceous age) in the Alberta Basin. Phase II concentrated on the design and implementation of a CO₂-micro-pilot test following procedures developed by Amoco Production Company for coals in the San Juan Basin in the U.S. The project is now in Phase III, which is to evaluate the design and implementation of a full-scale pilot project. Burlington Resources has successfully injected CO₂ into relatively high permeability coal seams in the San Juan Basin and stimulated CBM production and recovery rates compared to primary production (a pressure depletion process). Additional tests are needed to demonstrate the concept for the low permeability coals of the Alberta Basin and elsewhere in the world.

RESULTS AND DISCUSSION

Following the successful completion of Phase I in the summer of 1997, Phase II proceeded in a timely manner and was completed in the spring of 1999. The primary goals of Phase II were the following: (1) to accurately measure data from a single well test involving a series of CO₂ injection/soak cycles followed by production of CO₂ and methane; (2) to history match the measured data with a comprehensive coal gas reservoir simulation model in order to obtain estimates of reservoir properties and sorption characteristics; and (3) to calibrate simulation models to predict the behaviour of a large-scale pilot project or full field development. The field test was carried out in an existing Gulf Canada well at the Fenn Big Valley location in the central Alberta Plains. Phase II was, in essence, the prelude to a full-scale 5-spot pilot test. The study concluded that a

full-scale pilot CO₂ sequestration/ECBM (enhanced coalbed methane recovery) project is possible in the above location (3).

The economic feasibility analysis of Phase II revealed that flue gas injection offers better economic return than pure CO₂ injection unless there is credit for the CO₂ avoided. At a rate of US\$1.00 per thousand standard cubic feet (MSCF) of CO₂ (US\$19 per tonne), the CO₂ would account for US\$2.00 per MSCF of methane sold, assuming that it takes at least 2 cubic feet of CO₂ injected for each cubic feet of methane produced. The CO₂-ECBM recovery mechanism is shown in Figure 2 (4-5). It might be advantageous to optimize the CO₂/N₂ composition of the flue gas when considering CO₂ storage/sequestration options. If flue gas is injected, the CO₂ would remain sorbed in the coal matrix while the majority of N₂, by being adsorbed less than CO₂, would be produced along with the methane. Flue gas injection would enhance CBM production rates by more than a factor of two (6). However, the early breakthrough of N₂ at the production well will cause an additional expense of having to separate N₂ from methane for sales. Pressure swing adsorption (PSA) systems are the optimum method to remove N₂ from the produced gas for small-scale/large N₂ content operations whereas cryogenic processes are favored for large field operations (7). Flue gas conditioning, compression, and N₂/CH₄ separation in surface facilities remain some of the technical challenges that will be addressed in Phase III.

Therefore, by combining CO₂ and N₂ for injection, the appearance of N₂ will be retarded compared to a pure N₂ injection stream and the methane production rate will be enhanced compared to a pure CO₂ stream [6]. However, gas separation will play a key role in the production of methane from coal beds and the most economic gas separation method for the injection gas stream will depend on the specified CO₂ concentration of this stream (7).

The three numerical models that were evaluated in Phase II adequately predicted the primary production of CBM. One such simulation, based on a 5-spot, 320-acre pattern, showed that CH₄ production rate increased by a factor of about 5 compared to primary production when flue gas was injected but methane production decreased rapidly (Figure 3). On the other hand, pure CO₂ injection resulted in methane production at lower rates but for much longer periods of time. Only one out of the three models evaluated was suitable to simulate flue gas injection. None of the three simulation software packages were capable of predicting the produced gas composition in the field test with any degree of accuracy. A better understanding of the process mechanisms involved, for example multiple gas sorption and diffusion, and changes in coal matrix volume due to sorption/desorption of gases is needed to guide any future development of the models.

Phase III was divided in two parts, to be conducted in stages from 1999 to 2001. Phase III-A evaluated the options for the treatment of flue gas, compression and associated economics to optimize CO₂ storage and CBM recovery both at the pilot and commercial scales. A second well was drilled and completed in the fall of 1999. Two flue gas micro-pilot tests, first of this kind in the world that involve injection of flue gas into a coal seam were carried out. Initially, core samples were taken from the second well and evaluated to determine the gas-in-place volume, gas composition, and gas storage capacity. The micro-pilot test was performed in the spring of 2000 by injecting a simulated flue gas steam consisting of two different ratios of N₂ and CO₂ to obtain greater methane recovery without any hindrance to CO₂ storage. The data will be used to finalize the design of the full-scale project that will be implemented in Phase III-B.

Phase III-B encompasses the implementation of a 5-spot field pilot, which would consist of four injection wells and one production wells, sized in a rectangular pattern between 20 and 40 acres. The objective of this phase would be to demonstrate the viability of a large-scale CO₂ storage/ECBM project and to obtain information on the specifications of the technology required to perform a full-scale development project. These specifications will be used to design flue gas collection and treatment facilities, compression, and gas production/separation facilities. The current plans call for the 5-spot pilot to be performed in the Fenn Big Valley site. Three additional wells will be drilled in 2001. These wells, along the one drilled in 1999 and the existing Gulf Canada well will comprise the 5 wells needed for the large pilot. Injection will begin in 2001 and will continue for 12 months.

If the large-scale pilot is successful, full-scale development could begin in 2003 either on the above site or at another suitable location in the Alberta Basin.

Although most of the work so far has focused on the Manville Group coals in the Fenn Big Valley area, a parallel study conducted by the Geological Survey of Canada evaluates the geological properties of other unminable coal seams in Alberta, such as those of the Edmonton and the Ardley groups (Upper Cretaceous-Lower Tertiary). The Edmonton coals are shallower than the Mannville coals and are located in closer proximity to major coal-fired power plants, thus making these coals favourable targets for CO₂ storage. On the other hand, the Ardley coals are being investigated because of their higher permeability and lower injection pressures and costs required for a successful pilot.

CONCLUSION

In conclusion, flue gas injection into coalbed reservoirs has scientific merit and is more economical than pure CO₂ injection for ECBM recovery purposes. Existing information on any field experience of injecting flue gas into geological formations is scarce. More work is needed on the gas treating, compression, and injection methods in order to allow us to determine the economics between CO₂ storage and methane production from coal beds.

REFERENCES

1. Natural Gas Potential in Canada, a Report by the Canadian Gas Potential Committee, 1997.
2. Gunter, W.D., Wong, S., Cheel, D.B., and Sjoström, G. Large CO₂ sinks: their role in the mitigation of greenhouse gases from an international, national (Canadian) and provincial perspective, *Applied Energy*, **61**, 209 (1998).
3. Wong, S., and Gunter, W.D. Testing CO₂-enhanced coalbed methane recovery, International Energy Agency Gas R & D Program, Greenhouse Issues, (45), November 1999, p. 1-3.
4. Wong, S., Foy, C., Gunter, W.D., and Jack, T. Injection of CO₂ for enhanced energy recovery: Coalbed methane versus oil recovery, Proc. 4th Int. Conf. on GHG Control Technologies, Interlaken, Switzerland (Reimer, P., Eliason B., and Wokaum, A. Eds.), 189, Pergamon, 1999.
5. Wong, S., Gunter, W.D., and Mavor, M.J. Economics of CO₂ sequestration in coalbed methane reservoirs, Proc. SPE/CERI Gas Technol. Symp. 2000, SPE 59785, April 3-5 2000, Calgary, Alberta, 631.
6. Wong, S., Gunter, W.D., Law, D., and Mavor, M.J. Economics of flue gas injection and CO₂ sequestration in coalbed methane reservoirs, Proc. 5th Int. Conf. on GHG Control Technologies, Cairns, Australia, August 13-16, 2000.
7. Ivory, J., Gunter, W.D., Law, D., Wong, S., and Feng, X., Recovery of CO₂ from flue gas, CO₂ sequestration, and methane production from coalbed methane reservoirs, Proc. Int. Symp. on Economaterials, Ottawa, Canada, August 20-23, 2000.

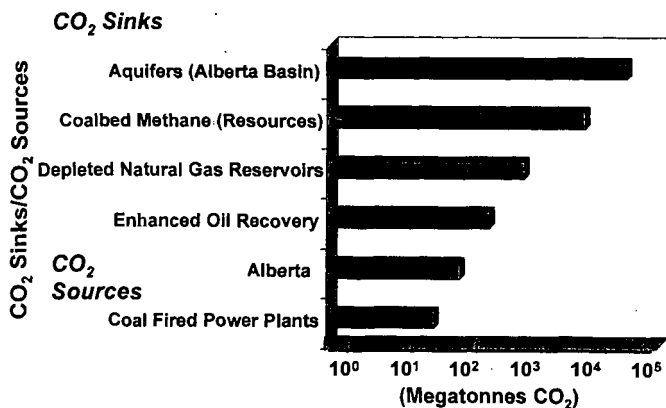


Figure 1 Emissions and greenhouse gas storage capacity in the Alberta basin.

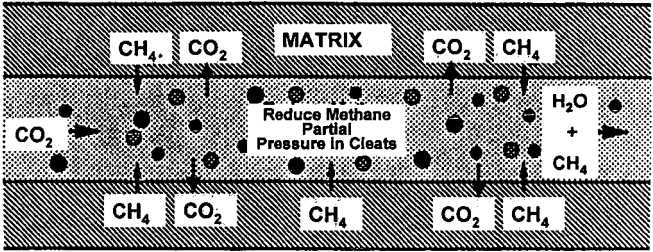


Figure 2 CO₂-enhanced coalbed methane recovery mechanism.

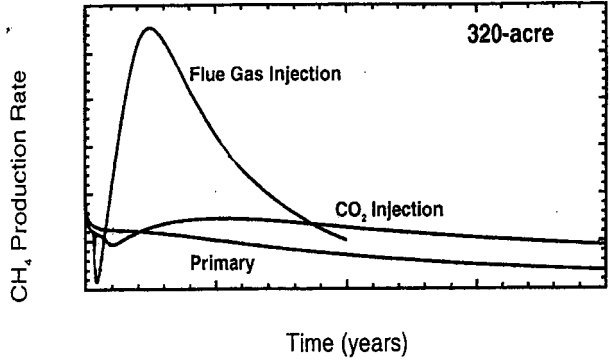


Figure 3 Coalbed methane production rate over time for primary recovery and as a result of pure CO₂ and flue gas injection.

MANAGING GREENHOUSE GAS EMISSIONS: STRATEGIES AND DEVELOPMENTS IN AUSTRALIA

B.C. Young, EnviroSAFE International Pty Ltd, Balwyn, VIC, Australia 3103
Email: byoung@envirosafe.com.au

D.J. Allardice, Allardice Consulting, Vermont, VIC, Australia 3133
Email: david.allardice@allardice.com.au

KEYWORDS

Greenhouse gas emissions, Australia's abatement programs, renewable energy

ABSTRACT

Australia is only a minor contributor to greenhouse gas (GHG) emissions globally but is a major contributor on a per capita basis. Owing to its dependence on coal-fired electricity generation, its energy intensive industries such as mining, aluminium, iron and steel, as well as its agriculture and land clearing practices, Australia's GHG emissions have already risen to 111% of the baseline 1990 levels. Consequently the Australian Government has moved from its previous 'no regrets' GHG abatement policies to issue new initiatives ranging from incentives and assistance programs on renewable energy, energy efficiency and alternative fuels, to a mandated target of 2% increase in renewable-based power generation (from 10% to 12%). Given the Government commitment of almost AUD\$1 billion over four years, these programs focus on the implementation of technologies available in the short-term rather than funding major long term development of new GHG abatement technologies.

INTRODUCTION

Australia, a large land mass approximately the area of continental USA containing about 19 million people, is rich in minerals and agricultural resources. It exports each year substantial quantities of raw and semi-processed minerals and metals as well as agricultural products. As a consequence of these factors, its energy use is high; for example, its electricity generation has increased from 155 TWh in 1990 to 179 TWh in 1998, with a further projected increase of over 40% by 2010. Australian energy use by source is shown in Table 1.

Greenhouse gas emissions worldwide exceed 41,000 million metric tons (tonnes) CO₂ equivalent annually, of which Australia's contribution is very small, about 1.4%. However, on a per capita basis at 26.7 tonnes CO₂ equivalent, Australia is amongst the highest emitters, 25 % higher than the USA and 2-3 times the annual per capita emissions of other developed countries, e.g. Germany at 12.6 tonnes. Further, by 1996, greenhouse gas emissions in Australia had increased to 111% of its 1990 baseline levels, already exceeding the emission target of 108% of 1990 baseline levels assigned at the Kyoto Greenhouse Summit in December 1997.

Australia in 1992 implemented a National Greenhouse Response Strategy, involving the voluntary cooperation and input by different levels of government, industry and the community for pursuing reduction of greenhouse gas (GHG) emissions. Shortly before the Kyoto meeting Australia moved from this "no-regrets" voluntary approach, e.g. the Greenhouse Challenge Agreement, to a more proactive strategy to combat and control the rising greenhouse gas emissions. In November 1997, the Prime Minister, Hon. John Howard announced a major policy statement entitled, *Safeguarding the Future: Australia's Response to Climate Change*, that included a AUD\$180 million package for addressing climate change and GHG emission issues. Since this announcement the Australian Government has expanded its initiatives and funding, to near AUD\$1 billion over 4-5 years, for a range of GHG emissions reduction projects.

This paper highlights various Government initiatives and programs. It also provides insight into selected key projects aimed at arresting Australia's continuing rise in CO₂ emissions.

GREENHOUSE ABATEMENT POLICIES/PROGRAMS

Underlying Australia's greenhouse abatement policies are the following premises:

1. Australia's competitive position in international markets should not be disadvantaged by policies and measures to reduce GHG emissions
2. Nuclear power is not a politically acceptable option in the short to medium term based on prevailing community attitudes.

The November 1997 Statement highlighted a range of financial incentives for energy efficiency and renewable energy programs along with mandating a 2 % increase in power generation from 'new' renewable energy sources. These policies and programs have subsequently been supplemented and expanded. The Australian Greenhouse Office (AGO) was formed to coordinate and implement the various greenhouse programs and measures, including the National Greenhouse Strategy (NGS).

Programs now being supported by the Australian Government include:

- Greenhouse Challenge – an expanded registry of companies, organizations and government authorities giving voluntary commitments to reduce their GHG emissions
- Renewable Energy Showcase Projects
- Renewable Energy Commercialisation Program
- Household Photovoltaic Scheme
- Alternative Fuels Conversion Program and Diesel Fuel/Alternative Fuels Grant
- Cities for Climate Protection™
- Efficiency Standards for Power Generation
- Bush (i.e. Outback) for Greenhouse
- International Greenhouse Partnerships (previously Activities Implemented Jointly)

The measure requiring a 2% increase in the use of 'new renewables' for power generation over existing levels by 2010 has also been strengthened to include a penalty of AUD\$40/MWh for non-attainment of the target.

The State and Local governments in Australia, having a degree of autonomy on energy and GHG matters, have strongly supported the Australian Government national programs as well as initiating State programs such as:

- The Green Power Program offering higher priced but renewables-based electricity
- Cogeneration and biomass generation incentives
- Energy efficiency labeling for household appliances
- Energy Smart programs and awards for companies, schools and other organizations

While the impact of these measures is difficult to quantify, there is general agreement that more action is required if Australia is to achieve its GHG targets. Carbon credit trading is an additional measure that various jurisdictions see as having potential to assist Australia meet its Kyoto obligations. The AGO has issued four discussion papers on the topic and is assessing the responses. Meanwhile the Sydney Futures Exchange is setting up electronic trading systems for a carbon credit market.

A major element of carbon trading schemes in Australia is sequestration credits from forestry activities. Forestry is largely a State responsibility and these carbon credit schemes vary from State to State. However, most State governments are actively pursuing forestry management programs and encouraging investment in future carbon sequestration credits. For example, TEPCO of Japan has significant forestry investments in NSW and Tasmania.

The Australian Government has also recently announced a model for a greenhouse trigger that would apply to actions or development projects that are likely to generate GHG emissions of over 500,000 tonnes of CO₂ equivalent in any 12 month period. This trigger could be applied under the Commonwealth's new Environment Protection and Biodiversity Act 1999. The proposed emissions threshold corresponds to approximately 10% of the average annual rise in Australia's total GHG emissions (1).

The current emphasis of the Australian Government funded greenhouse abatement programs is in maximising reductions in GHG emissions via demonstration, commercialisation and enhanced market acceptance of available or near-term renewable energy and energy efficiency technologies. A more detailed report summarising the various programs and including pertinent web sites, has been published elsewhere (2).

RENEWABLE ENERGY DEVELOPMENTS

2% Renewable Energy Target: The mandated 2% Renewable Target has been defined as 9500 GWh (about 2800MW) of green power that electricity suppliers are required to obtain from new renewable sources. Currently some 10 % of Australia's electricity is generated from renewable sources. Table 2 gives a breakdown of renewable energy sources for 1998

Beginning in 2001 with an additional 400 GWh of new renewables-based electricity, the measure will be phased in steps reaching 9500 GWh in 2010. As a minimum, the target amount is to be maintained through the period 2010-2020.

This 2% Target measure has already provided a significant boost to developing the renewable energy industry in Australia, and could stimulate at least AUD\$2 billion investment. Hence it is a major driver to develop new renewable energy sources for reducing GHG emissions.

SWERF Waste-to Energy Facility in NSW: Energy Developments Limited (EDL) is constructing a Solid Waste Energy Recycling Facility (SWERF) in Wollongong, NSW following a Renewable Energy Showcase Grant of \$2 million from the AGO. Based on 10 years development, the SWERF project will convert household trash to 'green' electricity with the potential for consuming 90% of the waste collected by Wollongong City Council currently going to landfill. Assuming a yield of 85% organic pulp (putrescibles, organics, paper, plastic), it is estimated that 100 tonnes of municipal solid waste will generate 90 MWh of electricity (3).

The EDL facility, costing AUD \$10 million for initial development, has been designed to separate recyclable materials, such as metals and glass, from unsorted household garbage and gasify the organic-based remainder using the Brightstar Environmental gasification technology. The gas is burned in reciprocating engines to generate electricity that is sent to the grid. The facility, having four 1.35 MW Gen-sets currently, is to be commissioned in July-August 2000. This demonstration phase will process some 20,000 tonnes per annum and, depending on a successful outcome, will be followed by two more distinct phases - 75,000 tonnes per annum and 150,000 tonnes per annum. The latter will generate up to 16 MW of electricity and substantially reduce the pressure on landfill sites.

Landfill-Gas to Electricity: EDL also operates 16 landfill-gas power generation facilities around Australia with a combined capacity of 72 MW. The conversion into electricity of methane gas resulting from anaerobic digestion of organic refuse avoided the release of 1.84 million tonnes of CO₂ in the 1998-99 financial year.

Bagasse/Wood Waste Generation: The construction of Australia's largest biomass project, costing AUD\$50 M, at Rocky Point Sugar Mill, Queensland, is scheduled for May 2000. The completed facility is to generate 30 MW of 'green' electricity from bagasse (typically 20-weeks sugarcane crushing season per year) and wood waste/green waste for use by consumers as well as steam and electricity for industrial users including the sugar mill and a nearby ethanol distillation plant.

The project is being jointly developed by the Heck Group (Rocky Point Sugar Mill owners) and Stanwell Corporation (power generator) supported by an AGO Showcase Grant of AUD \$3 million (4).

BP Solar Olympic Athletes Village: BP Solar, now BP Solarex following the merger of BP Oil with Amoco, is completing the installation of a 1 kW solar cell on each roof of the 650 houses at the Athletes Village for the 2000 Olympics in Sydney. The 12 solar laminates on each roof incorporate BP Solarex's high efficiency (17 %) Laser Grooved Buried Grid mono-crystalline technology.

In Australia, BP Solarex manufactures solar cells from multi-crystalline and mono-crystalline technology. The Solarex facility in 1999 received a Renewable Energy Commercialisation Grant of AUD \$482,000 to upgrade its multi-crystalline solar cell fabrication facility (4). By the end of year 2000, the company will be producing 13 MW of solar cell panels from its Sydney factory, with a projected output of 20 MW by the end of 2001.

CONCLUSIONS

The Australian Government has made a major commitment of almost \$1 billion towards achieving its Kyoto obligations through its financial support of diverse renewable energy and energy efficiency programs. The focus of the programs is on maximising reductions in GHG emissions via the demonstration, commercialisation and improved market acceptance of renewable energy and energy efficient technologies.

It is widely accepted that further measures will be needed for Australia to achieve its Kyoto targets. Options could include carbon credit trading, setting efficiency targets for major GHG emitters, and minimising the GHG impact of major development projects.

At this stage, there is no substantial government funding of high risk R&D projects as is common in USA, Japan and Germany. The Australian Government, however, supports fundamental greenhouse research activities through several CSIRO Divisions (e.g. global warming and climate change at the Division of Atmospheric Research; carbon fixing in forests and crops at the Division of Forestry) and various Cooperative Research Centres (e.g. CRC for Greenhouse Accounting; CRC for Renewable Energy; CRC for Clean Power from Lignite).

Increased joint government and industry funding of innovative technical solutions will be required to make further reductions in GHG emissions from Australia's particular energy generation and resource use as we move closer towards the Kyoto target dates of 2008-2012 and beyond.

ACKNOWLEDGMENTS

The authors express their thanks to New Energy and Industrial Technology Development Organization (NEDO), Sydney Representative Office, Australia for funding the Report (2) on which this paper is essentially based.

REFERENCES

- (1) Environment Australia: www.environment.gov.au, May 2000.
- (2) Allardice, D.J. and Young, B.C. *Greenhouse Gas Fixation and Utilisation Policy and Technology in Australia*, Report to NEDO (Sydney Representative Office): March 2000, 76p.
- (3) Toms, P. *Sustainable Utilisation of Green Waste and Urban Biomass – A Case Study of Wollongong's Electricity Plant and Solid Waste to Energy Recycling Facility*, IIR Conference on Waste Minimisation and Recycling 31 Aug – 1 Sep 1999, 17p.
- (4) Australian Greenhouse Office: www.greenhouse.gov.au/renewable/recp.
- (5) ABARE: *Australian Energy: Market Developments and Projections to 2014-15*, Canberra, 1999.
- (6) Schaap, H. *Data: Electricity Supply Association of Australia*, Melbourne, 1998.

Table 1. Australian Energy Use 1997-1998*

Source	Amount (%)
Crude oil	34
Black coal	29
Brown coal	13
Natural gas	18
Renewables	6

*Source: ABARE (5)

Table 2. Mix of Renewable Energy sources in Australia in 1998*

Source	Capacity (MW)	Generation (GWh)
Large hydro	7580	16,000
Small hydro	200	700
Biomass	330	800
Landfill gas	15	20
Sewage gas	49	90
Black liquor	6	40
Wind	2.7	4.8
Grid photovoltaic	0.14	0.3
Solar thermal	0.045	<1
Remote area power systems	14	<2
TOTAL	8,200	17,700

*Source: ESAA data (6)

A LIFECYCLE ASSESSMENT FRAMEWORK FOR EVALUATING THE REDUCTION OF CARBON DIOXIDE THROUGH INJECTION IN ACTIVE OR DEPLETED RESERVOIRS

Anne-Christine Aycaguer and Miriam Lev-On
BP Amoco HSE
333 S. Hope Street, PAC 1667
Los Angeles, CA 90071

Keywords: CO₂ storage, enhanced oil recovery, depleted reservoirs

Abstract

Several industries are conducting research to reduce their greenhouse gas (GHG) emissions because of the growing concerns over the GHG's effect on the atmosphere. In the petroleum industry, sequestration in active or depleted reservoirs seems a feasible solution towards lowering these emissions. Furthermore, injection in depleted reservoirs is said to offer important storage capacity, whereas injection in active reservoirs for enhanced oil recovery (EOR) combines GHG storage with the production of additional oil.

This paper presents a systematic approach to investigating and comparing the benefits of CO₂ storage in depleted versus EOR reservoirs. The benchmark is the potential for net CO₂ sequestration over the lifetime of the reservoir. An example applying a lifecycle assessment to an ARCO (now BP Amoco) project in West-Texas is described. The analysis on depleted reservoir storage is still in progress. However, preliminary results with EOR suggest GHG emissions from this power intensive process are small compared to the storage capacity of the formation, leading to a significant reduction of GHG emissions.

Introduction

With the burning of fossil fuel, arise anthropogenic emissions of greenhouse gases which enhance the natural greenhouse effect and could contribute to changing global climates. The petroleum and power industries are considering projects to reduce their emissions. Solutions include the offset of emissions by reforestation and forest management projects, as well as the reduction in emissions through energy efficiency improvements at their facilities, and sequestration of greenhouse gases in the oceans or underground in aquifers or fossil fuel reservoirs.

Fossil fuel reservoirs are very attractive as storage for greenhouse gases (especially carbon dioxide) because of existing infrastructure and/or a good understanding of the reservoirs. Two types of reservoirs can be used for that purpose: depleted reservoirs and reservoirs still active where enhanced oil recovery (EOR) can be applied.

Depleted reservoirs have not been employed for the storage of carbon dioxide yet. However, for many years now, they have been an essential link in the supply chain to ensure uninterrupted availability of natural gas during periods of high-energy demand such as winter. When the demand is low and excess capacity occurs, natural gas is stored in depleted reservoirs. It is recovered later on when necessary. In 1997, there were at least 410 underground reservoirs in the United States used for natural gas storage, with a total working gas capacity of 108 billion cubic meters (Thompson, 1997). Depleted reservoirs are located throughout the U.S. All areas of the United States with known oil and gas reservoirs also have depleted reservoirs. Both depleted oil reservoirs and depleted gas reservoirs can be used for storage of carbon dioxide and it is estimated the storage potential for these formations is around 794 billion metric tonnes worldwide (Stevens and Taber, 1999). This is a large potential for storage compared to the 6.6 billion metric tonnes of greenhouse gases in carbon dioxide equivalent emitted by the U.S. in 1997 (adapted from EPA, 1999).

For the case of active reservoirs, enhanced oil recovery is initiated when pumping techniques no longer produce enough oil for the fields to remain economically attractive. Supercritical carbon dioxide (CO₂) is injected in the reservoir and serves as an efficient solvent by reducing the viscosity of the oil, and thus enabling the oil to flow more readily to the producing wells. The carbon dioxide usually originates from naturally occurring CO₂ reservoirs, and in some cases CO₂ comes from processing plants. Reservoirs suitable for EOR are mostly located in the Permian Basin, TX, but can also be found in Alaska, California, Kansas, Oklahoma and the Texas Panhandle (Moritis, 1998). The current production from CO₂ EOR accounts for about 30 thousand cubic meters of oil per day from a total of 63 projects, or about 3% of total U.S. oil production (Moritis, 2000). Typically, an average of 530 to 1750 cubic meters of CO₂ is injected per cubic meter of oil recovered (Beike and Holtz, 1996). The overall storage potential in EOR reservoirs is estimated to about 129 billion metric tonnes (Stevens and Taber, 1999). Therefore, reservoirs using CO₂ for enhanced oil recovery present the advantage of being able to store large quantities of CO₂ while providing the economic incentive of oil production.

This presentation will compare the two storage options (depleted reservoirs versus EOR reservoirs) following a life cycle assessment methodology. Based on a currently operated EOR reservoir in the Permian Basin, we will investigate the storage potential as well as the emissions generated by the energy intensive process which includes the injection of the CO₂, its separation, capture and compression. The EOR reservoir analysis reflects the actual data from the case study with CO₂ originating from natural reservoirs and from the recycled CO₂-rich stream of the processing plant (attached to the EOR process for the treatment of the produced gas stream). The depleted reservoir case is a virtual case, a modification of the same reservoir to fit a depleted situation.

Methods –Life Cycle Assessment

To determine the environmental burden associated with the injection of CO₂ in active or depleted reservoirs, we chose to use a life cycle assessment (LCA) in order to capture the impacts from “cradle to grave.” The LCA can be used for product/process comparison, pollution prevention or simply for understanding one process/product’s impacts on the environment. An LCA’s major strength is the objectivity of the environmental analysis, and the elimination of externalities in project management regarding environmental issues.

The LCA follows a very structured methodology. We focused our efforts here on the inventory analysis and the impact analysis. Simply, the process is broken down into small entities, therefore facilitating the determination of input streams (resource requirement) and output streams (emissions) for each entity. The impact analysis provides a quantitative or qualitative characterization of the streams into and out of the system.

This presentation will be limited to greenhouse gas emissions and to the boundary of the facility. The scope of this work includes the extraction of oil/gas from the reservoir, the processing of the gas phase (extraction and separation of the usual components such as CO₂, H₂S, natural gas liquids), compression of the separated CO₂ stream, and underground injection in the reservoir either for use in EOR or simply for long term storage. Because we are investigating an existing reservoir under EOR, the study will be limited to the estimated 40-year lifetime of the reservoir.

A functional throughput unit was selected as a normalizing factor in order to allow for comparison among alternative approaches. In the case of EOR, and other methods of oil production in general, the net quantity of crude oil produced is the valued commodity. Therefore, releases to the environment and resources needed throughout the processes are quantified and indexed to the quantity of crude oil produced by the facility.

This LCA analysis uses specific site data for field emissions and storage as well as for electricity generation. The data used to determine the emissions are in part from direct sampling, and in part estimates based on applicable emission factors (E&P Forum, 1994; EPA, 1998; AP-42, 1998; IPCC, 1996). To remain conservative, the results presented below rely mainly on the E&P Forum emission factors or the EPA emission factors when no corresponding E&P Forum emission factors were available. The storage capacity is determined by performing a mass balance on the amount of CO₂ injected and the amount of CO₂ produced along with the oil.

Results and Discussion

A significant part of a life cycle assessment has to do with resource utilization or the use of natural resources to perform the process or obtain the desired product. Resources include both the natural resources used directly by on-site devices and indirect resources for generation of the grid power used by the facility. In our example, the resources consist of gas and coal, but remain regional variables and would be different for other part of the US. For the oil recovery process linked to enhanced oil recovery the resources also include CO₂. This paper is not going to discuss this aspect in order to better focus on emissions and storage.

The greenhouse gases emitted by the EOR processing can be divided into the direct and indirect emissions. Indirect emissions are attributable to electricity generated outside of the facility boundaries and transported through the grid to power equipment within the system investigated. In our case study, we found indirect emissions account for 13.5% of total CO₂ emissions, about 0.1% of CH₄ emissions, and approximately 0.8% of N₂O emissions.

Direct emissions originate from the use of on-site equipment fired by natural gas. On-site fired equipment demands more power than equipment receiving electricity from the grid and therefore emissions are higher. Direct emissions account for 59.2% of CO₂ emissions, approximately 2% of methane emissions, and 84.1% of N₂O emissions.

The rest of the on-site emissions are accounted for by process equipment leakage and routine maintenance that could result in fugitive methane emissions. In addition, flaring associated with the separation plant is also included and constitutes the remaining of the emissions presented. The system's total CO₂ emissions amounted to 0.3 kg / kg of oil produced. The EOR process also emitted 0.0015 kg of methane / kg of oil produced, and 2.1 10⁻⁵ kg of N₂O / kg of oil produced.

Simultaneously, the process contributed to storing 3 kg of CO₂ / kg of oil produced, and 0.18 kg of methane / kg of oil produced. Table 1 provides a summary of the emissions from the EOR process per kg of crude oil produced. The mass balance for carbon dioxide exhibits process emissions as positive quantities, while the amount stored in the reservoir is shown as a negative number. This highlights the CO₂ storage potential of an oil reservoir.

Table 1 Mass balance of greenhouse gas emission for the EOR process (kg / kg of oil produced)

	Carbon Dioxide		Methane		Nitrous Oxide	
	On-site	Off-site	On-site	Off-site	On-site	Off-site
Emission	0.31	0.05	0.002	1.5 x 10 ⁻⁶	2 x 10 ⁻⁵	1.6 x 10 ⁻⁷
Storage	3		0.2			
Balance	-2.6		-0.2		2 x 10 ⁻⁵	

Our results suggest the EOR process using CO₂ as a solvent contributed to limiting the amount of greenhouse gases reaching the atmosphere over the lifetime of the reservoir (40 years). This table includes both the CO₂ recycled and the CO₂ originating from natural reservoirs. Only the recycled CO₂ would have been vented under normal EOR operations. Close to 45% of the CO₂ injected in the reservoir over the 40 year period

came from the recycling plant. We found that all of the CO₂ recycled is ultimately stored in the formation and 20% of the CO₂ purchased from natural CO₂ reservoirs is stored again in the EOR reservoir.

The part of the analysis related to storage of carbon dioxide in depleted reservoirs is still in progress. Therefore, we are unable to provide a comparison of both types of storage at this time, but will present the complete results of the study at the conference. However, we expect emissions for depleted reservoir storage to be in the same order of magnitude than for the EOR process. The depleted reservoir storage capacity should be significantly higher because EOR requires injection of additional fluids in the reservoir, like water, to boost production. Also injection in depleted reservoir is easier to monitor because nothing is actually removed from the reservoir.

Conclusion

The first part of the analysis demonstrates the CO₂ storage potential of an oil reservoir in the Permian Basin, TX, through the use of enhanced oil recovery. Concurrent with the storage possibilities in an active reservoir, we estimated the greenhouse gas emissions originating from the range of equipment used and from flaring practices and fugitive emissions. The results suggest the EOR process is not only a major CO₂ user, but could also be a significant way to store the CO₂ underground. This study, so far, also illustrates that the overall sequestration efficiency could be enhanced by utilizing captured and recycled CO₂ from process vents and stack effluents, instead of using CO₂ from natural reservoirs.

The second part of the study on injection of CO₂ in depleted reservoirs will be presented at the conference. We will analyze and compare both storage options focusing on storage capacity and emissions associated with separation and compression of the CO₂ stream. Incentives might play a significant role in the implementation and widespread use of these storage options.

Acknowledgements

The authors acknowledge fruitful discussions with Bruce Johnson, Tom Krawietz, Margaret Lowe, Barry Petty, Joe Sinner, and Clifton Yocom from ARCO Permian, TX, and thank them for providing data for this case study and for their support throughout this research.

References

- Beike, D.K., M.H. Holtz. 1996. "Integrated geologic, engineering, financial assessment of gas displacement recovery in Texas." Proceedings of the Permian Basin Oil and Gas Recovery Conference, Midland, Texas, 27-29 March. SPE 35167.
- E&P Forum. 1994. Methods for estimating atmospheric emissions from E&P Operations. Report No 2.59/197, September 1994.
- EPA. 1998. Inventory of US greenhouse gas emissions and sinks 1990-1996. Environmental Protection Agency, March 1998.
- EPA. 1999. Inventory of US greenhouse gas emissions and sinks 1990-1997. Environmental Protection Agency, March 1999.
- IPCC, 1996. Revised 1996 IPCC Guidelines for national greenhouse inventories. The Intergovernmental Panel on Climate Change.
- Moritis, G. 2000. "EOR weathers low oil prices." *Oil and Gas Journal*. March. 20.

Stevens, S.H., J.J. Taber. 1999. "Barriers to overcome in implementation of CO₂ capture and storage (disused oil and gas fields)." IEA Report PH3/22.

Thompson, J. M. 1997. "U.S. underground storage of natural gas in 1997: existing and proposed." Energy information administration, Natural Gas Monthly September 1997.

A TOOL TO FACILITATE MODELING AND PILOT PROJECTS FOR SEQUESTRATION OF CARBON DIOXIDE IN SALINE FORMATIONS

Keywords: greenhouse gasses, capture and storage

Hovorka, Susan D., Martha L. Romero, Andrew G. Warne, William A. Ambrose, Thomas A. Tremblay, and Ramón H. Treviño, Bureau of Economic Geology, The University of Texas at Austin

ABSTRACT

Saline water-bearing formations that extend beneath much of the continental United States are attractive candidates for disposal of CO₂ produced during power generation or by other industrial processes. We have quantified the characteristics of saline formations that assure that gas can be efficiently injected into the selected subsurface unit and that it will remain sequestered for suitably long time periods. A GIS data base of these geologic attributes of 21 saline formations is available to support data analysis and comparison with CO₂ source locations. Attributes include depth, permeability, formation thickness, net sand thickness, percent shale, sand-body continuity, top seal thickness, continuity of top seal, hydrocarbon production from interval, fluid residence time, flow direction, CO₂ solubility in brine (P, T and salinity), rock mineralogy, water chemistry, and porosity. Variations in formation properties should be considered in order to match a surface greenhouse gas emissions reduction operation with a suitable subsurface disposal site.

INTRODUCTION

For CO₂ sequestration to be a successful component in U.S. emission-reduction strategies requires a favorable intersection of a number of variables such as the market for electricity, fuel source, power and industrial plant design and operation, a suitable geologic host for sequestration, and a suitable pipeline or right-of-way from the plant to the injection site. The concept of CO₂ sequestration in saline water-bearing formations (saline "aquifers") isolated at depths below potable aquifers became of widespread interest several years ago (Bergman and Winter, 1995) and continues to evolve. Saline formations are attractive because large volumes of prospective sink underlie many parts of the United States. Significant barriers remain, however, including high costs and potential citizen concerns about the safety and effectiveness of this process. Our contribution to the U.S. effort to reduce greenhouse gas emission via underground sequestration is a data base of formations that may have potential for sequestering CO₂. This data base can be used to (1) match CO₂ sources with prospective sinks, (2) conduct preliminary feasibility analysis, and (3) build various types of economic and process models. Our goal is to provide low-cost but realistic data that can support the search for viable options for CO₂ sequestration.

The scope of our investigations is saline water-bearing formations outside of oil and gas fields. We are accepting the concept of hydrodynamic trapping (Hitchon, 1996), in which the CO₂ is isolated from the atmosphere and potable water supplies by very long (>1,000 yr) travel times between the injection site and these environments. A structural trap for the CO₂ is not required. We are also focusing on onshore sites near large or closely spaced commercial power plants and other industrial centers with point-source emissions of CO₂. This definition allows exploration for large volumes of saline formations that may be optimal injection sites near sources where sequestration could be undertaken at minimal cost.

METHODS

In the feasibility phase of our project, we (1) mapped the 1996 carbon emissions of power plants to identify basins where sinks would be useful, (2) collected informal information on the areal distribution of industrial CO₂ sources, (3) identified 16 parameters that describe the properties of reservoirs and seals in potential sinks, and (4) tested the feasibility of collecting these data in saline formations.

During Phase II of our project, we compiled regional scale information and quantitatively mapped the 16 parameters for at least one target saline formation in 21 basins. This data compilation is based entirely on literature review, employing regional summaries, water-supply papers, state survey and U.S. Geological Survey maps and publications, oil and gas resource assessments, waste injection literature, and unpublished data sources including theses and contract reports. We used recent stratigraphic overviews to identify at least one potential saline

aquifer in areas with CO₂ sources. Then we conducted a literature search using GeoRef (<http://georef.cos.com/>) and other online resources and consulted local experts to locate, acquire, and compile the required information. We ranked the quality of data for each parameter as follows: (1) detailed data digitized from the cited source, (2) generalized or schematic data from the cited source, (3) detailed data interpreted during this project, (4) sparse or descriptive data interpreted during this project, and (5) little or no data, values based on analog data.

Raw data showing the spatial distribution of each parameter was digitized. In most basins, the raw data consisted of one or more paper maps, which were scanned and georeferenced using Cartesian projection and latitude-longitude as calibration points, digitized using NDS Mapper software, attributed, and imported into ESRI ArcView GIS (geographic information system). One source of error in the data base lies in unknown projection and imprecise registration of the source maps. A few data sets were obtained in digital format (for example, from N. Gupta Battelle Memorial Institute, USGS online sources, and an unpublished oil field data base compiled by M. Holtz, Bureau of Economic Geology).

Data were then manipulated in GIS and spreadsheet software to standardize highly variable raw data. Once in ArcView the maps were reprojected in meters and in Albers Equal Area projection, and the spreadsheet data were standardized into common units. Variability in original data is the major source of error in the data set; however, standardization is necessary for interbasinal comparisons, and we think that the precision is adequate for the intended purpose of supporting the search for CO₂ sequestration options. Site-specific follow-up studies will be required at any potential sequestration prospect to confirm relationships observed at a regional scale.

We did not attempt a comprehensive survey of potential saline formations. Saline formations were selected using the following informal criteria: (1) the formation has geographic and geologic potential to serve as a sink for areas of point-source CO₂ emissions, (2) sufficient data were located to map some of the parameters, and (3) inclusion of the formation contributes a geologically diverse set of potential sinks to be used for modeling experiments.

RESULTS

During the feasibility phase of evaluation of parameters that describe the properties of reservoirs and seals in potential sinks, we decided that the state of the science was too immature to determine which variables are critical. We therefore decided to compile diverse data. Variables were selected either because other workers have used them for models or basin assessment (for example Hendriks and Blok, 1995; Holloway and van der Straaten, 1995; Koide and others, 1995; Hitchon, 1996; van der Meer, 1996; Weir and others, 1996; Gupta and others 1998) or because they are commonly used in reservoir evaluation or for underground waste disposal site evaluation. These diverse data sets will then facilitate further evaluation and modeling.

Six parameters were selected primarily to describe injectivity. Injectivity controls how fast CO₂ can be injected into the saline formation without excessive pressure buildup. Depth is a primary constraint on the density of the injected CO₂. At typical temperature and pressure 800 m approximates the critical point, below which CO₂ requires less volume, which improves injectivity. Permeability and formation thickness are the rock variables that determine the flow rate from a well. Net sand (net high permeability strata) describes the thickness of the strata that accept fluid and are used for capacity assessment. Percent shale and sand-body continuity are indexes to the internal heterogeneity of the injection unit; they are needed to model the behavior of the CO₂ after it is injected.

Ten parameters were collected primarily to assess how effective the unit would be at trapping the CO₂. Under most conditions, CO₂ at critical point will be buoyant in brine. The top seal is defined as the low-permeability unit above the prospective injection unit that will limit leakage of the injected CO₂ upward into potable water and the atmosphere. The thickness of the top seal as well as its continuity can be used to calculate the rate of escape of CO₂ to assure that trapping will be effective. Production of oil or gas from the interval can provide a pathway for more rapid release of CO₂ to the atmosphere; pragmatically it raises issues of mineral rights. Injection of CO₂ in producing intervals can be beneficial to production, maintaining pressure and helping to mobilize oil. Use or reuse of hydrocarbon reservoirs for CO₂ sequestration has been considered in a number of studies, such as Holtz and others (1999), and is therefore not the focus of our study. Because we are using a hydrodynamic trapping assumption, fluid residence time

and flow direction are important in assessing effectiveness of lateral trapping in the formation and identifying potential short lateral paths for leakage to fresh water or the atmosphere. Temperature, pressure, and salinity are major variables in calculating CO₂ solubility in brine. Mineral trapping, in which CO₂ reacts with minerals in the rock, can also provide a very long term trapping mechanism (Hitchon, 1996); therefore, we compiled rock mineralogy and brine chemistry to permit assessment of the role of this process. Porosity is a simple variable for assessing the total volume of storage in the saline formation.

We identified 21 candidate formations in onshore U.S. basins, including Los Angeles, Powder River, Sevier, Mojave, South Carolina, Alabama, North Carolina, Appalachian, Illinois, Texas Gulf Coast, East Texas, Florida, Black Warrior, Denver, Williston, Michigan, San Juan, Palo Duro, and Anadarko. Data sets of 16 parameters for the target saline formation in each basin have been compiled and digitized. In many basins, several potential prospects were identified. We selected one or two formations to characterize in this study and note the potential for additional resource in overlying and underlying formations.

DISCUSSION

When we proposed this study, we thought that saline formations were generally poorly known because they are unused. We expected to have to interpolate information from oil and gas producing areas and aquifers. However, during the feasibility phase as well as the assessment phase, we found that data describing saline formations at a regional scale are moderately abundant. Data are derived from regional studies integrating areas productive for resources as well as assessment of saline formations themselves for potential for deep well injection of waste or saline water resources. In many places more detail can be extracted from sources such as well records and regulatory information from various types of injection, including waste and gas storage.

Capacity for CO₂ sequestration in different basins is highly variable. Primary causes of variability are formation thickness and permeability. For example, much larger volumes of CO₂ could be injected into thousands of feet of high-permeability sand typical of the Tertiary of the Gulf Coast than in the few hundred feet of older and less permeable basal Cambrian sandstones of the Midwest. In addition, quality of seals varies greatly, from thick, ductile mudstones to brittle and potentially highly fractured carbonate rocks. Many areas contain layered seal and permeable strata that may have the potential for greater protectiveness than a single thick seal. However, feasibility of implementing a sequestration project may not require optimal geologic conditions; other variables may bring a lower capacity sink into use.

We did not attempt a comprehensive survey of potential saline formations; therefore, our study is not intended as a refinement of the total volume assessment of Bergman and Winter (1995) or as a tool for evaluating all the sequestration options at a given site. It is, however, suitable for meeting our goal to provide realistic data that can support the search for viable options for CO₂ sequestration. In addition, our study provides a template for additional data compilation to create a detailed national assessment of capacity. This flexible data base can be used for construction of other scenarios, for example, combination of CO₂ utilization and geologic sequestration.

The data base is available to researchers in ArcView format from the Bureau of Economic Geology (contact us at <http://www.beg.utexas.edu/>).

CONCLUSIONS

Variations in formation properties should be considered in order to match a surface greenhouse gas emissions reduction operation with a suitable subsurface disposal site. In this environment, where cost is a critical limiting factor, matching CO₂ capture processes with an optimal subsurface site for sequestration can be essential. This data base provides a vehicle for assessing the interaction between surface variables such as the nature of the source and type of capture and infrastructure and subsurface geologic variables.

ACKNOWLEDGMENTS

This project was funded by DOE under contract number DE-AC26-98FT40417.

REFERENCES

- Bergman, P. D., and Winter, E. M., 1995, Disposal of carbon dioxide in aquifers in the U.S.: *Energy Conversion and Management*, v. 36, p. 523-526.

- Gupta, Neeraj, Naymik, T. G., and Bergman, Perry, 1998, Aquifer disposal of carbon dioxide for greenhouse effect mitigation: Proceedings of the 23rd International Conference on Coal Utilization and Fuel Systems, March 9-13, Clearwater, Florida.
- Hendriks, C. A. and Blok, K., 1995, Underground storage of carbon dioxide: Energy Conversion and Management, v. 36, p. 539-542.
- Hitchon, Brian, ed., 1996, Aquifer disposal of carbon dioxide: hydrodynamic and mineral trapping – proof of concept: Alberta, Canada, Geoscience Publishing Ltd, 165 p.
- Holloway, Sam, and van der Straaten, Rieks, 1995, The Joule II project: the underground disposal of carbon dioxide: Energy Conversion and Management, v. 36, no. 6-9, p. 519-522.
- Holtz, M. H., Nance, P. K., and Finley, R. J., 1999, reduction of greenhouse gas emissions through underground CO₂ sequestration in Texas oil and gas reservoirs, The University of Texas at Austin, Bureau of Economic Geology final report prepared for EPRI through the Department of Energy, WO4603-04, 68 p.
- Koide, H., Takahashi, M. Tsukamoto, H. and Shindo, Y, 1995, Self-trapping mechanism of carbon dioxide in aquifer: Energy Conversion and Management, v. 36, p. 505-508.
- van der Meer, L. G. H., 1996, Computer modeling of underground CO₂ storage: Energy Conversion and Management, v. 37, no. 6-8, p. 1155-1160.
- Weir, G. J., White, S. P., and Kissling, W. M., 1996, Reservoir storage and containment of greenhouse gasses: Transport in Porous Media: v. 23, p. 37-60.

ANALYSIS OF VISCOUS FINGERING IN TWO-DIMENSIONAL FLOW CELL BY FRACTAL DIMENSION

Olubunmi M. Ogunsola, Everett R. Ramer, Duane H. Smith

National Energy Technology Laboratory, U.S. Department of Energy,
P. O. Box 880, Morgantown, WV 26507-0880, 304-285-4313, ogunsola@netl.doe.gov

KEYWORDS: Fractal dimension, Viscous fingering, CO₂ sequestration

INTRODUCTION

The potential global warming effects of increased carbon dioxide (CO₂) in the atmosphere have recently gained national and international attention. Consequently, the search for different ways to reduce CO₂ emissions has increased, and among the options available is sequestration of CO₂ by injection into deep brine formations. However, when a less viscous fluid, such as CO₂ is used to displace a more viscous fluid, such as brine, a flow instability phenomenon known as viscous fingering occurs. During this type of flow, the less viscous fluid forms fingers extending into the more viscous fluid. This phenomenon is significant to CO₂ sequestration in brine-saturated formations, because it will govern how much volume is available for CO₂ storage. Researchers desire to maximize the saturation of sequestered CO₂. A greater understanding of the flow patterns might yield insight that could ultimately lead to the increase of CO₂ sequestered. One way of observing the complex flow patterns that occur during immiscible displacements is to use an artificial porous medium made by etching channels of random width into glass plates. Since this medium is transparent, images of the flow can be recorded and used to characterize the geometry of the flow. Fractal dimension is one method that has been used to describe random geometries, including porosity (Hildgen et al, 1997), aggregates formed in different fluid mechanical environments (Logan and Kilps, 1995), and characterization of waste water treatment systems (Bellouti et al, 1997). The fractal dimension is used in this study to characterize relative saturations of air under different fluid flow conditions.

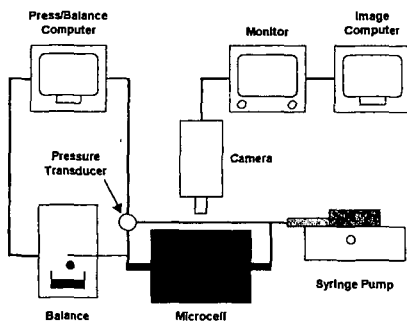


Figure 1: Experimental flow system

EXPERIMENTAL

The experimental flow system (see Figure 1) consists of a micro flow cell, which simulates the porous medium; a syringe pump, which provides a constant-volume-rate injection of fluid into the flow cell; a pressure transducer for measuring the pressure drop across the flow cell; and a balance for measuring the mass of the displaced fluid. The flow cell is made by etching channels of random width into a glass plate and fusing a second, flat plate to it, thereby creating a network of enclosed channels connected to inlet and outlet manifolds. A picture of one of the micro flow cells having random distribution of different channel widths used in this study is shown in Figure 2.



Figure 2: Flow cell showing pattern formed by injection of air into a water-saturated cell. The cell inlet is on left and the outlet on right.

Channel widths for cell #1 are in the range of 175-575 μm and for cell #2 are in the range of 260-1305 μm . In the experiment, the cell was first flooded with water to residual gas saturation. Then air was injected while the pressure drop across the cell and the mass of water displaced were recorded. Digital images of the cell were taken at regular intervals, usually 5 seconds, with a CCD camera. A computer program was developed to analyze the images for saturation and relative permeability calculations. Experiments were performed at different capillary numbers by use of different flow rates.

ANALYSIS

We use the box counting method (Aker, 1997) to analyze the pattern formed by the viscous fingers. In this method the image is covered with an array of square boxes, each box of size L , and the number of those boxes N that cover the injected-air pattern is counted. The relationship between N and the size of the box can be represented by

$$N(L) \sim L^{-d} \quad (1)$$

where d is the box-counting dimension and is a function of the geometry of the pattern. For example, if all the channels of the cell were filled with air, N would be proportional to L^{-2} . Or, if the air were to flow straight across the cell from entrance to exit filling only one channel, N would be proportional to L^{-1} . Since the actual pattern of the air flow is somewhere between these two extremes, N will be proportional to L^{-d} , where $1 < d < 2$. A log-log plot of the box counts can be used to determine d , as shown in Figure 3.

RESULTS AND DISCUSSION

Results from three experiments are discussed in this paper. These were conducted using two flow cells, and fixed injection rate Q and slightly different mobility ratios M . The mobility ratio is defined as ratio of the viscosity of the displaced fluid to that of the displacing fluid. The experimental conditions are shown in Table 1.

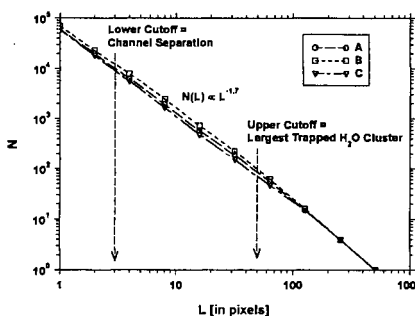


Table 1. Experimental Conditions

Experiment	Flow Cell	Fluids	Channel Width [μm]	Q [ml/min]	M
A	#1	Water and gas	175-575	0.87	53.76
B	#2	Water and gas	260-1305	0.90	53.76
C	#1	Nacl soln. and CO_2	175-575	0.91	72.53

The fractal dimensions of the flow patterns for these experiments are presented in Figure 3. The data plotted are for the ultimate flow patterns observed at the end of each experiment. The plots of data from the dynamic phase of the experiment, when the flow patterns are changing, are parallel to the plots of the ultimate values. Fractal dimensions of 1.7 were obtained with water and air as the immiscible fluids. When a sodium chloride solution and CO_2 were used (experiment C), no change in d was observed. We also noted that the injection rate does not change the value of d over the range of injection rates used.

Thus, in our work we found that d does not depend on the physical properties of the flow cell; the mobility ratios, although the two mobility ratios are relatively close; and on the level of air saturation of the cell. This implies that d is more of a characteristic of the flow patterns than any other parameter. The values of d obtained in our studies characterize viscous fingers for diffusion-limited aggregation (DLA) (Meakin, 1983). Figure 4 shows the correlation between fractal dimension and saturation.

CONCLUSIONS

These experiments demonstrate that fractal dimension is a function of fluid saturation but is independent of physical properties of the porous media. This analysis will be useful for

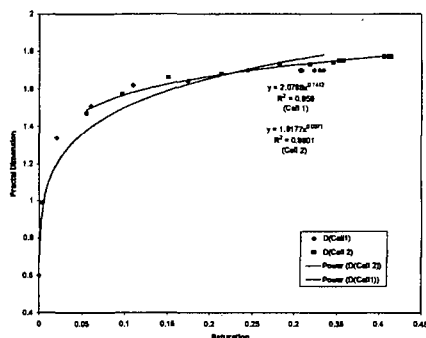


Figure 4: Fractal Dimension as a Function of Saturation

determining the fraction of the porous media that the displacing fluid will occupy. This is critical in the case of CO_2 sequestration into brine-saturated formations, because the more volume of space occupied by CO_2 during sequestration the more effective the process is.

Acknowledgments: Olubunmi Ogunsola was a National Research Council Sr. Associate. Her associateship and this work were funded by the Office of Fossil Energy, U.S. Department of Energy.

References

1. Bellouti, M. *Wat. Res.* **1997**, 31, 1227.
2. Aker, E. *PhD Dissertation, University Institute Oslo*, 1997.
3. M. Ferer, M.; G. Bromhal, and D. H. Smith, "Pore-Level Modeling of Carbon Dioxide Sequestration in Deep Aquifers," *Fuel Division preprint*, Washington, DC, August 20-24, 2000.
4. B.E. Logan and J. R. Kilps, *Wat. Res.* **1995**, 29, 443.
5. P. Meakin, *Phys. Rev. A* **1983**, 27, 2616.
6. M. Rahman, *J. of Food Engineering* **1997**, 32, 447.
7. P.Hildgen et al, *Physica. A* **1997**, 234, 593.

Pore-Level Modeling of Carbon Dioxide Sequestration in Deep Aquifers

Duane H. Smith, US DOE, National Energy Technology Laboratory, Morgantown, WV 26507-0880 and Dept. of Physics, West Virginia University; Grant S. Bromhal, Department of Civil and Environmental Engineering, Carnegie- Mellon University, Pittsburgh, PA 15213-3890; and M. Ferer, Department of Physics, West Virginia University, Morgantown, WV 26506-6315

KEYWORDS: CO₂ sequestration, Pore-level modeling; Immiscible drainage

ABSTRACT

Underground injection of gas is a common practice in the oil and gas industry. Injection into deep brine-saturated formations is a commercially proven method of sequestering CO₂. However, it has long been known that the immiscible displacement of a connate fluid by a less-dense and less-viscous fluid produces gravity override and unstable displacement fronts. These phenomena allow only a small fraction of the pore volume of a brine-saturated formation to be available for sequestration. A better understanding of the fluid displacement process could lead to reduced capital and operating costs by increasing CO₂ sequestration in deep aquifers.

We have developed a pore-level model of the immiscible injection of a non-wetting fluid (CO₂) into a porous medium saturated with a wetting fluid (brine). This model incorporates a distribution of different "pore-throat" radii, the wettability of the formation (i.e., the gas-liquid-solid contact angle), the interfacial tension between the fluids, the fluid viscosities and densities, and all other parameters that appear in the capillary pressure or the capillary, Bond, or fluid-trapping numbers. The computer code for the model maintains a constant injection velocity to within a few percent.

This model has been used, with experimental values of viscosities and interfacial tensions, to study the high-pressure injection of carbon dioxide into brine-saturated porous media. Results are presented for the applied pressures, fluid-front geometries, residual saturations, and numbers of blocked throats.

INTRODUCTION

The possible effects of rising atmospheric concentrations of carbon dioxide on global climate are of worldwide concern. The U. S. Department of Energy and its National Energy Technology Laboratory have instituted programs to study various methods of sequestering CO₂. [1], [2] Underground injection of gas has long been a common practice in the oil and gas industry.[3] Injection into deep brine-saturated formations is a commercially proven method of sequestering CO₂. [4] However, it has long been known that the immiscible displacement of a connate fluid by a less-dense and less-viscous fluid produces gravity override and unstable displacement fronts.[5] These phenomena allow only a small fraction of the pore volume of a brine-saturated formation to be available for sequestration.[6] A better understanding of the fluid displacement process could lead to new technologies for alleviating these mobility control problems[5] and to reduced capital and operating costs for CO₂ sequestration in deep aquifers.

We have developed a pore-level model of the immiscible injection of a non-wetting fluid (CO₂) into a porous medium saturated with a wetting fluid (brine).[7] This model, which is an extension of an earlier model for two miscible fluids,[8] incorporates a distribution of different "pore-throat" radii, the wettability of the formation (i.e., the gas-liquid-solid contact angle), the interfacial tension between the fluids, the fluid viscosities and densities, and all other parameters that appear in the capillary pressure or the capillary, Bond, or fluid-trapping numbers. This model has been used, with experimental values of viscosities[9] and interfacial tensions,[10] to study the high-pressure injection of carbon dioxide into brine-saturated porous media. Results are presented for a variety of capillary numbers, showing trends in the applied pressures, fluid-front geometries, and residual saturations.

DESCRIPTION OF THE MODEL

This pore-level model of injection of carbon dioxide into a water-wet porous medium incorporates, as realistically as possible, both the capillary pressure blocking the invasion of narrow throats and the viscous pressure drop in a flowing fluid. The two-dimensional model consists of a square lattice of pore bodies with unit volume at the lattice sites and connecting throats, which are of unit length and have randomly chosen cross-sectional areas between 0 and 1. We choose to inject the carbon

dioxide along a diagonal; if we had chosen to inject along one side of the square lattice, we would have the artificial situation of one-half of the throats perpendicular to the average pressure gradient, making them more susceptible to capillary blocking because of a reduced pressure drop. This model is similar in spirit to other recent modeling efforts; but our model has some features which should make it more physical than other models: e.g. pore throats with real volumes, pore bodies with finite volume, constant velocity (giving a meaningful capillary number), and multiple checks on whether pores are blocked or unblocked.[11],[12],[13]

When the interface is in one of the pore throats, the radius of curvature, R , of the meniscus is fixed by contact angle, θ , and the radius of the pore throat, r ;

$$R = r / \cos\theta. \quad (1)$$

Therefore, the pressure drop across the meniscus is fixed at the capillary pressure

$$P_{\text{cap}}(R) = \frac{2 \sigma \cos\theta}{r}, \quad (2)$$

where σ is the surface tension. Thus the flow velocity is given by the throat conductance times the total pressure drop across the throat, see Fig. (1a).

$$q = g_{\text{throat}} (P_{\text{nw}} - P_w - P_{\text{cap}}). \quad (3a)$$

Here, pressure P_{nw} is the pressure in the non-wetting, CO_2 -filled pore body, and P_w is the pressure in the wetting water-filled pore body. The transmissibility (conductance) of the throat is given by Poiseuille's law [14]

$$g_{\text{throat}} = \frac{1}{8\pi\mu_w} \frac{A_{\text{throat}}^2}{(x + (1-x)/M)} \quad (3b)$$

where μ_w is the viscosity of water, A_{throat} is the cross-sectional area of the throat, (randomly chosen from a uniform distribution between 0 and 1), x is the fraction of the throat of length 1 which is water-filled, and M is the ratio of the water viscosity to that of the carbon dioxide. From Eq. (3a), the CO_2 advances if the pressure difference between the CO_2 -filled pore and the water-filled pore exceeds the capillary pressure. Otherwise the CO_2 will retreat.

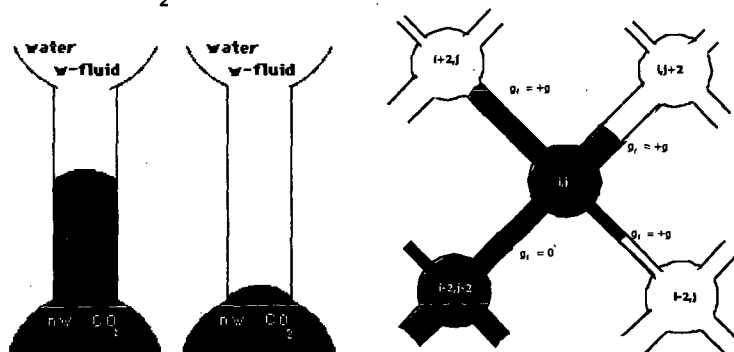


Fig. 1a Meniscus in throat
Fig. 1b Meniscus at inlet
Blocking is possible in 1.b (see Eq. (5))

Fig. 2 Example for determining g_f in Eq. (6).

If the interface is at the entrance to a throat Fig. (1b)), the throat will be blocked if the pressure difference is positive but not large enough to overcome the capillary pressure in Eq. (2). In this case, the positive pressure difference creates a meniscus with a radius of curvature, R , satisfying the equation

$$P_{\text{cap}}(R) = \frac{2 \sigma \cos\theta}{R} = P_{\text{nw}} - P_w, \quad (4)$$

where this radius of curvature is larger than the radius R in Eq. (1) needed to enter the throat. Therefore the throat is blocked ($q = 0$) whenever a positive pressure drop is too small to push the meniscus into the throat, i.e., whenever

$$0 < P_{\text{nw}} - P_w < \frac{2 \sigma \cos\theta}{r}. \quad (5)$$

If the pressure drop in Eq. (5) is negative (q is negative ; $q = g_{throat} (P_{nw} - P_w)$), the water re-invades the pore body ; and if the pressure drop exceeds the capillary pressure, the non-wetting fluid advances; q is positive and given by Eq. 3a.

Volume conservation of the incompressible fluid dictates that the net volume flow, q , out of any pore body must be zero. Using the above rules for the flow velocities, requiring that the net flow out of pore body (i,j) be zero leads to the following equation for $P_{i,j}$:

$$(g_{i-2,j-1} + g_{i,j+1} + g_{i-1,j} + g_{i+1,j})P_{i,j} = \quad (6)$$

$$(g_{i-2,j-1} P_{i-2,j-2} + g_{i,j+1} P_{i+2,j+2} + g_{i-1,j} P_{i-2,j} + g_{i+1,j} P_{i+2,j}) + (gf_{i-2,j-1} P_{cap,i-2,j-1} + gf_{i,j+1} P_{cap,i,j+1} + gf_{i-1,j} P_{cap,i-1,j} + gf_{i+1,j} P_{cap,i+1,j})$$

Here the array gf is zero if there is no meniscus in the throat; for a meniscus in the throat $gf = +g$ or $-g$ depending on the direction of CO_2 advance in the throat (Fig. 2).

To determine the pressure field one iterates (Eq. 6) until stability is achieved (the residual is less than some small value); i.e. until

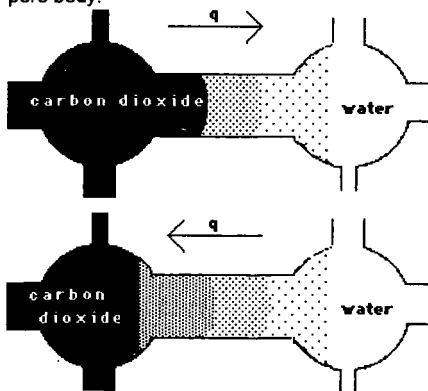
$$R = \sum (P_{new} - P_{old})^2 < \varepsilon, \quad (7)$$

where ε is chosen to be small (e.g. $10^{-6} > \varepsilon > 10^{-8}$). This value of ε was adjusted to minimize run-time without seriously sacrificing mass-conservation.

At a given time step, once the pressure field is determined for the initial choice of conductances, the interface is scanned to determine if there are changes in the throat blockages because of changes in the pressure drops. With these new conductances, the pressure field is redetermined by iterating Eq. (6). With the new pressure field, changes in the blockages are re-determined. This procedure continues until there are no further changes in the blockages, or until the changes occur only in throats that have alternated (blocked to unblocked) three times or more.

Once the pressure field has been determined and there are no more changes in throat blockage (excluding the oscillating blockages discussed above), we know the pressure field that will advance the interface. We choose a time interval that will advance the fluid one-half unit volume through the throat with the largest flow velocity.

Flow can increase the amount of non-wetting fluid (CO_2) within the pore throat, or through the pore throat into the pore body (Fig. 3a). Similarly, backflow can cause the interface to retreat within the pore throat (Fig. 3b) or through the pore throat into the pore body.



Flow Rules: Fig. 3a) Top ; 3b) Bottom
Fig. 3a) flow can advance the interface through the throat into the pore body
Fig. 3b) the interface can retreat from a pore body into the throat and into the next pore body

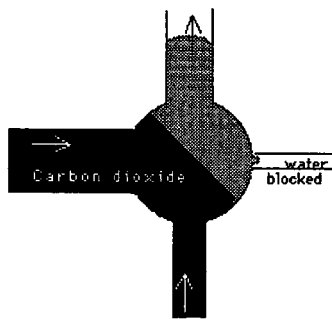


Fig. 4 If the flow over-fills a pore body at a given step, the over-filling is shared by the unblocked throats

If the pore body becomes over-filled by carbon dioxide, the excess fluid is shared proportionally by the outflow throats (Fig. 4). However, if at these pressures the

carbon dioxide is blocked from entering any throats, the last time interval is recalculated so that the fluid will just fill the pore body with an excess of 5% or less. Similarly, if the water backflow fully re-invades a pore body, the excess water is shared by the outflow throats.

If the carbon dioxide occupies two adjacent pores, without fully occupying the throat between them, there is a trapped plug of water in the throat. This plug will remain trapped in the throat unless the pressure drop across the throat is large enough to mobilize the plug of wetting fluid. The pressure drop across the throat must be larger than the capillary pressure to push the water out of the throat. If the pressure drop is large enough, we allow this water to reside in the pore until such a time as that pore is fully re-invaded by water. This assumption that the water remains in the pore is unphysical, because it is more favorable to have the wetting fluid re-invade the narrower throats filled with non-wetting fluid. The fraction of wetting fluid (water) participating in this unphysical process is calculated in the program. On the other hand, if water re-invades two adjacent pore bodies, without re-invading the connecting throat, the non-wetting carbon dioxide is moved to the low-pressure pore body.

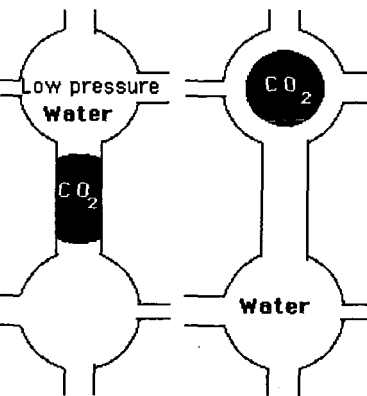


Fig 5a) Trapped CO₂ will be moved to the lower pressure pore body.

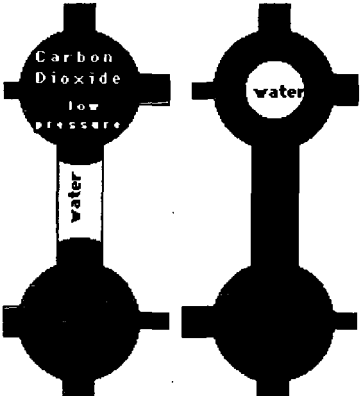


Fig. 5b) Trapped water will be moved to the low pressure pore body for a pressure drop exceeding the capillary pressure

A throat is considered to be on the interface, if the pore body at one end contains some water and if the pore body at the other end is fully invaded by carbon dioxide (or was fully invaded and is not yet fully re-invaded by water due to backflow).

RESULTS

We have chosen parameters appropriate to high-pressure injection of carbon dioxide injection into a typical brine saturated reservoir: an interfacial tension, $\sigma = 21 \frac{\text{dynes}}{\text{cm}}$, a contact angle of $\theta = 0^\circ$, and a viscosity of the high pressure CO₂, $\mu = 0.05 \text{ cp}$. [9,10,15]

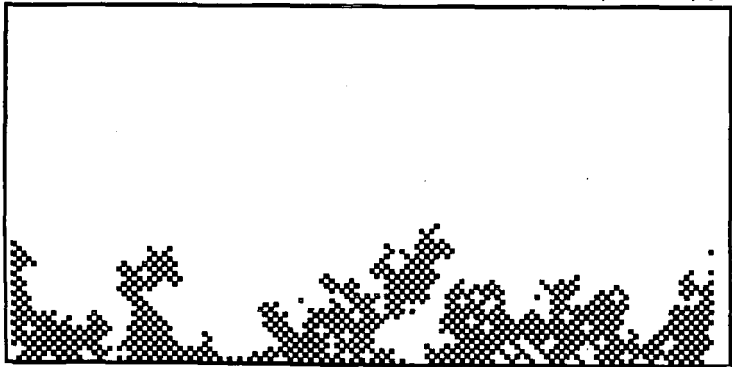


Figure 6) The flow pattern, the black pores are occupied by carbon dioxide.

We chose the scale of the medium (length of a typical throat) to be $\ell = 100 \mu\text{m}$; thus, in our model porous medium, the largest throats will have a radius of $56 \mu\text{m}$, and the smallest capillary pressure (in this largest throat) will be $P_{\text{cap,min}} = 7500 \frac{\text{dyne}}{\text{cm}^2}$. Using these values of the parameters, we have run this program on a 70×70 square lattice array, adjusting the pressure drop, ΔP , to maintain a constant flow velocity $q = \frac{q^* \ell^3}{8\pi \text{ sec}}$ with $q^* = 116.0 \pm 1.4$. For these parameters the capillary number is 3×10^{-5} .

Figure 6 shows the flow pattern after 10,000 time steps. The black areas are invaded by carbon dioxide. At this time the saturation is 24%.

As mentioned, the velocity is approximately constant; small variations are within a standard deviation of less than 2%. To maintain this constant velocity, the pressure drop shows wide variations (see Fig. 7).

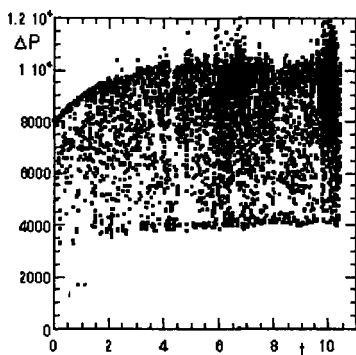


Figure 7) Pressure drop across the porous medium as a function of injection time.

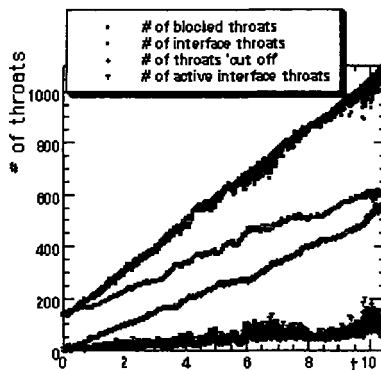


Figure 8) Number of throats of different types as a function of injection time.

Figure 8 shows the dramatic effect of capillary blocking of the throats, near the end of this simulation there are 600 throats on the interface. Of these 600 throats, only 90 are active with the rest being blocked. The total number of blocked throats consists of the 510 interfacial throats that are blocked and the 560 throats that have trapped, immobilized water (as in Fig. 5b, with the pressure drop being too small to mobilize the trapped water).

Additional computer runs will lead to a greater understanding of the role of capillary trapping in CO_2 sequestration and of the effectiveness of different sequestration schemes.

1. U. S. Department of Energy, Office of Fossil Energy. *Carbon Sequestration*, February 1999.
2. U. S. Department of Energy, National Energy Technology Laboratory. *Carbon Sequestration*, June 1999.
3. Hadlow, R. E. In *Proc. 67th Annual Tech. Conf. Soc. Petrol. Engrs.*, Washington, DC, 1992, SPE 24928.
4. Hanisch, C. *Environ. Sci. Tech.* **1998**, 32, 20A-24A.
5. Smith, D. H., ed. *Surfactant-Based Mobility Control: Progress in Miscible-Flood Enhanced Oil Recovery*, American Chemical Society, Washington, DC, 1988.
6. Hendriks, C. *Carbon Dioxide Removal from Coal-Fired Power Plants*, Kluwer Academic Publishers, Dordrecht, 1994.
7. Ferer, M., G. S. Bromhal and D. H. Smith. In *Proc. Pittsburgh Coal Conference*, Pittsburgh, PA, September 11-14, 2000, paper # 53.
8. Ferer, M., J. Gump and D. H. Smith. *Phys. Rev. E* **1996**, 53, 2502-2508.
9. Michels, A., A. Botzen and W. Schurman. *Physica* **1957**, 23, 95-102.
10. Chun, B.-S. and G. T. Wilkinson. *Ind. Eng. Chem. Res.* **1995**, 34, 4371-77.
11. van der Marck, S. C., T. Matsuura & J. Glas. *Phys. Rev. E* **1997**, 56, 5675-5687.
12. Pereira, G. *Phys. Rev. E* **1999**, 59, 4229-4242.
13. Akers, E. A Simulation for Two-Phase Flow in Porous Media, Dissertation, Univ. of Oslo, Oslo, Norway (1996) www.fys.uio.no/~eaker/thesis/thesis.html.
14. Lenormand, R., E. Touboul and C. Zarcone. *J. Fluid Mech.* **1988**, 189, 165-187.
15. Vesovic, V. and W. A. Wakeham. *J. Phys. Chem. Ref. Data* **1990**, 19, 763-808.

IMPROVED GEOLOGIC SEQUESTRATION USING CARBON DIOXIDE THICKENERS

Chunmei Shi, Zhihua Huang, Jianhang Xu, Sevgi Kilic, Eric Beckman and Robert Enick
Chemical and Petroleum Engineering
1249 Benedum Engineering Hall
University of Pittsburgh
Pittsburgh, PA 15261

KEYWORDS: geologic sequestration, carbon dioxide, viscosity

ABSTRACT

The sequestration capacity of deep saline aquifers and abandoned oils reservoirs may be increased if dense carbon dioxide can be thickened. Random copolymers of 71 mol% fluoroacrylate and 29% styrene are the most effective CO₂ thickeners, inducing 2-200 fold increases in viscosity at concentrations of 0.1-5.0 wt%. The fluoroacrylate content of the copolymer assures CO₂ solubility, while the π - π stacking of the phenyl groups induces substantial viscosity increases. Non-fluorous analogs of these thickeners are being developed to dramatically reduce their cost.

INTRODUCTION

The focus of this paper is the sequestration of CO₂ in geologic formations, such as oil reservoirs, gas reservoirs, aqueous formations and deep and unmineable coal formations (DOE 1999). This mode of sequestration has already been initiated Sleipner West off the coast of Norway. At this site, CO₂ is separated from a natural gas off-shore production well, and then re-injected into an aquifer 1000 m under the North Sea. About 1 million tonnes of CO₂ are sequestered each year in this manner. The technologies associated with the injection of CO₂ into subterranean porous media containing water, gas and oil have been studied for decades. Of particular relevance is the use of CO₂ to recover oil from sandstone or limestone formations. This CO₂ EOR technology provides a basis for understanding the phenomena involved in the flow of CO₂ in porous media. The 70 oil fields in the world that use CO₂ to displace oil from the formation sequester large volumes of CO₂ in the reservoir at the end of the project. The bulk of the CO₂ currently used for these EOR projects is derived from natural CO₂ reservoirs, however. It is expected that in the future, CO₂ derived from power plant flue gas may be used for EOR.

Another advantage of geologic sequestration is that a significant capacity for geologic sequestration exists in the US. Although estimates of the capacity for geologic sequestration can vary widely, they indicate a substantial potential for sequestration relative to anthropogenic CO₂ emissions. Worldwide emission has been estimated to be 21.8 Gt CO₂/yr, or 5.9 Gt C/yr (Rubin, et al. 1992). The US generates 4.8 Gt CO₂/yr, or 22% of these emissions. The US CO₂ output from all electric generating plants is 35% of this total, 0.46 GtC/yr, or 1.7 Gt/yr of CO₂, or 30.6 TSCF/yr of CO₂. These sequestration capacity estimates for domestic geologic formations include 1-130 GtC for deep saline aquifers (Bergman and Winter, 1995), 10-25 GyC for natural gas reservoirs, 0.3GtC/yr for active gas fields (Baes, et al. 1980), 0.14 Gt/yr for depleted and abandoned oil reservoirs (DOE, 1993), 3 Gt CO₂ (Winter and Bergman, 1993) -30 Gt CO₂ (Johnson, et al. 1992) for depleted oil and natural gas reservoirs. A worldwide estimate 320 Gt CO₂ has also been made (Koide, et al, 1992).

There is an aspect of CO₂ sequestration into geologic formations that may significantly diminish the capacity of aquifers and oilfields. Although the permeability or porous media to oil, water and CO₂ are of the same order of magnitude, the viscosity of the CO₂ is significantly less than the viscosity of oil or water. At sequestration conditions, the viscosity of CO₂ will be on the order of magnitude of 0.1 cp. Oil viscosity can be 0.2-20 cp, while brine viscosity is on the order of 1 cp. These low ratios (less than unity) of the displacing fluid (CO₂) to the displaced fluid (water or oil) result in poor vertical sweep efficiency as the CO₂ preferentially flows through low permeability layers and poor areal sweep efficiency as viscous fingers of CO₂ bypass oil in each layer. These effects become more pronounced as the viscosity ratio becomes smaller. A substantial reduction in the effective volume for sequestration may occur because of the poor sweep efficiency of CO₂ in an aquifer. For example, a comparison of the sequestration capacity estimates of The Netherlands indicated that a reduction of about an order-of-magnitude reduction of the sequestration capacity of an aquifer may occur if the effects of the low-viscosity of CO₂ on sweep efficiency are accounted for (van Engelenberg and Blok, 1991; van der Meer, 1992, van der Meer, et al. 1992). Therefore, if the viscosity of the CO₂ could be increased to a value

comparable to that of the fluid being displaced (water or oil), a significant increase in the sequestration capacity of aquifers and oilfields could be realized. An inexpensive CO₂-thickener that is capable of elevating the M to a value of unity would enhance the sequestration capacity of aquifers and oilfields. The ideal thickener would be effective in dilute concentrations, easy to dissolve in CO₂, inexpensive, non-volatile, readily available in large quantities, environmentally benign and safe. Carbon dioxide thickeners had not been designed and synthesized until the late 1990's (Enick, 1998).

MATERIAL AND METHODS

Four novel types of CO₂ thickeners, semifluorinated trialkyltin fluorides, telechelic polyfluoro-urethane ionomers, fluorinated small hydrogen bonding compounds (Shi et al. 1999) and fluoroacrylate-styrene copolymers (Huang, et al. 2000) have been recently identified. Only the fluoroacrylate-styrene copolymers have exhibited the ability to induce dramatic increases in viscosity at dilute concentrations, however. The fluoroacrylate-styrene copolymer was composed of two monomers, a fluoroacrylate and styrene. These monomers were bulk-polymerized. The fluoroacrylate portion of the random copolymer imparted significant carbon dioxide solubility to the polymer. The styrene was relatively CO₂-phobic and interacted with the styrene functionalities of neighboring polymers in solution via "π-π stacking". These intermolecular associations lead to the formation of macromolecular structures in solution that can induce tremendous increases in solution viscosity. The optimal composition of the copolymer was 29 mol% styrene-71 mol% fluoroacrylate. Greater concentrations of styrene led to marked decreases in CO₂ solubility and viscosity enhancement. Falling cylinder viscometry results for this copolymer were measured in a high pressure, windowed, variable volume view cell manufactured by D.B. Robinson.

Unfortunately, these types of fluoroacrylate-styrene copolymers suffer an inherent disadvantage. The copolymer is predominantly fluoroacrylate and this fluorinated monomer is currently *very expensive*. Once injected into the aquifer, the thickener cannot be recovered and recycled, therefore all of the thickener will be "lost" to the reservoir. 3M uses fluoroacrylate monomers in their products, and the lowest price of their fluoroacrylate polymers is on the order of \$50-100/lb. Even at \$50/lb, the 0.1wt% (1000 ppm) copolymer would add approximately \$100/ton CO₂ injected in chemical costs alone. At a concentration of 0.01 wt% (100 ppm) the added cost of this chemical would be \$10/ton, and at 0.001 wt% the cost would be \$1/ton CO₂. The economics of sequestration would therefore require this type of thickener to be effective at concentrations as low as 0.001 wt% (1 ppm). Although it is reasonable to expect a significant viscosity increase at 0.1wt%, it is highly unlikely that *any* thickener can be effective at concentrations of 0.01 wt% or less.

Therefore our objective was to identify an environmentally benign, CO₂-thickener that is two orders of magnitudes less expensive than the fluoroacrylate-styrene copolymer. Clearly, the copolymer must contain *no fluorine*, and preferably it should be composed of *only carbon, hydrogen and oxygen*. If this can be achieved, it is quite reasonable to expect that an affordable CO₂-thickener can be identified for geologic sequestration applications. Our strategy for designing an inexpensive CO₂-thickener was (a) to identify a highly CO₂-philic polymer, (b) to maximize its molecular weight, and (c) to modify its structure to incorporate CO₂-phobic functional groups that lead to viscosity-enhancing macromolecular structures in solution. The results of the first step (a) will be presented. An example of a highly CO₂ soluble, non-fluorous copolymer was obtained by copolymerizing CO₂ and a cyclic ether to form an ether-carbonate copolymer (Sarbu, et al. 2000). This was done by copolymerizing either propylene oxide (PO), ethylene oxide (EO), or cyclohexene oxide (CHO) with CO₂ using sterically hindered aluminum catalysts, Figure 1. Note that CO₂ is a raw material for the synthesis of the CO₂-thickening compound. Although this may result in a marginal increase in the amount of CO₂ sequestered in an aquifer, the foremost advantage is that lost cost of CO₂ will lower the price of this copolymer. Polymerizations using these aluminum catalysts give yields in the range of 200 – 1200 g polymer/g catalyst. The polymerizations are typically living in character, with molecular weight distributions less than 1.5 (typically 1.1) and absolute molecular weights governed by the ratio of monomer to initiator. ²⁷Al NMR showed that these catalysts exhibit only one Al species, unlike typical aluminum catalysts used in CO₂/oxirane copolymerizations that exhibit "multi-site" behavior. The extent to which CO₂ is incorporated into the polymer is a function of temperature, pressure, and catalyst type.

Phase results of mixtures of CO₂ and these new CO₂-philic functional groups will be presented. Solubility was determined using standard, non-sampling, visual cloud point determination via isothermal compressions and expansions of a mixture of specified overall composition. The same view cell used for the viscometry was employed for the solubility measurements.

RESULTS

A comprehensive falling cylinder viscometry study was conducted with the 29 mol% styrene-71 mol%fluoroacrylate copolymer. Figure 2 illustrates the effect of shear rate and polymer concentration on relative solution viscosity. The relative solution viscosity is the ratio of solution viscosity to the viscosity of neat CO₂ at the same temperature and pressure. The solution is shear-thinning at all concentrations. At 5 wt% in liquid CO₂, a 250-fold increase was observed at low shear rates. Even at concentrations as low as 0.2 wt%, a significant increase in the viscosity was detected at very high shear rates. The sequestration target area for desired viscosity increase and shear rate in the formation are also illustrated in this figure. It is apparent that this copolymer may be able to induce a 10-fold increase in solution viscosity at the low shear rates associated with CO₂ sequestration.

Copolymers of PO and CO₂ proved to be remarkably CO₂-philic; Figure 3 shows that a 250 repeat unit PO/CO₂ copolymer with 15.4% carbonate units exhibits lower miscibility pressures [8] than a fluoroether (poly(hexafluoropropylene oxide) whose chain length is significantly lower (175 repeats). It should be noted that a PO homopolymer of 250 repeat units would exhibit miscibility pressures beyond the capacity of our instrument. Therefore this copolymer is composed of two readily available monomers, one of the monomers is CO₂, the copolymer exhibits greater CO₂-solubility than PO, and the copolymer is more CO₂-soluble than fluoroether polymers of comparable length.

DISCUSSION

Although fluorinated copolymers are effective carbon dioxide thickening agents, their high cost will prohibit their implementation in large-scale geologic sequestration projects. Non-fluorous copolymers have therefore been proposed as means of reducing the cost of the thickening agent. The first of three steps required for developing an effective thickener, the identification of a highly CO₂ soluble moiety, has been addressed. The PO/CO₂ copolymer is one of several novel polymers that has demonstrated CO₂-philicity greater than one of the previously established CO₂ fluorinated ethers of a comparable number of repeat units. The next steps in the development of a thickening agent, increasing the MW of the copolymer and introducing CO₂-phobic associating functionalities, have not been completed.

CONCLUSIONS

Fluoroacrylate-styrene copolymers remain the most effective carbon dioxide thickening agent yet identified. Extrapolations of high shear rate falling cylinder viscometry results demonstrated that 2-20 increases in CO₂ viscosity may be realized at concentrations of 0.1 wt%. Process economics dictate that the maximum concentration of this fluorinated copolymer be only 0.001 wt%. Despite the effectiveness of this thickening agent, it is not a viable candidate for increasing the capacity of geologic sequestration formations. Non-fluorous copolymers may be viable, however, because of their significantly lower cost. PO/CO₂ copolymers, for example, exhibit solubility comparable to CO₂ fluorinated ethers of comparable repeat units. These non-fluorous copolymers must be modified, however, to make them effective thickeners.

ACKNOWLEDGMENTS

We would like to thank the US DOE National Petroleum Technology Office, the US DOE National Energy Technology Laboratory, Air Products, Cabot Oil and Gas, and Normex International for their financial support of this work.

REFERENCES

- Baes, C., Beall, S. and Lee, D., 1980, "The Collection, Disposal and Storage of Carbon Dioxide," 495-519 in *Interactions of Energy and Climate*, Bach, W., Pankrath, J. and Williams, J., eds., D. Riedel Publishing.
- Bergman, P. and Winter, E., 1995, "Disposal of Carbon Dioxide in Aquifers in the US," *Energy Consers. Mgmt.* 36:523-526.
- DOE, July 1993, "A Research Needs Assessment for The Capture, Utilization and Disposal of Carbon Dioxide from Fossil Fuel-Fired Power Plants," Volume II Topical Reports, DOE/ER-30194.
- DOE, Feb. 1999, "Carbon Sequestration, State of the Science," Office of Science, Office of Fossil Energy, US Department of Energy
- Enick, 1998, A Literature Review of Attempts to Increase the Viscosity of Dense Carbon Dioxide, DOE report DE-AP26-97FT25356
- Z. Huang, C. Shi, S. Kilic, J. Xu, E. Beckman, and R. Enick, "Fluoroacrylate-Styrene Copolymers as Thickening Agents for Liquid Carbon Dioxide" *Macromolecules* (in press)
- Johnson, H., Vejtasa, S., Pelling, J., Biasca, F., Simbeck, D., and Dickensen, R., 1992, "Screening Analysis of CO₂ Utilization and Fixation," US DOE Report DOE/FE/61680-H2, SFA Pacific, Inc., Mountain View, CA.
- Koide, H., Tazaki, Y., Noguchi, S., Nakayama, S., Iijima, M., Ito, K., Shindo, Y., 1992, "Subterranean Containment and Long-Term Storage of Carbon Dioxide in Unused Aquifers and in depleted Natural Gas Reservoirs," *Energy Conversion and Management*.
- Rubin, E., Cooper, R., Frosch, R., Lee, T., Marland, G., Rosenfeld, A., Stine, D., "Realistic Mitigation Options for Global Warming," 1992, *Science* 257, 148.
- Sarbu, T., Styrance, T., Beckman, E., "Non-fluorous Polymers with Very High Solubility in Supercritical CO₂ Down to Low Pressures," *Nature* 405 (2000)165-168.
- Shi, C.; Huang, Z.; Kilic, S.; Xu, J.; Enick, R.; Beckman, E.; Carr, A.; Melendez, R.; Hamilton, A.; "The Gelation of CO₂: A Sustainable Route to the Formation of Microcellular Materials," *Science* 286, 19 Nov. 1999, 1540-1543.
- van der Meer, L., "Investigations Regarding the Storage of Carbon Dioxide in Aquifers in the Netherlands," 1992, *Energy Conversion and Management*.
- van der Meer, L., Griffioen, J., Geel, C., Feb. 1992, "Investigations regarding the Storage of Carbon Dioxide in the Netherlands," IGG-TNO report OS.92-24-A, 1-105.
- van Engelenberg, B. and Blok, K., 1992, "Prospects for the Disposal of Carbon Dioxide in Aquifers," Department of Science, Technology and Society, Univ. of Utrecht, The Netherlands, Report No. G-91006.
- Winter, E. and Bergman, P., "Availability of Depleted Oil and Gas Reservoirs for the Disposal of Carbon Dioxide in the United States," presented at the 29-31 Mar 1993 IEA Carbon Dioxide Disposal Symposium, Oxford, UK.

Figure 1. Copolymer of CO₂ and Propylene Oxide

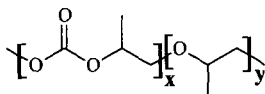


Figure 2. Effect of Shear Rate and Copolymer Concentration on Solution Viscosity of Fluoroacrylate-Styrene Copolymer/CO₂ Mixtures

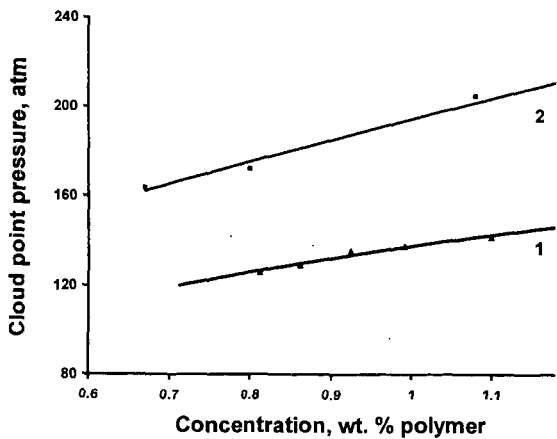
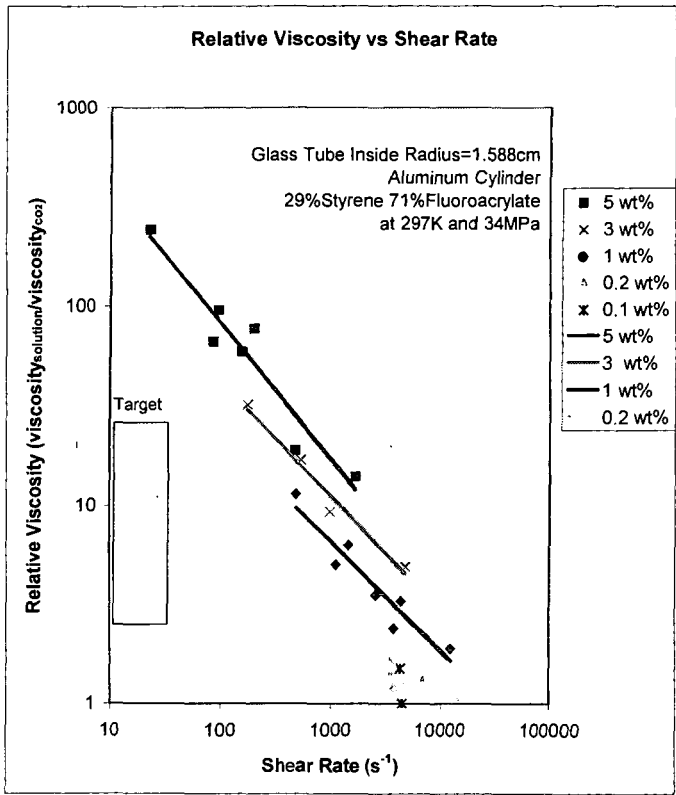


Figure 3. 295K, Cloud point pressure vs concentration in CO₂ for 1. PO/CO₂ copolymer with 250 repeat units and 2. polyperfluoropropyleneoxide polymer with 175 repeat units

INCORPORATING CO₂ SEQUESTRATION AND COALBED METHANE RECOVERY INTO HYDROGEN PRODUCTION FROM COAL - ECONOMICS AND ENVIRONMENTAL ASPECTS

by
Pamela Spath
Wade Amos
National Renewable Energy Laboratory
1617 Cole Blvd.
Golden, CO 80401

KEYWORDS: Hydrogen production, coal gasification, CO₂ sequestration

ABSTRACT

A hydrogen production process using pressure swing adsorption (PSA) for purification results in a concentrated CO₂ gas stream. In a typical natural gas steam reforming process this stream is used to fuel the reformer. However, because coal gasification takes place at high temperatures the synthesis gas contains very little CH₄ and other hydrocarbons, therefore, reforming is not required. An analysis was performed to examine hydrogen production via gasification of low sulfur western coal with CO₂ sequestration of the PSA off gas. This stream is then used to displace methane from unmineable coalbeds and the methane is utilized within the gasification-to-hydrogen system. Several processing schemes were evaluated: a reference case, a CO₂ sequestration only case, a maximum hydrogen production case, and a hydrogen/power coproduction case. The purpose of the analysis was to examine the technoeconomic feasibility, CO₂ emissions, and energy balance of these systems. This paper discusses the cases examined and presents the results of this study.

INTRODUCTION

A collaborative effort to study the feasibility of producing hydrogen from low Btu western coal with an emphasis on CO₂ sequestration and coal bed methane recovery was undertaken by National Renewable Energy Laboratory (NREL) and the Federal Energy Technology Center (FETC). Four cases which are outlined in Table 1 were studied in this analysis.

Table 1: Cases Examined

Case	Title	Description
1	reference case	coal gasification, shift, & H ₂ purification
2	CO ₂ sequestration only	reference case with CO ₂ sequestration only added
3	maximum H ₂ production	H ₂ production via the syngas, CO ₂ sequestration, & additional H ₂ production via steam methane reforming of the coalbed methane
4	H ₂ /power coproduction	H ₂ production via the syngas, CO ₂ sequestration, & power production via the coalbed methane

SYSTEM DESCRIPTION

Because Wyodak coal is inexpensive to produce and is available in an abundant supply, it was selected as a suitable low-rank Western coal for this study. The coal is assumed to be mined from the Wyoming region, gasified to produce hydrogen, then the CO₂-rich off gas is injected into unmineable coal beds. Coal gasification is via the Destec gasifier which is a two-stage entrained, upflow gasifier that operates at an exit temperature of 1,038°C (1,900°F) and a pressure of 2,841 kPa (412 psia). The feed is a coal/water slurry and for hydrogen production, the gasifier is oxygen blown in order to minimize the amount of nitrogen in the syngas.

The synthesis gas leaving the gasifier contains entrained particles of char and ash. Particulate removal is performed through cyclone separators and ceramic candle type hot gas filters. The coal gas is primarily comprised of H₂, CO, CO₂, and H₂O and, since there is less than 0.1 mol% CH₄, reforming of the syngas is not necessary. However, in order to maximize hydrogen production, shift reactors are needed to convert the carbon monoxide to hydrogen. Because the syngas from the gasifier contains approximately 1,400 ppm of H₂S, the majority of the sulfur must be removed prior to shift conversion. Hot gas clean up (HGCU) followed by a ZnO bed is the most economical sulfur removal choice because it avoids cooling and reheating the syngas stream, in addition to avoiding condensing out the majority of the steam that is required for shift conversion. The transport desulfurizer technology from the Piñon Pine Project located near Reno, Nevada was used in the HGCU process step. This technology has an absorber/regenerator system where sulfur compounds

are absorbed on a zinc oxide based sorbent. When the sorbent is regenerated, SO_2 is captured and converted to sulfuric acid. Because the gasifier operates at a high temperature, a steam cycle was incorporated into the process design. Stepwise cooling of the synthesis gas produced steam that was used to generate electricity or to fulfill the plant steam requirements. Finally, hydrogen purification is done using a pressure swing adsorption unit.

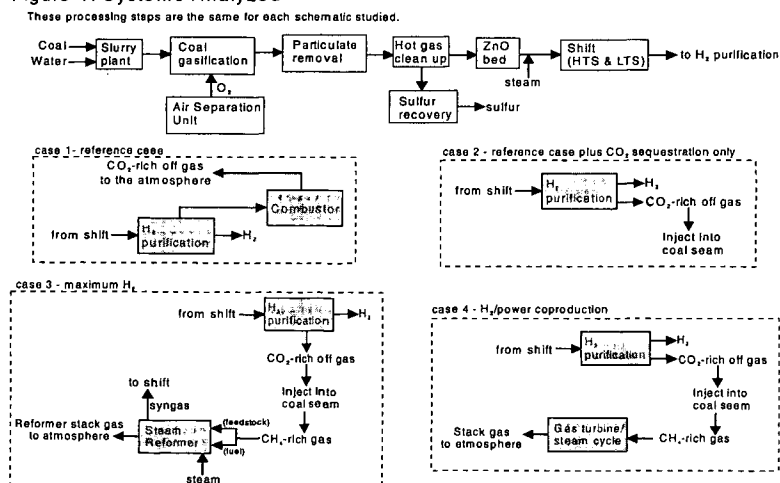
The analysis assumes that two molecules of CO_2 were injected for every one molecule of CH_4 released from the coalbed (Gunter *et al.*, 1996 and Hendriks, 1994). The off gas from the hydrogen purification unit containing primarily CO_2 (68 mol%; 93 wt%) was compressed from 2.6 MPa (372 psi) to a pressure of 8 MPa (1,160 psi). The analysis also assumed that new wells needed to be drilled and that they were connected by a CO_2 distribution system.

SCHEMES EXAMINED

In order to compare the economics as well as the overall CO_2 emissions from each schematic studied in this joint venture, a reference case was analyzed which included only the process steps associated with coal gasification, shift, and hydrogen purification (i.e., none of the steps associated with CO_2 sequestration or coalbed methane recovery were included in the reference case). Three other process schemes were examined in this study and compared to the reference case. Figure 1 depicts the reference case as well as the other three schemes (Note: The overall heat integration for each option is not shown.). The top portion of the figure shows the process steps that are the same for each schematic up to hydrogen purification while the operations inside the dashed boxes represent the steps that differ among the four options.

Scheme one represents the reference case (case 1). The PSA off gas is typically used to fuel the reformer in steam methane reforming plants but, due to the composition of the gasifier syngas, this scenario did not require a reformer. Therefore, the PSA off gas would be combusted, the heat would be used by another source (i.e., in producing steam), and the flue gas emitted to the atmosphere. The second scheme is the reference case with CO_2 sequestration only added to it and thus coalbed methane is not recovered (case 2). Scheme number three is maximum hydrogen production (case 3). The off gas is injected into the coal seam and a portion of the recovered methane is reformed to produce synthesis gas. This gas is then shifted and purified to produce more hydrogen. Part of the recovered coalbed methane is used to fuel the reformer. The fourth scheme is to produce hydrogen from the synthesis gas, to inject the CO_2 -rich off gas into the coalbed, and to produce power from the recovered methane (case 4). For this scenario, power is produced using a natural gas turbine and steam cycle.

Figure 1: Systems Analyzed



RESULTS - MATERIAL & ENERGY BALANCE

The material and energy balance for each case studied is given in Table 2. The coal feed rate is the same for each option and the resulting amount of hydrogen does not change except for the maximum hydrogen production case (case 3). Additionally, all of the cases examined, except maximum hydrogen production (case 3), produce some amount of power.

Table 2: Material & Energy Balances at 100% Capacity

Case	Coal (as received) (kg/hr)	Coalbed CH ₄ (kg/hr)	H ₂ (kg/hr)	Electricity required (MW)	Energy ratio
Reference	113,393	0	8,011	-12	0.83 ¹ 0.58 ²
CO ₂ sequestration only	113,393	0	8,011	-4	0.57
Maximum H ₂	113,393	47,366	18,739	3	0.67
H ₂ /power coproduction	113,393	36,419	8,011	-241	0.50

Energy ratio defined as (energy out of the system/energy into the system):

$$\frac{(H_2)(HHV_{H_2}) + (STM_{st})(\Delta H_{sh}) + e_{exp} + (off)(HHV_{off})}{(Coal_t)(HHV_{coal}) + (CH_4)(HHV_{CH_4}) + e_{imp}}$$

H₂ = hydrogen produced (kg)

HHV_{H₂} = higher heating value of hydrogen (GJ/kg)

STM_{st} = steam produced which is sold (kg)

ΔH_{sh} = enthalpy difference between incoming water and steam produced which is sold (GJ)

e_{exp} = exported electricity (GJ equivalents)

off = off gas produced (kg) - reference case only

HHV_{off} = higher heating value of off gas (GJ/kg) - reference case only

Coal_t = coal feed rate (kg)

HHV_{coal} = higher heating value of the coal (GJ/kg)

CH₄ = methane feed rate (kg)

HHV_{CH₄} = higher heating value of the methane (GJ/kg)

e_{imp} = imported electricity (GJ equivalents)

¹This is the energy ratio with an off gas energy credit.

²This would be the energy ratio if there were no off gas energy credit.

RESULTS - CO₂ BALANCE

To adequately determine the overall effect of CO₂ for each option studied, the CO₂ balance must incorporate CO₂ emissions in addition to those emitted from the process itself. For example, each case produces electricity, except for the maximum hydrogen production case (case 3), and for these cases (cases 1, 2, and 4) a CO₂ emissions credit must be taken for displacing electricity from the grid. Because the maximum hydrogen production case (case 3) requires some grid electricity, the system must be debited (rather than credited) with CO₂ emissions equivalent to the plant's net electricity requirement. Additionally, for the two options that recover coalbed methane (case 3 and 4), each of those systems must be credited with CO₂ emissions that are avoided from natural gas production and distribution via today's normal routes of gas and oil wells. Table 3 summarizes the CO₂ emissions for each of the cases examined.

Table 3: CO₂ Balance at 100% Capacity

Case	Overall CO ₂ to atm (kg/hr)	Avoided electricity CO ₂ (kg/hr)	Avoided natural gas CO ₂ (kg/hr)	Electricity CO ₂ (kg/hr)	Process CO ₂ (kg/hr)
Reference	195,707	-10,037	N/A	N/A	205,744
CO ₂ sequestration only	-3,667	-3,667	N/A	N/A	0
Maximum H ₂	65,985	N/A	-12,694	2,619	43,070
H ₂ /power coproduction	-109,065	-200,575	-9,760	N/A	101,270

Process CO₂ defined as:

Reference = flue gas resulting from combusting CO₂-rich PSA off gas

CO₂ sequestration only = none

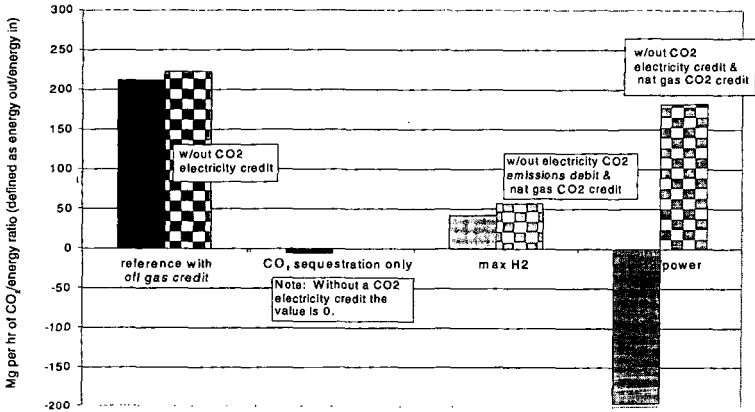
Maximum H₂ = CO₂ in the reformer flue gas

H₂/power coproduction = CO₂ in the natural gas combined cycle stack gas

For the reference case (case 1), the CO₂ emissions are primarily a result of the hydrogen production process. The overall CO₂ emissions for the CO₂ sequestration only case (case 2) are actually slightly negative instead of zero because of the CO₂ credit for the displaced grid electricity. The hydrogen/power coproduction case (case 4) also results in a negative amount of CO₂ emissions. This is due to the large credit in CO₂ emissions from displacing a significant quantity of grid electricity. In this analysis, grid electricity was assumed to be the generation mix of the mid-continental United States, which according to the National Electric Reliability Council, is composed of 64.7% coal and

coal-fired power plants generate large quantities of CO₂. There are still a large amount of process emissions from this system but these are overshadowed by the avoided CO₂ emissions. Even though the maximum hydrogen case (case 3) sequesters CO₂, some CO₂ is generated when the off gas is burned in the reformer. Also, some electricity is required for this case which results in additional CO₂ emissions. However, overall it is not correct to compare the emissions on a per system or a per amount of hydrogen produced basis because many of these cases generate power (refer to Table 2) and all of the cases produced energy in the form of steam. Additionally, for two of the cases (case 3 and 4), the additional hydrogen or power is produced from coalbed methane and the energy content of this feedstock must be taken into consideration. To correctly compare each system, they must be examined on an energy wide basis. If the CO₂ emissions were examined per the amount of hydrogen produced from each system then the results would be misleading. Therefore, the CO₂ emissions were divided by the energy ratio of the system and the results can be seen in Figure 2. For comparison, the CO₂ emissions were also plotted assuming that no CO₂ credits or debits were taken for grid electricity and natural gas production and distribution. It is evident that the only case that is greatly affected by this, and would most definitely be misrepresented, is the hydrogen/power coproduction case (case 4). Hydrogen/power coproduction (case 4) and CO₂ sequestration only (case 2) are the only cases that result in a negative amount of CO₂ emissions. However, the maximum hydrogen production case (case 3) does emit significantly less CO₂ than the reference case (case 1).

Figure 2: CO₂ Emissions per Energy Ratio @ 90% Capacity Factor



RESULTS - COST OF HYDROGEN

The plant gate hydrogen selling price was determined using a cash flow analysis with an after-tax internal rate of return (IRR) of 15%. However, because the hydrogen production plant must be located at the coal mining site in order to sequester CO₂ into unmineable coalbeds, it is not likely that the consumer will be "over the fence". Therefore, the cost to store and transport the hydrogen must be added to the plant gate cost in order to determine the delivered cost of the hydrogen. For this study, because the hydrogen plant is assumed to be sited far from any users, two likely storage and transportation options were examined: (1) bulk delivery for a distance of 1,610 km (one way) and (2) pipeline delivery with 3 km to nearest infrastructure; no storage; an additional 1,610 km pipeline distance for delivery to end user for which the cost is shared by 5 companies. Table 4 gives the plant gate cost as well as the delivered cost for each of the cases examined in this study. The cheapest storage method for the bulk delivery option was determined to be liquid/rail based on previous work at NREL (Amos, 1998). The maximum hydrogen production and hydrogen/power coproduction cases (case 3 and 4) were found to be more economical than the reference case (case 1). Pipeline delivery added \$4.67/GJ to the plant gate cost and bulk delivery added \$8.78/GJ.

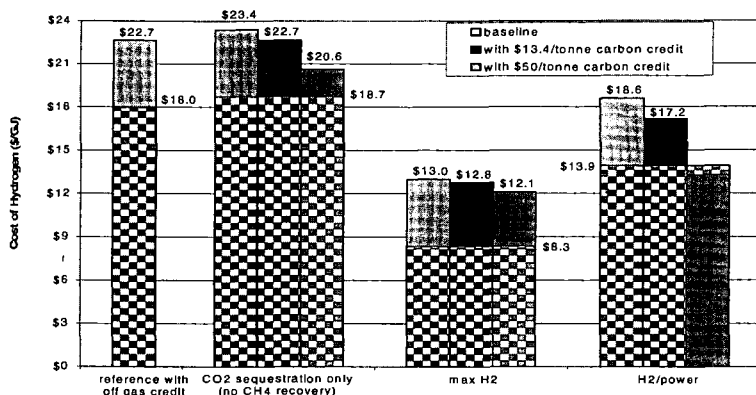
Table 4: Cost of Hydrogen

Case	Plant gate hydrogen selling price (\$/GJ)	Delivered cost of hydrogen (\$/GJ)	
		Bulk delivery (1,610 km - liquid/rail)	Pipeline delivery (1,610 km - shared)
Reference	17.98	26.76	22.65
CO ₂ sequestration only	18.72	27.50	23.39
Maximum hydrogen	8.34	17.12	13.01
H ₂ /power coproduction	13.92	22.70	18.59

RESULTS - CARBON TAX

By comparing the hydrogen selling price of the reference case (case 1) with that of the CO₂ sequestration only case (case 2), a carbon tax that would represent a break-even point was calculated. The hydrogen selling price for the CO₂ sequestration only case (case 2) would be reduced to \$17.98/GJ, the reference (case 1) with off gas credit case cost, if a carbon tax of \$13.4/tonne of carbon was mandated. Additionally, to examine the affect of a higher tax, a carbon tax of \$50/tonne of carbon was applied to the analysis. Figure 3 shows the plant gate selling price (denoted by the checkered sections), the cost of hydrogen for the baseline pipeline delivery option, and how the two carbon tax values affect the delivered cost of hydrogen for each of the four cases examined in this study. A carbon tax has the greatest effect on the hydrogen/power coproduction case (case 4). A \$50/tonne of carbon tax brings the delivered price of hydrogen below the plant gate selling price with the delivered cost being reduced from \$18.6/GJ to \$13.3/GJ. The delivered cost of hydrogen from the CO₂ sequestration only case (case 2) is reduced by \$2.8/GJ while a carbon tax has a small effect of the maximum hydrogen case (case 3) with a reduction of about \$1/GJ.

Figure 3: Delivered Cost of Hydrogen (Pipeline -1,610 km) with a Carbon Tax



CONCLUSIONS

Four process schemes were evaluated in this coal gasification, hydrogen production study. The economics favor sequestering CO₂, recovering coalbed methane, and making hydrogen or power (case 3 and 4). However, due to the CO₂ emissions generated from the steam methane reformer, additional hydrogen production via natural gas is not necessarily the most environmentally friendly option from a CO₂ standpoint (case 3). Coal fired power plants emit large quantities of CO₂, therefore optimizing hydrogen production with electricity generation, as in case 4, is a means of lowering the CO₂ emissions from power generation in the U.S. Because of the high temperatures, coal gasification to hydrogen production does not require a steam methane reforming step, and adding CO₂ sequestration only (case 2), results in almost no CO₂ being emitted to the atmosphere for a minimal cost. Mandating a carbon tax would make sequestering the CO₂ economically viable. However, for all of the cases examined in the analysis it should be noted that there is much debate about the fate of the sequestered CO₂ and its long term environmental effects.

ACKNOWLEDGEMENTS

We would like to acknowledge the Department of Energy's Office of Fossil Energy and Office of Energy Efficiency and Renewable Energy for funding this work. We would also like to recognize Harold Chambers, Diane Revay Madden, and Denny Smith at FETC and Walter Shelton at EG&G Technical Services of West Virginia who provided coal gasification data for this study.

REFERENCES

1. Gunter, W.D.; Gentzis, T.; Rottenfusser, B.A.; Richardson, R.J.H. (September 1996) "Deep Coalbed Methane in Alberta, Canada: A Fuel Resource with the Potential of Zero Greenhouse Gas Emissions." Proceedings of the Third International Conference on Carbon Dioxide Removal. Cambridge, Massachusetts.
2. Hendriks, C. (1994). *Carbon Dioxide Removal from Coal-Fired Power Plants*. Kluwer Academic Publishers. Dordrecht, Netherlands.
3. Amos, W.A. (1998). *Costs of Storing and Transporting Hydrogen*. National Renewable Energy Laboratory, Golden, CO, TP-570-25106.

GEOTHERMAL POWER PRODUCTION UTILIZING SUPERCRITICAL CO₂ COMBINED WITH DEEP EARTH CARBON SEQUESTRATION

Donald W. Brown

Earth and Environmental Sciences Division, MS-D443

Los Alamos National Laboratory

Los Alamos, NM 87545

KEYWORDS: hot-dry-rock (HDR) geothermal energy, heat mining using supercritical carbon dioxide, deep-earth carbon sequestration

ABSTRACT

For equivalent levels of electric power production, a deep man-made geothermal reservoir designed to supply the heat requirements for power generation would sequester, per unit time, about as much CO₂ as that produced by a typical coal-fired power plant. The deep earth carbon sequestration would be accomplished by the gradual diffusion of CO₂ into the unfractured rock mass surrounding the highly pressurized geothermal reservoir.

INTRODUCTION

A new engineered geothermal energy concept using supercritical CO₂ (SCCO₂) to both create the *man-made* geothermal reservoir and for heat transport to the surface is here proposed. This concept builds on the extensive Hot Dry Rock (HDR) research and development effort conducted by Los Alamos National Laboratory (LANL) at Fenton Hill, NM. This previous field testing convincingly demonstrated the viability of the HDR heat-mining concept, based on the results obtained from the production testing of two separate confined reservoirs for almost a year each. However, using SCCO₂ instead of water in a closed-loop HDR system offers three significant advantages over the original Los Alamos concept:

- The very significant wellbore density difference between the cold SCCO₂ in the injection well (about 0.96 g/cc) and the hot SCCO₂ in the production wells (about 0.39 g/cc) would provide a very large buoyant drive (i.e., thermal siphoning), markedly reducing the circulating pumping power requirements over those of a comparable water-based HDR system.
- The inability of SCCO₂ to dissolve and transport mineral species from the geothermal reservoir to the surface would eliminate scaling in the surface piping, heat exchangers, and other surface equipment.
- HDR reservoirs at temperatures in excess of 374°C (the critical temperature for water) could be developed without the problems associated with silica dissolution in water-based systems, potentially providing increased thermodynamic efficiency for the surface power-conversion equipment.

Thermodynamic and systems analyses show that SCCO₂, because of its unique properties, is nearly as good as water when used for heat mining from a confined HDR reservoir (see Brown, 2000). Even though the mass heat capacity of SCCO₂ is only two-fifths that of water, for equivalent reservoir operating conditions, the ratio of fluid density to viscosity (a measure of the reservoir flow potential) is 1.5 times greater for SCCO₂ than for water, primarily due to the viscosity of SCCO₂ which is 40% that of water. Therefore, the rate of geothermal energy production using SCCO₂ would be about 60% that of water. However, on a net power production basis, when pumping power requirements are considered, the power production from an SCCO₂-HDR system would almost equal that of a water-based HDR system.

The commercial development of this new renewable energy concept, given the ubiquitous worldwide distribution of the HDR geothermal resource, could be a significant contributor to providing clean, renewable sources of energy for the 21st century. Further, this new geothermal energy concept would help in mitigating global warming since a supercritical-CO₂-based HDR system would also sequester significant amounts of CO₂ deep in the earth by fluid diffusion into the rock mass surrounding the reservoir. To put this statement in perspective: Such an HDR power plant, based on long-term reservoir pressurization/fluid-loss studies carried out by LANL at Fenton Hill, would have the capability of continuously sequestering, by fluid diffusion into the rock mass surrounding the HDR reservoir, about as much CO₂ as that produced by a typical coal-fired power plant, each on a per MW-electric generation basis [24 tons of CO₂ per day per MW(e)].

THE HOT DRY ROCK CONCEPT AND RESOURCE BASE

HDR geothermal energy, which utilizes the natural heat contained in the earth's crust, can provide a widely available source of nonpolluting energy. The earth's heat represents an almost unlimited source of indigenous energy that could begin to be exploited worldwide within the next decade through the LANL-developed heat-mining concept. The feasibility of this concept has already been demonstrated by LANL through a sequence of field experiments at the Fenton Hill HDR test site extending over more than 20 years.

As depicted in Figure 1, hydraulic fracturing techniques developed by the oil industry would be used to create a very large stimulated volume of hot crystalline rock containing significant artificial permeability. This permeability would be created by pressure dilating the multiply interconnected array of pre-existing -- but hydrothermally resealed -- natural joints and fractures contained in a previously almost completely impermeable rock mass. This hydraulically stimulated region (the HDR reservoir) would then be connected to the surface through a pair of production wells, forming a closed-loop circulating system to transport the geothermal heat to the surface to be used in heating a secondary working fluid in a Rankine power cycle, or alternatively, to be used nearby for direct heating applications. In effect, we would be mining heat in a fashion analogous to the way other earth resources are obtained, but without any attendant pollution since the only thing that would be produced in this closed-loop process would be heat.

Numerous estimates place the accessible HDR resource base somewhere between 10 and 13 million quads in the US, and over 100 million quads worldwide (Tester et al., 1989). Figure 2 provides estimates of the geothermal temperature gradient distribution across the US and clearly shows that the moderate-grade (30° to 45°C/km) HDR resource is well distributed. Kron and Heiken (1980) estimate the high-grade US HDR resource base, with gradients greater than 45°C/km, to be in excess of 650,000 quads. Thus, on almost any basis, the amount of potentially usable thermal energy in the HDR resource is vast -- literally orders of magnitude larger than the sum total of all fossil and fissionable resources (see Figure 3 for a resource comparison on a worldwide basis). Even if only a small fraction of the accessible HDR resource base is ultimately extracted, the impact on the US energy supply could be far-reaching.

PRIOR RESEARCH

During the period from 1974 through 1995, LANL was actively engaged in field-testing and demonstrating the Hot Dry Rock (HDR) geothermal energy concept at their Fenton Hill HDR test site in the Jemez Mountains of north-central New Mexico (Brown, 1995a). This testing ended with the very successful demonstration of sustained energy production from the deeper HDR reservoir during a series of flow tests referred to as the Long-Term Flow Test (LTFT), conducted from April 1992 through July 1995 (Brown, 1994 and 1995b). Although that program has now ended, a vast amount of information was obtained concerning the characteristics and performance of confined HDR reservoirs during this extended period of testing. For instance, a recent report (Brown, 1999) summarizes the data from the LTFT supporting the existence and long-term stability of a highly pressurized region of jointed rock at a depth of 3.6 km, which is quite germane to studying the deep sequestration of carbon dioxide in basement rock associated with an HDR geothermal power-production system.

THE SCCO₂-HDR CONCEPT

In this new concept for engineered geothermal reservoirs, which embodies much of the original HDR concept developed and demonstrated by LANL, SCCO₂ would be used for both the fracturing fluid and the heat transport fluid for deep-earth heat-mining systems. As envisioned, a three-well HDR system -- two production wells and one injection well -- would be employed to best access the fractured reservoir region (Brown and DuTeaux, 1997). As shown schematically in Figure 1, the heat contained in the hot geofluid would be transferred to a secondary working fluid in a high-pressure heat exchanger included as part of the surface power plant.

A major contributing factor to the enhanced performance of an SCCO₂-HDR system is the very significant buoyant drive across the reservoir, arising from the marked density contrast between the hot fluid rising in the production wells and the cold, much more dense fluid in the injection well. For example, for an appropriate set of SCCO₂ surface operating conditions for the HDR reservoir depicted in Figure 1 -- a mean injection pressure of 30 MPa at 40°C and a surface production backpressure of 30 MPa at 250°C, the mean fluid density in the injection wellbore would be 0.96 g/cc and the corresponding mean fluid density in the production wellbores would be 0.39 g/cc, providing a density difference of about 0.57 g/cc. At a reservoir depth of 4 km, this augmented buoyant drive provided by using SCCO₂ instead of water as the geofluid would add an additional 22 MPa (3200 psi) to the pressure differential driving fluid across the reservoir. For the case of laminar flow which is the accepted flow regime in HDR reservoirs, this would more than double the production flow rate compared to a water-based HDR system with the same reservoir flow impedance and injection pressure, potentially providing a thermal power potential exceeding that of an equivalent water-based HDR system.

RESERVOIR CREATION

The engineered HDR reservoir region, probably approaching an ultimate volume of 1/2 cubic kilometer or more, would be created by hydraulically fracturing a deep region of essentially impermeable, hot, crystalline rock using SCCO_2 instead of water as the fracturing fluid. This would be accomplished by pumping SCCO_2 from the surface down a high-pressure tubing string, and injecting this fluid into a packed-off (i.e., pressure-isolated) interval of openhole wellbore for a period of several weeks or more, at a rate in the range of 20 to 40 kg/s.

Initially, as the pressure in the packed-off interval rapidly increases, one or more of the more favorably oriented natural joints intersecting the wellbore would start to open under a combination of tensile (hoop) stresses at the wellbore surface and normal opening stresses from fluid invasion into the somewhat more permeable (than the adjacent rock) hydrothermally sealed natural joints. As pumping continues, these joints would progressively open and interconnect, forming a multiply connected region of pressure-dilated joints in the rock mass surrounding the packed-off wellbore interval, thus creating the fractured HDR reservoir.

Based on over 20 years of reservoir testing at Fenton Hill, NM, this opening of an array of natural joints is in stark contrast with the originally envisioned formation of one or more large, near-vertical, penny-shaped fractures created by hydraulic fracturing (Brown, 1995a). Based on the Laboratory's extensive experience with hydraulic fracturing of deep basement rock using water, there appears to be no limitation to using SCCO_2 for similar operations. It should be noted that hydraulic fracturing of sedimentary formations using SCCO_2 , as reported by Yost et al. (1994), is now routinely done to increase the productivity of petroleum reservoirs where special reservoir conditions warrant this type of stimulation to minimize formation damage from water-based fracturing fluids.

POST-HYDRAULIC-FRACTURING FLUID COMPOSITION IN THE RESERVOIR REGION

From laboratory measurements on core samples of Precambrian crystalline rock obtained from depths between 1.2 and 2.8 km at Fenton Hill, a mean in-situ rock mass porosity of 0.9×10^{-4} has been determined (Simmons and Cooper, 1977). In contrast, following reservoir creation by hydraulic fracturing and the accompanying dilation of the pressure-stimulated array of joints, the mean reservoir porosity was about 1.2×10^{-3} [24,700 m^3 of water injected into a pressure-accessible volume of 20 million m^3 (Brown et al., 1999)]. Therefore, using an analogy to the deeper Fenton Hill HDR reservoir, the fracture volume occupied by the SCCO_2 would be about 13 times greater than the initial microcrack pore volume in the rock mass. For this situation, the SCCO_2 would tend to dissolve almost all of the original pore fluid (essentially a brine), with the mineral constituents previously dissolved in the pore fluid being left behind as mineral precipitates. Figure 4 shows the solubility, at 250°C, of water in SCCO_2 and SCCO_2 in water as a function of pressure. For an HDR reservoir with a rock temperature of 260°C at a depth of 4 km, and with a surface injection pressure of 30 MPa, one would anticipate about a 24 mol% solubility of water in SCCO_2 . This solubility is equivalent to a 10% solubility by weight, which would imply that all the previously existing pore fluid within the microcrack pore structure of the rock would end up being dissolved by the SCCO_2 diffusing into the rock mass.

CO₂ SEQUESTRATION IN THE ROCK MASS SURROUNDING THE HDR RESERVOIR

Again, from experience gained from extensive field testing of the deeper HDR reservoir at Fenton Hill, the fluid loss from a 1/2 cubic kilometer pressure-stimulated reservoir volume, at a mean reservoir injection pressure of 30 MPa (4350 psi) above hydrostatic, is predicted to be about 3 kg/s for a 10-MW(e) power system, which is equivalent to 100,000 tons per year. Although not a very large number in absolute terms, over the predicted 20-year lifetime of a suitably engineered HDR reservoir, this diffusional loss of SCCO_2 into the rock mass immediately adjacent to the HDR reservoir would be very significant -- about 2 million tons of CO_2 sequestered deep in the earth for each 10-MW(e) HDR power plant. This is in addition to the 48,000 ton inventory of SCCO_2 circulating through the reservoir and the surface power plant for such a 10-MW(e) HDR power system.

This leads to an ancillary benefit at the periphery of the HDR fractured region, where the SCCO_2 would be slowly diffusing outward to the far field from the pressurized reservoir. In the surrounding rock mass, the pre-existing water-filled network of interconnected microcracks would be slowly flushed with SCCO_2 , leaving behind mineral precipitates which would tend to slowly plug off the microcrack porosity and seal the reservoir boundaries over time -- which, from the normal point of view, are almost impermeable already (with a permeability in the range of several hundredths of a microdarcy).

SUMMARY AND CONCLUSIONS

In a confined reservoir, which is one of the unique characteristics of a true man-made HDR reservoir, as contrasted with a natural hydrothermal geothermal reservoir, the chemistry and/or

nature of the circulating fluid can be specified by the operator (Brown et al., 1999). For this reason, the choice of SCCO₂ as the working fluid is possible, and alters considerably the potential for designing unique features into such engineered geothermal systems.

As an ancillary benefit from the standpoint of carbon sequestration, the slow diffusional loss of SCCO₂ from the pressurized HDR reservoir region outward into the surrounding unfractured -- and therefore *confining* -- rock would, over the long term, provide a considerable amount of carbon storage within the microcrack volume of this rock mass.

In this preliminary study of the SCCO₂-HDR concept, it was not possible to consider all the ramifications or nuances of using a geofluid other than water as the heat transport fluid in an engineered heat-mining concept. However, the advantages of using SCCO₂ in a power-producing man-made HDR geothermal system appear to be considerable.

REFERENCES

- Brown, D. W. (1994), Summary of Recent Flow Testing of the Fenton Hill HDR Reservoir, Proc., 19th Workshop on Geothermal Reservoir Engineering, Jan. 18-20, 1994, Stanford University, Stanford, CA, SGP-TR-147, pp. 113-116.
- Brown, D. (1995a), The US Hot Dry Rock Program -- 20 Years of Experience in Reservoir Testing, Proc. World Geothermal Congress, 1995, Florence, Italy, v. 4, pp. 2607-2611.
- Brown, D. (1995b), 1995 Verification Flow Testing of the HDR Reservoir at Fenton Hill, New Mexico, Geothermal Resources Council Trans. **19**, 253-256.
- Brown, D. (1999), Evidence for the Existence of a Stable, Highly Fluid-Pressurized Region of Deep, Jointed Crystalline Rock From Fenton Hill Hot Dry Rock Test Data, Proc., 24th Workshop on Geothermal Reservoir Engineering, Jan. 25-27, 1999, Stanford University, Stanford, CA, SGP-TR-162, pp. 352-358.
- Brown, D., (2000), A Hot Dry Rock Geothermal Energy Concept Utilizing Supercritical CO₂ Instead of Water, Proc., 25th Workshop on Geothermal Reservoir Engineering, Jan. 24-26, 2000, Stanford University, Stanford, CA, SGP-TR-165, pp. 233-339.
- Brown, D. and R. DuTeaux, (1997), Three Principal Results From Recent Fenton Hill Flow Testing, Proc., 21st Workshop on Geothermal Reservoir Engineering, Jan. 17-27, 1997, Stanford University, Stanford, CA, SGP-TR-155, pp. 185-190.
- Brown, D., R. DuTeaux, P. Kruger, D. Swenson, and T. Yamaguchi (1999), Fluid Circulation and Heat Extraction from Engineered Geothermal Reservoirs, *Geothermics* **28**, 553-572.
- Kron, A. and G. Heiken (1980), Geothermal Gradient Map of the United States -- Exclusive of Alaska and Hawaii, Los Alamos Scientific Laboratory map LA-8478-MAP.
- Shyu, G., N. Hanif, K. Hall and P. Eubank (1997), Carbon dioxide--water phase equilibria results from the Wong-Sandler combining rules, *Fluid Phase Equilibria* **130**, 73-85.
- Simmons, G. and H. Cooper (1977), "DSA of the Microcracks in More GT-2 Core: Interpretation and Implications," final technical report to the Los Alamos Scientific Laboratory under Subcontract X67-69648-1, unpublished, 34 p.
- Tester, J., D. Brown and R. Potter (1989), Hot Dry Rock Geothermal Energy -- A New Energy Agenda for the 21st Century, Los Alamos National Laboratory report LA-11514-MS, July 1989, 30 p.
- Yost II, A.B., R.L. Mazza, and R.E. Remington II (1994), Analysis of Production Response of CO₂/Sand Fracturing: A Case Study, SPE Paper #29191, 1994 Eastern Regional Conference & Exhibition, Charleston, NC.

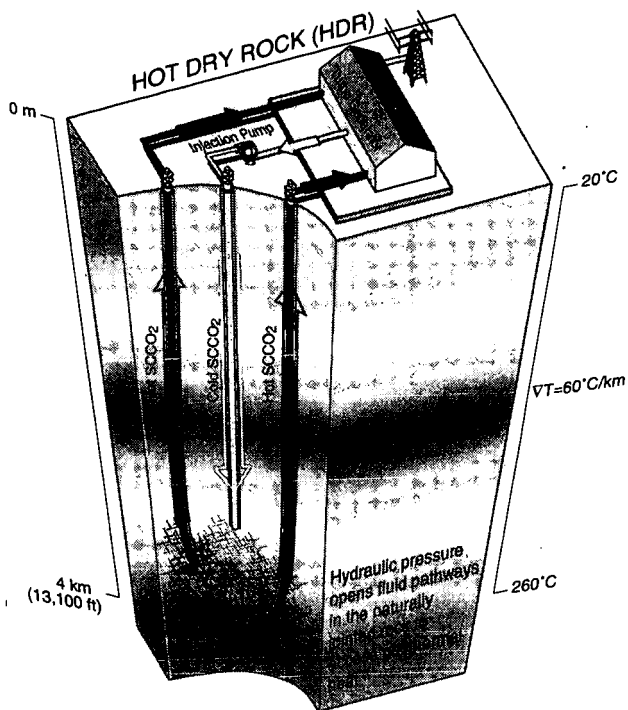


Figure 1: HDR-SCCO₂: A System Engineered for Geothermal Heat Mining Using Supercritical CO₂.

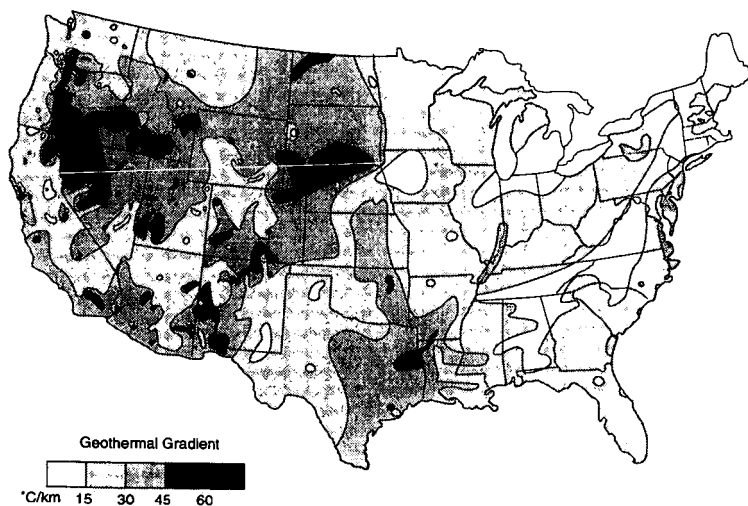


Figure 2: The Distribution of Geothermal Temperature Gradients in the "Lower 48" States.

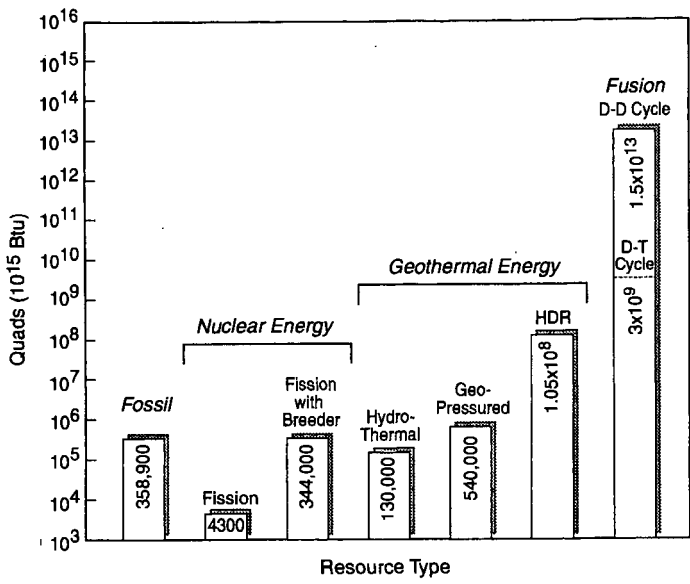


Figure 3: Worldwide nonrenewable resources.

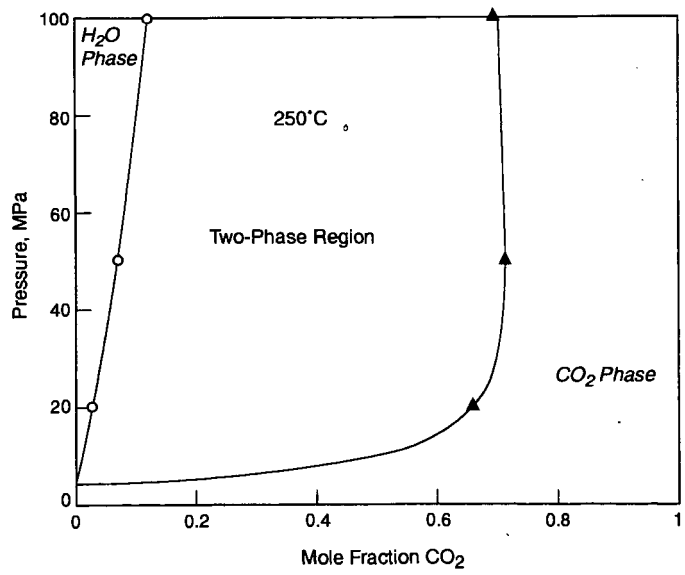


Figure 4: Phase diagram for $\text{CO}_2 + \text{H}_2\text{O}$ at 250°C . Adapted from Shyu et al. (1997).

Tri-reforming: A New Process Concept for Effective Conversion and Utilization of CO₂ in Flue Gas from Electric Power Plants

Chunshan Song*

Applied Catalysis in Energy Laboratory, The Energy Institute and
Department of Energy & Geo-Environmental Engineering, Pennsylvania State University
209 Academic Projects Building, University Park, PA 16802

KEYWORDS: Tri-reforming, CO₂ Conversion, Flue Gas, Power Plants

INTRODUCTION

CO₂ conversion and utilization are a critically important element in chemical research on sustainable development. The prevailing thinking for CO₂ conversion and utilization begins with the use of pure CO₂, which can be obtained by separation. In general, CO₂ can be separated, recovered and purified from concentrated CO₂ sources by two or more steps based on either absorption or adsorption or membrane separation. These separation and purification steps can produce pure CO₂ from flue gases of power plants but add considerable cost to the CO₂ conversion or sequestration system [DOE/OS-FE, 1999]. Even the recovery of CO₂ from concentrated sources requires substantial energy input [Weimer et al., 1996]. According to US DOE, current CO₂ separation processes alone require significant amount of energy which reduces a power plant's net electricity output by as much as 20% [DOE/FE, 1999a]. While new technology developments could make this recovery easier to handle and more economical to operate in power plants, it is highly desirable to develop novel ways to use CO₂ in flue gases without separation.

SOURCES OF CO₂ EMISSIONS

A recent paper showed the data on CO₂ emissions from the consumption of fossil fuels during 1980-1997 in the world based on government reports on statistics [EIA/IEO, 1998, 1999]. The three major fossil fuels used worldwide are coal, petroleum, and natural gas. A very large amount of CO₂ is emitted every year, and the total amount of annual emissions is also increasing rapidly. The current top 10 major producers of CO₂ in terms of total annual emission include US, China, Russia, Japan, India, Germany, UK, Canada, South Korea, and Italy. CO₂ emissions from many other countries, particularly developing countries, are increasing rapidly.

Table 1 CO₂ Emissions from Different Sectors in the U.S. (in Million Metric Tons of Carbon)

CO ₂ Emissions Sources	1980	1985	1990	1995	1997
CO ₂ from Residential Sector	248.4	245.8	253.1	270.3	286.5
CO ₂ from Commercial Sector	178.3	189.7	206.8	217.9	237.2
CO ₂ from Industrial Sector	484.6	424.7	454.1	465	482.9
CO ₂ from Transportation Sector	378.1	384.4	432.1	458.5	473.1
CO ₂ from End-Use Total	1289.4	1244.6	1346.1	1411.7	1479.6
CO ₂ from Electric Utilities*	418.4	439	476.9	495.3	523.4

*Electric Utility emissions are distributed across end-use sectors.

Sources: DOE, EIA, 1998, 1999

Table 1 summarizes the CO₂ emissions from different sectors in the U.S. [EIA/AER, 1998, 1999]. A clear trend is that all the end-use sectors of energy are major contributors of CO₂, and electric power industry is no longer the only major CO₂ emitter. In other words, everyone in the society is responsible for the increased CO₂ production, either by using electricity in various places and by consuming fuels for transportation and for other purposes. Table 2 specifically indicates the CO₂ emissions from the U.S. electricity-generating units in electric utilities and non-utilities based on coal, natural gas and petroleum [EIA/AER, 1998, 1999]. Coal is the dominant fossil fuel for the electricity-generating units. On the other hand, it is projected that the share of natural gas-fired units will increase significantly in the near future, due to the heightened concerns for environmental issues and the fact that natural gas is viewed as a premium fuel and is environmentally cleaner than either coal or petroleum.

* Contact: E-mail: csong@psu.edu; Fax: 814-865-3248

Table 2. CO₂ Emission from Electricity-Generating Units in the U.S. (in Million Metric Tons of Carbon)

CO ₂ Emissions Sources	1990	1995	1997
Coal-Fired Units at Electric Utilities	409.9	434.3	471.3
Petroleum-Fired Units at Electric Utilities	25.3	13.0	15.0
Gas-Fired Units at Electric Utilities	39.2	44.5	36.0
Other Units at Electric Utilities	1.2	0.8	1.0
Emissions at Electric Utilities, Total	475.5	492.7	523.4
Coal-Fired Units at Nonutilities	17.8	24.6	25.3
Petroleum-Fired Units at Nonutilities	4.3	7.3	7.4
Gas-Fired Units at Nonutilities	39.2	57.6	53.2
Other Units at Nonutilities	37.4	45.9	48.4
Emissions at Nonutilities, Total	98.7	135.5	134.4
CO ₂ from Coal-Fired Units, Total	427.7	458.9	496.6
CO ₂ from Petroleum-Fired Units, Total	29.6	20.3	22.4
CO ₂ from Gas-Fired Units, Total	78.4	102.1	89.3
CO ₂ from Other Units, Total	38.5	46.8	49.4
Total CO₂ Emissions from Generators	574.2	628.1	657.7

Sources: DOE, EIA, 1998, 1999

ADVANTAGES OF USING FLUE GAS FOR CO₂ CONVERSION

As can be seen from Table 2, flue gases from fossil fuel-based electricity-generating units represent the major concentrated CO₂ sources in the US. If CO₂ is to be separated, as much as 100 megawatts of a typical 500-megawatt coal-fired power plant would be necessary for today's CO₂ capture processes based on the alkanolamines [DOE/FE, 1999a]. Therefore, it would be highly desirable if the flue gas mixtures can be used for CO₂ conversion but without pre-separation of CO₂. Based on our research, there appears to be a unique advantage of directly using flue gases, rather than pre-separated and purified CO₂ from flue gases, for the proposed tri-reforming process.

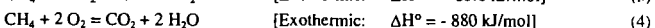
Typical flue gases from natural gas-fired power plants may contain 8-10% CO₂, 18-20% H₂O, 2-3% O₂, and 67-72% N₂; typical flue gases from coal-fired boilers may contain 12-14 vol% CO₂, 8-10 vol% H₂O, 3-5 vol % O₂ and 72-77% N₂ [Miller and Pisupati, 1999]. The typical furnace outlet temperature of flue gases is usually around 1200°C which will decrease gradually along the pathway of heat transfer, while the temperature of the flue gases going to stack is around 150°C [Miller and Pisupati, 1999]. Current toxic emission control technologies can remove the SO_x, NO_x and particulate matter effectively, but CO₂ and H₂O as well as O₂ remain largely unchanged.

In the proposed tri-reforming process, CO₂ in the flue gas does not need to be separated. In fact, H₂O and O₂ along with CO₂ in the waste flue gas from fossil-fuel-based power plants will be utilized for tri-reforming of natural gas for the production of synthesis gas.

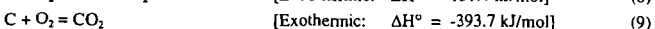
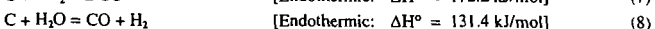
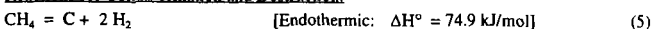
PROPOSED TRI-REFORMING PROCESS

The tri-reforming refers to simultaneous oxy-CO₂-steam reforming of natural gas (eqs. 1-4). It is a synergetic combination of endothermic CO₂ reforming (eq. 1) and steam reforming (eq. 2) and exothermic partial oxidation of methane (eqs. 3 and 4).

Tri-reforming of Natural Gas:



Reactions for Coke Formation and Destruction:



The tri-reforming (Figure 1) is an innovative approach to CO₂ conversion using flue gases for syngas production. Coupling CO₂ reforming and steam reforming can give syngas with desired H₂/CO ratios for methanol (MeOH) and Fischer-Tropsch (F-T) synthesis. Steam reforming is widely used in industry for making H₂ and syngas [Rostrup-Nielsen, 1993; Armor, 1999; Gunardson and Abrardo, 1999]. When CO-rich syngas for oxo synthesis and syngas with H₂/CO ratio of 2 are needed for F-T synthesis and methanol synthesis, steam reforming alone can not give the desired H₂/CO ratio [Gunardson, 1998]. Steam reforming gives too high a H₂/CO ratio (≥ 3) and thus need to import CO₂ for making syngas with H₂/CO ratios of 2 or lower.

CO₂ reforming (dry reforming) of CH₄ has attracted considerable attention worldwide [Ashcroft et al., 1991; Rostrup-Nielsen et al., 1993], and the research up to 1998 has been reviewed [Bradford and Vannice, 1998]. A simple estimate of energetics indicates that CO₂ reforming is 20% more endothermic than steam reforming (eq. 2 vs eq. 1), and so it does cost more energy. However, it can be done and is indeed necessary for adjusting H₂/CO ratio for making MeOH or F-T synthesis gas. There are two industrial processes that utilizes this reaction, including SPARG [O'Connor and Ross, 1998; Gunardson, 1998] and Calcor [Teuner, 1987; Kurz and Teuner, 1990]. CO₂ reforming of methane suffers from a major problem of carbon formation (eqs. 5 and 6), particularly at elevated pressures [Song et al., 2000; Sinivasa et al., 2000]. When CO₂ reforming is coupled to steam reforming, this problem can be effectively mitigated. This carbon formation in CO₂ reforming can be reduced by the addition of oxygen.

Direct partial oxidation of CH₄ to produce syngas [Dissanayake et al., 1991; Hickman et al., 1993] and partial combustion of CH₄ for energy-efficient autothermal syngas production [Pena et al., 1996] are being explored. These reactions are important but the catalytic partial oxidation is more difficult to control. The major operating problems in catalytic partial oxidation are the over-heating or hot spot due to exothermic nature of the oxidation reactions, and consequently coupling the exothermic reaction with an endothermic reaction could solve this problem [Ruckenstein and Hu, 1998].

The combination of dry reforming with steam reforming can accomplish two important missions: to produce syngas with desired H₂/CO ratios and to mitigate the carbon formation problem that is significant for dry reforming. Integrating steam reforming and partial oxidation with CO₂ reforming could dramatically minimize or eliminate carbon formation on reforming catalyst thus increase catalyst life and process efficiency. Therefore, the proposed tri-reforming can solve two important problems that are encountered in individual processing. The incorporation of O₂ in the reaction generates heat in situ that can be used to increase energy efficiency and O₂ also reduces or eliminates the carbon formation on the reforming catalyst. The tri-reforming can thus be achieved with natural gas and flue gases using the 'waste heat' in the power plant and the heat generated in situ from oxidation with the O₂ that is already present in flue gas.

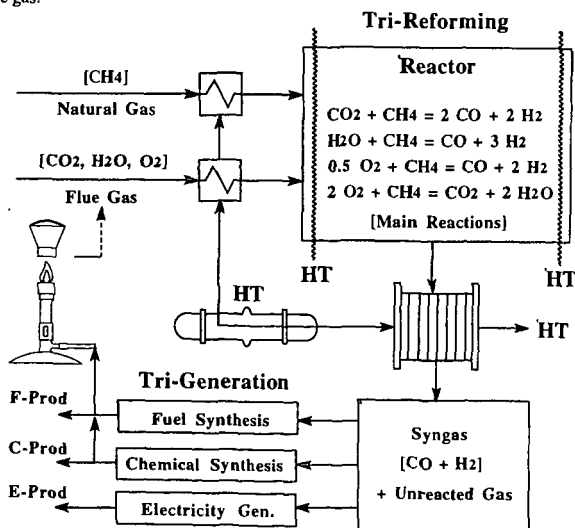


Figure 1. Conceptual design of proposed tri-reforming process in the recently proposed CO₂-based tri-generation system (Version 2 in May 2000).

As illustrated in Figure 1, the tri-reforming is the key step in the recently proposed CO₂-based tri-generation of fuels, chemicals, and electricity [Song, 1999, 2000]. In principle, once the syngas with desired H₂/CO ratio is produced from tri-reforming, the syngas can be used to produce liquid fuels by established routes such as Fischer-Tropsch synthesis, and to manufacture industrial chemicals by methanol and oxo synthesis. Syngas can also be used for generating electricity either by IGCC type generators or by using fuel cells.

The proposed tri-reforming concept is consistent, in general, with the goals of Vision 21 EnergyPlex concept [DOE/FETC, 1999b, 1999c] being developed by the U.S. DOE. The goals of Vision 21 EnergyPlex (plants) include greater efficiency of power generation (>60% with coal, >75% with natural gas), greater overall thermal efficiency (85-90%), near zero-emissions of traditional pollutants, reduction of greenhouse gas (40-50% reduction in CO₂ emission), and coproduction of fuels [DOE/FE, 1999b].

The challenges and feasibility issues and related literature information have been discussed recently [Song, 1999, 2000]. Current flue gases contain inert N₂ gas in high concentrations, and thus the conversion process design requires the considerations on how to dispose inert gas. It is possible that oxygen-enriched air or oxygen will be used in power plants in the future. If that becomes a reality, then the proposed tri-reforming process will be even more attractive because of much lower inert gas concentration and thus higher system efficiency. Another challenge is how to deal with the small amounts of NO_x, SO_x and other toxic substances that are present in most flue gases.

IS TRI-REFORMING FEASIBLE?

We have not found any previous publications or reports on reforming using flue gases or CO₂ conversion using flue gases related to the proposed concept [Song, 1999, 2000]. Our computational thermodynamic analysis shows there are benefits of incorporating steam (H₂O) and oxygen (O₂) simultaneous in CO₂ reforming of natural gas or CH₄ [Pan et al., 1999; Pan and Song, 2000]. On the other hand, some recent laboratory studies with pure gases have shown that the addition of oxygen to CO₂ reforming [Vernon et al., 1992; Choudhary et al., 1995; O'Connor and Ross, 1998; Ruckenstein and Hu, 1998] or the addition of oxygen to steam reforming of CH₄ [Choudhary et al., 1998] can have some beneficial effects in terms of improved energy efficiency or synergetic effects in processing and in mitigation of coking. A feasibility analysis by calculation showed that utilizing CO₂/H₂O/O₂/CH₄ for making synthesis gas is feasible [Tjajopoulos and Vasalos, 1998]. Inui and coworkers have studied energy-efficient H₂ production by using mixture of pure gases including CH₄, CO₂, H₂O and O₂ [Inui et al., 1995]. Choudhary and coworkers have reported on their laboratory experimental study on simultaneous steam and CO₂ reforming of methane over Ni/MgO-SA in the presence of O₂ at atmospheric pressure; they have shown that it is possible to convert methane into syngas with high conversion and high selectivity for both CO and H₂ [Choudhary et al., 1998]. Ross and coworkers have shown that a PtZrO₂ catalyst is active for steam and CO₂ reforming combined with partial oxidation of methane [Hegarty et al., 1998]. Therefore, the proposed tri-reforming of flue gas from power plants appears to be feasible and safe, although its demonstration requires detailed experimental studies, computational analysis as well as engineering evaluations.

CONCLUDING REMARKS

A new process concept, tri-reforming, is proposed for effective conversion and utilization of CO₂ in the waste flue gases from fossil fuel-based power plants in the 21st century. The CO₂, H₂O and O₂ in the flue gas need not be pre-separated because they will be used as co-reactants for the tri-reforming of natural gas. In the tri-reforming (simultaneous oxy-CO₂-steam reforming) process, the flue gas and natural gas are used as chemical feedstock for production of synthesis gas (CO+H₂) with desired H₂/CO ratios.

The proposed tri-reforming is a synergetic combination of CO₂ reforming, steam reforming, and partial oxidation of natural gas. The tri-reforming process solves some of the major problems in CO₂ reforming, in steam reforming, and in partial oxidation. It also makes use of the 'waste heat' in the power plant and heat generated in situ from oxidation with the O₂ that is already present in flue gas. This tri-reforming process could be applied, in principle, for natural gas-based or coal-based power plants and IGCC power plants.

Another important feature of the proposed tri-reforming is that this is the first innovative approach to conversion and utilization of CO₂ in flue gases from power plants without CO₂ separation. Many

questions remain to be answered, and further research is needed in order to establish and demonstrate this new process concept.

Acknowledgments

The author wishes to thank his coworkers (Mr. W. Pan and Dr. S. T. Srinivas) at PSU and Dr. John Armor of Air Products and Chemicals Inc. for helpful discussions on reforming. The author is also grateful to his colleagues (B. Miller and S. Pisupati) for helpful discussions on power plant flue gas.

References

- Armor J.N. Appl. Catal. A: General, 1999, 176, 159-176.
- Ashcroft A. T., Cheetham A. K., Green M. L.H., Vernon P.D.F. Nature, 1991, 352 (6332), 225-226.
- Bradford M.C.J. and Vannice M.A. Catal. Rev., 1999, 41 (1), 1-42
- Choudhary V.R., Rajput A.M., and Prabhakar B. Angew. Chem. Int. Ed. Engl., 1994, 33 (20), 2104-2106.
- Choudhary V.R., Rajput A.M., and Prabhakar B. Catal. Lett., 1995, 32 (3-4), 391-396.
- Choudhary, V.R. and Mamman, A. S. J. Chem. Technol. Biotechnol., 1998, 73 (4), 345-350.
- Dissanayake D., Rosynek M.P., Kharas K.C.C. and Lunsford J.H. J Catal., 1991, 132 (1), 117-127.
- DOE/FE. Capturing Carbon Dioxide. Office of Fossil Energy, U.S. DOE, 1999a.
- DOE/FE. Project Facts-Advanced Power and Fuel Technologies. The Vision 21 EnergyPlex Concept. DOE/FE-0364, Office of Fossil Energy, U.S. DOE, 1999b.
- DOE/FETC. Vision 21 Program Plan-Clean Energy Plants for the 21st Century. Federal Energy Technology Center, Office of Fossil Energy, U.S. DOE, 1999c.
- DOE/OS-FE. Carbon Sequestration. State of the Science. Office of Science and Office of Fossil Energy, U.S. DOE, February 1999.
- EIA/AER, Annual Energy Review (AER) 1997, Energy Information Administration, U.S. DOE. Report No. DOE/EIA-0384(97), July 1998.
- EIA/AER. Annual Energy Review (AER) 1998, Energy Information Administration, U.S. DOE, 1999.
- EIA/IEO. International Energy Outlook (IEO), Energy Information Administration, U.S. DOE. DOE/EIA-0484(97), July 1998.
- EIA/IEO. International Energy Outlook (IEO), Energy Information Administration, U.S. DOE, 1999.
- Gunardson, H. Industrial Gases in Petrochemical Processing. Marcel Dekker, New York, 1998. 283 pp.
- Gunardson, H.H. and Abrardo, J.M., Hydrocarbon Processing, 1999, 87 (April issue).
- Hegarty M.E.S., O'Connor A.M. and Ross J.R.H. Catal. Today, 1998, 42 (3), 225-232.
- Hickman D.A., Hauptfear E.A., and Schmidt L.D. Catal. Lett., 1993, 17 (3-4), 223-237.
- Inui T., Saigo K., Fujii Y., and Fujioka K. Catal. Today, 1995, 26 (3-4), 295-302.
- Kurz G. and Teuner S. ERDOL KOHLE ERDGAS P., 1990, 43 (5), 171-172.
- Miller, B. and Pisupati, S. Personal Communication on Power Plants and Flue Gases. Pennsylvania State University, November 24, 1999.
- O'Connor A.M. and Ross J.R.H. Catal. Today, 1998, 46 (2-3), 203-210.
- Pan, W., Srinivas, T.S. and Song, C. Proc. 16th Annual International Pittsburgh Coal Conference. Pittsburgh, PA, October 11-15, 1999, Paper No. 26-2.
- Pan, W., and Song, C. Am. Chem. Soc. Div. Petrol. Chem. Prepr., 2000, 45 (1), 168-171.
- Pena M.A., Gomez J.P., and Fierro J.L.G. Appl. Catal. A: Gen., 1996, 144 (1-2), 7-57.
- Rostrup-Nielsen JR. Catal. Today, 1993, 18 (4), 305-324.
- Rostrup-Nielsen JR. and Hansen J.H.B. J. Catal., 1993, 144 (1), 38-49.
- Ruckenstein E. and Hu Y. H. Ind. Eng. Chem. Res., 1998, 37 (5), 1744-1747.
- Song, C. Proc. 16th Annual International Pittsburgh Coal Conference, Pittsburgh, PA, October 11-15, 1999, Paper No. 16-5.
- Song, C. Am. Chem. Soc. Div. Petrol. Chem. Prepr., 2000, 45 (1), 159-163.
- Song, C., Srinivas, S.T., Sun, L., and Armor, J.N. Am. Chem. Soc. Div. Petrol. Chem. Prepr., 2000, 45 (1), 143-148.
- Srinivas, S. T., Song, C., Pan, W. and Sun, L. Am. Chem. Soc. Div. Petrol. Chem. Prepr., 2000, 45 (2), 348-351.
- Teuner S. Hydrocarbon Process., 1987, 66 (7), 52-52.
- Tjaitjopoulos, G. J. and Vasalos, I. A. Ind. Eng. Chem. Res., 1998, 37, 1410-1421.
- Weimer, T., Schaber, K., Specht, M. and Bandi, A. Am. Chem. Soc. Div. Fuel Chem. Prepr., 1996, 41 (4), 1337-1340.

THE POTENTIAL ROLE OF GEOLOGIC STORAGE AND CARBON DIOXIDE IN A SUSTAINABLE FOSSIL FUELS FUTURE

David J. Beecy, U.S. Department of Energy

Frank M. Ferrell, U.S. Department of Energy

James K. Carey, Energetics, Incorporated

ABSTRACT

Various geologic settings are beginning to be examined as possible sinks for storage of CO_2 . These include depleting and depleted oil and gas reservoirs, deep unmineable coal seams, and deep saline or brine formations. It is well known that there are many methanogens in nature which convert CO_2 to CH_4 . Some of these are extremeophiles, existing at high temperatures and pressures. At least one has been the subject of genome mapping. It is also known that "directed development" is a methodology that is being utilized to develop "designer microbes" with selected or enhanced traits. The concept described here is that through a coordinated biological, chemical, and geophysical effort, either designer microbes or biomimetic systems can be developed to produce closed-loop fossil fuel systems. In such systems, geologic repositories of CO_2 could be converted to CH_4 , thereby closing the fuel cycle in a sustainable manner.

Keywords: carbon sequestration, global climate change, methanogenesis

INTRODUCTION

This paper is an early output from an ongoing investigation of the state-of-the-art related to the concept of geologic storage of CO_2 with subsequent conversion to methane. In most of the areas reviewed, the research has been performed for reasons other than that which is the focus of this paper—carbon management in response to global climate change. For example, hydrocarbon seeps have been studied to develop better oil exploration techniques, thermal vents have been studied to better understand their environmental impacts, and hydrocarbon emissions from natural sources have been studied for knowledge about global climate change.

We believe that there is a need and opportunity to bring together researchers and knowledge from diverse fields to identify and conduct focused scientific and technologic research to determine the potential of options discussed in this paper along with other novel concepts that may emerge.

Due to growing concern about the effects of increasing carbon dioxide in the atmosphere, the United States and 160 other countries ratified the Rio Mandate, which calls for "... stabilization of greenhouse gas concentrations in the atmosphere at a level that would prevent dangerous anthropogenic interference with the climate system." While the level of greenhouse gases that represents "stabilization" is open to debate, a range of 350-750 parts per million (ppm) is widely discussed. As shown in the various scenarios in Figure 1, all of these scenarios are significantly lower than a "business as usual" scenario (IS92A). When one considers the anticipated growth in the global population and the global economy over the next 50-100 years, even modest stabilization will require enormous amounts of fossil energy with very low greenhouse gas emissions. Many energy producers are now recognizing the major role that carbon sequestration must play if we are to continue to enjoy the economic and energy security benefits which fossil fuels bring to the world's energy mix.

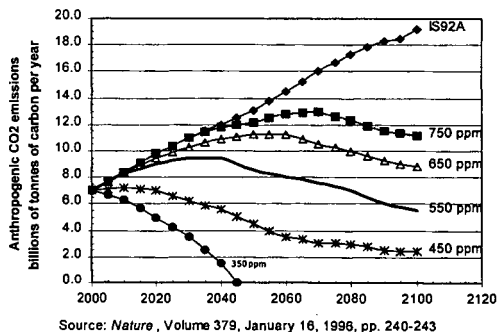


Figure 1. Scenarios for the Stabilization of
Global Carbon

Under virtually any stabilization and market scenario, fossil fuels will remain the mainstay of energy production for the foreseeable future. To achieve any level of atmospheric stabilization that is ultimately deemed acceptable, there are three basic approaches: 1) reduce the carbon content of fuels, 2) improve the efficiency of energy use, and 3) capture and sequester the carbon. The approach of sequestration is comparatively new, and is now discussed as both a technology and policy option to mitigate global climate change (1). In the United States, sequestration has joined the first two approaches within the Department of Energy (DOE) as a valuable option, with funding of sequestration R&D activities (2). A report prepared jointly by the U.S. DOE Office of Science and the DOE Office of Fossil Energy (DOE/FE) identified five pathways to sequestration (3).

- Capture and sequestration
- Sequestration in geologic formations
- Ocean sequestration
- Sequestration in terrestrial ecosystems (soils and vegetation)
- Chemical, biological and other advanced concepts for CO₂ fixation or reuse.

Within the DOE/FE, the Carbon Sequestration Program has further delineated these research pathways and the current R&D activity within the pathways (4). Figure 2 shows the program's research areas. Together they cover the carbon sequestration life cycle of capture, separation, transport, and storage or reuse. A recent report by DOE/FE outlines the national needs, benefits, strategy, plans, and milestones for the program (5). Within this context is an emphasis on enhancing natural CO₂ sequestration processes, including enhancement of storage in various geologic formations, in soils and biomass, and through enhanced mineralization.

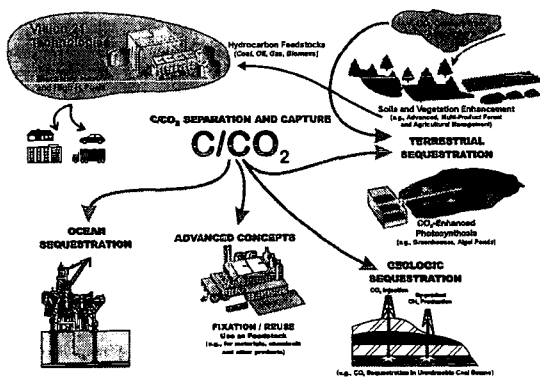


Figure 2. Carbon Sequestration Pathways

DISCUSSION

Natural CO₂ reservoirs are relatively common. They are in fact commercially exploited for CO₂ production for commodity use. In addition to these comparatively pure CO₂ reservoirs, CO₂ is found in many other formations. Reservoirs of various kinds exist throughout the world containing mixtures of CO₂, methane, and various other fluids. Many of these geologic settings are being examined as possible sinks for storage of CO₂. These include depleting and depleted oil and gas reservoirs, deep unmineable coal seams, and deep saline or brine formations. In one current commercial project CO₂ is being sequestered under the North Sea (1). The Norwegian oil company Statoil is recovering CO₂ from natural gas processing, and injecting approximately one million tons per year of CO₂ into a sandstone layer. This is a saline formation under the sea associated with the Sleipner West Heirndel gas reservoir. The amount being sequestered is equivalent to the output of a 250-MW gas-fired power plant.

Methanogenesis is a biological process which is widely found in nature. Methanogenic bacteria generate methane by several pathways, principally the fermentation of acetate and the reduction of CO₂ (6)(7). Generally a consortium, or food chain of microbial organisms, operates together to effect a series of biochemical reactions in the production of methane in energy-yielding cellular processes. Methanogens are anaerobic bacteria of the family Archaea, and are found in such diverse environments as landfills, digestive systems of animals, in deep ocean vents, and in coal seams. Chemosynthetic communities are found in close association with cold hydrocarbon seeps, for example, and demonstrate complex relationships that include the mineralization of CO₂ as well as methanogenesis (8). In one location, sampling of hydrocarbon gases from ocean-floor cold hydrocarbon seeps in Monterey Bay, California suggest that most of the methane produced is microbial in origin (9). In coal seams, methanogens may increase coalbed methane production. Laboratory study of microbially enhanced coalbed methane processes indicate that microbial consortia can increase gas production through conversion of coal and enhancement of formation permeability, leading to the potential for substantially increased methane production (10).

In general, methane in the earth's crust may be formed by both biogenic (that is, the conversion of organic matter) and abiogenic processes. The vast majority appears to be biogenic in origin, and results from a combination of microbial production and thermogenic processes (11). It is believed that 20% of the natural gas in the earth is from methanogens, of which 2/3 is by acetate fermentation and 1/3 by CO_2 reduction (7). While the portion generated by methanogen varies, there is strong evidence that it may be the predominant mechanism in some fields. For example, in the Terang-Sirusan Field in the East Java Sea, methane is generated exclusively by methanogens using the CO_2 -reduction pathway (12). Furthermore, recent study of oil and gas fields in the Gulf of Mexico shed light on the rate of methane evolution. It appears that they may be significant recharge of reservoir methane in a timeframe (decades) that is significant to commercial uses (13).

Developments in genetic decoding, gene sequencing, identification of novel enzymes, and selection of desirable traits have the potential to result in enhanced CO_2 to CH_4 conversion processes. The potential exists for both improved biological processes using engineered biological systems, or processes that mimic biologically-based catalysts and processes (biomimetics). For example, advances in the "directed development" of microorganisms offers the potential for enhancing biochemical processes and pathways of interest for commercial applications (14).

In the area of biological or biomimetic advanced concepts, a number of potential CO_2 sequestration pathways have been discussed, including mineralization of CO_2 to carbonates. One such approach is the enzymatic catalysis of CO_2 to carbonic acid and thence to carbonate materials (15). A second major pathway is methanogenesis. Extremophile organisms have been isolated from deep-sea ocean vents where they live at high temperatures and pressures. One such organism, *Methanococcus jannaschii*, was first isolated at a hydrothermal vent in the Pacific Ocean, and is currently the subject of genome mapping under the U.S. DOE Microbial Genome Mapping Program (16). These extremophile characteristics may be compatible with conditions in oil- and gas-producing formations. Alternatively, compatible characteristics could be obtained through directed development.

The conceptual system proposed here would close the carbon-cycle loop for fossil energy by converting CO_2 produced by power plants into CH_4 for subsequent power production. It would consist of the following.

- The development of an enhanced microbial consortium to produce CH_4 at a commercially-useful rate.
- The use of depleting or depleted oil or gas reservoirs, or saline reservoirs, as storage sites for captured CO_2 . CO_2 has historically been widely used in enhanced oil recovery operations.
- The use of the enhanced microbial consortium in a reservoir to convert the stored CO_2 to CH_4 .
- The reservoir would largely be left alone for a period of 10 years to several decades while the microbial consortium operated, with reservoir monitoring to assess gas composition.
- As CH_4 evolved over time, it would be produced through the existing field well and collection structure.

Figure 3 depicts the general concept and the geologic setting. An alternative approach would be to perform the conversion above-ground in rapid-contact reactors. This would assume a biomimetic pathway with kinetics greatly enhanced over the reservoir approach.

CONCLUSIONS

The attainment of "closed-loop" fossil fuel carbon cycles could provide the energy supply needed for economic security and environmental quality over the next century while renewable energy sources develop. Geologic storage of CO_2 with subsequent biological or biomimetic conversion to CH_4 would provide one such closed cycle. While

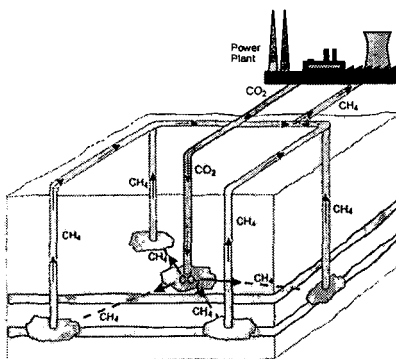


Figure 3. Closed-Loop-Carbon-Cycle Power Production

there appears to be a sound fundamental basis for this and related approaches, several areas of research are indicated.

- A better understanding of emerging sequestration processes in various geological settings is required.
- The kinetics of known microbial conversions appear to be relatively slow; increases of many orders of magnitude will be required for processes of commercial scale.
- Related factors, such as growth cofactors needed to sustain a healthy microbial population, the source of hydrogen for CO₂ conversion, and the mechanisms to remove waste products in a geological setting must be determined.
- While the approach would build on natural geophysical and biochemical processes combined with novel or enhanced enzyme and energy pathways, our present understanding of these processes is fragmented in this context. A systematic assessment of the linkages and relationships of the geologic, chemical, and biological components will be necessary.
- Public acceptance of the process as a safe, benign mechanism for commercial-scale applications must be assured.

If these barriers can be resolved, the concept would provide significant benefits.

- The closed loop process would enable continued use of hydrocarbon fuels without requiring a totally decarbonized fuel product or total conversion of the energy infrastructure to a hydrogen-based economy.
- The approach would expand geologic sequestration options to include essentially unlimited value-added production of a fuel form (beyond what could be achieved through CO₂-enhanced oil recovery or CO₂-enhanced recovery of coal-bed methane, where CO₂ enhances production only of the existing gas- or oil-in-place).
- The process would support sustainable, closed-loop energy production without the large surface-area requirements and impacts of biomass, wind, or photovoltaic systems.
- When combined with other pathways to permanent sequestration (e.g., mineralization), it would provide a more robust basis for a zero-carbon fossil energy infrastructure.

The authors wish to interest researchers from various disciplines in beginning an open and extended dialogue on the potential of novel concepts, such as one discussed here, in developing science and technology options to mitigate global climate change. The role of novel science and technology approaches will be critical to the development of effective mechanisms to stabilize greenhouse gas concentrations.

ACKNOWLEDGMENTS

We are indebted to our associates at the U.S. Department of Energy, with whom we have had discussions and who have provided valuable information on topics related to bacterial genomes and other microbial research: Gregory L. Dilworth, Daniel W. Drell, Anna L. Palmisano, and Nicholas B. Woodward.

We have also received information from numerous researchers outside of the DOE that proved invaluable. We would like to express our appreciation to Dr. Jean K. Whalen, Woods Hole Oceanographic Institute, for information on the topics of marine sediments, marine geomicrobiology and reservoir recharge; to Dr. James G. Ferry of Pennsylvania State University for information on enzyme mechanisms and functional genomics; to Dr. Martin Schoell of Chevron for information on the origins and concentrations of biogenic methane; to Dr. William Gunter of the Alberta Research Council for information on gas generation and characteristics in Canadian formations; to Drs. Keith Kvenvolden and William Dillon of the United States Geological Survey for information on methane occurrence in fluid seeps; to Dr. Roger Sassen of Texas A&M University for information on natural gas hydrates and hydrocarbon seeps in the Gulf of Mexico; to Dr. Gillian M. Bond of New Mexico Tech for information on the catalytic hydration of CO₂ and the formation of carbonates; and to Dr. Frances H. Arnold of the California Institute of Technology for information on protein design and the evolution of new biocatalysts.

REFERENCES

- (1.) H. Herzog, B. Eliasson, O. Kaarstad, "Capturing greenhouse gases," *Scientific American*, pp. 73-79, February 2000.
- (2.) "US warms to carbon sequestration research," *Nature*, volume 401, p. 315, September 23, 1999.
- (3.) *Carbon Sequestration State of the Science*, U.S. Department of Energy, www.fetc.doe.gov/products/gcc, April 1999.
- (4.) *Carbon Sequestration R&D Program Plan: FY 1999-FY 2000*, U.S. Department of Energy, www.fetc.doe.gov/products/gcc, June 1999.
- (5.) *Carbon Sequestration: Overview and Summary of Program Plans* (draft), U.S. Department of Energy, April 2000.
- (6.) J.G. Ferry, "Biochemistry of methanogenesis," *Critical Reviews in Biochemistry and Molecular Biology*, volume 27(6), p. 473-503, 1992.
- (7.) M.J. Whiticar, E. Faber, M. Schoell, "Biogenic methane formation in marine and freshwater environments: CO₂ reduction vs. acetate fermentation - Isotope evidence," *Geochemica et Cosmochemica Acta*, volume 50, p. 693-709, 1986.
- (8.) R. Sassen, H.H. Roberts, P. Aharon, J. Larkin, E.W. Chinn, R. Carney, "Chemosynthetic bacterial mats on cold hydrocarbon seeps, Gulf of Mexico continental slope," *Organic Geochemistry*, volume 20, number 1, p. 77-89, 1993.
- (9.) T.D. Lorenson, K.A. Kvenvolden, F.D. Hostettler, R.J. Rosenbauer, J.B. Martin, D.L. Orange, "Hydrocarbons associated with fluid venting processes in Monterey Bay, California," United States Geological Survey, 2000.
- (10.) A.R. Scott, "Improving coal gas recovery with microbially enhanced coalbed methane." *Coalbed Methane: Scientific, Environmental, and Economic Evaluations*, July 1999, p. 89-111.
- (11.) M. Schoell, "Multiple origins of methane in the earth," *Chemical Geology*, volume 71, p. 1-10, 1988.
- (12.) R.A. Noble, F.N. Henk Jr., "Hydrocarbon charge of a bacterial gas field by prolonged methanogenesis: an example from the East Java Sea, Indonesia," *Organic Geochemistry*, volume 29, p. 301-314, 1998.
- (13.) J.K. Whelen, "Buried treasure, recharging oil and gas reservoirs in the Gulf of Mexico," *Geotimes*, p. 14-18, January 2000.
- (14.) F.H. Arnold, et al., www.che.caltech.edu/faculty/fha, 2000.
- (15.) G.M. Bond, G. Egeland, D.K. Brandvold, M.G. Medina, J. Stringer, "Enzymatic Catalysis and CO₂ Sequestration," *World Resource Review*, volume 11, no. 4, p. 603-619, 1999.
- (16.) *Microbial Genome Program*, U.S. Department of Energy, p. 19, www.ornl.gov/hgmis/publicat/microbial, 2000.

THE SEQUESTRATION OF CARBON DIOXIDE TO THE DEEP OCEAN BY FERTILIZATION

Michael Markels, Jr. and Richard T. Barber

KEYWORDS: CO₂ sequestration/ Ocean fertilization/ Iron fertilization

ABSTRACT

The sequestration of carbon dioxide (CO₂) to the deep ocean by the fertilization of high nutrient, low chlorophyll (HNLC) ocean waters can be an answer to the concerns arising from the increasing CO₂ content of the atmosphere. This approach has the potential to sequester CO₂ for 1000 to 2000 years for a cost of about \$2.00/ton of CO₂. A technology demonstration is planned to fertilize 5,000 square miles of the equatorial Pacific that is expected to sequester between 600,000 and 2,000,000 tons of CO₂ in a period of 20 days. The concept is that fertilization of HNLC waters with chelated iron will cause a bloom of phytoplankton that sink below the thermocline into deep water. Five recent ocean experiments have observed iron stimulation of phytoplankton growth, but the effects were difficult to quantify in these 9 to 28 square-mile experiments because eddy diffusion along the edges of the patch diluted the bloom. This problem will be minimized in the planned technology demonstration because its large area reduces the impact of exchange at the edges.

INTRODUCTION

The CO₂ content of the atmosphere has increased from about 280 ppm to about 365 ppm during the last 60 years¹. During the 1980's the rate of increase of CO₂ in the atmosphere, in terms of carbon metric tons, was about 3.3 gigatons of carbon per year (GtC/yr). Fossil fuel emissions were about 5.5 GtC/yr (20 Gt CO₂/yr*) and terrestrial emissions were about 1.1 GtC/yr during that period, so about 3.3 GtC/yr, 60% of fossil fuel emissions, were sequestered naturally. Of this, about 2.0 GtC/yr was absorbed by the oceans and 1.3 GtC/yr by the land.² The remaining 40%, 2.2 GtC (8.1 GtCO₂/yr, contributed to the increasing atmospheric CO₂ concentration. This increase in the CO₂ content of the atmosphere has led to concerns that this increase will result in global climate change, which, over time, can have adverse effects on weather, sea level and human survival. This concern has led to the 1992 Rio Treaty, the IPCC Working Group³ and the Kyoto Protocol of 1997, which call for a reduction of emissions of 34% by 2050 and a reduction of 70% from the then-expected emissions by 2100⁴. These reductions, if put into effect, would have serious adverse effects on the economy of the United States, causing loss of jobs, decrease in our standard of living and a reduction in the life span of our citizens. These required reductions would not address the concerns that demand an approach to permit the reversal of atmospheric CO₂ increase, should this become necessary.

THE CURRENT APPROACH

The current approach to the problem of atmospheric CO₂ increase is to take specific actions now to reduce the risk of adverse consequences in the future. These actions are to increase the efficiency of energy production and use and to change our standard of living to reduce our dependence on energy in our lives. Energy efficiency can often be increased, but we have been doing this for over 200 years, so there is not a lot of gain remaining before we run into thermodynamic barriers. Even at 100% efficiency we still add CO₂ to the atmosphere, so this can never address peoples' concerns. We can also address the other side of the problem, which is to increase the rate at which CO₂ is removed from the atmosphere. If we could increase this enough we could bring the net increase in CO₂ emissions to zero, providing a solution to the problem of peoples' concerns.

CO₂ is removed from the atmosphere by plants using the Sun's energy to convert it to biomass. This biomass may be used as food by bacteria, fungi and animals that obtain energy by reacting it with oxygen from the air and respiring CO₂ back to the atmosphere. Over time, a portion of the biomass formed has been sequestered in the earth and in the ocean bottom, forming fossil fuels that we burn to obtain energy to support our standard of living. Numerous projects have been undertaken to increase tree growth in the tropics, which reduces the CO₂ content of the atmosphere. These projects suffer from a short lifetime, generally 20 to 50 years, and the difficulty of assuring that forest fires, poaching, etc., will not result in an early recycling of the carbon to the atmosphere. Other CO₂ sequestering technologies have been proposed, including injection of liquid CO₂ into geological formations or into the deep ocean. These suffer from high cost, since the flue gases have to be cooled, separated to make pure CO₂, compressed to a liquid, transported to the site and then injected down a well or into the deep ocean. The projected cost is in the range of \$300 per ton of carbon.

* 1GtC = 3.67 Gt CO₂

OCEAN FERTILIZATION

Another approach is to sequester CO_2 to the deep ocean by causing a bloom of plant life that then sinks to the deep waters where it remains for about 1600 years. This process is possible because large areas of the oceans have excess, unused plant nutrients and much less than expected phytoplankton biomass, the so-called HNLC waters. The difference is that the HNLC waters are deficient in one or more of the micronutrients required for plants to grow. While several essential metals may be involved in the limitation of growth in HNLC areas, iron has been shown to be the major micronutrient. Generally, 100,000 moles of carbon biomass require 16,000 moles of fixed nitrogen, 1,000 moles of soluble phosphorous and one mole of available iron. The main difficulty is the iron. Since surface ocean waters are highly oxygenated, any soluble iron is soon converted to Fe^{+++} and precipitates as $\text{Fe}(\text{OH})_3$. A shovel full of earth is about 5.6% iron on the average. The ocean, on the other hand, has 0.000000001 or less moles per liter of iron. The first problem, then, is how to add iron to the ocean so that it will be available to the phytoplankton (plants). The phytoplankton themselves exude organic chelating compounds into the ocean that protect the iron that is there from precipitation. Adding iron in the form of a chelate so that it does not precipitate but remains available for plant fertilization can mimic this natural process.⁵ An essential element that may be in short supply in nutrient-depleted, tropical ocean waters is phosphorous. Most phosphates are soluble and can be added directly to the ocean. Since the phosphate may attack the iron chelate, it may be necessary to keep the concentrations of both fertilizers low. This can be done by adding them to the ocean separately in the form of small floating pellets that release the fertilizing element slowly over a period of days.⁶ This process has been tested in the Gulf of Mexico with good results. The remaining required essential element is fixed nitrogen. Bluegreen algae or, as they are more properly called, cyanobacteria, have the ability to fix nitrogen, so inducing a bloom of nitrogen fixers might supply this requirement.

When the fertilizer mixed with water is added to the tropical ocean surface it mixes rapidly in the warm waters (the mixed layer) and starts the phytoplankton bloom. The plants, mostly diatoms, multiply rapidly, increasing their numbers by two to three times per day, until they run out of one of the required nutrients. They then cease growing, lose the ability to maintain buoyancy and presumably sink through the thermocline. The sinking biomass is trapped in the cold, dense waters where it is eaten by animal life and bacteria. This slowly converts the biomass back to CO_2 in the deep waters. Where high concentrations of biomass reach the bottom and are covered by mud and debris, anoxic digestion may occur. The methane produced is converted to methane hydrates by the high pressure of the deep ocean. It has been estimated that there is more carbon in the methane hydrates of the deep ocean floor than all the terrestrial fossil fuels combined. It is worth noting that the addition of CO_2 in this low concentration, natural process is not expected to have any adverse environmental impact on the ocean, which now has about 85 times as much dissolved inorganic carbon as the atmosphere.

Since our objective is to sequester CO_2 to the deep ocean it is important that we minimize the proportion of the biomass produced that is processed by animal life and bacteria in the mixing layer above the thermocline. This can be done by fertilizing in pulses, so that the slower-growing animal life cannot multiply effectively before the diatoms have bloomed, died and gone below the thermocline, a period of less than 20 days.⁷ We must also test the waters we intend to fertilize in order to add the correct amount and mix to produce the optimum result. To achieve this we select the waters for fertilization to include a strong, shallow thermocline, tropical sunshine and high nutrient, low chlorophyll (HNLC) conditions. These waters can be found in the tropical Pacific near the equator west of the Galapagos Islands. The cool wind-driven currents go directly to the west before reaching the Line Islands of Polynesia. These HNLC waters can sequester about 0.4 $\text{GtCO}_2/\text{yr.}$, a significant proportion of the 8.1 $\text{GtCO}_2/\text{yr.}$ from fossil fuels that is not sequestered naturally.

TECHNOLOGY EXPERIMENTS TO DATE

The technology of ocean fertilization as a means of CO_2 sequestration is still in its infancy. Accurate estimates of the results of ocean fertilization cannot be obtained from bottle experiments. The iron tends to stick to the walls, increasing the response by as much as 100 times. Therefore, ocean voyages were started in 1993 to determine the response. The first voyage in the equatorial Pacific, IronEx I, spread 880 lbs. of Fe as FeSO_4 on a 25 square mile patch resulting in an increase in phytoplankton, but no measurable decrease in the CO_2 content of the water. This was due to the sinking of the patch under an intrusion of barren warmer water. A second voyage in the same area of the equatorial Pacific, IronEx II, spread 990 lbs. of Fe as FeSO_4 on 28 square miles of the ocean surface.⁸ In order to mitigate the effect of iron precipitation, the iron was added in three infusions, half on day zero, one-fourth on day three and one-fourth on day seven. This resulted in a bloom of diatoms. The chlorophyll increased by a factor of 27 times, while the CO_2 partial pressure was reduced by 90 μatm in the patch.

Ocean Farming, Inc. (OFI) has undertaken two voyages in the nutrient-depleted tropical waters of the Gulf of Mexico. Voyage 1 was carried out in the Gulf of Mexico in early January 1998. Three, 9 square mile, patches were fertilized: one with iron, only; one with iron and 6.35 times the molar ratio of phosphorous to iron; and one with iron and 63.5 times the molar ratio of phosphorous to iron. The iron was in the form of a chelate to protect it from precipitation and the phosphorous was in the form of phosphoric acid. The ocean and weather conditions, including a very deep thermocline and high winds, caused the fertilizer to mix much more rapidly, both vertically and horizontally, than planned. The result was a bloom of large diatoms to 4.3 times their initial concentration in a little over one day. After that, the mixing diluted the signal to about 1.5 times the initial chlorophyll concentration. These results, while giving a positive indication of a large bloom were not definitive and did not provide a verifiable measure of phytoplankton increase over the period of the expected bloom of about two weeks.

Voyage 2 was carried out in the Gulf of Mexico in early May 1998. One 9 square mile patch was fertilized using the enhanced chelated iron-containing pellets. The ocean conditions were much more benign (no one got seasick) and we were able to follow the patch for six days. The pellets acted as expected, discharging the chelated iron over a period of four days. The result was a bloom of large diatoms that averaged five times background and reached seven times background. Further increase in phytoplankton was restricted by the absence of the next required fertilizing element, probably phosphorous, nitrate or both. However, extrapolating over the increased size to the patch gave an estimated 600 tons of diatoms per ton of fertilizer pellets, or 1,800 tons of diatoms per ton of chelated iron added to the waters. Both voyages in the Gulf of Mexico were in low nutrient, low chlorophyll (LNLC) waters, which are not favorable to the production of large blooms.

A fifth voyage, SOIREE, has been conducted in the Southern Ocean south of New Zealand. Full reporting is not yet available, but preliminary data indicate that a successful bloom was achieved in those HNLC waters.

These experiments have added greatly to our knowledge of the biodynamics and chemistry of the ocean. Other recent measurements have further increased our understanding. These have included the tethered buoy systems (TAO buoys) as well as the SeaWiFS satellite, instrumented buoys and drifter systems. These systems have, for the first time, provided continuous measurements of the ocean surface as well as at depth, instead of isolated measurements from intermittent ship cruises. This great increase in data has provided enough understanding that we can now design a technology demonstration aimed at proving the CO₂ sequestration potential of ocean fertilization.

PLANNED TECHNOLOGY DEMONSTRATION

All of these previous experimental voyages, while providing a compelling case for iron fertilization in HNLC waters, did not provide a solid basis for evaluating the potential for carbon sequestration. The fertilized patches were all so small that they were all edge; that is, the diffusion in the ocean surface waters is so great that the result of the fertilization, especially the amount of the biomass that sinks below the thermocline, could not be measured. Therefore, we have designed a technology demonstration using the long-lived chelated iron fertilizer in the HNLC waters of the equatorial Pacific Ocean. The fertilized patch will be 5,000 square miles in area and designed to sequester between 600,000 and 2,000,000 tons of CO₂. The patch will be laid by a chemical tanker that will traverse a spiral path⁹ starting at a floating buoy that is maintained as the center of the pattern at all times. When the 5,000 square mile (80 miles in diameter) patch has been completed, in approximately four to five days, the commercial ship will return to port. It will leave a patch with an iron concentration of 2 to 4 nM Fe in the ocean, an increase of about 20 to 40 times background. Based on patch dissipation rates determined from the IronEx studies in the same general Pacific location, the reduction in concentration from diffusion for the center of the patch is expected to be about 2% during the 20 days of the test. A scientific team on a research vessel using the most advanced technology, including direct measurement of the sinking biomass under the patch will measure the response to the fertilization. The research vessel will continuously transact the patch, taking samples to compare with the background measurements made before the patch is laid and, later, outside of the patch. The academic team will measure all relevant environmental impacts until the impacts vanish, which is expected to take about 20 days. The ocean area of the test site is shown in Figure 1. This area is over 2,000 miles from any reef system and in waters 10,000 to 15,000 feet deep that have high oxygen content. Therefore, anoxia that can occur in shallow waters will not be a problem. Red tide and noxious algae typically occur only in shallow waters so should not be a concern. We will not be adding any new organisms to the ocean, only increasing the numbers of those already there. This controlled experiment will parallel the upwellings that occur off of the coast of Peru in all but the El Niño conditions, so we expect the environmental impacts to be benign.

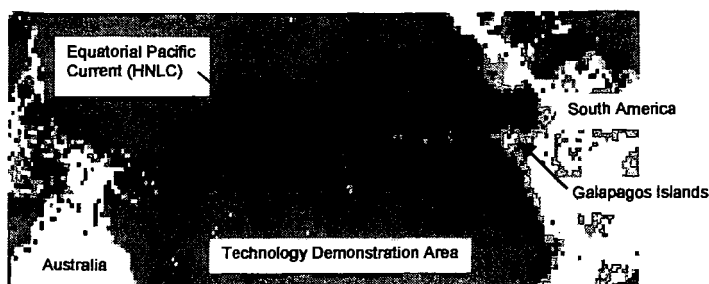


Figure 1. Location of Planned Technology Demonstration

POSSIBLE COMMERCIALIZATION

Should the increasing CO_2 content of the atmosphere be determined to have adverse impacts, the further demonstration of this technology can provide a solution, relieving the concerns regarding the continuous increase of these adverse impacts. CO_2 sequestering could then be carried out in the equatorial Pacific and in other HNLC waters, especially off of Antarctica, the main areas of the oceans that have a high capacity of sequestering CO_2 . For instance, if all the CO_2 in the atmosphere were sequestered in the ocean, it would raise the average concentration of CO_2 in the ocean by only about 1.2%. The ocean chemistry would not be altered significantly and the increase in outgassing of the CO_2 would be minimal.

The cost of sequestering CO_2 on a commercial scale is expected to be about \$1.00 per ton of CO_2 . The sales price for CO_2 sequestering credits, should they become tradable, would be about \$2.00 per ton of CO_2 , to include the cost of verification, overhead and profit. It is expected that these credits would be highly valued since they would not suffer from the problems of fire hazard, leakage and additionality the forest projects for CO_2 sequestering face.

CONCLUSION

Many approaches for dealing with the increase in the CO_2 content of the atmosphere have been proposed, but sequestration by ocean fertilization has received little attention. It is new, far away and poorly understood by many. The initial reaction is that not enough is known to warrant attention at this time. While this reaction may have had merit in the past, the last few years have seen a great increase in knowledge about the oceans, especially the equatorial Pacific, where moored and floating buoy systems, research vessel voyages and continuous satellite monitoring have all greatly increased our knowledge and understanding. The last remaining piece of the puzzle is to quantify the response of this HNLC ocean water to iron fertilization, which can be done by the large experiment described here. We now know enough to design and carry out this technology demonstration experiment, which can lead to solving the problem of peoples' concerns rather than just working on it, thereby saving time and costs while greatly reducing the risk of adverse consequences.

REFERENCES

- ¹ US Department of Energy (1999) *Working Paper On Carbon Sequestration Science And Technology*, p. 1-1
- ² US Carbon Cycle Plan 1999, p. 7
- ³ IPCC (Intergovernmental Panel on Climate Change) 1996
- ⁴ Wigley, T.M.L., R. Richards and J.A. Edmonds "Economics and Environmental Choices in the Stabilization of Atmospheric CO_2 Concentrations" *Nature* 379, 18 Jan 96, pp. 240-243
- ⁵ Markels, Jr., Michael, US Patent No. 5,433,173, *Method of Improving the Production of Seafood*, 18 Jul 1995
- ⁶ Markels, Jr., Michael, US Patent No. 5,535,701, *Method of Improving the Production of Seafood in the Ocean*, 18 Jul 1996 and US Patent No. 5,967,087, *Method of Improved Seafood Production in the Barren Ocean*, 19 Oct 1999
- ⁷ Markels, Jr., Michael, US Patent No. 6,058,919, *Method of Sequestering Carbon Dioxide*, 02 May 2000
- ⁸ Frost, W.F.; "Phytoplankton bloom on iron rations"; *Nature* 10 Oct 96, pp. 495,508,511,513 & 475
- ⁹ Markels, Jr., Michael, US Patent Application No. 09/521,885, *Method of Sequestering Carbon Dioxide with Spiral Fertilization*, filed 9 Mar 2000.

Thermodynamics of Conversion of Methane Clathrate Hydrate to Carbon Dioxide Hydrate Within Porous Media

Duane H. Smith, U.S. Department of Energy, National Energy Technology Laboratory, Morgantown, WV 26507-0880 and, Department of Physics, West Virginia University, Morgantown, WV 26506

Kal S. Seshadri, Parsons Infrastructure and Technology Group; Morgantown, WV 26507-0880

Key Words: carbon dioxide hydrate, equilibrium conditions of gas hydrates decomposition, enthalpies of gas hydrates dissociation.

INTRODUCTION

Environmental concerns about rising concentrations of atmospheric carbon dioxide are stimulating R&D on a variety of carbon dioxide sequestration options. In energy-supply research, it has been estimated that natural gas hydrates in arctic and seafloor formations contain more energy than all other fossil fuel deposits (coal, oil, and natural gas) combined.¹ From data in the literature it is known that the conversion of bulk methane hydrate to bulk carbon dioxide hydrate is thermodynamically favored.¹ Thus, it has been proposed that the sequestration of CO₂ and the production of natural gas might be performed simultaneously by the injection of carbon dioxide into deposits of natural gas hydrates and the conversion of CH₄ hydrate to the hydrate of CO₂.^{2,3}

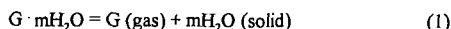
However, natural gas hydrates usually are found distributed within the pores of sediments,¹ and the thermodynamic parameters of methane hydrate are affected by the size of the pores in which the hydrates form.⁴⁻⁶ Recently we have measured the temperature-pressure equilibria and heats of formation of CO₂ hydrates in silica gel of various pore diameters. These measurements show how the temperature-pressure equilibrium of CO₂ hydrate depends on the pore size, and allow us to estimate the effect of pore size on the heat of dissociation of CO₂ hydrate. Bulk natural gas hydrates almost always occur in the "sII" crystal structure, because the presence of as little as one percent propane is sufficient to change the structure from the "sI" form of pure methane hydrate.¹ Measurements on the formation of hydrate(s) in pores by various multi-component natural gases have not yet been performed. Nevertheless, by comparing thermodynamic data for hydrates of CO₂ and CH₄ in porous media, we can explore whether calculations performed for the conversion of bulk natural gas hydrate to bulk carbon dioxide hydrate need to be corrected for pore-size effects.

EXPERIMENTAL METHOD

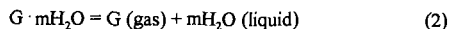
Carbon dioxide hydrate was synthesized within the pores of silica gel following the method described by Handa⁶ for hydrates of methane and propane. The silica gel was obtained from Aldrich; according to the vendor, the pore diameter of the Davisil™ material was 15.0 nm. Pore diameter and surface area also were determined by the BET method.⁷ The mesh size of the silica gel was 200-425, and the purity of the carbon dioxide (Matheson Coleman) was 99.99%. Sample temperatures were established by immersing the pressure cell in the fluid of a NesLab model RTE-140 chiller bath, which kept the temperature constant to within 0.05 K. Bath temperatures were read with a Hart Scientific model 1006 MicroTherm thermometer, traceable to NBS standards, with a sensitivity of 0.001 K. Pressures were measured by means of a calibrated Serta pressure transducer and readout with a sensitivity of 0.0068 MPa and an accuracy of 0.11% of full scale (20.40 MPa).

RESULTS

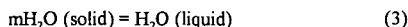
Figure 1 illustrates the equilibrium pressure vs. temperature curves for the hydrates of carbon dioxide (present work) and methane⁶ in 15 nm diameter pores. The carbon dioxide pressure-temperature data were converted to fugacities⁸ and plotted vs. 1000/T (Fig. 2). The carbon dioxide hydrate data in Figs. 1 and 2 are for two different equilibria:



and



where G is the "guest" molecule. Reactions (1) and (2) are in equilibrium at the (lowest) quadruple point. Linear regressions were performed to the data of Fig. 2 above and below the quadruple point, respectively. The regression equations were $\ln f = 17.671 - 4.7237/T$ ($R^2 = 0.9992$) and $\ln f = 18.184 - 4.8599/T$ ($R^2 = 0.9927$), respectively. The quadruple point (i.e., point of intersection of the two regressions) was $T_Q = 266.9$ K, $P_Q = 0.98$ MPa. As suggested by (1) and (2), the quadruple point determined by the equilibrium



is essentially independent of pressure over the change of quadruple point pressure induced either by pore effects or by changes of the "guest" component (CO_2 or CH_4). Hence, the quadruple point temperature is principally determined by the effect of pore size on the melting point. Using differential scanning calorimetry, Handa measured the melting point of ice in 15 nm diameter pores to be 267.5 K.⁹ Thus, the value for the quadruple point temperature found from the carbon dioxide hydrate data compares favorably with the expected value. From Handa's pressure-temperature data for methane hydrate we calculate $T_Q = 267.4$ K. The quadruple point temperature is $T_Q = 273.1$ K for bulk hydrates of CO_2 and CH_4 . Thus, the effect of pore size on the quadruple point temperature is simple: it is essentially the same for all guest-molecule compositions. For 15 nm diameter pores, the quadruple point temperature is lowered by 5.6 K.

Next, the enthalpies for equilibria (1) and (2) were estimated from the data plotted in Fig. 2, by means of the Clausius-Clapeyron equation. As listed in Table 1, these calculations yielded the values 35.59 kJ/mole for equilibrium (1) and, 39.10 kJ/mole for equilibrium (2) of CO_2 hydrate. Also listed in Table 1 are the enthalpies that we have calculated from Kamath's data for methane and carbon dioxide hydrates in sand packs¹⁰ and calorimetric data by Handa⁵ for methane hydrate in 15 nm silica gel. Additional data for CO_2 hydrates in porous media may be found in ref. 11.

REFERENCES

1. Sloan, E. D. *Clathrate Hydrates of Natural Gases*; Marcel Dekker: New York, 1998.
2. Komai, T.; Yamamoto, Y. *Third International Conference on Gas Hydrates*, Salt Lake City, July 18-22, 1999.
3. Komai, T.; Yamamoto, Y.; Ikegami, S. *ACS Div. Fuel Chem. Preprints* **1997**, *42*, 568.
4. Makogon, Y. F. *Hydrates of Natural Gas*; PennWell: Tulsa, 1981.
5. Handa, Y. P. *J. Chem. Thermo.* **1986**, *18*, 915.
6. Handa, Y. P.; Stupin, D. *J. Phys. Chem.* **1992**, *96*, 8599.
7. Brunauer, S.; Emmett, P. H.; Teller, E. *J. Am. Chem. Soc.* **1938**, *60*, 30.
8. Pitzer, K. S.; Curl, R. F. *J. Am. Chem. Soc.* **1957**, *79*, 2369.
9. Handa, Y. P.; Zakrzewski, M.; Fairbridge, C. *J. Phys. Chem.* **1992**, *96*, 8594.
10. Kamath, V. A. University of Pittsburgh, Ph.D. Dissertation, 1984, Univ. Microfilms No. 8417404.
11. Smith, D. H.; Seshadri, K. S. *Proc. Seventeenth Annual Pittsburgh Coal Conference*, Pittsburgh, Sept. 11-15, 2000, paper no. 55.

Table 1. Heats of Dissociation (kJ/mole) for Hydrates of Methane and Carbon Dioxide in Sand and in 15 nm Diameter Pores

Guest	Medium	Heat of Dissociation (kJ/mole)	
		reaction (1)	reaction (2)
CH_4	15 nm pores ^(a)	15.83	45.92
CH_4	sand ^(b)	15.22	68.84
CO_2	15 nm pores ^(c)	35.59	39.10
CO_2	sand ^(b)	25.43	82.43

^(a)Heat measured calorimetrically by Handa⁵

^(b)Heats calculated in the present work from the equilibrium pressure-temperature data of Kamath¹⁰

^(c)Heat obtained in the present work

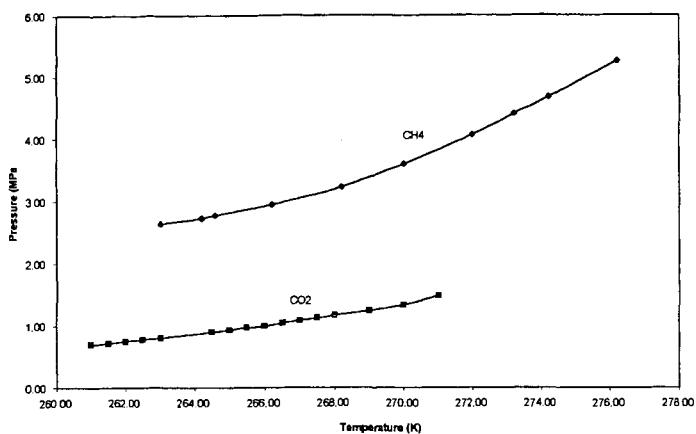


Figure 1. Equilibrium pressure-temperature for hydrates of CO₂ and CH₄ in 15 nm diameter pores of silica gel.

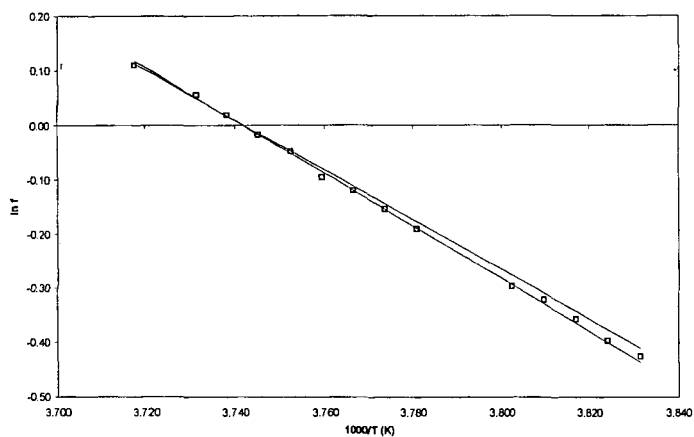


Figure 2. Logarithm of the fugacity, f , vs. inverse temperature, $1/T$, for CO₂ hydrate in 15 nm diameter pores of silica gel.

Reformation and Replacement of CO₂ and CH₄ Gas Hydrates

Takeshi Komai, Taro Kawamura and Yoshitaka Yamamoto
National Institute for Resources and Environment, MITI, Japan
16-3, Onogawa, Tsukuba, Ibaraki, 305-8569 Japan
E-mail:koma@nire.go.jp

Keywords: Gas Hydrate, Methane Hydrate, Carbon Dioxide Hydrate, Reformation, Replacement

INTRODUCTION

Large amounts of gas hydrates, clathrate compounds of water and gases formed under high pressure and low temperature, are found in marine sediments and permafrost. To extract methane gas from its reservoir in a practical method, it is necessary to obtain fundamental information on the mechanism underlying the formation and dissociation of gas hydrates and their properties, including kinetics and crystal growth. We have proposed an advanced method of gas hydrate production, by which methane gas is extracted from the reservoir by replacing methane with carbon dioxide at the molecular level. This method would be feasible to achieve the sequestration of carbon dioxide into the sediments. The main purposes of this research are to elucidate the mechanism underlying hydrate reformation and replacement and accumulate practical data for completing the original concept of the proposed method. We have carried out experiments on the dynamics on reformation and replacement of gas hydrates using an apparatus consisting of a high pressure vessel and a Raman spectroscopy. In this paper we present the experimental results concerning the behavior of gas hydrate reformation and replacement, and some discussion on the dynamics and the mechanism of gas hydrate formation.

EXPERIMENTAL

The experimental apparatus, in which the formation and replacement of gas hydrate could be observed, was designed and constructed, so that the several conditions of pressure, temperature and concentration of gases could be precisely controlled. Fig.1 illustrates the schematic diagram of the apparatus and measuring system used in the experiment. The pressure cell, made of stainless steel with a 3.2 ml internal volume, can be used at a pressure condition of up to 20 MPa. It contains a glass window for observing Raman scattering of monochromatic lights, a thermoelectric temperature control module, and some nozzles for the introduction of gas and liquid components. The pressure cell is installed on a constant temperature plate filled with a cooling agent methanol, where the temperature can be controlled with an accuracy of ± 0.1 K. It is equipped with transducers for detecting and controlling pressures with an accuracy of ± 0.05 MPa. The observation system of the Raman spectroscopy and a CCD camera are mounted in the apparatus as shown in Fig.2.

As a preliminary experiment, samples of CH₄ gas hydrate were synthesized from fine ice crystals and pressurized CH₄ gas, and stored as solid-phase pellets under extremely low temperature. The procedures of the experiment on reformation and replacement of gas hydrates are as follows. A pellet of CH₄ gas hydrate sample with a volume of 0.8 ml is placed into the pressure cell at a low temperature (< 253 K), and remaining volume of the pressure cell is filled with pressurized CO₂ gas. The internal pressure and flow rate of the gas can be adjusted using a fluid supplier system. The flow rate of CO₂ is set to approximately 5 ml/min. The reformation of CO₂ gas hydrate is observed during the changes in temperature of entire system. CH₄ gas hydrate no longer exists in this condition. The experiment on replacement is conducted under the conditions where both CO₂ and CH₄ gas hydrates can exist in the solid phase. An optical cell and the Raman spectroscopy system are installed on the glass window for detecting the nucleation and change of component of the hydrate structure. The gas components are analyzed by gas chromatography.

RESULTS AND DISCUSSION

a) Reformation of CO₂ and CH₄ gas hydrates

There are many differences of formation properties between CO₂ and CH₄ gas hydrates, such as the phase equilibrium and the formation rate. Fig.3 shows the pressure-temperature relationship of formation obtained at the first run of CO₂ and CH₄ gas hydrates. A first run is a situation of nonequilibrium formation without any gas hydrate nuclei in dissolved solution. The upper curve represents the relationship between nonequilibrium formation temperature T_f and pressure P_f , the lower curve, that between dissociation temperature T_d and pressure P_d . The center curve corresponds to the three-phase equilibrium estimated using the thermodynamic theoretical approach (Sloan). It can be seen that the relation between $P_f(T_d)$ and $T_f(T_d)$ is approximately linear in a semilog plot. In addition, it was found that the formation relation greatly differs from the theoretical data of phase equilibrium. The differential temperatures between nonequilibrium

formation and dissociation for CO_2 gas hydrate were slightly higher than those for CH_4 gas hydrate. At the second and third runs, reformation of gas hydrates occurred under conditions of higher temperatures and/or lower pressures than those at the first run. However, a supercooling temperature higher than 1.5 K was necessary for gas hydrate reformation in the case of CO_2 . These properties may reveal interesting phenomena concerning the mechanism of gas hydrate nucleation under nonequilibrium conditions.

b) Solid-phase formation of CH_4 gas hydrate samples

CH_4 gas hydrate samples were synthesized in the solid phase for the replacement experiment using fine grains of ice crystal (average diameter: 0.1 mm) and the solution in which CH_4 gas hydrates were dissociated at a temperature slightly higher than the equilibrium temperature. It took a relatively short time to achieve nucleation of gas hydrate using the dissociated solution. When the temperature was set 2.0 K lower than the equilibrium temperature, the reformation of CH_4 gas hydrate could be achieved within 24 hours. Fig.4 shows the result of Raman spectroscopic analysis for CH_4 gas hydrate obtained using the procedure. A sharp Raman shift appears around $2905/2915\text{ cm}^{-1}$, indicating the existence of Type-I CH_4 gas hydrates. According to a more precise analysis, the hydration number of the obtained samples was in the range of 6.4 to 6.0, that is, the ratio of occupancy in small cages can be estimated to be approximately 85-95 percent.

c) Formation rate of CO_2 gas hydrate in quasi-liquid phase

The formation rate of CO_2 gas hydrate was measured in situ observation using Raman spectroscopy; results are shown in Fig.1. The nucleation of gas hydrate was initiated from fine ice crystals under a temperature lower than 273 K. After setting ice crystals into the pressure cell, CO_2 gas was introduced to maintain the pressure inside the cell at 1.6 MPa. Fig.5 illustrates the trend of the Raman shifts obtained from 10 minutes to 2170 minutes after nucleation. Four Raman shift peaks were observed, in which peaks of around 1276 cm^{-1} and 1381 cm^{-1} are due to the existence of guest in the CO_2 gas hydrate structure. It was found in Fig.5 that the values of peak strength increase with time after the nucleation of gas hydrate. As the peak strength closely corresponds to the numbers of molecules in the structure, the formation rate of gas hydrate can be estimated from the peak strength. Fig.6 shows the formation rates of CO_2 gas hydrate obtained at temperatures from 254.5K to 274.5K. The formation rates of gas hydrate changed greatly with temperature, especially in the range between 269 K and 275 K. This suggests that the existence of quasi-liquid phase water, a type of slightly melting ice, plays an important role in promoting formation of gas hydrate at the gas-solid interface. Based on the behavior of CO_2 formation, the optional temperature for the replacement process was set around 273-275 K.

d) Replacement of CO_2 and CH_4 gas hydrates in solid phase

The replacement experiment on CO_2 and CH_4 gas hydrates was carried out using a bulk scale testing apparatus. Samples of CH_4 gas hydrate were synthesized in the solid phase from fine ice crystals and the dissociated solution. A preliminary process was performed under the conditions mentioned in the experimental procedure. During the process of replacement, the pressure of CO_2 was 2.0 MPa and the temperature was $274 \pm 0.5\text{ K}$. Fig.7 illustrates the Raman shifts obtained from the replaced hydrate sample observed 1 hour following CO_2 introduction. Two typical peaks appeared in the Raman spectra, $2905/2915\text{ cm}^{-1}$ for CH_4 hydrate and around $1275/1380\text{ cm}^{-1}$ for CO_2 hydrate. This means that both CH_4 and CO_2 gas hydrates coexist in the structure of the replaced hydrate sample. Based on quantitative analysis, the ratio of occupancy for $\text{CO}_2 / \text{CH}_4$ gas hydrates in the replaced hydrate sample were 40 and 45 percent, respectively. The portion of CO_2 gas hydrate in the sample increased with time. Fig.8 shows the trend of $\text{CO}_2 / \text{CH}_4$ components in the solid hydrate after CO_2 introduction as a function of time. The data were obtained from in situ observation and the analysis of peak strength of Raman shifts. This result indicates that the replacement of guest elements in solid gas hydrates could be achieved within a short period of 12 hours, if the pressure and temperature are precisely controlled in the pressure cell. It is also considered that a period of 2 hours is sufficient for nucleation of CO_2 hydrate at the surface of sample, and then crystal growth proceeds as a result of CO_2 transport into the solid hydrate. Because the transport of CO_2 gas should be fast in porous media, the in situ replacement of CO_2 gas hydrate may be used for the extraction of gas hydrates from their reservoirs. More systematic researches are necessary to elucidate the phenomenon underlying gas hydrate replacement.

CONCLUSIONS

Experimental studies on the dynamics and behavior of reformation and replacement of gas hydrates was carried out using a specially designed apparatus. It was shown that reformation of gas hydrates easily occurred in the quasi-solid structure when the dissociated solution is used. The rate of reformation of CO_2 gas hydrate was observed by Raman spectroscopy. The results of the bulk scale experiment showed that replacement of CO_2 gas hydrate could be achieved within a period of 12 hours in pure samples of CH_4 gas hydrate that had been synthesized as solid crystal, if

the pressure and temperature are precisely controlled in the pressure cell. The replacement of guest elements in CO_2 and CH_4 gas hydrates may be quite innovative from both aspects, the extraction of gas hydrates and sequestration of CO_2 , to maintain the global environment and stability of marine sediments.

ACKNOWLEDGMENTS

The authors gratefully acknowledge Dr. F. Kiyono and Mr. H. Haneda in NIRE for assistance in developing the original concept of the extraction system, and Dr. K. Nagashima and Dr. Seong-Pil Kang for advice in completing the theoretical analysis.

REFERENCES

- Sloan, E. D., *Clathrate Hydrates of Natural Gases*, Marcel Dekker, 111-192, (1990)
 Uchida, T., Hondoh, T. and Mae, S.: Effects of Temperature and Pressure on the Transformation Rate from Air Bubbles to Hydrate Crystals, *Ann. Glaciol.*, 20, 143-147, (1994)
 Matsumoto, R.: Feasibility of Methane Hydrate under the Sea as a Natural Gas Resource, *J. Jap. Assoc. Petroleum Tech.*, 60(2), 147-156, (1995)
 Ogaki, K., Takano, K.: Methane Exploitation by Carbon Dioxide, *J. Chem. Eng. Japan*, 29, 478-483 (1996)
 Holder, G.D., Zett, S.P. and Pradhan, N.: Phase Behavior in Systems Containing Clathrate Hydrates: A Review., *Reviews in Chemical Engineering*, 5, 1-70, (1988)
 Komai, T., Yamamoto Y.: Dynamics of Reformation and Replacement of CO_2 and CH_4 gas hydrates, 3rd Int. Gas Hydrate Symposium, Utah, USA, (1999) (in press)

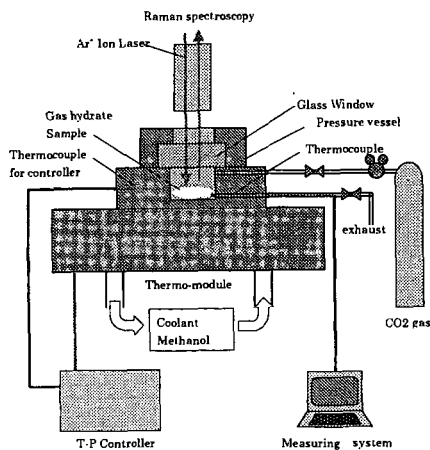


Fig.1 Schematic diagram of the experimental setup for gas hydrate formation.

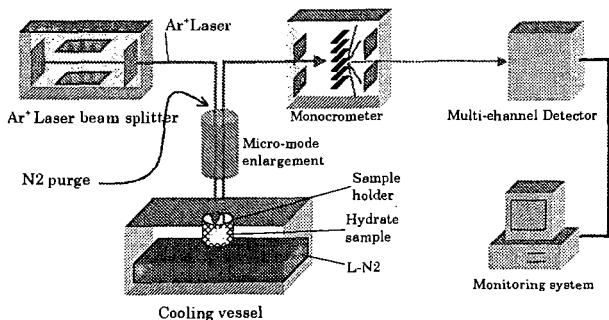


Fig.2 Raman spectroscopy apparatus for observing gas hydrate structure and component.

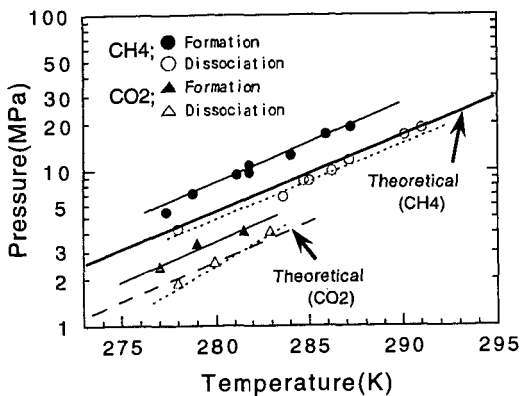


Fig.3 The relations of formation/dissociation P and T for CO_2 and CH_4 gas hydrates.

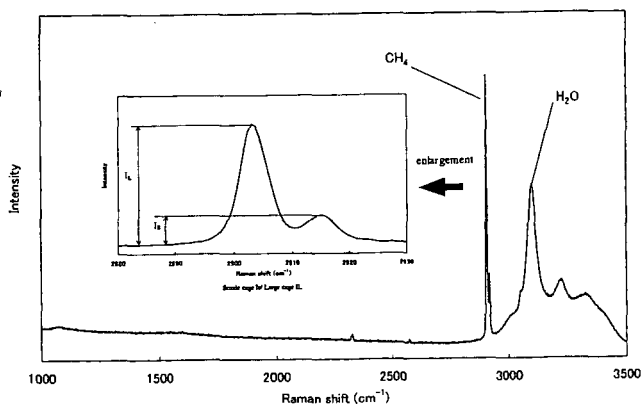


Fig.4 Raman shift for a sample of CH_4 gas hydrate made from ice crystals

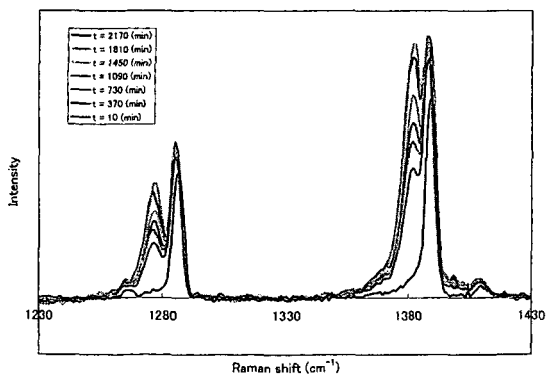


Fig.5 Changes in Raman shifts observed for CO_2 gas hydrate formation.

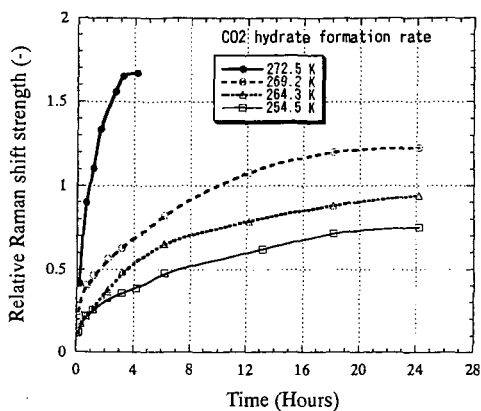


Fig.6 The trend curves of the formation rate of CO_2 gas hydrate under different temperatures.

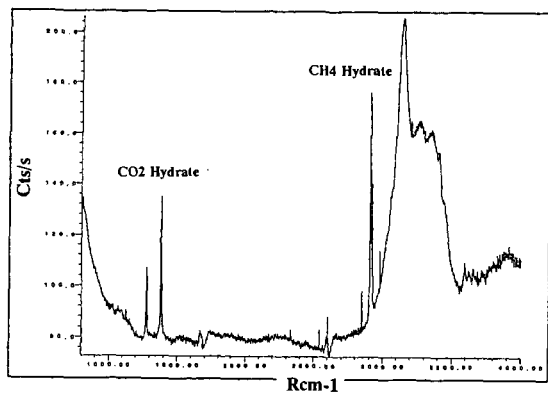


Fig.7 Raman shift for a sample of replacement from CH_4 to CO_2 gas hydrates.

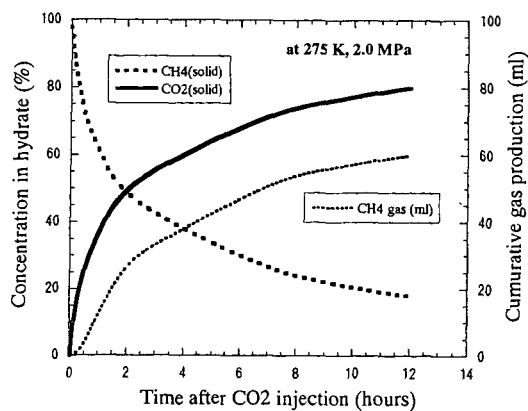


Fig.8 The trend curves of CO_2 and CH_4 components in replaced gas hydrate sample and the cumulative CH_4 production.

DIRECT OBSERVATION OF THE FATE OF OCEANIC CARBON DIOXIDE RELEASE AT 800M

Edward T. Peltzer, Peter G. Brewer,
Gernot Friederich and Gregor Rehder
Monterey Bay Aquarium Research Institute
Moss Landing, CA 95039

Keywords: bubbles, carbon dioxide, clathrate hydrate, ocean sequestration

ABSTRACT

The rise rate and dissolution rate of freely released CO_2 in the ocean were measured to provide fundamental data regarding carbon sequestration in the upper ocean. These experimental observations were accomplished using MBARIs advanced remotely operated vehicle (ROV) technology. Small amounts of liquid CO_2 were released at 800 m depth and ambient temperature (4.4°C). The rising droplets were contained within an open ended acrylic chamber and were imaged with an HDTV camera. The mean rise rate for a droplet of initially 1 cm diameter observed over a one hour period was 12.4 cm/sec. The rise rate was initially about 10 cm/sec and it gradually increased to about 15 cm/sec as the bubble rose. The mean dissolution rate was $3.7 \mu\text{mol}/\text{cm}^2/\text{sec}$. Visual contact of the rising droplets was maintained for up to 1 hour and over 400 m initially suggesting a slow dissolution rate and long bubble lifetimes. However, 90% of the mass loss occurred within 30 minutes and 200 m of the release point.

INTRODUCTION

Concern about the rising levels of atmospheric CO_2 and the continued use of fossil fuels to meet ever increasing energy demands lead to consideration of the disposal of fossil fuel CO_2 in the ocean as a means of ameliorating greenhouse gas induced climate change (1,2). While many models of this process have been formulated (3,4), and various laboratory simulations have been carried out (5), there have been few direct oceanic experiments reported. With the availability of advanced ROV technology at MBARI, it was thought possible to carry out a controlled release of liquid and gaseous CO_2 in the open ocean, and to observe the processes taking place. In earlier work (6) we reported on contained experiments involving CH_4 and CO_2 to form hydrates. Here we present an initial experiment addressing the more difficult problem of observing and accurately measuring the behavior of a rising stream of freely released liquid CO_2 . We choose this approach in order to evaluate the effectiveness of intermediate depth releases when all the co-varying properties of salinity, temperature, and pressure are present, and to represent the fluid dynamics of a rising cloud of liquid CO_2 droplets in the ocean.

In order to properly evaluate whether it is wise to proceed with any ocean disposal option, an accurate description of the fate of CO_2 injected into ocean water is necessary. At shallow depths (above about 350 m, depending upon the local temperature gradient) CO_2 is a gas, and readily dissolves. Below this depth, we encounter the gas hydrate phase boundary where a shell of CO_2 -hydrate may be generated (7,8) on the bubble/droplet surface. Such a hydrate skin or shell, could have profound consequences; both slowing the rate of dissolution, increasing bubble lifetimes and increasing the thickness of the layer where the bulk of the CO_2 dissolves. Below about 400 m depth, pure CO_2 will exist as a liquid. Due to the relatively high compressibility of liquid CO_2 in comparison to seawater, the density ratio will invert at high pressure such that below about 2800 m depth a gravitationally stable release can be achieved (9). Release of CO_2 at depths deeper than this, may promote rapid and massive solid hydrate formation, and may lead to long oceanic residence times and effective sequestration from the atmosphere. The potential cost and technical difficulty of this deep injection scenario suggests the need to evaluate alternate injection scenarios at shallower depths.

While laboratory studies of the CO_2 clathrate-hydrate phase boundary and the solid phase have both been successful, it is difficult for a laboratory study to simulate the behavior of freely released material in motion, in a complex physical regime. Thus, several mathematical models have been devised to simulate this process and differing conclusions were reached. Holder et al. (10) modeled the behavior of a rising CO_2 plume incorporating a constantly growing film of solid hydrate. With time, this film slows the rise rate since CO_2 -hydrate is more dense than either seawater or liquid CO_2 , and eventually causes the combined mass to sink. Herzog et al. (3) modeled the dissolution rate of liquid CO_2 between 500 and 2000 m without the hydrate effects. They concluded that if the initial droplet radius is less than 1 cm, then complete dissolution would occur within less than 200 m. Very complete sets of model calculations incorporating plume dynamics have been carried out (3,4,11), and yet no field data exist to compare these models against.

EXPERIMENTAL

The experiments were executed beginning at 800m depth in Monterey Bay, off the coast of central California, during October 12-13, 1999, using the ROV *Ventana*. The ROV was equipped with an HDTV camera to observe the CO₂ released and the video tape recorded from this camera provides a permanent record of the work. The system captures images with a specially modified Sony HDC-750 high-definition television camera which digitizes the picture data and formats it to the SMPTE 292M HDTV interface standard with 2:1 interlace. The resolution of the images is 1035 pixels vertically and 1920 pixels horizontally which is about five times the resolution of conventional video. The image data is recorded with a Panasonic HD2000 high-definition video tape recorder without any further transcoding steps.

An earlier attempt at observing the free release of CO₂ had shown that it was impossible to maintain a CO₂ droplet cloud that was free to move in all dimensions within the field of view. Effects of the vehicle motions, strong lateral forcing due to local currents, and the similarity of appearance of a droplet of liquid CO₂ to the ubiquitous gelatinous marine organisms, all combined to frustrate continuous observation. Therefore a simple imaging box (89 cm long, 25 cm deep, and with a transparent face 30 cm wide) was constructed. It was open to the ocean at top and bottom, and mounted directly in front of the camera. The purpose of this box was to restrain lateral motions, while permitting free upward motion of the droplet plume. A meter scale within the box provided dimensional control within the imaged field. Additionally, the opaque back of the box hid the visually distracting marine snow in the background. The liquid CO₂ injector was modified slightly from that described earlier (9), and used a piston assembly, operated by the vehicle hydraulic system, to deliver 128 mL of liquid per stroke through a 1/8-inch orifice mounted on the back of the imaging box. Smaller volumes were delivered with partial strokes. A CTD instrument mounted on the ROV provided depth, temperature and salinity information for the duration of the experiment. The experiment depth was chosen to match plans for a future large-scale release of CO₂ off the coast of Hawaii (12).

With the known dimensions of the bubble box, and the meter scale attached to the rear wall, we have numerical reference points with which to quantify the images of droplets during ascent. The time at which an image was recorded was logged on the same time base as the vehicle depth (pressure), temperature, etc. Frame grabs from the HDTV video tape provide a convenient means to measure droplet dimensions by comparison to the numerical scale.

At first glance, this experiment is disarmingly simple, however experience has shown that there is more here than meets the eye. It requires the precise piloting of a 3 ton vehicle, subject to oceanic forcing in 3 dimensions, while imaging a small cloud of droplets with millimeter precision for one hour over hundreds of meters of ascent. The successful completion of this experiment is a tribute to the skill of the ROV pilots and engineers.

RESULTS

Two CO₂ release experiments were carried out. In the first experiment, the droplets rose from 800 m to 625 m depth during the course of 21 minutes, at which time the droplet escaped from the bubble box. In a second release, a droplet was followed from 800 m to 340 m depth during a period of about 1 hour. The depth versus time curve for the second release is shown in Figure 1. Small errors in positioning the bubble in the vertical center of the box are assumed to be negligible when compared to the over 400 m rise of the experiment. The temperature profile recorded during this experiment is overlain on the relevant portion of the phase diagram for CO₂ in seawater in Figure 2. Note that visual contact with the bubble was lost just below the hydrate phase boundary. The nearness of this significant boundary attracted our attention initially, but the evidence suggests that the visual loss of the bubble at this point was coincidental.

A mean ascent rate of 12.8 cm/sec was observed during the first release and 12.4 cm/sec for the second, longer, experiment. Close inspection of the data revealed a measurable increase in velocity with decreasing pressure and concomitant diminishing droplet diameter. By fitting a second-order polynomial to the depth versus time data, we were able to better estimate (from the first derivative of this equation) that the rise rate was 10.2 cm/sec initially, increasing gradually to 14.9 cm/sec just before contact was lost with the bubble. A dramatic change in rise rate coincident with the transition from droplet to bubble on crossing the liquid-to-gas phase boundary, was not observed. While the data can be smoothly fit with a second order polynomial (see Figure 1) with no evidence of a discontinuity at that point, data above this phase boundary are sparse. As the droplets rose, they shrink from dissolution, expand from pressure release, and encounter progressively warmer and less dense seawater. The net result of this complex process is the small and relatively simple to model increase in rise rate versus time that was observed.

The ideal experiment of a single purely spherical droplet proved unrealistic. Early we observed that bubble collisions were frequent, and that rafts of CO₂ droplets remained strongly attached to

each other and that these rafts persisted for very long periods. At the same time, one could recognize a distinctively shaped unit and follow it within the droplet cloud. One such unit was found which later formed a droplet pair. The changing dimensions of this droplet pair during their ascent are given in Table 1. These complex shapes, rotating in three dimensions present varying aspect ratios to the camera and frame grabs were carefully selected to remove this effect.

Occasionally, droplets collided with and stuck to the walls of the bubble box. It was possible to free the droplet with a sudden lateral ROV motion, but the possibility of mass loss to the walls, rather than by dissolution remains. Furthermore, boundary flow occurs along the walls of the bubble box as the vehicle rose, and droplets were consistently drawn to this region. In spite of these difficulties it proved possible to maintain the droplets in free flow for the greater part of the ascent suggesting that any bias due to boundary effects is small. Images, from an alternate experiment, where droplets of liquid CO₂ were allowed to rise freely while the ROV was held stationary and thus no boundary flow effects are present, are being analyzed to determine the extent of the impact of the boundary flow upon the measured rise rates.

Table 1 presents the data on droplet size versus depth. Additionally, these data are plotted versus time in Figure 3. From these observations, and literature values on the density of liquid CO₂ as a function of pressure and temperature, it is possible to calculate the mass loss with time. These results show that droplet diameter changes as a linear function of time, and gives a dissolution rate for liquid CO₂ of 3.7 $\mu\text{mol}/\text{cm}^2/\text{sec}$. This result compares well with the results of Aya et al. (5) from laboratory pressure vessel studies at 30 MPa and 4.5°C. The laboratory measurements yield a value of 1.7 or 2.8 $\mu\text{mol}/\text{cm}^2/\text{sec}$ with and without a hydrate skin, respectively. The slightly higher rate obtained in the natural environment, may be due to the lower pressures involved and the complex physical situation, or the dynamics of a rising droplet stream (13,14).

In earlier work (6,9), we have demonstrated that within the phase boundary, CO₂ hydrate forms readily, almost instantaneously, on vigorous mixing of CO₂ and seawater. In these experiments, hydrate formation is usually recognizable by a change in optical reflectivity at interface of the phases, and by a white cloudy appearance. Based upon the imagery we obtained, it is not possible to state with certainty, whether the droplets followed here maintained a hydrate skin. Immediately after injection, the droplets appear to have a stiff surface skin, and droplet rafts formed and maintained a stick like shape. As the droplets rose they became more rounded, and soon appeared to be hydrate free. It is possible that some hydrate may have formed inside the release tube and was carried out with the droplets. However it is impossible, on the basis of these observations, to say whether the dissolution rate observed was affected by a molecular boundary layer of hydrate, or whether the relatively slow dissolution is simply the result of the high degree of immiscibility between liquid CO₂ and seawater.

The choice of a scenario for the long term sequestration of anthropogenic CO₂, either via a rising stream of CO₂, or via the formation of a sinking plume with hydrate formation (9) has yet to be made. The results presented here should allow a more accurate prediction of the CO₂/pH field, and the environmental effects, surrounding an injection point. However, a critical property for the longer term will be the effectiveness of the process in terms of sequestration. For example, the depths chosen here cover the 27.3 - 26.8 (σ_θ) isopycnal surfaces. While the 26.8 surface is the most dense seawater to outcrop seasonally at the surface in the North Pacific, Warner et al. (15) have recently mapped the ventilation age of this surface demonstrating that it was relatively recently (12-32 years) exposed to contact with the atmosphere. This probably represents the shallowest depth at which disposal in this ocean basin is likely to be effective as a sequestration option, although other shallow disposal scenarios have also been considered (13,14).

The small-scale ROV experiments described here are a "first effort" to evaluate these processes, and appear to offer an effective way to approach the problem without the costs and problems associated with larger-scale releases. We were not yet able with these small quantities to easily simulate some of the changes in local seawater density, and "peeling" of the plume predicted by large scale fluid dynamic modeling (11). At the same time, it should be recognized that the results reported here pertain to isolated bubbles moving in a more or less undisturbed ocean. Differences with the large-scale releases will no doubt be found. It is not only possible to extend these studies to include biological effects (16) but it is also desirable and this work is in progress.

ACKNOWLEDGEMENTS

The authors would like to thank the Captain and crew of the RV *Point Lobos*, and the pilots of the ROV *Ventana*. Without their skilled support, this research would not have been possible. This work was supported by a grant to MBARI from the David and Lucile Packard Foundation.

REFERENCES

1. C. Marchetti, *Climate Change* **1**, 59 (1977).
2. N. Handa and T. Ohsumi, *Direct Ocean Disposal of Carbon Dioxide* (Terra Scientific Publishing, Tokyo, 1995).
3. H. Herzog, D. Golomb, S. Zemba, *Envir. Prog.* **10**, 64 (1991).
4. H. Drange, P. Haugan, *Tech. Rep. 54, NERSC* (1992).
5. I. Aya, K. Yamane, H. Nariai, *Energy* **22**, 263 (1997).
6. P. G. Brewer, F. M. Orr, Jr., G. Friederich, K. A. Kvenvolden, D. L. Orange, *Energy Fuels* **12**, 183 (1998).
7. E. D. Sloan Jr., *Clathrate Hydrates of Natural Gases* (Dekker, New York, 1990).
8. W. J. North, V. R. Blackwell, J. J. Morgan, *Environ. Sci. Technol.* **32**, 676 (1998).
9. P. G. Brewer, G. Friederich, E. T. Peltzer, and F. M. Orr, Jr., *Science* **284**, 943 (1999).
10. G. D. Holder, A. V. Cugini, R. P. Warzinski, *Environ. Sci. Technol.* **28**, 276 (1995).
11. G. Alendal, H. Drange, *J. Geophys. Res.* In Press.
12. E. Adams, H. Herzog, *Tech. Rept., MIT* (1998).
13. P. Haugan, H. Drange, *Nature* **357**, 318 (1992).
14. R. Clift, J. R. Grace, M. E. Weber, *Bubbles, Drops and Particles* (Academic Press, New York, 1978).
15. M. J. Warner, J. L. Bullister, D. P. Wisegarver, R. H. Gammon, R. F. Weiss, *J. Geophys. Res.* **101**, 20,525 (1996).
16. M. N. Tamburri, E. T. Peltzer, G. E. Friederich, I. Aya, K. Yamane, P. G. Brewer, *Mar. Chem.*, In Press.

Table 1

Measured Liquid CO₂ Droplet Characteristics during Ascent from 800m Depth

Elapsed Time (min)	Depth (m)	Temp. (°C)	Droplet Diameter (cm)		CO ₂ Density (g/cc)	Amount of CO ₂ (millimoles)		Rise Rate (cm/s)
			(a)	(b)		(a)	(b)	
0	804.5	4.398	1.10		0.9423	14.92		10.2
14.23	706.3	4.740	0.75		0.9310	4.67		11.3
23.13	649.1	4.994	0.60	1.10	0.9235	2.37	14.63	12.0
29.82	602.1	5.165	0.45	0.90	0.9171	0.99	7.96	12.5
43.08	496.8	5.449	0.20	0.80	0.9021	0.09	5.50	13.5
49.73	447.3	5.995		0.45	0.8910		0.97	14.0
61.65	341.2	7.291		0.25	0.8632		0.16	14.9

The initial droplet tracked (a) was joined at about 650 m depth by a second, larger, bubble (b) which became attached. No change in rise rate could be detected due to the attachment, and the changing size of each droplet could be independently determined. The mean density of liquid CO₂ during the rise of the droplets was 0.92 (a) and 0.90 (b), respectively. Thus, a 1 cm³ droplet contains 21.1 (a) or 20.4 (b) millimoles CO₂. We calculate the dissolution rate (Γ) from the slope of:

$$(r_t - r_0) = -V_m \times \Gamma \times (t - t_0), \quad [1]$$

where V_m is the specific volume (mmol/cm³), r_0 and r_t are initial droplet radius and droplet radius at time t , and t_0 and t are initial time and the time elapsed since t_0 . The observed dissolution rate was 3.7 $\mu\text{mol}/\text{cm}^2/\text{sec}$.

The rise rate was determined by fitting a second-order polynomial to depth versus time to obtain:

$$Z_t = -2.250 \times 10^{-2} \times t^2 - 6.145 \times t + 799.2, \quad [2]$$

then taking the first derivative of equation [2] to yield the rise rate at time, t :

$$R_t = -0.0450 \times t - 6.145. \quad [3]$$

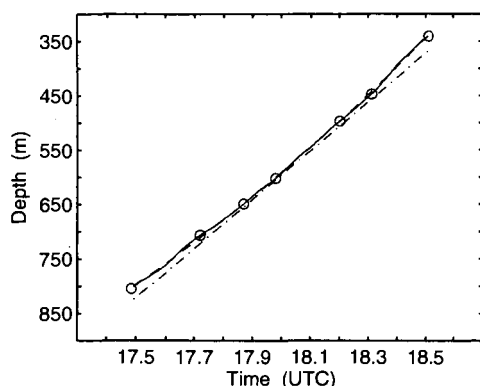


Figure 1. Plot of the observed ROV depth vs time for the second CO_2 release (solid line) and selected droplets (o). The mean rise rate for this release is shown as the dot-dash line tangent to the mid-point of the data curve. The dashed line is the second order polynomial fit to depth.

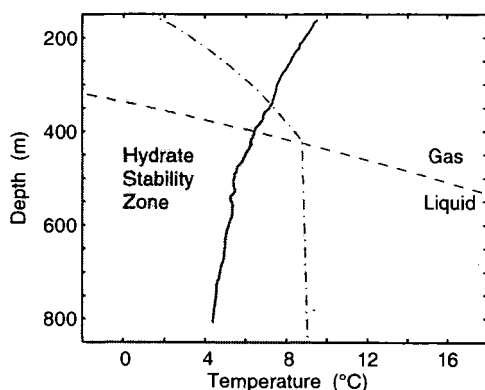


Figure 2. The observed ocean temperature profile recorded during the droplet rise experiments, overlaid on the CO_2 phase diagram for seawater. While the injection point is far inside the region for hydrate formation, the droplet crossed the liquid-to-gas phase boundary at about 400 m depth, and visual contact with the droplet was lost at about 340 m depth.

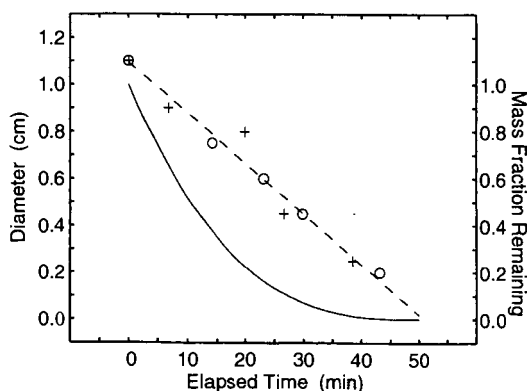


Figure 3. Plot of the changing droplet diameter with time, and remaining mass fraction of the droplets. The droplet size derived from HDTV video analysis, as listed in Table 1, is shown by circles (a) and crosses (b), respectively. The dashed line indicates the trend of diameter versus time calculated from equation (1) with a dissolution rate of $3.7 \mu\text{mol}/\text{cm}^2/\text{sec}$. The solid line shows the calculated remaining mass fraction relative to the initial mass of the CO_2 droplets.

ANALYTICAL AND EXPERIMENTAL STUDIES OF DROPLET PLUMES WITH APPLICATION TO CO₂ OCEAN SEQUESTRATION

E. Eric Adams, Brian C. Crounse, Timothy H. Harrison, and Scott A. Socolofsky
Dept. Civil & Envir. Engrg., Massachusetts Institute of Technology,
Cambridge, MA 02139

1. Abstract

This paper describes a numerical model of a steady-state plume in linear stratification driven by a buoyant dispersed phase, such as bubbles or droplets. The model was developed specifically to simulate CO₂ sequestration plumes. It extends the hybrid double-plume model of Asaeda & Imberger (1993) by incorporating droplet dynamics (dissolution, hydrate formation, and phase changes), by introducing a self-regulating detrainment criterion, and by allowing multiple intrusions to overlap. The model is calibrated to data from the literature and is applied to study the sensitivity of a CO₂ plume to ambient stratification.

2. Introduction

Several techniques for transferring CO₂ to the deep ocean have been proposed; buoyant droplet plumes injected around 1000 m depth are the simplest and least costly (Adams & Herzog 1996). Although the oceans and atmosphere will eventually equilibrate (on the order of 1000 years), the intent of such a sequestration strategy is to minimize atmospheric CO₂ concentrations over the next few hundred years, by which point CO₂ emissions will have significantly decreased (Adams & Herzog 1996). This paper examines the design of such a CO₂ injection.

This paper presents a numerical model for a two-phase plume in stratification that extends the hybrid double-plume model of Asaeda & Imberger (1993). The model currently neglects the effects of a crossflow in order to minimize the number of dynamic processes involved. This is deemed acceptable since the no-current case probably represents a worst-case scenario in terms of dilution of the dissolved CO₂. Because the dissolution of CO₂ increases the density of the seawater, there is a feedback on the plume dynamics. After presenting the model, this paper explores the relative importance of stratification and CO₂ dissolution for controlling the resultant plume structure.

3. Model Formulation

The spatial evolution of a two-phase plume in stratification is controlled by four primary processes: buoyant forces acting upon the droplets and plume water, dissolution of the droplets, turbulent entrainment of ambient water into the plume, and buoyant detrainment, called peeling. Qualitative two-phase plume behavior depends on the values of the droplet buoyancy flux, B , droplet slip velocity, u_s , and the strength of the ambient density stratification, N . Asaeda & Imberger (1993) and Socolofsky (in prep.) have identified four classes of two-phase plumes in stratification, illustrated in Figure 1. Type 1 plumes act like plumes in unstratified surroundings, flowing to the water surface without interruption. Type 2 plumes exhibit one or more intermediate peeling events, where plume water is stripped from the rising droplets by buoyant forces. The peeled water descends until it becomes forms a neutrally buoyant intrusion flow. Type 1* is a variant of Type 2 where the droplet slip velocity is low enough that the droplets partially peel along with the plume water. A Type 3 plume occurs when the droplet slip velocity is very high, so that the droplet core does not effectively transport ambient fluid. The progression from Type 1* to Type 3 can be correlated with the dimensionless slip velocity (Socolofsky, in prep.),

$$U_N = \frac{u_s}{(BN)^{1/4}} \quad (1)$$

The vertical evolution of plume structure can be predicted with an integral model. Integral models describe the plume flow as a one-dimensional problem by assuming a profile shape independent of height for each variable describing a plume property. Although this similarity assumption is not strictly valid for a two-phase plume in stratification, models based on similarity have been successful (Asaeda & Imberger 1993, Wüest et al. 1992, Turner 1986, McDougall 1978). Here, we choose top-height profiles (variables are assumed constant over the plume width) for both the inner, rising plume of water and droplets, and for the outer, falling annular plume of water only. Asaeda & Imberger (1993) introduced this type of double plume.

We formulate the model in terms of the governing flux variables. The mass flux of bubbles, W_b , is given by their number flux, N_b , their nominal diameter, d_b , and their density, ρ_b , yielding

$$W_b(z) = \frac{1}{6} \pi d_b^3(z) N_b \rho_b(z) = Q_b(z) \rho_b(z) \quad (2)$$

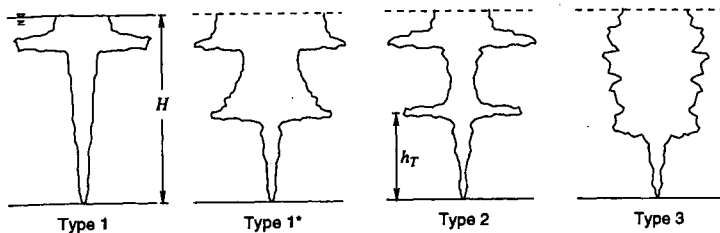


Figure 1. Schematic of characteristic two-phase plume behavior in stratification.

The size and density of bubbles are tracked in a bubble sub-model that accounts for dissolution, hydrate formation and phase changes. Denoting X as the cross-sectional fraction of the inner plume occupied by bubbles, we define the volume flux, Q , of plume water as

$$Q_i(z) = \int_0^b (1 - X(z)) u_i(z) 2\pi r dr = \pi b^2 u_i \quad (3)$$

where u is the average water velocity and b is the plume width. The subscript i indicates an inner-plume value. The momentum flux, M , includes the momentum of both the bubbles and the droplets

$$M_i(z) = \gamma \int_0^b (1 - X(z)) u_i^2(z) \rho_i(z) 2\pi r dr + \gamma \int_0^b X(z) (u_i(z) + u_b(z))^2 \rho_b 2\pi r dr \quad (4)$$

where u_b is the bubble slip velocity and γ is a momentum amplification term, first introduced by Milgram (1983), that accounts for the fact that the model formulation implicitly ignores turbulent momentum transport. Because $X \ll 1$ and $u_b = O(u_i)$, the second term in (4) can be ignored giving $M_i = \gamma \pi b^2 u_i^2 = \gamma \rho_i Q_i u_i$.

The buoyant forces generating the plume result from changes in density. For this model, density is tracked through changes in salinity flux, S , heat flux, J , and the dissolved CO_2 flux, C . The salinity flux is defined from the local plume salinity, s , such that

$$S_i(z) = Q_i(z) s_i(z). \quad (5)$$

The heat flux of the plume is defined from the local water temperature, T , yielding

$$J_i(z) = Q_i(z) \rho_i c_p(z) T_i(z) \quad (6)$$

where c_p is the heat capacity of the fluid. Finally, the dissolved CO_2 flux is defined from the local dissolved CO_2 concentration, c ,

$$C_i(z) = Q_i(z) c_i(z). \quad (7)$$

Thus, (2) through (7) define the model state variables for the inner plume.

The state variables for the outer plume are nearly identical. The primary difference is that, because the outer plume is assumed to be annular, the volume flux of the outer plumes is defined as

$$Q_o(z) = \pi (b_o^2 - b_i^2) u_o \quad (8)$$

where the subscript, o , indicates an outer plume value. Defining z as the upward spatial coordinate and specifying that the outer plume flow downward, the velocity u_o is negative and u_i is positive. Using (8) and changing the subscripts in (2) to (7) from i to o yield the flux equations for the outer plume.

The plume develops by exchanging fluid with the ambient and by exchanging fluid between the inner and outer plumes. The entrainment hypothesis, introduced by Morton et al. (1956), states that the entrainment flux across a turbulent shear boundary is proportional to a characteristic velocity in the turbulent layer. In this model, we have defined three entrainment fluxes: E_i entrains from the ambient or from the outer plume into the inner plume, E_o entrains from the inner plume into the outer plume, and E_a entrains from the ambient into the outer plume. The entrainment relationship for counterflows is not well known. Here, we adopt the relationship used by Asaeda & Imberger (1993):

$$E_i(z) = 2\pi b_i \alpha_i (u_i - u_o) \quad (9)$$

$$E_o(z) = 2\pi b_o \alpha_o u_o \quad (10)$$

$$E_a(z) = 2\pi b_o \alpha_a u_o \quad (11)$$

where the α 's are entrainment coefficients.

The final exchange equation accounts for buoyant detrainment, which has been modeled in a variety of ways. Liro (1992) assumed that a fixed fraction of plume fluid was ejected when the net buoyancy flux across the plume approached zero. Asaeda & Imberger (1993) assumed that all of the plume fluid detrained when the net momentum approached zero. Based on experiments, peeling is better predicted when the net momentum approaches zero. For this model, a self-regulating peeling criterion is introduced. We know that peeling occurs when the drag from the bubbles can no longer support the negative buoyancy of the fluid. The simplest parameterization that behaves similarly to experiments gives the peeling flux as

$$E_p(z) = \varepsilon \left(\frac{u_b(z)}{u_i(z)} \right)^2 \left(\frac{B_i(z)}{u_i^2(z)} \right) \quad (12)$$

where ε is a non-dimensional fitting parameter of order 0.01, and B is the buoyancy flux, defined as

$$B_i(z) = gQ_i(z) \frac{\rho_a(z) - \rho_i(z)}{\rho_i} \quad (13)$$

where ρ_a is the ambient density. The relationship in (12) makes it easier for outer plumes to overlap and makes it possible to simulate the continuous peeling nature of Type 3 plumes, which were first defined by Asaeda and Imberger (1993).

With these definitions, the plume conservation equations can be readily defined. From mass conservation, we have:

$$\frac{dQ_i}{dz} = E_i + E_o + E_p \quad (14)$$

$$\frac{dQ_o}{dz} = E_i + E_o + E_p + E_a \quad (15)$$

Momentum conservation states that the momentum changes in response to the applied forces, which gives the following equations

$$\frac{dM_i}{dz} = g \left(\frac{Q_p}{(u_i + u_b)} (\rho_a - \rho_b) + \pi b_i^2 (\rho_a - \rho_i) \right) + E_i \rho_o u_o + E_o \rho_i u_i + E_p \rho_i u_i \quad (16)$$

$$\frac{dM_o}{dz} = -g\pi(b_o^2 - b_i^2)(\rho_a - \rho_o) + E_i \rho_o u_o + E_o \rho_i u_i + E_p \rho_i u_i + E_a \rho_a u_a \quad (17)$$

The conservation of salt, heat and dissolved CO₂ flux follow from the mass conservation equation, yielding for the inner plume:

$$\frac{dS_i}{dz} = E_i s_o + E_o s_i + E_p s_i \quad (18)$$

$$\frac{dJ_i}{dz} = c_p \rho_r (E_i T_o + E_o T_i + E_p T_i) + \frac{dW_b}{dz} \Delta H_{diss} \quad (19)$$

$$\frac{dC_i}{dz} = E_i c_o + E_o c_i + E_p c_i \quad (20)$$

and for the outer plume:

$$\frac{dS_o}{dz} = E_i s_o + E_o s_i + E_p s_i + E_a s_a \quad (21)$$

$$\frac{dJ_o}{dz} = c_p \rho_r (E_i T_o + E_o T_i + E_p T_i + E_a T_a) \quad (22)$$

$$\frac{dC_o}{dz} = E_i c_o + E_o c_i + E_p c_i + E_a c_a \quad (23)$$

The last term in (19) accounts for the energy released by dissolving CO₂. The densities ρ_i and ρ_o are determined by an equation of state which is a function of s , T , and c . dW_b/dz is calculated by the bubble sub-model.

The model begins with integration of the inner plume from the point of release to the point where the droplets disappear or the water surface is reached. Once the inner plume integration is complete, the outer plume segments are integrated. The integration of each outer plume section continues until the momentum flux approaches zero. Then, the next outer plume section is initialized and integrated. This cycle repeats until the solution converges to a steady result (typically 10 iterations).

4. Results

Literature data were available for an unstratified bubble plume and for a single-phase plume ($u_b=0$) in stratification. For both these cases the outer plume did not develop, so only values for α_i could be calibrated. Data for the unstratified case were from Milgram (1983) for a 50 m deep spring. The model matched the trend and magnitude of the measured plume velocities for a value of $\alpha_i =$

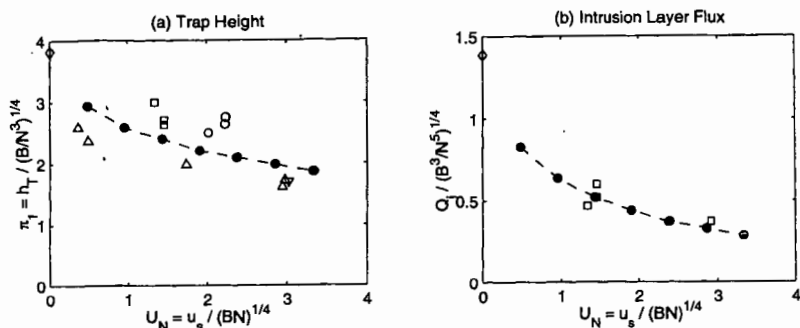


Figure 2. Model predicted (a) trap height and (b) intrusion layer volume flux versus experimental data. Up and down triangles are from Reingold (1994), open circles are from Asaeda and Imberger (1993), right-pointing triangles are from Lemckert and Imberger (1993), and squares are from experiments described in Socolofsky (in prep.). Model predictions are represented by the filled circles.

0.12. In the stratified case, the trap height relationship $h_T = 3.8(B/N^3)^{1/4}$ was tested. The model reproduced the scale-dependence of h_T on B and N for $\alpha = 0.11$.

Additional calibration data for two-phase plumes in stratification were available from Socolofsky (in prep.). The height of the first peeling event, h_T , and the volume flux in the resulting intrusion, Q_i , can be correlated with U_N . Calibrating to the trap-height relationship gives values of $\alpha = 0.07$, $\alpha_0 = 0.11$, and $\alpha_0 = 0.11$. Figure 2 shows the model predictions for trap height and intrusion layer flux, compared to experimental data.

The ambient density gradient, characterized by the buoyancy frequency, varies somewhat with geographic location and strongly with depth. To investigate the model sensitivity to stratification, a base-case CO_2 injection scenario was defined. Table 1 summarizes the base case along with scenarios featuring decreased and increased stratification.

Variable	Decreased Stratification	Base Case	Increased Stratification
Release Depth	800 m	800 m	800 m
Droplet Diameter	0.5 cm	0.5 cm	0.5 cm
Droplet Density	940 Kg/m^3	940 Kg/m^3	940 Kg/m^3
Flow rate	1.1 L/s	1.1 L/s	1.1 L/s
Buoyancy Frequency	0.0016 s^{-1}	0.0032 s^{-1}	0.0064 s^{-1}

Table 1. Simulation scenarios for CO_2 sequestration sensitivity analysis.

Figure 3 shows the model results for the three sequestration scenarios in Table 1. Although the total plume rise heights are about the same (the bubbles completely dissolve at the same height), the intrusion levels and fluxes differ. The volume flux to the intrusion layers decreases with increasing stratification because their descent is arrested more quickly in higher stratification, which leads to less cumulative entrainment and less total dilution. The mean concentration of excess CO_2 and the resulting change in pH in the intrusions are summarized in Table 2.

Case	Intrusion excess CO_2
Decreased stratification	0.03 Kg/m^3
Base case	0.06 Kg/m^3
Increased stratification	0.13 Kg/m^3

Table 2. Intrusion excess CO_2 concentration and change in pH for the three cases simulated.

The near-field dilution of the CO_2 reported in Table 2 is controlled by the competition between the stratification and the solution density effect of the CO_2 . Over the range of buoyancy frequencies sampled, the concentration of CO_2 in the intrusion layers is nearly proportional to the buoyancy frequency.

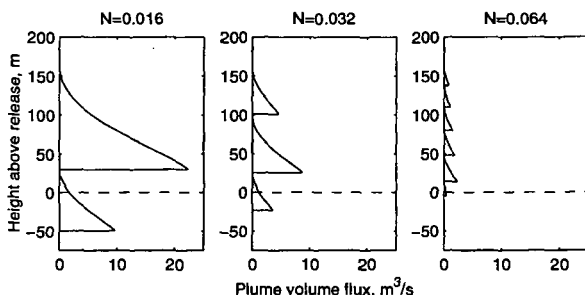


Figure 3. Sensitivity of plume structure to ambient stratification. The solid lines represent the volume flux profiles of the outer plume sections. The inner plume volume flux profiles are omitted for clarity.

5. Conclusions

A numerical model has been presented that extends our modeling abilities for a buoyant CO_2 plume in the deep ocean. The newly introduced detrainment relationship (12) provides a convenient numerical solution for downdraught flows that overlap, as is the case for CO_2 plumes. Although the entrainment relationship for the resulting counterflow is not well understood, the density feedback of the CO_2 dissolution provides a large enough driving force that the outer plume dominates the structure, and the dilution in the outer plume becomes insensitive to reasonable values for the entrainment coefficients. Thus, the near-field dilution of a CO_2 plume is controlled by the balance between the negative buoyancy of the dissolving CO_2 and the stratification, rather than by the buoyancy of the bubbles.

6. Acknowledgements

This work was supported by the MIT Sea Grant College Program, the National Energy Technology Laboratory of the U.S. Department of Energy, and the Deep Spills Task Force, comprised of the Minerals Management Service of the U.S. Department of Interior and a consortium of 13 member oil companies of the Offshore Operations Committee.

7. References

- Adams, E. E. & Herzog, H. J. (1996), Environmental impacts of ocean disposal of CO_2 , Technical Report MIT-EL 96-003, Energy Laboratory, MIT.
- Asaeda, T. & Imberger, J. (1993), 'Structure of bubble plumes in linearly stratified environments', *J. Fluid Mech.* **249**, 35-57.
- Lemckert, C. J. and Imberger, J. (1993), 'Energetic bubble plumes in arbitrary stratification', *J. Hydr. Engrg.* **119**, 680-703.
- Liro, C. R., Adams, E. E., Herzog, H. J. Modeling the Release of CO_2 in the Deep Ocean, Technical Report MIT-EL 91-002, Energy Laboratory, MIT.
- McDougall, T. J. (1978), 'Bubble plumes in stratified environments', *J. Fluid Mech.* **85**, 655-672.
- Milgram, J. H. (1983), 'Mean flow in round bubble plumes', *J. Fluid Mech.* **133**, 345-376.
- Morel, F. M. M. & Hering, J. G. (1993), *Principles and Applications of Aquatic Chemistry*, Wiley-Interscience, New York.
- Morton, B., Taylor, G. I., & Turner, J. S. (1956), 'Turbulent gravitational convection from maintained and instantaneous sources', *Proc. R. Soc. London Ser. A* **234**, 1-23.
- Reingold, L. S. (1994), An experimental comparison of bubble and sediment plumes in stratified environments, M.S. Thesis, Dept. of Civ. & Environ. Engrg., MIT, Cambridge, MA.
- Socolofsky, S. A., Crounse, B. C. & Adams, E. E. (2000), 'Bubble and droplet plumes in stratification 1: Laboratory studies' in Proc. IAHR 5th Int. Symp. Strat. Flow, Vancouver, BC, July 10-13.
- Socolofsky, S. A. (in prep.), Laboratory Experiment of Multi-phase Plumes in Stratification and Crossflow, Ph.D. Thesis, Dept. Civ. & Environ. Engrg., MIT, Cambridge, MA.
- Turner, J. S. (1986), 'Turbulent entrainment: the development of the entrainment assumption, and its application to geophysical flows', *J. Fluid Mech.* **173**, 431-471.
- Wüest, A., Brooks, N. H. & Imboden, D. M. (1992), 'Bubble plume model for lake restoration', *Wat. Resour. Res.* **28**, 3235-3250.

EXPERIMENTS TO INVESTIGATE CO₂ OCEAN SEQUESTRATION

Stephen M. Masutani¹, Masahiro Nishio², Guttorm Alendal³, and Gérard C. Nihous⁴

¹University of Hawaii, Hawaii Natural Energy Institute
2540 Dole Street, Holmes 246, Honolulu, Hawaii 96822 USA

²Mechanical Engineering Laboratory, Department of Energy Engineering
1-2 Namiki, Tsukuba, Ibaraki 305-8564 JAPAN

³Nansen Environmental & Remote Sensing Center
Edvard Griegsvei 3A, 5037 Solheimsvei, Bergen N-5037 NORWAY

⁴Pacific International Center for High Technology Research
2800 Woodlawn Drive, Suite 180, Honolulu, Hawaii 96822 USA

KEYWORDS: CO₂; ocean sequestration; environmental impact

ABSTRACT

An international collaboration to investigate the sequestration of CO₂ in the deep ocean was initiated in December 1997. The program is being funded by agencies of the governments of Japan, the U.S., Norway, Canada, and Australia; and Asea Brown Boveri (ABB) of Switzerland. The investigation comprises both experimental and modeling components. During the first phase of the program which runs through March 2002, a field experiment will be conducted in the summer of 2001 in which liquid CO₂ will be injected through various nozzles at a depth of approximately 800 m in the ocean at flow rates ranging from about 0.1 to 1 kg/s. Data will be obtained to develop and validate models that can be applied to predict induced changes to sea water chemistry. This paper describes the planned field experiment and presents selected results from laboratory and modeling studies that have been conducted to support the field experiment.

INTRODUCTION

Anthropogenic emissions of greenhouse gases may precipitate significant changes in global climate. The magnitude and extent of these changes are being actively investigated and debated. Carbon dioxide (CO₂) currently is the most important of these gases due to the preponderant quantities being released into the atmosphere by the combustion of fossil fuels. The latest Intergovernmental Panel on Climate Change (IPCC) assessment indicates that more than 80% of the heat trapping potential of anthropogenic greenhouse gas emissions is associated with CO₂ (UNFCCC, 1997).

International negotiations to establish practices that will stabilize atmospheric concentrations of greenhouse gases have been underway since 1992. In 1997, the Kyoto Protocol established legally-binding greenhouse gas emissions targets for Annex I industrialized countries. For the majority of these countries, the Protocol mandates that a 5% to 8% reduction of CO₂ emissions from 1990 levels be achieved sometime between 2008 and 2012 (UNFCCC, 1998).

Although renewables are being promoted to reduce greenhouse gas emissions, a major transition away from fossil fuels appears unlikely in the near-term. At present, practical and economic factors favor approaches such as increasing the percentage of electricity generated by nuclear power plants, energy conservation, switching from coal and oil to a lower-carbon fuel such as natural gas, and upgrading the efficiencies of fossil fuel energy systems.

Another approach to reduce greenhouse gas emissions into the atmosphere from fossil fuel combustors is to develop techniques to recover, reuse, and/or dispose of the 'fossil' CO₂ released by these devices. One technique that has emerged as a primary candidate for the control of atmospheric carbon emissions involves extraction of CO₂ from flue gases, followed by liquefaction and sequestration underground or in the deep ocean.

Removal and liquefaction of CO₂ from the effluent streams of industrial fossil fuel combustors can be accomplished utilizing existing technologies, albeit at substantial cost (Mori *et al.*, 1993; Herzog *et al.*, 1996). The technical viability of the concept as a means to stabilize emissions therefore depends on whether long term (i.e., of the order of centuries) sequestration of the captured CO₂ from the atmosphere can be achieved. Given the limited range of reuse options, huge quantities of CO₂ will need to be disposed of in an environmentally safe, and cost effective manner. Disposal in the ocean and in subterranean sites such as deep coal seams, spent gas and

oil wells, aquifers, salt domes, and rock caverns has been considered. While geological storage has the potential for very long term sequestration from the atmosphere—of the order of millennia—the world's oceans have a larger capacity to absorb CO₂. It has been estimated that the oceans can accept orders of magnitude more CO₂ than the amount that would be released by oxidation of all known recoverable fossil fuels reserves

The oceans currently remove at least 2 Gigatonnes (i.e., 2×10^{12} kg) of the 6-7 Gigatonnes of carbon released annually by human activity into the atmosphere. Over time, about 80% of this anthropogenic carbon is expected to find its way into the oceans. The slow process of exchange between the surface and deep zones of the ocean, however, constitutes a bottleneck that results in the accumulation of CO₂ in the atmosphere. While direct injection of CO₂ into the depths of the ocean would circumvent this bottleneck, associated impacts on the marine environment in the region surrounding the discharge need to be investigated. CO₂ readily goes into solution in sea water to form dissolved CO₂, and carbonate and bicarbonate ions (Millero & Sohn, 1992). One consequence of this process, however, is a depression of pH. While calcareous materials present in the deep ocean will buffer this effect, and dilution should limit acute changes in sea water chemistry, accurate quantification of these changes is not possible with existing data and models.

Laboratory experiments to investigate CO₂ ocean disposal phenomena have been pursued for over a decade (Masutani & Nihous, 1997). While these experiments have yielded important information, they will never be able to simulate completely the complex, large-scale discharge process. To address this limitation, an R&D program comprising a sequence of three field experiments of increasingly larger scale was authorized via a cooperative agreement signed in December 1997 by representatives of the Governments of Japan, the United States, and Norway. Since its inception, the Governments of Canada and Australia, and Asea Brown Boveri (ABB) of Switzerland, a private sector entity, have joined the program as sponsors.

EXPERIMENTAL PROGRAM

The experimental program has been described previously by Masutani & Nihous (1999), and Masutani (2000). Under the cooperative agreement, three separate field experiments will be conducted in the following sequence: (1) short-term tests of direct release of pure CO₂ at a depth of about 800 m at an open ocean site; (2) longer duration experiments to evaluate acute and chronic biological impacts; and (3) operation of an ocean sequestration test facility over several years to obtain extended-term operational data. Work on the first phase (short-term) field experiment officially was initiated following the signing of the cooperative agreement in December 1997 and will continue through the spring of 2002.

Liquid CO₂ released in the deep ocean is hydrodynamically unstable and will break up into a dispersed droplet phase. Within the depth regime that is accessible using existing pipeline technologies (say, $\leq 1,500$ m), the CO₂ droplets are buoyant and will rise as a plume through the density-stratified water column. A thin, solid hydrate phase may form on the droplet surface that impedes, but does not prevent dissolution (Aya & Yamane, 1992; Teng *et al.*, 1995; Hirai *et al.*, 1995). Sea water will be entrained into the rising droplet plume and transported upward to depths where the ambient water is less dense. Dissolution of CO₂ increases the density of the sea water in the plume. At various points in its ascent, heavy, CO₂-enriched sea water peels away from the plume and subsides to a level of neutral buoyancy (Liro *et al.*, 1992). This CO₂-enriched sea water subsequently is diluted and dispersed by ocean turbulence and currents.

The complex dynamics of the droplet plume in the stratified deep ocean, the effects of hydrates, and dilution and dispersion of CO₂-enriched sea water must be understood in order to address the issues of marine environmental impacts and the effectiveness of sequestration. Models currently are not capable of simulating the behavior of the CO₂ effluent with an acceptable level of confidence, and the fundamental physics of the process are not completely understood.

During the first field experiment, data will be obtained on changes induced in sea water chemistry by the release of pure CO₂. A preliminary sampling of biota and a study of the effects of the discharged CO₂ on naturally occurring bacteria populations also are planned. The specific objectives are:

1. investigate CO₂ droplet plume dynamics through qualitative flow visualization (using mobile video cameras) and quantitative measurements of velocity and pH in the plume and on its margins;
2. clarify the effects of hydrates on droplet dissolution through visualization of the droplet phase and measurements of the vertical extent of droplet rise using scalar indicators (either pH or other added tracers);

3. trace the evolution of CO₂-enriched sea water that peels from the plume by mapping the velocity and relevant scalar (e.g., pH or dissolved inorganic carbon) fields; and
4. assess potential impacts on marine biota by quantifying variations in bacterial biomass, production, and growth efficiency associated with induced changes in seawater pH.

Experiments are scheduled for the summer of the year 2001 at a facility on the west coast of the island of Hawaii. A series of tests with combined duration of about 40 hours will be conducted over two weeks. During these tests, pure liquid CO₂ will be pumped from refrigerated storage tanks installed on a ship to a depth of about 800 m through a small suspended conduit (3 to 6 mm i.d.). The liquid CO₂ will be discharged through different injectors installed at the end of the conduit. The discharge rate will be varied between 0.1 kg/s and 1 kg/s. A range of CO₂ discharge conditions (i.e., mass flow rate; injection velocity; droplet size) will be examined.

Data will be collected employing both fixed and mobile diagnostics. A video system mounted on an ROV (remotely-operated vehicle) will provide flow images of the CO₂ droplet plume. pH sensors and acoustic current profilers will be moored on the sea floor along with the ROV transponders to monitor ambient conditions. Detailed mapping of the scalar and velocity fields will be performed utilizing ROV-mounted instruments that will include conventional salinity, temperature, and pH probes. The ROV will collect data along a three dimensional survey path through the droplet plume and the region of CO₂-enriched sea water generated by the discharge. Water and sediment samples will be collected for chemical and biological analysis and CTD casts will be performed to supplement the data obtained with the moored arrays and ROV.

RESULTS

To support the planning and design of the 2001 field experiment, oceanographic surveys and modeling and laboratory studies are being conducted. A brief overview of this work is provided in this section.

An oceanographic survey of the experimental site off the west coast of the island of Hawaii was conducted during the first week of August 1999. A second survey is scheduled for October 2000. Data has been obtained that: (1) documents the background currents and sea water chemistry and density, and quantifies spatial and temporal variations of these quantities; (2) characterizes ambient bacterial production rates and their response to pH variations; and (3) characterizes the local benthic communities. During the survey, the performance of three methods to measure pH—a conventional glass electrode on the CTD; a novel IS-FET (ion specific field effect transistor) instrument; and shipboard photometric analysis of sea water samples—were compared and evaluated. Accurate and reliable measurements will be critical during the 2001 field experiment, since pH is a primary indicator of the released CO₂. Selected results from the 1999 oceanographic survey have been posted on the project website (<http://www.co2experiment.org>).

Laboratory experiments are being conducted to evaluate injectors and to address concerns related to flow instabilities, flow rate control, and hydrate blockage. Tests are being performed in pressure facilities at the Southwest Research Institute and the University of Hawaii (UH). Figures 1 and 2 present representative video frames obtained in a series of experiments at UH in which liquid CO₂ was pumped into a large pressure vessel to assess the performance of a multiple orifice prototype injector and to investigate hydrate blockage phenomena.

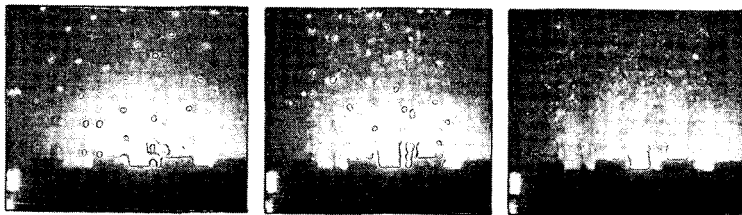


Figure 1 CO₂ injection into a laboratory pressure vessel. The frames show injection at different flow rates through an injector consisting of seven 2 mm diameter ASME sharp-edged orifices; water pressure = 56 bar; water temperature = 2°C.

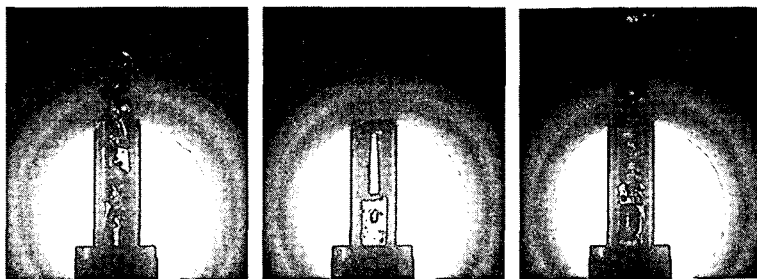


Figure 2 Liquid CO₂ and water flow through a clear nozzle used to investigate hydrate blockage; water pressure = 56 bar; water temperature = 3°C.

Estimates of the height of the droplet plumes and changes in the pH and dissolved CO₂ fields induced by the injection of liquid CO₂ during the experiment are needed to optimize the test plan and instrumentation; and for the Environmental Assessment report and permit applications. Several modeling activities have been pursued by the project team. The most sophisticated supercomputer model produces time-dependent spatial distributions of pH and dissolved and undissolved CO₂ concentrations for user-specified injection scenarios (Alendal *et al.*, 1998). Figure 3 presents one set of results for the Hawaii experiment site when liquid CO₂ is injected at 790 m at a rate of 1 kg/s in a 5 cm/s cross current. It is assumed that the injector produces a monodispersion of 14 mm diameter droplets. The mass transfer coefficient used in these simulations approximates the dissolution of liquid CO₂ droplets covered with a hydrate film. The results imply that the droplet plume will rise less than 150 m before dissolving completely. The lowest pH detected by the simulation for this case was about 6.1 (ambient pH = 7.5).

SUMMARY

A research program to investigate the feasibility of sequestering CO₂ in the deep ocean as a means to reduce the build-up of greenhouse gases in the atmosphere was initiated through an international cooperative agreement signed in December 1997. The program is funded by agencies of the Governments of Japan, the United States, Norway, Canada, and Australia; and Asca Brown Boveri. The program consists of a series of three separate field experiments of increasing magnitude and duration. The first field experiment will be conducted in Hawaii during the summer of 2001. Quantitative data will be obtained on the dissolution and transport of pure CO₂ released at a depth of about 800 m.

To support the planning and design of the field experiment, oceanographic surveys of the site, modeling studies, and laboratory experiments are being pursued. The modeling results suggest that, at the maximum test injection rate of 1 kg/s, a plume comprising relatively large 14 mm diameter droplets will rise less than 150 m before dissolving completely. The lowest pH detected by the simulation for this case was about 6.1 (ambient pH = 7.5). Laboratory studies indicate that a wide range of CO₂ droplet sizes can be generated through appropriate design and operation of the injector. Droplet size is a principal factor that determines the extent of the affected water volume and the magnitude of induced changes to sea water chemistry. Tests also are being performed to assess the potential of hydrate blockage and to devise strategies to avoid this problem.

ACKNOWLEDGMENTS

Support by the Research Institute of Innovative Technology for the Earth (RITE) via subcontracts through the Pacific International Center for High Technology Research and the U.S. Department of Energy under Contract No. DE-FG22-95PC95206 is gratefully acknowledged. This support does not constitute an endorsement by the Department of Energy of the views expressed herein. Experiments at UH were partially supported by the Japan Industrial Technology Association (JITA).

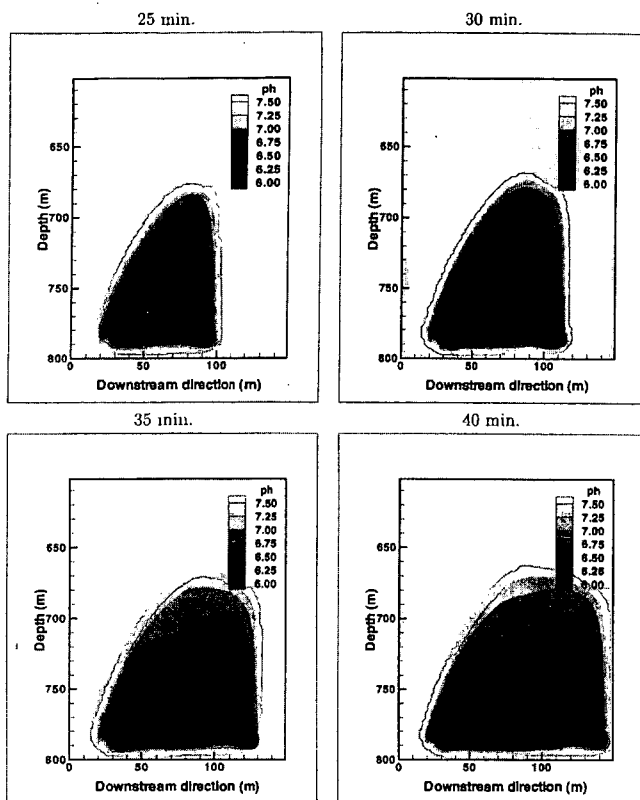


Figure 3 Supercomputer model predictions of pH distributions at different times after the start of injection; ambient pH is 7.5. 14 mm droplets of CO₂ are injected continuously at 1 kg/s at 790 m; mass transfer is assumed to be inhibited by a hydrate film.

REFERENCES

- Alendal G., H. Drange, and F. Thorkildsen, "Two-Phase Modelling of CO₂ Droplet Plumes," Technical Report No.153, NERSC, October 1998.
- Aya, I. And K. Yamane, "Stability of Clathrate-Hydrate of Carbon Dioxide in Highly Pressurized Water," *Proc. Winter Ann. Meeting of ASME*, HTD-Vol. 215, 17, 1992.
- Herzog, H. E. Drake, and E. Adams, "CO₂ Capture, Reuse and Storage Technologies for Mitigating Climate Change," White Paper prepared for U.S. Department of Energy, DE-AF22-96PC01257, 1996.
- Hirai, S., K. Okazaki, N. Araki, Y. Yazawa, H. Ito, and K. Hijikata, "Transport Phenomena of Liquid CO₂ in Pressurized Water Flow with Clathrate Hydrate at the Interface," *Energy Convers. Mgmt* 36(6-8), 471 (1995).
- Liro, C.R., E. Adams, and H. Herzog, 1992. "Modeling the Release of Carbon Dioxide in the Deep Ocean" *Energy Convers. Mgmt* 33(5-8), 667 (1992).
- Masutani, S.M. and G.C. Nihous, "Rig Techniques and Experiments," in *IEA Greenhouse Gas R&D Programme Report on Ocean Storage of CO₂, Workshop 4-Practical and Experimental Approaches* (W. Omerod, ed.), IEA Greenhouse Gas R&D Programme, Cheltenham, UK, 1997.
- Masutani, S.M., "A Field Experiment to Investigate CO₂ Ocean Sequestration," *Proc. Deep Sea and CO₂ 2000*, 2000.
- Masutani, S.M. and G.C. Nihous, "An Update on the International Field Experiment on CO₂ Ocean Sequestration," invited paper, in *Proc. 2nd International Symposium on Ocean Sequestration of Carbon Dioxide*, 1999.
- Millero, F.J. and M.L. Sohn, *Chemical Oceanography*, CRC Press, Boca Raton, FL, 1992.
- Mori, Y., S.M. Masutani, G.C. Nihous, L.A. Vega, and C.M. Kinoshita, "Pre-combustion Removal of Carbon Dioxide from Hydrocarbon-fuelled Power Plants," *Fuel* 72(9), 1293 (1993).
- Teng, H., C.M. Kinoshita, and S.M. Masutani, "Hydrate Formation on the Surface of a CO₂ Droplet in High-Pressure/Low-Temperature Water," *Chemical Engineering Science* 50(4), 559 (1995).
- UNFCCC, Document FCCC/SBI/1997/19/Add.1, from <http://www.unfccc.de/>, 1997.
- UNFCCC, Document FCCC/CP/1997/7/Add.1, from <http://www.unfccc.de/>, 1998.

DEVELOPMENT OF A HIGH-PRESSURE WATER TUNNEL FACILITY FOR OCEAN CO₂ STORAGE EXPERIMENTATION

Robert P. Warzinski and Ronald J. Lynn

U.S. Department of Energy, National Energy Technology Laboratory
P.O. Box 10940, Pittsburgh, PA 15236-0940

Anne M. Robertson and Igor V. Haljasmaa

University of Pittsburgh, Department of Mechanical Engineering
648 Benedum Hall, Pittsburgh, PA 15260

KEYWORDS: carbon dioxide, ocean sequestration, water tunnel

INTRODUCTION

The rising atmospheric levels of greenhouse gases, primarily CO₂, due to the production and use of energy is a topic of global concern. Stabilization may require measures other than fuel switching to lower carbon energy sources, increased use of renewable energy, and improvements in efficiencies. A new way of potentially limiting atmospheric increases of CO₂ while maintaining energy diversity is carbon sequestration which entails the capture and non-atmospheric storage of the carbon emitted from energy production and use. A recent report describes the key areas of research and development presently viewed as necessary to understand the potential of carbon sequestration for managing carbon emissions (1).

One potential storage option is to directly introduce CO₂ into the ocean at depths greater than about 500 m (1,2). Part of the carbon sequestration research program at the National Energy Technology Laboratory (NETL) of the U.S. Department of Energy has involved work in this area (3,4). This work has focused primarily on the impact on this storage option of the possible formation of the ice-like CO₂ clathrate hydrate (CO₂ · nH₂O; 6 < n < 8; referred to hereafter simply as hydrate) as either discrete particles or as coatings on drops of liquid CO₂. All of this prior work was performed in a small (less than 40 cm³) pressure vessel. While useful data on the formation, dissolution, and relative density of the hydrate were obtained, realistic simulation of the oceanic environment was not possible owing to contact of the species of interest with foreign (glass, stainless steel) materials in such a vessel. These foreign materials can influence hydrate formation and dissolution by acting as nucleation sites and providing unnatural heat transfer characteristics, both important factors in crystallization processes.

To attempt to overcome these limitations and provide a more realistic simulation of the deep ocean environment, a High-Pressure Water Tunnel Facility (HWTF) is being constructed that will permit experimental observations on objects such as CO₂ drops, hydrate particles or hydrate-covered CO₂ drops to be made without contact with materials other than seawater. The HWTF will permit the observation of buoyant objects in a windowed test section through the use of a countercurrent flow of water and special design features that provide for radial and axial stabilization. This paper describes the status of the experimental and theoretical efforts associated with the development of the HWTF.

DISCUSSION

In 1981, Maini and Bishnoi published work on the development of a high-pressure water tunnel to study hydrate formation on freely suspended natural gas bubbles in a simulated deep ocean environment (5). Their design considerations formed a starting point for the work at NETL on ocean sequestration of CO₂. As summarized in their paper, the hydrodynamic conditions necessary for holding an object in free suspension in such a device consist of: 1) the drag on the object should be equal to the force of buoyancy; 2) the axial velocity of the liquid should gradually increase with height to provide stability against vertical displacement; 3) the velocity distribution over a cross section of the liquid column should be axially symmetric with a local minimum at the center to provide stability against lateral displacement; and 4) the flow should be free of large-scale turbulence. To achieve the desired velocity profiles, an observation section with a tapered inner diameter and various flow conditioning devices inserted above and possibly below this section can be used.

A simplified schematic drawing of a water tunnel device is shown in Figure 1 (only inner diameters are shown). This device is placed in a flow loop that provides for recirculation of water through the system. For a positively buoyant object, the flow of water or seawater enters the top of the water tunnel and passes through a stilling section (not shown in Figure 1). At the end of the stilling section, a flow conditioning element is placed to provide the velocity profile required for radial stabilization of the buoyant object in the test section immediately below it.

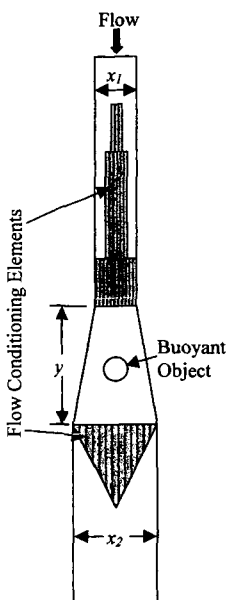


Figure 1. Schematic diagram of a water tunnel device

automatically moved across the section's diameter to obtain information related to local velocities. A computer-controlled positioning system translates the pitot tube across the test section and obtains the measurements needed to determine a velocity profile at this point in the system.

An example of velocity profile data obtained in this manner over a range of flow rates is shown in Figure 2. Only an upstream flow conditioning element similar to the top one in Figure 1 was used to create the velocity profiles shown in Figure 2.

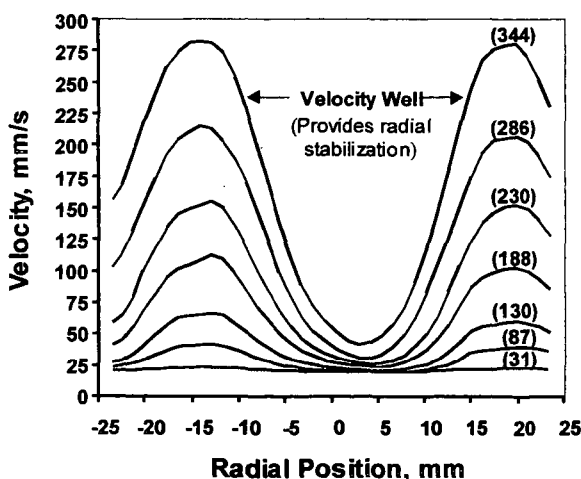


Figure 2. Velocity profiles obtained in LWTF test section using a pitot tube inserted 7.5 cm below the flow conditioning element. Each curve was obtained at a different total flow rate (average flow in cm^3/s shown in parentheses). Radial position is measured from the center of the test section.

The top flow conditioning element shown in Figure 1 represents a bundle of small tubes of different length. Various other configurations are possible. Increasing the length of the tubes in the center results in more head loss in this region and results in flow redistribution with the desired local velocity minimum in the center of the water tunnel. The diameter of the test section increases from top to bottom ($x_2 > x_1$) which provides the downstream axial velocity drop required for axial stabilization. At the exit of the test section, another flow conditioning element may be used. In Figure 1, this lower element depicts another possible tube bundle shape that could be used. A final stilling section is located after the test section (again not shown in Figure 1). Design variables affecting the velocity profile in the test section include the geometries of the conditioning elements and the divergent test section.

Both experimental and theoretical work is in progress at NETL to determine the required design parameters needed for stabilization of CO_2 in a HWTF over the range of anticipated ocean injection conditions. A Low-Pressure Water Tunnel Facility (LWTF) of similar internal dimensions ($x_1 = 5.08 \text{ cm}$, $x_2 = 6.35 \text{ cm}$) has been built to test various designs and provide information for the theoretical treatment of this problem. It consists of the water tunnel which is constructed of plexiglass pipe, a 5.08 cm ID flow loop of PVC plastic pipe, and a variable-speed centrifugal pump for water circulation. An ultrasonic flow sensing system is used to measure the total flow rate in the loop. An S-shaped pitot tube was fabricated and calibrated at NETL for insertion through ports in the test section and is

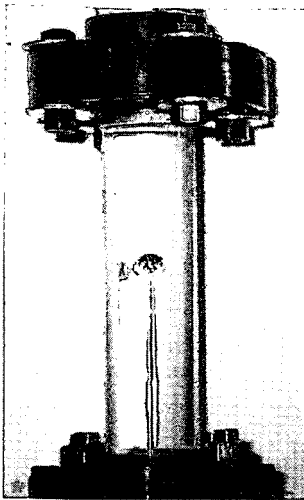


Figure 3. Air bubble stabilized in the test section of the LWTF.

Figure 3 shows an air bubble stabilized in the test section of the LWTF. Similar stability was also achieved using plastic spheres of varying size and density. A single flow conditioning element similar to the one shown in Figure 1 at the top of the test section was used. It consisted of a tube bundle containing longer tubes in the center.

In previous work (5,6), different types of flow conditioning elements were used; however no systematic analyses were performed to relate possible configurations of the flow conditioning elements to the velocity profile and the resulting positional stability of the buoyant object. Presently, in the work at NETL, theoretical optimization of flow conditioning element configuration is being pursued. This work is divided into two steps:

1. Given the mass and density of the bubble or drop (hereafter referred to as fluid particle), determine the optimal velocity profile to stabilize the position of the fluid particle;
2. Given the optimal velocity profile, find the geometry of the flow conditioning element(s) which not only produce such a profile, but also minimize

degeneration of it through the test section.

The optimum velocity profile for fluid particle stabilization is expected to vary with the regime of flow. Prior work by various researchers on bubbles and on rising and falling drops in different fluids reveals a variety of regimes, the realization of which depends on a small number of non-dimensional parameters. A non-dimensional analysis is therefore necessary to determine the relevant independent parameters for the anticipated regimes in a water tunnel device.

If a uniform flow of an incompressible fluid past the fluid particle is considered and if the effects of the wall and flow inside the fluid particle are ignored, then there are six parameters of interest, which are summarized below in Table 1.

Table 1. Parameters of Interest for Flow Analysis

Variable	Definition	Dimensions (MLT)
D_e	Effective Diameter	L
U	Free Stream Velocity	L/T
ρ_l	Liquid Density (water)	M/L^3
$\Delta\rho$	Density Differential ($\rho_l - \rho_g$)	M/L^3
μ_l	Viscosity of Liquid	$M/(LT)$
γ	Surface Tension	M/T^2

There are three primary dimensions for the six physical and geometric parameters: mass, length, and time (MLT). From the Buckingham Pi Theorem, it follows that there will be three independent dimensionless numbers for this system. The choice of these dimensionless parameters is not unique, which means there is some freedom to choose parameters which are the most suitable for this analysis.

It is helpful to relate the definitions of the dimensionless numbers to characteristic values of the effective forces acting on the fluid particle. Four considered effective forces are shown below in Table 2.

Table 2. Effective Forces Acting on a Fluid Particle

Effective Forces	Characteristic Magnitudes
Viscous Forces	$\mu_l U D_e$
Buoyancy Forces	$\Delta\rho g D_e^3$
Surface Tension Forces	γD_e
Inertial Effects	$\rho_l U^2 D_e^2$

Displayed in Table 3 are the definitions of commonly used dimensionless numbers for bubbles in uniform flow. Various triplets of these dimensionless numbers are used in the literature (7,8):

Table 3. Dimensionless Variables for Flow Analysis

Non-dim. Variable	Name	Ratio of Physical Phenomena	Definition
Re	Reynolds Number	Inertial/viscous	$\rho_l U D_e / \mu_l$
Ca	Capillary Number	Viscous/surface tension	$\mu_l U / \gamma$
Eo	Eotvos Number	Buoyancy/surface tension	$(\Delta \rho g D_e^2) / \gamma$
We	Weber Number	Inertial/surface tension	$(\rho_l U^2 D_e) / \gamma$
Wg	Inertial Buoyancy Parameter	Inertial/buoyancy	$(\rho_l U^2) / (\Delta \rho g D_e)$
Cg	Viscous Buoyancy Parameter	Viscous/buoyancy	$(\mu_l U) / (\Delta \rho g D_e^2)$
Mo	Morton Number		$(\Delta \rho g \mu_l^4) / (\rho_l \gamma^3)$

Reference 7 considers shape regimes for fluid particles as a function of Re and Eo numbers. There exist two limiting cases where the analysis can be significantly simplified:

Case 1. Small Re and Eo numbers, under which the fluid particle has an almost spherical shape. Often, this regime is realized for very small particles (<0.5mm in diameter), or for the slow motion of the fluid particle caused by a very small buoyant force (small difference in density). In this case the terminal velocity of the fluid particle can be expressed (9,10) as:

$$U_{term} = \frac{1}{K} \frac{D_e^2 g \Delta \rho}{\mu_l} \quad (1)$$

(constant K spans from 12 to 36 in different theories and is believed to depend on surface active impurities in the liquid).

Case 2. Large Re and Eo numbers, under which the fluid particle has a spherical cap shape with a well determined front boundary and an unstable, wavy rear boundary caused by the wake behind the fluid particle. Often, this regime is realized for large bubbles (> 2 cm³ volume), when inertial effects dominate viscous effects and surface tension. Then, the terminal velocity of the fluid particle can be expressed (7) as:

$$U_{term} = \frac{2}{3} \sqrt{g R \frac{\Delta \rho}{\rho_l}} \quad (2)$$

where R is radius of curvature of the fluid particle at the stagnation point.

For intermediate values of Re and Eo, different kinds of transitional regimes occur which are essentially unstable. Therefore, it would be beneficial to design experiments corresponding to one of the limiting cases outlined above.

The liquid CO₂ particle/seawater system is expected to exhibit Case 1 behavior since the densities of seawater and CO₂ are not that different under anticipated direct ocean injection conditions. Owing to its greater compressibility, at depths greater than about 2700 m, liquid CO₂ can even be more dense than seawater. Sphericity of the fluid particle can significantly simplify both the theoretical analysis and experimental observations. Past experimental works show that for a small Re number, fluid particles of almost spherical shape exhibit a rectilinear motion. As the Reynolds number is increased, the wake behind the particle begins to oscillate and further increases in Reynolds number lead to periodic shedding of the vortices (9). Absence of lateral oscillations and significant wakes behind the fluid particle at low Reynolds numbers makes this regime very attractive for initial experiments involving hydrate formation. Hence, it would be useful to determine the optimum size of the fluid particle, small enough to be in the spherical regime, but big enough for meaningful observations. Preliminary non-dimensional analysis shows that at the depths of about 2400-3000 m, a CO₂ fluid particle of 1-cm diameter should be close to spherical. When the optimum size of the fluid particle is determined, optimum flow conditioning elements for this particular size can be developed.

The HWTF has been designed to permit investigation of other species, such as other flue gas components (N₂, O₂, SO₂) and natural gas components, which may have properties quite

different than those of CO₂. In these cases, behavior more like Case 2 may be encountered. The modeling work will eventually be extended to develop flow conditioning elements for such systems.

In conjunction with the measurements being made using the LWTF, a preliminary simplified analytical evaluation of the flow conditioning system used in LWTF has been completed. This evaluation provides an approximation for the velocity distribution immediately downstream of the flow conditioner due to different resistances across the tube bundle system. Having a data base of different profiles corresponding to different flow conditioners will permit the appropriate design of the flow conditioner to be selected to meet the desirable velocity profile for fluid particle stabilization. It will then be used to guide the design of the flow conditioning elements for the HWTF.

In order to avoid the assumptions inherent in the simplified analytical evaluation, full three-dimensional finite element analysis (FEA) of the flow through the conditioning element will be performed. This numerical approach enables both a more accurate model of the actual element geometry and the exploration of the velocity profile degeneration downstream of the conditioning element.

The numerical domain will include a straight section upstream of the spoiler, the spoiler system, and the diverging/converging test section downstream of the spoiler. The straight upstream section is included since the velocity profile immediately upstream of the flow conditioning element is not known a priori. This length of the upstream section is made long enough to approximate fully developed inlet conditions. If necessary, the actual inlet geometry of the experimental device can be included. From this three dimensional analysis, velocity profiles throughout the test chamber can be obtained.

The theoretical analyses described above is a sizeable analytical and numerical challenge. This work is not only necessary for the design optimization of the flow conditioning elements and internal geometry of the HWTF for CO₂ ocean sequestration research, but will also be useful in utilizing the device in applications involving different fluids.

ACKNOWLEDGEMENTS

The authors wish to thank Jerry Foster and Jay Levander for their assistance in developing the LWTF.

REFERENCES

1. *Carbon Sequestration Research and Development*, U.S. Department of Energy Report, DOE/SC/FE-1, 1999, available NTIS.
2. Herzog, H. *Greenhouse Gas Control Technologies*, B. Eliasson, P.W.F. Riemer, and A. Wokaun, eds., Pergamon, Amsterdam, 1999, 237-242.
3. Warzinski, R.P., G.D. Holder *Ibid*, 1061-1063.
4. Warzinski, R.P., R. J. Lynn, G.D. Holder *Third International Conference on Gas Hydrates, Annals of the New York Academy of Sciences*, in press, 1999.
5. Maini, B.B. & P.R. Bishnoi *Chem. Engng. Science* **36**, 1981, 183-189.
6. Moo-Young, M., G. Fulford, I. Cheyne. *Ind. Eng. Chem. Fundam.*, **10**(1), 1971, 157-160.
7. Clift, R., J. R. Grace, M. E. Weber. *Bubbles, Drops, and Particles*, Academic Press, 1978.
8. Leal, L.G. *Computational Studies of Drop and Bubble Dynamics in a Viscous Fluid*, Drops and Bubbles, Third International Colloquium, 1988, 147-168.
9. Batchelor, G.K. *An Introduction to Fluid Dynamics*, Cambridge Univ. Press, 1967.
10. L.-S. Fan, K. Tsuchiya, *Bubble wake Dynamics in Liquids and Liquid-Solid Suspensions* (Butterworth - Heinemann), 1990.

**CHARACTERISTICS AND PERFORMANCE
OF A DEEP OCEAN DISPOSAL SYSTEM
FOR LOW-PURITY CO₂ GAS BY GAS LIFT EFFECT**

Takayuki Saito
National Institute for Resources and Environment
Onogawa 16-3, Tsukuba
Ibaraki 305-8569, Japan
(Permanent address: Shizuoka University
3-5-1 Johoku, Hamamatsu
Shizuoka 432-8561, Japan)

Sanai Kosugi
Sumitomo Metal Industries Ltd.
8-2, Honshio-cho, Shinjuku-ku
Tokyo 160-0003, Japan

Takeo Kajishima
Osaka University
2-1 Yamadaoka, Suita
Osaka 565-0871, Japan

Katsumi Tsuchiya
Tokushima University
Minamijosanjima-cho, Tokushima
Tokushima 770-0814, Japan

KEYWORDS: Gas lift effect, Ocean disposal, Carbon dioxide

ABSTRACT

Progressive Gas Lift Advanced Dissolution (P-GLAD) system has been newly developed to mitigate the global warming. The system dissolves low-purity CO₂ gas in seawater at shallow portions and sequesters CO₂ at the deep ocean. The system is an inverse-J pipeline set in the ocean between 200 and 3000m in depth. Usual methods of deep-sea sequestration such as storage of liquid CO₂ at the deep-sea floor and deep-sea releasing of liquid CO₂ consume huge amount of energy, because these need high-purity capture and liquefaction of CO₂. To realize deep-sea sequestration with low energy consumption and low environmental impact, we utilize a gas-lift effect to dissolve low-purity CO₂ into seawater and transport CO₂ solution to a great depth. The present paper describes basic characteristics and performance of the system for low-purity CO₂ gases. We also discuss cost estimate including a system for capture of CO₂ gas and construction of P-GLAD.

INTRODUCTION

The global warming mainly due to the increase of atmospheric CO₂ concentration is getting serious. A countermeasure that can economically and effectively treat huge amount of CO₂ (23Gt/year) emitted by human activities should be developed. Ocean sequestration of CO₂ is a hopeful option to mitigate the increase in the atmospheric CO₂ concentration, because the ocean has been absorbing and sequestering CO₂ through the history of the earth, and the absorption capacity is enormous [Hoffert, 1979]. Several ideas of ocean disposal of CO₂ have been proposed. They are categorized as follows: a) storage of liquid CO₂ on the deep-sea floor deeper than about 3000m, in the idea CO₂ is stored on the deep sea floor as CO₂ ponds covered with CO₂ gas hydrate [Ohsumi, 1993]; b) direct release of liquid CO₂ into the intermediate depth water of 1000-3000m [Liro, 1992]; c) direct release of gaseous CO₂ into shallow water and use of gravity current [Haugan, 1992], the idea is direct release of gaseous CO₂ into the seawater at a depth of 200-400m and expecting sink of CO₂-rich seawater to the deep-sea by the density difference between the solution and ambient seawater.

Long term isolation, more than several hundreds years, of CO₂ from the atmosphere is expected in the methods a) and b), because the initial injection point is in intermediate or deep water. Though deeper initial injection assures longer-term isolation, these two methods need high-purity capture and separation, and liquefaction of CO₂. Higher-purity separation of CO₂ from exhausted gas consumes larger energy. They inevitably consume huge amount of extra energy in these preprocessing. The deep initial injection brings the deep ocean secondary environmental impact, namely acidity by dense CO₂ solution. Since the method c) need no liquefaction, it improves an amount of energy consumption. Density and/or temperature layers in the ocean, which grow in middle and low latitude area, prevent sinking of CO₂ solution to a great depth. In this case, long-term isolation is no longer expected.

A method of the ocean sequestration has to isolate huge amount of CO₂ from the atmosphere for long term, several hundreds or thousand years, with low cost, low energy consumption and low environmental impact. To realize this, the preprocessing should be low-purity separation and no

liquefaction; besides the disposal method should be able to deal with low-purity CO₂ gas. We have been improving GLAD system, which is an ocean sequestration system for pure CO₂ gas using gas lift effect [Saito, 1996; Saito 1997; Saito, 2000; Kajishima, 1995; Kajishima, 1997]. We have developed P-GLAD (Progressive Gas Lift Advanced Dissolution, See Fig.1) system [Saito, 1999a, b] for low-purity CO₂ gas. In the present paper, we discuss performance, cost estimate and environmental receptivity of P-GLAD by experimental and numerical simulation. First, we describe experimental results on solubility and pumping performance of the system. Second, essence of numerical method is explained. Agreement of numerical results with experimental ones is discussed. Third, acidity of the solution released from the system is discussed. Finally, based on these discussions cost estimate for P-GLAD and comparison of the cost with usual method are performed.

EXPERIMENT

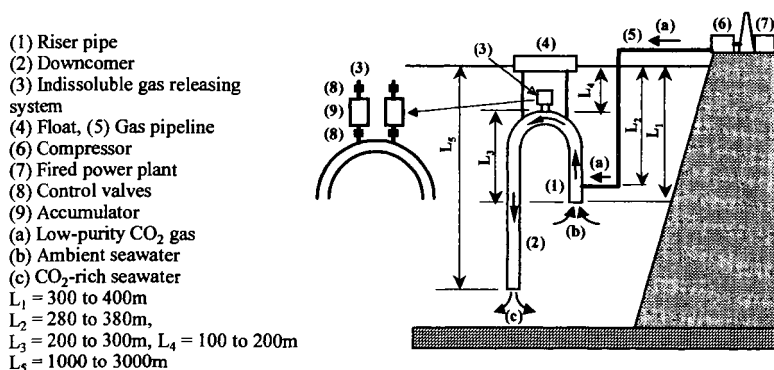
Experimental setup used in the present investigation, a laboratory-scale P-GLAD system, is illustrated in Fig. 2. The riser pipe (1) and the downcomer (2) are made of acrylic transparent pipes of 25mm in diameter and 7.69m in height. The riser is connected to two pressure vessels (4) made of stainless pipe of 106.3mm in diameter and 8.19m in height. The downcomer is placed inside the vessel. The top of the riser is equipped with an indissoluble gas-releasing device (3), which releases indissoluble gases of N₂ and O₂. Low-purity CO₂ gas, mixture of pure CO₂ gas (99.9% purity) and pure air (CO<1ppm, CO₂<1ppm and CH₄<1ppm) well mixed in a gas-mixing accumulator (10), is injected into the riser through a gas injector (5). The gas-injector has an annular structure; the inner pipe of acrylic resin with 25mm in diameter is equipped with 108 small capillaries of 0.78mm in diameter; outer pipe is made of stainless steel of 106.3mm in diameter.

Tap water is supplied at the top of each pressure vessel after filtration by a 1μm filter. Our experiments were performed under overflowing condition. The temperatures of the supplied water and the gas-liquid mixtures were between 287 and 290K.

MESUREMENT

Superficial velocity of the liquid phase J_L was measured using an electromagnetic flowmeter (A), the temperature and static pressure in the riser using thermo couples (B) and pressure transducers (C), respectively. We measured and controlled mass flow rate of each gas, Q_{CO_2} and Q_{AIR} using mass flow controllers (E) and (F).

Performance of solubility of the laboratory-scale P-GLAD is calculated from CO₂ molar concentration of the gas phase in the riser [Saito, 1999a]. First, we visualized and recorded the bubbly flows in the riser using two sets of high-speed video systems of 500 frames/s and stroboscopes of 10μs of flushing rate (C). Second, we analyzed the images by digital image processing. Third, bubble characteristics such as volume, surface area, location and velocity were calculated from the processing results. Finally, the molar concentration and solubility were calculated from the above characterization of bubbles.



The main part of the P-GLAD system is an inverse-J pipeline (1) and (2), and an indissoluble gas releasing system (3). The low-purity CO₂ gas (a) is injected into the riser pipe (1) at a depth between 200 and 400m. An upward current occurs in the pipe by a gas-lift effect. CO₂ included in the bubbles dissolves into seawater while the bubbles rise in the riser. Ambient seawater (b) is flowing at the bottom of the riser. Indissoluble gas of N₂ is released at the top of the riser by an indissoluble gas releasing system (3). The downcomer (2) is used as a transportation pass of the CO₂-rich seawater (c) to a great depth between 1000 and 3000m. An additional downward current is generated in the downcomer owing to the density difference between the CO₂-rich and ambient seawater. Thus, the bubble dissolution and the transportation of CO₂-rich seawater to great depths are enhanced in the P-GLAD system by the gas lift effect.

Fig.1 Concept and principle of the P-GLAD system

- (1) Dissolution pipe
 - (2) Drainpipe
 - (3) Indissoluble gas releasing device
 - (4) Pressure vessels
 - (5) Gas injector
 - (6) Observing windows
 - (7) Camera lifter
 - (8) CO₂-gas cylinder
 - (9) Pure-air cylinder
 - (10) Gas mixing accumulator
- (A) Electromagnetic flowmeter
 - (B) Thermo couplers
 - (C) Pressure transducers
 - (D) High-speed video systems & strobes
 - (E) & (F) Mass flow controller

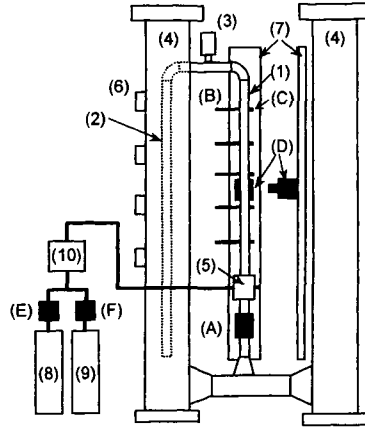


Fig. 2 Experimental setup

NUMERICAL SIMULATION

The Lagrange method was applied for the each bubbles, and the Euler method for the liquid phase. Conservation laws of mass and momentum for each phase were employed. Trapp & Mortensen scheme was used in our computation [Trapp, 1993]. In the present investigation, applying the Lagrange method mass conservation law of dispersed gas phase is expressed as following equation.

$$\frac{d}{dt}(\rho_p V_p) = -k_L M_p (C_s - C) A_p \quad (1)$$

where k_L represents the mass transfer coefficient, $V_p (= 4\pi r_p^3/3)$ the bubble volume, $A_p (= 4\pi r_p^2)$ the surface area, and r_p the equivalent diameter of bubble. Density of gas phase ρ_p is calculated from the ideal gas equation. C_s is the molar concentration of CO₂ on the bubble surface and defined as saturated concentration of CO₂ calculated from Henry's law. C is the molar concentration of CO₂ in the solution, estimated by the equation of convective diffusion.

$$\frac{dC}{dt} + J_i \frac{dC}{dx} = D_i \frac{d^2 C}{dx^2} + q_s \quad (2)$$

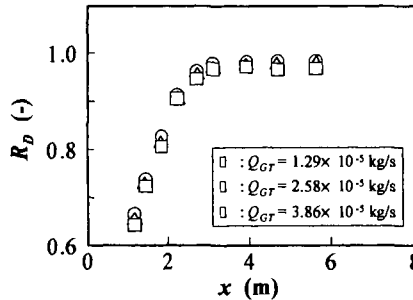


Fig. 3 Axial profiles of dissolution ratio in the riser. $Q_{GT} = Q_{CO_2} + Q_{AIR}$

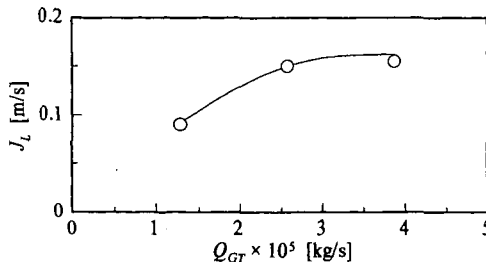


Fig. 4 Superficial velocity of liquid phase in the riser as a function of gas injection rate.

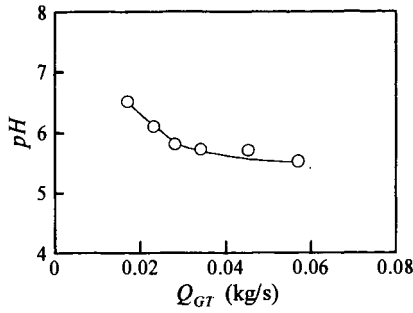


Fig. 5 Acidity of CO₂ solution discharged from the laboratory P-GLAD.

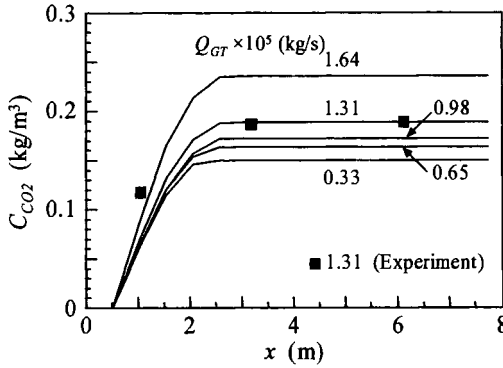


Fig. 6 Computational results on CO₂ concentration in solution compared with experimental ones.

q_g represents the rate of dissolution, $J_l [(1 - \alpha)u_l]$ the superficial velocity of liquid phase, α the void fraction, u_l the velocity of liquid phase. D_T is the turbulent diffusion coefficient calculated from liquid phase flow of Reynolds number $J_l D/\nu$ using $k-\varepsilon$ model, where ν is kinematic viscosity.

EXPERIMENTAL AND COMPUTATIONAL RESULTS

Defining CO₂ gas dissolution ratio as $R_D = Q_{CO_2, dis}/Q_{CO_2}$, the axial profile is plotted in Fig. 3, where $Q_{CO_2, dis}$ represents the mass of CO₂ dissolved in liquid phase, and Q_{CO_2} the mass of CO₂ included in injected gas. R_D rapidly increases for $z < 3$ m, and most of the CO₂ gas injected dissolves into the water phase in the section. The maximum values of R_D are 0.979, 0.955 and 0.964. P-GLAD shows satisfactory performance of CO₂ gas dissolution.

Superficial velocity of liquid phase J_L , namely lifted water velocity, is shown in Fig. 4 as a function of gas injection rate Q_{GT} . J_L gradually increases with increase in Q_{GT} before 3×10^{-5} kg/s. After the value, J_L is almost saturated. In higher gas injection rate, it was observed that indissoluble gas remained at the top of the riser. As a result, saturation of J_L occurs owing to increase in friction loss there.

Acidity of CO₂ solution discharged from laboratory-scale P-GLAD is plotted in Fig. 5 as a function of gas injection rate. The acidity increases with increase in gas injection rate. The value of pH is in the range between 5.5 and 6.5 in the present investigation. The acidity is moderate. Besides the acidity is controllable by adjusting the gas injection rate.

Figure 6 shows computational results on CO₂ concentration in solution and comparison of them with those of the experiment. Computational results show a good agreement with the experimental ones. Therefore, our numerical modeling and computational scheme is reasonable.

COST ESTIMATE

Before cost estimate, we carried out experiments using a large-diameter-pipe loop (150mm in diameter). Large-scale structure and turbulence mechanism of bubbly flows in a large diameter pipe were obtained [Mudde & Saito, 2000]. We performed cost estimate of P-GLAD for 1,000MW fired power plant listed in Table 1 on the basis of above experimental and numerical results. Gas transportation plant, CO₂ capture and separation plant, and dimension of P-GLAD

Table 1 Dimension of fired power plant.

Generating capacity	1,000MW
Location	Seaside
Rate of CO ₂ discharge	100kg/s (360ton/s)

Table 2 Gas transportation plant.

Compressor power	40,000kw
Compressor location	Power plant site
Length of pipeline	100km
Diameter of pipe	0.5m
Material of pipe	High-tension steel

Table 3 CO₂ capture and separation plant.

Method	PSA (1 stage)
Adsorption	Under atmospheric pressure
Degassing	Under vacuumed
Dewatering tower	$\phi 12.5\text{m} \times \text{H}36\text{m} \times 16\text{units}$
Number of adsorption/de-gassing tower	$\phi 6\text{m} \times \text{L}40\text{m} \times 16\text{units}$
Adsorption material for CO ₂	Zeorite
Adsorption material for water	Activated aluminum + Zeorite

Table 4 Dimension of P-GLAD.

Riser	$\phi 0.5\text{m} \times \text{H}300\text{m} \times 90\text{units}$, High-tension steel
Downcomer	$\phi 0.5\text{m} \times \text{L}10\text{km} \times 90\text{units}$, Rain-forced FEP steel
Gas injection depth	200m
Releasing depth	1000m
Float	$\phi 11.6\text{m} \times \text{W}150\text{m}$
Anchoring	Tension leg

Table 5 Cost estimate of P-GLAD and comparison of the cost with that of a usual method (direct release of liquid CO₂).

	P-GLAD (US\$/ton-CO ₂)	Usual (US\$/ton-CO ₂)
Capture & separation	26	43
Liquefaction	0	64
Transportation	30	7
Sequestration	12	12
Total	68	126

are listed in Table 2 to Table 4, respectively. We estimated a total cost of the ocean sequestration by P-GLAD considering construction, operation, labor cost (in Japan), land cost (in Japan), tax (in Japan), interest and a price reduction. The result is summarized in Table 5.

Total cost of P-GLAD is a half of that of a usual method. Economical feasibility of P-GLAD is very higher than that of a usual method such as direct release of liquid CO₂ into intermediate depth water.

CONCLUSION

We discussed performance and characteristics of P-GLAD (Progressive Gas Lift Advanced Dissolution system) experimentally and numerically. We obtained P-GLAD has satisfactory performance as an ocean sequestration system of low-purity CO₂ gas. On the basis of these results, we performed cost estimate of a total system of P-GLAD. P-GLAD showed highly economical feasibility.

REFERENCE

- Haugan, P. M. & Drange, H., *Nature*, Vol. 357, 318, (1992).
Hoffert, M. I., Wey, Y. C., Callegari A. J. & Broecker, W. S., (1997), *Climatic Change*, Vol. 1, 59.
Kajishima, T., Saito, T. and Nagaosa, R., (1995), *Energy Conve. and Manag.*, Vol. 36, 467.
Kajishima, T., Saito, T. and Nagaosa, R., (1997), *Energy*, Vol. 22, 257.
Liro, C. R., Adams, E. E. & Herzog, H. J., (1992), *Energy Conve. and Manag.*, Vol. 33, 667.
Mudde, R. F. and Saito, T., submitted to *J. of Fluid Mech.*, (2000)
Ohsumi, T., *Energy Conversion and Management*, Vol. 34, 1059, (1993).
Saito, T., Kajishima, T., Tsuchiya, K. and Kosugi, S., (1999a) *Chem. Eng. Sci.*, Vol. 54, 4945.
Saito, T., Kajishima, T., and Tsuchiya, K., (1999b), applied to EU, US and Australian patent.
Saito, T. and Kajishima, T., (1996), *ACS, Division of Fuel Chemistry*, Vol. 41, 1441.
Saito, T. and Kajishima, T., (1997), US patent, No. 5662837.
Saito, T., Kajishima, T. and Nagaosa, R., (2000), reviewed in *ES & T*.
Trapp, J. A. and Mortensen, G. A., *J. of Comput. Phys.*, Vol. 107, 367, (1993)

An Integrated Approach to Utilization of Coal for Specialty Chemicals, Materials and Advanced Jet Fuels

Chunshan Song* and Harold H. Schobert

Applied Catalysis in Energy Laboratory, The Energy Institute, and
Department of Energy & Geo-Environmental Engineering, Pennsylvania State University
209 Academic Projects Building, University Park, PA 16802-5000

Keywords: Coal Utilization, Chemicals, Materials, Fuels

ABSTRACT

This paper will discuss an approach in research for more effective conversion and comprehensive (fuel and non-fuel) utilization of coal for making specialty organic chemicals, carbon-based materials and advanced thermally stable jet fuels. It also discusses shape-selective synthesis of specialty chemicals and polymer materials from coal-derived liquids.

1. INTRODUCTION

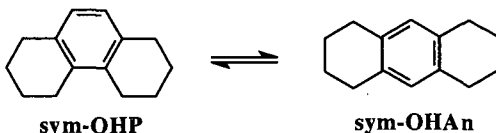
This article is a selective overview for recent research in our laboratory that was designed for more effective conversion and comprehensive utilization of coal for making specialty organic chemicals, carbon-based materials and advanced thermally stable jet fuels. We are taking an integrated approach for both non-fuel and fuel uses that make effective uses of the unique structural features of coals. The non-fuel uses of coal has been discussed at length in our previous reviews that were written in response to the invitations by the late Prof. Frank Derbyshire [Song and Schobert, 1993, 1996].

2. SPECIALTY CHEMICALS

Coal-derived liquids contain various 1-ring to 4-ring aromatic structures. Many of the 2-4 ring structures are not readily available from petroleum, and thus the coal tars are still the major sources of the 2- to 4-ring aromatic chemicals in the world today. Our attention on chemicals has focused on shape-selective catalytic synthesis of value-added chemicals from polycyclic aromatic compounds that are rich in coal liquids and some refinery streams. As outlined in recent reviews [Song, 1998, 1999], we are studying ring-shift isomerization of phenanthrene derivatives to anthracene derivatives, shape-selective alkylation of naphthalene, shape-selective alkylation of biphenyl, conformational isomerization of cis-decahydronaphthalene, and shape-selective hydrogenation of naphthalene, and regio-selective hydrogenation of hetero-aromatic compounds, as described below.

Ring-Shift Isomerization. Phenanthrene and its derivatives are rich in various coal-derived liquids such as coal tars, but their industrial use is still very limited. On the other hand, anthracene and its derivatives have found wide industrial applications. We have found that some mordenite and ion-exchanged Y zeolite catalysts selectively promote the transformation of sym-octahydrophenanthrene (sym-OHP) to sym-octahydroanthracene (sym-OHAN), which we call ring-shift isomerization, as shown in Scheme I. The selectivity and activity of the catalysts also depend on the reaction conditions. This reaction is in distinct contrast to the well-known ring-contraction isomerization which results in methylindane-type products.

Scheme I



Under mild conditions, some zeolites can afford over 90% selectivity to sym-OHAN with 50% conversion of sym-OHP. This could provide a cheap route to anthracene and its derivatives, which are valuable chemicals in demand, from phenanthrene that is rich in liquids from coal. Possible uses of sym-OHAN include the manufacturing of anthracene (for dyestuffs), anthraquinone (pulp agent), and pyromellitic dianhydride (the monomer for polyimides such as Du Pont's Kaption).

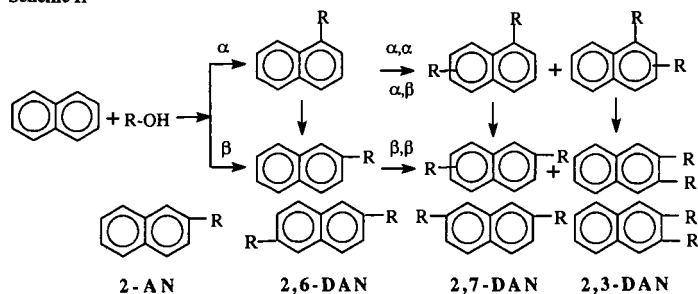
Shape-selective alkylation of naphthalene.

Due to the demand for monomers for making the advanced polymer materials such as PEN and PBN, 2,6-dialkyl substituted naphthalene (2,6-DAN) is needed now for making the monomers for PEN, PBN and LCPs. In tars or liquids derived from coal, naphthalene and its derivatives are major components. Shape-selective alkylation over molecular sieve catalysts can produce 2,6-DAN. There are ten possible DAN isomers (Scheme II). The β,β -selective alkylation over molecular sieve catalysts can produce 2-alkylnaphthalene, 2,6-, 2,7-, and 2,3-DAN [Frankel et al., 1986; Komatsu et al., 1994]

The key challenge is to obtain 2,6-DAN with high selectivity, which means increasing the ratio of 2,6/2,7-DAN. Many reports have been published on synthesis of 2,6-DIPN (diisopropylnaphthalene) [Katayama et al., 1991; Moreau et al., 1992] because isopropylation can give much higher selectivity to the 2,6-isomer than the methylation, and an excellent review has been published by Sugi and Kubota [1997]. The results from our laboratory showed that by using partially dealuminated mordenite catalysts, selective alkylation of naphthalene can be achieved with over 65% selectivity to 2,6-DIPN by using isopropanol with 2,6-DIPN/2,7-DIPN ratio of about 3 or using propylene as the alkylating agent with 2,6-DIPN/2,7-DIPN ratio of >2 . We also found some simple and effective methods for enhancing the shape selectivity to 2,6-DIPN by using water and chemically dealuminated mordenite.

* Corresponding author: Email: csong@psu.edu; Fax: 814-865-3248; Tel: 814-863-4466

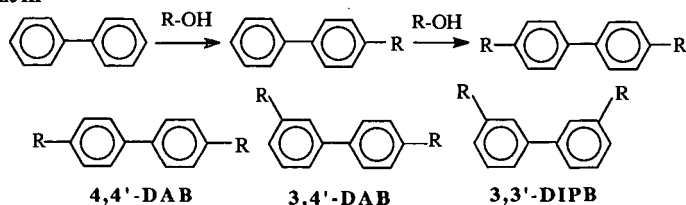
Scheme II



Shape-selective Alkylation of Biphenyl. Biphenyl and its derivatives are present in coal-derived liquids, although at concentrations lower than those of naphthalene derivatives. Shape-selective alkylation of biphenyl (Scheme III) can produce 4,4'-dialkyl substituted biphenyl (4,4'-DAB), the starting material for monomer of some LCP materials represented by Xydar. Proton-form mordenite can be used as shape-selective catalyst for isopropylation of biphenyl.

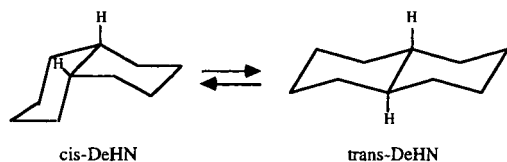
Lee et al. [1989] first demonstrated the beneficial effect of dealumination for selective formation of 4,4'-diisopropylbiphenyl (4,4'-DIPB). Sugi and coworkers have carried out a series of studies on biphenyl isopropylation over mordenites [Sugi and Kubota., 1997]. They have reported on the influence of propylene pressure, effects of $\text{SiO}_2/\text{Al}_2\text{O}_3$ ratio of mordenites, on shape-selectivity and coke deposition, and impact of cerium exchange of sodium mordenite. It was shown in our report that dealumination of some commercial mordenites by acid treatment first increases then decreases their activity, but increases their selectivity toward 4,4'-DIPB in isopropylation with propylene. More recently, we have found that addition of water to dealuminated mordenite is a simple method to inhibit deactivation of the partially dealuminated mordenite catalysts without losing activity and selectivity.

Scheme III



Conformational Isomerization. Commercial decalins obtained from naphthalene hydrogenation are almost equimolar mixtures of cis-decalin and trans-decalin. In the course of studying sym-OHP isomerization using decalin as solvent, we accidentally found that cis-decalin isomerizes to trans-decalin over ion-exchanged Y zeolite and mordenite catalysts at low temperatures (250°C), as shown in Scheme IV. This reaction would require a temperature of above 400°C in the absence of a catalyst.

Scheme IV



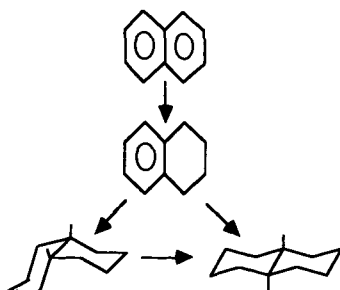
The catalytic reactions were mainly conducted at 200-250 °C for 0.15-8 h under an initial pressure of 0.79 MPa N_2 or H_2 using six catalysts: a hydrogen Y zeolite, a lanthanum ion-exchanged Y zeolite, a hydrogen mordenite, and three noble metal loaded mordenites. Pt- and Pd-loaded mordenites displayed the highest selectivity towards trans-DeHN (nearly 100%), with a trans-DeHN/cis-DeHN ratio of about 13 under H_2 at 200°C; however, they are less effective under N_2 . Pre-reduction of Pt/HM30A could improve its catalytic effectiveness in N_2 atmosphere.

By using mordenite-supported platinum or palladium catalysts, it is possible to achieve over 90% conversion with 95% selectivity at 200°C. trans-Decalin has substantially higher thermal stability at temperatures above 400°C. Possible applications of this process are high-temperature heat-transfer fluids and advanced thermally stable jet fuels, which can be used both as heat sinks and as fuels for high-Mach aircraft.

Shape-Selective Hydrogenation of Naphthalene. Complete hydrogenation of naphthalene in conventional processes produces mixtures of cis- and trans-decalin. Our work on selective naphthalene hydrogenation is motivated from the accidental finding on zeolite-catalyzed isomerization of cis-decalin and from the need to tailor the formation of desired isomers from two-ring compounds. Our previous studies on naphthalene hydrogenation showed that certain catalysts

show higher selectivity towards *cis*-decalin or *trans*-decalin. More recently, we found that mordenite and Y zeolite-supported Pt and Pd catalysts can selectively promote the formation of *cis*-decalin or *trans*-decalin, as shown in Scheme V.

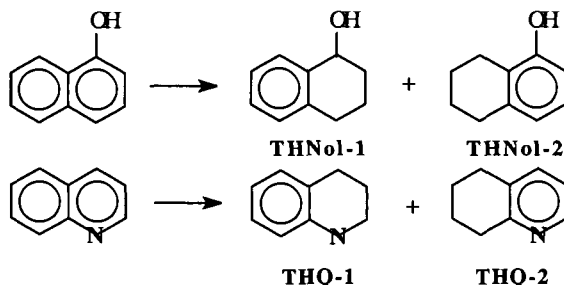
Scheme V



Now we can produce *cis*-decalin, with over 80% selectivity (or over 80% *trans*-decalin) at 100% conversion by using some zeolite-supported catalysts at 200°C. *cis*-Decalin may have potential industrial application as the starting material for making sebacic acid. Sebacic acid can be used for manufacturing Nylon 6,10 and softeners. There is also an industrial need for selective production of tetralin, a hydrogen-donor solvent, from naphthalene. Partial passivation of some zeolite-supported noble metal catalysts by sulfur can make them highly selective for the production of tetralin during metal-catalyzed hydrogenation of naphthalene at low temperatures.

Regio-Selective Hydrogenation. More recently we have begun to explore regio-selective hydrogenation of heteroatom-containing aromatic compounds. Examples of such compounds are 1-naphthol and quinoline shown in Scheme VI. Partial hydrogenation of 1-naphthol can give 1,2,3,4-tetrahydro-1-naphthol (THNol-1) and 5,6,7,8-tetrahydro-1-naphthol (THNol-2). Under fuel hydrotreating conditions, hydrogenolysis of C-O bond can also take place. It is of interest to see whether we can selectively produce THNol-1. We are conducting experimental work on regio-selective hydrogenation over various metal catalysts supported on zeolites, alumina and titania. As in the case of naphthalene hydrogenation described above, the type of metal and support were found to be important for achieving regio-selectivity (for example, to THNol-1) (Shao et al., 2000). Similarly, for partial hydrogenation of quinoline, either 1,2,3,4-tetrahydroquinoline (THQ-1) or 5,6,7,8-tetrahydroquinoline (THQ-2) can be produced. It is interesting to clarify how can one of the two isomers be produced selectively under practically useful conditions for catalytic processing. The hydroaromatic products of regio-selective hydrogenation have some unique applications, e.g. as hydrogen donors or radical scavengers for stabilizing fuels at high temperatures [Andresen et al., 1999; Venkatraman et al., 1998].

Scheme VI



3. CARBON MATERIALS

Since all coals are carbon-rich solids, they are potential starting materials for other, higher value materials via conversion to new carbon-based solids. It is now well known that various useful carbon-based materials and composite materials can be made from coals, coal tars, petroleum pitch, and coal liquids from liquefaction and coal pyrolysis, as shown in Table 1 [Song and Schobert, 1993].

Table 1. List of Some Coal-Based Carbon Materials

Materials That Can be Made Using Coal	Materials from Coal-derived Liquids
Metallurgical coke	Pitch-based carbon fibers
Activated carbon adsorbents	Mesocarbon microbeads
Molecular sieving carbons	Carbon Electrodes
Graphite and graphite-based materials	Binder pitches
Composite (coal/polymer) materials	Activated carbon fibers
Fullerenes or "bucky-balls"	Mesophase-based carbon fibers
Carbon nano tubes	Carbon whiskers or filament
Diamond-like films	Carbon fiber reinforced plastic
Intercalation Materials	Carbon-based Honeycomb

Production of activated carbons from coals has been of interest for years. Excellent reviews, with abundant historical information, has been published by Derbyshire and colleagues [Derbyshire et al., 1995; Derbyshire, 1998]. Activated carbons are used mainly as adsorbents for liquid- and gas-phase applications. The amount of coals used worldwide for producing activated carbons is about 200,000 t/y [Golden, 1992], a significant fraction of the world's annual production of activated carbons, estimated to be about 450,000 t from all feedstocks. Significant growth potential exists for this application, primarily for water and air purification. The liquid-phase applications of activated carbons produced from bituminous coals by chemical activation include water purification, decolorizing, food processing, and gold recovery; the gas-phase applications cover air purification, gas treatment, and solvent recovery [Jagtøyen et al., 1993]. Activated anthracites produced by air treatment prior to steam activation are microporous with a significant fraction of the pores having molecular dimensions [Gergova et al., 1995]. This suggests that molecular sieve materials could be produced from anthracites.

Current graphite technology uses petroleum cokes as the filler material. Molded graphite articles have a wide range of applications, from high-tonnage uses as electrodes in electric arc furnaces, a \$US2.2 billion business in 1991 [Pierson, 1993], to specialty graphites for high-technology uses in chemical vapor deposition and epitaxial deposition devices. Meta-anthracite, of very limited value (\approx \$US25/ton) because of its poor combustion performance, may be a superior filler for molded graphites, even better than the more conventional anthracites. For example, non-catalytic graphitization of meta-anthracite at 2400°C yields a product having a 0.3363 nm d-spacing [Morrison et al., 1996], compared with the 0.335 nm value of pure graphite. The value of meta-anthracite as a replacement for petroleum coke in graphite production would exceed its value as a fuel by about a factor of ten.

The amount of coals used worldwide for producing molecular sieving carbons (MSC) is estimated to be 3,000 tonnes/year [Golden, 1992]. The application MSC for gas separation by pressure-swing adsorption is now commercially viable. In the United States, MSC is used for air separation by Air Products and Chemicals Inc. It is likely that more companies will be engaged in producing MSC in the next century.

Coal tar pitches are raw materials for carbon fibers and mesocarbon microbeads [Derbyshire et al., 1994]. Liquids from coal extraction and liquefaction can be used for making carbon fibers and graphitic materials [e.g., Zondlo et al., 1993]. Kimber and Gray [1976] also noted potential advantages in using coal-based coke for making carbon electrodes.

4. ADVANCED JET FUELS

One commercially available route to make liquid fuels from coal is the well-known SASOL route incorporating coal gasification as the first step and the Fischer-Tropsch synthesis as the second step. The fuels from Fischer-Tropsch synthesis using either natural gas- or coal-derived syngas are good as diesel fuels. However, for jet fuel applications, there is an unique structural advantage of coal that can lead to superior fuels. There are some unique compositional advantages of coal-derived liquids for making jet fuels, with respect to the high-temperature thermal stability required for future supersonic and hypersonic jet aircraft. The USAF has established a long-term goal to develop advanced jet fuels called JP-900 that are stable at high temperatures up to 900 °F (482 °C) [Edwards et al., 1997].

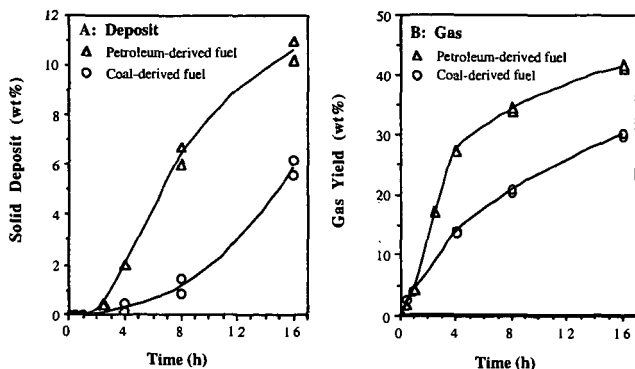


Figure 1. Formation of solid deposit (A) and gases (B) from petroleum-derived JP-8P and coal-derived JP-8C jet fuels at 450°C for 0.5-16 h under nitrogen atmosphere (100 psi, cold).

As can be seen from Figure 1, compared to conventional petroleum derived jet fuels, the coal-derived jet fuels display greater thermal stability at temperatures above 400 °C in the pyrolytic regime, in terms of much lower degree of decomposition and significantly less amount of solid deposit [Lai et al., 1992; Song et al., 1993]. This is because coal-derived jet fuels are rich in cycloalkane and the aromatic compounds in coal-derived jet fuels can be dominated by hydroaromatic structures. Cycloalkanes are more stable than the n-alkanes with the same or less carbon number, and the stability of alkylated cycloalkanes decreases with increasing length or carbon number of the side chain [Lai and Song, 1996; Song and Lai, 1998]. At temperatures above 400°C, decomposition of long-chain paraffins in jet fuels is dominated by radical-chain reactions [Song et al., 1994a]. Hydroaromatic compounds such as tetralin are hydrogen donors which can serve as radical

scavengers in pyrolytic reactions which inhibit the thermal decomposition of reactive hydrocarbons [Song et al., 1994b; Yoon et al., 1996]. Studies on model paraffinic jet fuels in the absence and the presence of added hydroaromatic compounds have also demonstrated that they are capable of suppressing the initial decomposition by retarding the radical reactions [Venkatraman et al., 1998; Andresen et al., 1999].

Coal-derived JP-8C fuel and a model jet fuel that contains mainly cycloalkanes and about 10% tetralin has been shown to be thermally stable at temperatures up to 482°C or 900 °F [Strohm et al., 1999].

The coal-based thermally stable jet fuels can be produced using liquids that are partially or wholly derived from coal, by one of the following strategies: (1) the use of by-product coal tars from coal carbonization or from coal gasification (pyrolysis); (2) the use of blends of coal tar distillates and petroleum refinery streams, which would enlarge the pool of available feedstock; (3) the use of by-product liquids from co-coking of coal and petroleum resids; and (4) the use of liquids from co-processing of coal and petroleum resids, which is a process alternative to the well-known direct liquefaction of coal.

5. CONCLUDING REMARKS

We must always keep in mind that coal is a valuable hydrocarbon source, that can have multiple and equally important uses for both non-fuel and fuel applications. As we move into the 21st century, coal may become more important both as an energy source and as the source of chemical feedstocks.

ACKNOWLEDGEMENTS

We wrote this preprint article for the ACS Symposium to honor the late Frank Derbyshire, the former editor of Fuel and a friend of us. We gratefully acknowledge the helpful discussions that we had with him in the past on the topic of non-fuel use and on coal conversion and utilization. We also thank our current and former coworkers at Penn State. Various portions of our research were supported through funding or donations of special samples from the U.S. Department of Energy, Federal Energy Technology Center, the Pennsylvania Energy Development Authority, PQ Co, Air Products and Chemicals Inc., and Duracell Co.

REFERENCES

- Andrésen, J. M., Strohm, J. J., Coleman, M. M. and Song, C. Am. Chem. Soc. Div. Fuel. Chem. Prepr., 1999, 44 (1), 194.
- Derbyshire, F. J., M. Jagtoyen, Y. Q. Fei, and G. Kimber. Am. Chem. Soc. Div. Fuel Chem. Prepr., 1994, 39 (1), 113.
- Derbyshire, F. Proceedings of 15th Annual International Pittsburgh Coal Conference, Pittsburgh, PA, September 14-18, 1998, Paper No. 22-1.
- Edwards, T., Harrison, W. E. and Schobert, H. H. 33rd AIAA/ASME/SAE/ASEE Joint Propulsion Conference and Exhibit, July 6-9, 1997, Seattle, WA, Paper no. AIAA 97-2848.
- Fraenkel, D., Cherniavsky, M., Ittah, B. and Levy, M. J. Catal., 1986, 101, 273.
- Gergova, K., Eser, S. and Schobert, H.H. Energy and Fuels, 1993, 7, 661.
- Golden, T.C. Air Products Co., personal communication, April 24, 1992.
- Jagtoyen, M., Groppo, J. and Derbyshire, F. Fuel Procs. Technol., 1993, 34, 85-96.
- Katayama, A., Toba, M., Takeuchi, G., Mizukami, F., Niwa, S.-i., Mitamura, S. J. Chem. Soc., Chem. Commun. 1991, 39-40.
- Kimber, G. M. and Gray, M.D. Amer. Chem. Soc. Symp. Ser., 1976, 21, 445.
- Lai, W.-C., Song, C., Schobert, H. H. and Arumugam, R. Am. Chem. Soc. Div. Fuel Chem. Prepr., 1992, 37 (4), 1671.
- Lai, W.-C. and Song, C. Fuel Processing Technology, 1996, 48 (1), 1.
- Lee, G. S., Maj, J. J., Rocke, S. C., Garces, J. M. Catal. Lett., 1989, 2, 243.
- Moreau, P.; Finiels, A.; Geneste, P.; Solofo, P. J. Catal., 1992, 136, 487.
- Morrison, J.L., Rusinko, F., Eser, S., Pisupati, S.V. and Scaroni, A.W. Unpublished report, The Pennsylvania State University, University Park, PA, 1996.
- Pierson, H.O. Handbook of Carbon, Graphite, Diamond and Fullerenes. Noyes Publications, Park Ridge, NJ., 1993.
- Shao, J., Holtzer, G. and Song C. Am. Chem. Soc. Div. Petrol. Chem. Prepr., 2000, 45 (1), 18.
- Song, C. and Schobert, H. H. Fuel Processing Technol., 1993, 34 (2), 157.
- Song, C., Eser, S., Schobert, H. H., and Hatcher, P. G. Energy Fuels, 1993, 7 (2), 234.
- Song, C., Lai, W.-C. and Schobert, H. H. Ind. Eng. Chem. Res., 1994a, 33 (3), 534.
- Song, C., Lai, W.-C. and Schobert, H. H. Ind. Eng. Chem. Res., 1994b, 33 (3), 548.
- Song, C. and Schobert, H. H. Fuel, 1996, 75 (6), 724.
- Song, C. and Schobert, H. H. Chemistry and Industry, 1996, No.7, 253.
- Song, C. and Lai, W.-C. Am. Chem. Soc. Div. Petrol. Chem. Prepr., 1998, 43 (3), 462.
- Song, C. Stud. Surf. Sci. Catal., 1998, 113, 163.
- Song, C. Am. Chem. Soc. Symp. Ser., 1999, 738, 248.
- Strohm, J. J., Andrésen, J. M., and Song, C. Am. Chem. Soc. Div. Petrol. Chem. Prepr., 1999, 44, 386.
- Sugi, Y.; Kubota, Y. Catalysis-Specialist Periodical Report, 1997, 13, 55.
- Venkataraman, A., Song, C., and Coleman, M. M. Am. Chem. Soc. Div. Petrol. Chem. Prepr., 1998, 43 (3), 364.
- Yoon, E., Selvaraj, L., Song, C., Stallman, J. and Coleman, M. M. Energy Fuels, 1996, 10 (3), 806.
- Zondlo, J.W., Stansberry, P.G. and Stiller, A.H. Proc. 10th Ann. Intl. Pittsburgh Coal Conf., 1993, 379.

CATALYTIC HYDROTREATMENT OF HETEROATOM SPECIES IN SOUTH BANKO COAL LIQUID DISTILLATE OVER CARBON SUPPORTED NiMo CATALYST

SD. Sumbogomurti*, K. Sakanishi**, I. Mochida*

* Institute of Advance Material Study, Kyushu University
Kasuga, Fukuoka 816-8580, Japan

** National Institute for Resources and Environment, Tsukuba, Ibaraki 305-8569, Japan

Abstract

Hydrotreatment of crude liquid oil produced from South Banko coal (SBCL) was carried out using alumina and carbon supported NiMo catalysts to find advantages of carbon support for up-grading coal liquid. Reactivity of representation sulfur, nitrogen and oxygen molecular species were measured to confirm the high activity of the catalyst against refractory species. NiMo supported on of ultrafine particle carbon black (Ketjen Black:KB) with extremely large surface area was found an excellent support for hydrotreatment catalyst to show much higher activity for the hydrodesulfurization(HDS), hydrodenitrogenation(HDN) and hydrodeoxygenation(HDO) of coal liquid than that of a commercial NiMo/Al₂O₃ catalyst.

Key words: coal liquids oil, hydrotreatment, carbon support catalyst

Introduction

As environmental protections become greater concern, it is very essential to treat hydrocarbons feed-stocks such as naphthas, middle distillate, gas oil, vacuum gas oil, vacuum resids, coal liquids to decrease the content of undesirable aromatic hetero atomic species. Noble metal catalysts, which are excellent for aromatics saturation, get fast poisoned by the sulfur and nitrogen compounds to lose their activity.

The support to replace alumina is one of targets approaches for this purpose. Carbon has been recognized an interesting support to showing higher catalytic activity for the HDS of thiophene than alumina support [1]. Such high activity of carbon-supported HDS catalyst has been attributed to the inertness of the carbon support as compared to the conventional alumina support [1]. Carbon has the additional advantage over other support of a great flexibility in the modification of both the porosity and surface area. Daly et al [2] have shown that the types of carbons affected the distribution of active sulfides on their surface. Vissers et al. [3] found that increasing of carbon surface area results in increasing HDS activity because of the lower sintering trend of the active phase. Schmitt and Castellion [4] also found that sulfides supported on carbon with larger mean pore size were more active for the HDS of gasoil. Drahoradova et al. [5] reported that NiMo on carbon showed higher hydrodenitrogenation (HDN) activity and lower inhibition of HDS activity with thiophene/pyridine feeds than alumina-supported NiMo. Mochida et al [6], also notified that nickel molybdenum sulfide supported on carbon (Ketjen Black) was more active for the hydrogenation of 1-methylnaphthalene than NiMo supported on alumina. Furthermore, carbon-based catalysts can be less expensive than alumina. Combustible carbon facilitates metals recovery and reduced volume of disposal [7].

The present study prepared KB supporting nickel-molybdenum sulfide catalyst and applied to the hydrotreatment of SBCL which contained much more aromatic and hetero atom species such nitrogen, sulfur and oxygen compounds. Its activity for hydrodesulfurization (HDS), hydrodenitrogenation (HDN) and hydrodeoxygenation (HDO) was compared with those of a commercially available alumina catalyst to find the advantages of carbon support in the hydrotreatment of highly polar feed.

Experimental

Feed

The sample used were two different cutting point of SBCL (A: bp < 300 °C; B: bp 200 ~ 350 °C) which was prepared at 450 °C, 15 Mpa using limonite catalyst in a BSU (Bench Scale Unit) pilot plant of Nippon Brown Coal Liquefaction Co. Ltd. and was supplied by courtesy of NEDO. Their properties are listed in Table 1.

Catalyst

A commercially available NiMo/ Al₂O₃ (NiO; 2 wt%, MoO₃; 10 wt%), was used as a reference. Carbon supported NiMo catalyst was prepared in the laboratory. Some properties of carbon black (Ketjen Black:KB EC 600JD) provided by Mitsubishi Chemical Co. are summarized in Table 2. Nickel and Molybdenum salt were impregnated simultaneously using Ni(Ac)₂ and MoO₂-AA in methanol. Ni(Ac)₂ and MoO₂-AA dissolved in methanol were mixed to the slurry KB methanol and were dispersed by ultrasonic for 40 min. The mixture was heated up to 40 °C for 120 min, followed by evaporation to remove solvent under reduced pressure. The catalyst precursor was then dried at 120 °C for 12 h in vacuum. It was presulfided in a 5 % of H₂S/H₂ flow at 360 °C for 2 h prior to the reaction.

Hydrotreatment procedures

Hydrotreatment of South Banko coal liquid distillate was performed in a 50ml magnetically stirred autoclave. The ratio of catalyst to feed was 10 wt%, and 10 g of feed was used. Feed was charged in to the autoclave together with catalyst, and the autoclave was flush with nitrogen three times to replace air and was then filled with pure hydrogen. The initial pressure of hydrogen was 10 MPa. The reaction time was counted from the point when the reaction temperature was reached to the prescribed temperature. The hydrogenated product was collected from the autoclave with acetone. The liquid product was then separated from the catalyst by vacuum filtration. After removal of acetone, the hydrogenated product was analyzed by GC-AED to calculate the extent of HDS, HDN and HDO.

Results

GC=AED chromatographs of SBCL (A) before and after hydrotreatment at 360 °C over NiMo/Al₂O₃ catalyst are illustrated in Figure 1 ~ 3. Figure 1 shows high reactivity of sulfur species, which allowed them complete removal under this condition. Nitrogen exhibited the lower reactivity and still much remained after the reaction as shown in Figure 2. Pyridines were the most reactive among nitrogen species. The nitrogen species left in the hydrotreated oil were found as anilines, methyl-, dimethyl-, trimethyl-anilines, quinoline and indoles. The oxygen compounds were further less reactive than other heteroatoms species as shown in Figure 3. Most of phenols still remained after the hydrotreatment over NiMo/Al₂O₃ catalyst at 360 °C. Dibenzofuran appeared the most refractory species.

Figure 4 & 5 illustrate both reactivities of SBCL (B) in the hydrotreatment at 360 °C over NiMo/Al₂O₃ and NiMo/KB. SBCL (B) of higher boiling range carried much less reactive species such as 4,6-dimethyldibenzothiophene and dimethylcarbazoles. Hence their heteroatom removal was much slow than that of SBCL (A). The carbon-supported catalyst was found more active than alumina supported one, shows better removal all heteroatoms. The advantage of carbon support decreases in order of S > N > O removal.

Discussion

The reactivity of heteroatom species in SBCL (A) is defined clearly in the order of S > N > O. Sulfur was easily removed became smaller content and least refractory species such as 4,6-dimethyldibenzothiophene. Nitrogen species are less reactive than sulfur species. Among the nitrogen species, very basic nitrogen species were removed at lower temperature, their

preferential adsorption being suggested. Anilines and alkyl anilines were less reactive. Oxygen species especially benzofuran were very unreactive.

KB supported NiMo catalyst was found much more active than alumina supporting ones especially against refractory species. Large surface area and very fine grains help its high dispersion of active phases over the surface and among the heteroatom species of the catalyst particles. The number of active site is believed to depend on the extent of sulfurization. Medium strength of chemical interaction between active phase and carbon support may be favorable for complete sulfurization.

The acidic polar support has been believed to help hydrogenation and C-X cleavage. It clearly accelerates the deactivation by coking through strong absorption. Carbon is certainly expected less deactivated. More chemical modification of carbon can be the target of the next research.

References.

1. J. C. Duchet, E. M. van Oers, V. H. J. de Beer and R. Prins, *J. Catal.* 80, 386 (1983)
2. F. P. Daly and J. S. Brinen, *App.Catal.* 11, 161 (1984)
3. J. P. R. Vissers, T. J. Lensing, V. H. J. de Beer and R. Prins, *Appl. Catal.* 3, 21 (1982)
4. J. L. Schmitt, Jr., and G. A. Castellion, *U.S.Patent* 4032435(1977)
5. Drahoradova, A; Vit, Z; Zdrzil, M. *Fuel* 1992, 71 (4), 455
6. Sakanishi K.; Mochida I., *Energy & Fuel* 1995, 9 (6), 995
7. Lillian A.R.; *Energy & Fuel* 1993, 7, 937-942

Table 1 Elemental analyses of feed

Sample	b.p(°C)	C*	H*	N*	S**	O***	H/C
A	< 300	84.97	10.37	0.84	667	3.74	1.46
B	200 - 350	85.59	9.09	1.74	770	3.49	1.27

* : wt%, ** : ppm, *** : differences

Table 2 Some Properties of Ketjen Black

Surface area (m ² /g)	1270
Volatile matter (%)	0.7
PH	9.0
Particle size (nm)	30
Apparent density (g/L)	115
Ash (%)	0.1
Ni (ppm)	1.5
V (ppm)	30
Fe (ppm)	100
Cu (ppm)	1
Mn (ppm)	1

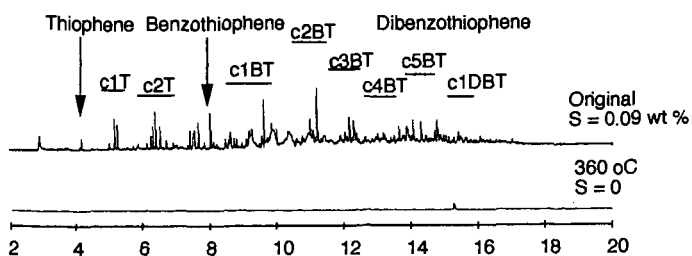


Figure 1 sulfur chromatograms of hydrotreated SBCL (A) over NiMo/Al₂O₃ catalyst

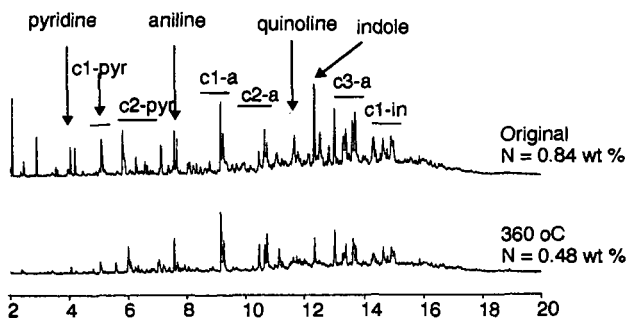


Figure 2 nitrogen chromatograms of hydrotreated SBCL (A) over NiMo/Al₂O₃ catalyst

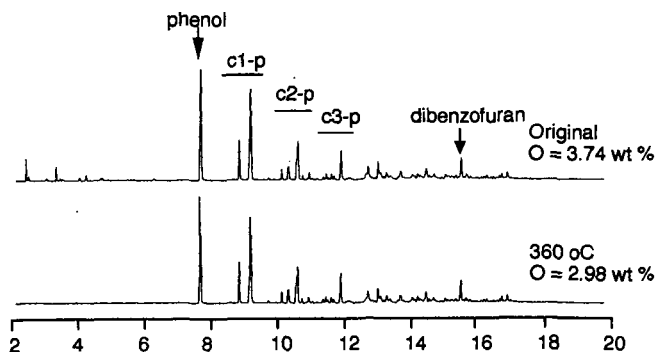


Figure 3 oxygen chromatograms of hydrotreated SBCL (A) over NiMo/Al₂O₃ catalyst

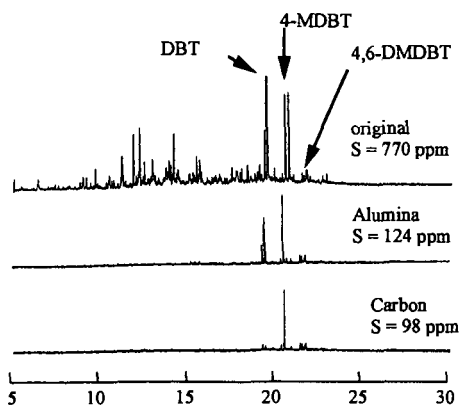


Figure 4 sulfur chromatogram of hydrotreated SBCL(B) over NiMo/Al₂O₃ and NiMo/carbon catalyst

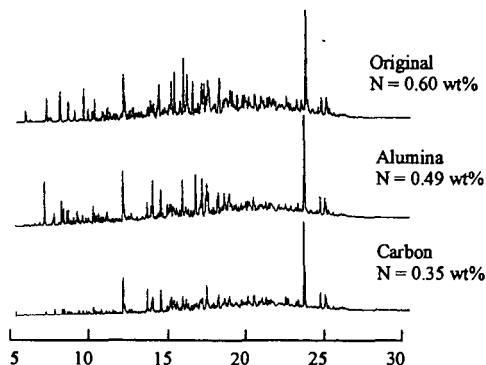


Figure 5 Nitrogen chromatograms of hydrotreated SBCL(B) over NiMo/Al₂O₃ and NiMo/carbon catalyst

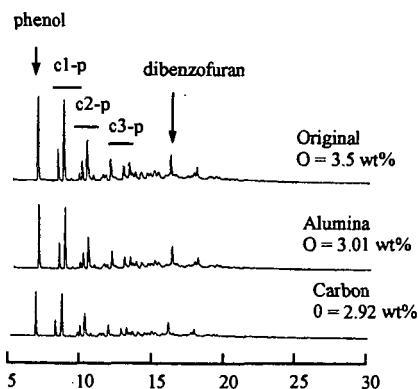


Figure 6 oxygen chromatographs of hydrotreated SBCL(B) over NiMo/carbon and NiMo/Al₂O₃ catalyst

ENHANCING ACTIVITY OF IRON-BASED CATALYST SUPPORTED ON CARBON NANO PARTICLES BY ADDING NICKEL AND MOLYBDENUM

Unggul Priyanto¹⁾, Kinya Sakanishi²⁾, Osamu Okuma³⁾, and
Isao Mochida¹⁾

1) Institute of Material Study, Kyushu University,
Kasuga, Fukuoka 816-8580, Japan

2) National Institute for Resources and Environment,
Tsukuba, Ibaraki 305-8569, Japan

3) The New Industry Research Organization, 1-5-2, Minatojima-minamimachi, Chuo-ku, Kobe
650-0047, Japan

Abstract

FeMoNi catalyst supported on carbon nanoparticles (Ketjen Black: KB) was tested in the liquefaction of sub-bituminous coals in an autoclave of 50 ml capacity. At 450°C and 15 MPa, the liquefaction of (an Indonesian coal) Tanito Harum coal with FeMoNi/KB catalyst (10% Fe, 5% Mo, 2% Ni, 83% KB) provided oil yield as high as 77wt% that is comparable to that obtained from liquefaction with NiMo/KB catalyst (2% Ni, 10% Mo, 88% KB). The ternary catalyst was also optimized for the highest activity in terms of loading amount and order of the active components.

Keywords: coal liquefaction; iron molybdenum nickel catalysts; carbon nanoparticle support

Introduction

In fundamental research, a number of catalytic materials have been examined to find better liquefaction catalyst. However, only iron and molybdenum have been attempted in demonstration plant and so far the greatest attention has been given to Fe catalysts because of their low cost and disposability even though their activity is rather poor. To enhance the activity of iron, active metals of higher price have been combined by expecting some synergistic activation. Moreover, the very fine particles as catalyst supports having high surface area are useful to give high dispersion of active metals on its surface. In addition, as carbon support, it has a weak interaction between the metal phase and the support, which allows the quantitative conversion of the metal oxide to the active sulfide form. Thus, the carbon-supported catalysts are very effective to carry more active and costly metals at lower loading.¹

The present authors have attempted to use the nickel-molybdenum sulfide supported on carbon nano particles (KB: Ketjen Black) to achieve excellent activity and recovery for repeated use in the liquefaction.² The authors also proposed FeNi sulfide on KB to reduce the cost of catalyst, which is superior to the NiMo/Al₂O₃ but inferior to the NiMo/KB.^{3,4}

In the present study, catalytic activities of ternary sulfide FeNiMo/KB were examined by loading least amount of Mo on carbon nanoparticles to obtain the activity that is comparable to that of NiMo/KB catalyst. The effect of catalyst preparation method to the activity of FeMoNi/KB catalyst was also investigated.

Experimental Section

Catalyst and Materials

Fe, Ni and Mo salts were impregnated on to KB by several impregnating methods using FeC₄H₂O₄ (fumarate), Ni(NO₃)₂ or Ni-(Ac)₂, and MoO₂-AA in methanol and water depending on the solubility of the salts. The catalysts prepared in the present study are listed in Table 1. A prescribed amount of Ketjen black (KB) was dispersed in methanol under ultrasonic irradiation for 15 min. A mixture of iron(II) fumarate and Ni(NO₃)₂ dissolved in methanol was mixed to the KB-methanol slurry with a small amount of nitric acid (1% vol.) as an additive. The slurry had been dispersed under ultrasonic irradiation and heated at 40°C for 2 h before the slurry was evaporated, and dried at 120°C for 12 h in vacuo. In the case of successive impregnation, nickel was first impregnated, being followed by iron. Other combinations of metal precursors, Mo/Ni, Fe/Mo, and Fe/Mo/Ni (the order of impregnation) were also impregnated on KB. These catalysts were presulfided by flowing 5% vol H₂S/H₂ at 360°C for 2 h prior to the reaction.^{2,3,5}

The elemental analyses of Tanito Harum, Yilan, and Shenmu coals are summarized in Table 2. Commercially guaranteed grade tetralin (TL) was used as a liquefaction solvent, and 1-methylnaphthalene was used as a reactant in the hydrogenation.

Liquefaction Procedure

Coal liquefaction was performed in an electromagnetic-driven autoclave of 50 ml capacity. 3 g of coal, 3 g of solvent and 0.09 g of catalyst were charged to the autoclave⁶. The liquefaction was performed under 15 MPa of hydrogen pressure at 450°C for 60 min. The heating rate to the reaction temperature was 20°C/min, and the stirring speed was 1300 rpm.

The liquid and solid products of coal liquefaction were recovered by THF. After the THF was removed by evaporation, the product was extracted in sequence with n-hexane, acetone, and THF. The n-hexane-soluble (HS), n-hexane-insoluble but acetone-soluble (HI-ACS), acetone-insoluble but THF-soluble (ACI-THFS), and THF-insoluble (THFI) substances were defined as oil (O) and

solvent, asphaltene (A), preasphaltene (PA), and residue (R), respectively. The gas yield was calculated by the weight difference between initial coal, solvent, and recovered product. The oil yield was calculated by subtracting the initial solvent weight from the total weight of HS. The reaction under the same conditions was repeated at least three times to make sure the experimental results that were within the errors of 1wt% daf coal base.

Hydrogenation of 1-methylnaphthalene

1-Methylnaphthalene (1-MN; 6g) and catalyst (1.5wt% based on 1-MN) were charged into a 50 ml magnetically stirred autoclave. Standard conditions for the hydrogenation were 60 min, 360°C, and 15 MPa of H₂ reaction pressure. The 1- and 5-methyltetralins and trace of tetralin were identified and quantified by GC-MS to calculate the hydrogenation activity and selectivity over the catalyst.

Results and Discussion

Effects of Ni or Mo on the catalytic activities of iron supported on KB

Figure 1 describes yields of Tanito Harum coal liquefaction at 450°C and 15 MPa with Fe(10%) based catalyst on KB. The addition of Mo from 2 to 3% improved the oil yield of 67 and 68%, respectively, which were much higher than that of Fe(20)/KB. FeNi/KB catalyst with Ni content of 15% provided oil yield as high as 73%. More Mo or Ni content tends to increase the activity of Fe based catalyst.

Activity of the NiMo/KB catalysts with various Mo content and effects of Ni addition to the FeMo/KB catalyst

Figure 2 shows the activity of NiMo/KB catalyst with various Mo contents and the effect of Ni addition to the FeMo/KB catalyst in the liquefaction of Tanito Harum coal. The activity of NiMo/KB catalyst increased in line with the increase of Mo content in the catalyst. The Ni Mo/KB catalyst with Mo content of 10% provided a very high oil yield of 78%.

The activity of FeMo/KB catalyst was improved by the addition of Ni. Fe(10)Mo(3)Ni(3)/KB gave higher oil yield than that of Fe(10)Mo(3)/KB (see Fig. 2e and 1c). The activity was governed by Mo content of 2 to 5% that provided oil yield from 70 to 77%. It must be noted that 5% Mo in FeMoNi/KB catalyst provided a comparable oil yield to that of Ni(2)Mo(10)/KB under the same conditions. Moreover, 3 and 5% Mo in FeMoNi/KB gave oil yield of 5% higher than those of NiMo/KB with the same as Mo contents.

Effects of catalyst preparation procedure on the catalytic activity of NiMo and FeMoNi on KB

Figure 3 shows the effects of catalyst preparation procedures. For NiMo/KB catalyst, successive impregnation method appeared definitely much better than simultaneous impregnation. In impregnation procedure, molybdenum was first impregnated. However, the order of Mo/Fe/Ni in the successive method gave the same oil yield as to that in simultaneous impregnation procedure (see Figure 3c and 3d), while the order of Fe/Mo/Ni provided a slightly higher oil yield (see Figure 3e). Successive impregnation appears to give higher activity when the most dominant metal component was loaded. The reason is that the metal component is generally better dispersed in the first impregnation than in the second one because the component gets more space on the support. However, the effects in the successive impregnation may not be so strong for the component of inferior majority such as Fe.

Comparison of various catalysts in the liquefaction of Yilan and Shenmu coals

Figure 4 compares the activities of FeNi/KB, FeMoNi/KB, NiMo/KB catalysts in the liquefaction of Yilan and Shenmu coals. The activities of Fe(10)Ni(10)/KB, Fe(10)Mo(3)Ni(3)/KB, Ni(2)Mo(10)/KB catalysts in the liquefaction of Yilan coal provided 65%, 72%, and 77% oil yields, respectively. FeMoNi/KB catalyst with less Mo content gave much higher oil yields than FeNi/KB catalyst. High oil yield compensated by low gas, asphaltene, and preasphaltene yields suggests high selectivity of FeMoNi/KB catalyst. In the liquefaction of Shenmu coal (bituminous coal), the oil yield by FeMoNi/KB catalyst was higher compared to FeNi/KB in spite of lower than that of NiMo/KB catalyst.

The activity of NiMo and Fe based catalysts supported on KB in the hydrogenation of 1-methylnaphthalene

Table 3 compares the activities of catalysts in the hydrogenation of 1-methylnaphthalene at 360 °C, 15 MPa H₂, and 60 min. The Mo content governed basically the hydrogenation activity. The Mo content of 2, 3, 5, and 10% in the Fe-based and NiMo catalysts on KB provided conversions of 16, 24, 47, and 94%, respectively, regardless of the other components. The catalysts prepared by successive impregnation procedure showed a little better activity than that by simultaneous impregnation.

Conclusion

The addition of small amount of molybdenum and nickel on the iron catalyst supported on carbon nanoparticles enhances the activity of the catalyst in the liquefaction of sub-bituminous and bituminous coals. However, the hydrogenation activity for aromatic ring of the catalyst is basically influenced by Mo content. The activity of FeMoNi/KB catalyst is slightly influenced by the order of impregnation sequences in the catalyst preparation procedure.

References

- (1) Derbyshire, Frank J.; *Catalysis in Coal Liquefaction: New Directions for Research*; IEA Coal Research; London; June 1988.

- (2) Sakanishi, K.; Hasuo, H.; Kishino, M.; Mochida, I. *Catalytic Activity of NiMo-sulfide Supported on a Particular Carbon Black of Hollow Microsphere in the Liquefaction of a Subbituminous Coal*; *Energy & Fuels* 1996, 10, 216-219.
- (3) Sakanishi, K.; Taniguchi, H.; Hasuo, H.; Mochida, I. *Iron-based Catalysts Supported on Carbon Nanoparticles of Hollow Structure for Coal Liquefaction*; *Ind. Eng. Chem. Res.* 1997, 36, 306
- (4) Mochida, I.; Sakanishi, K.; Suzuki, N.; Sakurai, M.; Tsukui, y.; Kaneko, T., *Catalysis Surveys from Japan* 1998, 2, 17.
- (5) Sakanishi, K.; Hasuo, H.; Mochida, I.; Okuma, O. *Preparation of Highly Dispersed NiMo Catalyst Supported on Hollow Spherical Carbon Black Particles*; *Energy & Fuels*, 1995, 9, 995
- (6) Priyanto, U.; Sakanishi, K.; Mochida, I. *Effects of Solvent Amount and Dispersed Catalyst in the Liquefaction of Indonesian and Chinese Coals*. Proceedings of the Tenth International Conference on Coal Science, I, 1999, Shanxi science & Technology Press, Taiyuan, China.

Table 1. Catalysts and Salts

Catalysts ^a	Fe salts	Ni salts	Mo salts
1. Fe(10)Ni(10)	FeC ₄ H ₂ O ₄	Ni(NO ₃) ₂	-
2. Fe(10)Ni(15)	FeC ₄ H ₂ O ₄	Ni(NO ₃) ₂	-
3. Fe(10)Mo(2)	FeC ₄ H ₂ O ₄	-	MoO ₂ -AA
4. Fe(10)Mo(3)	FeC ₄ H ₂ O ₄	-	MoO ₂ -AA
5. Fe(10)Mo(2)Ni(2)	FeC ₄ H ₂ O ₄	Ni(NO ₃) ₂	MoO ₂ -AA
6. Fe(10)Mo(3)Ni(3)	FeC ₄ H ₂ O ₄	Ni(NO ₃) ₂	MoO ₂ -AA
7. Fe(10)Mo(5)Ni(2)	FeC ₄ H ₂ O ₄	Ni(NO ₃) ₂	MoO ₂ -AA
8. Ni(3)Mo(3)	-	Ni-(Ac) ₂	MoO ₂ -AA
9. Ni(2)Mo(5)	-	Ni-(Ac) ₂	MoO ₂ -AA
10. Ni(2)Mo(10)	-	Ni-(Ac) ₂	MoO ₂ -AA

^a Numbers in parentheses indicate the weigh percent of metals.

Table 2 Elemental Analysis of Coals Used in The Present Study

	C ^a	H ^a	N ^a	O ^a	S ^a	Ash ^b	H/C	O/C
Tanito Harum Coal	71.2	5.5	1.6	21.7	0.16	3.9	0.93	0.23
Yilan Coal	76.1	5.6	1.3	16.7	0.22	3.8	0.88	0.167
Shenmu Coal	78.8	5.1	1.1	14.7	0.21	3.9	0.78	0.14

^a in Wt % (d.a.f.)

^b Wt.% in

Table 3 Hydrogenation of 1- Methylnapthalene ^a

Catalysts	Conversion % ^b
Fe(10)Ni(10)/KB (simultaneous impregnation)	14
Fe(10)Ni(10)/KB (successive impregnation)	16
Fe(10)Mo(2)Ni(2)/KB (simultaneous impregnation)	16
Fe(10)Mo(3)Ni(3)/KB (simultaneous impregnation)	24
Fe(10)Mo(3)Ni(3)/KB (successive impregnation)	28
Fe(10)Mo(5)Ni(2)/KB (successive impregnation)	47
Ni(2)Mo(10)/KB (simultaneous impregnation)	94
Ni(2)Mo(10)/KB (successive impregnation)	98

^a Catalysts, 0.09 gr; 1-methylnapthalene, 6 g

^b Reaction conditions : 360 °C; 15 MPa; 60 min; stirring speed : 1300 rpm.

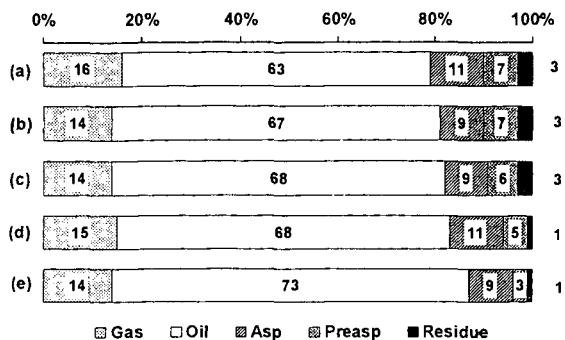


Figure 1. Effect of Ni or Mo addition to the Fe(10)/KB on the liquefaction of Tanito Harum coal : (a) Fe(20)/KB; (b) Fe(10)Mo(2)/KB; (c) Fe(10)Mo(3)/KB; (d) Fe(10)Ni(10)/KB, (e) Fe(10)Ni(15)/KB.

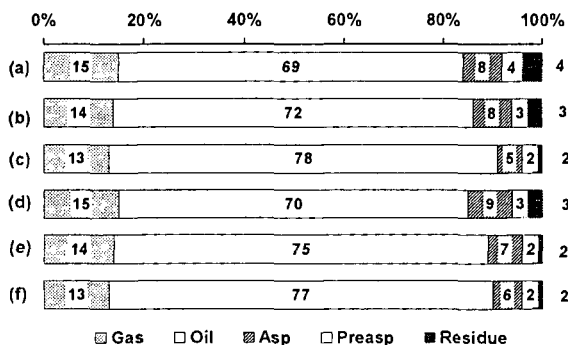


Figure 2. Activity of the NiMo/KB catalysts with variable Mo content and Effect of addition of Ni to the FeMo/KB catalysts on the liquefaction of Tanito Harum coal : (a) Ni(3)Mo(3)/KB; (b) Ni(2)Mo(5)/KB; (c) Ni(2)Mo(10)/KB; (d) Fe(10)Mo(2)Ni(2)/KB; (e) Fe(10)Mo(3)Ni(3)/KB; (f) Fe(10)Mo(5)Ni(2)/KB.

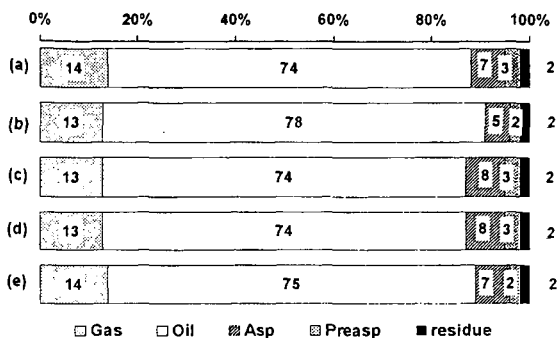


Figure 3 Effect of preparation method on the catalytic activity of Mo-based catalysts in the liquefaction of Tanito harum coal : (a) Ni(2)Mo(10) simultaneous impregnation process; (b) Ni(2)Mo(10) successive impregnation process; (c) Fe(10)Mo(3)Ni(3) simultaneous impregnation; (d) Fe(10)Mo(3)Ni(3) successive impregnation process I* , (e) Fe(10)Mo(3)Ni(3) successive impregnation process II**.

* Mo was firstly impregnated

** Fe was firstly impregnated

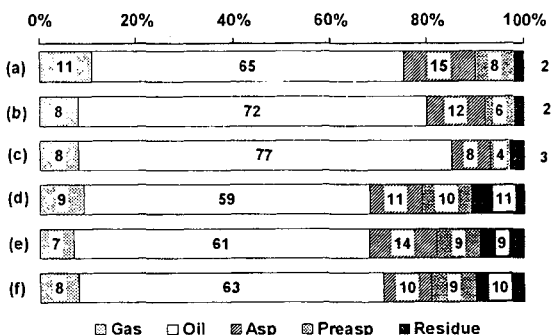


Figure 4 Activities of Fe(10)Ni(10)/KB, Fe(10)Mo(3)Ni(3)/KB, and Ni(2)MO(10)/KB catalyst in the liquefaction of Yilan, and Shenmu coals with tetralin solvent. (a), (b), (c) Yilan coal; (d), (e), (f) Shenmu coal; (a), (d), Fe(10)Ni(10)/KB catalyst, (b), (e) Fe(10)Mo(3)Ni(3)/KB catalyst, (c), (f) Ni(2)MO(10)/KB catalyst.

CO and CO₂ Hydrogenation Over Co/SiO₂ Catalyst

Y. Zhang, D. Sparks, M. E. Dry and B. H. Davis
Center for Applied Energy Research, University of Kentucky,
Lexington, KY 40511

Summary

CO and CO₂ hydrogenation was studied in a fixed bed reactor on a Co/SiO₂ catalyst. Reaction was carried out at 220°C, 350psig, H₂:CO=2:1, H₂:CO₂ = 2:1, with a total flow rate of 150 mL/min (3NL/hr/g catalyst) and a H₂+CO, H₂+CO₂ or H₂+CO+CO₂ flow rate of 50 mL/min(1NL/hr/g catalyst). CO, CO₂ and CO,CO₂ mixture feed gas were used respectively for comparison. The results indicated that in the presence of CO, CO₂ hydrogenation hardly occurred. For the cases of only CO or only CO₂ hydrogenation, the activity of the two were similar but the selectivity was very different. For CO hydrogenation, normal Fischer-Tropsch synthesis product distribution were observed with an α of about 0.80; in contrast, the CO₂ hydrogenation product contained about 70% methane. Thus, CO₂ and CO hydrogenation appears to follow different reaction pathways.

Introduction

Fixation of carbon dioxide has become of greater interest in recent years, primarily because of its impact on the environment through the greenhouse effect. One approach that has attracted attention is to produce synthesis gas through its reaction with methane even though the syngas produced only has a H₂/CO ratio of 1 for the idealized reaction. Another option is to recycle carbon dioxide to a gasification unit; however, there is a limit to the amount of carbon dioxide that can be utilized in this manner. Another approach is to hydrogenate carbon dioxide in Fischer-Tropsch synthesis (FTS) plants; this has become an attractive approach even though one must find a source of hydrogen to accomplish this.

For high temperature (330-350°C) FTS the water-gas-shift (WGS) reaction is sufficiently rapid that it is nearly at the equilibrium composition. The hydrogenation of CO₂ at high temperatures is possible and occurs in the fluid bed reactors operated by Sasol and Mossgas. However, the use of a slurry phase bubble column reactor is very attractive since its use allows the FTS reaction to be carried out isothermally. In the liquid phase synthesis, lower temperatures must be utilized (220-240°C) with either a cobalt or iron catalyst. It was of interest to compare the FTS reactions of CO and CO₂ with a cobalt catalyst. In this initial work a simple catalyst formulation has been utilized: cobalt supported on a silica without any promoters.

Experimental

The catalyst was prepared by three incipient wetness impregnations of silica (Davisil 644, 100-200 mesh, 300 m²/g, and pore volume of 1.15 cm³/g) with aqueous cobalt nitrate to produce a final loading of 15 wt.%. The material was dried in a fluidized bed and then calcined for 4 hrs. in an air flow at 400°C. Three grams of the calcined catalyst was diluted with 15 g of glass beads and placed in a fixed bed reactor where it was reduced in a H₂(33%)/Ar flow for 10 hours at 350°C. The reaction conditions were: 220°C, 24 atm (2.4MPa), H₂/CO = 2/1, 3 NL/hr/g catalyst total gas flow, 1 NL/hr/g catalyst synthesis gas flow. Analysis of the gaseous products was accomplished using gas chromatography.

Results.

The conversion of CO and CO₂ during 10 days on-stream are given in figure 1. Compared to the CO conversions of the same and another similar Co-silica catalyst, it appears that the initial CO conversion is about the same in the CSTR and in the fixed bed reactor; however, the activity decline is more rapid in the fixed bed reactor. The run data and conversions for the fixed bed reactor are compiled in table 1.

There was a decline in activity during the period between collecting the first two samples. The exit gas from the CO₂ conversions contained more CO₂ than the calibration gas so that CO₂

conversions were calculated from the mass balance for the other gaseous and liquid products; thus, there is some uncertainty in the absolute CO₂ conversion data but the trend shown in Table

Table 1 Run conditions and results from the conversion of CO and CO₂ with a cobalt-silica catalyst.

sample No.	time on stream(hrs)	feed gas	conversion(%)
1	17.3	CO	52.2
2	39.47	CO	45.8
3	44.47	CO ₂	31.2.
4	61.97	CO	24.4
5	70.47	CO ₂	23.1
6	90.97	CO ₂	20.5
7	109.97	CO	18.6
8	117.22	CO ₂	24.5
9	134.47	CO+CO ₂	CO, 53.5% CO ₂ , 3.98%
10		methanol	
11	206.22	CO+CO ₂ (different flow rate)	CO: 9.86% CO ₂ : 6.1%
12	226.89	CO ₂	22.8

1 and figure 1 are certainly valid. Thus, with the cobalt catalyst the conversion of CO and CO₂ occur at about the same rate. This is in contrast to the observations with an iron catalyst under low temperature FTS conditions where the rate of conversion of CO₂ is considerably lower than for CO (1-6).

A striking difference for the cobalt catalyst is the formation of methane. Under the same reaction conditions, the amount of methane produced is much higher for the CO₂ reactant (figure 2). Whenever CO₂ was the reactant, methane accounted for greater than 70% (based on carbon). However, under the same reaction conditions and with the same catalyst, methane accounted for less than 10% of the products. Similar results are reported by Riedel et al. (6). This requires that methane be formed by two pathways or that a common reaction intermediate and reaction pathway does not occur with CO and CO₂.

During period 9, the feed was changes so that equal amounts of CO and CO₂ were present in the feed and the flows of Ar, H₂ and (CO + CO₂) were the same as when either pure CO or CO₂ was converted. Under competitive conversions, CO was converted much more rapidly than CO₂, clearly showing that CO is adsorbed on the Co catalyst to a much greater extent than the CO₂. Whereas the total carbon oxide conversion is about the same expected from the trend of the previous runs, the conversion of CO accounted for more than 90% of the total conversion of the carbon oxides. A similar result was obtained following the conversion of methanol except that there was not as dramatic a difference as would be expected from the trend of the previous conversions. The CO conversion following the period of methanol feed was lower than expected from the trend of the prior periods. Since the water partial pressure was much higher during the conversion of methanol, it is anticipated that irreversible, or slowly reversible, damage of the catalyst occurred during the exposure to the high water partial pressure conditions.

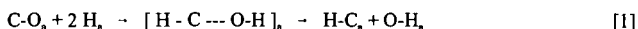
Following the first conversion of the mixture of CO and CO₂, methanol was substituted for the carbon oxides feed. Because of the limitations of the liquid pump, the feed during this period was only H₂ and methanol. The total flow was 4 NL/hr/g catalyst and the H₂/methanol molar ratio

was 2/1. Thus, the H₂/carbon ratio in the feed was the same as when CO and/or CO₂ was the feed but the flow rate of methanol was four times that of the carbon oxide. Under the reaction conditions used the conversion of methanol was about 50% whereas the conversion of CO or CO₂ was slightly less than 25%. Thus, considering the higher flow rate (4 times higher) and higher conversion (2 times higher) of methanol, the total carbon converted with the methanol feed was about 8 times greater than for the carbon oxides. Thus, the relative rate is rapid enough that any methanol intermediate could be converted to methane so that methanol would not be detected in the liquid sample; unfortunately, in this preliminary run the analysis of the gas sample did not provide a measure of the amount of methanol in the gas phase. The only significant products from the conversion of methanol under the FTS conditions were methane and water; thus, any methanol formed during the reaction could have been converted to methane.

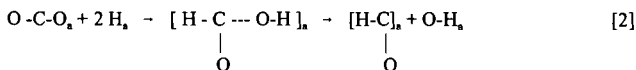
Discussion.

The difference in the product distributions obtained from the hydrogenation of CO and CO₂ preclude a common reaction pathway for FTS unless there is a second reaction pathway for the conversion of CO₂, but not CO, to methane. Furthermore, if there is a second pathway, then the FTS with CO₂ occurs at about only 20% of the rate with CO.

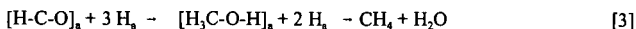
Based on the preliminary data, it is proposed that the conversion of CO and CO₂ occurs by different reaction pathways. It is assumed that the hydrogenation and breaking of the two C-O bonds of the CO₂ provide the source of the different pathways. In this proposal, the breaking of the C-O bond, presumably by the addition of adsorbed H to form C-O-H, competes with, and probably leads, the addition of adsorbed H to form the C-H bond. Thus, for CO the following reaction pathway could apply:



In the case of CO₂ the reaction is more complex since there are two C-O bonds that must be broken prior to, or simultaneous with, the formation of the C-H bond. If it is assumed that similar rates apply for the formation of the first O-H and C-H bonds as in the case of CO we would have a different situation, idealized in reaction [2]:



If reaction [2] is valid, it is then a matter of the hydrogenation of the adsorbed oxygen species to produce the adsorbed intermediate (methanol) and its subsequent hydrogenation:



Based on the carbon mass balance, about 75% of the hydrogenation of CO₂ would proceed by reaction [3] and the remainder would involve the breaking of the second C-O bond to continue along the normal FTS reaction pathway that is followed by CO hydrogenation. At this time, while the above mechanism accounts for the products that are produced from the hydrogenation of CO₂, it is very speculative. ¹⁴C-tracer studies are planned that should provide some evidence to establish whether the speculation has merit.

The results to date for the hydrogenation of CO₂ indicate that it will not be commercially attractive using typical FTS catalysts based on iron or cobalt.

Acknowledgment

This work was supported by US DOE contract number DE-AC22-94PC94055 and the Commonwealth of Kentucky. The funds to support Professor Dry's visit were provided by the Commonwealth of Kentucky.

References

1. L. Xu, S. Bao and B. H. Davis, Role of CO_2 oxygenates and alkenes in the initiation of chain growth during the Fischer-Tropsch synthesis, (M. de Pontes, R. L. Espinoza, C. P. Nicolaides, J. H. Scholz and M. S. Scurrell, eds.) *Natural Gas Conversion IV (Studies in Surface Science and Catalysis)* **107**, 175 (1997).
2. L. Xu, S. Bao, D. J. Houpt, S. H. Lambert and B. H. Davis, Role of CO_2 in the initiation of chain growth and alcohol formation during the Fischer-Tropsch Synthesis, *Catal. Today*, **36**, 347 (1997).
3. L. Xu, S. Bao, L.-M. Tau, B. Chawla, H. Dabbagh and B. H. Davis, Role of CO_2 in the initiation of chain growth during the Fischer-Tropsch Synthesis, *11th Ann. Int. Pittsburgh Coal Conf. Proc.*, **88**, 1994.
4. L. Xu, S. Bao, L.-M. Tau, B. Chawla, H. Dabbagh and B. H. Davis, Role of CO_2 in the initiation of chain growth during the Fischer-Tropsch synthesis, *Preprints ACS Fuel Chem. Div.*, **40**, 153 (1995).
5. L. Xu, S. Bao, L.-M. Tau, B. Chawla, H. Dabbagh and B. H. Davis, Role of CO_2 in the initiation of chain growth during the Fischer-Tropsch synthesis, *Proc. 211th National Mtg., ACS, Petrol. Div.*, 246-248 (1996).
6. T. Riedel, M. Claeys, H. Schulz, G. Schaub, S.-S. Nam, K.-W. Jun, M.-J. Choi, G. Kishan and K.-W. Lee, Comparative study of Fischer-Tropsch synthesis with H_2/CO and H_2/CO_2 syngas using Fe- and Co-based catalysts, *Appl. Catal. A: General*, **186**, 201-213 (1999).

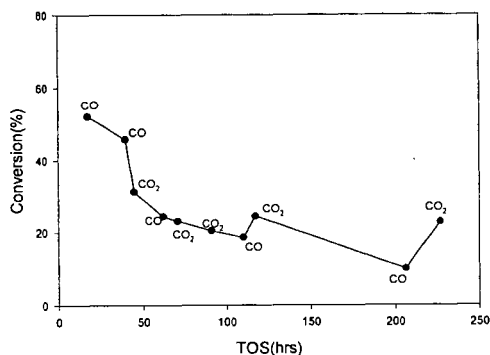


Fig. 1 CO and CO_2 conversion as a function of time on stream

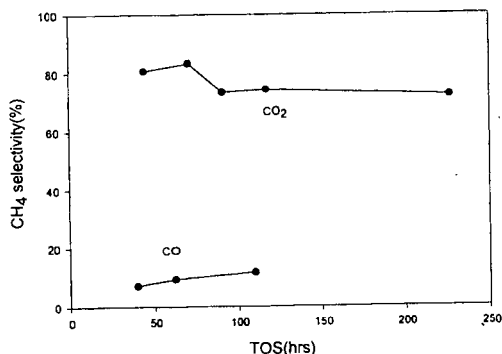


Fig. 2 Methane selectivity as a function of time on stream

References

1. L. Xu, S. Bao and B. H. Davis, Role of CO_2 oxygenates and alkenes in the initiation of chain growth during the Fischer-Tropsch synthesis, (M. de Pontes, R. L. Espinoza, C. P. Nicolaides, J. H. Scholz and M. S. Scurell, eds.) *Natural Gas Conversion IV (Studies in Surface Science and Catalysis)* **107**, 175 (1997).
2. L. Xu, S. Bao, D. J. Houpt, S. H. Lambert and B. H. Davis, Role of CO_2 in the initiation of chain growth and alcohol formation during the Fischer-Tropsch Synthesis, *Catal. Today*, **36**, 347 (1997).
3. L. Xu, S. Bao, L.-M. Tau, B. Chawla, H. Dabbagh and B. H. Davis, Role of CO_2 in the initiation of chain growth during the Fischer-Tropsch Synthesis, *11th Ann. Int. Pittsburgh Coal Conf. Proc.*, **88**, 1994.
4. L. Xu, S. Bao, L.-M. Tau, B. Chawla, H. Dabbagh and B. H. Davis, Role of CO_2 in the initiation of chain growth during the Fischer-Tropsch synthesis, *Preprints ACS Fuel Chem. Div.*, **40**, 153 (1995).
5. L. Xu, S. Bao, L.-M. Tau, B. Chawla, H. Dabbagh and B. H. Davis, Role of CO_2 in the initiation of chain growth during the Fischer-Tropsch synthesis, *Proc. 211th National Mtg., ACS, Petrol. Div.*, 246-248 (1996).
6. T. Riedel, M. Claeys, H. Schulz, G. Schaub, S.-S. Nam, K.-W. Jun, M.-J. Choi, G. Kishan and K.-W. Lee, Comparative study of Fischer-Tropsch synthesis with H_2/CO and H_2/CO_2 syngas using Fe- and Co-based catalysts, *Appl. Catal. A: General*, **186**, 201-213 (1999).

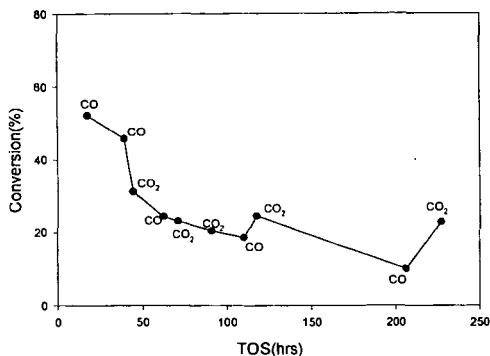


Fig.1 CO and CO_2 conversion as a function of time on stream

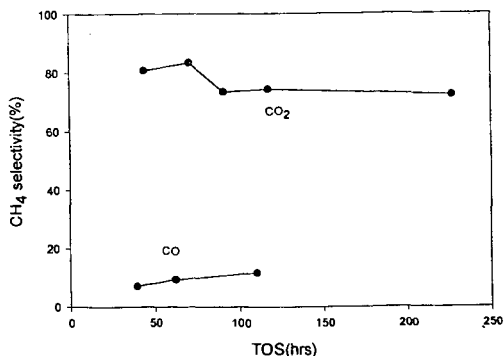


Fig. 2 Methane selectivity as a function of time on stream

OXIDATION OF SHORT CARBON FIBERS BY OXYGEN PLASMA

A. Martinez-Alonso and J. M.D. Tascón,
INCAR,CSIC, Apartado 73, Oviedo, N/A, 33080, Spain,
J.P. Boudou,
Université Pierre et Marie Curie, CNRS, 4, Place Jussieu, 75252Paris Cedex05, France
M.Chehimi
University Paris VII, ITODYS, 1, rue Guy de la Brosse, 75005Paris, France,
J. F. Watts
University of Surrey, Guildford, Surrey, N/A, GU2 5XH, United Kingdom

INTRODUCTION

Oxidation of carbon fibers is a method commonly used to improve their adhesion to matrices in the preparation of composite materials (1). The aim of this work is to evaluate the possibility and convenience of further increasing surface oxidation in short isotropic carbon fibers by the use of a cold oxygen plasma, not only in terms of the amount of oxygen introduced but also paying attention to the type of functionality achieved.

EXPERIMENTAL

Short, isotropic pitch carbon fibers, S-233 from Osaka Gas. Studied fibers include as supplied fibers plus two set of fibers submitted to oxygen plasma treatments of varying severity: 50W/1 min and 150 W / 5 min. All three sets of fibers (untreated and after oxygen plasma treatment) were characterized by C1s and O1s X-ray Photoelectron Spectroscopy (XPS, VG Scientific, Source : Al Mono Standard, CAE 20eV, Step 0.2 eV) (2) and by programmed pyrolytic degradation of oxygen complexes (TPD-MS).

RESULTS AND DISCUSSION

In Figure 1, XPS showed that the oxygen plasma treatment produces a strong surface oxidation. However, at higher power and longer time of exposure (150W/5min), the surface oxidative effect slightly declines. The same trend reversal due to a more drastic plasma treatment was already observed during oxidation of an activated carbon (3). Figure 2 shows a relative increase of the of -C=O and -C-O- region (<287 eV for C1s and <533 eV for O1s) with increase of the treatment intensity.

TPD agrees with results obtained by XPS. CO_2 evolution showed a promotion of the acidic COO- functionality (carboxylic groups, anhydrides, lactones) in the fiber treated at 50 W / 1 min which recedes for the more severely treated fiber where basic surface groups become predominant.

CONCLUSIONS

XPS and TPD showed that oxygen plasma treatments increase the oxidation levels of short carbon fibers. This enrichment is compensated by a selective removal of the surface acidic groups on the most exposed surface. Different predominant functionalities can be achieved by varying the treatment conditions.

LITERATURE CITED

- (1) Paiva, M.C., Montes-Morán, M.A., Martínez-Alonso, A., Tascón, J.M.D. and Bernardo, C.A., Proceedings, 22nd Biennial Conf. on Carbon, ACS, San Diego, CA, USA, 180-181 (1995).
- (2) Vickers, P.E., Watts, J.F., Perruchot, C., Chehimi, M.M., Carbon, 38, 675-689 (2000).
- (3) Boudou, J.P., Martínez-Alonso, A. and Tascón, J.M.D., Carbon, 38, 1021-1029 (2000)

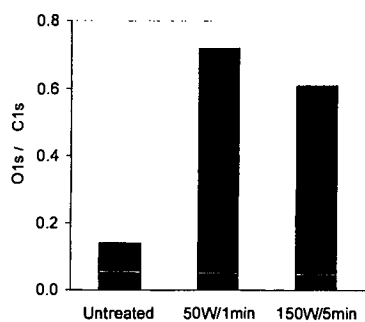


Figure 1. Effect of the plasma treatment on the XPS O1s / C1s ratio

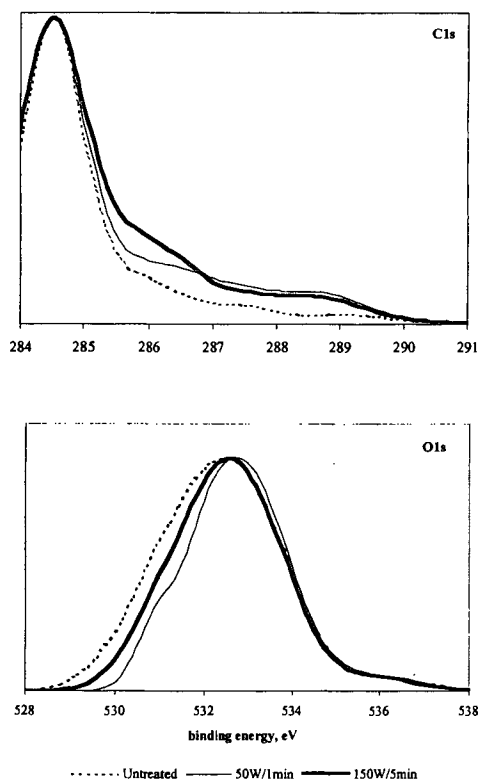


Figure 2 : Effect of the plasma treatment on the shape of the C1s and O1s spectra (normalized to the maximum of the untreated sample)

CARBON DEPOSITION ON Fe, Ni, AND Cr AND THEIR ALLOYS IN SUPERCRITICAL JET FUEL ENVIRONMENT

Orhan Altin, Fan Zhang, Bhabendra K. Pradhan and Semih Eser

Laboratory for Hydrocarbon Process Chemistry
The Energy Institute, 209 Academic Projects Building,
The Pennsylvania State University, University Park, PA 16802, USA

Key words: carbon deposit, sulfur, jet fuel, Ni, Fe, Cr, SEM, TPO.

INTRODUCTION

The formation of carbon deposits on metal surface from decomposition of jet fuel is a major concern in the development of advanced aircraft in which the fuel is also used as a heat sink (1). Metal surface composition can strongly affect carbon deposition from thermally stressed jet fuel or model hydrocarbon (2). Carbon deposition on heat exchanger surfaces, filters, injectors and control valves can pose serious operational problems. Depending on the temperature and pressure of the system and the activity of metal surfaces, the deposition may be catalyzed by metal surfaces with the formation of filamentous carbon, or other forms of carbonaceous solids (3, 4).

A considerable volume of research has been carried out on Fe and Ni containing catalysts/or alloys over the past two to three decades to investigate their catalytic activity for the formation of carbonaceous deposits from various hydrocarbons under different conditions (5-7). Jet fuels may contain up to 2000 ppm sulfur that can have a significant effect on solid deposit formation from thermal stressing of fuels on metal surfaces. The effects of sulfur compounds on carbon deposition are not clear. Ohla and Grabke (8) reported that sulfur retarded graphitic carbon formation on iron, but the growth of graphitic carbon on nickel was accelerated by sulfur. Trimm and Turner (9) observed both the facilitation and retardation effect of sulfur on carbon deposition from a mixture of propane and hydrogen on pre-sulfided nickel, copper, iron and stainless steel surfaces. They suggested that the formation of stable metal sulfides on surfaces inhibit carbon deposition, whereas the formation, and subsequent decomposition of labile metal sulfides accelerated the deposition process.

The main objective of this study is to investigate and characterize the carbon and sulfur based solid deposit formation from jet fuel (JP-8) stressing on pure Ni, Fe and Cr and binary alloys of Fe/Ni (55/45), Fe/Ni (64/36) and Ni/Cr (80/20) surfaces.

EXPERIMENTAL

Thermal stressing of a JP-8 fuel (120 ppm constituent sulfur) was carried out in the presence of pure Ni, Fe, and Cr and Fe/Ni (55/45), Fe/Ni (64/36), and Ni/Cr (80/20) foil surfaces. The 15x0.3x0.01 cm coupons were placed at the bottom of a 20 cm, 0.63 cm (O.D) and 0.4 cm (I. D.) glass-lined tube reactor. The reaction system was heated to 500°C for 2 hours under argon flow at 500 psig prior to the introduction of the JP-8. Then, the preheated fuel at 250°C was introduced to the reactor. The reactor temperature and the fuel pressure were kept constant throughout the experiments at 500°C, and 500 psig, respectively. The flow rate of jet fuel was maintained at 4 ml/min. After 5 hours of stressing, the foils were cooled down under argon flow in the reaction system.

The stressed foils were analyzed using LECO-RC412 Multiphase Carbon analyzer to determine the total amount of carbon deposition on the foils as well as temperature programmed oxidation (TPO) burn-off profiles (10). In TPO experiments, the CO₂ evolution was measured by two IR cells as a function of time while heating the sample from 100°C to 900°C at a constant rate of 30°C/min under O₂ flowing at 750 ml/min. The carbon deposits were also examined by field emission SEM (FESEM), SEM with energy dispersive x-ray spectroscopy (EDS), and x-ray diffraction (XRD).

RESULTS AND DISCUSSION

As shown in Table 1, the thermal stressing of JP-8 fuel on Ni and Fe and their alloys resulted in large amounts of carbonaceous solid deposits as compared to Cr and binary alloy with Ni, Ni/Cr (80/20). Total amounts of deposits were measured by using the LECO multi-phase carbon analyzer and the results were calculated in terms of μg of carbon per cm^2 surface area of the metal foil. The amount of carbon deposited on pure Ni, and Fe surfaces is 100, and 132 $\mu\text{g}/\text{cm}^2$,

respectively. The two binary alloys of Fe and Ni (with a relatively small difference in their bulk compositions) collected substantially different amounts of deposits. The alloy with 55% Fe and 45% Ni collected 55 $\mu\text{g}/\text{cm}^2$ carbon deposit (lower than that collected on pure Fe, or Ni), whereas 64% Fe and 36% Ni collected 389 $\mu\text{g}/\text{cm}^2$ (much higher than that collected on either pure metal surface). As expected, the addition of Cr to Ni reduced the deposit formation significantly. The binary Ni/Cr alloy collected 6 $\mu\text{g}/\text{cm}^2$ carbon deposit.

Table 1. The amount of carbon deposits collected on Ni, Fe, Fe/Ni (55/45), Fe/Ni (64/36), and Ni/Cr (80/20) surfaces. JP-8 was thermally stressed at 500°C and 500 psig for 5h at a flow rate of 4 ml/min.

Metal	Amount of deposit ($\mu\text{g}/\text{cm}^2$)
Ni	132
Fe	100
Fe/Ni (55/45)	55
Fe/Ni (64/36)	389
Ni/Cr (80/20)	6

Figure 1 shows the SEM micrographs of deposits formed from JP-8 stressing at 500°C on pure Ni, and Fe surfaces. In Figure 1a, it is seen that Ni surface is completely covered with filamentous deposits formed all over the surface. Most of the filaments have twisted shapes and they are longer than 5 μm in length. High magnification images from FESEM examination showed that some of the filaments contain metal particles at their tips. An EDS elemental map analysis indicated that the surface contains high concentrations of sulfur in addition to carbon. The sulfur compounds present in jet fuel such as, thiophene and benzothiophene and their alkylated homologs appear to react with metal surfaces at high rates. An XRD analysis clearly showed the formation of Ni_3S_2 on the nickel surface upon stressing with JP-8.

The thermal stressing of JP-8 at 500°C on pure Fe surface produced two different sulfur-containing structures besides the carbon deposits. Figures 1b and 1c show hexagonal, tetragonal and monoclinic structures of Fe_{1-x}S , pyrrhotites, and FeS, troilite formed on pure Fe surface. In Figure 1b, a carbon deposit in amorphous form was also observed as bright overlayer between the sulfide crystals. There was no filamentous deposit observed on the Fe surface. The formation of highly crystalline sulfide structures may inhibit the catalytic effect of Fe surface to form carbon filaments. Trimm and Turner (9) also observed similar behavior during propane stressing in the presence of H_2S on the Fe surface. The authors reported that the Fe surface did not produce much carbon deposit when H_2S is present, but without H_2S , the Fe surface collected a significant amount of carbon deposit.

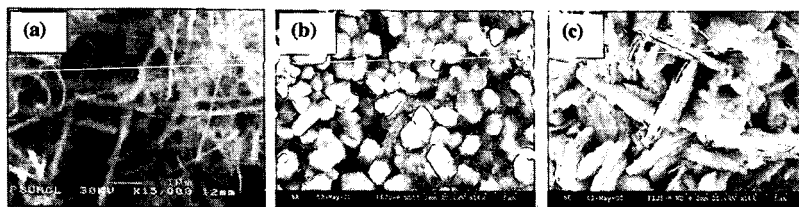


Figure 1. SEM micrographs of carbon deposits from thermal stressing of JP-8 at 500°C and 500 psig for 5h at flow rate of 4 ml/min on Ni (a), and Fe (b and c) surfaces.

Figures 2a, 2b and 2c show carbon and sulfur deposit structures on binary alloys of Fe/Ni (55/45), Fe/Ni (64/36) and Ni/Cr (80/20). No distinctive filamentous carbon morphology was observed on the surfaces of the deposited coupons. The deposits on the two Fe/Ni binary alloys appeared to have particulate morphologies with different surface coverage and particulate size. The bright carbon deposit structures seen on the Fe/Ni (55/45) surface in Figure 2a covered the whole alloy surface. The average particulate size of the deposits is 0.2 μm . However, on the Fe/Ni (64/36) shown in Figure 2b, deposits collected more on isolated areas without covering the surface completely. The average size of the particulate deposits is 0.5 μm , larger than that observed on the other binary Fe/Ni alloy. From these observations and the TPO results, one can suggest that the Fe/Ni (64/36) alloy has a higher activity towards carbon deposition than the Fe/Ni (55/45) alloy. This difference in surface activity can be attributed to differences in surface composition and metallic phases present in these alloys among other factors, such as

impurities and physical characteristics of the alloy surfaces. Figure 2c shows that addition of Cr to Ni significantly reduced the surface activity towards sulfur and carbon corrosion. A relatively small amount of deposits observed on the surfaces consist of sulfide flakes and small particles of solid carbon.

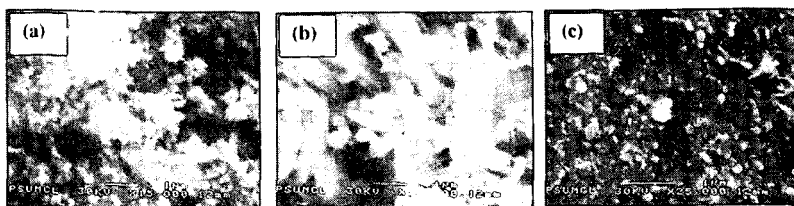


Figure 2. SEM micrographs of carbon deposits from thermal stressing of JP-8 at 500°C and 500 psig for 5h at flow rate of 4 ml/min on Fe/Ni (55/45)(a), Fe/Ni (64/36) (b) and Ni/Cr (80/20) (c) alloy surfaces.

The TPO profiles shown in Figure 3 indicate that on the pure Ni surface there are mainly two types of deposit structures that exhibit different reactivities in oxygen, giving two CO₂ evolution peaks centered at 375 and 750°C, respectively. The lower temperature peak can be attributed to reactive deposits, such as disordered, or amorphous deposits, and metal carbide (Ni₃C) particles. The higher temperature peak, on the other hand, should result from the oxidation of more ordered, e.g., graphitic, structures, produced around the metal particles in filamentous carbon structures.

On the Fe surface, three peaks were observed at 150, 275 and 450°C burn-off temperatures. The first low temperature peak can be related to the evaporation of trapped hydrocarbon molecules in the porous deposit structure, and the second broad peak results probably from the highly reactive carbon deposits formed between the sulfide crystals (Figure 1b). The third peak that appeared at around 450°C can be attributed to the oxidation of different iron carbides, e.g., Fe₃C₂, Fe₃C, and FeC, or of the more ordered carbon deposits formed on metal surfaces. No carbides were identified by XRD, probably because their quantity is very small compared to that of sulfides on the Fe surface.

The TPO profiles of the binary alloys of Fe and Ni are also shown in Figure 3. The heavy deposition on Fe/Ni (64/36) alloy is particularly noteworthy. The three major TPO peaks of the deposited alloys appeared at 150, 250-300 and 400°C. It is interesting that the high temperature peak (750°C) seen on the deposited nickel surface is absent on the deposited alloy surfaces. Similar to pure Fe TPO profiles, the first two peaks of alloys can be ascribed to the evaporation and oxidation of the trapped hydrocarbons, and the oxidation of the highly reactive solid deposits. The third very sharp peak at 400°C, probably results from the presence of an active alloy phase (Fe and Ni), which seems to catalyze the oxidation of the carbon deposits, as well.

As seen in Figure 2c, the amount of deposit on Ni/Cr alloy surface was very low compared to that obtained on Ni/Fe alloys. The TPO profile of the carbon deposits on Ni/Cr surface showed only one broad peak at 375°C that can be attributed to the oxidation of amorphous deposits and metallic carbides of Ni and Cr.

CONCLUSIONS

The catalytic effect of Ni and Fe surfaces resulted in significant amount of carbon deposits during the thermal stressing of JP-8 fuel in a flow reactor producing both filamentous, crystalline, amorphous, and metal carbide deposits. The sulfur compounds in the jet fuel lead to the formation of metal sulfides that cause surface corrosion and increase the surface area available for carbon deposition. The binary alloys of Fe and Ni further increased both carbon and sulfur deposition depending on the Fe content. The Cr addition to Ni, however, inhibited the catalytic activity of Ni significantly compared to the Ni and Fe alloys.

ACKNOWLEDGMENTS

This work was funded by the Air Force Wright Laboratory/Aero Propulsion and Power Directorate, Wright Patterson AFB. We thank Prof. H. H. Schobert of PSU for his support and Dr. T. Edwards of AFWL/APPD for helpful comments and discussion.

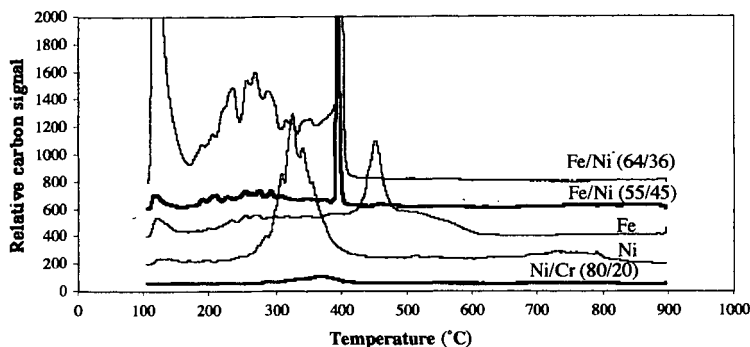


Figure 3. TPO profiles of deposits from JP-8 stressing at 500°C and 500 psig for 5h at a flow rate of 4 ml/min on pure Ni and Fe and Fe/Ni (55/45), Fe/Ni (64/36) and Ni/Cr (80/20) alloys.

REFERENCES

- 1) Edwards, T., Zabarnick, S., *Ind. Eng. Chem. Res.*, 3117, 32 (1993).
- 2) Li, J., Ph. D. Thesis, The Pennsylvania State University, 1998.
- 3) Edwards, T., Atria, J. V. ASME paper 97-GT-143, 1997.
- 4) Linne, D. L., Meyer, M. L., Edwards, T.; Eitman, D. A. 33rd Joint Propulsion Conference and Exhibit, AIAA, ASME, SAE, and ASEE, paper AIAA-97-3041, 1997.
- 5) Baker, R. T. K., *Carbon*, 315, 27 (1989).
- 6) Derbyshire, F. J., Trimm, D. L., *Carbon*, 189, 13 (1975).
- 7) Derbyshire, F. J., Presland, A. E. B., Trimm, D. L., *Carbon*, 111, 13 (1975).
- 8) Ohla, K., Grabke, H.J., *Werkstoffe und Korrosion*, 33, 341 (1982).
- 9) Trimm, D. L., Turner, C. J., *J. Chem. Tech. Biotechnol.*, 31, 285 (1981).
- 10) Altin, O., Eser, S., *Ind. Eng. Chem. Res.*, 642, 39(3) (2000).

A LANDMARK PAPER ON CARBON-SUPPORTED CATALYSTS: THE REAL STORY REVEALED BY THE SCIENCE CITATION INDEX

Ljubisa R. Radovic

*Department of Energy and Geo-Environmental Engineering
The Pennsylvania State University, University Park, PA 16802*

KEYWORDS: Carbon-supported catalysts, Carbon surface chemistry, Citation Index

INTRODUCTION

In the 1980's there was a resurgence of interest in understanding carbon as a catalyst support. It had been well documented by then that high catalyst dispersion can be achieved on carbon supports under certain conditions. This was attractive because it had also been established that carbon-supported hydrotreatment catalysts are much less prone to deactivation by coke deposition than the conventional alumina-supported catalysts. At Penn State, conditions were ideal to fully understand the virtues of carbon-supported catalysts and to rationalize the potential pitfalls in their preparation. Frank Derbyshire had just arrived from Mobil R&D and, being an expert in coal hydroprocessing, was eager to renew his studies on the catalytic properties of carbon. Alan Scaroni had been conducting an extensive study of coking propensities of carbon and alumina. And there was also the support of Phil Walker, with his encyclopedic knowledge of carbon materials and pioneering expertise in their use as catalyst supports.

Prior work had shown that "catalyst activity is strongly influenced by the interaction between the carbon surface and the deposited metal species" [1]. However, the exact nature of this influence was not clear [2]. Therefore, Derbyshire and his collaborators set out to "investigate the importance of surface functional groups on [sic] the activity of carbon-supported MoS₂ catalysts" [1]. In contrast to much of the previous work, in which "the carbons used ... were of different origin and varied in their chemical structure, textural properties and content of impurities," in this study "a single metal salt precursor and a single parent carbon were selected."

Offered below is a summary of the seminal importance of this study, even though its findings and conclusions, seen in hindsight, were somewhat ambiguous. While necessarily subjective, such an account is not only appropriate as a contribution to the symposium in memory of Frank Derbyshire but arguably also as a record of equal value (if not greater) as the more "objective" accounts offered by scientometricians or historians of science. Historians of science typically direct their efforts only at the "big stories," thus leaving us ignorant of the instructive historical context of "everyday science," where wheel reinventions are much more common. The Citation Index, an increasingly popular and potentially powerful tool, is too often used only by librarians and science administrators, as an end in itself rather than the means toward a more incisive analysis of the impact of a scientific publication.

HIGHLIGHTS OF "THE INFLUENCE OF SURFACE FUNCTIONALITY ON THE ACTIVITY OF CARBON-SUPPORTED CATALYSTS" [1]

Figure 1 reproduces the key results of this study. A "somewhat hydrophobic" polymer-derived carbon was subjected to widely varying oxidizing (a) and nitriding (b) treatments prior to their incipient wetness impregnation with ammonium heptamolybdate dissolved in a mixture of 90% H₂O/10% ethanol. Catalytic activity was determined at 450 °C by monitoring asphaltene conversion in batch hydrogenation tests of a process-derived coal liquefaction solvent. The extent of coke formation was determined by monitoring the weight gain of the catalyst after reaction. The effectiveness of carbon pretreatment was analyzed by elemental analysis and FT infrared spectroscopy. Maximum oxygen incorporation occurred when the carbon was treated in conc. HNO₃ and H₂SO₄ (ca. 25.3 and 20.1% O, respectively, vs. 1.4% in the parent carbon); nitrogen content increased from <0.05 to 0.53 and 0.87% after NH₃ treatment at 400 and 600 °C, respectively.

In contrast to the unclarified and largely detrimental effects of carbon oxidation, nitriding "was found to have a distinct effect in enhancing catalyst activity," and the authors proposed that this is because "nitrogen-containing surface groups ... provide preferential sites for the adsorption of Mo species." Even though the authors did not identify these sites, they argued prophetically that "the affinity between a particular carbon surface and the [selected catalyst] precursor will depend upon the compatibility of the two chemical structures."

IMPACT OF "THE INFLUENCE OF SURFACE FUNCTIONALITY ON THE ACTIVITY OF CARBON-SUPPORTED CATALYSTS" [1]

The story told by the Science Citation Index (Institute of Scientific Information, Philadelphia, PA), as of June 2000, is summarized in Figure 2. Not a widely cited paper, one would conclude, but such a conclusion would be a misleading one. As emphasized by Radovic and Rodríguez-Reinoso [2], this was the "first explicit attempt to clarify the influence of surface functional groups on the activity of carbon-supported catalysts." Intriguingly, however, most of the (non-self-) citing studies listed in Figure 2, even some of the most recent ones, do not identify it as such. Instead, the context of most citations is arguably peripheral and too often simply wrong.

(a) Inspired by Ref. 1, Guerrero-Ruiz et al. [3] performed a similar study of the role of nitrogen and oxygen surface groups in the behavior of carbon-supported iron and ruthenium CO hydrogenation catalysts, with ambiguous results.

(b) Abotsi and Scaroni [4-6] further pursued the issues raised in Ref. 1, emphasizing that "the activities of carbon-based catalysts are dependent on the nature and concentration of carbon surface functional groups." In particular, they were among the first investigators to appreciate [5] the crucial role of carbon surface charge [2]. Unfortunately, they mixed up the conditions of development of surface charge: it is the positively charged carbons, and not negatively charged ones (see p. 110 in Ref. [5]) that "are generally produced at high temperatures," and this turned out to be one of the keys to the preparation of highly dispersed molybdenum catalysts using anionic precursors [2, 7, 8].

(c) Groot et al. [9] echoed the underlying theme in Ref. 1, that chemical treatments should create catalyst anchoring sites on the support surface, and argued that "carbon blacks have a low density of functional (oxygen-containing) groups," which might serve as such sites.

(d) García and Schobert [10] mention Ref. 1 in passing, as a study of "hydrodesulfurization of thiophenes" [sic]. In a subsequent study by the same group [11], Ref. 1 is again misquoted as a study in which, presumably, "limits [in achievable liquefaction conversion] have been observed beyond which further increases in Mo addition no longer have a significant effect."

(e) The study of Solar et al. [7] is a direct descendant of Ref. 1, and its success in providing some of the key answers regarding the role of carbon surface chemistry [2] was largely due to the fact that Ref. 1 had asked the right questions. The studies by Suh et al. [12], Martín-Gullón et al. [13], Kim et al. [14], Jansen and van Bekkum [15], Krishnakutty and Vannice [16], Bastl [17], Dandekar et al. [18], Vázquez et al. [19] and Aksoylu et al. [20] fall into the same category. In a recent study, de la Puente and coworkers [21, 22] revisited the topic of the interaction between Mo and activated carbons, did cite Ref. 1 in the appropriate context, but failed to recognize that the key issues had been largely resolved in the intervening period [2]. Disregarding the fact that adsorption of molybdate anions is suppressed by carbon oxidation, largely because of the presence of acidic functional groups (e.g., COOH), these authors concluded, rather paradoxically, that "acidic groups were acting as chemical anchorage centers." It is not clear how "oxygenated surface groups ... can act as chemical anchorage sites for molybdate ions." They argued that "[w]hen using incipient-wetness impregnation, electrostatic repulsions seem to be less important than other factors such as the hydrophilicity of the sample and the distribution of oxygen-containing surface groups;" they did not provide measurements of catalytic activity to support these interesting claims.

(f) Klinik and Grzybek [23] cite Ref. 1 as, presumably, a study which has shown that "the effect of oxidation [of carbon using concentrated HNO₃] depends on the structure of the starting material. A subsequent study by the same senior author [24] uses Ref. 1 to support the argument that "some bigger pores (macropores)" are formed during oxidation of an activated carbon.

(g) In what is perhaps the most intriguing one of all the inappropriate citations, Sakanishi et al. [25] invoke Ref. 1 after saying that "fine particles of a Mo-based catalyst are applied in a moving bed." Along the same lines, Mochida and Sakanishi [26] further invoke Ref. 1 in vain by saying that "titanium and carbon have recently been examined as supports for iron and Ni-Mo sulfides."

Many other studies, especially in the 1990s, had as their *main* theme the effect of surface chemistry on the dispersion and activity of carbon-supported catalysts, and they are the ones that should have given, but did not, due credit to the pioneering effort of Derbyshire and his colleagues. Several examples will be provided during the presentation.

SUMMARY

Figure 3 is an attempt to synthesize our collective knowledge of the influence of surface functionality on the activity of carbon-supported catalysts. Its roots can be traced to the incisive questions posed by Frank Derbyshire and his colleagues in Ref. 1, as well as to improved understanding of "the compatibility of the two chemical structures" [1]. Apart from the effects of wetting and pore size distribution, carbon surface functionality governs the extent of adsorption of the catalyst precursor and the extent of its reduction or conversion to active state. Thus, for example, in catalyzing the oxygen transfer reactions illustrated here, the optimum surface chemistry is the one that (a) provides the anchoring sites for the catalyst precursor (e.g., carboxyl groups for ion exchange with cationic precursors), (b) allows favorable electrostatic interaction between the support and catalyst precursor (e.g., adsorption of anions at a pH less than the point of zero charge of the carbon), (c) prevents excessive catalyst mobility on the support surface, and (d) also facilitates the achievement of an intermediate oxidation state of the active phase, which in turn promotes oxygen transfer from the gas phase to the carbon surface.

The two-tiered value of the Science Citation Index to researchers, as opposed to librarians and research administrators, has been demonstrated here. On one hand it provides a quick start in the evaluation of scientific impact of a peer-reviewed publication. On the other hand, its increased use along the lines suggested here will hopefully force us all to be more careful, more selective and more responsible in collecting the lists of references for our publications. Perhaps sometime soon this important, yet too often neglected, activity will again be regarded as an opportunity to give credit where credit is really due and not as a matter of convenience, tradition and even nuisance. Had this been the case with Ref. 1, its "objective impact" would have been much closer to the admittedly subjective but arguably more appropriate evaluation presented here.

REFERENCES

1. Derbyshire, F. J., V. H. J. de Beer, G. M. K. Abotsi, A. W. Scaroni, J. M. Solar, and D. J. Skrovanek, *Appl. Catal.*, 1986. 27: p. 117.
2. Radovic, L. R. and F. Rodríguez-Reinoso, in *Chemistry and Physics of Carbon*, Vol. 25, P. A. Thrower, Editor. 1997, Marcel Dekker: New York. p. 243.
3. Guerrero-Ruiz, A., I. Rodríguez-Ramos, F. Rodríguez-Reinoso, C. Moreno-Castilla, and J. D. López-González, *Carbon*, 1988. 26: p. 417.
4. Abotsi, G. M. K., A. W. Scaroni, and F. J. Derbyshire, *Appl. Catal.*, 1988. 37: p. 93.
5. Abotsi, G. M. K. and A. W. Scaroni, *Fuel Process. Technol.*, 1989. 22: p. 107.
6. Abotsi, G. M. K. and A. W. Scaroni, *Carbon*, 1990. 28(1): p. 79.
7. Solar, J. M., C. A. León y León, K. Osseo-Asare, and L. R. Radovic, *Carbon*, 1990. 28(2/3): p. 369.
8. Solar, J. M., V. H. J. de Beer, F. J. Derbyshire, and L. R. Radovic, *J. Catal.*, 1991. 129: p. 330.
9. Groot, C. K., P. J. G. D. van de Gender, W. S. Niedzwiedz, A. M. van der Kraan, V. H. J. de Beer, and R. Prins, *Bull. Soc. Chim. Belg.*, 1988. 97: p. 167.
10. García, A. B. and H. H. Schobert, *Fuel*, 1989. 68: p. 1613.
11. Dutta, R. and H. Schobert, *Catal. Today*, 1996. 31: p. 65.
12. Suh, D. J., T.-J. Park, and S.-K. Ihm, *Carbon*, 1993. 31(3): p. 427.
13. Martín-Gullón, A., C. Prado-Burguete, and F. Rodríguez-Reinoso, *Carbon*, 1993. 31(7): p. 1099.
14. Kim, K. T., Y. G. Kim, and J. S. Chung, *Carbon*, 1993. 31(8): p. 1289.
15. Jansen, R. J. J. and H. v. Bekkum, *Carbon*, 1994. 32(8): p. 1507.
16. Krishnankutty, N. and M. A. Vannice, *Chem. Mater.*, 1995. 7: p. 754.
17. Bastl, Z., *Collect. Czech. Chem. Commun.*, 1995. 60: p. 383.
18. Dandekar, A., R. Baker, and M. A. Vannice, *Carbon*, 1998. 36: p. 1821.
19. Vazquez, P., et al., *Appl. Catal. A*, 1999. 184(2): p. 303.
20. Aksoylu, A., M. Madalena, A. Freitas, and J. Figueiredo, *Appl. Catal.*, 2000. 192: p. 29.
21. de la Puente, G. and J. Menéndez, *Solid State Ionics*, 1998. 112(1-2): p. 103.
22. de la Puente, G., A. Centeno, A. Gil, and P. Grange, *J. Colloid Interf. Sci.*, 1998. 202: p. 155.
23. Klinnik, J. and T. Grzybek, *Fuel*, 1992. 71: p. 1303.
24. Grzybek, T., *Fuel*, 1990. 69(5): p. 604.
25. Sakanishi, K., H.-U. Hasuo, I. Mochida, and O. Okuma, *Energy & Fuels*, 1995. 9: p. 995.
26. Mochida, I. and K. Sakanishi, *Adv. Catal.*, 1994. 40: p. 39.

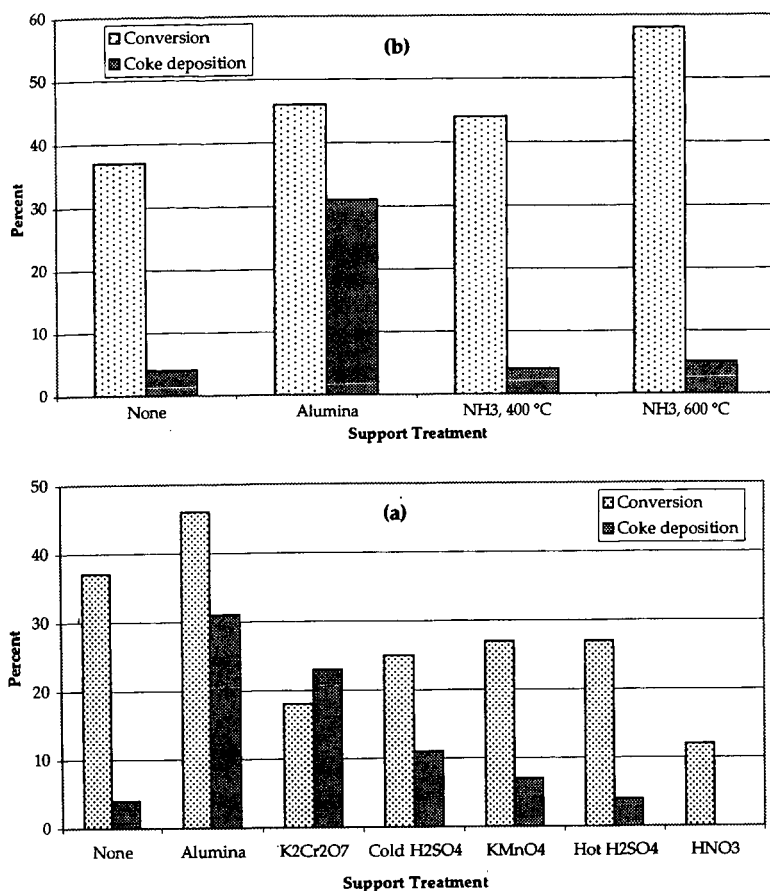


FIGURE 1. Effect of carbon surface functionality on the performance of sulfided Mo/C catalysts: (a) oxidative treatments; (b) nitriding treatments (from Ref. 1).

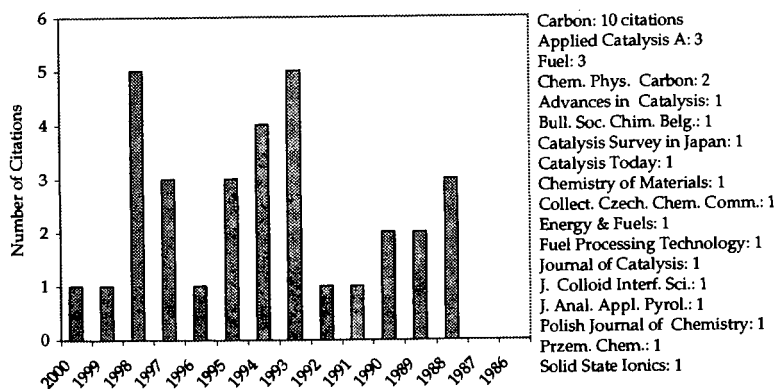


FIGURE 2. Summary of the Citation Index search for Ref. 1, as of June 2000.

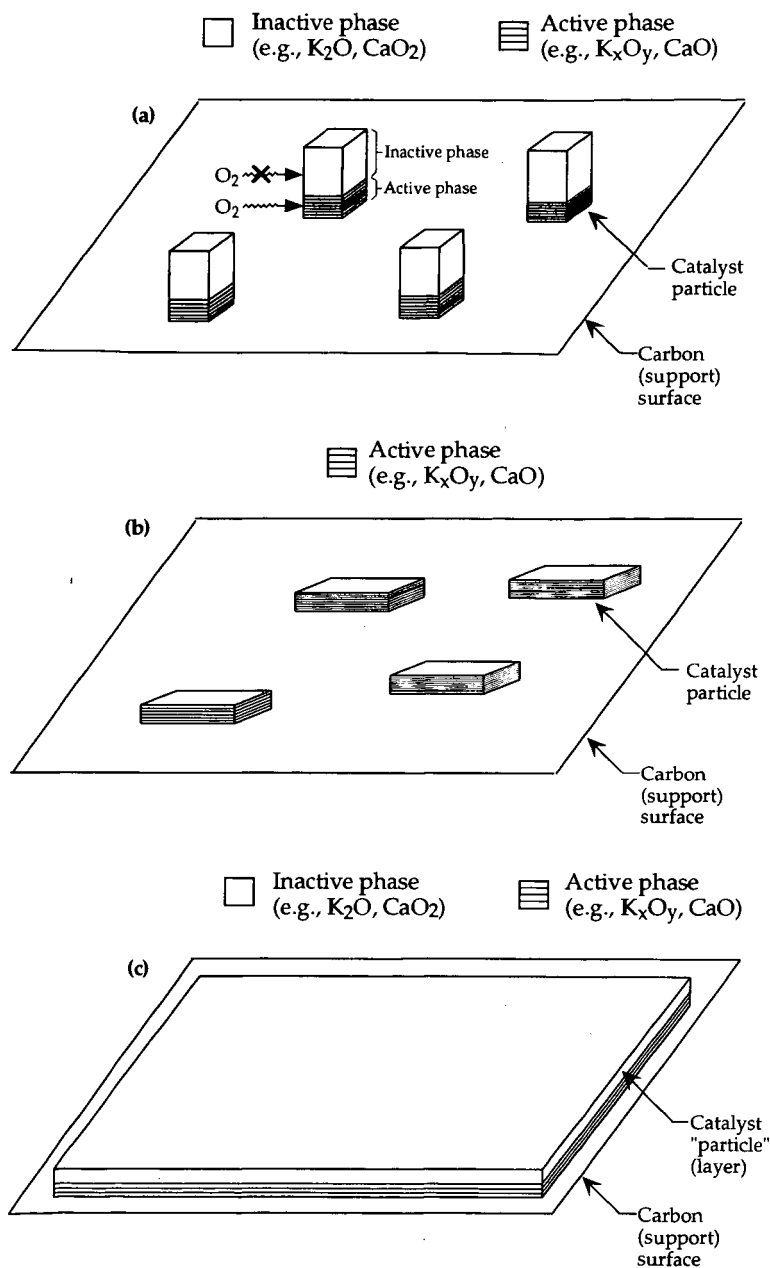


FIGURE 3. Summary of the influence of carbon surface functionality on the dispersion (and thus catalytic activity) of carbon-supported catalysts: (a) intermediate dispersion (activity); (b) high dispersion (activity); (c) low dispersion (activity).

LIQUEFACTION OF INDONESIAN COALS WITH BOTTOM RECYCLE USING FeNi CATALYST SUPPORTED ON CARBON NANOPARTICLES

Unggul Priyanto¹⁾, Kinya Sakanishi²⁾, Osamu Okuma³⁾, and
Isao Mochida¹⁾

1) Institute of Material Study, Kyushu University,
Kasuga, Fukuoka 816-8580, Japan

2) National Institute for Resources and Environment,
Tsukuba, Ibaraki 305-8569, Japan

3) The New Industry Research Organization, 1-5-2, Minatojima-minamimachi, Chuo-ku, Kobe
650-0047, Japan

Abstract

A series of coal liquefaction with bottom recycle was performed using FeNi catalyst supported on carbon nanoparticles (Ketjen Black: KB) at 450°C for single- and two-stage. In the single-stage, FeNi/KB catalyst gave excellent catalytic activity providing oil yield over 74% with successful reduction of catalytic loading to 0.15 wt% Fe and 0.15 wt% Ni d.a.f coal base.

Keywords: coal liquefaction; bottom recycle; iron nickel supported on KB

Introduction

The main key of catalyst cost reduction for direct liquefaction of coal are recovery and repeated use of the catalyst. The major difficulty for the catalyst recovery comes from the mineral presence in coal. There are two approaches for catalyst recovery and regeneration. The first one is to eliminate or reduce the mineral in the coal, and another one is to design catalysts of ultrafine particle size and low specific gravity for recovery.¹

Dow Chemical Co developed very small particles of molybdenum sulfide used as catalysts and were recovered and recycled with a novel hydroclone process.² The catalyst support can also provide such functions. The authors proposed a novel type of liquefaction catalyst with high activity and functions for recovery and repeated use.³⁻⁶ NiMo and FeNi sulfides supported on particular carbon nanoparticles are catalysts, which can provide high distillate yields and can be separated from the solid residue by gravimetric separation for repeated use.

One of the major contributions for recycle of the catalyst or drastic reduction of its amount is to recycle non-distillate coal liquefaction products back to the initial stage of the process, which is termed as bottom recycle.⁷ It has been recognized that large polycondensed aromatic rings from non-distillate products are very effective to disperse solvents for the very polar initial products of coal dissolution. Moreover, they can be hydrogenated easily to hydro aromatic structures, and have ability to shuttle hydrogen between unreacted coal, reacting molecules, and solvent components.^{8,9}

In the present study, liquefaction of Tanito Harum and Adaro coals (Indonesian coals) was performed by using FeNi/KB catalyst to examine the effect of bottom recycle on the oil yield and the performance of H-donor (tetralin):

Experimental Section

Catalyst and Materials

A prescribed amount of Ketjen black was dispersed in methanol by ultrasonic irradiation for 15 min. Then, iron(II) fumarate and Ni(NO₃)₂ dissolved in methanol were mixed to the KB-methanol slurry with a small amount of nitric acid (1% vol.) as an additive to prepare FeNi/KB catalyst. The slurry was dispersed by ultrasonic, and then, heated at 40°C for 2 h before the slurry was dried at 120°C for 12 h in vacuo. The catalyst was presulfided by flowing 5% vol H₂S/H₂ at 360°C for 2 h prior to the reaction.

The elemental analysis of Tanito Harum coal is summarized in Table 1. Commercially guaranteed grade tetralin (TL) was used as liquefaction solvent.

Liquefaction Procedure

Coal liquefaction was performed in an electromagnetic-driven autoclave of 50 ml capacity at 450°C for single stage, 380°C and 450°C for two-stage liquefaction.¹⁰ Three grams of coal, 3 grams of solvent, and 0.09 grams of catalyst were charged to the autoclave.¹¹ The single- and two-stage liquefaction was performed under 15 MPa of hydrogen pressure. The heating rate to the reaction temperature was 20°C/min. The stirring speed was 1300 rpm. For two-stage liquefaction, the first stage was performed at 380°C for 15 min, and then the reactor was cooled down. Hydrogen gas was renewed after releasing out gaseous products. The second stage reaction was carried out at 450°C, 15 MPa for 105 min.

The liquefaction with repeated use of catalyst was done by recycling asphaltene, preasphaltene, residue, and used catalyst from run 1 to run 2 after they were separated from oil as illustrated in Figure 1. The liquefaction with bottom recycle was performed in 7 runs as illustrated in Figure 2. After the third run, a third of asphaltene, preasphaltene, residue, and used

catalyst was purged to prevent the accumulation of ash and unconverted materials. The remainder was recycled to the following run. To keep the the sulfidation state of the catalyst, CS₂ was added in every run.¹²

The liquid and solid products of coal liquefaction were recovered with THF. After THF was removed by evaporation, the product was extracted in sequence with n-hexane, acetone, and THF. The n-hexane-soluble (HS), hexane-insoluble but acetone-soluble (HI-ACS), acetone-insoluble but THF-soluble (ACI-THFS), and THF-insoluble (THFI) substances were defined as oil(O) and solvent, asphaltene(A), preasphaltene(PA), and residue(R), respectively. The gas yield was calculated by weight difference between initial coal and recovered product. The oil yield was calculated by subtracting the solvent weight from the total weight of HS. The reaction under the same conditions was repeated at least three times to make sure the experimental result that were within 1wt% daf coal base.

Results and Discussion

Recycle of Heavy Residual Product and Repeated used of FeNi/KB catalyst

Table 1 describes results of residual product recycle in the single-stage liquefaction of Tanito Harum coal with FeNi/KB catalyst using process as illustrated in Figure 1. The liquefaction process in run 2 gave 69% oil yield that was comparable to that of run 1. It must be noted that there was no addition of fresh catalyst in run 2. It means that the activity of repeated use of FeNi/KB catalyst in run 2 was still high enough. Moreover, the oil yield was increased by hydrogenation of asphaltene and preasphaltene. The asphaltene, preasphaltene, and residue yields in the run 2 was average value of run 1 and 2.

Effects of Reaction Procedure with Bottom Recycle Mode on the single-stage Liquefaction

Figure 3 describes effect of reaction process results in the single-stage liquefaction of Tanito Harum coal with FeNi/KB catalyst. The liquefaction yields from single run were showed in Figure 3a, and the yields from liquefaction with bottom recycle were showed in Figure 3b.

The liquefaction with heavy residual recycle was performed in 7 successive runs (see Figure 2). In the run 1 to 3, the liquefaction was done by utilizing bottoms recycle without purging to obtain the recycled catalyst/fresh catalyst ratio of 2. The liquefaction with bottom recycle provided average oil yield of 74%, which was 5% higher than that of liquefaction without bottom recycle. It is also be noted that the liquefaction only used fresh catalyst of 0.045 g each run compared to liquefaction without bottom recycle that used 0.09 g catalyst. It was suggested that high recycle ratio (recycled catalyst/fresh catalyst ratio) can improve significantly oil yields.

Table 3 shows liquefaction yields from liquefaction of Tanito Harum coal with bottom recycle each run. The lowest oil yields was obtained in the first run, which only carried the total catalyst of 0.045 g. In the second run, the oil yield highly improved in line with the addition of fresh catalyst. The highest improvement of oil yield occurred in this run followed by increasing gas yield reaching 18%. Large oil yield may be due to the conversion of asphaltene and preasphaltene sent from the first run.

The highest oil yield occurred in the third run. In this run, the total catalyst (fresh and used catalyst) reached 0.135 g. The highest oil yield in this run may be caused by a number of total catalyst that still had high activity and heavy residual products from previous runs. After the third run, the oil yield tended to decrease down to 74%, which showed the decrease of the catalyst activity. The oil yield appeared to be constant from the fifth run. In those run the activity of catalyst and a number of heavy residual products recycled become stationary.

Table 4 summarizes the conversion of tetralin into naphthalene after liquefaction of 60 min at 450°C, 15 MPa. Single-stage liquefaction with bottom recycle in the second run allowed 16% conversion that was much lower than that of liquefaction without bottom recycle (21% conversion), indicating that polynuclear aromatic ring of crude liquid bottom can aid in utilizing gaseous hydrogen. However, in the sixth run allowed 20% conversion inspite of higher total catalyst than that of the second run. This indicated the decrease of catalyst activity in the run.

Effects of Reaction Procedure with Bottom Recycle Mode on the Two-stage Liquefaction

Figure 4 illustrates results of the two-stage liquefaction of Adaro coal with FeNi/KB catalyst. The liquefaction yields from single-stage, two-stage, and two-stage with bottom recycle was showed on Figures 4a, 4b, and 4c respectively. Single- and two-stage liquefaction of Adaro coal provided 68% and 80% oil yields respectively (see Figure 4a and 4b). The two-stage liquefaction with bottom recycle provided average oil yield of 82% that was 2% higher than that of liquefaction without bottom recycle. The combination of two-stage and bottom recycle gave very high oil yield.

Table 5 summarizes gas and oil yields from two-stage liquefaction of Adaro coal with bottom recycle in several runs. The highest oil yield occurred in the third run. After the fifth run, the oil yield tended to be constant.

Conclusions

The liquefaction of coal with bottom recycle mode in the present study successfully improved oil yield, hydrogen transfer efficiently, and reduction of catalyst amount required. In this procedure, FeNi catalyst supported on carbon nanoparticles showed an excellent catalytic activity in the liquefaction with bottom recycle mode that can keep its activity in the repeated use.

References

- (1) Mochida, I.; Sakanishi, K.; 'Advances in Catalysis', Academic Press, 1994, 8, 25.
- (2) Whitehurst, D.D., Ed., 'Coal Liquefaction Fundamentals' ACS Symp. Ser., Vol.139, Washington DC, 1980.
- (3) Sakanishi, K.; Hasuo, H.; Mochida, I.; Okuma, O. *Preparation of Highly Dispersed NiMo Catalyst Supported on Hollow Spherical Carbon Black Particles; Energy & Fuels*, 1995, 9, 995.
- (4) Sakanishi, K.; Hasuo, H.; Kishino, M.; Mochida, I. *Catalytic Activity of NiMo-sulfide Supported on a Particular Carbon Black of Hollow Microsphere in the Liquefaction of a Subbituminous Coal; Energy & Fuels* 1996, 10, 216-219.
- (5) Sakanishi, K.; Taniguchi, H.; Hasuo, H.; Mochida, I. *Iron-based Catalysts Supported on Carbon Nanoparticles of Hollow Structure for Coal Liquefaction; Ind. Eng. Chem. Res.* 1997, 36, 306.
- (6) Sakanishi, K.; Hasuo, H.; Kishino, M.; Mochida, I. *Solvent-free Liquefaction of Brown and Sub-bituminous Coals Using NiMo Sulfide Catalyst Supported on Carbon Nanoparticles; Energy & Fuels* 1998, 12, 284.
- (7) Mochida, I.; Sakanishi, K.; Suzuki, N.; Sakurai, M.; Tsukui, Y.; Kaneko, T., *Catalysis Surveys from Japan* 2, 1998, 17.
- (8) Derbyshire, F.J.; Whitehurst, D.D.; *Study of Coal Conversion in Polycondensed Aromatic compounds; Fuel* 1981, 60, 655.
- (9) Derbyshire, F.J.; Varghese, P.; Whitehurst, D.D., *Synergistic Effects between light and Heavy Solvent Components during Coal liquefaction, Fuel* 1982, 61, 859.
- (10) Priyanto, U.; Sakanishi, K.; Mochida, I. *Optimization of Two-stage Liquefaction of Indonesian Coals Using FeNi Catalyst supported on carbon nanoparticles*, Proceedings of International Conference on Clean and Efficient Coal Technology in Power Generation, 1999, Jakarta, Indonesia.
- (11) Priyanto, U.; Sakanishi, K.; Mochida, I. *Effects of Solvent Amount and Dispersed Catalyst in the Liquefaction of Indonesian and Chinese Coals*. Proceedings of the Tenth International Conference on Coal Science, I, 1999, Shanxi science & Technology Press, Taiyuan, China.
- (12) Derbyshire, F.J.; Davis, A.; Lin, R.; Stansberry, P.G.; Tetter, M.T. *Coal Liquefaction by Molybdenum Catalysed Hydrogenation in the Absence of Solvent; Fuel Process. Technol.* 1986, 12, 127.

Table 1 Elemental Analyses of Coals Used in The Present Study

	C ^a	H ^a	N ^a	O ^a	S ^a	Ash ^b	H/C
Adaro Coal	66.6	5.3	0.9	26.7	0.44	3.0	0.96
Tanito Harum Coal	71.2	5.5	1.6	21.7	0.16	3.9	0.93

^a in Wt % (d.a.f.)

^b in Wt. %

Table 2 Liquefaction yields from Single-stage Liquefaction of Tanito Harum Coal with Repeated used Catalyst

Run	Total catalyst g	Gas Yield Wt %	Oil yield Wt %	Asp ^a Wt %	Preasp ^a Wt %	Residue ^a Wt %
1	0.09	15	69	-	-	-
2	0.09	15	69	10	5	1

^a average value of run 1 and 2

Table 3 Liquefaction yields from Single-stage Liquefaction of Tanito Harum Coal with Bottom Recycle

Run	Total catalyst g	Gas Yield Wt % (d.a.f)	Oil yield Wt % (d.a.f)	Asp Wt % (d.a.f)	Preasp Wt % (d.a.f)	Residue Wt % (d.a.f)
1	0.045	14 ^b	67 ^b	-	-	-
2	0.09	18 ^b	75 ^b	-	-	-
3	0.135	16 ^b	77 ^b	7 ^a	3 ^a	1 ^a
4	0.135	15 ^b	76 ^b	7 ^b	2 ^b	1 ^b
5	0.135	15 ^b	74 ^b	10 ^b	1 ^b	1 ^b
6	0.135	15 ^b	74 ^b	9 ^b	2 ^b	1 ^b
7	0.135	15 ^b	74 ^b	9 ^b	2 ^b	1 ^b

^a average value of run 1, 2, and 3

^b relative value of each run based on its coal feed

Table 4 Conversion of Tetralin during Coal Liquefaction ^a

Reaction Process	Total Catalyst g	Tetralin Conv (%)
Single-stage	0.09	21
Single-stage with bottom recycle ^b	0.09	16
Single-stage with bottom recycle ^c	0.135	20

^a Reaction Condition : 450°C, 60 min, 15 MPa; stirring speed : 1300 rpm.

^b in the second run (see table 3)

^c in the sixth run

Table 5 Gas and Oil Yields from Two-stage Liquefaction of Adaro Coal with Bottom Recycle

Run	Total Catalyst g	Gas Yield ^a Wt %	Oil Yield ^a Wt %
1	0.045	13	74
2	0.09	19	84
3	0.135	14	87
4	0.135	14	85
5	0.135	14	85
6	0.135	15	81
7	0.135	15	81

^a relative value of each run based on its coal feed

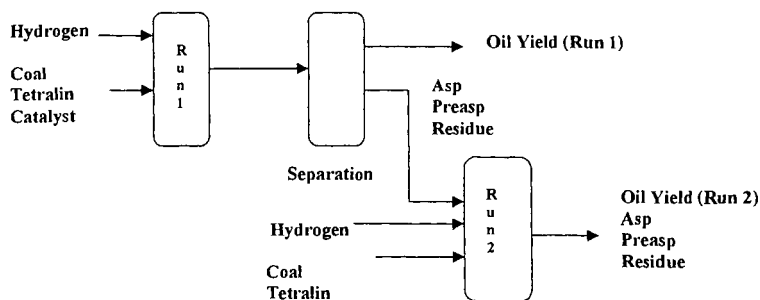
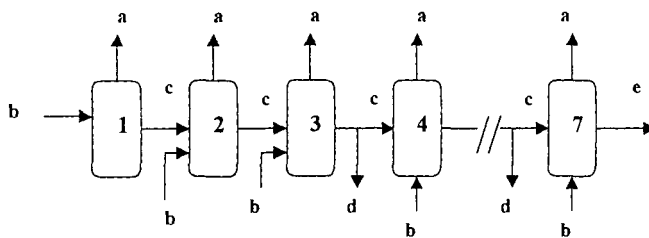


Figure 1 Coal liquefaction process in series



a Oil Yield
b Feed of coal(3 g), tetralin(3 g), and catalyst(0.045)
c Yields of Asphaltene, preasphaltene, repeated use catalyst, and residue
d Purge of asphaltene, preasphaltene, used catalyst, residue
e Last output of oil, asphaltene, preasphaltene, and residue

Figure 2. Liquefaction Process with Bottom Recycle

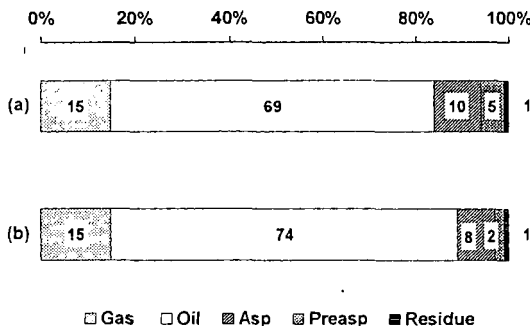


Figure 3. Effects of reaction process in the single-stage liquefaction of Tanito Harum coal with FeNi/KB catalyst, reaction conditions: 450°C, 15 MPa. Reaction processes: (a) Single stage at 60 min (b) Single-stage with bottom recycle performed for 60 min as given on Fig.2. For (a) coal/solvent/catalyst = (3 g)/(3 g)/(0.09g) and (b), coal/solvent/catalyst = (3 g)/(3 g)/(0.045 g)

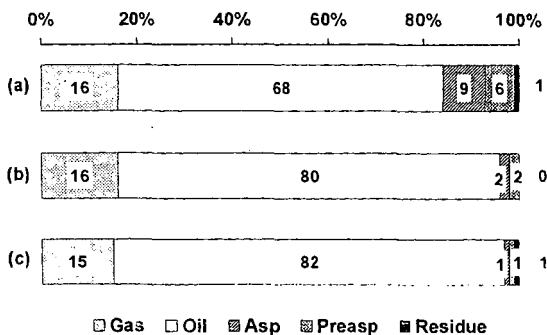


Figure 4. Effects of reaction process in the single- and two-stage liquefaction of Tanito Harum coal with FeNi/KB, Reaction Process: (a) is single-stage, and (b) is two-stage while (c) is two-stage with bottom recycle as given by Figure 2. Reaction times: (a) single-stage at 60 min; (b) 15 min at the first stage and 105 min at the second stage; (c) 15 min at the first stage and 105 min at the second stage each run. For (a) and (b), coal/solvent/catalyst = (3 g)/(3 g)/(0.09 g); For (c), coal/solvent/catalyst = (3 g)/(3 g)/(0.045 g).

LIQUEFACTION PATHWAYS OF SUBBITUMINOUS AND BITUMINOUS COALS

Burtron H. Davis and Robert A. Keogh

Center for Applied Energy Research

2540 Research Park Drive

Lexington, KY 40511

KEYWORDS: coal liquefaction, reaction pathways

INTRODUCTION

Lumped parameter kinetic models have successfully been used to describe industrially significant and complex chemical processes such as catalytic cracking (e.g. 1), catalytic reforming (e.g. 2) and addition polymerization (e.g. 3). The complexity of the liquefaction process has necessitated the use of this approach in studying the thermal and catalytic pathways of this process. In this work, the lumped parameters used are the standard solubility class: a) oil plus gases (O+G), b) asphaltenes and preasphaltenes (A+P) and, c) coal insoluble organic matter (IOM). The lumped solubility classes produced from the thermal liquefaction of a large number of U.S. bituminous coals were plotted on a ternary plot. The resulting data suggested a common pathway for all of the bituminous coals. A Wyodak coal was also studied to determine the pathway of a subbituminous coal for comparison.

EXPERIMENTAL

The description and the range of values of some of the key coal properties of the 69 high volatile bituminous coals used in the initial study are given in Table 1. The properties of the three coals (W. Ky. #9, W. Ky. #6 and Wyodak) used in the more extensive studies are given in Table 2.

All of the liquefaction experiments were done in 50 mL batch microautoclaves using a hydrogen atmosphere. Details of the liquefaction procedure and solubility class determinations are given elsewhere (4). In this work, oils are defined as pentane solubles, asphaltenes are benzene soluble and pentane insoluble, preasphaltene are pyridine soluble and benzene insoluble and IOM are pyridine insoluble. In the catalytic experiments, all catalysts, with the exception of Shell 324, were sulfided *in-situ* by adding twice the stoichiometric amount of dimethyldisulfide required to sulfide the metal of the catalyst. The Shell 324 catalyst was presulfided prior to the additions of coal and liquefaction solvent to the reactor.

RESULTS AND DISCUSSION

The lumped parameters obtained from the thermal liquefaction of the initial 69 coals at a 15 min. residence time and three reactions temperatures (385°C, 427°C, 445°C) were plotted in a ternary graph (Figure 1). These data suggest a common liquefaction pathway for all of the coals. A Western Kentucky #6 and #9 were selected to verify the apparent pathway. Reaction conditions were selected to cover a maximum range of conversions.

The thermal liquefaction pathway of the W. Ky. #6 coal is shown in Figure 2. As can be seen in Figure 2, the thermal pathway over a large range of conversions is identical to the pathway suggested in Figure 1 for the diverse set of coals. There appears to be two distinct stages in the liquefaction of these coals. In the initial stage, the primary reaction is the conversion of the coal to asphaltenes plus preasphaltenes. This reaction continues until the A+P and coal conversion reaches a maximum yield. During this stage, the oil plus gas yield remains relatively constant. In the second stage of the thermal pathway, the primary reaction is the conversion of A+P to O+G. The coal conversion increases very little in this stage of the pathway. At the higher temperature and long residence times, the pathway appears to change again. Both the O+G and A+P yields decrease suggesting the possibility of retrograde reactions are taking place. These results suggest that these bituminous coals have a common thermal liquefaction pathway.

The pathway defined for the bituminous coals indicates that a maximum in the A+P yields is achieved before there is a substantial increase in the O+G yield. It is desirable to change the pathway in such a manner as to achieve increases in the O+G yield as coal conversion increases. A supported catalyst (Shell 324) and an oil-soluble catalyst precursor (molybdenum naphthenate) were utilized in an attempt to favorably alter the liquefaction pathway to increase the O+G yields as coal conversion increases. The same W. Ky. #6 sample was used in the catalytic studies. The results of these experiments are shown in Figure 3. The pathway defined using both catalysts are similar to

the defined thermal pathway for this coal. The major effect of catalyst addition on the pathway is to increase the rate of production of the intermediate, A+P, and has no major effect on the selectivity defined by the solubility classes. Therefore, the observed data for the thermal and catalytic processes of the bituminous coals are consistent for the following series of reactions:



A subbituminous Wyodak coal was studied next to determine if the lower rank coal has the same thermal and catalytic pathway as those defined for the bituminous coals. The results of similar experiments performed for the Wyodak coal are shown in Figure 4. Both the thermal and catalytic pathways defined for the Wyodak coal are significantly different from the pathways defined for the bituminous coals. For the subbituminous coals, as conversion increases, there is a parallel increase in both the O+G and A+P yields. These yields continue to increase until a maximum in coal conversion is achieved. The major reaction taking place after these maxima have been achieved is the conversion of A+P to O+G with little additional coal conversion taking place. This stage is similar to the second stage of the bituminous coal pathway. The addition of a catalyst does not alter the subbituminous coal pathway (Figure 4). As was observed with the bituminous coals, the addition of a catalyst only increases the rate of production of the intermediates and does not alter the selectivity defined by the thermal pathway.

CONCLUSIONS

The utilization of a lumped solubility class parameters plotted on a ternary plot show that the bituminous coals studied have a common liquefaction pathway. Attempts to change thermal pathway by catalyst addition were unsuccessful. The addition of a catalyst only increased the rates of production of products. The addition of a catalyst had no effect on the selectivity defined by the pathway.

The pathway defined for a subbituminous coal was significantly different than that defined for the bituminous coals. For the subbituminous coal, as conversion increases in the first stage, both the O+G and A+P yield increase. In the first stage for the bituminous coal only the A+P yield show a substantial increase in yield with conversion and the O+G yields remain fairly constant. The second stage of the pathway for the subbituminous coal, the primary reaction in the conversion of A+P to O+G which is similar to the second stage of the bituminous coal pathway. The addition of a catalyst to the subbituminous coal had no effect on the selectivity of the pathway.

ACKNOWLEDGMENT

This work was supported by the Commonwealth of Kentucky and DOE contract #DE-FC88PC8806.

REFERENCES

1. Weekman, V. W., *AIChE Monograph Series*, **75** (1979).
2. Smith, R. B., *Chem. Eng. Prog.*, **55** (1959).
3. Platzer, N., *Ind. Eng. Chem.*, **62** (1970).
4. Keogh, R. A., Hardy, R. H., Taghizadeh, K., Meuzelaar, H. L. C. and Davis, B. H., *Fuel Proc. Tech.*, **37** (1994).

Table 1							
Make-up of Sample Set and Range of Key Properties							
A. Distribution of Samples by State:				B. Distribution by ASTM Rank Classification:			
Kentucky		36		High volatile bituminous A, B, C			
Indiana		22					
Ohio		10					
West Virginia		1					
C. Ranges of Key Properties							
	Wt.% V.M. (daf)	Wt.% C(daf)	Wt.% Total S. (daf)	Wt.% Org.S. (daf)	Wt.% Pyr.S. (daf)	Vol% Vitrinite (dmmf)	R _o max
minimum	34.27	76.04	.70	.55	.03	80.06	.388
maximum	48.34	86.48	13.78	4.72	8.87	92.70	.984
mean	43.15	80.67	4.15	2.25	1.70	86.78	.606

Table 2			
Coal Analyses			
Ultimate (wt.%, daf)	Wyodak	W. KY. #6	W. Ky. #9
Carbon	82.87	76.80	71.02
Hydrogen	5.42	5.41	5.42
Nitrogen	1.72	1.90	1.37
Sulfur	5.15	8.41	1.00
Oxygen ¹	4.84	7.40	21.29
Reflectance (R _{o max})	.77	.54	---
1. By difference.			

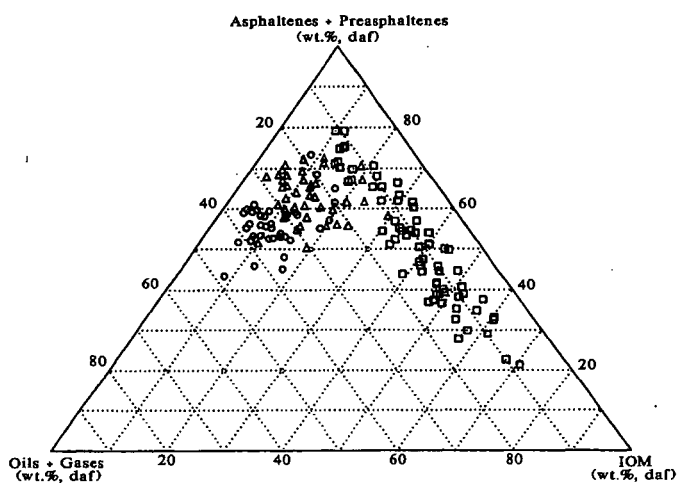


Figure 1. Solubility class distribution of the liquefaction products obtained from the thermal dissolution of bituminous coals using a 15 min. residence time, 3 reactions temperatures (385°C, □; 427°C, Δ, 445°C, ○) and a H₂ atmosphere (ca. 2000 psig @ 445°C).

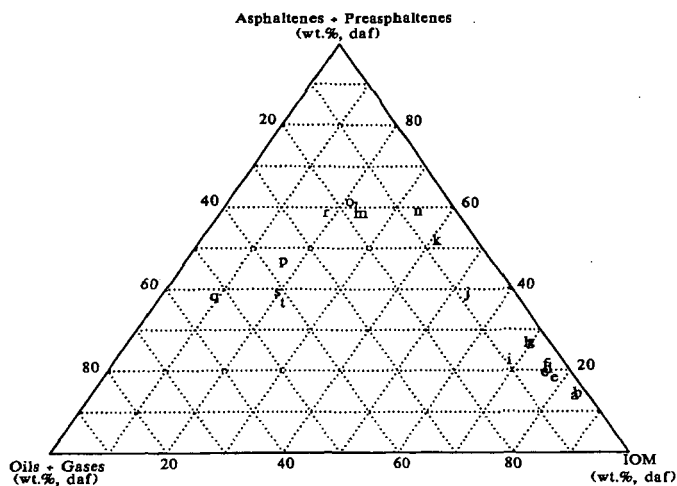


Figure 2. The thermal liquefaction pathway of a W.Ky. #6 bituminous coal using a H_2 atmosphere (ca. 2000 psig @ 445°C) using various reactor temperatures and residence times (325°C and 2.5 min., l; 5 min., b; 10 min., c; 15 min., d; 20 min., e; 30 min., f; 40 min., g; 60 min., h; 385°C and 5 min., i; 15 min., j; 30 min., k; 60 min., l; 90 min., m; 427°C and 5 min., n; 15 min., o; 30 min., p; 60 min., q; 445°C and 5 min., r; 15 min., s; 30 min., t).

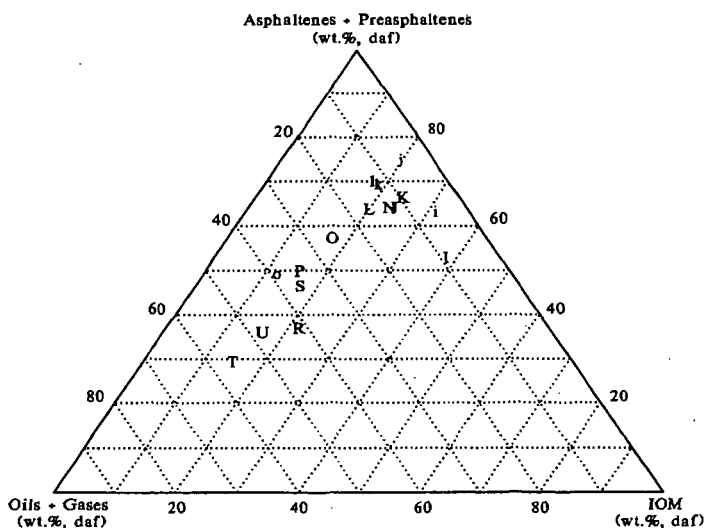


Figure 3. The catalytic liquefaction pathway of a W.Ky. #6 bituminous coal using a H_2 atmosphere (ca. 2000 psig @ 445°C) and a Shell 324 catalyst (385°C and 5 min., I; 15 min., J; 30 min., K; 60 min., L; 427°C and 5 min., N; 15 min., O; 30 min., P; 445°C and 5 min., R; 15 min., S; 30 min., T; 60 min., U) and a molybdenum naphthenate catalyst (385°C and 5 min., i; 15 min., j; 30 min., k; 40 min., l; 427°C and 15 min., o).

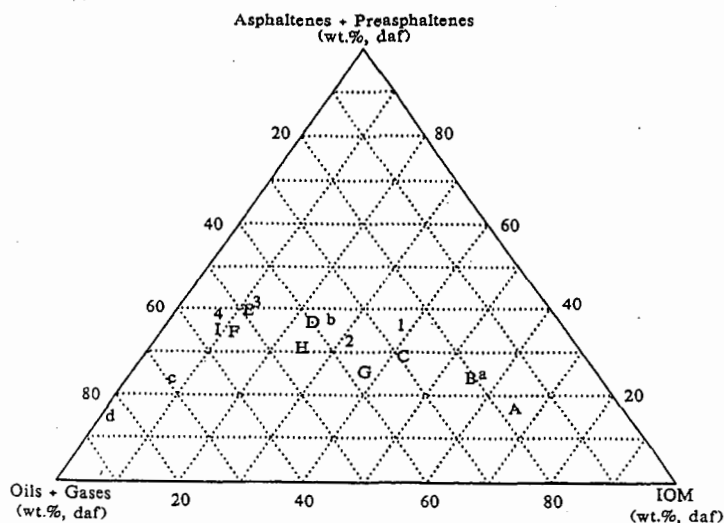


Figure 4. Thermal and catalytic liquefaction pathway for a Wyodak coal using a H_2 atmosphere (ca. 2000 psig @ 445°C) and a number of different reactor temperature and residence times (No catalyst: 385°C and 5 min., A; 15 min., B; 30 min., ; 427°C and 15 min., D; 30 min., E; 60 min., F; 445°C and 5 min., G; 15 min., H; 30 min., I; ultrafine Fe_2O_3 : 385°C and 15 min., 1; 30 min., 2; 427°C and 15 min., 3; 30 min., 4; No naphthenate: 385°C and 5 min., a; 15 min., b; 427°C and 30 min., c; 60 min., d).

MOLECULAR COMPOSITION OF COAL LIQUID OIL CHARACTERIZED BY GAS CHROMATOGRAPHY WITH ATOMIC EMISSION DETECTOR

SD. Sumbogo Murti*, K. Sakanishi**, I. Mochida*

* Institute of Advance Material Study, Kyushu University
Kasuga, Fukuoka 816-8580, Japan

** National Institute for Resources and Environment,
Tsukuba, Ibaraki 305-8569, Japan

Heteroatom-containing species in the coal liquid oils (CLO) were identified and quantified by the aid of gas chromatography with atomic emission detector (GC-AED). Four different CLOs from different rank coals, processes and cut points were investigated in the present study. Thiophene and its derivatives were found to be the major sulfur compounds, pyridines and anilines, and phenols were the major nitrogen and oxygen compounds, respectively in the oils of boiling range < 300 °C. An oil of boiling range (300 – 420°C) carried more dimethyldibenzothiophenes and benzoquinolines. The correlation between feed coal and liquid product was discussed in terms of the compositions of heteroatomic compounds.

Key words: coal liquid oil, heteroatomic compounds, GC-AED

INTRODUCTION

Coal liquefaction has been expected to supply liquid transportation fuels to moderate the indispensable dependence on the petroleum products since the supply of crude oil may not meet the increasing demand in near future [1]. Coal liquid oil (CLO) of gas oil fraction tends to carry more heteroatoms such as sulfur, nitrogen and oxygen than the corresponding petroleum product [2]. Higher content of such heteroatoms causes serious problems to produce the pollutants, and to cause the poor stability in storage. Furthermore, they may play as inhibitor and poison in the catalytic refining processes, where molybdenum or tungsten sulfide promoted by cobalt or nickel supported on alumina or silica alumina have been usually applied as catalyst [3-6].

It is very necessary to quantify the heteroatom-containing molecular species in the coal liquids to clarify their chemical roles and behaviors in the hydrotreatment. Molecular level analyses of sulfur species in gas oil and their reactivity have been reported [7]. Although GC-MS can be applied to measure all species, identification of all molecular species is very tedious.

The present study reports the distribution of heteroatom containing compounds (sulfur, nitrogen and oxygen) in CLOs by the aid of gas chromatography equipped with atomic emission detector (GC-AED). AED is a multi-element detector that can measure more than 20 elements [8,9]. Recently it has been applied to the quantitative analyses of sulfur, nitrogen compounds in gas oil and metal containing compounds in vacuum gas oil [10]. Molecular distribution of heteroatom species may reflect compositional characteristic of starting coal, efficiency of liquefaction process for heteroatom removal, and their cutting point.

EXPERIMENTAL

Coal liquids sample

Crude liquid oils used in this study were supplied from liquefaction pilot plants in Japan, using 4 coals as listed in Table 1. Analyses of 4 raw coals are summarized in Table 2. Basic and non-basic fractions of SBCL-B were separated by acid extraction.

Gas Chromatography with Atomic Emission Detector

The identification of heteroatom containing compounds in the CLO was carried out using a HP 6890 with split/splitless injector port gas chromatograph (GC) with a HP G2350A atomic emission detector (AED) system. The chromatographic separation was done on a 30 m HP-1MS 0.32 internal diameter capillary column with film thickness of 1.0 µm (HP).

Carbon, sulfur, nitrogen and oxygen atomic emissions at 179, 181, 174 and 171 nm were used to obtain the high selectivity. Two injections of 1 µl were carried out with every

sample. The first injection was for determination of carbon, sulfur, nitrogen, while the second one was for oxygen. Hydrogen was used for the major reagent gas for both analyses. Oxygen and pure methane was added for the former analyses while 10 % methane in nitrogen was for latter analyses. The HP AED ChemStation was used to control the GC-AED and to perform the data acquisition and peak integration.

Results

Figure 1 shows the carbon, sulfur, nitrogen, and oxygen chromatograms of SBCL measured by GC-AED. Thiophenes, and dibenzothiophenes derivatives were the major compound identified in the SBCL. Pyridines, aniline and phenols and their derivatives were nitrogen and oxygen compounds respectively.

The carbon chromatograms from 4 CLOs are shown in Figure 2. The sample contained paraffinic hydrocarbon up to C17 for SBCL-A because of its end point of 300 °C, and C12 for the others of cutting point of 260°C. C9 and C10 were found to be the highest peak found in the tatter samples. Chromatograms of sulfur compounds in coal liquid distillates are illustrated in Figure 3. The sulfur species observed in CLOs were mostly thiophene and alkyl-substituted thiophenes. Thiophene content in SBCL-A was relatively small compared to those of the others three CLOs. Benzothiophene and its derivatives appeared in SBCL-A at longer retention times corresponding to their higher boiling points. Figure 4 illustrates the nitrogen chromatograms. The nitrogen components identified in CLO were mostly pyridine, aniline and their derivatives. Quinoline, indole and alkyl-substituted indoles were found only in SBCL.

The chromatograms of oxygen species in coal liquid distillates are illustrated in Figure 5. Phenols and alkyl-substituted phenols were the major oxygen compounds found in CLOs, although dibenzofuran was identified only in SBCL-A.

Chromatograms of SBCL-B are illustrated in Figure 6,7 and 8 for carbon (hydrocarbon), sulfur and nitrogen, respectively. SBHD contained paraffinic hydrocarbon of C17 to C29. Dibenzothiophene (DBT) and its derivatives were found as major sulfur species. Basic nitrogen species identified in SBHD are mostly aniline, quinoline, benzoquinoline and their derivatives.

Discussion

GC-AED was confirm to be able to identify basically all molecular species in CLO of boiling range up to 420 °C. The content and distribution of heteroatoms containing species in CLOs appear to reflect the liquefaction process, rank of feed coals as well as boiling range although very similar species were usually contained. Sulfur levels of South Banko, Adaro, and Ikeshima oils were much the same around 0.1 wt% except for Tanitoharum, although the contents of sulfur in the raw coals were significantly different. The distributions of sulfur species in the former three oils are different. SB carried dimethyl, trimethyl BT and dibenzothiophene in the boiling range < 300 °C, while Adaro and Ikeshima oils did not carried. TH oil carried similar species to those of Adaro and Ikeshima, although the sulfur level of the former oil was certainly less than the latter oils. Major difference was observed in the content of thiophene.

Nitrogen content appears more different in oils. The CLO carried nitrogen of 0.4 – 0.9 wt%, which was much larger than Sulfur. The CLOs of the same boiling range appear to carry the respective nitrogen content, which reflected the contents of the raw coals. The distribution of nitrogen species in the four oils is similar although SB carried quinoline and indoles due to the higher boiling range. TH oil carries more aniline, methyl and dimethylanilines compared to others.

Oxygen contents in CLO reflected the oxygen contents in the starting feeds. CLO carried oxygen of 1 – 3.7 wt%, which was the largest heteroatom found. SB of the highest oxygen content produced the much oxygen compound in the oil. The three feed shows the similar content. During liquefaction processing, most of oxygen were found phenols. Dibenzofuran believed to be refractory oxygen species was found only in SB.

The representative aromatic and non-aromatic fraction of SBHD as illustrated in Figure 6, were clearly separated according to the standard procedure of ASTM D-2549. The percentages of aromatic and non-aromatic fraction were 82.1 and 17.9 wt%, respectively. It is clear that the humping reflects the aromatic fraction. Overlapped peaks of aromatic, condensed

naphenic-aromatic, aromatic olefin and heteroatom species such sulfur, nitrogen and oxygen lead to the humping. Non-aromatic fraction contains a series of normal paraffins.

The higher boiling point of SBCL-B contained much complex heteroatoms and mostly refractory species. 4-methyldibenzothiophene (61ppm) and 4,6-dimethyl dibenzothiophene (12 ppm) of refractory sulfur species were clearly identified. Benzoquinoline and its derivative also identified as the major nitrogen species. Such complex heteroatom compounds with three or more benzene ring believed to be difficult to remove by catalytic up grading, using conventional commercial catalyst. Inhibitor such oxygen compound and basic nitrogen species in CLOs, forces us to design better catalyst and better process for up-grading such a crude in a current transportation fuel.

Conclusions

- Gas chromatography with atomic emission detector is very powerful for characterization and identification heteroatom species of whole molecular species in petroleum and coal liquid oil.
- Thiophenes, benzothiophene as sulfur compound, pyridine, aniline as nitrogen compounds, phenols as oxygen compound were identified in CLOs of lighter boiling point. Dibenzothiophene, quinoline, indole, dibenzoquinoline, dibenzofuran and their derivatives were only found in SB due to its higher cutting boiling range.

References:

1. Mochida, I., Sakanishi, K., Suzuki, N., Sakurai, M., Tsukui, Y., Kaneko, T., *Catalyst Surveys from Japan*, 1998, 2, 17-30.
2. Yanai, S., Komatsu, N., Shimasaki, K., *proceeding, The 6th Japan - China Symposium on Coal and CI Chemistry*, Miyagi, Japan, 1998, 196 - 199
3. Albro, T. G., Dreifuss, P. A., Wormsbecher, R. F., *HRC & CC* 1993, 16, 13 - 17
4. Dorbon, M., Ignatiadis, I., Schmitter, J. M., Arpino, P., Guichon, G., Toulhoat, H. A., *Fuel* 1984, 63, 565 - 570.
5. Fathoni, A. Z., Batts, B. D. *Energy Fuel* 1992, 6, 681 - 693
6. Schmichitter, J. M., Vajta, Z., Arpino, P. J., *Advances in Organic Gheochemistry*, 1979, Pergamon Press Oxford, 1980, 67 - 76
7. Whitehurst, D. D.; Isoda, T.; Mochida, I. *Adv.Catal.* 1998, 42, 345-471
8. Albro, T. G., Dreifuss, P. A., Wormsbecher, R. F., *HRC&CC* 1993, 16, 13 - 17
9. Quimby, V., Giarocco, J., McCleary, K. A., *HRC & CC* 1993, 15, 705 - 709
10. Senghan Shin, Kinya Sakanishi, Isao Mochida submitted to *Fuel and Energy*

Table 1. Ultimate analyses of CLOs

CLO	Process	b.p.(°C)	C ^a	H ^a	N ^a	S ^a	O(diff)	H/C
South Banko (SBCL-A)	NBCL	< 300	84.97	10.37	0.84	0.09	3.74	1.46
South Banko (SBCL-B)	NBCL	300-420	87.89	9.29	0.77	0.07	1.98	1.27
Adaro (ADCL)	NEDOL	< 260	87.78	10.16	0.35	0.10	1.61	1.39
Tanitotharum (THCL)	NEDOL	< 260	86.84	10.84	0.84	0.05	2.23	1.50
Ikejima (UCL)	NEDOL	< 260	88.48	9.94	0.51	0.10	0.97	1.35

a : wt% ; diff : differences

Table 2. Analyses of raw coals

Coal	C ^a	H ^a	N ^a	S ^a	O(diff)	H/C
South Banko coal	71.3	5.4	1.3	0.5	21.5	0.91
Adaro coal	74.2	5.2	0.9	0.0	19.7	0.84
Tanitotharum coal	75.9	5.8	1.8	0.2	16.3	0.92
Ikejima coal	81.8	6.1	1.4	1.4	9.3	0.89

a : wt% ; diff : differences

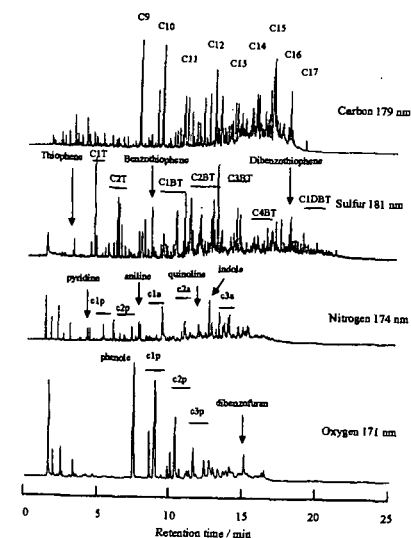


Figure 1 : chromatograms of carbon, sulfur, nitrogen and oxygen species in SBCL

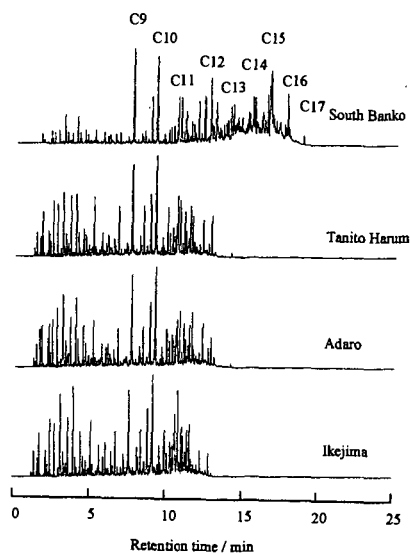


Figure 2 GC-AED chromatograms of carbon in CLOs

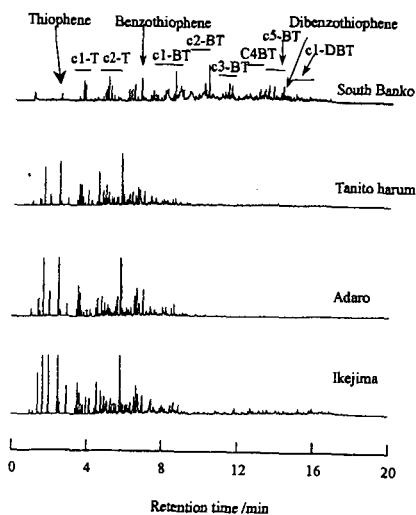


Figure 3 GC-AED chromatogram of sulfur in CLOs

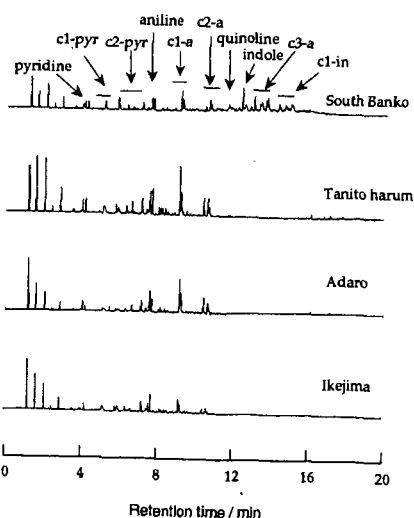


Figure 4 GC-AED chromatograms of nitrogen in CLOs

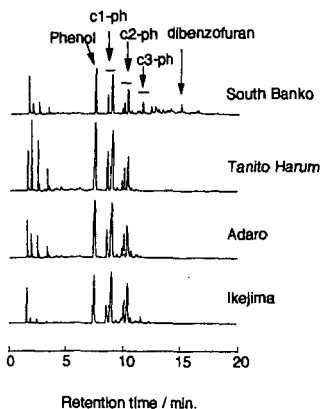


Figure 5 GC-AED chromatograms of oxygen in CLOs

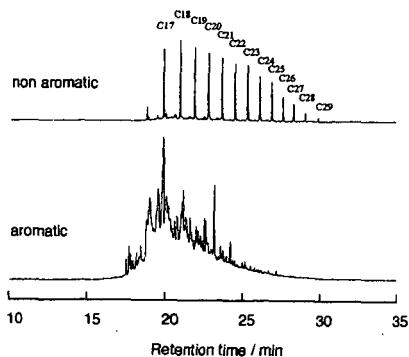


Figure 6 AED chromatograms of aromatic and non aromatic hydrocarbon in SBCL-B

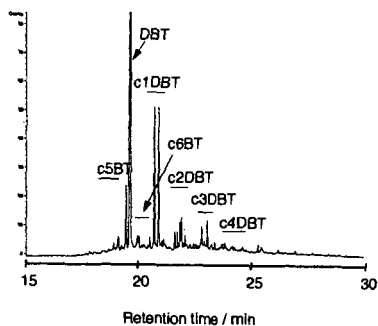


Figure 7. AED chromatograms of Sulfur compounds in SBCL-B

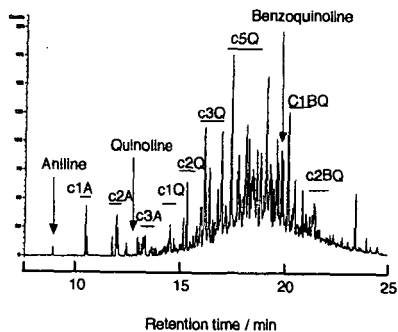


Figure 8. AED chromatograms of basic nitrogen compounds in SBCL-B

Behavior of additives on the coal solubility and aggregation

Chong Chen* and Masashi Iino

Institute for Chemical reaction Science, Tohoku University
Sendai 980-8577, Japan

Abstract

A very small amount of additives significantly increases the extraction yield of Upper Freeport coal in NMP/CS₂ mixed solvent from 63% to 78–84%. Twenty additives were tested. The most effective ones are TCNE, TCNQ, PDA, 1,1,2,3,3-pentacyanopropenide (PCNP) and acetate anion. In addition, the effect of PCNP anion and acetate anion on the aggregation of coal extract was observed by Size Exclusion Chromatography. The result indicates that anions prevent the aggregation of the coal extracts.

Introduction

NMP/CS₂ mixed solvent has good extractability for some bituminous coals, e.g., ~60% for Upper Freeport coal and Zao Zhuang coal¹. The purpose of adding additives into this mixed solvent is to further increase the coal solubility. Some of them increase the extraction yield of Upper Freeport coal from ~60% to ~80%^{2,3}. Unfortunately, only a few additives are effective among the twenty additives we tested. In addition to their effect on coal extractability, some additives also prevent the aggregation coal molecules in solution, which was investigated by Size Exclusion Chromatography (SEC). The effect of TCNE on coal aggregation is hard to observe by SEC because of the strong interaction of TCNE with the polystyrene column⁴. Some anionic additives significantly increase coal extractability. They do not strongly interact with the column⁵. Their effect on coal aggregation was investigated by comparing the SEC eluted by NMP or NMP/anionic additive.

Experimental

Extraction of coal with NMP/CS₂ containing additive was carried out according to the method described in ref. 1. All the additives are commercial product except for NMP-1,1,2,3,3-pentacyanopropenide (PCNP), which was prepared by the author³.

SEC was run on the polystyrene column (7.8_300mm, particle size 13μm, TOSOH Co., Japan) and eluted by NMP and additive modified NMP with a flow rate of 1.0ml/min.

The effect of anionic additives on pyridine-phenol hydrogen bond was observed by ¹H-NMR in CDCl₃.

Results and discussion

Table 1 presents the extraction yield of Upper Freeport coal extracted by NMP/CS₂ with or without additives. Some of these additives are strong electron acceptors or donors. In previous works, the charge-transfer interaction between coal and additive was considered to be responsible for breaking coal-coal interaction. However, the correlation of the electron acceptability or donate ability with coal extractability did not support this assumption⁶. In addition, TCNE was found converted to PCNP anion in NMP. This anion was as effective as TCNE, although it is not an electron acceptor³. The result rules out the formation of a charge-transfer complex between coal and TCNE as a main route to break coal-coal interaction.

TCNQ is another effective additive. The pathway of its interaction with coal is probably related to the interaction of TCNQ with solvent⁷. It is found that TCNQ forms radical anion in NMP but does not in THF and chlorobenzene. TCNQ is also effective in NMP but not in THF and chlorobenzene. TCNQ radical anion formed in NMP may have some relations with its effect on coal solubility. The mechanism is under investigation.

Aniline and *p*-dimethyl-aniline(PDA) are also very effective in increasing coal extractability as shown in table 1. Their electron donating ability with increased coal extractability was also not well correlated⁸. Instead, the hydrogen bonding formed between additive and coal was thought to be a factor. Comparing the effect of aniline and dimethylaniline; PDA and TMPDA, methylated amines are less effective. The result indicates that hydrogen bonding formation may affect the extraction of coal, because dimethylaniline and TMPDA have weaker ability to form hydrogen bonds with coal.

* Current address: Department of Chemistry, Lehigh University, Bethlehem 18015, USA

Anion is an effective additive found recently^{3,5}. The most effective ones are PCNP anion and acetate anion. They increase UF coal extractability from 62% to 78~84%. Hydrogen bonding with coal may also be a factor to break coal-coal interaction, which will be discussed later.

These additive are also effective in increasing the solubility of PI fraction, which is a fraction from coal extract that dissolves in NMP/CS₂ but not in pyridine. Two PI fractions were prepared by different method. PI(1) was prepared by washing extract with pyridine under ultrasonic radiation at room temperature, while PI(2) was washed by pyridine with Soxhelt extraction, in which more pyridine solubles were removed(unfortunately, the accurate weight loss was not measured, roughly estimated about 10~20%). The solubility of the two PI in NMP/CS₂ is significant different as shown in table 2. The more pyridine solubles is removed the lower solubility is. It seems that the PI(2) becomes more associated. Both PI fractions are associated by non covalent bonding, but the effect of these additive on them is different. TCNE is always the most effective one. Over 90% of PI was dissolved in NMP/CS₂ with addition of TCNE for the two PI fractions. However, TCNQ, DDQ and others become less effective for PI(2). Some of them even cause stronger association of coal, and decrease the solubility of PI(2). The difference between PI(1) and PI(2) is that PI(1) still has more pyridine solubles which is difficult to remove at room temperature. In other words, PI(2) is heavier than PI(1). The major structure difference between PS and PI is that PI has higher heteroatom, OH content. Accordingly, PI(2) should have higher heteroatom, OH content and aromaticity, which may give rise to the stronger non-covalent interaction in PI(2). If the additive breaks the covalent bond to increase the coal solubility, their effect will not be so dependent on the lighter fraction(pyridine soluble) reminded in PI. These results demonstrate that additives break the non-covalent interaction but not the covalent bond in coal.

Based on the observation of the structure of additives listed in Table 1, the effective ones usually have symmetrical and delocalized structure. Most anionic additives are effective. Among those effective additive, TCNE, TCNQ and aniline, PDA were well discussed. Here, we force our interest on organic anion, e.g., PCNP anion and acetate anion.

The behavior of the two anionic additives on coal molecular aggregation was investigated by SEC. The use of NMP as an eluent minimized the sample adsorption on the polystyrene column⁹⁻¹¹. The separation is mainly size based¹⁰. The SEC chromatogram of coal extract exhibits bimodal peaks. The first one appearing near exclusion limit of the column is assigned to those stronger aggregated molecules⁵. Another one resolved by the column eluting at longer retention time corresponds to the less aggregated portion⁵. Addition of small amount of PCNP or acetate anion into the NMP eluent results in the disappearance of the peak near exclusion limit of the column, but no effect on the peak at longer retention time. This change indicates the size of coal molecular aggregates decreased. The effect of anion on coal molecular aggregation depends on the nature of the anion. Addition of LiBr into NMP eluent shifts all the peaks to longer retention time, which was considered due to the decrease of solvent solubility because some precipitates appeared in NMP/LiBr¹². Addition of PCNP anion and acetate anion increases the Upper Freeport coal solubility in NMP/CS₂ from 60% to 78% and 84%, respectively, but addition of same amount of LiBr does not increase coal solubility at all. Accordingly, the change of SEC behavior by adding PCNP and acetate anion is due to the disruption of the coal molecular aggregation. The reversible effect of additive on SEC was also found. Some materials eluted near exclusion limit still appear when injection of the sample containing anion additive onto the column eluted by NMP. The result indicates a partial reversible aggregation of coal extracts.

The mechanism of anion increasing coal extractability is under investigation. We are not very sure whether the new hydrogen bonds formed between coal molecules and anion will break the coal-coal interaction or not. The change of OH proton signal in NMR spectrum of pyridine-phenol mixture by addition of 0.1% PCNP anion may provide some information for better understanding the mechanism of PCNP anion increasing coal extractability. As described in figure 2, for the pyridine-phenol mixture, hydrogen bonded OH proton shows a broad peak in low field. Addition of 0.1% PCNP anion (NMP-1,1,2,3,3-pentacyanopropenide) shifts of this proton signal up field appearing as a sharp peak. The result indicates that the chemical environment of this proton changed. Pyridine-phenolic OH hydrogen bond is a major hydrogen bond in coal. NMR result

indicates that PCNP anion affects this hydrogen bond. If this is related to coal solubility increase is awaiting further investigation.

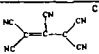
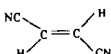
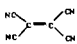
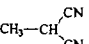
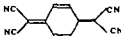
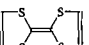

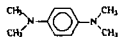
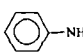
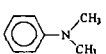
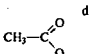
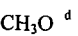
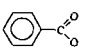
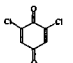
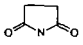
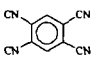
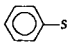
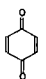
Acknowledgment

The authors are grateful to the JSPS for financial support of this work.

References

1. Iino, M.; Takanohashi, T.; Ohsuga, H.; Toda, K. *Fuel* 1988, 67, 1639-1647
2. Liu, H-T.; Ishizuka, T.; Takanohashi, T.; Iino, M. *Energy Fuels* 1993, 7, 1108-1111
3. Chen, C.; Kurose, H.; Iino, M. *Energy Fuels* 1999, 13, 1180-1183
4. Takanohashi, T. private communication
5. Chen, C.; Iino, M. *Fuel* Preparing for submission
6. Chen, C.; Iino, M. *Prep. Pap. Am. Chem. Soc. Div. Fuel Chem.* 1999, 44(3), 606-609
7. Chen, C.; Iino, M. *Energy Fuels* 1999, 13(5), 1105-1106
8. Giray, E. S.; Chen, C.; Takanohashi, T.; Iino, M. *Fuel* 2000, in press
9. Lafleur, A. L.; Nakagawa, Y. *Fuel* 1989, 68, 741
10. Domin, M.; Herod, A.; Kandiyoti, R.; Larsen, J. W.; Lazaro, M-J.; Li, S.; Rahimi, P. *Energy Fuels* 1999, 13, 552-557
11. Johnson, B. R.; Bartle, K. D.; Herod, A. A.; Kandoyoti, R. *J. Chromatogr. A* 1997, 758, 65-74.
12. Herod, A. A.; Shearman, J.; Lazaro, M.-J.; Johnson, B. R.; Bartle, K.D.; Kandiyoti, R. *Energy Fuels* 1998, 12, 174-184

Table 1 Extraction yield of Upper Freeport coal from NMP/CS₂^a

Additives ^b	Structure	Extraction yield wt%	Additives ^b	Structure	Extraction yield wt%
PCNP anion		84.1			53.9
TCNE		81.3			60.2
TCNQ		80.0	TTF		61.9
PDA		78.6	TMPDA		60.4
Aniline		71.7			60.1
Acetate		78.6			61.8
		75.0			49.7
		69.5			49.8
		68.0			39.3
	OH ^d	66.1			

^a) extraction yield with no additive added, 62.8%; ^b) amount of additive, ~0.2mmol/g-coal;

^c) from NMP-1,1,2,3,3-pentacyanopropene ^d) tetrabutylammonium salt.

Table 2. Solubility of PI fraction in NMP/CS₂ with or without additive

Additive (~0.2mmole/g-coal)	Solubility of PI (wt%)	
	PI(1)	PI(2)
No	66.4	20.8
TCNE	99.5	89.5
TCNQ	94.3	52.9
DDQ	88.8	6.9
1,2,4,5-Tetracyanobenzene	71.2	10.5
Benzoquinone	76.1	10.2
2,6-Dichloro- <i>p</i> -benzoquinone	67.4	8.5

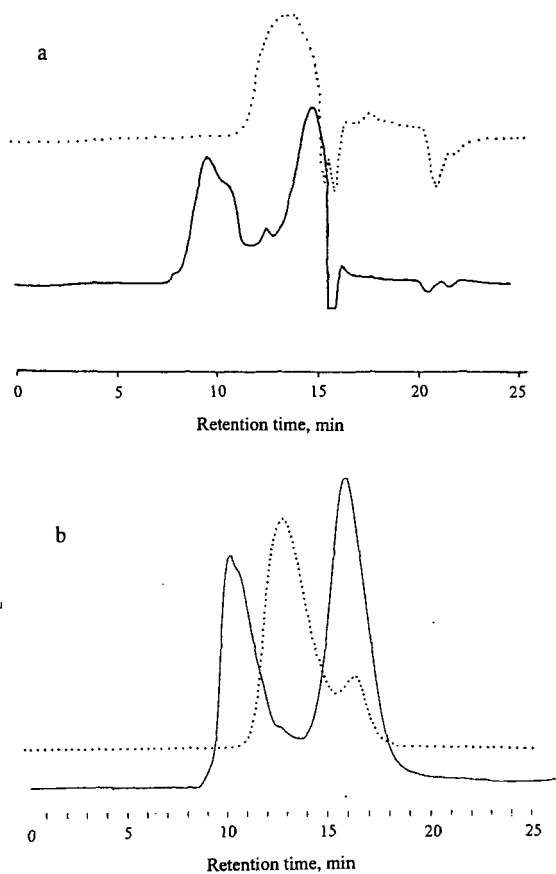


Figure 1. Size Exclusion Chromatograph of UF coal extract eluted by NMP(solid line) and NMP containing anion additive(dot line). (a) additive, 5mM NMP-PCNP; detected by RI detector; (b) additive, 10mM Tetrabutylammonium acetate, detected by UV at 300nm

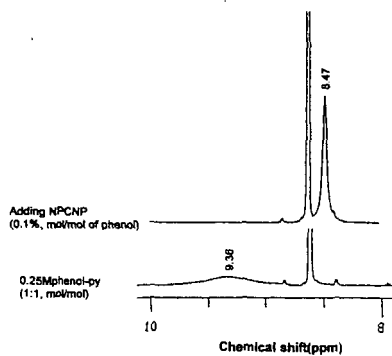


Figure 2. Shift of hydrogen bonded proton(phenol-pyridine) by adding NMP-PCNP. Solvent, CDCl_3

AN IMPREGNATED ACTIVATED CARBON FOR THE SEPARATION OF VOC MIXTURES INTO THEIR INDIVIDUAL COMPONENTS

J.P. Boudou,

Université Pierre et Marie Curie - Case 124, CNRS, 4, Place Jussieu, 75252 Paris, France

F. Payot

Laboratoire de Chimie du Solide Minéral, Université Henri Poincaré BP 239

54506 Vandœuvre les Nancy, France

Deposition of impregnation chemicals on the internal surface of suitable activated carbon optimizes the existing properties of the activated carbon for the chemisorption of certain gas pollutants giving a synergism between the chemicals and the carbon. Various qualities of impregnated activated carbon are available and have been used for many years in the fields of gas purification, civil and military gas protection and catalysis. For the manufacture of impregnated activated carbon, an activated carbon of suitable quality for the particular application is impregnated with solutions of salts or other chemicals which, after drying or other after-treatment steps, remain on the internal surface of the activated carbon. Usually, homogeneous distribution of the impregnating agents on the internal surface without any blocking of the micropores and macropores is considered to be important to keep the impregnation agent accessible for the reactants. However, in this case, the impregnated activated carbon is not selective: the adsorptive removal of further gas impurities can also take place.

In this work, we propose a new impregnated activated carbon for the selective removal and the fractionation of VOC's mixtures in exhaust humid gas. One seeks to separate by adsorption and thermodesorption on activated carbon four organic solvents: chlorinated (dichloromethane: DCM, 1,2-dichloroethane: DCE) and oxygenated (methanol: MET, methylethylketone: MEK) present in low concentration ($< 0.5 \text{ mole/m}^3$) in wet air (c. 70% of relative humidity). While seeking to avoid any degradation, the solvents must be selectively trapped at ambient temperature and selectively thermodesorbed by electric heating under a flow of nitrogen. Thermodesorption must perfectly regenerate the activated carbon in order to make it possible to apply a sequence of cycles of adsorption-desorption modulated in temperature. That implies a high selective adsorption capacity and a fast desorption at low temperature.

A preliminary work undertaken on carbon adsorbents chemically activated with phosphoric acid (SA 1817 from Atochem and Picazine from Pica), or on activated carbon oxidized by a mixture of nitric and sulfuric acid, showed us that, after washing, the residual mineral acid (acid phosphoric or acid sulfuric) gave a beginning of selectivity to the carbonaceous supports: the chlorinated solvents (DCM, DCE) tend to be better retained on the acid loaded support than the oxygenated ones (MET, MEK). We took benefit from this observation by impregnating the carbonaceous support (activated carbons in grains or fiber) with a mineral substance (ZnCl_2) having acid properties by simple cold agitation in aqueous concentrated solutions (c. 1.25 g ml^{-1}). Electron microscopy showed that the grains are coated with the product of impregnation and the adsorptiometry put in evidence that the impregnation plugs the whole porosity of the carbonaceous material. However the effect of the support is very important. Various supports were tested (powdered /granular from coal or coconut, carbon cloth). The best results were obtained with the most mesoporous activated carbons - for instance with a granular activated carbon prepared with the lignite of Lubstov (Poland) at the University of Wrocław (Table 1).

The most remarkable result is that on the ZnCl_2 impregnated CA, the DCM and the DCE are not retained at all, whereas methanol and MEK are trapped and completely desorbed by isothermal heating at 100°C during a few minutes under a flow of nitrogen, while on the non-impregnated support, the peaks of desorption of the oxygenated VOC "strongly tails". The impregnated support remains perfectly stable during more than 15 cycles of adsorption in a flow of air charged with 70% moisture followed by a thermodesorption at 150°C under a nitrogen flow (Figure 1). The disadvantage of the method lies in the fact that the impregnation's product is toxic, corrosive and hygroscopic. That implies constraints of storage, and requires to use reactor protected from corrosion and to work in short cycles of adsorption-desorption. In fact, MEK breakthrough appears before that of methanol and water. The improvement of the process is currently in hand by seeking a better acidic substance of impregnation for the selective removal of ppm concentration of various VOC's and HAP's in humid effluents.

Table 1. Porosity parameters of the activated carbon (AC) before and after impregnation

	Pore volume, $\text{cm}^3 \text{g}^{-1}$			BET m^2
	Micropores	Mesopores	Micro+Meso	
Non-impregnated AC	0.205	0.504	0.709	740
ZnCl_2 impregnated AC	0.028	0.057	0.085	17

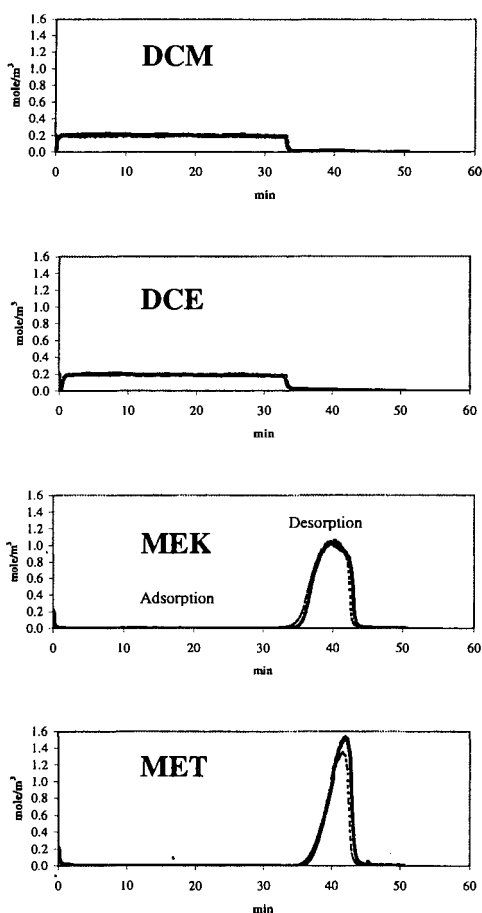


Figure 1. Profile of dynamic adsorption at 25°C and desorption at 150°C of a mixture of dichloromethane (DCM), 1,2, dichloroethane (DCE), methylethylketone (MEK) and methanol (MET) (individual VOC concentration : 0.2 mole / m^3 , water vapour concentration : 70% of the saturation pressure at 25°C, flow rate : 20 ml/min) on a column filled with 83 mg of ZnCl_2 -impregnated activated carbon (impregnation rate : c. 50 wt %, dashed line : 2nd adsorption-desorption cycle, solid line : 15th adsorption-desorption cycle). The adsorption stage is stopped at the breakthrough point of MEK.

ACTIVATED CARBON FIBERS AND FILMS PREPARED FROM POLY(VINYLIDENE FLUORIDE) BY USING A CHEMICAL CARBONIZATION

Junya Yamashita*, Toyonari Hirano, Masatoshi Shioya, Takeshi Kikutani and
Toshimasa Hashimoto

Department of Organic and Polymeric Materials, Tokyo Institute of Technology,
2-12-1 O-okayama, Meguro-ku, Tokyo 152-8552, Japan

* Present address: Carbon Materials Division, Energy Resources Department, National
Institute for Resources and Environment,
16-3 Onogawa, Tukuba-shi, Ibaraki 305-8569, Japan

KEYWORDS: Activated carbons, Chemical dehydrofluorination, Adsorptive properties

1. INTRODUCTION

Activated carbons with excellent adsorptive properties have been used in many fields such as separation of mixtures and removal of contaminant impurities. The granular activated carbons have been produced mainly from palm shells and coal. As compared with the granular activated carbons, activated carbon fibers prepared from synthetic fibers have an advantage to process into various shapes such as fabrics and papers. Furthermore, high adsorption-desorption rate of activated carbon fibers is also advantageous. The activated carbon fibers produced by conventional methods, however, are microporous and they are insufficient for the purpose of adsorbing large molecules.

Recently, several attempts have been made to introduce mesopores into carbons. For example, mesoporous carbons have been obtained by steam activation of the carbons derived from mixtures of pitch and metal complexes [1-3]. It is considered, however, that the metal residues in these carbons bring about unfavorable effects for the application to catalyst supports. Thus, new methods to prepare the mesoporous carbons free from metal complexes are required.

The present authors have obtained carbon fibers and films with various average pore sizes by applying a combination of dehydrofluorination and high-temperature heat-treatment to poly(vinylidene fluoride) (PVDF) [4]. In this study, PVDF-based carbons derived with this method were further activated. The porous structure and adsorptive properties of the resulting activated carbons were investigated by using nitrogen gas and methylene blue as adsorbates.

2. EXPERIMENTAL

The PVDF fibers with small diameters in a range of 7-10 μm were prepared by firstly spinning bicomponent fibers which consisted 261 continuous filaments of PVDF core fibers and polystyrene matrix and secondly dissolving the matrix. The bicomponent fibers were spun using a melt-spinning technique with the spinning temperature at 290°C and the take-up velocity of 100 m min⁻¹. For dissolving the matrix, the bicomponent fibers were soaked in tetrahydrofuran at 50°C for 90 min. Then, obtained PVDF fibers were washed in methanol and dried under reduced pressure.

PVDF films with a thickness of about 120 μm were prepared by hot-pressing PVDF pellets at 200°C and quenching them between steel plates at room temperature. The films were cut into the sizes of 7.5 mm by 10 mm.

The dehydrofluorination of PVDF fibers and films were carried out by using one of the strongest organic base, 1,8-diazabicyclo[5.4.0]undec-7-ene (DBU), under a swollen state. The degree of swelling was controlled by using a mixture of a swelling solvent, dimethylformamide (DMF), and a nonsolvent, ethanol (EtOH), with a volume ratio of DMF/EtOH = 2/3. The PVDF fiber bundles and films by the amounts corresponding to the number ratio of DBU/(vinylidene fluoride unit) = 4/1 were soaked in a DMF-EtOH solution of 1.0 M DBU at 70°C. During this treatment, a slight tension was applied to the fiber bundle. After the treatment, the fibers and films were washed in methanol for 1 h and

dried under reduced pressure. In the following, 'untreated PVDF' will refer to the PVDF that was not dehydrofluorinated.

The dehydrofluorinated fibers and films were heated at a rate of $2^{\circ}\text{C min}^{-1}$ up to desired temperatures below 1300°C in a nitrogen atmosphere. During the heat-treatments, the fibers were slightly tensioned, and the films were held between two graphite plates in order to reduce wrinkling. The untreated PVDF films were also heat-treated under the same conditions by placing them on a glassy carbon plate in order to avoid adhesion of the products to the substrate.

The carbonized fibers and films were activated using carbon dioxide gas. First, the specimens were heated at a heating rate of $10^{\circ}\text{C min}^{-1}$ up to 850°C under nitrogen gas flow. Then, the flowing gas was changed to carbon dioxide and the specimen was activated at 850°C for a desired duration. The flowing gas was changed back to nitrogen, and the specimen was left to cool in the furnace down to room temperature. The flow rate of both nitrogen and carbon dioxide gasses was $500\text{ cm}^3\text{ min}^{-1}$. The duration of activation was determined so that the mass loss during activation relative to the carbonized PVDF ($\Delta M_{\text{act}}/M_{\text{heat}}$) reached about 70% for all the specimens.

The pores developed in the carbon fibers and films were characterized with small-angle X-ray scattering (SAXS) by using a diffractometer (Rigaku), the PSPC and pinhole-collimated $\text{CuK}\alpha$ radiation. Specimens were prepared by aligning the carbon fibers and stacking the carbon films. The specimen-to-detector distance was 360mm and a height-limiting slit with 0.43 mm gap was attached at the X-ray entrance of the PSPC. Since SAXS of the pores in the PVDF-based carbon fibers and films was isotropic, it was possible to convert the SAXS profiles into those obtainable with an infinitely-long-slit collimation of the incident X-ray beam. From the converted profiles, the radius of gyration (R_g) of the pores was estimated according to a method proposed by the present authors [5,6]. If the pores are of spherical shape, their diameter D is given by $(28/3)^{1/2} R_g$. If the pores are of cylindrical shape, aligned in parallel to each other, and R_g is estimated with this analysis method from the equatorial intensity distribution of the cylinders, their diameter D is given by $81/2 R_g$.

The nitrogen gas adsorption-desorption isotherm was measured at 77K using an automatic gas adsorption apparatus (Autosorb-1, Quantachrome). From the isotherms measured, BET surface area, total pore volume and average pore diameter were calculated. Pore size distribution was determined from the desorption isotherm by applying the Barrett-Joyner-Halenda method to the desorption isotherm [7].

Adsorptive properties against methylene blue (MB) adsorbate which is accessible to the pores with diameters larger than 1.5 nm [8] was measured. The MB dye used showed 13.0% mass loss when heated at 135°C for 12 h under reduced pressure due to evaporation of water. By taking into account the degree of hydration of MB, aqueous solutions of MB with various concentrations in a range of 25-500 g m^{-3} were prepared. The carbon specimen of about 10 mg, dried at 135°C for 12 h under reduced pressure, was mixed with the solution of MB of 10 cm^3 in a test tube and shaken at 30°C for 24 h. The concentration of MB in the solution sampled by using a hypodermic syringe was measured. The adsorption of MB per unit mass of the specimen was calculated from the difference in the concentrations of MB in the solution before and after the specimen was added to the solution. The concentration of MB was determined by measuring the optical absorbance of the solution with a visible spectrometer (UV-2200, Shimadzu) and using a calibration curve which had been constructed based on Beer's law.

3. RESULTS AND DISCUSSION

3.1. Dehydrofluorinated fibers and films

As dehydrofluorination progresses, the color of PVDF fibers and films was turned from white into black initially at the surface of the materials and eventually over the entire cross section. From the masses of the specimen before and after dehydrofluorination, the

mass loss during dehydrofluorination relative to the mass of the starting PVDF ($\Delta M_{chem}/M_{PVDF}$) was calculated. With increasing dehydrofluorination time, the $\Delta M_{chem}/M_{PVDF}$ value decreases and at a dehydrofluorination time of 12 h, these values reached 16 and 13%, respectively, for the fibers and films [4]. With the increase of $\Delta M_{chem}/M_{PVDF}$, the fluorine content decreased and the carbon content increased almost linearly [4]. Thus, $\Delta M_{chem}/M_{PVDF}$ will be used as the measure of the degree of dehydrofluorination.

3.2. Heat-treated fibers and films

During heat-treatment, untreated PVDF melted and only granular carbon was derived. On the contrary, dehydrofluorinated PVDF maintained its macroscopic precursor geometry during heat-treatment even though $\Delta M_{chem}/M_{PVDF}$ was as small as 2%. As a result, carbon fibers and films could be obtained without causing wrinkling and/or fragmentation. It is considered that multiple C-C bonds were introduced into the PVDF molecules by dehydrofluorination, which prevented fusion of PVDF during high-temperature heat-treatment.

During heat-treatment, rapid decomposition took place in the temperature range of 300–400°C, and the pores were formed in this temperature range. The change of the pore size with increasing heat-treatment temperature above 400°C was small.

The R_3 values of the pores in PVDF-based carbon fibers and films carbonized at 1300°C are plotted against $\Delta M_{chem}/M_{PVDF}$ in Fig. 1. For comparison, R_3 values of the pitch-, polyacrylonitrile- and phenol-based carbon fibers prepared in our laboratory at the carbonization temperature of about 1300°C were 1.2, 0.8 and 0.9 nm, respectively. In these cases, R_3 values represent the size of the pore cross section perpendicular to the fiber axis. For the commercial activated carbon granule derived from palm shells, R_3 value was 2.1 nm. By applying a slight dehydrofluorination, the pore size of the PVDF-based carbon increases as compared with that of the carbon derived from untreated PVDF. By applying an intensive dehydrofluorination, on the other hand, the pore size decreases. Thus, the pore size of the PVDF-based carbon can be controlled in a range of 0.3–2.3 nm by changing the degree of dehydrofluorination.

From the nitrogen gas adsorption, it was obtained that the PVDF-based carbon granule derived from untreated PVDF by heat-treatment at 1300°C had BET surface area of 761 m² g⁻¹, total pore volume of 0.46 ml g⁻¹ and average pore diameter of 2.41 nm. On the other hand, the PVDF-based carbon prepared by dehydrofluorination to a $\Delta M_{chem}/M_{PVDF}$ value of 7% and heat-treatment at 1300°C did not adsorb detectable amount of nitrogen gas. Thus, the pores detected with SAXS have closed structure. In order to make the pores in PVDF-based carbons accessible with adsorbate, activation was carried out.

3.3. Activated carbon fibers and films

In the nitrogen gas adsorption-desorption isotherms of PVDF-based activated carbon films shown in Fig. 2, a steep increase of the amount of adsorption is found at low relative pressure region. This indicates that micropores are developed in the PVDF-based activated

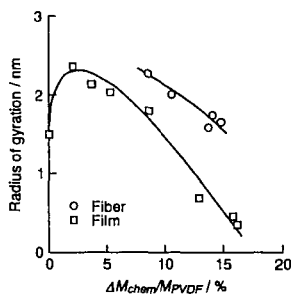


Fig. 1 Radius of gyration (R_3) of pores in PVDF-based carbon fibers and films versus $\Delta M_{chem}/M_{PVDF}$. Heat-treatment temperature was 1300°C. At the value of $\Delta M_{chem}/M_{PVDF}$ of 0%, film was pulverized during heat-treatment.

carbons. For the activated carbon films which were prepared by applying dehydrofluorination to a $\Delta M_{chem}/M_{PVDF}$ value of 2%, the isotherm has a large hysteresis loop indicating the existence of mesopores. The hysteresis loop gradually diminishes and disappears at $\Delta M_{chem}/M_{PVDF}$ of 13%.

Pore size distributions of PVDF-based activated carbon films are shown in Fig. 3. Mesopores with a diameter of 2-4 nm are developed even though dehydrofluorination is not applied. In this case, however, the material is granular. By applying dehydrofluorination to a $\Delta M_{chem}/M_{PVDF}$ value of 2%, noticeable amount of mesopores with a diameter of 4-8 nm are formed. Intensive dehydrofluorination decreases the amount of mesopores.

As shown in Fig. 4, the average pore diameter, determined by nitrogen gas desorption, of PVDF-based activated carbon films is almost in proportion to the R_3 value determined by SAXS for the carbon films before activation. Therefore, the pore structure of the PVDF-based activated carbon films reflected that of the carbon films before activation.

Adsorption of MB, at equilibrium concentration of 3.0×10^{-4} mol l⁻¹, on PVDF-based activated carbon fibers and films are plotted against $\Delta M_{chem}/M_{PVDF}$ in Fig. 5. For comparison, the MB adsorption properties of various activated carbon granules cited from literature [2] are shown in Table 1. PVDF-based activated carbons exhibit superior adsorptive properties against MB. With appropriate preparation conditions, MB adsorption of 1.7×10^{-3} mol g⁻¹ was achieved.

4. SUMMARY

By using a combination of chemical dehydrofluorination and high temperature heat-treatment, the PVDF-based activated carbon fibers and films were highly mesoporous and showed superior adsorptive properties against MB.

The advantage of PVDF-based activated carbon prepared in the present study is that it does not contain impurity such as metal particles. This will be preferable for the application of activated carbons to catalyst supports or electrodes of electric double-layer capacitor.

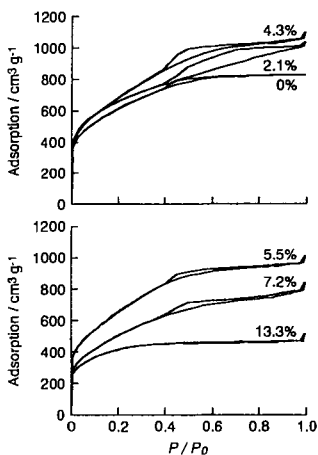


Fig. 2 Nitrogen gas adsorption-desorption isotherms at 77K, of PVDF based activated carbon films. The value of $\Delta M_{act}/M_{heat}$ was about 70% for all specimens. Values of $\Delta M_{chem}/M_{PVDF}$ are shown in the figure. At the value of $\Delta M_{chem}/M_{PVDF}$ of 0%, film was pulverized during heat-treatment.

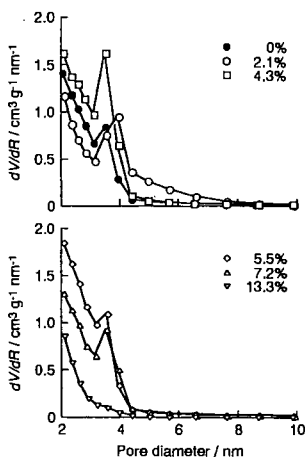


Fig. 3 Pore size distributions of PVDF based activated carbon films. The value of $\Delta M_{act}/M_{heat}$ was about 70% for all specimens. Values of $\Delta M_{chem}/M_{PVDF}$ are shown in the figure. At the value of $\Delta M_{chem}/M_{PVDF}$ of 0%, film was pulverized during heat-treatment.

Furthermore, the pore size is controllable in a wide range by changing the degree of dehydrofluorination. The good processability of PVDF into various geometries is also advantageous for applications.

Acknowledgements

The authors wish to thank Dr. A. Yasumori at Tokyo Institute of Technology for the measurements of nitrogen gas adsorption.

References

- [1] Oya A, Yoshida S, Alcaniz-Monge J, Linares-Solano A. *Carbon* 1995;33:1085.
- [2] Tamai H, Kakii T, Hirota Y, Kumamoto T, Yasuda H. *Chem Mater* 1996;8:454.
- [3] El-Merroui M, Tamai H, Yasuda H, Kanata T, Mondori J, Nadai K, Kaneko K. *Carbon* 1998;36:1769.
- [4] Yamashita J, Shioya M, Nakatani M. *Carbon* 1998;36:1240.
- [5] Takaku A, Shioya M. *J Mater Sci* 1990;25:4873.
- [6] Shioya M, Nakatani M, Kitano H, Takaku A, Araki Y, Takahashi Y, Suzuki T. *Carbon* 1996;34:1229.
- [7] Barrett EP, Joyner LG, Halenda PP. *J Am Chem Soc* 1951;73:373.
- [8] Zheng T, Liu Y, Fuller EW, Tseng S, Sacken U, Dahn JR. *J Electrochem Soc* 1995;142:2581.

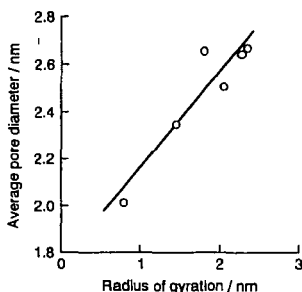


Fig. 4 Average pore diameter of PVDF based activated carbon films versus radius of gyration of PVDF based carbon films before activation. $\Delta M_{act}/M_{heat}$ was about 70% for all specimens. At the value of $\Delta M_{chem}/M_{PVDF}$ of 0%, film was pulverized during heat-treatment.

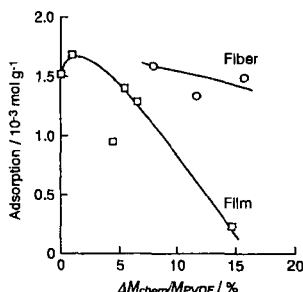


Fig. 5 Adsorption of methylene blue at equilibrium concentration of $3.0 \times 10^{-4} \text{ mol l}^{-1}$ at 30°C , on PVDF based activated carbon fibers and films versus $\Delta M_{chem}/M_{PVDF}$. The value of $\Delta M_{act}/M_{heat}$ was about 70% for all specimens. At the value of $\Delta M_{chem}/M_{PVDF}$ of 0%, film was pulverized during heat-treatment.

Table 1 Adsorption of methylene blue on various granular activated carbons.

Precursor	Adsorption / $10^{-3} \text{ mol g}^{-1}$
Palm shell	0.12
Coconut husk	0.20*
Bituminous coal	0.55*
Pitch	0.10*
Pitch/Y(naphthoate) ₃	0.15*
Pitch/Y(OiPr) ₃	0.16*

*Values were cited from reference [2].

SYNTHESIS OF ISOTROPIC CARBON FIBERS FROM PITCH PRECURSORS

Frank Derbyshire, Rodney Andrews, Adam Berkovich, David Jacques,
Marit Jagtoyen & Terry Rantell

University of Kentucky Center for Applied Energy Research,
2540 Research Park Drive, Lexington, KY. 40511-8410, USA

KEYWORDS: *Isotropic pitch, coal extracts, carbon fibers.*

1. INTRODUCTION

Pitch is used extensively as a binder and as an impregnant in the production of bulk carbon and graphite materials. Traditionally, coal tar pitch, a coke oven by-product, has been the major source of such materials. However, the range of carbons that can be obtained from coal is considerably expanded through the derivation of high molecular weight liquids or pitches by solvent extraction, hydropyrolysis, direct liquefaction as well as coking, each of which effectively serves to liberate the coal structural units. The composition of the liquids can be altered to a greater extent through the selection of the coal and reaction parameters, allowing considerable latitude in the preparation of precursors for different end products. The heavy liquid products and bottoms from crude oil processing represent an alternative source of these materials.

Relatively small quantities of both petroleum and coal tar pitch are also used as precursors for the production of carbon fibers. General purpose carbon fibers are produced by melt blowing isotropic pitch and high performance carbon fibers by melt spinning mesophase pitch. For isotropic pitch fibers, the principal steps involve the removal of entrained particulates by a solids separation process and elevation of the softening point. The ability to produce fine filaments from a pitch (spinnability) is very sensitive to the rheological properties of the pitch. For isotropic pitches exhibiting Newtonian flow properties, the glass transition temperature, T_g , and softening point can be used as characterization parameters. Once formed, the "green" pitch fibers need to be rendered infusible, or stabilized, to prevent the fibers melting and sticking together during carbonization.

In this paper the synthesis of carbon fibers from a range of isotropic pitch precursors of different origins have been examined to ascertain their suitability for fiber production. The overall aims were: to investigate the basic relationships between the composition and properties of the precursors and the ability to form fibers by melt spinning and to elucidate the mechanisms and kinetics of fiber stabilization and carbonization. The structure and properties of the carbon fibers were determined.

2. EXPERIMENTAL

Starting materials for the pitch precursors were obtained from several sources. Two coal tar pitches originating from industrial coking plants were obtained, both derived from bituminous coals (EF4 & 60FDR4). A third coal tar pitch was the by-product from the gasification of a North Dakota lignite (DR8). Several laboratory-prepared coal extracts were produced by the solvent extraction of coal under a range of conditions. These included the liquefaction of a West Virginia bituminous coal in tetralin under a high-pressure hydrogen atmosphere (FO79) and the extraction of a North Dakota lignite in a hydrogen donor solvent (47FDR). A third coal extract was produced by the dissolution of a Kentucky bituminous coal in a high boiling coal-derived solvent (7FDR2). Reaction temperatures in these tests were around 400°C with residence times of 60 minutes. Coal conversions were all high at >90%daf coal. In addition, some coal extracts were prepared by the solvent extraction of coal under very mild conditions (ACKy, ACPa & ACWy). Here, bituminous coals from Western Kentucky and Pittsburgh, and a Wyoming subbituminous coal, were extracted in anthracene oil at temperatures of around 350°C and residence times of 60 minutes. Extraction yields were correspondingly lower, ranging from 40 to 70%daf coal depending upon coal type. Two other feedstocks were used: a pitch derived from shale oil asphaltenes (F2DR) and a petroleum pitch (A500) that is used commercially to produce general purpose carbon fibers and activated carbon

fibers. The origins and the principal characteristics of these starting materials represent a diverse range of properties, Table 1. via soxhlet extraction

It is important to minimize the amount of particulate solids present in the feedstocks since their presence can disrupt the fiber forming process, result in non-uniform fiber production and also provide a source of weakness within the product carbon fiber. Where necessary, solids were removed by filtration or by extracting a soluble fraction from the reaction products using tetrahydrofuran (THF) or N-methyl pyrrolidone (FO79). For most of the precursors it was necessary to elevate the softening point of the solids-free feedstock to fall within the preferred range for fiber spinning, 230 to 260°C. This was generally achieved by vacuum distillation. Softening points were determined using a Mettler Apparatus (ASTM D3461-85, 1989). The solubility of the pitches in both quinoline and THF were determined to provide a guide to the molecular weight distribution. The pitches were also characterized by measurement of the elemental composition and by Fourier transform infrared spectroscopy (FTIR) and solid state ^{13}C nmr spectroscopy. The FTIR transmittance spectra were acquired using a Nicolet 20 SX spectrometer at 4 cm^{-1} resolution. The samples were mixed with KBr to give a 0.5% concentration in KBr and pressed into a pellet for analysis. The solid state ^{13}C nmr measurements were carried out at the University of Strathclyde using a Bruker MSL100 instrument with MAS at 5.0kHz. Once suitable pitches had been prepared, fibers were produced as single filaments by extruding the pitch through a die and drawing the diameter down into a fine filament by winding up on a rotating drum. Tows of fiber were cut into convenient lengths and stabilized by heating in air at rates of between 0.1 and $5^\circ\text{C}/\text{min}$. The process of stabilization by air oxidation serves to cross-link the fiber structure, rendering it infusible and preventing softening during subsequent heat treatment. The stabilized fibers were then carbonized by heating in an inert atmosphere to a temperature of 1100°C for 60 minutes. The yield and linear dimensions of the fibers were measured after each stage to monitor the major changes that were occurring during stabilization and carbonization. The physical properties of the carbonized fibers - diameter, tensile strength, elastic modulus (ASTM D3379, D638M) and electrical resistivity were also determined.

3. RESULTS and DISCUSSION

Broadly, these studies have confirmed that, the higher the softening point of the pitch from any one source, the higher the heating rate that can be used for fiber stabilization without incurring problems of fiber deformation or fusing. It is also clear that the maximum effective heating rate decreases with increasing fiber diameter, a result that was not unexpected when diffusional limitations are considered. However, it was apparent that some precursors can be stabilized significantly faster than others despite their exhibiting a similar or even lower softening temperature, Figure 1.

The processes that occur during stabilization include a small loss of volatile matter (depending upon the softening point and boiling point distribution), the uptake of oxygen, and possibly some loss of carbon as CO_2 , with a consequential change in the mass of the fibers. A contraction in the fiber dimensions is also observed. For most of the precursors, the uptake of oxygen compensates for volatile loss, and there is a net weight gain that can be as much as 10%. However, for the oil shale fibers there was a net weight loss of similar proportions. Not surprisingly, an inverse correlation between weight increase and the contraction in fiber length is observed, where a positive weight gain corresponds to a smaller dimensional change. These phenomena can be related to the precursor composition. In particular, there is a general trend of increasing weight gain and decreasing linear contraction, as the carbon content of the pitch increases. This implies that the uptake of oxygen primarily involves its combination with carbon, and these cross-linking reactions reduce volatile loss. The loss of labile hydrogen and heteroatom-containing species will contribute to the liberation of volatiles that increase the weight loss (or reduce the net gain) and increase the extent of dimensional contraction.

These same observations translate to the subsequent step of carbonization. In this case, there is always a weight loss of between approximately 20 to 45% with a corresponding net carbon yield from pitch feedstock to carbon fiber of between 50 and 86%. The corresponding overall linear

contraction was between 28 and 12%. The net carbon yield increases with precursor carbon content, (and decreases with the content of H, N, O and S), while the overall dimensional contraction follows an inverse trend. If such fibers were incorporated into a brittle matrix, the change in axial dimensions upon further thermal processing can introduce significant internal stresses. Therefore, careful selection of fiber and matrix for compatibility is necessary.

The mechanical and electrical properties of carbon fibers are, to some extent, controlled by the distribution of flaws and defects in the fibers. However, the tensile strength has been found to increase with precursor carbon content and carbon yield, Figure 2. The values for the materials studied here range from about 0.1 to 1.1 GPa. Pitches derived from bituminous coals via coking or solvent extraction produce fibers that are generally stronger than those from petroleum pitch. In contrast, the fibers derived from low-rank coals and oil shale were relatively weak. Similarly, the fibers generated from low rank coals with low aromaticities tend to have higher electrical resistivities.

The pitches derived from bituminous coal and the petroleum pitch sample are all strongly aromatic, while the pitches derived from low rank carbonaceous deposits are highly aliphatic. The lignite and shale oil samples were the most aliphatic and, significantly, were also the two samples for which it was not possible to increase the softening point by distillation to a value in the preferred temperature range, 230-260°C. The coal tar pitch DR8, is rich in oxygen groups, with both C-O bonds and carbonyl groups present. This may be expected since its lignite precursor will also be rich in oxygen. Two other pitches derived from low rank sources, 47FDR4 (lignite) and F2DR (shale oil) are also rich in C-O bonds. The elemental analysis data confirm the high oxygen contents of these pitches, ranging from 2.5 to 4.8%, compared with 0.5% or less for the pitches from higher rank sources.

4. CONCLUSIONS

Feedstocks suitable for generating isotropic carbon fibers were prepared from a wide range of pitch precursors. The differences in the properties and chemical composition of the feedstocks have been related to the processing and properties of the resultant carbon fibers:

- The higher the softening point of the pitch, the greater the stabilization rate at which the fibers could be processed. However, this can be offset by an increase in fiber diameter, which reduces the maximum achievable rate. For some of the feedstocks, (shale oil, subbituminous coal extract and petroleum pitch) significantly higher stabilization rates could be obtained compared to other feedstocks of similar softening point.
- During stabilization, weight gain increases with increasing carbon content in the precursor pitch, and correspondingly, the axial contraction is less for those fibers from pitches of higher carbon content. These changes are related to the uptake of oxygen and formation of cross-links within the pitch structure, reducing the loss of volatiles.
- The combined effects of stabilization and carbonization gave carbon yields of between 50 to 86% of the green fibers, with a corresponding overall axial contraction between 28 and 12%. The net carbon yield on conversion from pitch to carbon fiber was found to increase with carbon content of the parent pitch. This implies that the pitches with higher heteroatom content suffer greater loss of material due to gasification. Similar relationships were found between axial contraction and carbon content, and axial contraction and heteroatom content.
- The tensile strength of the derived fibers ranged from 0.1 to 1.1 GPa. The strength increased with aromaticity, increasing molecular size, and decreasing heteroatom content in the precursor, while the electrical resistivity of the fibers tended to decrease with these properties.

ACKNOWLEDGEMENTS

The authors wish to thank Paige Presler and Beverly Moore who diligently performed much of the characterization work and Peter Stansbury and John Zondlo at West Virginia University for supplying the FO79 pitch. Financial support was provided by the University of Kentucky Center for Applied Energy Research and the Commonwealth of Kentucky and also by Dept. of Energy contract DE-AC22-91PC91040.

Table 1: Analysis of Prepared Pitch

Source	Sample No.	Ultimate Analysis (wt%, daf)					Insolubility (wt%)		Softening point (°C)	Car / Cal (FTIR)	f_{ar} ($^{13}C_{amu}$)
		C	H	O	N	S	QI	THFI			
Coal Tar Pitch	EF4	93.6	3.7	0.5	1.6	0.6	0.5	38	245	35.1	>0.99
Coal Tar Pitch	60FDR4	94.4	3.9	0.0	1.3	0.5	0.2	31	240	29.9	>0.99
Coal Tar Pitch	DR8	88.4	6.5	3.4	1.3	0.3	0.5	0.5	225	0.05	0.65
Coal Extract	FO79	-	-	-	-	-	3.7	-	213	-	-
Coal Extract	47FDR	87.9	5.3	4.8	1.4	0.5	0.5	6	240	0.03	0.66
Coal Extract	7FDR2	90.2	4.3	2.5	1.8	1.1	0.1	58	260	0.59	0.91
Coal Extract	ACKy	91.1	4.5	1.7	1.7	1.0	<0.1	<0.1	230	-	-
Coal Extract	ACPa	-	-	-	-	-	<0.1	<0.1	230	-	-
Coal Extract	ACWy	85.7	5.8	6.8	1.4	0.3	<0.1	<0.1	220	-	-
Shale Oil	F2DR	84.9	6.6	3.6	2.3	2.5	0.6	1.3	210	0.04	0.61
Petroleum Pitch	A500	92.9	4.6	0.3	0.3	1.9	0.0	22	258	0.60	0.91

Oxygen by difference; QI = Quinoline insolubles; THFI = Tetrahydrofuran insolubles.
 f_{ar} is the fraction of aromatic carbon relative to the total carbon content.

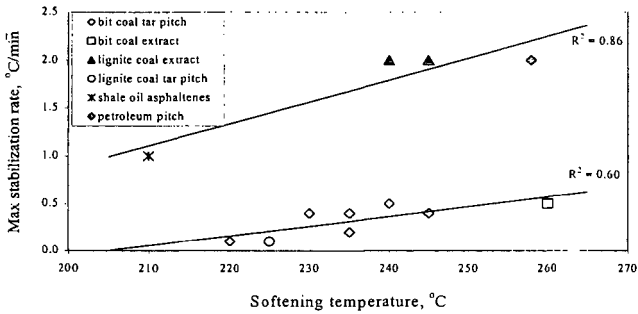


Figure 1 Dependence of Stabilization Rate on Pitch Softening Point

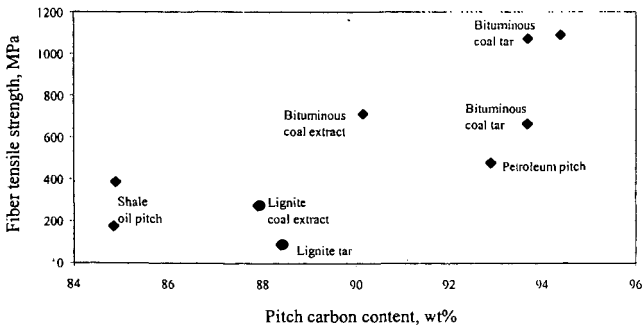


Figure 2 Tensile Strength of Fibers as a Function of Pitch Carbon Content

NOVEL CARBON ADSORBENTS FOR FUEL GAS STORAGE DERIVED FROM LIGNOSULFONATE WASTE

Emmanuelle Alain¹, Brian McEnaney¹, Oleksandr Kozynchenko^{2,3}, and Vladimir Strelko²

¹ Materials Research Centre, Department of Engineering and Applied Science, University of Bath, Bath, BA2 7AY, United Kingdom.

² National Academy of Sciences, Institute of Sorption and Problems of Endoecology, Kiev, Ukraine.

³ MAST Carbon Ltd, Henley Park, Guilford, GU3 2AF, United Kingdom

KEYWORDS carbon adsorbents, fuel gas, lignosulfonate waste

INTRODUCTION

There has been a resurgence of interest in using adsorbent carbons for fuel gas storage (natural gas and hydrogen). Molecular simulations of adsorption at ambient temperatures of methane (as a model for natural gas) [1] in slit-shaped carbon pores indicate an optimal micropore width for methane storage of ~11 Å. Thus, to optimise the storage capacity requires maximisation of micropore volume, of about this width, and minimisation of mesoporosity, macroporosity and void space between the carbon particles [2]. A storage system for road vehicles powered by natural gas requires a delivered volumetric capacity of ~150 v/v. These requirements have prompted the development of a number of routes for fabrication of highly microporous carbon monoliths with storage capacities that approach or meet the target [e.g., 2-5]. Thus, future work should be aimed towards the development of carbon monoliths by inexpensive and flexible methods. In this paper we report the preparation and characterisation of activated carbon monoliths from lignosulfonate resins derived from waste products in the paper pulp industry.

EXPERIMENTAL

Precursor Materials. Lignin is a high molecular weight, polyphenolic biopolymer and an important constituent of wood (~30 wt% dry basis). Lignosulfonates are waste products of the paper pulp industry formed by treatment of wood with strong alkali solutions saturated with sulphur dioxide. The lignosulfonate used in this study was received as a sodium salt from the Kondopoga plant in the north of European Russia. Spherical lignosulfonate resins were produced by emulsion, polycondensation reactions with cross-linking reagents; the details of the formulations used for the polymerisations are proprietary.

Carbon Microbeads. Spherical resin beads, M1, were carbonised in flowing argon by heating to 900 °C to produce carbon beads, M2. Heating in flowing carbon dioxide at 900 °C for different times produced two activated carbons M3 and M4 with 44 and 55 wt% burn-off respectively. A third activated carbon bead sample (59 wt % burn-off), L5, was made in the same way, but starting from a resin produced from a different polymerisation formulation.

Resin and Carbon Discs. The resin microbeads were pressed into resin discs (4.0 x 0.1 cm), A-1, at 100 °C and 3.2 kN cm⁻². Carbon discs, A-3, were prepared from A-1 by carbonisation in CO₂ at 600 °C for 1.5 h. An activated carbon disc, D-4, was prepared by addition of the activation catalyst potassium acetate (2 wt% K⁺) to resin microbeads prior to pressing into discs. The discs were then carbonised/activated by heating to 600 °C for 1.5 h. The burn-off of the activated carbon discs was estimated as 25-30%. The various routes for the production of carbons from the resin microbeads are summarised in Figure 1.

Characterisation Methods. The general morphology of the bead and disc samples was studied using SEM (JEOL 6310). Samples were spread on a graphite pad and gold sputtered. The packing density of the bead samples and piece (bulk) densities of the disc samples were measured using standard methods. Surface areas and micropore volumes were determined from N₂ adsorption at 77 K (Micromeritics ASAP 2010). Methane adsorption at 298 K and up to 8 bar was measured gravimetrically using a Hidden Intelligent Gravimetric Analyser.

RESULTS AND DISCUSSIONS

Microscopy. The spherical resin, M1, Figure 2(a), consists mainly of agglomerated spheres with a wide range of diameters (70-800 µm); only the largest microbeads are isolated. The extent of agglomeration in the carbon spheres, M2, and the activated spherical carbon, M3, M4, is much reduced and many more isolated particles are found, Figure 2(b)-(c). There is evidence for preferential attack at former points of contact in the case of the activated carbon

beads and broken particles reveal that some are solid spheres while others have hollow centres (shells). The same observations apply to the L5 sample. A comparison of the resin disc A-1, the carbon disc A-3 and the activated carbon disc D-4, Figure 3, illustrates the volumetric shrinkage (~67%) that occurs upon carbonisation. SEM of the discs, Figure 2 (d), shows that the pressing process leads to agglomeration of the resin microbeads and in some areas of the discs there is a transformation to a continuous structure.

Nitrogen Isotherms. Adsorption of nitrogen at 77 K on the carbon microbeads M2, Figure 4(a), and the activated carbons M3 and M4 indicate qualitatively that the carbons are microporous. For the activated carbons there is hysteresis at high relative pressures ($P/P_0 > 0.8$) that is type H1 in the IUPAC classification [6]. This is attributed to condensation in the interstices between the carbon spheres. The isotherm of the carbon material L5, Figure 4(b) shows hysteresis of type H3 that is indicative of a small amount of mesoporosity. This shows that the pore structure of the carbon beads can be controlled to some extent by varying the polymerisation conditions. The nitrogen adsorption isotherms for the carbon discs, A-3 and D-4, at low relative pressure, Figure 4(c), are more rectangular than those for the loose spherical carbons, indicating that they contain narrow micropores. Type H4 hysteresis is seen, indicative of microporosity with a type I isotherm. The gravimetric adsorptive capacities of the carbon discs are clearly less than those of the carbon microbeads, as reflected in the BET surface areas of the carbons, Table 1, and the micropore volumes, V_0 , determined using the Dubinin-Astakhov equation.

Methane Adsorption. Gravimetric isotherms for adsorption of methane at 298 K on activated carbons M4 and L5 and activated carbon disc D-4 are in Figure 5. It is notable that the gravimetric methane uptake by the activated carbon disc D-4 up to ~4 bar is comparable to the uptake by the activated carbon beads M4 and L5. This is in contrast to nitrogen uptake by these carbons, Figure 4.

The maximum pressure attainable in this study is 8 bar, but the practical target storage pressure for methane is 34 bar. We have shown previously [7] that the gravimetric capacity at 34 bar, $n(P)$, can be estimated accurately by extrapolation from the lower pressure data using the Tóth adsorption isotherm equation [8]:

$$n(P) = \left(\frac{mP}{b + P^t} \right)^{1/t} \quad (1)$$

where m , b and t are parameters of the equation obtained by curve fitting. Estimates of $n(P)$ at 34 bar and measured values for 1 bar for the activated carbon microbeads M4 and L5 and the activated carbon disc D-4 are given in Table 2. As indicated in Figure 5, the gravimetric capacity, $n(P)$, for the activated carbon discs D-4 at 34 bar is lower than those for the activated carbon spheres M4 and L5, but the reverse is true at 1 bar. This is another indication that the carbon discs have narrower micropores than do the carbon microbeads.

Volumetric Methane Capacities. The key criterion for evaluating the suitability of activated carbons for natural gas storage is the volumetric capacity expressed as volume of methane at 298 K per volume of activated carbon, including inter-particle voids. Three methane capacities can be taken into account: the adsorbed, the stored and the delivered capacities. The *adsorbed capacity*, V_a , is defined as the excess volume of methane adsorbed in micropores per volume of activated carbon. The adsorption isotherm expressed as gravimetric methane uptake, $n(P)/\text{mmol g}^{-1}$ vs. P is an excess isotherm which measures the excess methane adsorbed in pores, excluding methane stored in the gas phase. It is given by

$$V_a = 24.465 n(P) \rho_a \quad (2)$$

where ρ_a is the packing density for powders or the bulk (piece) density for monoliths. The *stored capacity*, V_s , is defined as the sum of methane stored in the adsorbed phase, V_a , and in the gas phase, V_g , at pressure, P , (3.4 MPa, 34 bar) where

$$V_g = \frac{PV_t \rho_a}{zP_0} \sim 36V_t \rho_a \quad (3)$$

and z is the compressibility of methane at P ($= 0.93$ at 34 MPa and 298 K), P_0 is a reference pressure (1 bar) and V_t , the total pore volume, including micropores, mesopores, macropores and inter-particle voids.

$$V_t = \left(1 - \frac{\rho_s}{\rho_c} \right) \sim (1 - 0.5 \rho_a) \quad (4)$$

where ρ_c is the skeletal density of solid carbon ($\rho_c \sim 2.0 \text{ g cm}^{-3}$). There is an uncertainty on whether or not the micropore volume should be included in the calculation of compressed methane gas in pores. If the micropores are fully occupied by adsorbed gas, then they should be

excluded from the calculation. In reality, the stored methane capacity should lie between the two extreme values:

$$V_s = V_a + 36(1 - 0.5\rho_a) \quad (5) \text{ (a) (b)}$$

$$V_s = V_a + 36(1 - 0.5\rho_a - V_0\rho_a)$$

The delivered capacity, V_d , is simply the difference between the stored capacity at the storage pressure (3.4MPa, 34 bar) and the stored capacity at the release pressure (0.1 MPa, 1 bar)

$$V_d = V_s(3.4\text{MPa}) - V_s(0.1\text{MPa}) \quad (6)$$

Table 2 shows that although the activated carbon beads M4 have the highest gravimetric methane capacity, the activated carbon disc has the highest stored and delivered capacity. Here, the lower gravimetric capacity of the discs is offset by their higher bulk density. By contrast, the delivered volumetric methane capacities of the carbon microbeads are modest due to the high volume fraction of inter-particle voids. The delivered capacities found for the activated carbon discs, D-4, approach the target value of 150 v/v. It is likely that this target can be achieved with further refinement of the microstructure of the carbons. For example the value of V_a (≈ 36 v/v) found for the discs D-4 at 1 bar is almost twice the values found for the loose activated carbon spheres. This is another reflection of the presence of narrow micropores in the carbon discs. The amount of methane retained in the discs at 1 bar can be reduced if the micropore size distribution can be widened slightly.

CONCLUSIONS

Porous spherical resins of different particle sizes can be produced by emulsion polycondensation of lignosulfonates with cross linking agents. These resin can be converted directly into activated carbon beads or pressed into discs that can be converted into activated carbon monoliths. The delivered volumetric capacities of the loose activated carbons are modest (~ 81 - 112 v/v) due to the high volume fraction of inter-particle voids. The delivered capacity of the activated carbon discs approach the target capacity of 150 v/v. The flexibility of the fabrication route for producing carbons from lignosulfonate resins suggests that this target can be reached with further development.

ACKNOWLEDGEMENT. We acknowledge financial support from the EU INTAS programme, Contract 96-1023 and EU TMR programme, Contract ERBFMBICT972773.

REFERENCES

1. Matranga, K.R., Myers, A.L. and Glandt, E.D., *Chem. Eng. Sci.*, **47** (1992) 1569
2. Chen, X.S., McEnaney, B., Mays, T.J., Alcaniz-Monge, J., Cazorla-Amoros, D. and Linares-Solano, A., *Carbon*, **35** (1997) 1251
3. Quinn, D.F. and MacDonald, J.A., *Carbon*, **30** (1992) 1097
4. Bose, T., Chahine, R. and Arnaud, J.M., *US Patent 4999330* (1991)
5. Manzi, S., Valladares, D., Marchese, J. and Zgrablich, G., *Adsorption. Sci. Tech.*, **15** (1997) 301
6. Gregg, S.J. and Sing, K.S.W., in *Adsorption, Surface Area and Porosity*, London, Academic Press (1982)
7. Alain, E., McEnaney, B., Mays, T.J., Strelko, V. and Kozynchenko, O., *Extended Abstracts 'Carbon '99'*, American Carbon Society, Charleston, SC, USA, (1999) 784
8. Valenzuela, D.P. and Myers, A.L., in *Adsorption equilibrium data handbook*, Prentice Hall, Englewood Cliffs, (1989) 8

Table 1. Particle bulk densities, ρ_a , BET surface areas, S_{BET} , and D-A micropore volumes, V_0 for activated lignosulfonate carbons.

Material	$\rho_a / (\text{g cm}^{-3})$	$S_{BET} / (\text{m}^2 \text{g}^{-1})$	$V_0 / (\text{cm}^3 \text{g}^{-1})$
Spherical activated carbons, M3	0.37	1202	0.64
Spherical activated carbons, M4	0.33	1610	0.92
Spherical activated carbons, L5	0.47	1235	0.58
Activated carbon discs, A-3	1.26	335	0.17
Activated carbon discs, D-4	0.95	676	0.33

Table 2. Methane capacities at 298 K for activated lignosulfonate carbon beads and discs.

Material	$n(P) / (\text{mmol g}^{-1})$ 34 & 1 bar ^b	V_a 34 & 1 bar ^b	V_s 34 bar ^c	V_d^c
Spherical activated carbons M4 (1) ^a	9.5 & 1.4	77 & 11	96~107	85~96
Spherical activated carbons M4 (2) ^a	9.1 & 1.4	73 & 11	92~103	81~92
Spherical activated carbons L5 (1) ^a	8.6 & 1.3	99 & 15	117~126	102~111
Spherical activated carbons L5 (2) ^a	8.7 & 1.3	100 & 15	118~127	103~112
Activated carbon discs D-4	6.5 & 1.6	152 & 36	159~170	123~134

a. Duplicate samples.

b. Values at 34 bar estimated using the Tóth equation, measured values at 1 bar.

c. Higher and lower values calculated using Equation 5 (a) and 5 (b) resp.

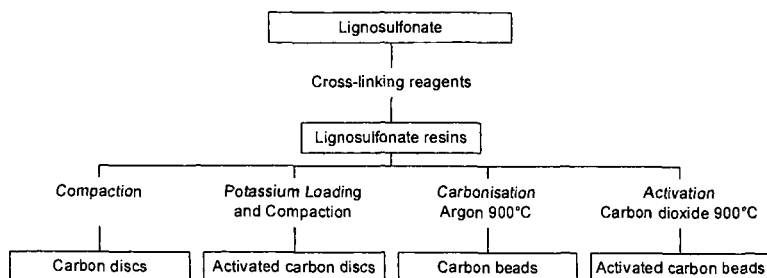


Figure 1. Flow diagram for production of the carbons derived from lignosulfonate resins.

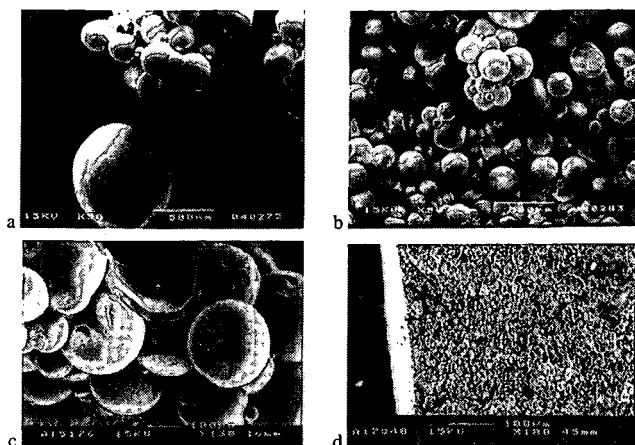


Figure 2 (a)-(d). SEM micrographs of the carbons

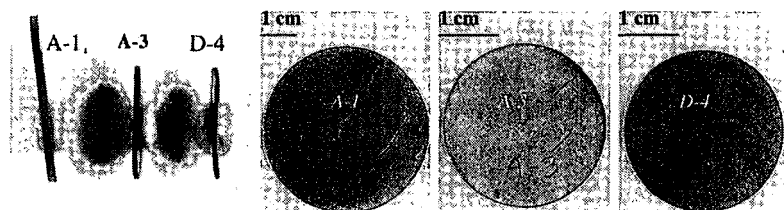


Figure 3. Optical macrographs of the discs

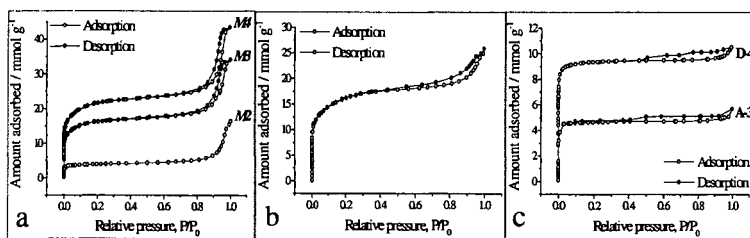


Figure 4. Nitrogen adsorption isotherms (a) M2-M4; (b) L5; (c) A-3, D-4.

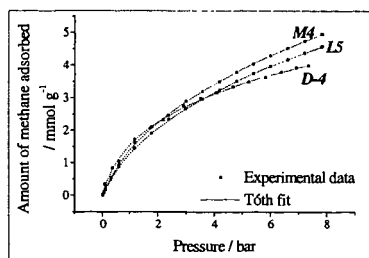


Figure 5. Measured methane isotherms at 298K and their Tóth fits.

MECHANISMS OF MERCURY CAPTURE AND BREAKTHROUGH ON ACTIVATED CARBON SORBENTS

Edwin S. Olson, Grant E. Dunham, Ramesh K. Sharma, Stanley J. Miller

Energy & Environmental Research Center, University of North Dakota

Grand Forks, ND 58202

KEYWORDS: mercury sorbent, activated carbon

ABSTRACT

An extensive series of studies was performed at the Energy & Environmental Research Center with mercury (Hg^0) sorbents in a thin bed using combinations of various flue gas constituents. This work determined that all the sorbents exhibited breakthrough in about 1 hour in the full flue gas mixture, and the mercury emitted after breakthrough is an oxidized mercury species. Trapping of the oxidized species and identification by mass spectrometry demonstrated that both carbon and metal oxide sorbents release the relatively volatile mercuric nitrate hydrate when both NO_2 , SO_2 , and water vapor are present in the gas phase. Further investigations of treated sorbents allow us to determine the role of oxidation and basic sites on the sorbent in the capture of mercury in NO_2 and SO_2 streams.

INTRODUCTION

There is currently intense interest in discovering effective sorbents for the control of mercury emissions in flue gas from coal-burning utilities. Extensive factorial evaluations of powdered sorbents were conducted at the Energy & Environmental Research Center in a bench-scale system consisting of a thin fixed-bed reactor in gas streams containing $15 \mu\text{g}/\text{m}^3$ of elemental mercury (Hg^0) in various flue gas components and simulated mixtures (1). One of the effective sorbents tested was the commercial powdered carbon sorbent Norit FGD, which is a lignite-derived activated carbon (LAC), and this carbon was selected for more extensive testing to determine the critical factors involved in mercury capture. The previous results showed that in an atmosphere containing an acid gas such as HCl or NO_2 , effective capture of Hg^0 from the gas phase occurred on activated carbon sorbents at temperatures of 100° to 150°C . Without either of these acid components in the gas stream, the carbon sorbents are ineffective, and immediate breakthrough occurred.

In tests conducted in the simulated flue gas containing NO_2 but not SO_2 , very little breakthrough was observed over an extended time period, indicating that the bound mercury form is quite stable. The capture is attributed to oxidation of the Hg^0 and concomitant reduction of NO_2 with formation of a low-volatile oxidized mercury species that remains bonded to the sorbent. Reactions of Hg^0 with NO and NO_2 in a glass container were previously reported to form mercuric oxide and mercuric nitrate/nitrite mixtures (2-3).

When SO_2 was added to the gas mixture containing the NO_2 , the mercury sorption rate was initially high (98% of inlet Hg^0 was sorbed); however, breakthrough occurred after 1 hr at the 225°F conditions. The breakthrough curve was relatively steep, increasing to 100% or greater emission after about 2 hr. Not only is mercury no longer sorbed, but mercury sorbed earlier in the experiment is released. Thus there is a significant interaction effect for SO_2 and NO_2 on the sorbent breakthrough time.

The mercury that is emitted from the sorbent after breakthrough is entirely an oxidized mercury species. In reactions conducted with NO_2 and SO_2 and no HCl , this volatile oxidized mercury product was identified as mercuric nitrate hydrate (4). The formation of the mercuric nitrate hydrate from reactions of Hg^0 and NO_2 was not reported in the early literature. It is surprising that SO_2 appears to facilitate the release of the volatile mercuric nitrate hydrate from the sorbent surface. The early breakthrough effect was observed for a number of different sorbents in the flue gas stream containing both NO_2 and SO_2 . This appears to be the controlling element in sorption capacity for mercury in flue gas. Since the effect lowers the capacity and defeats the effectiveness of all the sorbents tested, is important to understand the nature of this interaction and to determine the carbon-related factors that determine the reactivity of the carbon sorbent and its ability to stabilize the oxidized mercury against release as volatile salts. An adequate model for the sorption and breakthrough mechanism is needed to design effective sorbents for mercury control in flue gas.

The work reported in this paper concerns the carbon-related factors that determine the breakthrough behavior in the NO_2 - SO_2 stream. Two of these factors are the role of inorganic matter

present in the carbon and the role of catalytic surfaces on the carbon. The hypotheses to be tested are that basic inorganic constituents of the carbons are able to bind mercury by forming relatively stable basic mercury salts and that these basic sites are exhausted by continued exposure to SO_2 . Release of Hg(II) would occur at breakthrough when the basic binding sites are exhausted.

The much higher reactivities observed previously for mercury sorption in air with catalytic carbons compared to noncatalytic carbons lead to the hypothesis that sorption in NO_2 can also occur at different types of sites and involve formation of different intermediate species. Comparison of the breakthrough curves for the two types of carbons should elucidate these mechanisms.

RESULTS

To determine whether inorganic sites on the activated carbons are an important factor in mercury sorption in flue gas, carbons with various levels of inorganic constituents were tested. The Norit FGD sorbent that is active for mercury capture in flue gas streams is a finely powdered unwashed LAC. This means that it has a relatively high ash or inorganic content. This carbon is produced from a lignite with high calcium content, so part of the calcium is present in the carbon as the oxide and gives the surface a basic nature. The granular form of the LAC carbon is also available commercially (Norit GAC 1240), but in contrast to the powdered FGD sorbent, the granular lignite-derived carbon is acid-washed to remove some of the inorganic material in the carbon. In previous studies in air, neither the GAC 1240 or the powdered FGD carbon were effective for mercury capture. A ground sample of the GAC 1240 had not been tested for mercury capture in flue gas streams, so it was important to determine if the lower amounts of inorganic constituents on the washed carbon result in shorter breakthrough times owing to a lower capacity for retaining oxidized mercury.

The sorption test performed with the ground sample of commercial acid-washed GAC 1240 in the synthetic flue gas stream showed that the sorption activity was excellent at the start, and breakthrough was not observed for 1.7 hr, compared to 1 hr for LAC. The extended breakthrough results from this experiment are, therefore, not consistent with the concept that basic inorganic material on the surface is required for effective mercury sorption.

To further test the hypothesis that basic surfaces are important for effective mercury control, the Norit FGD carbon was washed with dilute nitric acid to remove basic calcium, iron, and sodium oxides. The demineralized carbon was tested in the synthetic flue gas stream, and results were compared with the initial FGD carbon under the same conditions of temperature, flow rate, and gas composition. The results with the washed FGD (Run 945) were identical to those from the original FGD carbon. Breakthrough occurred at 1 hr and later sampling showed that most of the Hg in the effluent from the sorbent bed was oxidized. Thus removal of basic sites by washing the sorbent with nitric acid did not result in less effective sorption.

Catalytic carbons were previously shown to exhibit very high mercury sorption activities in air streams (5). Not only were high initial kinetics for sorption observed, but the activities decreased only very gradually over several days of testing. But is this higher sorption activity for the catalytic carbons in air also observed in the simulated flue gas system?

The results of testing a catalytic carbon in the bench-scale simulated flue gas showed that the sorption curve is very similar to that of the LAC sorbent and that breakthrough occurred at the same 1-hr point in the experiment as observed for the LAC. Only oxidized mercury is observed in the emission after breakthrough. Thus the catalytic carbon is subject to the same NO_2 - SO_2 interaction as the LAC.

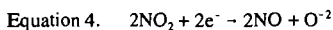
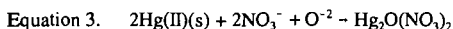
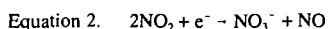
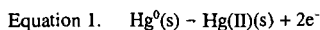
DISCUSSION

The results with washed carbons do not support the hypothesis that basic inorganic residues in the carbon are involved in binding oxidized mercury, since shorter breakthrough times resulting from failure to bind Hg(II) at basic inorganic sites were not observed. The better capacity exhibited by the ground sample of GAC 1240 may be explained by the cleaning effect of the acid in removing basic salts that are plugging the carbon pores and, therefore, improve internal mass transport. Secondly, the removal of inorganic material may expose more carbon surface and, therefore, more oxidation sites, which may overcome the negative effect expected for removal of the basic sites. Thirdly, there may be other binding sites on the carbon structure that would have been exposed by the removal of the basic inorganic sites. It is possible that some residue from the wash solution somehow improved the capacity of the GAC 1240.

The experiments do not, however, rule out the involvement of inorganic matter since it could be argued that the washing procedure removed mineral matter only from the mesopores. This would improve the internal mass transfer, but still leave some basic sites available on the micropore surface for converting the Hg(II) to nonvolatile basic salts. Thus the failure of the experiments to demonstrate decreased capacity does not reject the basic inorganic residue hypothesis, but other experiments must be conducted to determine which effects are occurring. The significantly better performance (longer breakthrough time) of the GAC 1240 cannot be adequately explained until further information on these factors is available.

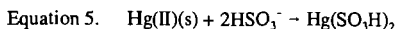
The air oxidation mechanisms of catalytic carbons appear to be quite different than those of noncatalytic carbons. Reactions with NO₂ could also involve different mechanisms and form different intermediate species in the two types of carbons. However, this work shows that the oxidation mechanisms using NO₂ as the primary oxidant (electron sink) may be the same in the catalytic and noncatalytic carbons. The similarity in breakthrough times for the two types of carbons appears to reject the hypothesis that intermediate species are different for the two carbons.

A simple model for the sorption reaction is that the adsorbed Hg⁰(s) is rapidly oxidized at an oxidation site on the carbon surface to a bound Hg(II) species utilizing electrons from the NO₂ (Equations 1-2). This reaction is likely to occur readily on any kind of carbon surface as well as other surfaces. In the absence of SO₂, the major species formed would be mercuric oxide or a basic mercuric nitrate/oxide (Equation 3), which is stable at 150°C, even in the stream containing NO₂. Oxide could be present on the sorbent surface initially (such as CaO) or could be produced from NO₂ as shown in Equation 4. The stable basic mercury salts collect in sites adjacent to the oxidation site, and the activated carbon is able to retain relatively large amounts of these forms. Thus this model is consistent with the behavior of both catalytic and LAC carbons.

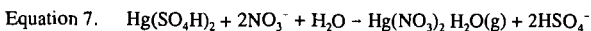
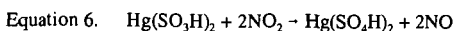


The role of SO₂ in the breakthrough mechanism is more difficult to understand. Since the oxidation of Hg⁰ is still 100% at breakthrough, it is unlikely that SO₂ is inhibiting the Oxidation Reaction 1 and, therefore, the oxidation sites. It must also not inhibit Reactions 2 and 4, since SO₂ can not provide the electron sink for Hg⁰ oxidation and is not normally reduced on a carbon surface. Therefore, SO₂ must be involved in the reactions leading to mercury stabilization on the sorbent or to bonding of the Hg(II) species formed in or subsequent to the oxidation.

Thus a direct involvement involving binding of SO₂ to an intermediate bound Hg(II) species seems more likely. In the presence of adsorbed SO₂, the Hg(II) may react to initially form mercuric sulfite or hydrosulfite (Equation 5). These species have Hg-S bonds and are expected to be nonvolatile. This nonvolatile species also collects in sites adjacent to the oxidation site. This form is consistent with the XAFS study (6) that concluded that mercury is bound by either sulfur or chloride on the sorbent.



Over time (1 hr), this form could be oxidized to mercury sulfate or bisulfate which results in forming Hg-O bonds (Equation 6). These bonds will be more labile, and interconversion to the volatile mercuric nitrate hydrate occurs (Equation 7). Since no Hg⁰ is emitted, the oxidation sites must still be functioning at breakthrough, only the bonding sites are becoming ineffective. This model is inadequate, however, because it predicts a gradual breakthrough from the start rather than the sudden one that is observed after 1 hr. Thus there seems to be other missing structural or reactivity factors that have not yet been considered.



The original hypothesis was that the LAC uses inorganic CaO sites to aid in the conversion of the oxidized Hg(II) (Equation 4) to the basic mercuric nitrate oxide that is not volatile and these sites are eventually converted to CaSO₃ or CaSO₄ that are inactive for stabilization. But this is not likely since removal of CaO did not shorten breakthrough.

The alternative model we now wish to consider is that SO_2 reacts with oxide at the carbon surface. By complexing these basic sites, this reaction may interfere with the formation of the stable basic mercuric oxide salt, as well as use up SO_2 that would bind directly to the mercury. Further experiments are needed to test this model.

ACKNOWLEDGMENTS

The support of the U.S. Department of Energy (Cooperative Agreement DE-FC26-98FT40320) is gratefully acknowledged.

REFERENCES

1. Miller, S.J.; Dunham, G.E.; Olson, E.S. "Mercury Sorbent Development for Coal-Fired Boilers," *In Proceedings of the Air Quality Conference*, McLean, VA, Dec. 1, 1998.
2. Pierce, W.C.; Noyes, W.A. *J. Amer. Chem. Soc.* **1928**, *50*, 2179.
3. Freeman, E.S.; Gordon, S. *J. Amer. Chem. Soc.* **1956**, *78*, 1813.
4. Olson, E.S.; Sharma, R.K.; Miller, S.J. Dunham, G.E. Mercury in the Environment, Proceedings of a Specialty Conference, VIP-91, Air & Waste Manag. Assoc., Minneapolis, MN, Sept 15, 1999, p 121.
5. Olson, E.S.; Sharma, R.K.; Miller, S.J.; Dunham, G.E. *Preprints: Div. Fuel Chem., Am. Chem. Soc.* **1998**, *43*, 867.
6. Huggins, F.E.; Huffman, G.P.; Dunham, G.E.; Senior, C.L. *Energy & Fuels* **1999**, *13*, 114.

ACTIVATED CARBONS IN EXTRACORPOREAL METHODS OF MEDICAL TREATMENT - TIME TO REACTIVATE THE IDEA?

Sergey Mikhlovsky

School of Pharmacy and Biomolecular Sciences

University of Brighton

Brighton BN2 4GJ, U.K.

KEYWORDS: Haemoperfusion, extracorporeal therapy, polymer-pyrolysed activated carbon

INTRODUCTION

The term "extracorporeal therapy" means a medical treatment utilising an extracorporeal circuit. Blood, plasma or another body fluid is passed through the extracorporeal purification device, where the toxic substances are separated and the purified fluid returns to the body. A range of extracorporeal therapies are available at present, based on physical (dialysis or filtration) or physicochemical (adsorption) mechanisms (Table 1).

Table 1. Physical and physico-chemical principles of extracorporeal therapy.

Method	Principle
Haemodialysis (HD)	Diffusion and convective transport through a semipermeable membrane, osmosis
Haemofiltration (HF)	Ultrafiltration and convective transport of solutes across a semipermeable membrane or filter
Combined HD/HF, or haemodiafiltration	Diffusion, ultrafiltration and convective transport
Apheresis and plasmapheresis	Membrane or centrifuge separation of blood into cells and plasma and further plasma fractionation using various methods
Haemoadsorption, or haemoperfusion (HP)	Physical adsorption, ion exchange or chemisorption

The concept of extracorporeal therapy (dialysis) can be traced back as early as 1913 [1], and the use of activated carbons in medicine for detoxification has been known since ancient Egypt and Greece [2], but real progress in the development and clinical applications of extracorporeal methods was made in 1960s-1980s. During these three decades commercial devices for extracorporeal treatment became available. Although extracorporeal adsorption was introduced along with dialysis and filtration, currently its use is limited to acute poisoning with low molecular drugs, whereas dialysis and filtration are widely used for the treatment of acute poisoning, acute and chronic organ failure and in various life support systems [3-6]. It is shown in this paper that recent progress in carbon science makes adsorption over activated carbons competitive to other extracorporeal methods. Current status, problems and prospects of extracorporeal adsorption therapy are discussed.

BIOCOMPATIBILITY OF ACTIVATED CARBONS

The first clinical use of charcoal in a HP device was reported by Yatsidis [7]. Haemoperfusion was carried out on a column of 200 g charcoal at a flow rate of 150-300 ml/min for 30-90 min. The results of the treatment of patients with terminal chronic renal failure were encouraging, and the charcoal column efficiently removed creatinine, uric acid and other uraemic metabolites. It was estimated that a 60-min HP was as efficient as a 4 to 6-hr HD. Blood perfusion over activated carbon was also successfully used for treatment of acute poisoning. However, this procedure induced hypotension, reduction in glucose, calcium and potassium concentration and damaged blood cells [8,9]. The most severe problem was the release of fine particles from the carbon granules causing microemboli. Despite thorough washing, microparticles of 5-35 µm size were persistently detected in the blood samples and washing solutions at the outlet of the carbon column. Use of plasma perfusion followed by its filtration to remove fine particles, instead of blood perfusion was suggested [10].

The problem of fine particle release from activated carbon granules was solved by coating them with a semipermeable membrane [9,11]. The most common commercially available activated

carbon haemoperfusion column 'Adsorba' is manufactured by Gambro, Sweden/Germany. In the 'Adsorba' column, Norit RXS extruded peat charcoal is coated with a 3-5 μm thick cellulose membrane. Coating carbon granules makes them more biocompatible but it also dramatically affects performance of a haemoperfusion column reducing the rate of diffusion to the carbon surface and efficiency of haemoperfusion. Adsorption of high molecular weight solutes is particularly affected. A thick membrane virtually cuts off HMW molecules and significantly reduces adsorption of "middle molecules" with molecular mass between 300 and 15,000 [12]. Removal of 'middle molecules' is essential as they play an important role in the development of many pathological conditions.

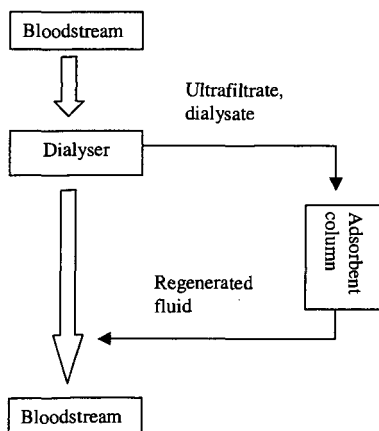
Use of coated adsorbents instead of uncoated dramatically reduces efficiency of haemoperfusion both in terms of adsorption capacity and rate of adsorption. Not surprisingly, information about the ability of coated activated carbons to remove even low molecular uraemic toxins is controversial [13]. As a result, HP has been limited in use to only acute poisoning with certain low molecular toxins [14].

UNCOATED ACTIVATED CARBONS FOR EXTRACORPOREAL THERAPY

The growing economic pressure on medical care provides a strong incentive for further development of adsorption therapy [15]. Patients in need of chronic extracorporeal treatment are usually of advanced age, and their number is rapidly increasing. For example, by the middle of this century the number of 75+ aged people will have doubled and the population over age 90 will have more than tripled in the U.K. [16]. This will result in a heavy burden on NHS. A similar situation is happening in other developed countries. Current expenditures on the treatment of chronic renal, liver and multiorgan failure – life threatening conditions in which HD and HF are widely used, far exceed the health care funding of all but a few nations [15]. Unless a cost-effective solution is found, this situation can only worsen.

An adsorption column could be used in-line with HD or HF to reduce the cost of treatment and achieve higher efficiency. Current dialysis membranes remove about 10-40% of middle molecular weight toxins. It has been found that up to 100% of this amount is removed by adsorption to the membrane surface which is about 1-2 $\text{m}^2 \text{g}^{-1}$ [17]. The surface area of an activated carbon is much higher. Thus, the capacity for removal of middle molecular weight toxins by adsorption far exceeds that of dialysis.

Use of dialysis or filtration technique inevitably results in a loss of large volume of water along with dissolved useful metabolites and nutrients. To compensate for such a loss, an isotonic and sterile replacement fluid is provided. In the treatment of intensive care patients who develop acute renal failure more than 50% of the total cost of HD or HF is associated with the purchase of replacement fluid [18]. In-line adsorption would increase efficiency of the extracorporeal procedure and reduce the loss of liquid by its recycling (Scheme).



Scheme.

In-line use of adsorbent column with HD or HF.

In this circuit the adsorbent does not come into contact with blood directly and the biocompatibility problem is reduced significantly.

A recently developed "BioLogic-DT" system combines haemodialysis and adsorption in one unit, utilising a carbon powder suspension to accelerate removal of toxins from blood [19]. In this system blood passes through a dialysis cellulose membrane package surrounded by a

suspension of fine particles of an activated carbon and a cation exchanger. The adsorbent and the blood are separated by a membrane. Removal of LMW toxins is accelerated by the adsorption mechanism that increases the concentration gradient across the dialysis membrane.

A similar approach has been suggested in a **Microspheres Based Detoxification system (MDS)** [20]. In this case blood is separated from plasma in the first circuit, and an adsorbent suspension is used in the secondary circuit for plasma purification. Although cellulose microbeads were used in the first instance, the system allows for the use of any other microparticles including activated carbon.

A specific problem with in-line carbon adsorption is related to its low adsorption capacity towards urea. Urea is one of the substances-markers of renal failure and it is efficiently removed from blood by dialysis. To tackle this problem, the ultrafiltrate regenerated by adsorption is infused into the additional diffusive dialyser that removes urea and then it is returned to the bloodstream. [21].

UNCOATED ACTIVATED CARBONS FOR DIRECT HAEMOPERFUSION

A much more challenging problem is synthesis of uncoated activated carbons that are as haemocompatible as coated adsorbents. Neither the exact nature of bio/haemocompatibility, nor the mechanism of 'blood-foreign surface' interactions are fully understood [22]. Despite this uncertainty, there is a general agreement that a haemocompatible material should meet the following criteria: (i) absence of thrombogenic, toxic, allergic or inflammatory reactions; (ii) no damage of blood cells or adjacent tissue; (iii) no undesirable changes in the blood composition; (iv) no immunological reaction; (v) no carcinogenic effect [23].

Carbon surface is considered to be rather biocompatible and some artificial organs are made from carbon materials. Such materials, however, have low surface area. The problem could be solved using activated carbons produced from synthetic polymers [24,25].

Using synthetic polymers as the precursor material eliminates any uncontrolled impurities. Coated activated carbons used for HP are made from natural raw materials. They have never been designed specifically for medical applications. In fact, they were technical grade carbons taken 'off the shelf' and used after a very simple pretreatment with hydrochloric acid and/or deionised water. Further pre-treatment such as electrolyte balancing is necessary to adjust the ionic composition of the carbon surface to the mineral composition of the blood. The fact that carbon surface contains a variety of functional groups having ion exchange properties, has been frequently ignored resulting in significant changes of pH and ion composition of the blood brought in contact with activated carbon.

It has been shown that two conflicting properties - large surface area and high mechanical strength - could be combined in polymer pyrolysed activated carbons. Thus a simple washing procedure removes microparticles from carbon granules eliminating the major concern about carbon biocompatibility.

Pore size distribution of activated carbons can be controlled by using porous polymeric precursors. In addition to micropores, polymer pyrolysed activated carbons have a unique mesoporous structure within 10-100 nm range which is predetermined by the pore size of the precursor.

It has been shown that mesoporous carbons possess high adsorption capacity towards middle and large protein molecules [26]. This is of particular importance for treatment of autoimmune diseases when removal of HMW immune complexes is necessary.

Activated carbons are considered to be non-specific adsorbents. Whilst high adsorption selectivity is desirable, nonspecific adsorption is also an advantage especially in the treatment of disorders with unknown etiology.

Despite chemical inertness of carbon, generation of chemically reactive functional groups such as $-COOH$, $-NH_2$ on its surface allows the use of carbon matrix for covalent binding of bioligands [27]. Carbon surface has been activated by oxidation and molecular bioligands have been attached covalently to the carboxylic functional groups via water soluble carbodiimide technique.

Carbon based bioselective adsorbents such as immuno-adsorbents could potentially combine the selectivity of a bioligand action and the nonspecific adsorptive capacity of the carbon matrix. The use of bioselective adsorbents for direct hemoperfusion would eliminate an expensive plasma separation stage.

CONCLUSIONS

The use of adsorbents for regeneration and recycling of dialysate or ultrafiltrate would decrease the volume of extracorporeal devices and replacement fluid, thus significantly reducing operational costs. Direct haemoperfusion over uncoated haemocompatible activated carbon offers more efficient, rapid and cost-effective means of medical treatment as in comparison with other extracorporeal techniques. Research in this area, almost abandoned in the 1980s, is becoming active again and very intensive development of adsorption methods should be expected.

ACKNOWLEDGMENTS

This work has been supported by the project INTAS 94-3033.

REFERENCES

1. Abel J.J., Rowntree L.G., and Turner B.B., *Trans. Assoc. Am. Physns*, 1913, **28**, 51.
2. Denti E., and Walker J.M., *Activated carbon: Properties, selection, and evaluation*, in Giordano, C. (Ed.), *Sorbents and Their Clinical Applications*, Academic Press, New York, NY, 1980, pp. 101-116.
3. Malchesky, P.S., *Artif. Organs*, 1994, **18**, 342.
4. Dunea, G., *Dialysis versus hemoperfusion in uremia*, in Giordano, C. (Ed.), *Sorbents and Their Clinical Applications*, Academic Press, New York, NY, 1980, pp. 375-385.
5. Miller, R., Kingswood, C., Bullen, C., and Cohen, S., *Brit. J. Hospital Med.*, 1990, **43**, 354.
6. Lopukhin, Yu.M., and Molodenkov, M.N., *Hemosorption*, C V Mosby, St Louis, 1979.
7. Yatzidis, H., *Proc. Eur. Dial. Transpl. Assoc.*, 1964, **1**, 83.
8. Rosenbaum, J.L., *Poisonings*, in Giordano, C. (Ed.), *Sorbents and Their Clinical Applications*, Academic Press, New York, NY, 1980, pp. 451-467.
9. Andrade, J.D., Van Wagenen, R., Chen, C., Ghavamian, M., Volder, J., Kirkham, R., and Kolff, W.J., *Trans. Am. Soc. Artif. Int. Organs*, 1972, **18**, 473.
10. Hagstam, K.E., Larsson, L.E., and Thysell, H., *Acta Med. Scand.*, 1966, **180**, 593.
11. Chang, T.M.S., *Trans. Am. Soc. Artif. Int. Organs*, 1966, **12**, 13.
12. Vanholder, R., De Smet, R., Vogeleere, P., and Ringoir, S., *Artif. Organs*, 1995, **19**, 1120.
13. Giordano, C., Esposito, R., Cirillo, D., Betuel, H., Fredel, A., Pluvio, M., Mazzola, G., Longhi, R., and Manzo, M. *International J Artif Organs*, 1984, **7**, 177.
14. Webb, D., *British J Hospital Medicine*, 1993, **49**, 493.
15. Friedman, E.A., *Artif. Organs*, 1992, **16**, 90.
16. *Fit for the Future: The Prevention of Dependency in Later Life*, Report of the Continuing Care Conference, H. Prophet, ed., June 1998.
17. Swinford, R.D., Baid, S., and Pascual, M., *Amer. J. Kidney Diseases*, 1997, **30**, Suppl. 4, S32.
18. Forni, L.G., and Hilton, P.J., *Current Concepts*, 1997, **336**, 1303.
19. Ash, S.R., *Artif. Organs*, 1994, **18**, 355.
20. Weber, C., Rajnoch, C., Loth, F., Schima, H., and Falkenhagen, D., *Int. J. Artif. Organs*, 1994, **17**, 595.
21. deFrancisco, A.L.M., Botella, J., Escallada, R., Hernandez, J., Malo, A.M., Garcia, R.P., Tomero, J.A.S., and Sanz, C., *Nephrol., Dial., Transplant.*, 1997, **12**, 528.
22. Colton, C.K., Ward, R.A., and Shaldon, S., *Nephrol., Dial., Transplant.*, 1994, **9** (Suppl. 2), 11.
23. Klinkmann, H., *The role of biomaterials in the application of artificial organs*, in Paul J P, Gaylor J D S, Courtney J M, Gilchrist T (Eds), *Biomaterials in Artificial Organs*, Macmillan Press, London, 1984, pp. 1-8.
24. Strelko, V.V., Korovin, Yu.F., Nikolaev, V.G., Kartel, N.T., and Adamenko, N.P., *Uncoated carbon sorbent SCN for direct hemoperfusion*, in Piskin E, Chang T M S (Eds), *Hemoperfusion and Artificial Organs*, Artificial Organs Society, Ankara, Turkey, 1982, pp. 144-146.
25. Lahaye, J., Nanse, G., Bagreev, A., Strelko, V., *Carbon*, 1999, **37**, 585.
26. Scorgie, K.A., Mikhaylovsky, S., Davies, J.G., Olliff, C., Lloyd, A., Phillips, G.J., Street, M., and Kingswood, C., *Carbon'99. 24th Biennial Conference on Carbon*. Amer. Carbon Soc., Charleston, SC, USA. Extended Abstracts, Vol. 1, pp. 150-151.
27. Mikhaylovsky, S.V., Strelko, V.V., Alekseyeva, T.A., and Komissarenko, S.V., *Biomat., Art. Cells, Art. Org.*, 1990, **18**, 671.

UNDERLYING MECHANISM OF DR EQUATION FOR ADSORPTION IN ACTIVATED CARBON

D. D. Do* and C. Nguyen
Department of Chemical Engineering
University of Queensland
St. Lucia, Queensland 4072
Australia

KEYWORDS: Dubinin-Radushkevich equation, Activated carbon, Adsorption

ABSTRACT: The Dubinin-Radushkevich (DR) equation is widely used for adsorption in microporous carbonaceous materials. This equation only yields a macroscopic behaviour of loading for a given pressure. In this paper, we apply our theory (Langmuir, 15, 3608, 1999) to explain the microscopic adsorption behaviour behind the DR equation.

INTRODUCTION

The Dubinin-Radushkevich (DR) equation is used to describe adsorption of sub-critical fluids in microporous solids such as activated carbon. The DR equation has the form

$$W/W_0 = \exp[-(A/E)^2], \quad A = RT \ln(P/P_0)$$

This equation provides the macroscopic information of the fraction of the total micropore volume occupied by the adsorbate molecules. It does not give any picture on how adsorption behaves microscopically, that is which micropores are filled and which are partially filled as it is well known that activated carbon has a rather broad pore size distribution. This information of microscopic distribution of adsorbed molecules is important in the study of mobility of adsorbed molecules. Here we apply a new method (Nguyen and Do, 1999) to describe the adsorption process in microporous carbonaceous materials with a pore size distribution. It is a structure based method, where enhancement of adsorption is allowed for due to the proximity of the pore walls. We will use this technique to investigate the adsorption in carbon micropores in an attempt to shed some light to the working mechanism of the DR equation.

THEORY

In our approach (Nguyen and Do, 1999) we adopt a common mechanism for the adsorption process occurring in carbonaceous pores as a sequence of surface layering followed by pore filling, irrespective of their sizes. The principal feature of this theory is the allowance for the enhancement in adsorption induced by the overlapping of the potential fields of opposite pore walls. This enhancement not only affects the adsorbed phase, but also the gas phase molecules occluded within the pore. The pressure exerted by these occluded molecules is calculated from:

$$p_p(r) = p \exp(-E_{av}/RT)$$

with E_{av} the average potential energy of the occluded molecules. These occluded molecules will provide source to build up adsorbed layers on the pore walls, following a mechanism akin to BET, but in this theory we take that these layers are enhanced due to the potential energy of interaction with the pore walls. The BET constant in a pore is calculated in terms of the BET constant of a corresponding flat surface as:

$$C_p(r) = C_s \exp[(Q_p(r) - Q_s)/RT]$$

where $Q_p(r)$ and Q_s are heats of adsorptions in pore and a flat surface, respectively. Adsorption in pores can be pictured as a process whereby gas phase molecules are drawn into the pore interior. Once inside, they are further pressed against each other as a result of the overlapping potential fields. If the pore pressure is beyond the corresponding vapor pressure, the adsorbed phase turns into liquid (albeit compressed liquid). It is, therefore, understood that in some narrow pores, due to the very large enhanced pressures, the adsorbed phase exists as liquid even at very low bulk pressures. This liquid filling process progresses to pores larger in size as the bulk pressure increases. This is essentially the micropore filling process described in the Dubinin theory (1960). In larger pores, adsorption occurs as a surface layering process, and this layer will grow until the following condition is satisfied:

$$r - t - \sigma_{HL}/2 = \gamma_{VM}/[RT \ln(P_0/P_p)]$$

when the complete pore filling will occur. Here r is the half width, γ is the surface tension and v_M is the liquid molar volume. The statistical thickness " t " is calculated from:

$$t(r) = t_m \frac{x_p(r)C_p(r)}{(1 - x_p(r))(1 - x(r) + x_p(r)C_p(r))}; \quad x_p(r) = \frac{P_p(r)}{P_0}$$

RESULTS & DISCUSSION

The fractional loading in the DR equation defined as $\theta = W/W_0$ accounts for adsorption in micropores only. This means that the contribution of larger pores on the uptake must be removed before they can be used with the DR equation. Furthermore, the DR equation provides only the macroscopic information. For example, when the change in the free energy, A , is equal to the characteristic energy of the system, the fractional loading is 0.37, meaning 37% of the micropore volume is occupied by the adsorbate molecules. Our approach models adsorption as a process occurring in all pores simultaneously, with the amount adsorbed in a pore dependent on the pore size. At a given pressure small micropores are completely filled, while larger micropores have a layer of adsorbate molecules. Knowing the volume of each pore, the overall fractional loading is calculated from:

$$\theta = \sum_j \theta_j w_j / \sum_j w_j$$

where θ_j is the pore fractional loading, and is equal to 1 for filled pores and equal to $t_j/(r_j - \sigma_{ss}/2)$ for pores having layers of adsorbate. This overall fractional loading is then compared with that calculated from the DR equation.

We illustrate this theory with nitrogen adsorption data at 77 K on an ACF sample. This ACF has a micropore volume of 0.24 cc/g, and a mean micropore half width of 0.66 nm. Fitting the DR equation with the data yields the characteristic energy of 6.9 kJ/mol. The distribution of pores calculated by our method is shown in Table 1 (columns 1 and 2) where we show 24 representative pores with their corresponding pore volumes. Using our theory we calculated the amounts adsorbed in each pore at three levels of pressure: 6×10^{-5} , 3×10^{-2} and 0.4, and these are shown in Table 1. To distinguish pores already filled, the amount adsorbed in these pores are printed bold. At the very low relative pressure of 6×10^{-5} , adsorption occurs mainly in the smallest micropores. The first three pore sub-ranges are filled completely with adsorbate while larger pores are layered with adsorbate molecules. The overall capacity calculated by our theory is 3.04 mmol/g, compared to 3.06 mmol/g calculated using the DR equation. Our approach provides a detailed distribution of this 3.04 mmol/g capacity. At a relative pressure of 3×10^{-2} , all pores having half width less than 0.588 nm are filled. This pore filling is progressed to pores of larger size when pressure increases. For example, at a reduced pressure of 0.4, the threshold pore size for complete filling is 1.266 nm, which is now in the mesopore range. Table 2 presents the results of the nitrogen adsorption onto the ACF sample at these three pressure levels calculated using the DR and our method. As seen in the table, the amount adsorbed calculated using the DR equation is by and large equal to the sum of the amounts adsorbed in all pores using our technique. The difference is more significant at the higher end of the pressure range, where adsorption in mesopores occurs in addition to that in micropores. This is because the DR equation, unable to deal with mesopores, underpredicts the data at high relative pressures, while our technique describes well the data at all pressure levels.

We now turn to the isosteric heat of adsorption, which can be calculated from the DR equation (Do, 1998) as:

$$-\Delta H = \Delta H_{vap} + E \left(\ln \frac{1}{\theta} \right)^{1/2} + \frac{E\delta T}{2} \left(\ln \frac{1}{\theta} \right)^{-1/2}$$

where δ is the coefficient of expansion of liquid adsorbate, which is very small. Figure 1 shows the plot of the isosteric heat of adsorption of nitrogen versus relative pressure at -196°C onto the ACF sample calculated from this DR equation. To calculate the heat of adsorption from our method, we assume that the adsorption heat is approximated by the decrease in the potential energy of adsorbate, when moved from the bulk into the interior of the pore. This is shown in Table 1 for all pores. Energy released is larger in smaller pores, and proportional to the pore volume. Since the ACF sample has a distribution of pores mostly in the range from 0.32 to 0.397 nm, most of the heat comes from the pores in that range. The total heat released at any overall loading (C_μ) is obtained by summing all the individual heats released in each pore. This is the cumulative heat produced when the amount of C_μ is loaded into a clean sample. For example, from Table 1 the cumulative heat at the relative pressure of 3×10^{-2} is 55 Joule, corresponding to an amount of 6.38 mmol loaded on 1 gram of the ACF sample. The isosteric heat of adsorption

is the heat released at a given loading C_μ , i.e. it is the incremental heat produced per unit mole when the loading is incrementally increased from C_μ to $C_\mu + \Delta C_\mu$ ($\Delta C_\mu \ll C_\mu$). This is applied for nitrogen adsorption onto ACF data, and the results are shown in Figure 1. The maximum possible isosteric heat for nitrogen is ~ 16.2 kJ/mol if all pores having half width equal to the solid-fluid collision diameter. The isosteric heat calculated using the DR equation and our technique are quite different. The comparison between the methods and/or the justification of the suitability can be made based on the experimental measurement of the isosteric heat of the system, which is not available at this stage.

We now address the question regarding the validity of the DR equation. Figure 2 shows the isotherms of nitrogen adsorption of representative pore sub-ranges in the form of $\log(C_\mu)$ versus $\log^2(1/x)$. As seen, none of the single pore isotherms can be considered to be a straight line. However, by adding up the individual isotherms, we get the overall isotherm shown as a dotted line, which is practically a straight line, supporting the suitability of the DR equation. It is clear that the DR equation is not applicable for adsorbents having a extremely narrow pore size distribution. Samples having very skewed PSDs can not also be described by DR equation. Thus, for the DR equation to be applicable, the porous solid must have a distribution of micropores, and that distribution must not be very skewed. This explains why the DR equation is not applicable to all microporous materials.

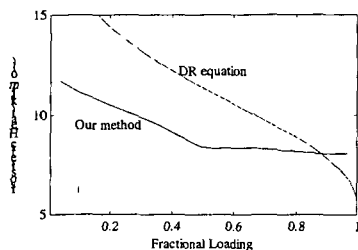


Figure 1: Plot of the isosteric heat versus loading

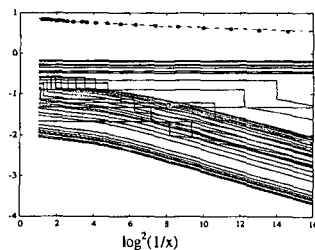


Figure 2: Plot of $\log(C_\mu)$ versus $\log^2(1/x)$

ACKNOWLEDGEMENT

Support from the Australian Research Council is acknowledged.

REFERENCES

- Do, D.D., "Adsorption Analysis: Equilibria and Kinetics", Imperial College Press, London, 1998.
- Dubinin, M.M., Chem. Rev., **60**, 235 (1960).
- Nguyen, C. and D. D. Do, Langmuir, **15**, 3608 (1999).

Table 1: Nitrogen adsorption onto ACF at 77 K at three relative pressures (per gram of sample).

Half width	Volume	$x = 6 \times 10^{-5}$		$x = 3 \times 10^{-2}$		$x = 0.4$	
		loading	energy	loading	energy	loading	energy
nm	cc	mmol	J	mmol	J	mmol	J
0.286	0.004	0.1256	1.32	0.1256	1.32	0.1256	1.32
0.320	0.047	1.3611	13.10	1.3611	13.10	1.3611	13.10
0.357	0.041	1.1914	10.84	1.1914	10.84	1.1914	10.84
0.397	0.029	0.2410	2.11	0.8267	7.24	0.8267	7.24
0.439	0.009	0.0367	0.31	0.2653	2.27	0.2653	2.27
0.485	0.007	0.0144	0.12	0.2069	1.74	0.2069	1.74
0.534	0.021	0.0241	0.20	0.6021	4.99	0.6021	4.99
0.588	0.030	0.0219	0.18	0.8551	7.03	0.8551	7.03
0.645	0.026	0.0136	0.11	0.3667	3.00	0.7624	6.23
0.706	0.018	0.0069	0.06	0.2249	1.83	0.5144	4.19
0.772	0.006	0.0018	0.01	0.0674	0.55	0.1688	1.37
0.843	0.005	0.0012	0.01	0.0490	0.40	0.1340	1.09
0.919	0.005	0.0010	0.01	0.0465	0.38	0.1382	1.12
1.001	0.006	0.0011	0.01	0.0516	0.42	0.1663	1.34
1.090	0.004	0.0007	-	0.0328	-	0.1141	-
1.266	0.002	0.0003	-	0.0159	-	0.0637	-
1.683	0.002	0.0002	-	0.0085	-	0.0155	-
2.249	0.002	0.0001	-	0.0066	-	0.0118	-
2.912	0.005	0.0003	-	0.0155	-	0.0278	-
3.805	0.006	0.0002	-	0.0144	-	0.0258	-
4.958	0.006	0.0002	-	0.0117	-	0.0208	-
6.444	0.009	0.0002	-	0.0134	-	0.0240	-
8.361	0.014	0.0003	-	0.0161	-	0.0288	-
9.214	0.007	0.0001	-	0.0071	-	0.0126	-
Micropore	0.254	3.042	28.39	6.240	55.09	7.318	63.87
overall	0.308	3.044		6.382		7.663	

Table 2: Nitrogen adsorption onto ACF sample calculated using our method and DR equation.

P/P_0	Overall capacity (mmol/g)		Micropore capacity (mmol/g)	
	Experimental	our method	DR eq.	our method
6×10^{-4}	3.03	3.04	3.06	3.04
3×10^{-2}	6.36	6.38	6.25	6.24
0.4	7.63	7.66	6.9	7.31

CHARACTERIZATION OF ADSORPTION ON CARBON NANOTUBES USING A PULSE MASS ANALYZER

Edward W. Bittner, Milton R. Smith, and Bradley C. Bockrath
National Energy Technology Laboratory
US Department of Energy
Pittsburgh, PA 15236

KEYWORDS: Carbon nanotubes, hydrogen, adsorption of organic compounds

INTRODUCTION:

In addition to their other special properties, carbon nanotubes also have excited considerable interest because of their potential to serve as hydrogen storage materials [1]. Several groups have reported [2-4] large values for hydrogen uptake by single walled nanotubes. Molecular simulation studies were used to identify critical structural properties that are important for development of an effective material for hydrogen storage [5]. A list of critical properties culled from the experimental and theoretical results includes the diameter of the tube, the relative number of tubes with open ends, the ease of penetration of the pore mouth to the interior of the tube, the ease of entrance into the extra-tubular space typically found between the single tube strands of rope-like structures, and the interaction potential between hydrogen and the carbon surface. In the work described below, a pulse mass analyzer similar to that originally developed to investigate the kinetics of coke deposition on cracking catalysts [6] was used to evaluate novel materials for storage potential. Direct measurements were made of weight changes in a packed bed of storage material caused by changes in the gas stream or by injection of small samples of volatile organic compounds. The amount of weight change found after injection of the samples and the "retention" time of the adsorbed material provided useful information on the characteristics of various nanotube samples. The method holds promise as an additional tool for characterization of adsorbents and storage materials.

EXPERIMENTAL:

Materials. The single wall nanotubes were obtained from Rice University (Tubes@Rice). "Fullerene Nanotubes" were used after grinding in a ball mill for ease of introduction into the sample holder, and are referred to below as raw Rice tubes. According to the analysis provided the average tube diameter is 1.36 nm. TGA analysis gave a residue weight after combustion corresponding to the expected amount of catalytic metals reported as incorporated during the synthesis. Analysis of the TGA residue by ICP led to the determination of 3.7 % nickel, 3.5 % Co, and 0.44 % Fe in the original material.

Equipment: Figure 1 is a block diagram for the apparatus including the pulse mass analyzer (PMA1500) manufactured by Rupprecht and Pataschnick. The PMA1500 is a mass measuring device that employs a tapered glass element that is stimulated to vibrate at its natural frequency. The element is made up of a long narrow hollow quartz glass tube that opens at the bottom to a 0.100 cc volume into which the sample is placed. Quartz wool and a retaining cap hold the sample in place. The element is mounted vertically in a holder in a stainless steel vessel. Carrier gas flows through the sample bed providing excellent contact. The frequency of vibration of the element is monitored via an optical system. With appropriate calibration the frequency changes are recorded as mass changes within the reactor using Equation 1. A stream of purge gas sweeps out carrier gas and other components once they have passed through the sample bed. In addition, a valve/loop injector allows pulses of reactant gases to be introduced into the carrier gas upstream of the sample chamber. Injection of volatile organic liquids was made by syringe through a heated injection port. Mass flow controllers (Brooks, 5850E) were used to regulate the flow of both carrier and purge gases. The instrument is able to work at pressures from 1- 60 atmospheres (Brooks backpressure regulator, 5866E) and at temperatures up to 700 C.

$$\Delta m = k / (1/f_1^2 - 1/f_2^2) \quad (1)$$

To determine k the instrument was equilibrated at a set temperature with no sample or sample-retaining cap and with flow rates of carrier and purge gases at nominal values. After the frequency of the vibrating element was recorded the sample-retaining cap of known mass was placed on the element and the frequency was measured a second time. Thus, k is established for the particular set of pressure, flow and temperature settings used. The constant k has a strong temperature dependency and re-calibration must be done when the temperature is varied.

Additional information was obtained from a quadrupole mass spectrometer (Ametek MA 100M) that sampled the exit gas stream through a 6-meter length of a capillary GC column. This detector was especially useful with the PMA in pulse mode. When a significant portion of an injection was not retained by adsorption on the sample the pulse of material passing through the bed was observed by the mass spectrometer. Materials that were retained and then slowly

bled from the sample remained below the detection limit and were not observed. The use of a capillary column as transfer tube provided an additional means to discriminate between compounds by observing the transit time between PMA and the spectrometer. For example, the transit time for ethanol was 3.5 min. while that for 2-propanol was 5.0 min.

Gas Density Experiment

The frequency of vibration depends on the mass of the tapered element and its contents, including the weight of the gas contained within the tapered element. For example, when the carrier gas was switched from nitrogen to helium a change in mass occurred due to the change in gas density inside the element. Cycling back and forth showed reproducible gas density changes (Figure 2). Because of this, the changes in mass due simply to changes in gas density must be taken into account when the results from adsorption experiments are considered.

Adsorption Experiments

The sample bed was packed with the carbon nanotube sample and heated using helium as carrier gas and nitrogen as purge gas both at 50 cc/min. All of the experiments were performed at atmospheric pressure. Each sample was pre-treated in situ by heating to either 200 C or 700 C for 4 hours before adsorption measurements were made. Then the temperature was set for the adsorption experiment (30 C, 100 C, or 200 C) and the PMA was allowed to equilibrate for about an hour. Organic compounds (typically 1.0 or 2.0 μ l as liquids), were injected into the pre-heated port (200 C) of the PMA where they vaporized rapidly in the carrier stream; the mass responses were recorded. For a carrier flow of 50 cc/min, a mass response was seen within 6 seconds, the time taken by the vaporized sample to reach the fixed bed. The mass changes were recorded as a function of time. For those compounds poorly adsorbed only a very small and transient change in mass was observed. For those strongly adsorbed, a large, rapid increase in mass was observed followed by a gradual decrease as the retained compound slowly desorbed. The gravimetric decay curve had a long tail resembling that associated with a poorly performing chromatographic column. Strongly adsorbed species took hours to desorb completely.

RESULTS:

Effect of adsorbate structure.

Hydrogen, carbon dioxide, and organic compounds were injected at 30 C, 100 C, and 200 C.

30 C. The sample holder was packed with 80.0 mg of raw Rice tubes and heated to 200 C in a stream of helium at 50.0 cc/min. with a purge gas of nitrogen at 50.0 cc/min. Following this pretreatment, the temperature of the PMA was equilibrated at 30 C for one hour. Individual pulses of hydrogen gas (3.90 mg., 1.95 mmoles) were introduced through the loop injector valve. A small peak was formed equivalent to a mass gain of 20- 25 μ g that returned to the baseline in a matter of seconds, indicating that only a small fraction of hydrogen injected was adsorbed then rapidly desorbed under these conditions. Pulses of CO₂ (12.8 mg., 0.291 mmoles) had a similar appearance. As typical of poorly retained compounds, hydrogen and carbon dioxide peaks appeared in the mass spectrometer following these injections and were of comparable size to those following injections into an empty reactor. Experiments conducted at a later time confirmed that little or no hydrogen adsorption occurred at 30 C by this sample, even under 27.0 atmospheres of hydrogen pressure flowing at 50 cc/min. for 3 hours. In these experiments the raw Rice tubes did not adsorb hydrogen or CO₂ to any significant extent at 30 C.

100 C. As before, pulses of hydrogen and carbon dioxide passed through the sample without significant adsorption. A series of organic compounds with similar boiling points, methanol (65.0 C), tetrahydrofuran (64.5 C), and n-hexane (68.0 C) was injected. Injections of methanol (2.0 μ l.) gave reproducible changes of 1.0 mg. corresponding to 63% of the material adsorbed. A small peak for methanol was also observed by the mass spectrometer, consistent with a partially or poorly adsorbed compound. THF was adsorbed more strongly than methanol. Duplicate injections gave 86 % and 89 % of the THF retained and each injection took approximately 60 minutes to desorb. The most strongly held compound of the series was n-hexane. Of two injections, 91% and 88% were retained and it required several hours at 100 C followed by heating to 200 C to remove it completely.

200 C. At 200 C another series of compounds of disparate polarity and structure but similar boiling points was used. These were ethanol (78.5 C), 2-propanol (82.0 C), 2-butanone (79.6 C), cyclohexane (81.0 C), cyclohexene (83.0 C), and benzene (80.0 C). Figure 4 shows the PMA responses and the data are summarized in Table 1. The most striking feature of Figure 4 is the wide range of retention. Alcohols are hardly retained. For ethanol, the amount adsorbed after each 0.790 mg. (1.0 μ l) injection was 0.230 mg, only 29 % of the mass injected. Desorption of the ethanol occurred within 30 seconds. About 55 % of the 2-propanol injected was retained and also desorbed rapidly. Markedly more of the cyclohexane (92 %) and cyclohexene (88 %) were

retained and each desorbed slowly. Among the three cyclic compounds, cyclohexene and benzene desorbed much more slowly than cyclohexane. The times required for the weight gain to diminish by one half (Table 1) were taken as a rough measure of relative retention.

Effect of pre-treatment temperature

After completing the adsorption experiments above, the raw Rice tubes were heated to 700 C to explore for effects due to the pretreatment temperature. This seemed appropriate because evidence has been presented [2,7] that functional groups are removed from tube openings by high temperature treatments, thus allowing for greater access to the interior of the tubes. The results show that the retention time increased significantly for some of the organic compounds compared with those found after pretreatment at 200 C (Table 1). For example, the retention time for cyclohexane doubled from 33 to 67 minutes. In general, the desorption curves for strongly retained compounds have long tails. Kinetic data from material pretreated at 200 C do not appear to obey a simple rate law. In contrast, the decay curves for all of the hydrocarbons sorbed onto nanotubes activated at 700 C were well described over the first 400 seconds by a second order rate law (eg. Figure 5). For comparison, the half lives were calculated in seconds for 1.0 mg starting weights of each as: cyclohexane (46), cyclohexene (88), benzene (89), and hexane (205). The result shows an increase in retention on introduction of one degree of unsaturation from cyclohexane to cyclohexene, but no further change on going to the aromatic compound benzene. A much greater increase was seen with n-hexane, the calculated half-life being nearly 4 ½ times that of its cyclic counterpart. This remarkable difference may be due to the ability of n-hexane to flex and bend to accommodate maximum interaction with the nanotube surface. This flexibility may allow either stronger binding to the exterior surface or alternatively, a greater tendency to be trapped within the tube. At present it seems unlikely that the desorption process can be successfully interpreted in terms of a single, well-defined adsorption site. Further studies with linear and branched hydrocarbons are needed to gain better insight into the adsorption process.

Table 1^a
Raw Rice Tubes, Pre-treated at 200 C and 700 C

COMPOUND	BP (C)	Den. (g/ml.)	Halfwidth ^b	Halfwidth ^c
			Sec.	Sec.
ETOH	78.5	0.789	13, 13	13
I-PROH	82.0	0.780	13, 13	15, 15
CYCLOHEXANE	81.0	0.779	33, 33	67, 67
BUTANONE	79.6	0.805	40, 40	-----
CYCLOHEXENE	83.0	0.811	67, 67	133, 133
BENZENE	80.0	0.880	77, 77	107
n-HEXANE	68.0	0.659	-----	313

a) 1.0 µl injections at 200 C, helium carrier 50 cc./min. nitrogen purge 50 cc./min., duplicates shown. b) Raw Rice tubes, pretreatment 200 C. c) Raw Rice tubes, pretreatment 700 C.

CONCLUSIONS:

The interactions of hydrogen and carbon dioxide as well as several organic compounds with carbon nanotubes were investigated with a pulse mass analyzer. The pulse mass analyzer proved to be a useful tool for elucidation of structure/adsorptivity relationships in these systems. Our findings indicate that neither hydrogen nor carbon dioxide has a great affinity for these materials as compared to the organic compounds tested. Within the organic sequences, we find that alcohols are not retained as well as hydrocarbons. Moreover, unsaturation may be beneficial for adsorption in some cases (cyclohexene versus cyclohexane), but in another case (hexane) the enhanced flexibility associated with saturation of the carbon chain perhaps leads to an even greater affinity for nanotubes.

REFERENCES:

1. M. S. Dresselhaus, K. A. Williams, P. C. Eklund, MRS Bulletin, 24, 45, (1999).
2. A. C. Dillon, K. M. Jones, T. A. Bekkedahl, C. H. Klang, D. S. Bethune, M. J. Heben, Nature, 386,377 (1997).
3. Y. Ye, C. C. Ahn, C. Witham, B. Fultz, J. Liu, A. G. Rinzier, D. Colbert, K. A. Smith, R. E. Smalley, App. Phys. Letts., 74, 2307 (1999).
4. C. Liu, Y. Y. Fan, M. Liu, H. T. Cong, H. M. Cheng, M. S. Dresselhaus, Science, 286, 1127 (1999).
5. Q. Wang, J. K. Johnson, J. Phys. Chem. B, 103,4809 (1999).
6. F. Hershkowitz, P. D. Madiera, Ind. Eng. Chem. Res., 32, 2969 (1993).
7. A. Kuznetsova, D. B. Mawhinney, V. Naumenko, J. T. Yates, Jr., J. Liu, R. E. Smalley, Chem. Phys. Lett., 321, 292 (2000).

ACKNOWLEDGMENT:

The authors acknowledge Shelia Hedges for her assistance in providing TGA analyses of the nanotube sample. This work was performed while MRS held a National Research Council-NETL Research associateship. This publication was supported in part by the appointment of EWB to the US Department of Energy Fossil Energy Faculty Research Program at NETL administrated by Oak Ridge Institute for Science and Education.

DISCLAIMER:

Reference in this work to any specific commercial product is to facilitate understanding and does not necessarily imply endorsement by the United States Department of Energy.

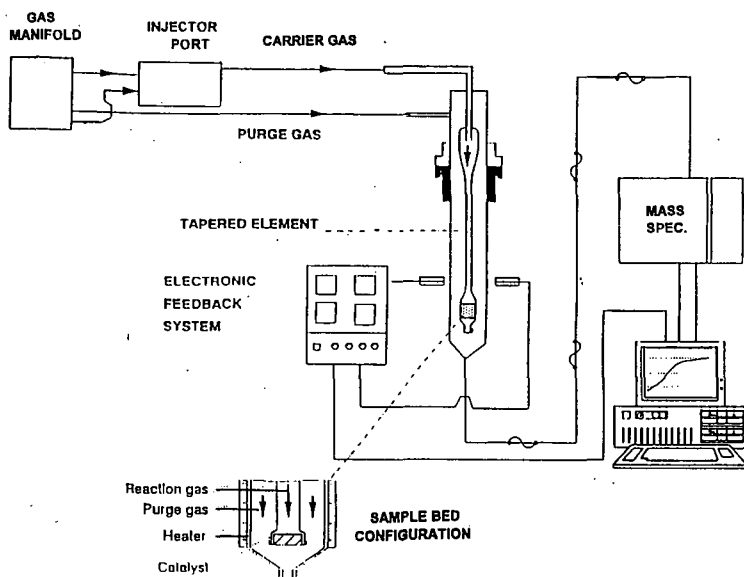


Figure 1 Block Diagram of the PMA1500

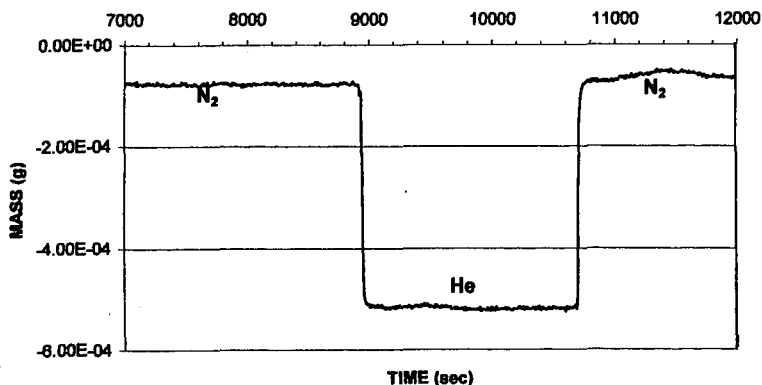


Figure 2 Gas Density Experiment, empty reactor, 30 C. carrier switch from 50cc/min N_2 to 50cc/min He to 50cc/min N_2 .

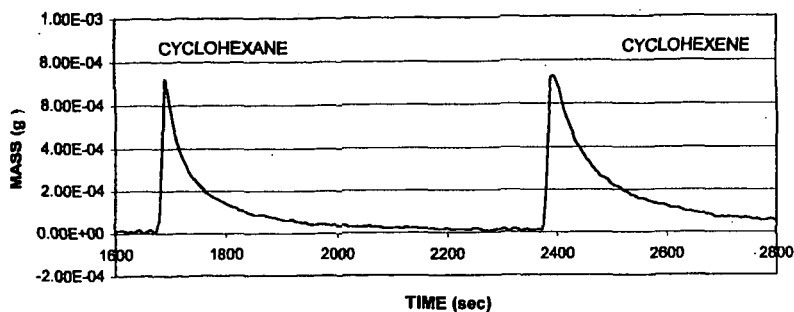


Figure 3 Raw Rice tubes at 200 C, 50 cc/min He carrier with 1.0 ul. injections of cyclohexane and cyclohexene, pretreated at 200 C

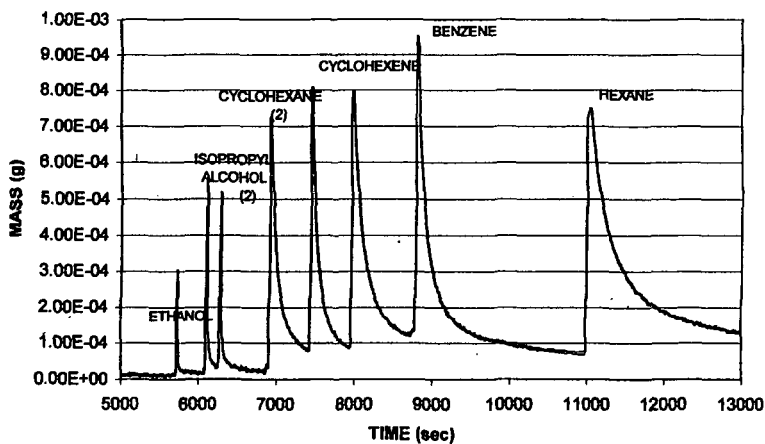


Figure 4. Raw Rice tubes at 200 C, helium carrier 50 cc/min., pre-treatment at 700 C, 1.0 ul. injections

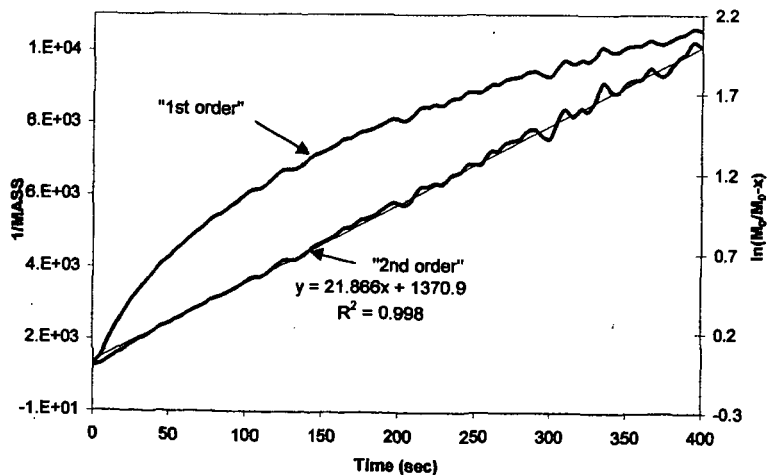


Figure 5. Rate dependence for loss of cyclohexane at 200 C (see Figure 4)

CARBON NANOTUBE ADSORBENTS

You Fa Yin, Tim Mays, Emmanuelle Alain and Brian McEnaney
Materials Research Centre, Department of Engineering and Applied Science,
University of Bath, BATH BA2 7AY, United Kingdom.

KEYWORDS: carbon nanotubes, adsorption, gas storage

INTRODUCTION

One of the more interesting applications proposed for carbon nanotubes is as storage media for fluids and solids. Of particular interest is their potential for fuel gas storage, especially hydrogen [1]. A full, experimental exploration of their potential in these fields must await developments in the production, purification and ordering of nanotubes. Meanwhile, it is possible to make some assessment of their potential as gas storage media using molecular simulations. The interior of an isolated open carbon nanotube can be viewed as a microporous or mesoporous cylindrical adsorption space (depending upon the nanotube diameter). Also, the interstices between nanotubes may provide additional adsorption space of nanometric dimensions. Therefore, we have been exploring the adsorption of gases in arrays of nanotubes using molecular simulations. In this paper we present some storage capacities for hydrogen at 298 and 77 K and nitrogen at 77 K in carbon nanotube arrays obtained from simulations and compare these to experimental measurements of adsorption in materials containing nanotubes.

MODELS AND SIMULATIONS

The model adsorption space consists of a unidirectional trigonal array of open or closed single wall carbon nanotubes, SWCNT, Figure 1. The diameter D and the nanotube separation G define the geometry of the array.

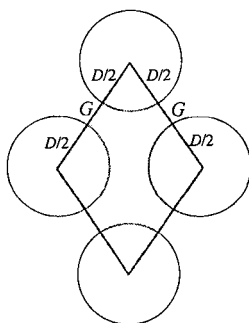


Figure 1. Model trigonal array of single-walled carbon nanotubes of diameter D and separation G . Circles are cross sections of nanotubes. The shaded area is the cross section of the simulation cell.

Table 1. Lennard-Jones potential parameters used for simulations of adsorption of H_2 and N_2 in SWCNT arrays. k_B is Boltzmann's constant.

Gas	LJ Parameter			
	$\sigma_{ff} / \text{\AA}$	$\sigma_{sf} / \text{\AA}$	$(\epsilon_{ff} / k_B) / K$	$(\epsilon_{sf} / k_B) / K$
Hydrogen	2.96	3.19	41.5	35.4
Nitrogen	3.572	3.494	93.98	53.52

We have also studied square arrays of SWCNT [2]. The Grand Canonical Monte Carlo Ensemble method [e.g., 3] was used to simulate equilibrium adsorption of gases in the model array. A single site Lennard-Jones (LJ) 12:6 pair potential was used to represent interactions between gas molecules. The interaction between an adsorbate molecule and a single nanotube was obtained by integration of the LJ potential over the nanotube surface; this potential is applicable to adsorption inside and outside tubes (endohedral and exohedral adsorption [4]). The LJ length (σ) and energy (ϵ) parameters for fluid-fluid (ff) and solid-fluid (sf) potentials are listed in Table 1. The cross section through the simulation cell, perpendicular to the length of the nanotubes, is a parallelogram, Figure 1. The length of the cell parallel to the nanotubes was

normally $10\sigma_H$, although this could be extended to increase the number of molecules in the cell and so reduce errors. The Peng-Robinson equation of state was used to calculate the chemical potentials of bulk gases [5]. The main output from the simulations was the average number of molecules adsorbed in the simulation cell as a function of pressure.

RESULTS AND DISCUSSION

Hydrogen Storage at 298 K and 77 K.

The amount of usable gas in a gas storage system is the delivered capacity, *i.e.*, the amount of gas stored at the higher (storage) pressure less the amount retained in the container at the lower (delivery) pressure. The delivered capacity can be expressed on a gravimetric or volumetric basis; here, a gravimetric basis is considered. For hydrogen, storage and delivery pressures were normally 70 and 1 bar respectively. For studies of the effects of storage pressure on the hydrogen capacity, the storage pressure was varied from 1 to 200 bar. The US DOE hydrogen plan for a fuel cell powered vehicle requires the storage system to have a delivered gravimetric capacity of 6.5 wt% H_2 [1].

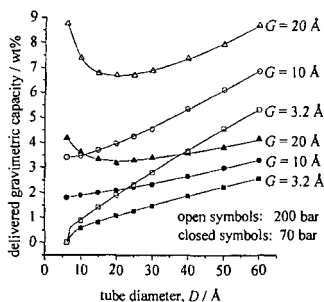


Figure 2. Delivered gravimetric hydrogen capacity at 298 K as a function of tube diameter in trigonal arrays of open single-walled carbon nanotubes with different separations G , for storage pressures of 70 and 200 bar.

Figure 2 shows the delivered gravimetric capacities of trigonal arrays of open SWCNT at 298 K and at storage pressures of 70 and 200 bar. For most of the arrays, capacity increases with increasing nanotube diameter, D , and tube separation, G . The effect of tube diameter on capacity is as expected while the effect of tube separation shows that exohedral adsorption in the interstices between the nanotubes is important. Significant amounts of hydrogen can be stored in the arrays, but none of them achieves the DOE target capacity at 298 K and a storage pressure of 70 bar. The DOE target capacity is achieved at 298 K and 200 bar storage pressure for SWCNT with a wide range of diameters in arrays with a spacing of 20 Å.

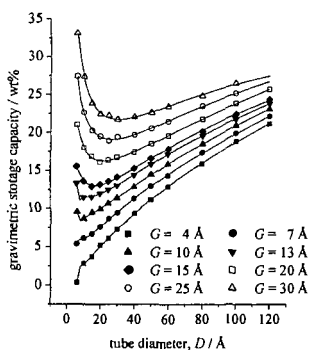


Figure 3. Gravimetric hydrogen storage capacity for trigonal arrays of open single-walled carbon nanotubes at 77 K and 70 bar as a function of tube diameter D and separation G .

The effects of increases in D and G on storage hydrogen capacities at 77 K and 70 bar, Figure 3, are broadly similar to those found at 298 K. The DOE target capacity is reached for arrays with a wide range of D and G values. For arrays with a spacing of 30 Å, the DOE target is exceeded by a considerable margin. The maximum delivered hydrogen capacity of ~33 wt% is reached with an array consisting of widely spaced narrow nanotubes ($D = 6$ Å, $G = 30$ Å) where exohedral adsorption dominates. The non-linear variations in capacity for arrays with $D < 30$ Å and $G > 7$ Å, Figure 3, are the result of complex geometrical factors affecting the space available for adsorption in the simulation cell. The volume of the simulation cell is proportional to $(D + G)^2$, while the mass of carbon in the cell is proportional to D . Thus, when $G \ll D$, the volume available per unit mass is $\sim D$, i.e., the capacities increase with D nearly linearly as in Figure 3. When $G \gg D$, the volume available per unit mass is $\sim 1/D$, i.e., the capacities decrease with increasing D .

Nitrogen Adsorption at 77 K. Figure 4 shows the gravimetric saturation capacity for nitrogen at 77 K and relative pressure $P/P_0 = 1$ for trigonal arrays of open SWCNT as a function of D and G . Qualitatively, the effects of increases in D and G on capacity are broadly similar to those found for hydrogen at 77 K, Figure 3. However, the gravimetric capacities for nitrogen at $P/P_0 = 1$ are more than 10 times higher than that for hydrogen at 70 bar in arrays of the same geometry. This is because (1) the critical temperature for nitrogen is much higher than for hydrogen, and (2) the molecular mass of nitrogen is 14 times that of hydrogen.

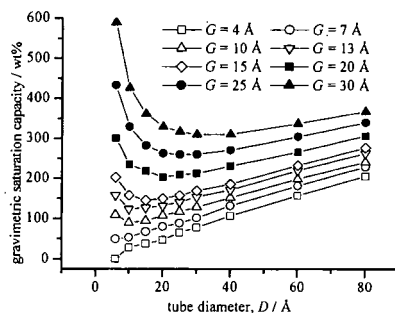


Figure 4. Gravimetric nitrogen saturation capacity for trigonal arrays of open single-walled carbon nanotubes at 77 K and relative pressure $P/P_0 = 1$ as a function of tube diameter D and separation G .

Comparisons of simulations with experiment.

In the case of nanotubes, comparisons between experimental and simulated gravimetric adsorption capacities are complicated because experimental amounts adsorbed have been measured on nanotube samples that have different purities and that have not been ordered into arrays. Also, as the foregoing shows, simulated gravimetric capacities depend upon the geometry of the array.

Comparison of hydrogen capacities at 298 and 77 K.

Table 2. Comparisons of gravimetric hydrogen storage capacities from experiments and molecular simulations.

System	T / K	P / bar	H ₂ capacity / wt%	Ref
SWCNT, 50% purity (E)	300	101	4.2	[6]
Trigonal array of open SWCNT (S)	298	100	4.7 max ^a	d
SWCNT, high purity (E)	80	72	8.25	[7]
Trigonal array of open SWCNT (S)	77	70	0-33 ^b	d

(E) – Experiment; (S) Simulation. a. $D = 60$ Å, $G = 10$ Å; b. $D = 6$ Å, $G = 30$ Å. d. this work

An experimental measurement of hydrogen capacity for 50% pure SWCNT at ambient temperatures and ~101 bar of 4.2 wt% [6], see Table 2, is in reasonable agreement with the hydrogen capacity at similar temperatures and pressures (4.7 wt%) obtained from simulations for trigonal arrays of open SWCNT with $D = 60$ Å, $G = 10$ Å. Molecular simulations of hydrogen storage at 77 K and 70 bar on trigonal arrays of open SWCNT with $D = 7$ Å, $G = 30$ Å, produce a

very high capacity (33 wt%, Table 2). This may be compared with an experimental measurement made on high purity SWCNT at similar temperatures and pressures [7] (8.25 wt%, Table 2). This simple comparison suggests that the experimental hydrogen capacities of nanotubes at 77 K can be increased substantially by developing ordered arrays.

Comparison of nitrogen capacities at 77 K. Some experimental measurements of adsorption of nitrogen on SWCNT have been reported by Alain *et al.* [8]. Here, a more precise comparison between simulation and experiment can be made because the dimensions of the nanotubes ($D \sim 13.8$ Å) are known from high-resolution transmission electron microscopy images. HRTEM also showed that the SWCNT were present in closed packed bundles with $G \sim 3.2$ Å. A comparison of the isotherm for these nanotubes measured using a volumetric apparatus with the results from simulations in trigonal arrays of open and closed SWCNT ($D = 13.8$ Å, $G = 3.2$ Å) is in Figure 5.

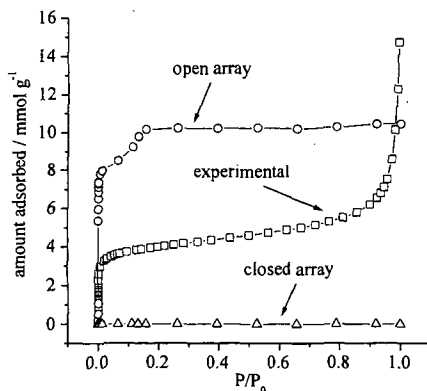


Figure 5. Comparison of experimental isotherms of nitrogen adsorbed at 77 K in single-walled carbon nanotubes to simulated isotherms for the same array geometry ($D = 13.8$ Å, $G = 3.2$ Å) with both open and closed nanotubes.

The simulations show that there is no adsorption in the array of closed SWCNT because the interstitial space is too small to admit nitrogen molecules. The simulated isotherm for the array of open SWCNT is close to Type I in the BDDT classification, indicating, as expected, that the nanotubes are behaving as microporous adsorbents. In the case of the experimental isotherm the steep rise at low relative pressures also indicates the presence of micropores. From the average bundle size and tube diameter [8], it is estimated that an average bundle contains about 50 nanotubes. Therefore, the specific surface area of the bundles is ~ 235 m² g⁻¹. The measured BET surface area of the nanotube sample is 302 m² g⁻¹ [8], larger than the estimated bundle surface area. It is believed that the majority of the SWCNT are closed, but it is possible that a small proportion are open so that they may make a contribution to the adsorption at low relative pressures. In addition, the impurities in the sample may also contribute to the BET surface area. The steep rise in adsorption at high relative pressures probably reflects condensation in the sample, possibly between the nanotube bundles. We are carrying out further simulations and experimental measurements of adsorption in carbon nanotubes to clarify these points.

CONCLUSIONS

Molecular simulations of adsorption of hydrogen at 298 K and 70 bar in ordered arrays of SWCNT show that significant storage occurs. However, this is $\sim 70\%$ of the DOE target capacity of 6.5 wt%. Experimental measurements of gravimetric hydrogen capacity at ambient temperatures and ~ 100 bar for carbon nanotube samples are similar to those predicted from simulations. The simulations also show that the target gravimetric hydrogen capacity can be achieved with ordered arrays of nanotubes at 77 K and 70 bar with a wide range of diameters and spacings. Experimental measurements of hydrogen capacity under similar conditions lie within the range predicted from simulations, but at $\sim 25\%$ of the predicted maximum capacity. Simulated and experimental measurements of nitrogen adsorption at 77 K on SWCNT both show some evidence for microporous adsorption. Also, the experimental isotherms show evidence for

capillary condensation at high relative pressures, possibly occurring between bundles of nanotubes.

ACKNOWLEDGEMENTS

The authors would like to thank the EU TMR programme, Contract ERBFMBICT972773 and the University of Bath for financial support and Dr W maser of CSIC, Zaragosa, Spain, for providing samples of SWCNT.

REFERENCES

1. Dillon, A. C., Jones, K. M., Bekkedahl, T. A., Kiang, C. H., Bethune, D. S. and Heben, M. J. (1997). Storage of hydrogen in single-walled carbon nanotubes. *Nature* **386**(6623), 377-379.
2. Yin, Y.F., Mays, T. J. and McEnaney, B. (1999). Adsorption of nitrogen in carbon nanotube arrays. *Langmuir* **15**, 8714-8718.
3. Allen, M. P. and Tildesley, D. J. (1987). Computer Simulation of Liquids. Clarendon Press, Oxford, p.127.
4. Yin, Y. F. and Mays, T. J. (1998). Adsorption in carbon nanotubes. *Carbon '98*, Strasbourg, France, 831-832.
5. Peng, D.Y. and Robinson, D.B. (1976). A new two-constant equation of state. *Ind. Eng. Chem. Fundam.* **15**, 59-64.
6. Liu, C., Fan, Y. Y., Liu, M., Cong, H. T., Cheng, H. M. and Dresselhaus, M. S. (1999). Hydrogen storage in single-walled carbon nanotubes at room temperature. *Science* **286**, 1127-1129.
7. Ye, Y., Ahn, C. C., Witham, C., Fultz, B., Liu, J., Rinzler, A. G., Colbert, D., Smith, K. A. and Smalley, R. E. (1999). Hydrogen adsorption and cohesive energy of single-walled carbon nanotubes. *Applied Physics Letters* **74**(16), 2307-2309.
8. Alain, E., Yin, Y. F., Mays, T. J. and McEnaney, B. (2000). Molecular simulation and measurement of adsorption in porous carbon nanotubes. *Stud. Surf. Sci. Catal.* **128**, 313-322.

POROSITY OF CARBON NANOTUBES

Marit Jagtoyen, James Pardue, Terry Rantell, Eric Grulke and Frank Derbyshire

University of Kentucky, Center for Applied Energy Research
2540 Research Park Drive, Lexington, KY 40511, USA

E-mail: jagtoyen@caer.uky.edu

Progress in the large-scale production of carbon nanotubes has opened up possibilities for new applications in some areas of adsorption and catalysis. In this paper we will discuss the characterization of single and multiwalled nanotubes by nitrogen, butane and methane adsorption. Nitrogen adsorption data will be used to calculate pore size distributions of the nanotubes. The incorporation of carbon nanotubes into pitch to change the porosity of the resultant activated carbon will also be discussed. By altering the pore structure of the pitch-based carbon fibers from highly microporous to a wider size distribution of micro and mesopores, new applications of the fibers can be envisaged in areas of environmental science and catalysis.

INTRODUCTION

Recently, methods have been developed at the University of Kentucky to synthesize high purity multiwalled carbon nanotubes (MWNT) in quantities that allow the study of the bulk properties of the material. Continuing work is aimed at improving both the rate of production, by operating on a larger scale, and a simplified process to reduce costs. The suitability of use of nanotubes in applications of gas adsorption, separation and catalysis has been investigated. Currently there is little reliable information available in the literature concerning the pore structure and surface properties of pure carbon MWNTs. Most work have been conducted on samples of low or uncertain purity that may contain high concentrations of amorphous and/or graphitic carbon as a contaminant. In contrast, materials produced at the Center for Applied Energy Research (CAER) are typically better than 95% pure MWNT.

The core diameter of single wall nanotubes (SWNT) is close to 1 nm, with little variation between samples, a value which falls in the range normally defined by micropores (pore entrance diameter < 2nm). MWNT, in contrast, show a small variation in core diameter, typically ranging from 3.5 to 7nm, and hence fall in the mesopore range (diameters 2 to 50nm). The uniformity of the nanotubes and thus the narrow distribution of pore sizes present in the sample, should make them excellent materials for gas separation applications. As an example, the diffusion rate of methane into MWNT bundles has been found to be up to ten times faster than that for butane, offering the prospect for the development of systems providing efficient molecular sieves.

Another objective of the current work is to use carbon nanotubes to modify the porosity of pitch-based activated carbon fibers (ACFs). These are normally derived from isotropic petroleum pitch precursors through a sequence of well-defined process stages, culminating in activation of the isotropic carbon fibers in steam or nitrogen, generating the high surface area and pore structure that is typified by a narrow distribution of micropores. The objective of dispersing mesoporous carbon nanotubes in the isotropic pitch before processing into activated carbon fibers is to produce fibers that are not only significantly more mesoporous, but also show significant improvements in other properties, e.g. strength and electrical conductivity. This could enable the procurement of activated carbon fibers with pore structures tailored to specific environmental applications. This paper will focus on the porosity characterization of multiwalled nanotubes and comparison with single walled tubes, and the introduction of these tubes into pitches to alter the pore structure of the product activated carbon.

EXPERIMENTAL

Single wall nanotubes (SWNTs) manufactured by Carbox Inc. using a carbon arc process with Ni/Y catalyst, were purified by refluxing in 2M nitric acid for 24 hours, filtered and then sonicated in dimethyl sulphoxide (DMSO) for 12 hours before drying. Multiwalled carbon nanotubes were produced at CAER by the catalytic decomposition of a ferrocene-xylene mixture at a temperature of about 700°C and at atmospheric pressure (1). Scanning electron microscopy (SEM) was used to estimate the purity of the MWNT samples. One of the MWNT samples was leached in hydrochloric acid to reduce the amount of iron catalyst from an as-produced concentration of about 5%, in order to determine its affect upon pore structure and accessibility. In a parallel series of experiments, the effect of the inclusion of carbon nanotubes in a pitch matrix precursor on the porosity of the active carbon derived from it was determined. A sample

of SWNT suspended in DMSO was dispersed in the pitch by intimately mixing the suspension with a solution of the pitch in a suitable solvent. A high power ultrasonic probe was used to ensure that the nanotubes were completely dispersed before the solvents were recovered by distillation. The pitch samples were then activated by heating in a steam atmosphere at 877°C to generate an active carbon. Characterization of the pore structures was carried out using an OMNISORB 610 instrument to obtain nitrogen adsorption isotherms at 77 K. The mesopore volume, surface area and pore size distribution were calculated using the BJH method (2).

RESULTS

Porosity of Nanotubes

Adsorption isotherms of SWNT and MWNT are compared in Fig. 1. The MWNT sample is ~100% purity as determined by SEM. The adsorption isotherms for both samples are typical of mesoporous carbons, with the MWNT giving considerably higher nitrogen adsorption. The mesopore size distribution of the two samples is shown in Figure 2. The multiwalled sample clearly has a higher mesopore volume with an average pore size of ~3.5 nm. This corresponds approximately to the diameter of the central core of the MWNTs as determined by transmission electron microscopy to be in the range of 3-7 nm, Figure 3. Elsewhere, it has been shown that the average pore diameter of MWNTs is 4-6 nm (3). The calculated mesopore volumes of MWNTs and SWNTs are shown in Table 1. The SWNT have a mesopore volume of 0.05 cc/g while that of the pure MWNT sample is about 0.45 cc/g.

Table 1. Mesopore volume of different nanotube samples.

Sample ID	Purity (% MWNTs)	Mesopore volume(cc/g)
SWNT	~100%	0.05
MWNT-A	~95%	0.47
MWNT-B	~100%, leached	0.48

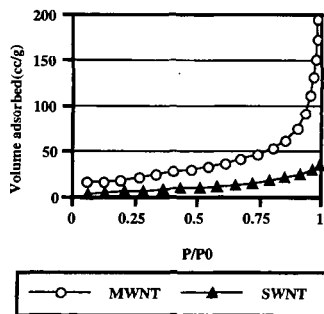


Figure 1. N₂ Adsorption isotherm of MWNT and SWNT

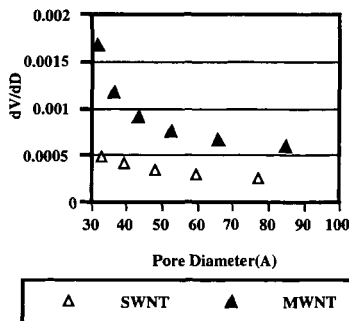


Figure 2. Pore size distribution of SWNT and MWNT

Observations by TEM have shown that small iron particles are present at the ends of the tubes, a consequence of their catalyzing nanotube growth. They are also found intermittently along the core of the innermost tube and in this location may not be accessible by the hydrochloric leaching agent. The acid treatment removes approximately 50% of the iron catalyst and probably improves access to the core of the MWNTs by removing iron from the ends. Even though the total mesopore volume is not significantly enhanced, Table 1, it does seem to broaden the mesopore size distribution slightly.

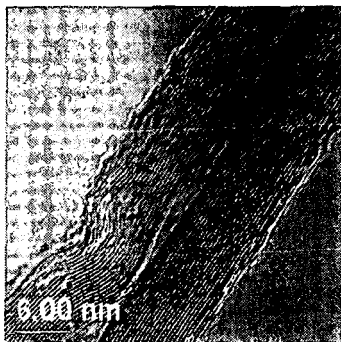


Figure 3. TEM micrograph of MWNT

Addition of SWNTs to pitch to modify the pore structure of activated carbons

A nitrogen adsorption isotherm of activated carbon derived from pitch powder is shown in Figure 4 together with that of the pitch with 5% SWNT incorporated. The pure petroleum pitch based carbon has a very microporous structure, illustrated by the flat isotherm, whereas the pitch with SWNT incorporated has a mesoporous structure, shown by the higher adsorption of nitrogen at high partial pressure. This isotherm is typical of a mesoporous activated carbon. The inclusion of SWNT in the precursor pitch has generated a high mesopore volume in the product active carbon without impairing the retained microporosity. The pore size distribution of the pitch with and without nanotubes is shown in Figure 5. It is evident that the activated carbon has a very narrow pore structure while the carbon with SWNT has a broader pore structure with more porosity in the mesopore range (20-500Å).

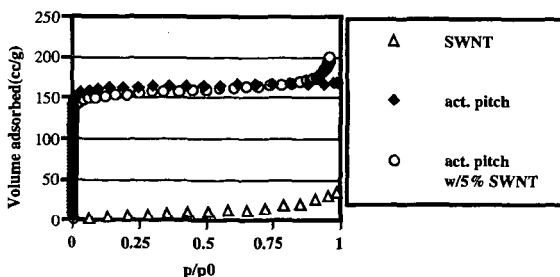


Figure 4. N₂ adsorption isotherms of activated pitch and activated pitch with SWNT

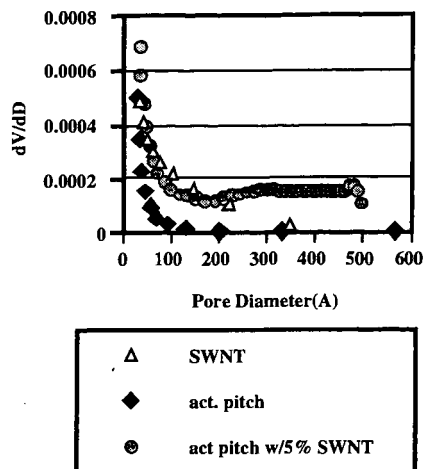


Figure 5. Pore size distribution of activated pitch and activated pitch with SWNT

ACKNOWLEDGEMENTS

The authors wish to acknowledge Rodney Andrews, David Jacques and Apparao Rao at the CAER for supplying samples of MWNTs and Carbolex Inc. for supplying SWNTs. We also acknowledge the financial support from the NSF MRSEC grant DMR - 9809686. The TEM micrograph was taken by X. Fan, Department of Chemical and Materials Engineering, University of Kentucky.

REFERENCES

1. Andrews, R., Jacques, D., Rao, A. M., Derbyshire, F., Qian, D., Fan, X., Dickey, E.C., Chen, J., Chem Phys Lets, 1999, April 16.
2. Gregg, S.J, Sing, K.S.W, in "*Adsorption, Surface Area and Porosity*", 2nd ed., Academic, London , 1982, 94-100.
3. Bonnamy, S., Gaucher, H., Metenier K., Pellenq, R., Nalimova V., Frackowiack, E. and Beguin, F., Abstract presented at the British Carbon Group, Leeds, 1998.